ELSEVIER

World Journal of Gastroenterology®

Supported by NSFC 2005-2006

Volume 11 Number 22
June 14, 2005

National Journal Award 2005

Contents

World Journal of Gastroenterology®
Volume 11 **Number** 22 **June** 14, 2005

Contents

World Journal of Gastroenterology®
Volume 11 **Number** 22 **June** 14, 2005

Contents

Editorial Coordinator for this issue: Umayal Rajarathinam

World Journal of Gastroenterology (*World J Gastroenterol , WJG*), a leading international journal in gastroenterology and hepatology, has an established reputation for publishing first class research on esophageal cancer, gastric cancer, liver cancer, viral hepatitis, colorectal cancer, and *Helicobacter pylori* infection, providing a forum for both clinicians and scientists, and has been indexed and abstracted in Index Medicus, MEDLINE, PubMed, Chemical Abstracts, EMBASE, Abstracts Journals, Nature Clinical Practice Gastroenterology and Hepatology, CAB Abstracts and Global Health. Impact factor of ISI JCR during 2000-2003 is 0.993, 1.445, 2.532 and 3.318 respectively. *WJG* is a weekly journal published jointly by The *WJG* Press and Elsevier Inc. The publication date is on 7th, 14th, 21st, and 28th every month. The *WJG* is supported by The National Natural Science Foundation of China, No. 30224801 and No.30424812, which was founded with a name of *China National Journal of New Gastroenterology* on October 1,1995, and renamed as *WJG* on January 25, 1998.

PUBLISHED JOINTLY BY
The WJG Press and Elsevier Inc

PRINTING GROUP
Printed in Beijing on acid-free paper by Beijing Kexin Printing House

 Print ISSN 1007-9327 CN 14-1219/R.

SPECIAL STATEMENT
All articles published in this journal represent the viewpoints of the authors except where indicated otherwise.

EDITORIAL OFFICE
Editor: *World Journal of Gastroenterology*,
The WJG Press, Apartment 1066 Yishou Garden, 58 North Langxinzhuang Road, PO Box 2345, Beijing 100023, China
Telephone: +86-(0)10-85381901-1023
Fax: +86-10-85381893
E-mail: wjg@wjgnet.com
http://www.wjgnet.com

Public Relationship Manager
Shi-Yu Guo
The WJG Press, Apartment 1066 Yishou Garden, 58 North Langxinzhuang Road, PO Box 2345, Beijing 100023, China
Telephone: +86-(0)10-85381901-1023
Fax: +86-10-8538 1893
E-mail: s.y.guo@wjgnet.com
http://www.wjgnet.com

SUBSCRIPTION INFORMATION
Foreign
Elsevier (Singapore) Pte Ltd, 3 Killiney Road #08-01, Winsland House I, Singapore 239519
Telephone: +65-6349 0200
Fax: +65-6733 1817
E-mail: r.garcia@elsevier.com
http://asia.elsevierhealth.com
Institutional Rates Print-2005 rates: USD1 500.00
Personal Rates Print-2005 rates: USD700.00

Domestic
Local Post Offices Code No. BM 82-261

Author Reprints
The WJG Press, Apartment 1066 Yishou Garden, 58 North Langxinzhuang Road, PO Box 2345, Beijing 100023, China
Telephone: +86-(0)10-85381901-1023
Fax: +86-10-85381893
E-mail: wjg@wjgnet.com
http://www.wjgnet.com

ADVERTISING
Rosalia Da Carcia
Elsevier Science
Journals Marketing & Society Relations Health Science Asia
3 Killiney Road #08-01, Winsland House 1 Singapore 239519
Telephone: +65-6349 0200
Fax +65- 6733 1817
E-mail: r.garcia@elsevier.com
http://asia.elsevierhealth.com

INSTRUCTIONS TO AUTHORS
Full instructions are available online at http://www.wjgnet.com/wjg/help/instructions.jsp If you do not have web access please contact the editorial office.

World Journal of Gastroenterology®

Editorial Board

2004-2006

Published by The WJG Press and Elsevier Inc., PO Box 2345, Beijing 100023, China
Fax: +86-(0)10-85381893 E-mail: wjg@wjgnet.com http://www.wjgnet.com

Bulgaria
Zahariy Alexandrov Krastev, *Sofia*

Canada
Wang-Xue Chen, *Ottawa*
Richard N Fedorak, *Edmonton*
Hugh James Freeman, *Vancouver*
Samuel S Lee, *Calgary*
Philip Martin Sherman, *Toronto*
Alan BR Thomson, *Edmonton*
Eric M Yoshida, *Vancouver*

China
Francis KL Chan, *Hong Kong*
Xiao-Ping Chen, *Wuhan*
Jun Cheng, *Beijing*
Chi-Hin Cho, *Hong Kong*
Zong-Jie Cui, *Beijing*
Da-Jun Deng, *Beijing*
Er-Dan Dong, *Beijing*
Sheung-Tat Fan, *Hong Kong*
Xue-Gong Fan, *Changsha*
Jin Gu, *Beijing*
De-Wu Han, *Taiyuan*
Shao-Heng He, *Shantou*
Fu-Lian Hu, *Beijing*
Wayne HC Hu, *Hong Kong*
Ching Lung Lai, *Hong Kong*
Kam Chuen Lai, *Hong Kong*
Wai-Keung Leung, *Hong Kong*
Zhi-Hua Liu, *Beijing*
Ai- Ping Lu, *Beijing*
Jing-Yun Ma, *Beijing*
Lun-Xiu Qin, *Shanghai*
Yu-Gang Song, *Guangzhou*
Peng Shang, *Xi'an*
Qin Su, *Beijing*
Yuan Wang, *Shanghai*
Benjamin Wong, *Hong Kong*
Wai-Man Wong, *Hong Kong*
Hong Xiao, *Shanghai*
Dong-Liang Yang, *Wuhan*
Xue-Biao Yao, *Hefei*
Yuan Yuan, *Shenyang*
Man-Fung Yuen, *Hong Kong*
Jian-Zhong Zhang, *Beijing*
Zhi-Rong Zhang, *Chengdu*
Xiao-Hang Zhao, *Beijing*
Shu Zheng, *Hangzhou*

Costa Rica
Edgar M Izquierdo, *San José*

Croatia
Marko Duvnjak, *Zagreb*

Denmark
Flemming Burcharth, *Herlev*
Peter Bytzer, *Copenhagen*
Hans Gregersen, *Aalborg*
Jens H Henriksen, *Hvidovre*
Fin Stolze Larsen, *Copenhagen*
Søren Møller, *Hvidovre*

Egypt
Abdel-Rahman El-Zayadi, *Giza*

Finland
Pentti Sipponen, *Espoo*

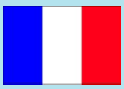

France
Charles Paul Balabaud, *Bordeaux*
Jacques Belghiti, *Clichy*
Pierre Brissot, *Rennes*
Franck Carbonnel, *Besancon*
Bruno Clément, *Rennes*
Jacques Cosnes, *Paris*
Francoise Degos, *Clichy*
Francoise Lunel Fabian, *Angers*
Gérard Feldmann, *Paris*
Jean Fioramonti, *Toulouse*
Rene Lambert, *Lyon*
Didier Lebrec, *Clichy*
Francis Mégraud, *Bordeaux*
Richard Moreau, *Clichy*
Jose Sahel, *Marseille*
Jean-Yves Scoazec, *Lyon*
Jean-Pierre Henri Zarski, *Grenoble*

Germany
HD Allescher, *Garmisch-Partenkirchen*
Rudolf Arnold, *Marburg*
Hubert Blum, *Freiburg*
Peter Born, *Muchen*
Heinz J Buhr, *Berlin*
Haussinger Dieter, *Düsseldorf*
Dietrich CF, *Bad Mergentheim*
Wolfram W Domschke, *Muenster*
Ulrich Robert Fölsch, *Kiel*
Peter R Galle, *Mainz*
Burkhard Göke, *Munich*
Axel M Gressner, *Aachen*
Eckhart Georg Hahn, *Erlangen*
Werner Hohenberger, *Erlangen*
RG Jakobs, *Ludwigshafen*
Joachim Labenz, *Siegen*
Ansgar W Lohse, *Hamburg*
Peter Malfertheiner, *Magdeburg*
Andrea Dinah May, *Wiesbaden*
Stephan Miehlke, *Dresden*
Gustav Paumgartner, *Munich*
Ulrich Ks Peitz, *Magdeburg*
Giuliano Ramadori, *Göttingen*
Tilman Sauerbruch, *Bonn*
Hans Seifert, *Oldenburg*
J Ruediger Siewert, *Munich*
Manfred V Singer, *Mannheim*
Jurgen M Stein, *Frankfurt*
Manfred Stolte, *Bayreuth*
Wolfgang R Stremmel, *Heidelberg*
Hans Ludger Tillmann, *Leipzig*
Siegfried Wagner, *Deggendorf*
Bertram Wiedenmann, *Berlin*

Greece
Arvanitakis C, *Thessaloniki*
Elias A Kouroumalis, *Heraklion*

Hungary
Simon A László, *Szekszárd*
János Papp, *Budapest*

Iceland
Hallgrimur Gudjonsson, *Reykjavik*

India
Sujit Kumar Bhattacharya, *Kolkata*
Chawla YK, *Chandigarh*
Radha Dhiman K, *Chandigarh*
Sri Prakash Misra, *Allahabad*
Kartar Singh, *Lucknow*

Iran
Reza Malekzadeh, *Tehran*

Israel
Abraham Rami Eliakim, *Haifa*
Yaron Niv, *Pardesia*

Italy
Giovanni Addolorato, *Roma*
Alfredo Alberti, *Padova*
Annese V, *San Giovanni Rotondo*
Giovanni Barbara, *Bologna*
Gabrio Bassotti, *Perugia*
Franco Bazzoli, *Bologna*
Adolfo Francesco Attili, *Roma*
Antomio Benedetti, *Ancona*
Giovanni Cammarota, *Roma*
Antonino Cavallari, *Bologna*
Dario Conte, *Milano*
Gino Roberto Corazza, *Pavia*
Guido Costamagua, *Roma*
Antonio Craxi, *Palermo*
Fabio Farinati, *Padua*
Giovanni Gasbarrini, *Roma*
Paolo Gentilini, *Florence*
Edoardo G Giannini, *Genoa*

Paolo Gionchetti, *Bologna*
Roberto De Giorgio, Bologna
Mario Guslandi, *Milano*
Giovanni Maconi, *Milan*
Giulio Marchesini, *Bologna*
Giuseppe Montalto, *Palermo*
Luisi Pagliaro, *Palermo*
Fabrizio R Parente, *Milan*
Perri F, *San Giovanni Rotondo*
Raffaele Pezzilli, *Bologna*
Pilotto A, *San Giovanni Rotondo*
Massimo Pinzani, *Firenze*
Gabriele Bianchi Porro, *Milano*
Piero Portincasa, *Bari*
Giacomo Laffi, *Firenze*
Enrico Roda, *Bologna*
Massimo Rugge, *Padova*
Vincenzo Savarino, *Genova*
Vincenzo Stanghellini, *Bologna*
Calogero Surrenti, *Florence*
Roberto Testa, *Genoa*
Dino Vaira, *Bologna*

Japan

Kyoichi Adachi, *Izumo*
Takashi Aikou, *Kagoshima*
Taiji Akamatsu, *Matsumoto*
Takafumi Ando, *Nagoya*
Akira Andoh, *Otsu*
Taku Aoki, *Tokyo*
Masahiro Arai, *Tokyo*
Tetsuo Arakawa, *Osaka*
Yasuji Arase, *Tokyo*
Masahiro Asaka, *Sapporo*
Hitoshi Asakura, *Tokyo*
Yutaka Atomi, *Tokyo*
Takeshi Azuma, *Fukui*
Nobuyuki Enomoto, *Yamanashi*
Kazuma Fujimoto, *Saga*
Toshio Fujioka, *Oita*
Yoshihide Fujiyama, *Otsu*
Hiroyuki Hanai, *Hamamatsu*
Kazuhiro Hanazaki, *Nagano*
Naohiko Harada, *Fukuoka*
Makoto Hashizume, *Fukuoka,*
Tetsuo Hayakawa, *Nagoya*
Kazuhide Higuchi, *Osaka*
Ichiro Hirata, *Osaka*
Keiji Hirata, *Kitakyushu*
Takafumi Ichida, *Shizuoka*
Kenji Ikeda, *Tokyo*
Kohzoh Imai, *Sapporo*
Fumio Imazeki, *Chiba*
Masayasu Inoue, *Osaka*
Hiromi Ishibashi, *Nagasaki*
Shunji Ishihara, *Izumo*
Toru Ishikawa, *Niigata*
Kei Ito, *Sendai*
Masayoshi Ito, *Tokyo*
Hiroaki Itoh, *Akita*
Hiroshi Kaneko, *Aichi-Gun*
Shuichi Kaneko, *Kanazawa*
Takashi Kanematsu, *Nagasaki*
Junji Kato, *Sapporo*
Mototsugu Kato, *Sapporo*
Shinzo Kato, *Tokyo*
Sunao Kawano, *Osaka*
Yoshikazu Kinoshita, *Izumo*
Masaki Kitajima, *Tokyo*
Tsuneo Kitamura, *Chiba*
Seigo Kitano, *Oita*
Hironori Koga, *Kurume*
Satoshi Kondo, *Sapporo*
Shoji Kubo, *Osaka*
Shigeki Kuriyama, *Kagawa*
Masato Kusunoki, *Mie*
Takashi Maeda, *Fukuoka*
Shin Maeda, *Tokyo*
Osamu Matsui, *Kanazawa*
Yasushi Matsuzaki, *Tsukuba*
Hiroto Miwa, *Hyogo*
Masashi Mizokami, *Nagoya*
Motowo Mizuno, *Hiroshima*
Morito Monden, *Suita*
Hisataka S Moriwaki, *Gifu*
Yoshiharu Motoo, *Kanazawa*
Akihiro Munakata, *Hirosaki*
Kazunari Murakami, *Oita*
Kunihiko Murase, *Tusima*
Masato Nagino, *Nagoya*
Yujl Naito, *Kyoto*
Hisato Nakajima, *Tokyo*
Hiroki Nakamura, *Yamaguchi*
Shotaro Nakamura, *Fukuoka*
Akimasa Nakao, *Nagoya*
Mikio Nishioka, *Niihama*
Susumu Ohmada, *Maebashi*
Masayuki Ohta, *Oita*
Tetsuo Ohta, *Kanazawa*
Susumu Okabe, *Kyoto*
Katsuhisa Omagari, *Nagasaki*
Saburo Onishi, *Nankoku*
Morikazu Onji, *Ehime*
Hiromitsu Saisho, *Chiba*
Hidetsugu Saito, *Tokyo*
Takafumi Saito, *Yamagata*
Isao Sakaida, *Yamaguchi*
Michiie Sakamoto, *Tokyo*
Iwao Sasaki, *Sendai*
Motoko Sasaki, *Kanazawa*
Chifumi Sato, *Tokyo*
Shuichi Seki, *Osaka*
Hiroshi Shimada, *Yokohama*
Mitsuo Shimada, *Tokushima*
Hiroaki Shimizu, *Chiba*
Tooru Shimosegawa, *Sendai*
Tadashi Shimoyama, *Hirosaki*
Ken Shirabe, *Iizuka City*
Yoshio Shirai, *Niigata*
Katsuya Shiraki, *Mie*
Yasushi Shiratori, *Okayama*
Yasuhiko Sugawara, *Tokyo*
Toshiro Sugiyama, *Toyama*
Kazuyuki Suzuki, *Morioka*
Hidekazu Suzuki, *Tokyo*
Tadatoshi Takayama, *Tokyo*
Tadashi Takeda, *Osaka*
Koji Takeuchi, *Kyoto*
Kiichi Tamada, *Tochigi*
Akira Tanaka, *Kyoto*
Eiji Tanaka, *Matsumoto*
Noriaki Tanaka, *Okayama*
Shinji Tanaka, *Hiroshima*
Kyuichi Tanikawa, *Kurume*
Tadashi Terada, *Shizuoka*
Akira Terano, *Shimotsugagun*
Kazunari Tominaga, *Osaka*
Hidenori Toyoda, *Ogaki*
Akihito Tsubota, *Chiba*
Shingo Tsuji, *Osaka*
Takato Ueno, *Kurume*
Shinichi Wada, *Tochigi*
Hiroyuki Watanabe, *Kanazawa*
Sumio Watanabe, *Akita*
Toshio Watanabe, *Osaka*
Yuji Watanabe, *Ehime*
Chun-Yang Wen, *Nagasaki*
Koji Yamaguchi, *Fukuoka*
Takayuki Yamamoto, *Yokkaichi*
Takashi Yao, *Fukuoka*
Hiroshi Yoshida, *Tokyo*
Masashi Yoshida, *Tokyo*
Norimasa Yoshida, *Kyoto*
Kentaro Yoshika, *Toyoake*
Masahide Yoshikawa, *Kashihara*

Lithuania

Sasa Markovic, *Japljeva*

Macedonia

Vladimir Cirko Serafimoski, *Skopje*

Malaysia

Andrew Seng Boon Chua, *Ipoh*
Jayaram Menon, *Sabah*
Khean-Lee Goh, *Kuala Lumpur*

Monaco

Patrick Rampal, *Monaco*

Netherlands

Louis MA Akkermans, *Utrecht*
Karel Van Erpecum, *Utrecht*
Albert K Groen, *Amsterdam*
Dirk Joan Gouma, *Amsterdam*
Jan BMJ Jansen, *Nijmegen*
Evan Anthony Jones, *Abcoude*
Ernst Johan Kuipers, *Rotterdam*
Chris JJ Mulder, *Amsterdam*
Michael Müller, *Wageningen*

Pena AS, *Amsterdam*
Andreas Smout, *Utrecht*
RW Stockbrugger, *Maastricht*
GP Vanberge-Henegouwen, *Utrecht*

New Zealand
Ian David Wallace, *Auckland*

Norway
Trond Berg, *Oslo*
Helge Lyder Waldum, *Trondheim*

Pakistan
Muhammad S Khokhar, *Lahore*

Philippines
Eulenia Rasco Nolasco, *Manila*

Poland
Tomasz Brzozowski, *Cracow*
Andrzej Nowak, *Katowice*

Portugal
Miguel Carneiro De Moura, *Lisbon*

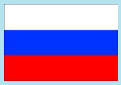

Russia
Vladimir T Ivashkin, *Moscow*
Leonid Lazebnik, *Moscow*
Vasiliy I Reshetnyak, *Moscow*

Singapore
Bow Ho, *Kent Ridge*
Francis Seow-Choen, *Singapore*

Slovakia
Anton Vavrecka, *Bratislava*

South Africa
Michael C Kew, *Parktown*

South Korea
Jin-Hong Kim, *Suwon*
Myung-Hwan Kim, *Seoul*
Yun-Soo Kim, *Seoul*
Yung-Il Min, *Seoul*
Jae-Gahb Park, *Seoul*
Dong Wan Seo, *Seoul*

Spain
Abraldes JG, *Barcelona*
Fernando Azpiroz, *Barcelona*
Ramon Bataller, *Barcelona*
Josep M Bordas, *Barcelona*
Maria Buti, *Barcelon*
Xavier Calvet, *Sabadell*
Antoni Castells, *Barcelona*
Manuel Daz-Rubio, *Madrid*
Juan C Garcia-Pagán, *Barcelona*
Genover JB, *Barcelona*
Javier P Gisbert, *Madrid*
Jaime Guardia, *Barcelona*
Angel Lanas, *Zaragoza*
Ricardo Moreno-Otero, *Madrid*
Julian Panes, *Barcelona*
Miguel Perez-Mateo, *Alicante*
Josep M Pique, *Barcelona*
Jesus Prieto, *Pamplona*
Luis Rodrigo, *Oviedo*

Sri Lanka
Janaka De Silva, *Ragama*

Swaziland
Gerd Kullak-Ublick, *Zurich*

Sweden
Lars Christer Olbe, *Molndal*
Curt Einarsson, *Huddinge*
Lars R Lundell, *Stockholm*
Xiao-Feng Sun, *Linkoping*

Switzerland
Christoph Beglinger, *Basel*
Michael W Fried, *Zurich*
Bruno Stieger, *Zurich*
Arthur Zimmermann, *Berne*

Turkey
Yusuf Bayraktar, *Ankara*
Figen Gurakan, *Ankara*
Cihan Yurdaydin, *Ankara*

United Kingdom
Axon ATR, *Leeds*
Paul Jonathan Ciclitira, *London*
Amar Paul Dhillon, *London*
Stuarts Forbes
Subrata Ghosh, *London*
Brian T Johnston, *Belfast*
David EJ Jones, *Newcastle*
Michael A Kamm, *Harrow*
Hong-Xiang Liu, Cambridge
Giorgina Mieli-Vergani, *London*
Nikolai V Naoumov, *London*
John P Neoptolemos, *Liverpool*
James Neuberger, *Birmingham*
Colm Antoine O'Morain, *Dublin*
Simon D Taylor-Robinson, *London*
Frank Ivor Tovey, *Basingstoke*
Min Zhao, *Foresterhill*

United States
Firas H Ac-Kawas, *Washington*
Gianfranco D Alpini, *Temple*
Paul Angulo, *Rochester*
Jamie S Barkin, *Miami Beach*
Todd Baron, *Rochester*
Kim Elaine Barrett, *San Diego*
Jennifer D Black, *Buffalo*
Xu Cao, *Birmingham*
David L Carr-Locke, *Boston*
Marc F Catalano, *Milwaukee*
Xian-Ming Chen, *Rochester*
James M Church, *Cleveland*
Vincent Coghlan, *Beaverton*
James R Connor, *Hershey*
Pelayo Correa, *New Orleans*
John Cuppoletti, *Cincinnati*
Peter V Danenberg, *Los Angeles*
Kiron Moy Das, *New Brunswick*
Hala El-Zimaity, *Houston*
Ronnie Fass, *Tucson*
Emma E Furth, *Pennsylvania*
John Geibel, *New Haven*
Graham DY, *Houston*
Joel S Greenberger, *Pittsburgh*
Anna S Gukovskaya, *Los Angeles*
Gavin Harewood, *Rochester*
Atif Iqbal, *Omaha*
Hajime Isomoto, *Rochester*
Dennis M Jensen, *Los Angeles*
Leonard R Johnson, *Memphis*
Peter James Kahrilas, *Chicago*
Anthony Nicholas Kalloo, *Baltimore*
Neil Kaplowitz, *Los Angeles*
Emmet B Keeffe, *Palo Alto*
Joseph B Kirsner, *Chicago*
Burton I Korelitz, *New York*
Robert J Korst, *New York*
Richard A Kozarek, *Seattle*
Shiu-Ming Kuo, *Buffalo*
Frederick H Leibach, *Augusta*
Andreas Leodolter, *La Jolla*
Ming Li, *New Orleans*
Lenard M Lichtenberger, *Houston*
Gary R Lichtenstein, *Philadelphia*
Josep M Llovet, *New York*
Martin Lipkin, *New York*

Manuscript reviewers of *World Journal of Gastroenterology*

PO Box 2345, Beijing 100023, China
www.wjgnet.com
wjg@wjgnet.com

ELSEVIER

World J Gastroenterol 2005;11(22):3331-3334
World Journal of Gastroenterology ISSN 1007-9327

Inhibitory effect of adeno-associated virus-mediated gene transfer of human endostatin on hepatocellular carcinoma

Hong Liu, Cheng-Hong Peng, Ying-Bin Liu, Yu-Lian Wu, Zhi-Ming Zhao, Yong Wang, Bao-San Han

Hong Liu, Ying-Bin Liu, Yu-Lian Wu, Zhi-Ming Zhao, Yong Wang, Bao-San Han, Department of Surgery, Second Affiliated Hospital, Zhejiang University College of Medicine, Hangzhou 310006, Zhejiang Province, China
Cheng-Hong Peng, Department of Surgery, Ruijin Hospital, Shanghai Second Medical University, Shanghai 200025, China
Supported by the National Natural Science Foundation of China, No. 20074031
Correspondence to: Dr. Hong Liu, Department of Surgery, Second Affiliated Hospital, Zhejiang University College of Medicine, 88 Jiefang Road, Hangzhou 310006, Zhejiang Province, China. lhong.lli@sohu.com
Telephone: +86-571-87932468
Received: 2004-06-29 Accepted: 2004-07-15

Abstract

AIM: To investigate the effect of adeno-associated virus-mediated gene transfer of human endostatin on the growth of hepatocellular carcinoma (HCC).

METHODS: HCC cell line Hep3B was infected with recombinant adeno-associated virus containing human endostatin gene (rAAV2-hEndo). The results of transfection were detected by RT-PCR and SDS-PAGE assay. MTT assay was used to observe the effects of supernatant of transfected cells on ECV304 cell proliferation. An animal model of HCC was established by injecting Hep3B cells subcutaneously into the back of nude mice. Intratumoral injection of rAAV2-hEndo, empty virus and phosphate-buffered saline were given sequentially. Serum endostatin was determined by ELISA, the inhibitory effect of endostatin on the growth of xenograft was assessed in 3 wk.

RESULTS: The results of RT-PCR and SDS-PAGE assay confirmed that rAAV2-hEndo successfully transfected Hep3B cells, and endostatin was secreted from Hep3B cells to medium. The supernatant of transfected cells markedly inhibited the proliferation of ECV304 cells ($P<0.01$). Intratumoral injection of rAAV2-hEndo (2×10^{10} v.g.) led to a sustained serum endostatin level of approximately (86.71±5.19) ng/mL. The tumor volume and microvessel density were less in rAAV2-hEndo group than in control groups ($P<0.01$).

CONCLUSION: Human endostatin can be stably expressed by adeno-associated virus-mediated gene transfer and effectively inhibit the growth of HCC.

Key words: Endostatin; Gene; Adeno-associated virus; Hepatocellular carcinoma

Liu H, Peng CH, Liu YB, Wu YL, Zhao ZM, Wang Y, Han BS. Inhibitory effect of adeno-associated virus-mediated gene transfer of human endostatin on hepatocellular carcinoma. *World J Gastroenterol* 2005; 11(22): 3331-3334
http://www.wjgnet.com/1007-9327/11/3331.asp

INTRODUCTION

Endostatin, a M_r 22 000 protein, was originally isolated from the supernatant of a cultured murine hemangioendothelioma cell line and represents a COOH-terminal fragment of collagen XVIII α1-chain[1]. It is a potent angiogenesis inhibitor that specifically inhibits the proliferation and migration of endothelial cells but has no effect on tumor cells or nonendothelial cell types[1-5]. Animal studies demonstrated that recombinant endostatin strongly inhibits the growth of a variety of murine and xenotransplanted human tumors[6-9]. The expression of endostatin is also associated with progression and prognosis of human hepatocellular carcinoma (HCC)[10-12]. In addition, elevated serum endostatin can inhibit tumor liver metastases by preferential targeting of hepatic sinusoidal endothelium[13,14]. In the present study, the recombinant adeno-associated virus vector containing human endostatin gene (rAAV2-hEndo) was constructed and used to transfect liver cancer cells. The data revealed that transfected cells could stably express active endostatin. Furthermore, our *in vivo* experiments showed that intratumoral injection of rAAV-hEndo could inhibit angiogenesis and growth of HCC.

MATERIALS AND METHODS

Reagents and cell lines

Recombinant adeno-associated virus (rAAV) was constructed in the Institute of Virology, Chinese Academy of Preventive Medicine. Human HCC cell line Hep3B was purchased from Shanghai Cancer Institute. Human umbilical vein endothelial cell line ECV304 was purchased from Institute of Biochemistry and Cell Biology, Chinese Academy of Sciences. The cells were incubated in DMEM (Gibco BRL) at 37 ℃ in a humidified 50 mL/L CO_2 atmosphere. All media were supplemented with 10% fetal calf serum, 100 U/mL penicillin, 100 μg/mL streptomycin, and 2 mmol/L L-glutamine.

Transfection in vitro

Hep3B cells were plated on 24-well plates at a density of

5×10^4 cells/well and incubated for 24 h. One of the wells was chosen to count cells. The cells were washed twice with PBS and incubated in 200 μL of serum-free medium with rAAV2-hEndo (1×10^5 v.g./cell) or AAV2 for 1 h. The medium was replaced by DMEM supplemented with 10% fetal calf serum, and cells were incubated for 72 h.

RT-PCR analysis

Total RNA was extracted from 10^7 transfected-Hep3B cells using the TRIzol reagent (Gibco BRL), and cDNA synthesis was performed using the reverse transcription system (Gibco BRL) according to the manufacturer's instructions. One microliter of cDNA was used as template and PCR amplification was carried out in a 50 μL reaction system . The primers were as follows: endostatin: 5'-AGT CGA ATT CAT GCA CAG CCA CCG CGA CTT CC-3', 5'-CTG TCG TCG ACC TA CTT GGA GGC AGT CAT G-3' (product size, 552 bp); β-actin: 5'-TCA CCC ACA CTG TGC CCA TCT ACG A-3', 5'-CAG CGG AAC CGC TCA TTG CCA ATG G-3' (product size, 295 bp). The following PCR cycling parameters were employed: at 95 ℃ for 5 min, followed by 35 cycles at 95 ℃ for 45 s, at 56 ℃ for 1 min, and at 72 ℃ for 1 min, then at 72 ℃ for 7 min. The PCR products were resolved on a 1.5% agarose gel.

SDS-PAGE analysis

AAV2 and rAAV2-hEndo-transfected Hep3B cells, and untransfected Hep3B cells were incubated in 24-well plates for 72 h respectively. The supernatant was collected, and 20 μL of 50-fold concentrated supernatant was used as SDS-PAGE samples. SDS-PAGE was performed according to a standard procedure under reducing conditions. Samples were loaded on 15% SDS-PAGE gel and run until the prestain molecular weight standard (Amersham Biosciences) revealed a good resolution, followed by staining with Coomassie Blue and destaining with methanol and acetic acid.

Endothelial cell proliferation assay

ECV304 cells (1×10^4 per well) were incubated in 96-well plates for 24 h. The cells were washed with PBS and the medium was replaced by 20 μL of 10-fold concentrated supernatant of transfected cells. Serum-free medium served as control. After 20 min, 80 μL DMEM supplemented with 10% fetal calf serum was added and cells were incubated for 24, 48, or 72 h, respectively. The viability of cells was determined by colorimetric MTT assay. Absorbance at 570 nm was read using a Model-550 ELISA plate reader (Bio-Rad).

Treatment of transplanted tumor

Hep3B cells were harvested and rinsed with serum-free medium. A total of 2×10^6 cells were inoculated subcutaneously into the back of 6-wk-old BALB/c nude mice. When the diameter of tumor reached about 0.5 cm, the mice were divided into three groups (8 mice/group). Two groups of mice were injected 100 μL rAAV2-hEndo or AAV2 (2×10^{11} v.g./mL). The control groups received PBS injection. Tumor size was monitored by measuring the longest and shortest dimensions thrice a week with a dial caliper, and tumor volume was calculated as width$^2\times$length$\times\pi/6$. The experiments were terminated in 3 wk. The serum samples of mice were collected by centrifugation at 10 000 *g*, and ELISA was performed to determine the serum level of endostatin according to the instructions of human endostatin EIA kit.

Detection of microvessel density

Tumor specimens were taken from the mice, embedded in paraffin and stained with hematoxylin-eosin. Five-micrometer-thick sections were mounted on silanized slides, which were processed according to the standard methods with ABC kit. The primary antibody used was polyclonal antibody of factor XVIII-related antigen (Dako, Glostrup, Denmark) at the dilution of 1:100. Diaminobenzine was used for color development. Negative controls were generated by substituting the primary antibody with distilled water. Neovascular hot spots were searched on duplicate slide set for each sample, which were frequently localized at or near the margin of tumors. Sections were scanned at low power (×40). Five areas with the greatest density of distinct positive microvessels were selected and a ×200 field in each was counted by two independent observers under an Olympus BX60 microscope. The mean value of the five fields was considered as the microvessel density (MVD) of each sample. Data were expressed as the number of microvessels per high power field.

RESULTS

Expression of endostatin in transfected cells

To evaluate the transcriptional expression of endostatin in rAAV2-hEndo transfected cells, RT-PCR was carried out and PCR products were analyzed under ultraviolet light after 1.5% agarose gel electrophoresis. A 552-bp fragment was visualized in PCR products amplified from transfected cells, but not from controls (Figure 1), indicating that endostatin gene was successfully transferred into Hep3B cells. On a reducing 15% SDS-PAGE gel, a distinct band of M_r 22 000, corresponding to endostatin, was seen in the supernatant of rAAV2-hEndo transfected cells only (Figure 2), confirming that endostatin could be stably expressed and secreted in Hep3B cells.

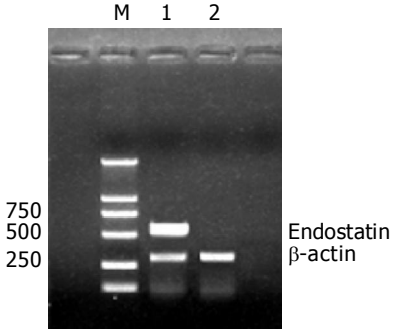

Figure 1 RT-PCR analysis of endostatin in transfected cells. M: DL2000 DNA marker; lane 1: PCR products amplified from rAAV2-hEndo transfected cells; lane 2: PCR products amplified from AAV2 transfected cells.

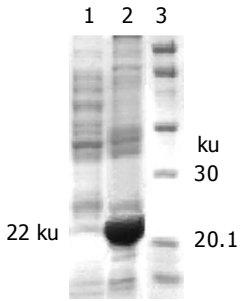

Figure 2 SDS-PAGE of the supernatant of transfected cells. Lane 1: concentrated supernatant of AAV2 transfected Hep3B cells; lane 2: rAAV2-hEndo transfected Hep3B cells; lane 3: molecular weight standard (Amersham Biosciences), myosin (M_r 220 000), phosphorylase (M_r 97 000), albumin (M_r 66 000), ovalbumin (M_r 45 000), carbonic anhydrase (M_r 30 000), trypsin inhibitor (M_r 20 100), lysozyme (M_r 14 300).

Antiangiogenic activities of endostatin

MTT assay was used to investigate the effects of endostatin on endothelial cell proliferation. ECV304 cells were incubated in supernatant of transfected cells for 24, 48 and 72 h. The optical densities in endostatin-transfected group (0.375±0.044, 0.481±0.025, 0.538±0.047) were lower than those in AAV2-transfected group (0.429±0.051, 0.740±0.031, 0.871±0.057) (P<0.05). However, the optical density in AAV2-transfected group had no significant difference from that of DMEM group (Figure 3), suggesting that endostatin expressed by rAAV2/Endo-transfected Hep3B cells could markedly inhibit ECV304 cell proliferation.

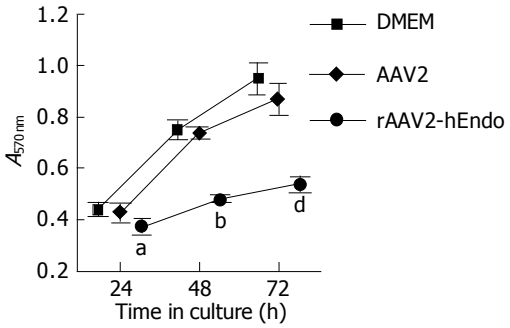

Figure 3 Proliferation inhibition of endothelial cells by supernatant from transfected and untransfected cells. [a]P<0.05, [b]P<0.01 and [d]P<0.01 *vs* AAV2-transfected group.

Determination of endostatin in vivo

The results of ELISA showed that intratumoral injection of rAAV2-hEndo (2×10^{10} v.g.) led to a sustained serum endostatin level of approximately (86.71±5.19) ng/mL. But in empty virus injection group and PBS-injection group, we did not detect the expression of endostatin, indicating that the endostatin could be efficiently expressed *in vivo* by adeno-associated virus-mediated gene transfer.

Effects of endostatin on HCC growth

After 3 wk, the tumor volume and MVD of rAAV2-hEndo injection group were significantly less than those in AAV2-injection group and PBS-injection group (P<0.01, Table 1).

The results of HE staining showed that necrosis of tissue increased, the number of blood vessels decreased and the distribution of tumor cells was asymmetrical in transplanted tumor treated with rAAV2-hEndo, compared with control groups (Figure 4).

Table 1 Effects of gene transfer of human endostatin on HCC xenograft (mean±SD)

Group	*n*	Volume (cm^3)	MVD (per HP)	Concentration (μg/L)
rAAV2-hEndo group	8	0.493±0.119[b]	18.50±4.38[b]	86.71±5.19
AAV2 group	8	0.992±0.194	44.88±6.22	Not determined
Control group	8	1.073±0.213	46.87±6.60	Not determined

[b]P<0.01 *vs* AAV2 and control group.

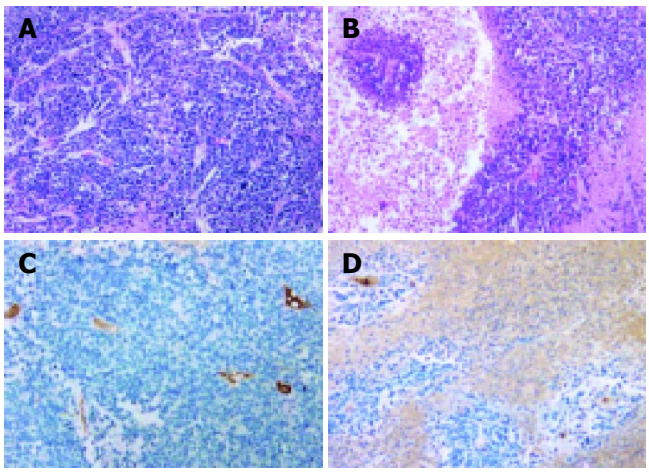

Figure 4 Immunohistochemical and HE staining of HCC xenograft. **A**: AAV2-transfected tissue (HE staining, ×200); **B**: endostatin-transfected tissue (HE staining, ×200); **C**: MVD of AAV2-transfected tissue (stained with factor VIII-related antigen, ×200); **D**: MVD of rAAV2-hEndo transfected tissue (stained with factor VIII-related antigen, ×200).

DISCUSSION

Generally, angiogenesis is essential for tumor growth and metastasis[15-19]. A variety of approaches demonstrate that interference with tumor-induced angiogenesis may be an effective strategy in cancer therapy. However, the most effective strategies require extended suppression of the angiogenic process. Gene therapy offers a possible approach to achieve sustained release of a therapeutically potent transferred gene product[20]. rAAV is currently considered as one of the most promising viral vectors for gene therapy, because of a unique combination of attractive properties[21,22]. Wild-type AAV2 is not associated with any human diseases, and has a broad range of host cells. rAAV vectors have the ability to efficiently transduce both mitotic and postmitotic tissues and the potential of site-specific integration. Previous studies demonstrated that a single administration of rAAV results in persistent expression of transgene and long-lasting phenotypic correction in rat model for more than 6 mo[23]. In addition, Ponnazhagan *et al*[24] reported that rAAV vectors accumulate predominantly in liver cells, suggesting that rAAV may possess hepatotropism.

Here we have constructed a novel recombinant adeno-associated virus vector with endostatin gene (rAAV2-hEndo)[25], which can successfully transfect Hep3B cells. The data indicate that endostatin expressed by transfected cells can markedly inhibit the proliferation of endothelial cells *in vitro*. In our study, intratumoral injection of rAAV2-hEndo (2×10^{10} v.g.) led to a sustained serum endostatin level of approximately (86.71±5.19) ng/mL, the tumor volume and MVD were significantly lower in endostatin-transfected group than in control groups, confirming that transfection of endostatin gene can effectively inhibit tumor cell-induced angiogenesis and suppress the growth of human HCC. Though the antitumor effect of rAAV2-hEndo is evident in HCC, the transplanted tumor did not resolve completely. It is possibly because endostatin has no toxicity to tumor cells and mostly acts on endothelial cells at the hyperplastic stage[26]. Recent studies have shown that combination of antiangiogenesis and conventional therapy improves antitumor effects[27-29], which may be a novel strategy for HCC therapy.

REFERENCES

1 **O'Reilly MS,** Boehm T, Shing Y, Fukai N, Vasios G, Lane WS, Flynn E, Birkhead JR, Olsen BR, Folkman J. Endostatin: an endogenous inhibitor of angiogenesis and tumor growth. *Cell* 1997; **88**: 277-285

2 **Boehm T,** Folkman J, Browder T, O'Reilly MS. Antiangiogenic therapy of experimental cancer does not induce acquired drug resistance. *Nature* 1997; **390**: 404-407

3 **Dhanabal M,** Ramchandran R, Volk R, Stillman IE, Lombardo M, Iruela-Arispe ML, Simons M, Sukhatme VP. Endostatin: yeast production, mutants,and antitumor effect in renal cell carcinoma. *Cancer Res* 1999; **59**: 189-197

4 **Ackley BD,** Crew JR, Elamaa H, Pihlajaniemi T, Kuo CJ, Kramer JM. The NC1/endostatin domain of *Caenorhabditis elegans* type XVIII collagen affects cell migration and axon guidance. *J Cell Biol* 2001; **152**: 1219-1232

5 **Dhanabal M,** Ramchandran R, Waterman MJ, Lu H, Knebelmann B, Segal M, Sukhatme VP. Endostatin induces endothelial cell apoptosis. *J Biol Chem* 1999; **274**: 11721-11726

6 **Yoon SS,** Eto H, Lin CM, Nakamura H, Pawlik TM, Song SU, Tanabe KK. Mouse endostatin inhibits the formation of lung and liver metastases. *Cancer Res* 1999; **59**: 6251-6256

7 **Perletti G,** Concari P, Giardini R, Marras E, Piccinini F, Folkman J, Chen L. Antitumor activity of endostatin against carcinogen-induced rat primary mammary tumors. *Cancer Res* 2000; **60**: 1793-1796

8 **Yokoyama Y,** Green JE, Sukhatme VP, Ramakrishnan S. Effect of endostatin on spontaneous tumorigenesis of mammary adenocarcinoma in a transgenic mouse model. *Cancer Res* 2000; **60**: 4362-4365

9 **Shi W,** Teschendorf C, Muzyczka N, Siemann DW. Adeno-associated virus-mediated gene transfer of endostatin inhibits angiogenesis and tumor growth *in vivo*. *Cancer Gene Ther* 2002; **9**: 513-521

10 **Musso O,** Theret N, Heljasvaara R, Rehn M, Turlin B, Campion JP, Pihlajaniemi T, Clement B. Tumor hepatocytes and basement membrane-Producing cells specifically express two different forms of the endostatin precursor, collagen XVIII, in human liver cancers. *Hepatology* 2001; **33**: 868-876

11 **Musso O,** Rehn M, Theret N, Turlin B, Bioulac-Sage P, Lotrian D, Campion JP, Pihlajaniemi T, Clement B. Tumor progression is associated with a significant decrease in the expression of the endostatin precursor collagen XVIII in human hepatocellular carcinomas. *Cancer Res* 2001; **61**: 45-49

12 **Dhar DK,** Ono T, Yamanoi A, Soda Y, Yamaguchi E, Rahman MA, Kohno H, Nagasue N. Serum endostatin predicts tumor vascularity in hepatocellular carcinoma. *Cancer* 2002; **95**: 2188-2195

13 **Solaun MS,** Mendoza L, De Luca M, Gutierrez V, Lopez MP, Olaso E, Lee Sim BK, Vidal-Vanaclocha F. Endostatin inhibits murine colon carcinoma sinusoidal-type metastases by preferential targeting of hepatic sinusoidal endothelium. *Hepatology* 2002; **35**: 1104-1116

14 **Miyashita M,** Tajiri T, Yanagi K, Shimizu T, Futami R, Sasajima K, Tokunaga A. Serum levels of vascular endothelial growth factor, basic fibroblast growth factor and endostatin in human metastatic liver tumors. *Hepatogastroenterology* 2003; **50**: 308-309

15 **Hanahan D,** Folkman J. Patterns and emerging mechanisms of the angiogenic switch during tumorigenesis. *Cell* 1996; **86**: 353-364

16 **Hahnfeldt P,** Panigrahy D, Folkman J, Hlatky L. Tumor development under angiogenic signaling: a dynamical theory of tumor growth,treatment response, and postvascular dormancy. *Cancer Res* 1999; **59**: 4770-4775

17 **Wu J,** Fan DM. Angiogenesis and antiangiogenesis therpy. *Shijie Huaren Xiaohua Zazhi* 2001; **9**: 316-321

18 **Abdollahi A,** Lipson KE, Sckell A, Zieher H, Klenke F, Poerschke D, Roth A, Han X, Krix M, Bischof M, Hahnfeldt P, Grone HJ, Debus J, Hlatky L, Huber PE. Combined therapy with direct and indirect angiogenesis inhibition results in enhanced antiangiogenic and antitumor effects. *Cancer Res* 2003; **63**: 8890-8898

19 **Chillemi F,** Francescato P, Ragg E, Cattaneo MG, Pola S, Vicentini L. Studies on the structure-activity relationship of endostatin: synthesis of human endostatin peptides exhibiting potent antiangiogenic activities. *J Med Chem* 2003; **46**: 4165-4172

20 **Li Z,** Pan X, Pan W, Cao GS, Wen ZZ, Fang GE, Qi ZT, Bi JW, Hua JD. Packaging and identification of recombinant adenovirus carrying endostatin soluble vascular endothelial growth inhibitor gene. *Shijie Huaren Xiaohua Zazhi* 2003; **11**: 741-744

21 **Nguyen JT,** Wu P, Clouse ME, Hlatky L, Terwilliger EF. Adeno-associated virus-mediated delivery of antiangiogenic factors as an antitumor strategy. *Cancer Res* 1998; **58**: 5673-5677

22 **Lu Y.** Recombinant adeno-associated virus as delivery vector for gene therapy--a review. *Stem Cells Dev* 2004; **13**: 133-145

23 **During MJ,** Xu R,Young D, Kaplitt MG, Sherwin RS, Leone P. Peroral gene therapy of lactose intolerance using an adeno-associated virus vector. *Nat Med* 1998; **4**: 1131-1135

24 **Ponnazhagan S,** Mukherjee P, Yoder MC,Wang XS, Zhou SZ, Kaplan J, Wadsworth S, Srivastava A. Adeno-associated virus 2-mediated gene transfer *in vivo*: organ-tropism and expression of transduced sequences in mice. *Gene* 1997; **190**: 203-210

25 **Wu ZJ,** Wu XB, Cao H, Dong XY, Wang H, Hou YD. A novel and highly efficient production system for recombinant adeno-associated virus vector. *Science in China* 2001; **31**: 423-430

26 **Bergers G,** Javaherian K, Lo KM, Folkman J, Hanahan D. Effects of angiogenesis inhibitors on multistage carcinogenesis in mice. *Science* 1999; **284**: 808-812

27 **Hanna NN,** Seetharam S, Mauceri HJ, Beckett MA, Jaskowiak NT, Salloum RM, Hari D, Dhanabal M, Ramchandran R, Kalluri R, Sukhatme VP, Kufe DW, Weichselbaum RR. Antitumor interaction of short-course endostatin and ionizing radiation. *Cancer J* 2000; **6**: 287-293

28 **Shi W,** Teschendorf C, Muzyczka N, Siemann DW. Gene therapy delivery of endostatin enhances the treatment efficacy of radiation. *Radiother Oncol* 2003; **66**: 1-9

29 **Plum SM,** Hanson AD, Volker KM, Vu HA, Sim BK, Fogler WE, Fortier AH. Synergistic activity of recombinant human endostatin in combination with adriamycin: analysis of in vitro activity on endothelial cells and *in vivo* tumor progression in an orthotopic murine mammary carcinoma model. *Clin Cancer Res* 2003; **9**: 4619-4626

Science Editor Wang XL and Guo SY **Language Editor** Elsevier HK

PO Box 2345, Beijing 100023, China
www.wjgnet.com
wjg@wjgnet.com

ELSEVIER

World J Gastroenterol 2005;11(22):3335-3338
World Journal of Gastroenterology ISSN 1007-9327

Nude mice multi-drug resistance model of orthotopic transplantation of liver neoplasm and Tc-99m MIBI SPECT on p-glycoprotein

Yu Han, Xiao-Ping Chen, Zhi-Yong Huang, Hong Zhu

Yu Han, Department of Hepatobiliary Surgery, The First Affiliated Hospital, Wenzhou Medical College, Wenzhou 325000, Zhejiang Province, China
Xiao-Ping Chen, Zhi-Yong Huang, Hong Zhu, Hepatic Surgery Center, Tongji Hospital, Tongji Medical College, Huazhong University of Science and Technology, Wuhan 430030, Hubei Province, China
Supported by the Science and Technology Special Fund of Ministry of Health, No. Wkz-2000-1-15
Correspondence to: Dr. Xiao-Ping Chen, Hepatic Surgical Center, Tongji Hospital, Tongji Medical College, Huazhong University of Science and Technology, Wuhan 430030, Hubei Province, China. chenxp@medmail.com.cn
Telephone: +86-27-83662599 Fax: +86-27-83662851
Received: 2003-05-12 Accepted: 2004-02-26

Abstract

AIM: To establish a model of drug-resistant neoplasms using a nude mice model, orthotopic transplantation of liver neoplasm and sporadic abdominal chemotherapy.

METHODS: Hepatocellular carcinoma cells HepG2 were cultured and injected subdermally to form the tumor-supplying mice. The orthotopic drug-resistant tumors were formed by implanting the tumor bits under the envelope of the mice liver and induced by abdominal chemotherapy with Pharmorubicin. Physical examination, ultrasonography, spiral CT and visual inspection were used to examine tumor progression. RT-PCR and immunohistochemistry were used to detect expression of mdr1 mRNA and its encoded protein p-glycoprotein (p-gp). Tc-99m sestamibi scintigraphy was performed by obtaining planar abdominal images at 20 min after injection, and the liver/heart ratios were calculated.

RESULTS: Post-implantation mortality was 0% (0/25), tumor implantation success was 90% (22/25), and the rate of implanting successfully for the second time was 100% (3/3). Tumor induction using Pharmorubicin was 80% (16/20). The mdr1 mRNA expression of the induced group was 23 times higher than that of the control group, and p-gp protein expression was 13-fold higher compared to the control group. The liver/heart ratio (as assessed *in vivo*, using Tc-99m radiography) was decreased significantly in the induced group as compared to the control group.

CONCLUSION: We have established an *in vivo* model of mdr1 in nude mice by orthotopic transplantation of liver neoplasm coupled to chemotherapy. We propose that identification of drug resistance as characterized by decreased 99mTc-ppm radiography due to enhanced clearance by p-gp may be useful in detecting *in vivo* drug resistance, as well as a useful tool in designing more effective therapies.

Key words: Orthotopic transplantation; Liver neoplasm; Sporadic abdominal chemotherapy

Han Y, Chen XP, Huang ZY, Zhu H. Nude mice multi-drug resistance model of orthotopic transplantation of liver neoplasm and Tc-99m MIBI SPECT on p-glycoprotein. *World J Gastroenterol* 2005; 11(22): 3335-3338
http://www.wjgnet.com/1007-9327/11/3335.asp

INTRODUCTION

The multidrug resistance (MDR), which develops in tumor cells, is a major obstacle to the success of cancer chemotherapy[1,2]. P-glycoprotein (p-gp) is a transmembrane protein that acts as an ATP-dependent efflux pump to remove drugs from cells. It is encoded by the mdr1 gene and has been shown to increase with the development of MDR[3]. Up to now, there are at least six members of mdr1, MRP, TopoIIα, GSTp1, MGMT and LRP in MDR family[4-8].

MDR models used currently are basically induced *ex vivo* and do not necessarily reflect living (*in vivo*) tumors accurately[9,10]. In the present study, we aimed to set up a nude mice mdr1 model of orthotopic transplantation of liver neoplasm by abdominal chemical therapy at intervals.

Methods including immunohistochemistry, RT-PCR and flow cytometry have been used in the diagnosis of drug resistance[11-13]. They have a common characteristic, which is that a specimen of target cancer tissue is essential. These methods are not useful in identifying non-resective liver neoplasms. A method that is convenient, rapid and overcoming these limitations would be advantageous in clinical assessment. Sestamibi is a cationic lipophilic agent, widely used for myocardial perfusion imaging to detect various tumors[14-16]. Recent evidence has shown that sestamibi is a suitable transport substrate for p-gp and could provide additional information about the p-gp status of tumor cells[17,18]. So we detected the level of p-gp protein by Tc-99m sestamibi on the nude mice models to evaluate the feasibility of this new way.

MATERIALS AND METHODS

Reagents and drugs

DMEM and TRIzol reagent (Gibco, USA), Pharmorubicin

(Pharmacia, USA), M-MLV reverse transcriptase and oligo $(dT)_{15}$ primer (Promega, USA), *Taq* DNA polymerase (Biostar, USA), 100-bp DNA ladder (SABC, China), monoclonal antibody JSB-1 (Wuhan Boster Biological Technology Co., Ltd, China) and Histostain™-Plus kit (Beijing Zhongshan Biotechnology Co., Ltd, China) were obtained. Mdr1 primers and β-actin primers were designed by using GeneFisher1.3 and produced by TaKaRa (Japan).

Establishment of nude mice model

HepG2 cells were injected subcutaneously at the back of each nude mouse at a concentration of 5×10^6 cells/0.1 mL to establish a model of tumor-bearing mice. Then, the orthotopic mdr1 model was established by implanting tumor bits under the envelope of the mice liver and inducing with abdominal chemotherapy using Pharmorubicin.

Inducing tumor

Ten days post-operatively, when the diameter of the tumor reached to 0.3-0.5 cm, the nude mice were grouped randomly into an inducing group ($n = 20$) and a control group ($n = 5$). Each mouse was injected with Pharmorubicin (10 μg/g ip, twice per week, for 6 wk). Mice in the control group were injected with saline.

Anatomy and pathology

Physical examination, ultrasonography, spiral CT, and visual inspection were used to examine the progression of the tumor. Tumor tissues were fixed with 10% neutral formaldehyde, then paraffin-embedded and sections were made. Following dissection of the mice, the size, number, form, and metastasis of the tumor were carefully observed.

RT-PCR analysis of mdr1

Mdr1 primer (174 bp): 5'-CAT TGG TGT GGT GAG TCA GG-3' and 5'-CTC TCT CTC CAA CCA GGG TG-3'; β-actin primer (247 bp): 5'-CCC AGA GCA AGA GAG GCA TC-3' and 5'-AGC ACA GCC TGG ATA GCA AC-3'.

Total RNA was isolated using the TRIzol reagent according to the manufacturer's instructions and reverse transcribed. cDNA was amplified in a 50 μL reaction containing 10× buffer (5.0 μL), cDNA (2.0 μg), primers (each 1.0 μL), 25 mmol/L $MgCl_2$ (3.0 μL), 10 mmol/L dNTPs (1.0 μL), and *Taq* polymerase (2.5 U). Each of total 30 PCR amplification cycles consisted of denaturation at 94 ℃ for 1 min, primer annealing at 57 ℃ for 45 s, extension at 72 ℃ for 45 s, for a total of 30 cycles. The PCR products were separated by electrophoresis on 2% agarose gels.

Determination of p-gp protein expression level

Tumor tissues were fixed with 10% neutral formaldehyde, then paraffin embedded and sections were made. The sections were stained with the monoclonal antibody JSB-1 followed by Streptavidin-Peroxidase kit (SP kit).

Tc-99m sestamibi SPECT

After administration of 7 MBq Tc-99m sestamibi (prepared according to the manufacturer's instructions), images were obtained at 20-min intervals. Planar abdominal images were acquired on 256×256 matrices using a low-energy high-resolution collimator. The liver/heart ratio was calculated by ROI (regions of interest) technique.

Image and statistical analysis

Image analysis was performed by using ImageTool 2.0 and statistical analysis by SAS 8.01. The Student's t test was performed to evaluate the significant differences between groups. Significance was determined at $P<0.01$.

RESULTS

Establishment of nude mice model

The implantation operation took approximately 12 min to complete. After 30 min, the mice became conscious and returned to normal activity by 60 min with a mortality rate of 0% (0/25). Successful tumor implantation rate was 90% (22/25), and the success rate of a second time implantation was 100% (3/3). Tumor induced successful rate was 80% (16/20).

Anatomy and pathology

The tumors were multilobular, hard, limited in one lobe of liver with an intact envelope. The tumors were clearly delimited from adjacent liver tissue but also appeared with abdominal metastasis (Figures 1A and B). Tumors of a diameter of approximately 0.5 cm could be detected by ultrasound and CT examination. The tumor manifests as a low-density echo by ultrasound and color Doppler flow imaging shows a developed artery spectrum. CT identified the tumors as a low-density lesion after reinforcement (Figures 1C and D). The pathological section showed that the tumor cells were heterogeneous in size and manifest karyomegaly. The nucleus was deeply dyed and appeared heterogeneous.

Expression of mdr1

RT-PCR assay demonstrated that the mdr1 mRNA expression was significantly stronger in the induced group than in the control group. The relative density of each band was scanned and expressed relative to β-actin. Expression of mdr1 in the induced group was 23-fold higher than that in the control group (56.11±5.82% induced *vs* 2.44±0.18% control group, $t = 20.4$, $P<0.01$) (Figure 2).

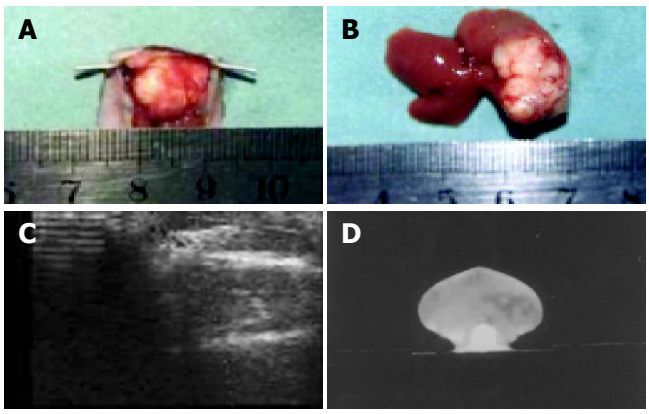

Figure 1 The specimen and images by Doppler and CT. **A:** Specimen of tumor model after 15 d of implantation; **B:** specimen of tumor model after 25 d of implantation; **C:** color Doppler image of tumor model after 25 d of implantation; **D:** contrast-enhanced abdominal CT image of tumor model after 20 d of implantation.

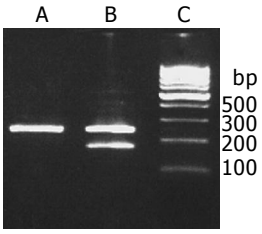

Figure 2 Mdr1 mRNA expression. lane A: Control group; lane B: induced group; lane C: 100-bp marker.

Immuohistochemistry

Immuohistochemical staining indicated that there was a significant expression of p-gp in the inducing group, with thick and buffy particles in the cell membrane and cytoplasm compared to the control group. The positive cells exhibited a nest distribution. P-gp protein expression in the induced group is 13-fold higher than that of the control group (t = 24.9, P<0.01, Figure 3).

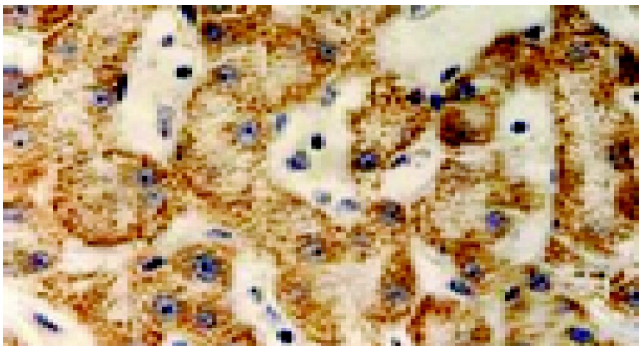

Figure 3 Expression of p-gp by using immunohistochemistry (SABC ×200).

Tc-99m sestamibi SPECT

The MIBI SPECT of the induced group showed a radioactivity deficiency in the tumor which contrasted with a radiographic dense area in the control group. The liver/heart ratio was significantly decreased in the induced group as compared to the control group. The average liver/heart ratio was 0.68±0.10 in the induced group and 1.86±0.32 in the control group (P<0.01, Figures 4A and B).

DISCUSSION

MDR of tumor cells is a major obstacle to the success of cancer chemotherapy[1,2]. A recent focus has been the recognition of the phenomenon of increased expression of p-gp protein encoded by the mdr1 gene, which is increased in liver neoplasms[19,20]. P-gp is a 170-ku membrane glycoprotein, which acts as an energy-dependent efflux pump exporting a variety of structurally and functionally unrelated compounds, including cytotoxic drugs, calcium channel blockers, calmodulin inhibitors, and peptides[21,22]. The importance of p-gp as a mechanism of drug resistance in cancer cells has been well characterized. However, many other associated genes have also been identified, such as MRP, TopoIIα, GSTp1, MGMT, LRP among others. The mechanisms of MDR induced by these other proteins is reportedly different

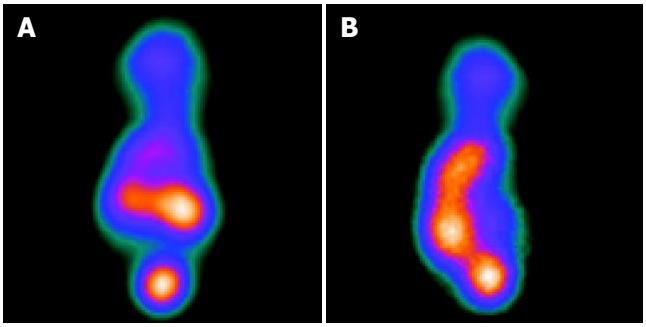

Figure 4 SPECT images of the nude mice model. **A:** SPECT of control group showing dense radioactivity; **B:** SPECT of control group showing deficiency radioactivity.

from p-gp[4-8]. It has been reported previously that p-gp is increased significantly in liver neoplasms[23-25].

Methods including immunohistochemistry, molecular biology (RT-PCR) and flow cytometry have been used in the diagnosis of drug resistance[11-13]. They have a common characteristic, which is that a specimen of target cancer tissue is essential. These methods are not useful in identifying non-resective liver neoplasms. A method that is convenient, rapid and overcoming these limitations would be advantageous in clinical assessment.

Previously, we used SMMC7721 MDR cells to assess drug resistance. The limitations were the length of time required for testing, and the trial-and-error methodology, which is problematic. Most of all, the cells are induced *ex vivo*, which is clearly different from the situation in clinical cancers. Establishment of a nude mice model of orthotopic liver neoplasm using abdominal chemotherapy would ideally represent the *in vivo* development of MDR of liver cancers. In the present study, we demonstrated that such a model is possible, with an inducing successful rate of 80% (16/20). The mdr1 mRNA expression of the induced group was 23 times that of the control group and p-gp protein expression was 13-fold the control group.

Tc-99m sestamibi is a cationic lipophilic agent developed for myocardial perfusion imaging. It is also used for diagnostic imaging of various tumors. Tc-99m sestamibi has been shown to be a substrate for p-gp, and accumulation of Tc-99m sestamibi in MDR cells is decreased or null. The washout rate of Tc-99m in tumor cells is determined by the quality of sestamibi in cells[26]. It has been reported that the MIBI SPECT in breast tumors could be useful in evaluating the level of p-gp expression[27-31]. Our present study demonstrates that, in the nude mice model of orthotopic liver neoplasm, the density of the sestamibi image in the tumors of the induced group is sparse (liver/heart: 0.68±0.10), while the sestamibi density in tumors of the control group was much higher (liver/heart: 1.86±0.32). This observation indicates the potential use of Tc-99m sestamibi as a p-gp probe for *in vivo* determination of p-gp transport function.

In conclusion, we have successfully established the nude mice mdr1 model of orthotopic liver neoplasm, and demonstrated the usefulness of SPECT by Tc-99m sestamibi for diagnosis of expression of p-gp. This model is representative of the clinical situations and could be of potential importance in the researches about the diagnosis and reversal of MDR.

REFERENCES

1 **Gottesman MM.** Multidrug resistance during chemical carcinogenesis: a mechanism revealed? *J Natl Cancer Inst* 1988; **80**: 1352-1353
2 **McGrath MS,** Rosenblum MG, Philips MR, Scheinberg DA. Immunotoxin resistance in multidrug resistant cells. *Cancer Res* 2003; **63**: 72-79
3 **Molinari A,** Calcabrini A, Meschini S, Stringaro A, Crateri P, Toccacieli L, Marra M, Colone M, Cianfriglia M, Arancia G. Subcellular detection and localization of the drug transporter P-glycoprotein in cultured tumor cells. *Curr Protein Pept Sci* 2002; **3**: 653-670
4 **Loe DW,** Deeley RG, Cole SP. Biology of the multidrug resistance-associated protein, MRP. *Eur J Cancer* 1996; **32A**: 945-957
5 **van Zanden JJ,** Geraets L, Wortelboer HM, van Bladeren PJ, Rietjens IM, Cnubben NH. Structural requirements for the flavonoid-mediated modulation of glutathione S-transferase P1-1 and GS-X pump activity in MCF7 breast cancer cells. *Biochem Pharmacol* 2004; **67**: 1607-1617
6 **Zhu Y,** Kong C, Zeng Y, Sun Z, Gao H. Expression of lung resistance-related protein in transitional cell carcinoma of bladder. *Urology* 2004; **63**: 694-698
7 **Kitange GJ,** Smith JS, Jenkins RB. Genetic alterations and chemotherapeutic response in human diffuse gliomas. *Expert Rev Anticancer Ther* 2001; **1**: 595-605
8 **Kunishio K,** Okada M, Miyake K, Matsumoto Y, Nagao S, Nishiyama Y, Ohkawa M. Report of two cases with germinoma treated by individual adjuvant chemotherapy based on the mRNA expression of drug-resistance gene. *No Shinkei Geka* 2004; **32**: 19-26
9 **Ishikawa H,** Nakata K, Mawatari F, Ueki T, Tsuruta S, Ido A, Nakao K, Kato Y, Ishii N, Eguchi K. Retrovirus-mediated gene therapy for hepatocellular carcinoma with reversely oriented therapeutic gene expression regulated by alpha-fetoprotein enhancer/promoter. *Biochem Biophys Res Commun* 2001; **287**: 1034-1040
10 **Bonn V,** Cheung RC, Chen B, Taghibiglou C, Van Iderstine SC, Adeli K. Simvastatin, an HMG-CoA reductase inhibitor, induces the synthesis and secretion of apolipoprotein AI in HepG2 cells and primary hamster hepatocytes. *Atherosclerosis* 2002; **163**: 59-68
11 **Rybarova S,** Boor A, Jurkovic I, Kocan P. Expression of LRP--lung resistance-related protein in the normal colorectal mucosa and in colorectal carcinoma. *Bratisl Lek Listy.* 2003; **104**: 179-183
12 **Hirano T,** Onda K, Toma T, Miyaoka M, Moriyasu F, Oka K. MDR1 mRNA expressions in peripheral blood mononuclear cells of patients with ulcerative colitis in relation to glucocorticoid administration. *J Clin Pharmacol* 2004; **44**: 481-486
13 **Piwnica-Worms D,** Chiu ML, Budding M, Kronauge JF, Kramer RA, Croop JM. Functional imaging of multidrug-resistant P-glycoprotein with an organotechnetium complex. *Cancer Res* 1993; **53**: 977-984
14 **Zhou J,** Higashi K, Ueda Y, Kodama Y, Guo D, Jisaki F, Sakurai A, Takegami T, Katsuda S, Yamamoto I. Expression of multidrug resistance protein and messenger RNA correlate with (99m)Tc-MIBI imaging in patients with lung cancer. *J Nucl Med* 2001; **42**: 1476-1483
15 Vergote J, Moretti JL, Kouyoumdjian JC, Garnier-Suillerot A. MRP1 modulation by PAK-104P: detection with technetium-99m-MIBI in cultured lung tumor cells. *Anticancer Res* 2002; **22**: 251-256
16 **Cayre A,** Cachin F, Maublant J, Mestas D, Feillel V, Ferriere JP, Kwiaktowski F, Chevillard S, Finat-Duclos F, Verrelle P, Penault-Llorca F. Single static view 99mTc-sestamibi scintimammography predicts response to neoadjuvant chemotherapy and is related to MDR expression. *Int J Oncol* 2002; **20**: 1049-1055
17 **Ramachandran C,** Khatib Z, Escalon E, Fonseca HB, Jhabvala P, Medina LS, D'Souza B, Ragheb J, Morrison G, Melnick SJ. Molecular studies in pediatric medulloblastomas. *Brain Tumor Pathol* 2002; **19**: 15-22
18 **Capella LS,** Gefe MR, Silva EF, Affonso-Mitidieri O, Lopes AG, Rumjanek VM, Capella MA. Mechanisms of vanadate-induced cellular toxicity: role of cellular glutathione and NADPH. *Arch Biochem Biophys* 2002; **406**: 65-72
19 **Huang CC,** Wu MC, Xu GW, Li DZ, Cheng H, Tu ZX, Jiang HQ, Gu JR. Overexpression of the MDR1 gene and P-glycoprotein in human hepatocellular carcinoma. *J Natl Cancer Inst* 1992; **84**: 262-264
20 **Warmann S,** Gohring G, Teichmann B, Geerlings H, Pietsch T, Fuchs J. P-glycoprotein modulation improves *in vitro* chemosensitivity in malignant pediatric liver tumors. *Anticancer Res* 2003; **23**: 4607-4611
21 **Chen CJ,** Chin JE, Ueda K, Clark DP, Pastan I, Gottesman MM, Roninson IB. Internal duplication and homology with bacterial transport proteins in the mdr1 (P-glycoprotein) gene from multidrug-resistant human cells. *Cell* 1986; **47**: 381-389
22 **Azzaria M,** Schurr E, Gros P. Discrete mutations introduced in the predicted nucleotide-binding sites of the mdr1 gene abolish its ability to confer multidrug resistance. *Mol Cell Biol* 1989; **9**: 5289-5297
23 **Itsubo M**, Ishikawa T, Toda G, Tanaka M. Immunohistochemical study of expression and cellular localization of the multidrug resistance gene product P-glycoprotein in primary liver carcinoma. *Cancer* 1994; **73**: 298-303
24 **Nagasue N,** Dhar DK, Makino Y, Yoshimura H, Nakamura T. Overexpression of P-glycoprotein in adenomatous hyperplasia of human liver with cirrhosis. *J Hepatol* 1995; **22**:197-201
25 **Soini Y,** Virkajarvi N, Raunio H, Paakko P. Expression of P-glycoprotein in hepatocellular carcinoma: a potential marker of prognosis. *J Clin Pathol* 1996; **49**: 470-473
26 **Marques-Santos LF,** Oliveira JG, Maia RC, Rumjanek VM. Mitotracker green is a P-glycoprotein substrate. *Biosci Rep* 2003; **23**: 199-212
27 **Yoon JH,** Bom HS, Song HC, Lee JH, Jaegal YJ. Double-phase Tc-99m sestamibi scintimammography to assess angiogenesis and P-glycoprotein expression in patients with untreated breast cancer. *Clin Nucl Med* 1999; **24**: 314-318
28 **Yeh JJ,** Hsu WH, Huang WT, Wang JJ, Ho ST, Kao A. Technetium-99m tetrofosmin SPECT predicts chemotherapy response in small cell lung cancer. *Tumour Biol* 2003; **24**: 151-155
29 **Dirlik A,** Burak Z, Goksel T, Erinc R, Karakus H, Ozcan Z, Veral A, Ozhan M. The role of Tc-99m sestamibi imaging in predicting clinical response to chemotherapy in lung cancer. *Ann Nucl Med* 2002; **16**: 103-108
30 **Kunishio K,** Morisaki K, Matsumoto Y, Nagao S, Nishiyama Y. Technetium-99m sestamibi single photon emission computed tomography findings correlated with P-glycoprotein expression, encoded by the multidrug resistance gene-1 messenger ribonucleic acid, in intracranial meningiomas. *Neurol Med Chir (Tokyo)* 2003; **43**: 573-580; discussion 581
31 **Liu Z,** Stevenson GD, Barrett HH, Kastis GA, Bettan M, Furenlid LR, Wilson DW, Woolfenden JM. Imaging recognition of multidrug resistance in human breast tumors using 99mTc-labeled monocationic agents and a high-resolution stationary SPECT system. *Nucl Med Biol* 2004; **31**: 53-65

Science Editor Kumar M and Guo SY **Language Editor** Elsevier HK

PO Box 2345, Beijing 100023, China
www.wjgnet.com
wjg@wjgnet.com

ELSEVIER

World J Gastroenterol 2005;11(22):3339-3345
World Journal of Gastroenterology ISSN 1007-9327

CIK cells from patients with HCC possess strong cytotoxicity to multidrug-resistant cell line Bel-7402/R

You-Shun Zhang, Fang-Jun Yuan, Guo-Feng Jia, Ji-Fa Zhang, Li-Yi Hu, Ling Huang, Ju Wang, Zong-Qing Dai

You-Shun Zhang, Fang-Jun Yuan, Guo-Feng Jia, Ji-Fa Zhang, Li-Yi Hu, Ling Huang, Ju Wang, Zong-Qing Dai, Institute of Liver Surgery, Dongfeng Hospital of YunYang Medical College, Shiyan 442008, Hubei Province, China
Co-first-authors: You-Shun Zhang and Fang-Jun Yuan
Correspondence to: Zong-Qing Dai, Institute of Liver Surgery, Dongfeng Hospital of YunYang Medical College, Shiyan 442008, Hubei Province, China. zlib125@163.com
Telephone: +86-719-8272282 Fax: +86-719-8224085
Received: 2004-06-08 Accepted: 2004-07-15

Abstract

AIM: To investigate the cytotoxicity of the cytokine-induced killer (CIK) cells from the post-operation patients with primary hepatocellular carcinoma (HCC) to multidrug-resistant (MDR) cell of HCC both *in vitro* and *in vivo*.

METHODS: A drug-resistant cell line was established by culturing human HCC cell line Bel-7402 in complete RPMI 1640 medium with increasing concentrations of adriamycin from 10 to 2 000 nmol/L. CIK cells were obtained by inducing the peripheral blood mononuclear cells with rhIFN-γ, monoclonal anti-CD3 antibody, rhIL-1α as well as rhIL-2, which were added into the culture. To detect the cytotoxicity of the CIK cells from HCC patients, the Bel-7402/R was taken as target (T) cells and CIK cells as effect (E) cells. Cytotoxic test was performed and measured by MTT. As to *in vivo* test, CIK cells were transfused into patients with HCC. The tumor specimens of the patients were obtained and immunohistochemistry was carried out to detect CD3, CD45, CD45RO as well as CD68.

RESULTS: A MDR 1 HCC cell line Bel-7402/R was established. Its MDR1 mRNA overexpressed which was shown by RT-PCR; the P-glycoprotein expression increased from 1.32% of parent cells to 54%. CIK cells expanded vigorously by more than 70-fold and the CD3+CD56+ increased by more than 600-fold after 3-wk incubation on average. The cytotoxicity of CIK from HCC patients to Bel-7402/R was about 50% and to L-02 below 10% (t = 8.87, P<0.01), the same as that of CIK from normal individuals. Each of the 17 patients received 1-5×10^{10} of CIK cell transfusion. No side effects were observed. After CIK treatment, the tumor tissue nodules formed and a large amount of lymphocytes infiltrated in the liver cancer tissue and CD3, CD45, CD45RO, and CD68 increased greatly which was shown by immunohistochemistry.

CONCLUSION: A stable MDR1 HCC cell line has been established which could recover from liquid nitrogen and CIK from HCC patients has strong cytotoxicity to MDR HCC cell. CIK adoptive immunotherapy is safe and has no side effects. Receivers improved their immunity to tumor evidently. CIK treatment may be a better choice for HCC patients after operation to prevent the recurrence, especially when tumors have developed drug resistance.

Key words: Hepatocellular carcinoma; Cytokine-induced killer; Cytotoxicity; Multidrug resistance; P-glycoprotein

Zhang YS, Yuan FJ, Jia GF, Zhang JF, Hu LY, Huang L, Wang J, Dai ZQ. CIK cells from patients with HCC possess strong cytotoxicity to multidrug-resistant cell line Bel-7402/R. *World J Gastroenterol* 2005; 11(22): 3339-3345
http://www.wjgnet.com/1007-9327/11/3339.asp

INTRODUCTION

Hepatocellular carcinoma (HCC) is one of the most common malignant tumors with a high mortality especially in China because of wide prevalence of HBV infection. Surgical operation is still the most effective and widely performed treatment, but the high frequency of recurrence after operation dramatically decrease the cure rate of HCC. To prevent recurrence of HCC, many measures have been taken such as regular chemotherapy after operation, intrahepatic arterial infusion of anticancer agents, transcatheter arterial embolization and recently, biotherapy[1-3] such as DC[4] cells and cytokine-induced killer (CIK) cells[5]. However, many patients' prognosis is poor and the 5-year survival rate usually is below 15-30%. Besides other reasons, drug resistance of the tumors induced in the chemotherapy plays an important role, which in turn protects the tumors against the chemical agents[6]. Among the many known biological mechanisms of drug resistance, multidrug resistance (MDR) is of particular interest[7,8]. MDR is associated with amplification or overexpression of the MDR1 gene and the expression of a transmembrane glycoprotein of 170 ku termed P-glycoprotein (Pgp). As a drug pump, it excludes the chemical drugs out of tumor cells and causes treatment failure.

CIK cells are generated according to a novel protocol[9] and several authors[10-13] have demonstrated that CIK possesses versatile anti-tumor advantages including easier generation from T cells, stronger cytotoxicity to tumor as well as more enhanced *in vivo* proliferation potency while compared with other adoptive immunotherapies. Shi *et al*,

and Wang *et al*, demonstrated that CIK treatment for HCC is effective and also safe. Now we show in this paper that multi-drug resistant HCC cell line Bel-7402/R, established by us, is also sensitive to CIK from HCC patients and positive pathological and immunohistochemical results were observed in one case whose tumor sample was verified as positive MDR1 expression by RT-PCR.

MATERIALS AND METHODS

Patients and controls

Seventeen HCC patients post-operation were enrolled in the study, including 16 cases of male and 1 female, aged 36-58 years with an average of 48.8 years. A written informed consent was obtained before CIK treatment which was certified by the Health Bureau of Hubei Province, China. Six of the patients were chosen randomly to take part in the *in vitro* test and six normal people from hospital staff were selected as normal controls.

Cell lines and culture conditions

All cell lines were grown[14] in complete medium (CM) namely RPMI 1640 (Gibco) with 100 mL/L calf serum, 25 mmol/L hepes, 2 mmol/L L-glutamine, 100 U/mL penicillin, 100 mg/mL streptomycin, and 50 μmol/L 2-mercaptoethanol (2-ME, all from Sigma). Some other agents were added according to research needs. Human HCC cell line Bel-7402 was a generous present from Professor Guanxin Shen, Department of Immunology, Tongji Medical School, Huazhong Science and Technology University. HCC cell line SMMC-7721 and embryo liver cell line L-02 were provided by the China Center for Type Culture Collection. Drug-resistance cell lines Bel-7402/R as well as SMMC-7721/R were induced by serially increasing adriamycin (ADM, Sigma) from 10 to 2 000 nmol/L in the culture.

CIK induction

CIK cells were prepared as described according to Schmidt-Wolf[9]. Briefly, for *in vivo* treatment peripheral blood mononuclear cells (PBMCs) were collected by CS-3000 Plus blood cell separator (Baxter, USA) or for *in vitro* test prepared by ficoll separation from post-operation patients with HCC (HCC group) or from volunteers as control group (normal group). The cells were grown in CM and 1 000 U/mL rhIFN-γ was added on d 0, after 24 h of incubation, 50 μg/L mouse monoclonal antibody (mAb) against CD3, 100 U/mL rhIL-1α (all from R&D Systems) and 1 000 U/mL rhIL-2 (Sunshine Pharma. Co., Ltd, China) were added. Cell density was about 1×106/mL and fresh CM with IL-2 was replaced every 3 d. Cell phenotypes were identified by FCM on d 0, 7, 14, 25. Cytotoxicities to target were determined after d 14. Cells were transfused back to patients between d 14 and 21 based on the cell number.

RT-PCR

Primers for MDR1 RT-PCR were designed based on the sequence in GenBank (NM000927), forward primer 5'-CAGGAGATAGGCTGGTTTGATG T-3' and backward primer 5'-TTAGCTTCCAACCACG TGTAAATC-3'. PCR was performed according to molecular cloning protocol, briefly as follows: after the collection of cultured cells or mincing of HCC tissue into small pieces, RNA was extracted by TRIzol reagent. Extracted RNA was solved in diethyl pyrocarbonate-treated water (DEPC water). RT-PCR was performed in 50 μL of mixture containing: 1 μL of extracted RNA, 1 μL of 10 μmoL of both forward and backward primers (synthesized by Sangon, Shanghai, China), 5 μL of 10× buffer (100 mmol/L of Tris-HCl, pH 8.0, 500 nmol/L of KCl, 0.1% gelatin, 1% Triton X-100), 1 μL of 10 mmol/L dNTP, 4 μL of 25 mmol/L MgCl2, 2.5 U of ribonuclease inhibitor, 200 U of M-MLV RT enzyme, 2 U of Taq polymerase, and DEPC water was added to the final volume of 50 μL. The reaction mixture was kept at 42 ℃ for 30 min to synthesize first cDNA, and at 94 ℃×3 min to denature DNA followed by 35 cycles of amplification consisting of 30 s of denaturing DNA at 94 ℃, 30 s of annealing DNA at 58 ℃ and 30 s of extending DNA at 72 ℃. β-actin served as control.

Flow cytometry analysis

All samples were pretreated before analyzed by FCM analyzer (Coulter: EPICX XL). For cell phenotype identification, cells were incubated for 30 min with mAb against CD3, CD4, CD56, coupled to FITC or PE. For the detection of Pgp, cells were fixed with 4% paraformaldehyde for 10 min, incubated with mouse anti-human p-170 for 30 min at room temperature, and stained with goat antimouse IgG coupled to FITC. For Pgp function determination[15], cells were incubated with Rhodamine 123 (Sigma) for 1 h before being trypsinized and washed.

Drug-resistance test

One hundred microliters of each parent or drug-resistant cells were distributed in 96-well culture microplates at 1×10^6/mL density in every well. ADM was added after a serial dilution from 40 μmoL to 36.25 nmoL. A triplicate of same samples was placed to control variation. Cells were incubated at 37 ℃ with 50 mL/L CO_2 for 48 h prior to the addition of 10 μL of MTT[18,20] (5 g/L, Sigma). After another 4 h of incubation, the plate was centrifuged at 3 000 r/min for 5 min, medium was discarded, 150 μL of DMSO was added to each well. Optical absorbance value was read at 570 nm by a microreader (BioRad 550, USA). Cell survival ratio (CSR) was calculated according to the formula: CSR = $A_{570\ \text{experiment}}/A_{570\ \text{control}}\times100\%$. The 50% inhibition concentration (IC_{50}) was determined by concentration-CSR curve.

Cytotoxicity test

One hundred microliters of target cells were seeded in a microplate at a 1×10^5/mL density and 0.1 mL of effect cells at a 1×10^6/mL density were mixed into each well (to reduce the influence of effect cell number, we deliberately made the E:T = 10:1). After 4 h of incubation, 10 μL of MTT was added. And following treatments were the same as in drug -resistant test. Cytotoxicity rate (CR) was calculated by the following formula: CR = $\{1-(A_{570\ \text{experiment}}-A_{570\ \text{E control}})/A_{570\ \text{T control}}\}\times100\%$.

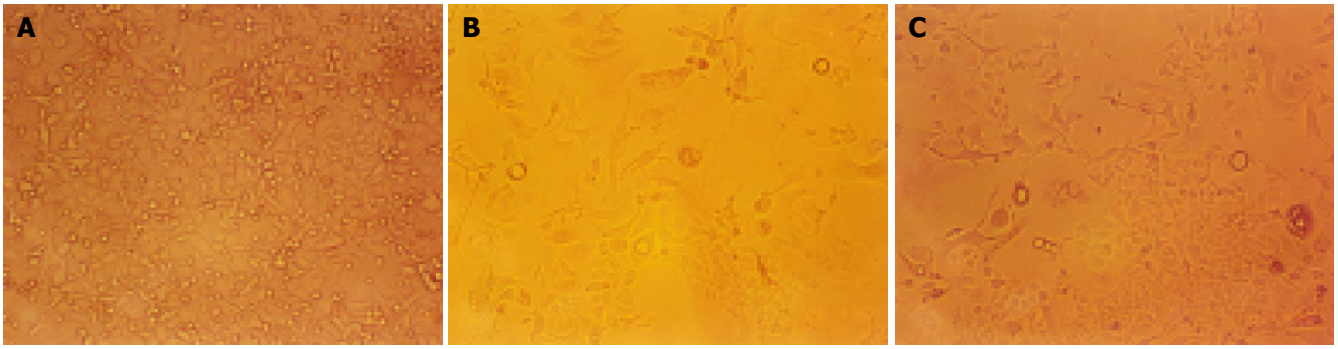

Figure 1 Morphological change of Bel-7402 during induction of drug-resistance. **A**: Parent cells; **B**: morphology change during culture; **C**: most of the cells died. Some "normal" cell islands appeared.

Immunohistochemistry

Specimens were HE stained and observed under a microscope. Cell markers were demonstrated by immunohistochemistry according to S-P protocol on slides with mAb against CD3, CD45, CD45RO, CD68 (Neomarker) as first antibody, goat anti-mouse antibody as second antibody.

Statistical analysis

Analysis was performed by using Student's *t* test, the data were expressed as mean±SD and $P<0.05$ was considered statistically significant.

RESULTS

Generation of CIK from PBMCs

The proliferation and phenotype of the PBMCs after CIK induction varied according to individual HCC patients. The cell number increase was more than 70-fold on average ($n = 17$) after 25-d incubation. CD3+CD56+ cells increased greatly by about 60-fold to more than 1 400-fold with an average of more than 600-fold (Table 1).

Induction of drug-resistant HCC cells

Bel-7402 HCC cell line under went drug-resistant induction test beginning with 10 nmol/L of ADM in the medium increased gradually to 200 or 2 000 nmol/L. Cells showed a series of changes (Figure 1) such as enlarged, polynuclear, discontinuous in plasma membrane (Figure 1B). Most of them died then some "normal" cell islands (Figure 1C) appeared, the same as the parent cell (Figure 1A). We designated the induced cells which survived in 200 nmol/L of ADM as Bel-7402/R-200, and those survived in 2 000 nmol/L of ADM, as Bel-7402/R-2000. After both grew in 2 mmol/L of ADM for 1 h, most of the former died and most of the latter still survived, indicating there might be some difference between the two. When MTT test was done to the parent cell and both drug-resistant cells, they showed different IC_{50} with ADM. IC_{50} of the parent Bel-7402 was 42 nmol/L, and of the induced cells, 2 000 and 8 000 nmol/L respectively (Figure 2). RT-PCR showed MDR1 overexpressed in induced cells and the parent cells generally gave negative results. Intracellular concentration of Rhodamine 123 was also determined by FCM (Figure 3), since Rhodamine 123 produces fluorescence itself and would be pumped out of cells if the Pgp existed. Bel-7402/R cells kept only 25.1%, 28.4% of Rhodamine 123 intracellularly each and the parent Bel-7402, 77.7%. Stained with anti-P-170 mAb (Figure 4), and determined by FCM, we found that only 1.32% of parent cells expressed P-170 and Bel-7402/R increased to 47%, 54% respectively.

Different from other reports, although it showed similar characters to Bel-7402/R in drug-resistance, the SMMC-7721/R only endured a smaller range of drug concentration (below 100 nmol/L of ADM) and it was difficult to recover from liquid nitrogen keeping.

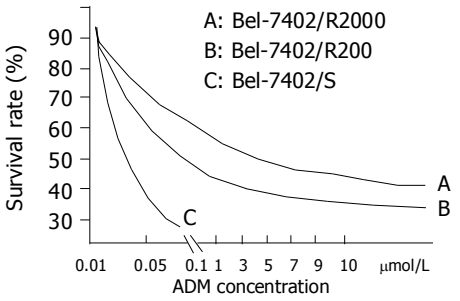

Figure 2 Survival-ADM concentration curves of three cells. A: Bel-7402/R-2000; B: Bel-7402/R-200; C: Bel-7402/S.

Table 1 Determination of CD3CD56 of CIK cells ($n = 6$)

CD3+(%)				CD3+CD56+(%)			
D 1		D 25		D 1		D 25	
Normal	HCC	Normal	HCC	Normal	HCC	Normal	HCC
59.5±7.8[a]	45.1±12.1[a]	93.3±6.5	89.4±5.1	3.2±1.6	2.4±2.1	20.6±13.4	19.1±11.7

[a]$P<0.05$ *vs* others.

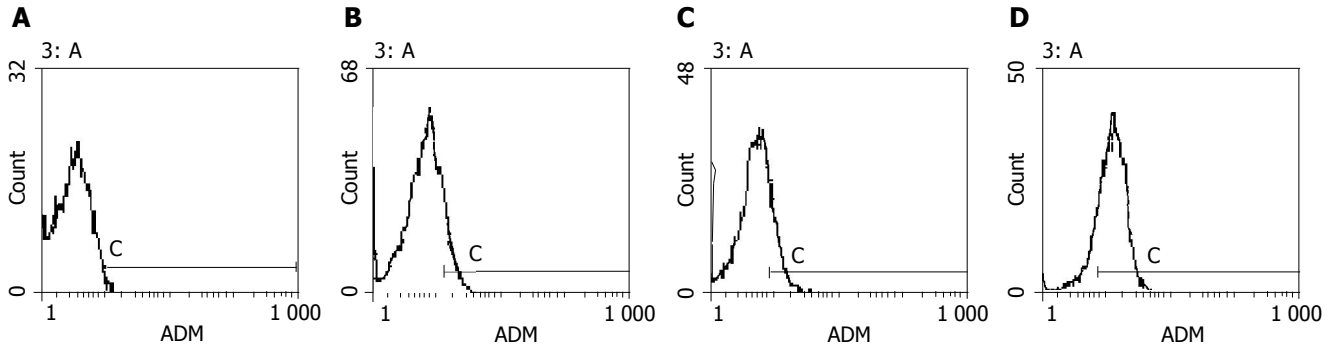

Figure 3 Rhodamine 123 excluding test detected by FCM. **A**: Control; **B**: Bel7402/r-2000; **C**: Bel7402/r-200; **D:** Bel7402/S.

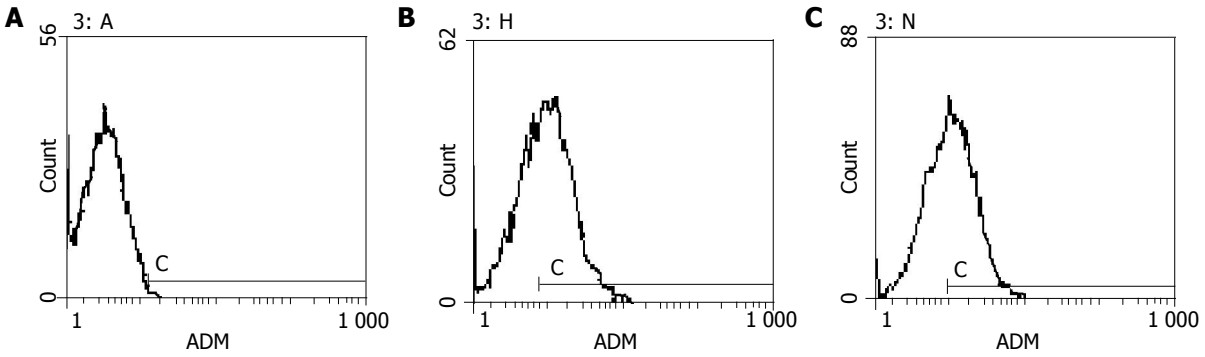

Figure 4 Indirect immunofluorescence on Pgp detected by FCM. **A**: Bel7402/s; **B**: Bel7402/r-200; **C**: Bel7402/r-2000.

Cytotoxicity of CIK to drug- resistant HCC cells

Shi *et al*, and Wang *et al*, have proven the CIK cells from HCC patients have stronger cytotoxicity to HCC cells and here we found that CIK both from normal persons and HCC patients had similar cytotoxicity to drug-resistant HCC cells (Figure 5) at different E∶T ratios, so we chose E∶T = 10∶1 to avoid bias produced by effect cell number in the test. The experiment wells contained 10^4 target cells mixed with 10^5 effect cells. Effect control (E control) included 10^5 effect cells only and target control (T control), 10^4 target cells only. Cytotoxicity of CIK from HCC patients to Bel-7402/S was 33-68% with an average of 50.7%. While to Bel-7402/R it was 37-64% with an average of 52.3% (P>0.05), the same as normal group. Cytotoxicity CIK from HCC patients to L-02, an embryo liver cell line, was under 10%, indicating no side effect to normal liver cells (Tables 2 and 3).

Table 2 Results of cytotoxicity of CIK to target cells

Patient Number	A value (rate of cytotoxicity)			
	7402/s[b](%)	7402/R[d](%)	L-02[bd] (%)	E control
1	0.802 (33)	0.743 (49)	1.011 (12)	0.485
2	0.913 (48)	0.895 (47)	1.201 (4)	0.627
3	0.681 (46)	0.599 (57)	0.888 (14)	0.379
4	0.630 (68)	0.602 (60)	0.959 (7)	0.401
5	0.711 (58)	0.802 (37)	1.001 (12)	0.479
6	0.987 (51)	0.903 (64)	1.302 (2)	0.718
T control	0.554	0.508	0.595	

t_a = 8.70, [b]P<0.01 t_t = 8.87, [d]P<0.01.

Table 3 Average of cytotoxicity and significance of difference (n = 6)

	7 402/s	7 402/R
HCC	50.7	52.3
Normal	57.1	54.7

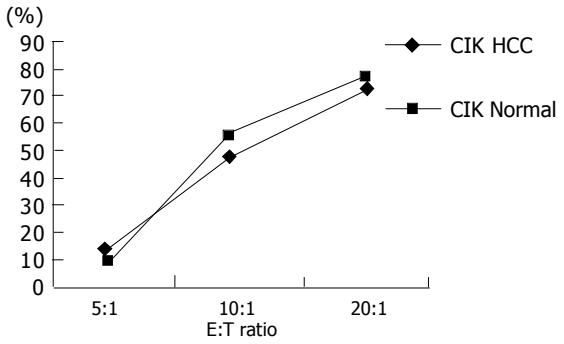

Figure 5 Cytotoxicity of CIK to Bel-7402 at different E:T ratios.

In vivo effect of CIK

Seventeen cases of recurrent HCC patients post-operation were recruited into our study, most of them with relapsed bulk tumors and no effective treatment. The results showed that CIK treatment for HCC was safe, effective, without side effects(data reported elsewhere). Here we only focus on one case whose tumor had been demonstrated MDR1 overexpression by RT-PCR and immunohistochemistry assay

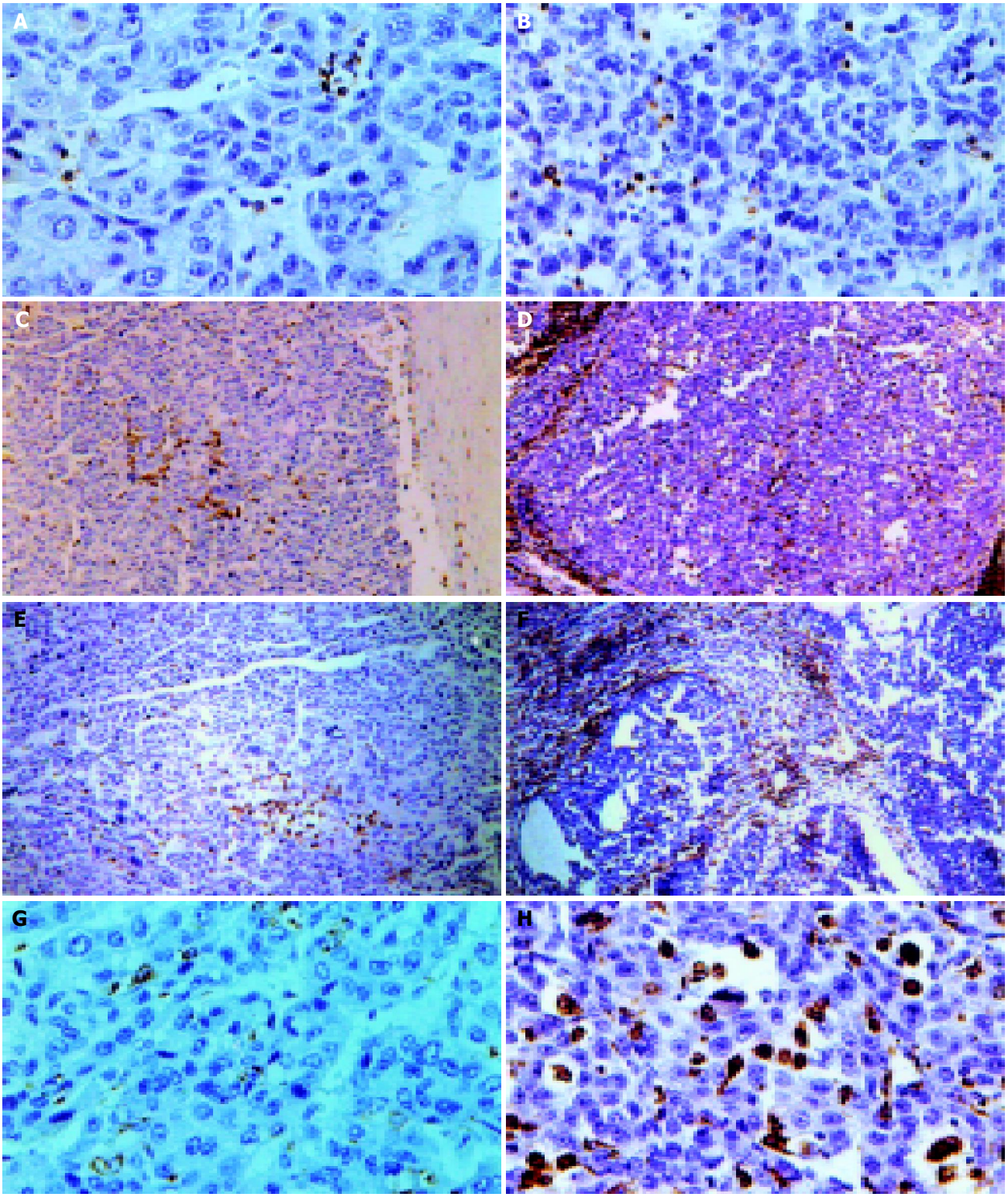

Figure 6 Immunohistochemistry results of the tumor specimen before and after CIK treatment, demonstrated that a large amount of lymphocytes with CD3, CD45, CD45RO, CD68 markers infiltrated in tumor after treatment. **A**: Immunohistochemistry with anti-CD3 to the specimen before treatment; **B**: with anti-CD3 to the specimen after treatment; **C**: immunohistochemistry with anti-CD45 to the specimen before treatment; **D**: with anti-CD45 to the specimen after treatment; **E**: immunohistochemistry with anti-CD45RO to the specimen before treatment; **F**: with anti-CD45RO to the specimen after treatment; **G**: immunohistochemistry with anti-CD68 to the specimen before treatment; **H**: with anti-CD68 to the specimen after treatment.

before and after operation was carried out. The patient was a male, 56 years old, relapsed about one year after liver tumor resection with pneumal metastasis and cancer embolus in portal vein, and received CIK treatment. After transfused 1.3×10^{10} CIK cells, the patient had improvement of nausea, vomiting and the windy abdomen, as well as his appetite. His ascites abated too. After another 3 mo a second operation was performed and the tumor sample underwent pathological and immunohistochemical assay. Compared with the specimen before CIK treatment the tumor became

nodular with a large amount of lymphocytes infiltration after treatment (Figure 6). CD3, CD45, CD45RO, CD68 positive cells increased vigorously (Table 4 and Figure 6) to 41, 283, 44, 77/HPF each from 0.1, 15, 3, 8/HPF before CIK treatment indicating the anti-tumor immunity was enhanced significantly since CD3, CD45 represent T cells, CD45RO is the marker of T memory subset, while CD68 is the marker of mono/macrophage.

Table 4 Comparison of immune cells in immunohistochemistry

	CD45	CD3	CD45RO	CD68
1	15.4 cells/HPF	0.15 cells/HPF	2.9 cells/HPF	8.0 cells/HPF
2	283 cells/HPF	41.3 cells/HPF	44.1 cells/HPF	77.7 cells/HPF
x-fold	18.4	275	15.2	9.7

1: before treatment. 2: after treatment. HPF: high power field.

DISCUSSION

Other than transgene models, several drug-resistant HCC cell lines induced by ADM have been established[17-19]. In our laboratory, we found that Bel-7402 is easier and has a wider range in drug-dose to induce drug-resistance than smmc-7721, as the latter is difficult to grow in >100 nmol/L of ADM and to recovered from liquid nitrogen preservation. Bel-7402/R still keep its resistance even revived from the liquid nitrogen and so it is easy to use. Our research demonstrated that MDR1 gene expression is one of important mechanisms of drug-resistance in our Bel-7402/R. At the same time, that Bel-7402/R-2000 was more resistant to the drug than Bel-7402/R200 reminded us that there should be some other reasons to be disclosed.

A number of studies[20,21] have illuminated that CIK possessed much stronger cytotoxicity than LAK to several kinds of cancer such as leukemia, renal cell carcinoma, melanoma[22], and proved that dendritic cells increased in serum of host after transfusion of CIK to HCC patients. Here we demonstrated CIK cells from HCC patients could equally kill drug-resistant HCC cell line as those from normal. One case of *in vivo* study also gave same results. Immunohistochemistry of specimens revealed large amounts of lymphocytes infiltrating into tumor; CD3+, CD45RO+, CD68+ cells were recruited there in great numbers. These observations may imply activation of anti-tumor immunity since CD45RO+ represents T memory subset while CD68+ is the marker of monocyte/macrophage[23]. Anti-CD3Ab can activate CD45RO+ T subset[24], so we deduced that the increase of CD45RO+ cells in the tumor locals may come from CIK.

CIK cell killing drug-resistant HCC cell line is of much benefit to HCC treatment. HCC is easy to induce drug-resistance. Because of tendency of metastasis and recurrence of HCC, post-operation chemotherapy is necessary. Since p-170 pumps drugs out of the cells, chemotherapy is not only useless to the drug-resistant tumor but produces the side effects to the host as well. CIK would be the better choice to kill the drug-resistant tumor. We suggest to perform CIK treatment to eradicate the remaining tumor cells after bulk tumor loads are removed by operation.

It is interesting that while CIK kills the tumor cells vigorously it has little effect on L-02 cells. Similar results were reported by Schmidt-Wolf *et al*[25]. They found that despite high cytotoxic activity of CIK against lymphoma cells, they had little toxicity against a subset of normal human hematopoietic progenitor cells. Some difference between Bel-7402 and L-02 has been reported recently by Shao *et al*[26], that LAPTM4B, a newly found HCC related antigen, was expressed in Bel-7402 but not in L-02. A polyclonal antibody against LAPTM4b has been produced. Monoclonal antibody against it is in process of production. It may be helpful to solve the problem.

REFERENCES

1 **Zhang YS,** Dai ZQ. Advances in Hepatoma Biotherapy Research. *Zhongguo Xiandai Putong Waike Jinzhan* 2001; **4**: 193-198
2 **Kline NE.** Promoting patient safety through the development of a pediatric chemotherapy and biotherapy provider program. *J Pediatr Oncol Nurs* 2004; **21**: 65-66
3 **Tan GH,** Wei YQ, Tian L, Zhao X, Yang L, Li J, He QM, Wu Y, Wen YJ, Yi T, Ding ZY, Kan B, Mao YQ, Deng HX, Li HL, Zhou CH, Fu CH, Xiao F, Zhang XW. Active immunotherapy of tumors with a recombinant xenogeneic endoglin as a model antigen. *Eur J Immunol* 2004; **34**: 2012-2021
4 **Rice AM,** Jones KL, Hart DN. DC preparations for therapy. *Cytotherapy* 2004; **6**: 99-104
5 **Hongeng S,** Petvises S, Worapongpaiboon S, Rerkamnuaychoke B, Pakakasama S, Jootar S. Generation of CD3+ CD56+ cytokine-induced killer cells and their *in vitro* cytotoxicity against pediatric cancer cells. *Int J Hematol* 2003; **77**: 175-179
6 **Bonin S,** Pascolo L, Croce LS, Stanta G, Tiribelli C. Gene expression of ABC proteins in hepatocellular carcinoma, perineoplastic tissue, and liver diseases. *Mol Med* 2002; **8**: 318-325
7 **van Brussel JP,** van Steenbrugge GJ, Romijn JC, Schroder FH, Mickisch GH. Chemosensitivity of prostate cancer cell lines and expression of multidrug resistance-related proteins. *Eur J Cancer* 1999; **35**: 664-671
8 **Warmann S,** Gohring G, Teichmann B, Geerlings H, Pietsch T, Fuchs J. P-glycoprotein modulation improves *in vitro* chemosensitivity in malignant pediatric liver tumors. *Anticancer Res* 2003; **23**: 4607-4611
9 **Schmidt-Wolf IG,** Negrin RS, Kiem HP, Blume KG, Weissman IL. Use of a SCID mouse/human lymphoma model to evaluate cytokine-induced killer cells with potent antitumor cell activity. *J Exp Med* 1991; **174**: 139-149
10 **Schmidt-Wolf GD,** Negrin RS, Schmidt-Wolf IG. Activated T cells and cytokine-induced CD3+CD56+ killer cells. *Ann Hematol* 1997; **74**: 51-56
11 **Schmidt-Wolf IG,** Lefterova P, Mehta BA, Fernandez LP, Huhn D, Blume KG, Weissman IL, Negrin RS. Phenotypic characterization and identification of effector cells involved in tumor cell recognition of cytokine-induced killer cells. *Exp Hematol* 1993; **21**: 1673-1679
12 **Kaneko T,** Fusauch Y, Kakui Y, Okumura K, Mizoguchi H, Oshimi K. Cytotoxicity of cytokine-induced killer cells coated with bispecific antibody against acute myeloid leukemia cells. *Leuk Lymphoma* 1994; **14**: 219-229
13 **Mehta BA,** Schmidt-Wolf IG, Weissman IL, Negrin RS. Two pathways of exocytosis of cytoplasmic granule contents and target cell killing by cytokine-induced CD3+CD56+ killer cells. *Blood* 1995; **86**: 3493-3499
14 **Zhang YS,** Huang L, Yuan FJ, Wang B, Dai ZQ. Research on effects of tumor vaccine to mouse hepatocellular carcinoma. *Yunyang Yixueyuan Xuebao* 2002; **21**: 8-12
15 **Shapiro AB,** Ling V. The mechanism of ATP-dependent multidrug transport by P-glycoprotein. *Acta Physiol Scand Suppl* 1998; **643**: 227-234

16 **Zhang YS,** Yao L, Huang L, Wang B, Dai ZQ. Observation on cytotoxicity of CD3AK. *Yunyang Yixueyuan Xuebao* 1999; **18**: 200-201
17 **Nakajima A,** Yamamoto Y, Taura K, Hata K, Fukumoto M, Uchinami H, Yonezawa K, Yamaoka Y. Beneficial effect of cepharanthine on overcoming drug-resistance of hepatocellular carcinoma. *Int J Oncol* 2004; **24**: 635-645
18 **He L,** Liu GQ. Effects of various principles from Chinese herbal medicine on rhodamine123 accumulation in brain capillary endothelial cells. *Acta Pharmacol Sin* 2002; **23**: 591-596
19 **Chu TM,** Lin TH, Kawinski E. Detection of soluble P-glycoprotein in culture media and extracellular fluids. *Biochem Biophys Res Commun* 1994; **203**: 506-512
20 **Schmidt-Wolf IG,** Finke S, Trojaneck B, Denkena A, Lefterova P, Schwella N, Heuft HG, Prange G, Korte M, Takeya M, Dorbic T, Neubauer A, Wittig B, Huhn D. Phase I clinical study applying autologous immunological effector cells transfected with the interleukin-2 gene in patients with metastatic renal cancer, colorectal cancer and lymphoma. *Br J Cancer* 1999; **81**: 1009-1016
21 **Alvarnas JC,** Linn YC, Hope EG, Negrin RS. Expansion of cytotoxic CD3+ CD56+ cells from peripheral blood progenitor cells of patients undergoing autologous hematopoietic cell transplantation. *Biol Blood Marrow Transplant* 2001; **7**: 216-222
22 **Marten A,** Ziske C, Schottker B, Renoth S, Weineck S, Buttgereit P, Schakowski F, von Rucker A, Sauerbruch T, Schmidt-Wolf IG. Interactions between dendritic cells and cytokine-induced killer cells lead to an activation of both populations. *J Immunother* 2001; **24**: 502-510
23 **Holness CL,** Simmons DL. Molecular cloning of CD68, a human macrophage marker related to lysosomal glycoproteins. *Blood* 1993; **81**: 1607-1613
24 **Gold JE,** Zachary DT, Osband ME. Adoptive transfer of *ex vivo*-activated memory T-cell subsets with cyclophosphamide provides effective tumor-specific chemoimmunotherapy of advanced metastatic murine melanoma and carcinoma. *Int J Cancer* 1995; **61**: 580-586
25 **Schmidt-Wolf IG,** Lefterova P, Johnston V, Scheffold C, Csipai M, Mehta BA, Tsuruo T, Huhn D, Negrin RS. Sensitivity of multidrug-resistant tumor cell lines to immunologic effector cells. *Cell Immunol* 1996; **169**: 85-90
26 **Shao GZ,** Zhou RL, Zhang QY, Zhang Y, Liu JJ, Rui JA, Wei X, Ye DX. Molecular cloning and characterization of LAPTM4B, a novel gene upregulated in hepatocellular carcinoma. *Oncogene* 2003; **22**: 5060-5069

Science Editor Zhu LH and Guo SY **Language Editor** Elsevier HK

PO Box 2345, Beijing 100023, China
www.wjgnet.com
wjg@wjgnet.com

ELSEVIER

World J Gastroenterol 2005;11(22):3346-3350
World Journal of Gastroenterology ISSN 1007-9327

Effect of lamivudine in HBeAg-positive chronic hepatitis B: Discordant effect on HBeAg and HBV DNA according to pretreatment ALT level

Tomoko Kurihara, Fumio Imazeki, Osamu Yokosuka, Kenichi Fukai, Tatsuo Kanda, Shigenobu Kawai, Hiromitsu Saisho

Tomoko Kurihara, Fumio Imazeki, Osamu Yokosuka, Kenichi Fukai, Tatsuo Kanda, Shigenobu Kawai, Hiromitsu Saisho, Department of Medicine and Clinical Oncology, Graduate School of Medicine, Chiba University, 1-8-1 Inohana, Chuou Ward, Chiba 260-8670, Japan
Correspondence to: Osamu Yokosuka, MD, Department of Medicine and Clinical Oncology, Graduate School of Medicine, Chiba University, 1-8-1 Inohana, Chuou Ward, Chiba 260-8670, Japan. yokosukao@faculty.chiba-u.jp
Telephone: +81-43-226-2086 Fax: +81-43-226-2088
Received: 2004-09-13 Accepted: 2004-10-08

Kurihara T, Imazeki F, Yokosuka O, Fukai K, Kanda T, Kawai S, Saisho H. Effect of lamivudine in HBeAg-positive chronic hepatitis B: Discordant effect on HBeAg and HBV DNA according to pretreatment ALT level. *World J Gastroenterol* 2005; 11(22): 3346-3350
http://www.wjgnet.com/1007-9327/11/3346.asp

Abstract

AIM: To clarify differences in antiviral effect of the drug in patients with different ALT levels, we examined the changes in HBV markers in patients with high or low ALT levels with or without lamivudine treatment.

METHODS: Thirty-seven HBeAg-positive patients were studied. Ten patients with ALT levels higher than 200 IU/L (group 1) and 8 patients with ALT below 200 IU/L (group 2) were treated orally with 100 mg/d of lamivudine. As untreated control, 9 patients with ALT above 200 IU/L (group 3) and 10 patients with ALT below 200 IU/L (group 4) were examined. ALT level, HBeAg/HBeAb status, and HBV DNA level were examined monthly for 11.9±0.4 mo.

RESULTS: The ALT level normalized in all 10 patients of group 1, 7/8 of group 2, 4/9 of group 3, and 1/10 of group 4 within 6 mo (groups 1 *vs* 2, P = NS; groups 1 *vs* 3, P = 0.002; groups 1 *vs* 4, P<0.0001). HBV DNA fell below the detection limit in all 10 patients of group 1, 7/8 of group 2, 0/9 of group 3, and 0/10 of group 4 within 6 mo (groups 1 *vs* 2, P = NS). HBeAg became seronegative in 7/10 patients of group 1, 1/8 of group 2, 3/9 of group 3, and 0/10 of group 4 within 12 mo (groups 1 *vs* 2, P = 0.02; groups 1 *vs* 3, P = NS).

CONCLUSION: Our data suggest that HBeAg-positive patients with higher ALT levels can be considered good candidates for lamivudine therapy, probably because lamivudine accelerates the natural seroconversion of HBeAg, accompanied by HBV DNA loss, in these patients.

Key words: Lamivudine; Chronic hepatitis B; HBeAg; HBV DNA; ALT

INTRODUCTION

Hepatitis B virus (HBV) infection is a worldwide problem with chronic carriers numbering an estimated 350 million, and with approximately 1.5 million in Japan[1]. Although the natural course of chronic HBV infection is variable, carriers are at risk for developing cirrhosis and hepatocellular carcinoma, and thus need to be followed up and monitored so as to be able to make timely decisions regarding intervention with antiviral therapy[2].

Lamivudine treatment is effective in suppressing HBV replication and decreasing the level of HBV DNA in patients with type B hepatitis[3], thereby improving liver function tests and leading to histological improvement[4-7]. HBeAg seroconversion was found in 17% of patients at 1 year of treatment and in 27% at 2 years[8].

The most troublesome problem of lamivudine treatment is the emergence of lamivudine-resistant strain during the treatment[9-13]. The risk of developing lamivudine resistance increases with the duration of treatment. Reactivation of hepatitis after the cessation of treatment is another problem[14-17]. In this context, knowing the effect of lamivudine on HBV in relation to the clinical status must be of major importance.

The effect of lamivudine was reported to be better in patients with ALT levels elevated to more than 5 times the upper limit of normal (ULN)[18,19]. It is known that such patients tended to seroconvert during interferon treatment[20,21]. Therefore, we studied the effect of lamivudine in relation to the level of ALT, comparing those with and without lamivudine.

The correlations of ALT, HBeAg, and HBV DNA alongside the status of precore and core promoter mutation have not been well demonstrated. We therefore compared the effect of lamivudine in terms of these parameters in a controlled trial.

MATERIALS AND METHODS

Patients

Between January 2000 and June 2001, 75 patients with HBeAg-positive chronic hepatitis B attended Chiba University

Medical Hospital every 1 to 3 mo. Asymptomatic carriers were not included. Eighteen of these patients began treatment with 100 mg/d of oral lamivudine during this period, while the remaining 57 patients chose not to undergo this treatment. Among them, 19 patients were selected as control, and they were not treated with antiviral drug such as lamivudine or interferon throughout the study. There were no patients positive for HCV-Ab, anti-human immunodeficiency virus antibody or hepatitis D virus antibody, or with a history of drinking over 80 g/d of alcohol. This study was performed in accordance with the Helsinki Declaration.

Thus, a total of 37 patients were classified into 4 groups according to lamivudine treatment and ALT level at enrollment, and they were examined for changes in ALT, HBV DNA and HBeAg/HBeAb. They consisted of 10 treated patients with ALT more than 200 IU/L (group 1), 8 treated patients with ALT less than 200 IU/L (group 2), 9 untreated patients with ALT more than 200 IU/L (group 3), and 10 untreated patients with ALT less than 200 IU/L (group 4) (Table 1). All patients in groups 1 and 2 were continuing lamivudine medication at the time of final observation.

Serologic markers

HBeAg and anti-HBe were examined by ELISA (Abbott Laboratories, Chicago, IL). Anti-HCV was determined by ELISA (Ortho Diagnostics, Tokyo, Japan). Serum HBV DNA was quantified by transcription-mediated amplification (TMA) assay (DNA probe Chugai-HBV, Chugai Diagnostics, Tokyo)[22]. The detection range of this assay was from 3.7 to 8.7-log genome equivalents/mL (LGE/mL).

Detection of precore and core promoter mutations

The G to A mutation at nucleotide (nt) 1 896 in the precore region (A1896 mutation) and the A to T mutation at nt 1 762 and G to A mutation at nt 1 764 in the core promoter region (T1762 and A1764 mutations) were determined by the direct sequence method after PCR amplification, basically as previously described[23]. The primers for the first PCR were 5'-TCGCATGGAGACCACCGTGA-3' (sense, nt 1 604-1 623) and 5'-ATAGCTTGCCTGAGTGC-3' (antisense, nt 2 076-2 060), and the primers for the second PCR were 5'-CATAAGAGGACTCTTGGACT-3' (sense, nt 1 653-1 672) and 5'-GGAAAGAAGTCAGAAGGC-3' (antisense, nt 1 974-1 957).

Determination of HBV genotypes

HBV genotype was determined from patients' sera using ELISA (HBV Genotype EIA; Tokushu-Meneki Laboratory, Tokyo, Japan) based on the method described by Usuda *et al*[24]. Cases in which the HBV genotype could not be determined by this method, we performed PCR of the S-gene region and analyzed the restriction fragment length polymorphism pattern[25].

Statistical analysis

Proportion of each clinical factor was compared between the groups using the χ^2 test and Fisher's exact probability test, and the group means were compared using the Student's *t*-test. The rates of HBV DNA loss, HBeAg loss, and ALT normalization among groups 1 to 4, and those of HBV DNA breakthrough during lamivudine treatment between groups 1 and 2 were analyzed by Kaplan-Meier method, and the difference in incidences was assessed by the log-rank test. The association between HBeAg loss during the follow-up period and clinical factors at baseline including age, sex, HBV-DNA level, the pattern of core promoter or precore mutation, and medication of lamivudine was examined by multivariate Cox regression analysis. *P* values less than 0.05 were considered significant.

RESULTS

Characteristics of patients at baseline

The characteristics of the 37 patients at baseline are shown in Table 1. The mean HBV DNA level was 7.4±1.4 LGE/mL in group 1, 7.5±0.9 in group 2, 7.2±1.5 in group 3, and 8.2±0.5 in group 4 (Table 1). The mean follow-up period was 11.9±0.4 mo (10-12 mo). All the patients had genotype C HBV except one case. Precore mutation was found in 3 patients, one each in groups 1, 2, and 3. Core promoter mutation was found in 50% of group 1, 71% of group 2, 89% of group 3, and 60% of group 4 patients (Table 1).

Outcome of ALT level in the four groups

The cumulative incidence of ALT normalization is shown

Table 1 Characteristics of patients with positive HBeAg at enrollment

	Group 1 (n = 10)	Group 2 (n = 8)	Group 3 (n = 9)	Group 4 (n = 10)	
Age in years (mean±SD)	38.8±9.7	40.0±9.1	34.1±12.9	31.2±10.2	P = 0.07
Gender (male/female)	10/0	6/2	4/5	7/3	P = 0.01
ALT (IU/L)	695±450	89±45	325±195	89±38	P = 0.01
HBV DNA (LGE/mL)	7.4±1.4	7.5±0.9	7.2±1.5	8.2±0.5	P = 0.06
Genotype (A/B/C)	0/0/10	1/0/6	0/0/9	0/0/10	P = NS
Precore (wild/mutant)	9/1	6/1	8/1	10/0	P = NS
Core promoter (wild/mutant)	5/5[e]	2/5	1/8	4/6	P = 0.14
Fibrosis stage (F1/F2/F3)	1/3/1	3/1/2	0/4/1	3/1/0	P = 0.06

Group 1, ALT ⩾ 200 and lamivudine-treated; group 2, ALT<200 and lamivudine-treated; group 3, ALT⩾200 and lamivudine-untreated; group 4, ALT<200 and lamivudine-untreated. LGE, logarithm genome equivalent.

for groups 1 to 4 by Kaplan-Meier method in Figure 1. The rates were different among the groups, and the differences between groups 1 and 3, and groups 1 and 4 were statistically significant (groups 1 and 3, $P = 0.002$; groups 1 and 4, $P<0.0001$). The incidence rates between groups 2 and 4, and groups 3 and 4 were also statistically different (groups 2 and 4, $P = 0.0002$; groups 3 and 4, $P = 0.031$). In patients given lamivudine, ALT normalized within 6 mo of starting the treatment in all 10 group 1 patients, 7/8 of group 2 patients, while in untreated patients, ALT normalized in 4/9 group 3 patients and remained abnormal in all the group 4 patients except one case within 6 mo.

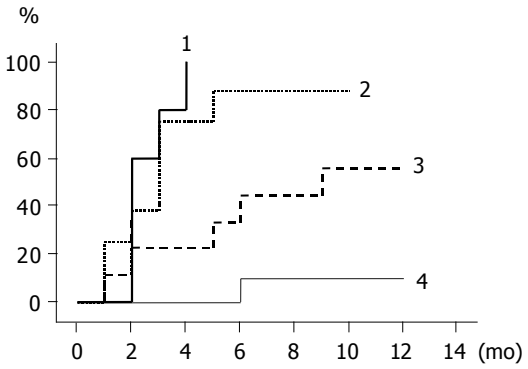

Figure 1 Cumulative incidence of ALT normalization of groups 1 to 4 by Kaplan-Meier method. Group 1 is indicated by thick line, group 2 by dotted line, group 3 by dashed line, and group 4 by thin line. Groups 1 *vs* 2, *P* = NS; groups 1 *vs* 3, *P* = 0.002; groups 1 *vs* 4, *P*<0.0001; groups 2 *vs* 3, *P* = NS; groups 2 *vs* 4, *P* = 0.0002; groups 3 *vs* 4, *P* = 0.031 (log-rank test).

Outcome of HBV DNA level in the four groups

The cumulative incidence of HBV DNA loss is shown by Kaplan-Meier method in Figure 2. Group 1 and 2 patients with lamivudine treatment had higher rates of HBV DNA loss compared to untreated group 3 and 4 patients, whose HBV DNA did not disappear during the follow-up period. HBV DNA levels declined in all the group 1 and 2 patients, falling below the detection limit in all 10 group 1 patients and in 7 of 8 group 2 patients within 6 mo. There was no statistical difference between groups 1 and 2.

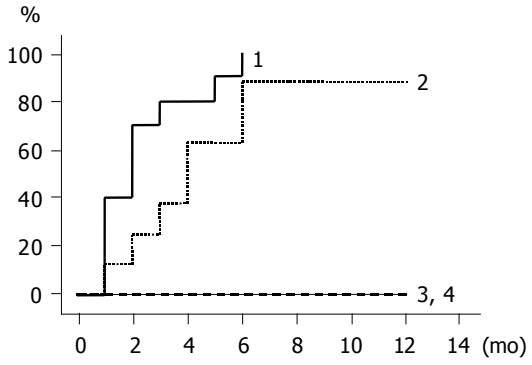

Figure 2 Cumulative incidence of HBV DNA disappearance of groups 1 to 4 by Kaplan-Meier method. Group 1 is indicated by thick line, group 2 by dotted line, group 3 by dashed line, and group 4 by thin line. Groups 1 *vs* 2, *P* = NS (log-rank test).

Outcome of HBeAg/anti-HBe status in the four groups

The cumulative incidences of HBeAg loss and HBeAg seroconversion are shown in Figures 3 and 4 respectively. Groups 1 and 3 patients with higher ALT levels had higher rates of HBeAg loss and HBeAg seroconversion compared to groups 2 and 4 patients with lower ALT levels. (Figure 3: groups 1 and 2, $P = 0.020$; Figure 4: groups 1 and 2, $P = 0.048$). HBeAg became seronegative in 7 of 10 group 1, 1 of 8 group-2, 3 of 9 group-3, and none of 10 group-4 patients within 12 mo, and became seroconverted in all patients with HBeAg loss except one patient of group 1.

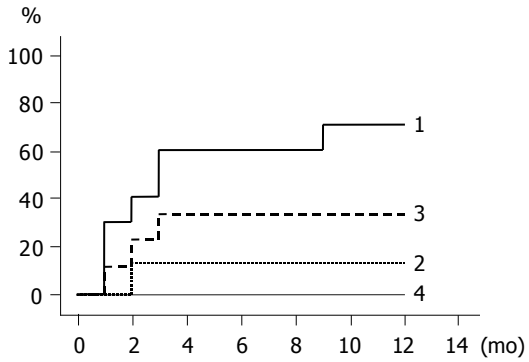

Figure 3 Cumulative incidence of HBeAg loss of groups 1 to 4 by Kaplan-Meier method. Group 1 is indicated by thick line, group 2 by dotted line, group 3 by dashed line, and group 4 by thin line. Groups 1 *vs* 2, *P* = 0.020; groups 1 *vs* 3, *P* = NS; groups 2 *vs* 3, *P* = NS (log-rank test).

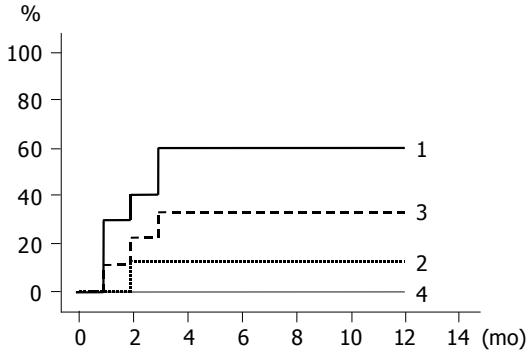

Figure 4 Cumulative incidence of HBeAg seroconversion of groups 1 to 4 by Kaplan-Meier method. Group 1 is indicated by thick line, group 2 by dotted line, group 3 by dashed line, and group 4 by thin line. Groups 1 *vs* 2, *P* = 0.048; groups 1 *vs* 3, *P* = NS; groups 2 *vs* 3, *P* = NS (log-rank test).

Incidence of breakthrough of HBV DNA

Breakthrough of HBV DNA in spite of continuous lamivudine medication was found in 1 patient of group 1 and in 3 of group 2 during the follow-up period. The cumulative rates of breakthrough at 1 year were 23.5% in the lamivudine-treated patients, 10% in group 1 in contrast to 42.9% in group 2 (P = NS).

HBeAg loss in relation to precore mutation or core promoter mutation

HBeAg became negative or seroconverted in 1 of 3 (33%) patients with precore mutation and in 10 of 33 (30%) without

precore mutation within 12 mo (P = NS by log-rank test). This result was not affected by lamivudine treatment: 1 of 2 (50%) patients with precore mutation *vs* 7 of 15 (47%) without precore mutation in those with lamivudine treatment (P = NS by log-rank test), and 0 of 1 (0%) *vs* 3 of 18 (17%) in untreated patients (P = NS by χ^2 test).

HBeAg became negative in 7 of 24 (29%) patients with core promoter mutation and in 4 of 12 (33%) without core promoter mutation within 12 mo (P = NS by log-rank test). HBeAg became negative in 4 of 10 (40%) with core promoter mutation and in 4 of 7 (57%) without mutation in those with lamivudine treatment (P = NS by log-rank test), and in 3 of 14 (21%) with core promoter mutation and in 0 of 5 (0%) without mutation in those untreated (P = NS by χ^2 test).

Factors associated with HBeAg loss

Multivariate Cox regression analysis showed that ALT above 200 IU/L was the only predictive factor with a relative risk of 13.158 associated with HBeAg loss among 7 factors (Table 2).

Table 2 Multivariate Cox regression analysis of factors associated with HBeAg loss

Variables		Relative risk	95% CI	*P*
Age <30 (yr)		1.0		
≥30 (yr)		1.995	0.236 - 16.898	0.526
Gender male		1.0		
female		5.247	0.294 - 93.594	0.260
ALT <200 IU/L		1.0		
≥200 IU/L		13.158	1.153 - 142.857	0.038
HBV DNA (LGE/mL)		0.751	0.479 - 1.178	0.212
Core promoter	wild	1.0		
	mutant	0.944	0.234 - 3.817	0.936
Precore	wild	1.0		
	mutant	0.749	0.050 - 11.236	0.834
Lamivudine	untreated	1.0		
	treated	9.826	0.765 - 126.290	0.079

DISCUSSION

Our study has confirmed that the effect of lamivudine on HBe seroconversion is different in patients with ALT more than 200 IU/L and in those with less than 200 IU/L. Although the two groups showed no differences in the rates of HBV DNA disappearance and ALT normalization, the response of HBeAg was quite different between the two groups, with patients with ALT more than 200 IU/L showing a higher seronegative rate than those with a lower level. A higher seroconversion rate for HBeAg was obtained in patients with higher ALT in the treatment with interferon[20,21]. Recently, Chien *et al*[18], reported that, in lamivudine treatment, HBeAg seroconversion rates were also higher in patients with ALT levels greater than 5 times the ULN compared with those less than this level (7/11, 64% *vs* 15/129, 12%), results compatible with those of the current study (6/10, 60% *vs* 1/8, 13%).

The state of HBeAg would be decided by the relative amounts of HBeAg and HBeAb. The production of HBeAg is influenced by HBV replication, precore mutation and/or basic core promoter mutation of HBV. Using a duck hepatitis B virus model, we already reported that both precore wild and mutant viruses reduced their viral DNA levels during lamivudine treatment[26]. As the presence of precore or basic core promoter mutant viruses did not affect the reduction of HBV DNA levels in the sera in the current study, the anti-HBe antibody production level might be the key factor for HBeAg loss and seroconversion.

Patients in untreated groups and with ALT more than 200 IU/L also showed higher rates of HBeAg seroconversion compared to those with ALT less than 200 IU/L in the present study. Liaw reported previously that patient with ALT levels less than and greater than 5 times the ULN have significantly different spontaneous HBeAg seroconversion rates[27]. Because hepatic injuries in patients with chronic hepatitis B are the consequence of cytotoxic T-cell mediated immune hepatocytolysis, higher ALT levels reflect stronger immunological attack of the host against infected HBV. Thus, it seems that patients with high ALT levels tended to have higher rates of HBeAg seroconversion without lamivudine treatment, and the seroconversion rate did not differ between treated (group 1) and untreated (group 3) patients with high ALT levels (Figure 4). However, the rates of ALT normalization and HBV DNA disappearance were quite different between the two groups, with higher rates of ALT normalization and HBV DNA disappearance observed in group 1. Therefore, lamivudine treatment plays a beneficial role in accelerating and maintaining the loss of HBeAg by inhibiting HBV replication in those patients with high ALT.

Our analysis revealed that patients with precore mutation showed no higher rates of HBeAg loss or seroconversion than those without it. Therefore, precore mutation might not be associated with HBeAg loss or seroconversion in lamivudine treatment, although the small number of patients with precore mutation at baseline, only three, and the total number of cases analyzed were too few to draw a definite conclusion. Kuwahara *et al*[28], reported that eight patients among 12 who lost HBeAg during lamivudine treatment still had precore wild strain, and precore mutant strain reverted to wild in 11 of 17 patients during lamivudine treatment. Maruyama *et al*[29], also reported that the emergence of precore mutant was a separate event from HBeAg seroconversion.

As for core promoter mutation, Asahina *et al*[30], reported it to be an independent predictive factor for HBeAg loss during lamivudine therapy in 60 patients with genotype C. However, we could not extract core promoter mutation as a predictive factor by multivariate regression analysis in the current study. This result applied not only to the total patients but also to those treated or untreated with lamivudine, although clinical features at baseline were slightly different between lamivudine-treated and untreated groups in the present study. Further studies will be needed for clarification on this issue.

The reported reappearance of HBV DNA in sera and ALT elevation with the emergence of YMDD mutant of HBV during lamivudine treatment, together with the reactivation of HBV replication and flare-up of hepatitis after cessation of the treatment, are important problems

indeed[9-13]. In the current study, patients with ALT more than 200 IU/L showed not only a higher rate of HBeAg seroconversion but also a lower incidence of breakthrough of HBV DNA compared to those with ALT less than 200 IU/L during lamivudine treatment. This implies that patients with ALT more than 200 IU/L can be considered good candidates for the treatment with lamivudine.

REFERENCES

1 **Lee WM.** Hepatitis B virus infection. *N Engl J Med* 1997; **337**: 1733-1745
2 **Lok AS,** McMahon BJ. Chronic hepatitis B: update of recommendations. *Hepatology* 2004; **39**: 857-861
3 **Dienstag JL,** Perrillo RP, Schiff ER, Bartholomew M, Vicary C, Rubin M. A preliminary trial of lamivudine for chronic hepatitis B infection. *N Engl J Med* 1995; **333**: 1657-1661
4 **Dienstag JL,** Schiff ER, Wright TL, Perrillo RP, Hann HW, Goodman Z, Crowther L, Condreay LD, Woessner M, Rubin M, Brown NA. Lamivudine as initial treatment for chronic hepatitis B in the United States. *N Engl J Med* 1999; **341**: 1256-1263
5 **Lai CL,** Chien RN, Leung NW, Chang TT, Guan R, Tai DI, Ng KY, Wu PC, Dent JC, Barber J, Stephenson SL, Gray DF. A one-year trial of lamivudine for chronic hepatitis B. Asia Hepatitis Lamivudine Study Group. *N Engl J Med* 1998; **339**: 61-68
6 **Suzuki Y,** Kumada H, Ikeda K, Chayama K, Arase Y, Saitoh S, Tsubota A, Kobayashi M, Koike M, Ogawa N, Tanikawa K. Histological changes in liver biopsies after one year of lamivudine treatment in patients with chronic hepatitis B infection. *J Hepatol* 1999; **30**: 743-748
7 **Dienstag JL,** Goldin RD, Heathcote EJ, Hann HW, Woessner M, Stephenson SL, Gardner S, Gray DF, Schiff ER. Histological outcome during long-term lamivudine therapy. *Gastroenterology* 2003; **124**: 105-117
8 **Liaw YF,** Leung NW, Chang TT, Guan R, Tai DI, Ng KY, Chien RN, Dent J, Roman L, Edmundson S, Lai CL. Effects of extended lamivudine therapy in Asian patients with chronic hepatitis B. Asia Hepatitis Lamivudine Study Group. *Gastroenterology* 2000; **119**: 172-180
9 **Seta T,** Yokosuka O, Imazeki F, Tagawa M, Saisho H. Emergence of YMDD motif mutants of hepatitis B virus during lamivudine treatment of immunocompetent type B hepatitis patients. *J Med Virol* 2000; **60**: 8-16
10 **Nafa S,** Ahmed S, Tavan D, Pichoud C, Berby F, Stuyver L, Johnson M, Merle P, Abidi H, Trepo C, Zoulim F. Early detection of viral resistance by determination of hepatitis B virus polymerase mutations in patients treated by lamivudine for chronic hepatitis B. *Hepatology* 2000; **32**: 1078-1088
11 **Liu CJ,** Chen PJ, Lai MY, Kao JH, Chen DS. Hepatitis B virus variants in patients receiving lamivudine treatment with breakthrough hepatitis evaluated by serial viral loads and full-length viral sequences. *Hepatology* 2001; **34**: 583-589
12 **Liaw YF,** Sung JJ, Chow WC, Farrell G, Lee CZ, Yuen H, Tanwandee T, Tao QM, Shue K, Keene ON, Dixon JS, Gray DF, Sabbat J. Lamivudine for patients with chronic hepatitis B and advanced liver disease. *N Engl J Med* 2004; **351**: 1521-1531
13 **Chang TT,** Lai CL, Chien RN, Guan R, Lim SG, Lee CM, Ng KY, Nicholls GJ, Dent JC, Leung NW. Four years of lamivudine treatment in Chinese patients with chronic hepatitis B. *J Gastroenterol Hepatol* 2004; **19**: 1276-1282
14 **Song BC,** Suh DJ, Lee HC, Chung YH, Lee YS. Hepatitis B e antigen seroconversion after lamivudine therapy is not durable in patients with chronic hepatitis B in Korea. *Hepatology* 2000; **32**: 803-806
15 **Lau DT,** Khokhar MF, Doo E, Ghany MG, Herion D, Park Y, Kleiner DE, Schmid P, Condreay LD, Gauthier J, Kuhns MC, Liang TJ, Hoofnagle JH. Long-term therapy of chronic hepatitis B with lamivudine. *Hepatology* 2000; **32**: 828-834
16 **Leung NW,** Lai CL, Chang TT, Guan R, Lee CM, Ng KY, Lim SG, Wu PC, Dent JC, Edmundson S, Condreay LD, Chien RN. Extended lamivudine treatment in patients with chronic hepatitis B enhances hepatitis B e antigen seroconversion rates: results after 3 years of therapy. *Hepatology* 2001; **33**: 1527-1532
17 **Ryu SH,** Chung YH, Choi MH, Kim JA, Shin JW, Jang MK, Park NH, Lee HC, Lee YS, Suh DJ. Long-term additional lamivudine therapy enhances durability of lamivudine-induced HBeAg loss: a prospective study. *J Hepatol* 2003; **39**: 614-619
18 **Chien RN,** Liaw YF, Atkins M. Pretherapy alanine transaminase level as a determinant for hepatitis B e antigen seroconversion during lamivudine therapy in patients with chronic hepatitis B. Asian Hepatitis Lamivudine Trial Group. *Hepatology* 1999; **30**: 770-774
19 **Perrillo RP,** Lai CL, Liaw YF, Dienstag JL, Schiff ER, Schalm SW, Heathcote EJ, Brown NA, Atkins M, Woessner M, Gardner SD. Predictors of HBeAg loss after lamivudine treatment for chronic hepatitis B. *Hepatology* 2002; **36**: 186-194
20 **Lok AS,** Ghany MG, Watson G, Ayola B. Predictive value of aminotransferase and hepatitis B virus DNA levels on response to interferon therapy for chronic hepatitis B. *J Viral Hepat* 1998; **5**: 171-178
21 **Wong DK,** Cheung AM, O'Rourke K, Naylor CD, Detsky AS, Heathcote J. Effect of alpha-interferon treatment in patients with hepatitis B e antigen-positive chronic hepatitis B. A meta-analysis. *Ann Intern Med* 1993; **119**: 312-323
22 **Kamisango K,** Kamogawa C, Sumi M, Goto S, Hirao A, Gonzales F, Yasuda K, Iino S. Quantitative detection of hepatitis B virus by transcription-mediated amplification and hybridization protection assay. *J Clin Microbiol* 1999; **37**: 310–314
23 **Sumi H,** Yokosuka O, Seki N, Arai M, Imazeki F, Kurihara T, Kanda T, Fukai K, Kato M, Saisho H. Influence of hepatitis B virus genotypes on the progression of chronic type B liver disease. *Hepatology* 2003; **37**: 19-26
24 **Usuda S,** Okamoto H, Iwanari H, Baba K, Tsuda F, Miyakawa Y, Mayumi M. Serological detection of hepatitis B virus genotypes by ELISA with monoclonal antibodies to type-specific epitopes in the preS2-region product. *J Virol Methods* 1999; **80**: 97-112
25 **Mizokami M,** Nakano T, Orito E, Tanaka Y, Sakugawa H, Mukaide M, Robertson BH. Hepatitis B virus genotype assignment using restriction fragment length polymorphism patterns. *FEBS Lett* 1999; **450**: 66-71
26 **Tomita T,** Yokosuka O, Tagawa M, Saisho H, Tamura S, Fukuda I, Omata M. Decrease of wild-type and precore mutant duck hepatitis B virus replication during lamivudine treatment in white Pekin ducks infected with the viruses. *J Hepatol* 2000; **32**: 850-858
27 **Liaw YF.** Hepatitis flares and hepatitis B e antigen seroconversion: implication in anti-hepatitis B virus therapy. *J Gastroenterol Hepatol* 2003; **18**: 246-252
28 **Kuwahara R,** Kumashiro R, Murashima S, Ogata K, Tanaka K, Hisamochi A, Hino T, Ide T, Tanaka E, Koga Y, Sata M. Genetic heterogeneity of the precore and the core promoter region of genotype C hepatitis B virus during lamivudine therapy. *J Med Virol* 2004; **72**: 26-34
29 **Maruyama T,** Kuwata S, Koike K, Iino S, Yasuda K, Yotsuyanagi H, Moriya K, Maekawa H, Yamada H, Shibata Y, Milich DR. Precore wild-type DNA and immune complexes persist in chronic hepatitis B after seroconversion: no association between genome conversion and seroconversion. *Hepatology* 1998; **27**: 245-253
30 **Asahina Y,** Izumi N, Uchihara M, Noguchi O, Nishimura Y, Inoue K, Ueda K, Tsuchiya K, Hamano K, Itakura J, Miyake S. Core promoter/pre-core mutations are associated with lamivudine-induced HBeAg loss in chronic hepatitis B with genotype C. *J Hepatol* 2003; **39**: 1063-1069

Science Editor Li WZ **Language Editor** Elsevier HK

PO Box 2345, Beijing 100023, China
www.wjgnet.com
wjg@wjgnet.com

ELSEVIER

World J Gastroenterol 2005;11(22):3351-3356
World Journal of Gastroenterology ISSN 1007-9327

Genes transactivated by hepatitis C virus core protein, a microarray assay

Min Liu, Shu-Lin Zhang, Jun Cheng, Yan Liu, Lin Wang, Qing Shao, Jian Zhang, Shu-Mei Lin

Min Liu, Shu-Lin Zhang, Shu-Mei Lin, Department of Infectious Diseases, The First Affiliated Hospital, Medical College, Xi'an Jiaotong University, Xi'an 710061, Shaanxi Province, China
Jun Cheng, Yan Liu, Lin Wang, Qing Shao, Jian Zhang, Gene Therapy Research Center, Institute of Infectious Diseases, The 302 Hospital of PLA, Beijing 100039, China
Supported by the National Natural Science Foundation of China, No. 39970674
Correspondence to: Dr. Min Liu, Department of Infectious Diseases, The First Affilated, Medical College, Xi'anJiaotong University, Xi'an 710061, Shaanxi Province, China. liumin3262@sohu.com
Telephone: +86-10-85323262 Fax: +86-10-85252512
Received: 2004-08-31 Accepted: 2004-10-11

Abstract

AIM: To explore the new target genes transactivated by hepatitis C virus (HCV) core protein and to elucidate the pathogenesis of HCV infection.

METHODS: Reverse transcribed cDNA was subjected to microarray assay. The coding gene transactivated by HCV core protein was cloned and analyzed with bioinformatics methods.

RESULTS: The expressive vector of pcDNA3.1(-)-core was constructed and confirmed by restriction enzyme digestion and DNA sequencing and approved correct. mRNA was purified from HepG2 and HepG2 cells transfected with pcDNA3.1(-)-core, respectively. The cDNA derived was subjected to microarray assay. A new gene named HCTP4 was cloned with molecular biological method in combination with bioinformatics method.

CONCLUSION: HCV core is a potential transactivator. Microarray is an efficient and convenient method for analysis of differentially expressed genes.

Key words: Hepatitis C virus; Core protein; Microarray assay

Liu M, Zhang SL, Cheng J, Liu Y, Wang L, Shao Q, Zhang J, Lin SM. Genes transactivated by hepatitis C virus core protein, a microarray assay. *World J Gastroenterol* 2005; 11(22): 3351-3356
http://www.wjgnet.com/1007-9327/11/3351.asp

INTRODUCTION

Hepatitis C virus (HCV) causes chronic liver disease, including chronic active hepatitis, liver cirrhosis and hepatocellular carcinoma[1-4]. About 170 million persons are infected with HCV worldwide and about 3.2% people are positive for anti-HCV in China. The pathogenesis of HCV infection is not clear[5,6].

The HCV core gene contains the most conserved sequence in the coding region of most HCV genotypes, which implies an important biological function. Since suitable viral culture systems are usually not available[7-9], analysis of HCV genome organization and viral-product function is important to understand the viral life cycle and the pathogenesis of HCV infection. In order to understand the pathogenesis of HCV infection, we investigated the transactivating effect of HCV core protein by microarray assay. Among 1 152 genes, 95 genes transregulated by HCV core protein are involved in signal transduction, cell proliferation, differentiation, apoptosis, immunosuppression. One new gene, HCTP4 was studied by microarrary assay.

MATERIALS AND METHODS

Construction and identification of expression vectors of HCV core

Plasmid pBRTM/HCV-1 (provided by Rice CM, USC Rockfeller University) containing full-length HCV cDNA (9 401 nt) was used to design polymerase chain reaction (PCR) primers for core (342-914 nt) of HCV. PCR product was cloned into pGEM-T. After its accuracy was verified, sequences of the genes of HCV core were ligated into plasmid pcDNA3.1(-)-core containing full-length of HCV core gene. pcDNA3.1(-) obtained from Invitrogen Co. was digested by *Eco*RI and *Bam*HI (Takara). PCR primers were as follows: sense primer, 5'-GAA TTC AAT GAG CAC GAA TCC TAA-3'; antisense primer, 5'-GGA TCC AGG CTG AAG CGG GCA CA-3' (Shanghai BioAsia Biotechnology Co., Ltd, China).

Expression of pcDNA3.1(-)-core in HepG2 cells

HepG2 cells were transiently transfected with pcDNA3.1 (-)-core using lipofectamine. At the same time, empty vectors transfected into cells served as control. HepG2 cells were plated at a density of 1×10^6 in RPMI 1640 containing 100 U/mL of penicillin, 100 μg/mL of streptomycin, and 100 mL/L heat-inactivated fetal bovine serum (FBS). Twenty-four hours after the cells growth reached 40-50% confluence, the cells were transfected with plasmids by using lipofectamine according to the manufacturer's protocol (Gibco Co., USA).

mRNA and cDNA isolation

Total cellular RNA was isolated using TRIzol (Invitrogen

Co., USA) according to the manufacturer's instructions. Then mRNA was reverse transcribed to generate Cy3 and Cy5 fluorescent-labeled cDNA probes.

Hybridization conditions

Hybridization of the fluorescent probe to the microchip was performed in 1× UniHyb solution at 37 ℃ for 30 min. DNA Probe was denatured before hybridization at 95 ℃ for 1 min and chilled on ice. A 2- to 3-μL spot from each probe was applied to the microarray and covered with a plastic cover slip (5 mm×5 mm) to prevent drying of the probe during incubation in the hybridization cassette (TeleChem International, Inc., USA). After hybridization, the slides were washed once with 2× SSC+0.2% SDS for 10 min at room temperature, once with 0.1× SSC+0.2% SDS for 10 min, and once with 0.1× SSC for 10 min and dried at room temperature.

Scanning and quantitation of microarrays

Fluorescent images of the microarrays were generated by scanning the slides using a ScanArray 3000 (General Scanning). The fluorescent signals from each spot were measured and compared using ImaGene 3.0 software. Analysis of collected data was performed on the basis of total fluorescence intensity measured from a fixed circular area of each oligonucleotide spot. Fluorescent signals with a statistically significant difference ($P<0.01$) from the background level were considered to be positive and the results were expressed as a ratio.

Cloning and identification of new gene HCTP4

Among 95 different genes, we found a new gene and named it HCTP4. The HCTP4 gene was amplified by PCR using HpG2 cell DNA. PCR primers were as follows: sense primer, 5'-CCA TGG ATG TCA CAA GTT AAA AGC TC-3'; antisense primer, 5'-GGA TCC TTA GCA GTG GAA TCG AGT GG-3' (Shanghai BioAsia Biotechnology Co., Ltd).

Study of HCTP4 by microarray assay

Briefly, the recombined expression plasmid pcDNA3.1(-)-HCTP4 was constructed, and HepG2 cells were transfected. Total mRNA was isolated from the HepG2 cells transfected with pcDNA3.1(-) and pcDNA3.1(-)-HCTP4, respectively. Microarray was conducted for screening of up- and down-regulated genes of HepG2 cells. Fluorescent signals with a statistically significant difference ($P<0.01$) from the background level were considered to be positive and the results were expressed as a ratio.

RESULTS

Identification of expression vector

Restriction enzyme analysis of pcDNA3.1(-)-core plasmid with *Eco*RI/*Bam*HI yielded two bands: 4 900 bp pcDNA3.1(-) and 573 bp HCV core. Analysis of PCR reaction products by agarose gel electrophoresis got a clear band of the expected size (573 bp). Sequence of the PCR product was correct (Figure 1).

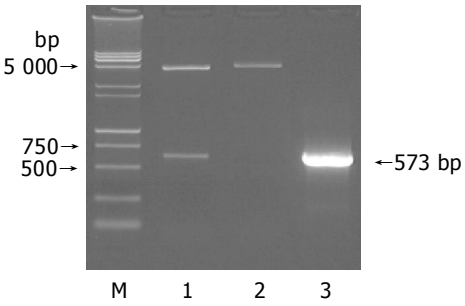

Figure 1 Eletrophoresis of pcDNA3.1(-)-core plasmid(A), cDNA(B) and HCTP4 (C) in 1% agarose gel. A: Lane 1: *Eco*RI/*Bam*HI; lane 2: *Hin*dIII; lane 3: plasmid; M: DNA Marker (15 000+2 000 bp).

Identification of HCV core transient expression

After being reverse-transcribed by three different Oligo dT, identification of cDNA by PCR yielded a common 573 bp band (Figure 2).

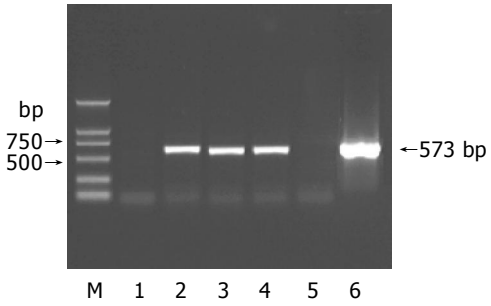

Figure 2 Eletrophoresis of cDNA in 1% agarose gel. Lane 1: negative control; lanes 2-4: total RNA; lane 5: blank control; lane 6: positive control; M: DNA Marker (2 000 bp).

Result of HCV core by microarray analysis

Approximately 45 up-regulated and 50 down-regulated genes were identified by HCV core in HepG2 cells. Some up- and down-regulated genes are shown in Tables 1 and 2.

Identification of RT-PCR products from HCTP4

Among 95 different genes, we found a new gene and named it HCTP4. The nucleotide sequence data of HCTP4 reported in this paper appear in the GenBank nucleotide sequence database under the following accession numbers AY734680. The production of HCTP4 PCR is 2 244 bp. (Figure 3).

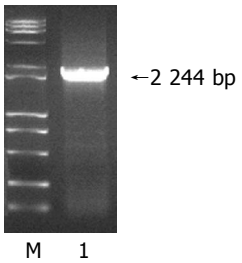

Figure 3 Eletrophoresis of HCTP4 in 1% agarose gel. Lane 1: HCTP4; M: DNA marker (15 000 bp).

Table 1 Up-regulated genes by HCV core

Accession numbers	Protein	Cy5/Cy3
NM_005657	Tumor protein p53 binding protein 1, TP53BP1	2.004
D50683	TGF-betaIIR alpha	2.072
NM_006595	Apoptosis inhibitor 5, API5	2.199
NM_000612	Insulin-like growth factor 2, IGF2	2.232
NM_002530	Neurotrophic tyrosine kinase, receptor	2.233
NM_000760	Colony stimulating factor 3 receptor, CSF3R	2.253
NM_014350	TNF-induced protein, GG2-1	2.358
NM_006290	Tumor necrosis factor, alpha-induced protein 3, TNFAIP3	2.359
NM_003151	Signal transducer and activator of transcription 4, STAT4	2.390
U07139	Voltage-gated calcium channel beta subunit	2.423
NM_000014	Alpha-2-macroglobulin, A2M	2.526
NM_012112	Chromosome 20 open reading frame 1, C20orf1	2.689
NM_002736	Protein kinase, cAMP- dependent, regulatory	2.710
NM_014575	Schwannomin interacting protein 1, SCHIP1	2.737
U47077	DNA-dependent protein kinase catalytic subunit, DNA-PKcs	2.787
AF352051	Proliferation potential-related protein	2.827
NM_003998	Nuclear factor of kappa light polypeptide gene enhancer in B-cells 1, p105, NF-κB1	3.005
NM_004728	DEAD/H box polypeptide 21	3.149
NM_005100	A kinase anchor protein 12, AKAP12	3.897
NM_005171	Activating transcription factor 1, ATF1	4.142
BC008959	Histocompatibility 13	4.760
NM_014863	B cell RAG associated protein, BRAG	5.769
NM_002291	Laminin, beta 1, LAMB1	10.334

Result of HCTP4 by microarray analysis

DNA microarray showed that 56 genes were up-regulated by HCTP4 in HepG2 cells (Table 3) and 52 genes were down-regulated by HCTP4 in HepG2 cells (Table 4).

DISCUSSION

Diverse functional activities of the HCV putative core protein are noted in a number of investigations[10-13]. We cotransfected HepG2 cells with pcDNA3.1(-)-core and pSV-lacZ and demonstrated that the HCV core was successfully expressed in transfected HepG2 cells. Expression of β-gal was 5.4-fold higher in cotransfected pcDNA3.1(-)-core and pSV-lacZ than in cotransfected empty pcDNA3.1(-) and pSV-lacZ. HCV core had a significant transactivating effect on early promoter of SV40, and increased the expression of downstream gene lacZ. This result indicates that the HCV core protein expressed in HepG2 cells retains its biological activity in terms of transcriptional activation, which is inconsistent with previous reports[14].

To understand the *trans*-action mechanism of the core protein, a microarray assay was used to identify the relative transactivating target genes of HCV core protein. Approximately 45 up-regulated and 50 down-regulated genes were identified by HCV core protein in HepG2 cells. The up-regulated genes include tumor protein p53 binding protein 1, apoptosis inhibitor 5, TGF-βIIR alpha, insulin-like growth factor 2, tumor necrosis factor α-induced protein 3, signal transducer and activator of transcription 4, α-2-macroglobulin and proliferation potential-related protein. The down-regulated genes include member 10 of a tumor necrosis factor receptor superfamily, apoptosis-related cysteine protease, leukocyte-associated Ig-like receptor 1, apoptosis-related RNA binding protein, leucine zipper, interleukin 1, interferon α, α and ω receptor 1. The results show that HCV core protein has multiple regulatory functions in host-cell transcription, apoptosis, cell transformation and lipid metabolism and may play a role in suppressing host

Table 2 Down-regulated genes by HCV core

Accession numbers	Protein	Cy5/Cy3
NM_000535	PMS2 postmeiotic segregation increased 2	0.122
NM_012096	Adaptor protein containing pH domain, PTB domain and leucine zipper motif, APPL	0.386
NM_003844	Tumor necrosis factor receptor superfamily, member 10a	0.388
NM_001226	Caspase 6, apoptosis-related cysteine protease	0.400
NM_001229	Caspase 9, apoptosis-related cysteine protease	0.429
NM_002287	Leukocyte-associated Ig-like receptor 1	0.440
AF090693	Apoptosis-related RNA binding protein	0.462
NM_021020	Leucine zipper, putative tumor suppressor 1 LZTS1	0.464
NM_000062	Serine or cysteine proteinase inhibitor	0.471
NM_000575	Interleukin 1, alpha	0.472
AF016266	TRAIL receptor 2	0.477
NM_003796	RNA polymerase II subunit 5 RPB5-mediating protein, RMP	0.485
NM_000629	Interferon alpha, beta and omega receptor 1,IFNAR1	0.494

Table 3 Up-regulated genes by HCTP4 protein

Accession numbers	Protein	Cy5/Cy3
NM_002599	Phosphodiesterase 2A, cGMP-stimulated (PDE2A)	2.011
NM_053274	FKBP-associated protein (FAP48), transcript variant 1	2.014
NM_012319	LIV-1 protein, estrogen regulated (LIV-1)	2.017
NM_007047	Butyrophilin,subfamily 3, member A2 (BTN3A2)	2.030
NM_021950	Membrane-spanning 4-domains, subfamily A, member 1 (MS4A1)	2.033
NM_000817	Glutamate decarboxylase 1 (GAD1)	2.048
NM_033625	Ribosomal protein L34 (RPL34)	2.055
NM_006526	Zinc finger protein 217 (ZNF217)	2.058
NM_112219	Esterase D	2.068
NM_000386	Bleomycin hydrolase (BLMH)	2.079
NM_006330	Lysophospholipase 1 (LYPLA1)	2.088
D21262	KIAA0035 gene	2.089
NM_003796	RPB5-mediating protein (RMP)	2.091
NM_004904	cAMP response element-binding protein (CRE-BPa)	2.096
AF012086	Ran binding protein 2 (RanBP2alpha)	2.118
NM_005836	Translational inhibitor protein p14.5 (UK114)	2.126
NM_003998	Heat shock 70 ku protein 8 (HSPA8)	2.138
NM_000816	Gamma-aminobutyric acid (GABA)A receptor, gamma 2 (GABRG2)	2.174
NM_003129	Squalene epoxidase (SQLE)	2.174
NM_022171	T-cell leukemia translocation altered gene (TCTA)	2.211
NM_006644	Heat shock 105 ku (HSP105B)	2.256
AF070674	Inhibitor of apoptosis protein-1 (MIHC)	2.281
NM_001892	Casein kinase 1, alpha 1 (CSNK1A1)	2.285
NM_001539	Heat shock protein, DNAJ-like 2 (HSJ2)	2.303
NM_013943	Chloride intracellular channel 4 (CLIC4)	2.325
NM_006407	Vitamin A responsive; cytoskeleton related (JVVA)	2.370
NM_014637	T-cell receptor rearranged beta chain gene V-region (V-D-J)V-beta-AT	2.395
M11952	Nuclear receptor subfamily 3, group C, member 1 (NR3C1)	2.396
NM_007268	Ig superfamily protein (Z391G)	2.445
NM_021129	Pyrophosphatase (inorganic) (PP), nuclear gene encoding mitochondrial protein	2.498
NM_002731	Protein kinase, cAMP-dependent, catalytic, beta (PRKACB)	2.525
D85606	Gene for cholecystokinin type-A receptor	2.635
NM_024824	Hypothetical protein FLJ11806 (FLJ11806)	2.730
AF072928	Myotubularin related protein 6	2.802

immune response[15-19].

The transregulation of HCV core protein is displayed extensively, one of the mechanisms of transregulation is that HCV core protein interacts with the promoters of genome in infected cells and affects the expression of gene. Another mechanism is that HCV core protein interacts with transcription factor in nuclei of infected cells and indirectly affects the expression of gene. HCV core protein interacts with various proteins which may be an important reason for hepatocellular damage and development of hepatocellular carcinoma. HCTP4 was identified and deposited in GenBank; the access number is AY734680. In order to investigate the function of HCTP4, cDNA microarray technology was employed. Approximately 56 up-regulated and 52 down-regulated genes were identified in HepG2 cells.

In the up-regulated genes by HCTP4, CLIC4 is differentially regulated in fibroblasts and its expression contributes to a collective stationary myofibroblast phenotype[20]. ZNF217 is a candidate oncogene on chromosome 20q13.2. ZNF217-transduced cultures give rise to immortalized cells. Overexpression of ZNF217 may be responsible for the development of hepatomas[21]. Inhibitor of apoptosis protein-1(MIHC) has effects on apoptosis[22]. JVVA is vitamin A-responsive and might be associated with cytoskeleton, which may play a role in the regulation of cell differentiation[23]. cAMP is an important signaling molecule for a variety of cellular functions and exerts its effects by activating the cAMP-dependent protein kinase (AMPK), which transduces the signal through phosphorylation of different target proteins. The inactive holoenzyme of AMPK is a tetramer composed of two regulatory and two catalytic subunits. cAMP causes dissociation of the inactive holoenzyme into a dimer of regulatory subunits bound to four cAMP and two free monomeric catalytic subunits[24,25].

In the down-regulated genes by HCTP4, TGFB is a multifunctional peptide that controls proliferation, differentiation, and other functions in many cell types. TGFB acts synergistically with TGFA (MIM 190170) in inducing transformation and as a negative autocrine growth factor. Dysregulation of TGFB activation and signaling may result in apoptosis[26]. LIM domains found in over 60 proteins, play key roles in the regulation of developmental pathways and function as protein-binding interfaces, mediating specific protein-protein interactions, thus becoming a candidate tumor suppressor gene[27]. HCTP4 may have effects on development of hepatomas. Saposins (sphingolipid activator proteins) A-D are 80-amino acid lysosomal glycoproteins encoded by a single gene, termed prosaposin. The proteolytic processing of prosaposin to individual

Table 4 Down-regulated genes by HCV core

Accession numbers	Protein	Cy5/Cy3
NM_001961	Eukaryotic translation elongation factor 2 (EEF2)	0.040
NM_002313	Actin binding LIM protein 1 (LIM), transcript variant ABLIM-1	0.214
NM_014680	KIAA0100 gene product (KIAA0100)	0.234
NM_003682	MAP-kinase activating death domain (MADD)	0.259
NM_001226	Prosaposin	0.266
NM_004728	DEAD/H box polypeptide 21 (DDX21)	0.313
NM_013975	Ligase III, DNA, ATP-dependent (LIG3)	0.317
NM_014889	Metalloprotease 1 (MP1)	0.347
NM_005770	Small EDRK-rich factor 2 (SERF2)	0.348
NM_005167	Ras homolog gene family, member C (ARHC)	0.368
NM_000208	Insulin receptor (INSR)	0.369
NM_003330	Thioredoxin reductase 1 (TXNRD1)	0.373
NM_005243	Ewing sarcoma breakpoint region 1 (EWSR1)	0.396
NM_016250	N-myc downstream-regulated gene 2 (NDRG2)	0.404
NM_001250	Tumor necrosis factor receptor superfamily, member 5 (TNFRSF5)	0.406
NM_003313	Tissue specific transplantation antigen P35B (TSTA3)	0.416
NM_004127	G protein pathway suppressor 1 (GPS1)	0.416
NM_002708	Protein phosphatase 1, catalytic subunit, alpha isoform (PPP1CA)	0.431
NM_001777	CD47 antigen (Rh-related antigen, integrin-associated signal transducer	0.444
NM_002199	Interferon regulatory factor 2 (IRF2)	0.454
NM_002087	Granulin (GRN)	0.469
NM_000660	Transforming growth factor, beta 1 (TGFB1)	0.475
NM_054012	Argininosuccinate synthetase (ASS)	0.478
NM_002084	Glutathione peroxidase 3 (GPX3)	0.493

saposins occurs predominantly in acidified compartments including lysosome. The physiological importance of this locus has been demonstrated by the genetic deficiencies of individual saposins or prosaposin that lead to various glycosphingolipid storage diseases[28,29]. Insulin is a pleiotropic hormone with multiple integrated metabolic and mitogenic signaling pathways upon binding to the cell surface insulin receptor[30]. HCTP4 interacts with prosaposin and insulin receptor and influences their biological functions. These results are associated with the nonregulation of sugar and lipid metabolism by HCV core[4,31]. Eukaryotes, in contrast to prokaryotes, contain more than one DNA ligase, and these enzymes have distinct roles in DNA metabolism. Five DNA ligase activities have been purified from mammalian cell extracts. Ligase III is more closely related to DNA ligase encoded by pox viruses rather than replicative DNA ligases such as mammalian DNA ligase 1, and may be involved in DNA repair and recombination[32]. Thioredoxin and thioredoxin reductase 1 (TXNRD1) are redox proteins that have been implicated in cellular events such as cell proliferation, transformation, and apoptosis[33,34]. DEAD box proteins characterized by the conserved motif Asp-Glu-Ala-Asp (DEAD) are putative RNA helicases. They are implicated in a number of cellular processes involving alteration of RNA secondary structure such as translation initiation, nuclear and mitochondrial splicing, ribosome and spliceosome assembly. Based on their distribution patterns, some members of this family are believed to be involved in embryogenesis, spermatogenesis, cellular growth and division. This gene encodes a DEAD box protein, which is an antigen recognized by autoimmune antibodies, unwinds double-stranded RNA, folds single-stranded RNA, and may play an important role in ribosomal RNA biogenesis, RNA editing, RNA transport, and general transcription[35]. MADD is intimately involved in anti-apoptotic and cell-survival processes[36]. N-myc downstream-regulated gene 2(NDRG2) is a member of the N-myc downregulated gene family, which belongs to the alpha/beta hydrolase superfamily. The protein encoded by this gene is a cytoplasmic protein that may play a role in neurite outgrowth. This gene may be involved in glioblastoma carcinogenesis[37]. TNFRSF5 is a member of the TNF-receptor superfamily. This receptor has been found to be essential in mediating a broad variety of immune and inflammatory responses including T cell-dependent immunoglobulin class switching, memory B cell development, and germ center formation[38,39].

In conclusion, HCV core protein and HCTP4 are related to chronic liver disease, liver cirrhosis and hepatocellular carcinoma.

REFERENCES

1 **Choo QL,** Kuo G, Weiner AJ, Overby LR, Bradley DW, Houghton M. Isolation of a cDNA clone derived from a blood-borne non-A, non-B viral hepatitis genome. *Science* 1989; **244**: 359-362

2 **Di Bisceglie AM,** Lyra AC, Schwartz M, Reddy RK, Martin P, Gores G, Lok AS, Hussain KB, Gish R, Van Thiel DH, Younossi Z, Tong M, Hassanein T, Balart L, Fleckenstein J, Flamm S, Blei A, Befeler AS. Hepatitis C-related hepatocellular carcinoma in the United States: influence of ethnic status. *Am J Gastroenterol* 2003; **98**: 2060-2063

3 **Siavoshian S,** Abraham JD, Kieny MP, Schuster C. HCV core, NS3, NS5A and NS5B proteins modulate cell proliferation independently from p53 expression in hepatocarcinoma cell lines. *Arch Virol* 2004; **149**: 323-336

4 **Bataller R,** Paik YH, Lindquist JN, Lemasters JJ, Brenner DA. Hepatitis C virus core and nonstructural proteins induce fibrogenic effects in hepatic stellate cells. *Gastroenterology* 2004; **126**: 529-540

5 **McHutchison JG.** Understanding hepatitis C. *Am J Manag Care* 2004; **10**: S21-S29

6 **Poynard T,** Yuen MF, Ratziu V, Lai CL. Viral hepatitis C. *Lancet* 2003; **362**: 2095-2100

7 **Trujillo-Murillo Kdel C,** Garza-Rodriguez Mdel L, Martinez-Rodriguez HG, Barrera-Saldana HA, Bosques-Padilla F, Ramos-Jimenez J, Rivas-Estilla AM. Experimental models for hepatitis C virus (HCV): new opportunities for combating hepatitis C. *Ann Hepatol* 2004; **3**: 54-62

8 **Ito T,** Mukaigawa J, Zuo J, Hirabayashi Y, Mitamura K, Yasui K. Cultivation of hepatitis C virus in primary hepatocyte culture from patients with chronic hepatitis C results in release of high titre infectious virus. *J Gen Virol* 1996; **77**(Pt 5): 1043-1054

9 **Bukh J.** A critical role for the chimpanzee model in the study of hepatitis C. *Hepatology* 2004; **39**: 1469-1475

10 **Sacco R,** Tsutsumi T, Suzuki R, Otsuka M, Aizaki H, Sakamoto S, Matsuda M, Seki N, Matsuura Y, Miyamura T, Suzuki T. Antiapoptotic regulation by hepatitis C virus core protein through up-regulation of inhibitor of caspase-activated DNase. *Virology* 2003; **317**: 24-35

11 **Kao CF,** Chen SY, Lee YH. Activation of RNA polymerase I transcription by hepatitis C virus core protein. *J Biomed Sci* 2004; **11**: 72-94

12 **Yasui K,** Wakita T, Tsukiyama-Kohara K, Funahashi SI, Ichikawa M, Kajita T, Moradpour D, Wands JR, Kohara M. The native form and maturation process of hepatitis C virus core protein. *J Virol* 1998; **72**: 6048-6055

13 **Ray RB,** Steele R, Basu A, Meyer K, Majumder M, Ghosh AK, Ray R. Distinct functional role of Hepatitis C virus core protein on NF-kappaB regulation is linked to genomic variation. *Virus Res* 2002; **87**: 21-29

14 **Chang J,** Yang SH, Cho YG, Hwang SB, Hahn YS, Sung YC. Hepatitis C virus core from two different genotypes has an oncogenic potential but is not sufficient for transforming primary rat embryo fibroblasts in cooperation with the H-ras oncogene. *J Virol* 1998; **72**: 3060-3065

15 **Lonardo A,** Adinolfi LE, Loria P, Carulli N, Ruggiero G, Day CP. Steatosis and hepatitis C virus: mechanisms and significance for hepatic and extrahepatic disease. *Gastroenterology* 2004; **126**: 586-597

16 **Ohkawa K,** Ishida H, Nakanishi F, Hosui A, Ueda K, Takehara T, Hori M, Hayashi N. Hepatitis C virus core functions as a suppressor of cyclin-dependent kinase-activating kinase and impairs cell cycle progression. *J Biol Chem* 2004; **279**: 11719-11726

17 **Crosse K,** Umeadi OG, Anania FA, Laurin J, Papadimitriou J, Drachenberg C, Howell CD. Racial differences in liver inflammation and fibrosis related to chronic hepatitis C. *Clin Gastroenterol Hepatol* 2004; **2**: 463-468

18 **Alonzi T,** Agrati C, Costabile B, Cicchini C, Amicone L, Cavallari C, Rocca CD, Folgori A, Fipaldini C, Poccia F, Monica NL, Tripodi M. Steatosis and intrahepatic lymphocyte recruitment in hepatitis C virus transgenic mice. *J Gen Virol* 2004; **85**: 1509-1520

19 **Sabile A,** Perlemuter G, Bono F, Kohara K, Demaugre F, Kohara M, Matsuura Y, Miyamura T, Brechot C, Barba G. Hepatitis C virus core protein binds to apolipoprotein AII and its secretion is modulated by fibrates. *Hepatology* 1999; **30**: 1064-1076

20 **Ronnov-Jessen L,** Villadsen R, Edwards JC, Petersen OW. Differential expression of a chloride intracellular channel gene, CLIC4, in transforming growth factor-beta1-mediated conversion of fibroblasts to myofibroblasts. *Am J Pathol* 2002; **161**: 471-480

21 **Nonet GH,** Stampfer MR, Chin K, Gray JW, Collins CC, Yaswen P. The ZNF217 gene amplified in breast cancers promotes immortalization of human mammary epithelial cells. *Cancer Res* 2001; **61**: 1250-1254

22 **Horrevoets AJ,** Fontijn RD, van Zonneveld AJ, de Vries CJ, ten Cate JW, Pannekoek H. Vascular endothelial genes that are responsive to tumor necrosis factor-alpha *in vitro* are expressed in atherosclerotic lesions, including inhibitor of apoptosis protein-1, stannin, and two novel genes. *Blood* 1999; **93**: 3418-3431

23 **Matsuda A,** Suzuki Y, Honda G, Muramatsu S, Matsuzaki O, Nagano Y, Doi T, Shimotohno K, Harada T, Nishida E, Hayashi H, Sugano S. Large-scale identification and characterization of human genes that activate NF-kappaB and MAPK signaling pathways. *Oncogene* 2003; **22**: 3307-3318

24 **Cartier C,** Hemonnot B, Gay B, Bardy M, Sanchiz C, Devaux C, Briant L. Active cAMP-dependent protein kinase incorporated within highly purified HIV-1 particles is required for viral infectivity and interacts with viral capsid protein. *J Biol Chem* 2003; **278**: 35211-35219

25 **Zidovetzki R,** Wang JL, Chen P, Jeyaseelan R, Hofman F. Human immunodeficiency virus Tat protein induces interleukin 6 mRNA expression in human brain endothelial cells via protein kinase C- and cAMP-dependent protein kinase pathways. *AIDS Res Hum Retroviruses* 1998; **14**: 825-833

26 **Fukuchi M,** Nakajima M, Fukai Y, Miyazaki T, Masuda N, Sohda M, Manda R, Tsukada K, Kato H, Kuwano H. Increased expression of c-Ski as a co-repressor in transforming growth factor-beta signaling correlates with progression of esophageal squamous cell carcinoma. *Int J Cancer* 2004; **108**: 818-824

27 **Kim AC,** Peters LL, Knoll JH, Van Huffel C, Ciciotte SL, Kleyn PW, Chishti AH. Limatin (LIMAB1), an actin-binding LIM protein, maps to mouse chromosome 19 and human chromosome 10q25, a region frequently deleted in human cancers. *Genomics* 1997; **46**: 291-293

28 **Ahn VE,** Faull KF, Whitelegge JP, Fluharty AL, Prive GG. Crystal structure of saposin B reveals a dimeric shell for lipid binding. *Proc Natl Acad Sci USA* 2003; **100**: 38-43

29 **Sun Y,** Qi X, Grabowski GA. Saposin C is required for normal resistance of acid beta-glucosidase to proteolytic degradation. *J Biol Chem* 2003; **278**: 31918-31923

30 **He HJ,** Kole S, Kwon YK, Crow MT, Bernier M. Interaction of filamin A with the insulin receptor alters insulin-dependent activation of the mitogen-activated protein kinase pathway. *J Biol Chem* 2003; **278**: 27096-27104

31 **Shintani Y,** Fujie H, Miyoshi H, Tsutsumi T, Tsukamoto K, Kimura S, Moriya K, Koike K. Hepatitis C virus infection and diabetes: direct involvement of the virus in the development of insulin resistance. *Gastroenterology* 2004; **126**: 840-848

32 **Bordone L,** Campbell C. DNA ligase III is degraded by calpain during cell death induced by DNA-damaging agents. *J Biol Chem* 2002; **277**: 26673-26680

33 **Lechner S,** Muller-Ladner U, Neumann E, Spottl T, Schlottmann K, Ruschoff J, Scholmerich J, Kullmann F. Thioredoxin reductase 1 expression in colon cancer: discrepancy between *in vitro* and *in vivo* findings. *Lab Invest* 2003; **83**: 1321-1331

34 **Anestal K,** Arner ES. Rapid induction of cell death by selenium-compromised thioredoxin reductase 1 but not by the fully active enzyme containing selenocysteine. *J Biol Chem* 2003; **278**: 15966-15972

35 **Henning D,** So RB, Jin R, Lau LF, Valdez BC. Silencing of RNA helicase II/Gualpha inhibits mammalian ribosomal RNA production. *J Biol Chem* 2003; **278**: 52307-52314

36 **Lim KM,** Chow VT. Induction of marked apoptosis in mammalian cancer cell lines by antisense DNA treatment to abolish expression of DENN (differentially expressed in normal and neoplastic cells). *Mol Carcinog* 2002; **35**: 110-126

37 **Deng Y,** Yao L, Chau L, Ng SS, Peng Y, Liu X, Au WS, Wang J, Li F, Ji S, Han H, Nie X, Li Q, Kung HF, Leung SY, Lin MC. N-Myc downstream-regulated gene 2 (NDRG2) inhibits glioblastoma cell proliferation. *Int J Cancer* 2003; **106**: 342-347

38 **Contin C,** Pitard V, Itai T, Nagata S, Moreau JF, Dechanet-Merville J. Membrane-anchored CD40 is processed by the tumor necrosis factor-alpha-converting enzyme. Implications for CD40 signaling. *J Biol Chem* 2003; **278**: 32801-32809

39 **Eeva J,** Postila V, Matto M, Nuutinen U, Ropponen A, Eray M, Pelkonen J. Kinetics and signaling requirements of CD40-mediated protection from B cell receptor-induced apoptosis. *Eur J Immunol* 2003; **33**: 2783-2791

Science Editor Wang XL and Guo SY **Language Editor** Elsevier HK

PO Box 2345, Beijing 100023, China
www.wjgnet.com
wjg@wjgnet.com

ELSEVIER

World J Gastroenterol 2005;11(22):3357-3362
World Journal of Gastroenterology ISSN 1007-9327

Correlation of serum leptin levels with anthropometric and metabolic parameters and biochemical liver function in Chinese patients with chronic hepatitis C virus infection

Zheng-Wen Liu, Ni Zhang, Qun-Ying Han, Jun-Tao Zeng, Yong-Lie Chu, Jian-Ming Qiu, Ya-Wen Wang, Lie-Ting Ma, Xiao-Qin Wang

Zheng-Wen Liu, Ni Zhang, Qun-Ying Han, Jun-Tao Zeng, Yong-Lie Chu, Jian-Ming Qiu, Department of Infectious Diseases, First Hospital, Xi'an Jiaotong University, Xi'an 710061, Shaanxi Province, China
Ya-Wen Wang, Lie-Ting Ma, Xiao-Qin Wang, Central Medical Laboratory, First Hospital, Xi'an Jiaotong University, Xi'an 710061, Shaanxi Province, China
Supported by the National Natural Science Foundation of China, No. 30170842
Correspondence to: Professor Zheng-Wen Liu, Department of Infectious Diseases, First Hospital, Xi'an Jiaotong University, Xi'an 710061, Shaanxi Province, China. zhengwenl@sohu.com
Telephone: +86-29-5324066 Fax: +86-29-5226360
Received: 2004-06-16 Accepted: 2004-07-22

Abstract

AIM: To determine serum leptin levels and investigate their correlations with anthropometric and metabolic parameters and biochemical liver function in patients with chronic hepatitis C virus (HCV) infection and their potential clinical implications.

METHODS: Forty-two chronic HCV-infected patients without anti-viral treatment were enrolled in this study, 30 patients had chronic hepatitis C, 10 had cirrhosis, and 2 had hepatocellular carcinoma (HCC). Thirty age- and sex-matched healthy individuals served as controls. Serum leptin levels were determined by ELISA. The biochemical liver function and serum lipids were determined at the same time. The height and body weight of patients and controls were measured, and body mass index (BMI) and body fat were calculated simultaneously. The correlations of serum leptin levels with anthropometric and metabolic parameters and biochemical liver function were assessed statistically.

RESULTS: The mean of serum leptin levels in patients with chronic hepatitis C, HCV-associated cirrhosis, HCV-associated HCC and control groups was (6.13±3.94), (5.25±4.21), (4.17±0.28), and (3.59±3.44) ng/mL, respectively. The serum leptin level in patients with chronic hepatitis C was significantly higher than that in controls. The serum leptin levels between cirrhotic patients and controls and between male and female cirrhotic patients had no significant difference. Serum leptin levels were positively-correlated with body fat, BMI, and apolipoprotein B (Apo B) in patients with chronic HCV infection. The serum alanine aminotransferase (ALT) levels were closely-correlated with BMI in patients with chronic hepatitis C.

CONCLUSION: HCV infection interferes with fat and lipid metabolism in patients with chronic HCV infection and leptin may play a role in hepatosteatosis.

Key words: Chronic hepatitis C; Leptin; Anthropometric parameter; Lipid metabolism

Liu ZW, Zhang N, Han QY, Zeng JT, Chu YL, Qiu JM, Wang YW, Ma LT, Wang XQ. Correlation of serum leptin levels with anthropometric and metabolic parameters and biochemical liver function in Chinese patients with chronic hepatitis C virus infection. *World J Gastroenterol* 2005; 11(22): 3357-3362
http://www.wjgnet.com/1007-9327/11/3357.asp

INTRODUCTION

Hepatitis C virus (HCV) infection is a worldwide public health problem[1,2]. HCV infection frequently leads to chronic hepatitis, which may progress to cirrhosis and even to hepatocellular carcinoma (HCC)[3]. The mechanisms responsible for the pathogenesis of chronic HCV infection are not well known. One of the common and prominent histopathologic features in patients with chronic HCV infection is the presence of hepatic steatosis, which is believed to be an important co-factor in accelerating the development of liver fibrosis[4-7]. Previous studies demonstrated that chronic HCV infection has close correlations with fat and lipid metabolism[8,9] and that there is a significant relationship between hepatic steatosis and fibrosis in chronic hepatitis C[10-12]. The relationship between body mass index (BMI), steatosis, and fibrosis in chronic HCV-infected patients suggests a role of steatosis in the progression of hepatitis C[13]. Recent attention has been focused on the liver profibrogenic role of leptin in animal models[14] and serum leptin levels have been investigated in European and North American patients with chronic HCV infection in terms of the important role of leptin in the regulation of body fat and lipid metabolism. These studies demonstrated that serum leptin levels correlate with hepatic steatosis in chronic hepatitis C[15], the levels of leptin increase according to the progression of the stage of fibrosis in chronic HCV-infected patients and the severity of liver fibrosis is

associated with high leptin levels in chronic hepatitis C[16]. Furthermore, clinical observations showed that fatigue, a common symptom in hepatitis patients, is associated with high circulating leptin levels in chronic hepatitis C[17] and interferon-alpha antiviral therapy can decrease and suppress leptin levels in chronic hepatitis C patients[18,19]. These data suggest that leptin may play a role in the regulation of hepatic fibrosis in patients with chronic HCV infection[20] although it is controversial[21].

There are differences in the relationship between body fat and BMI among different ethnicities[22] and comparisons of anthropometric measurements showed that Asians have lower BMI but higher body fat than whites[23]. Leptin levels have been shown to be associated with anthropometric parameters such as BMI, total body fat, and subcutaneous fat. Moreover, gender, ethnicity, body composition, and fat distribution have effects on serum leptin concentrations[24,25]. However, no report has documented the role of leptin in Chinese patients with chronic HCV infection so far.

In this study, serum leptin levels in Chinese patients with chronic HCV infection without antiviral treatment were investigated, and their relationships with simultaneously determined anthropometric measurements, metabolic parameters, and biochemical liver function were analyzed to elucidate the role of leptin in Chinese patients with chronic HCV infection and the potential clinical significance.

MATERIALS AND METHODS

Patients

Forty-two HCV-infected patients were studied. All patients were anti-HCV positive and had detectable serum HCV RNA except for two HCC patients. Thirty of them were clinically diagnosed with chronic hepatitis C, 10 with HCV-associated cirrhosis, and two with HCV-associated HCC. All patients had at least two documented occasions of increased serum alanine aminotransferase (ALT) levels 6 mo prior to enrollment, which were higher than the upper normal limit measured at intervals of more than 2 mo. Alcoholics and intravenous drug users or homosexual persons and patients with usage of hepatotoxic drugs, herbal medicine or immuno-suppressive therapy within the past 6 mo were excluded, and none of these patients had chronic renal failure, clotting abnormalities, hemophilia, serious neurological disorders, obesity, chronic viral hepatitis B or delta, HIV infection, autoimmune disease (anti-nuclear antibody titer >1:40), and/or inheritable disorders such as hemochromatosis, alpha-1-antitrypsin deficiency or Wilson's disease, and other metabolic disorders such as diabetes and thyroidism. None of the patients had any antiviral therapies before recruitment and all of them had stable body weight for at least 4 wk before enrollment. All the cirrhotic and HCC patients had no ascites. Informed consent was obtained from all patients. Thirty healthy age- and gender-comparable blood donors served as controls.

Methods

Blood samples were obtained from all subjects after overnight fasting. Samples were centrifuged and sera were stored at -25 ℃. Body height (m) and weight (kg), waist and hip circumference (cm) were taken with standard methods. BMI was calculated by weight/height^2. Fat distribution in abdomen (waist-to-hip ratio, WHR) was calculated by waist circumference/hip circumference. Body fat was calculated according to the formulae 1.2×BMI+0.23×age-16.2 and 1.2×BMI+0.23×age-5.4 for male and female subjects, respectively.

Serum anti-HCV was detected by ELISA using commercially available diagnostic kits for antibody to HCV from Sino-American Biotechnology Company (Zhengzhou, China). Quantification of serum HCV RNA was performed using commercial HCV fluorescence PCR diagnostic kits manufactured by Daan Gene Co., Ltd. (Zhongshan University, Shenzhen, China). The sensitivity of this HCV RNA assay was 80 copies/mL. Serum-soluble leptin levels were determined by commercial ELISA kits (R&D Systems Inc., Minneapolis, MN, USA). The sensitivity was 0.02 ng/mL. It had no cross reaction with interleukin (IL)-1, IL-2, IL-4, IL-6, IL-8, fibroblast growth factor, epidermal growth factor, platelet-derived growth factor, tumor necrosis factor (TNF), soluble TNF-receptor II, and interferon. Intra- and inter-assay variabilities were <10.5%. Serum total cholesterol, triglyceride, HDL cholesterol, LDL cholesterol, Apo AI, Apo B, and biochemical liver function were assayed on an automatic analyzer (HITACHI 7170A, Hitachi Koki Co., Ltd., Hitachinaka City, Japan).

Statistical analysis

Data were expressed as mean±SD and analyzed with SPSS 11.0 software. Statistical analysis was performed using two-tailed Fisher's exact test, two-tailed Student's *t*-test, χ^2 test, and analysis of covariance wherever appropriate. Correlation tests between parameters were performed by multiple linear regression and multiple correlation analysis. A P value less than 0.05 was considered statistically significant.

RESULTS

Comparison of serum leptin levels between patients with chronic HCV infection and controls

The demographic and anthropometric characteristics in patients with chronic HCV infection and controls are shown in Table 1. The age, body height and weight, waist and hip circumference, BMI, WHR, and body fat were not statistically different between patients with HCV infection and controls (Table 1).

Table 1 Demographic characteristics in patients with HCV infection and controls (mean±SD)

	Patients	Controls	t	P
Number (male/female)	25/17	18/12	0.002[1]	0.968
Age (yr)	44.93±14.35	39.43±12.33	1.696	0.094
Height (m)	1.67±0.08	1.66±0.07	0.925	0.358
Weight (kg)	64.86±15.08	64.00±9.18	0.312	0.756
WC (cm)	81.88±9.59	81.45±12.97	0.137	0.892
HC (cm)	94.25±8.46	94.00±7.92	0.084	0.933
BMI (kg/m^2)	22.94±4.59	23.14±3.09	0.225	0.822
WHR	0.87±0.74	0.87±0.11	0.220	0.827
Body fat (%)	26.21±7.63	24.96±7.25	0.714	0.478

WC: waist circumference, HC: hip circumference, BMI: body mass index, WHR: waist-to-hip circumference ratio, body fat (%): percent of body fat, [1]χ^2 test.

Considering the possible effects of BMI, WHR, and body fat on the levels of serum leptin, analysis of covariance was performed using BMI and body fat as covariate as determined by pre-analysis. The serum leptin level in patients with chronic HCV infection was significantly higher than that in controls ($F = 5.610$, $P = 0.021$, Table 2). Comparisons of serum leptin levels were further performed according to gender in term of the effects of gender on leptin concentrations due to differences in body composition and body fat distribution between male and female patients[26,27]. The results showed that serum leptin level in male and female patients was significantly higher than that in male and female controls ($F = 17.269$, $P<0.001$; $F = 4.002$, $P = 0.056$, Table 2). Serum leptin levels in female individuals were significantly elevated compared with those in male individuals ($F = 9.341$, $P = 0.005$ for patients and $F = 16.080$, $P<0.001$ for controls, Table 2).

Table 2 Comparison of serum leptin levels between patients with HCV infection and controls (mean±SD)

	Patients[2]	Controls[3]	*F*	*P*
No. (male/female)	25/17	18/12	0.002[1]	0.968
Male	3.58±2.06	1.44±1.06	17.269	<0.001
Female	9.13±3.59	6.83±3.23	4.002	0.056
Total	5.83±3.89	3.59±3.44	5.610	0.021

[1]χ^2 test, [2]$F = 9.341$, $P = 0.005$, male *vs* female; [3]$F = 16.080$, $P<0.001$, male *vs* female.

Comparisons of serum leptin levels between chronic HCV-infected patients at different clinical stages and controls

The demographic, anthropometric, biochemical, and virological characteristics in HCV-infected patients at different clinical stages are shown in Table 3.

The serum leptin levels in patients with chronic hepatitis C, HCV-associated cirrhosis, HCV-associated HCC and controls were compared by analysis of covariance. The serum leptin levels in patients with chronic hepatitis C were significantly higher than those in controls ($P = 0.003$). The serum leptin levels in patients with HCV-associated cirrhosis and HCV-associated HCC were not significantly increased as compared with controls ($P = 0.752$ and $P = 0.822$, respectively). The serum leptin levels in patients with chronic hepatitis C were not statistically different from those in patients with HCV-associated cirrhosis ($P = 0.074$) and HCV-associated HCC ($P = 0.397$). The serum leptin levels between patients with HCV-associated cirrhosis and HCV-associated HCC had no significant difference ($P = 0.952$). The serum leptin level in male patients with chronic hepatitis C were obviously different ($F = 12.454$, $P = 0.002$) from that in female patients. However, the serum leptin levels between male and female patients with HCV-associated cirrhosis were not statistically different ($F = 0.054$, $P = 0.823$, Table 4).

Correlation analysis of factors associated with serum leptin and ALT levels

Factors possibly-associated with serum leptin levels in patients

Table 3 Demographic, anthropometric, biochemical, and virological characteristics in chronic HCV-infected patients at different clinical stages (mean±SD)

	Chronic hepatitis C	HCV-associated cirrhosis	HCV-associated HCC
No. (male/female)	17/13	6/4	2/0
Age (yr)	41.03±14.10	53.70±9.93	59.5±12.02
Height (m)	1.68±0.09	1.66±0.05	1.69±0.04
BMI (kg/m^2)	23.01±3.39	22.71±7.59	22.97±4.53
WHR	0.86±0.07	0.87±0.08	0.95±0.02
Body fat (%)	25.79±6.52	27.72±11.23	25.05±2.67
LDL (mmol/L)	2.05±1.01	1.41±0.82	2.24±0.19
CHO (mmol/L)	4.09±2.05	3.22±1.08	5.55±1.06
TG (mmol/L)	1.51±1.03	0.81±0.45	1.52±0.47
HDL (mmol/L)	1.13±0.43	1.07±0.40	1.34±0.74
Apo AI (mg/L)	1.36±0.40	1.17±0.44	1.45±0.72
Apo B (mg/L)	0.55±0.27	0.39±0.19	0.71±0.13
ALT (U/L)	93.19±83.08	45.4±35.86	20.5±0.71
AST (U/L)	67.96±50.65	77.70±62.11	48.50±20.51
GGT (U/L)	50.27±41.22	49.80±53.79	92.00±18.38
HCV RNA (copies/mL)	(6.4±12)×10^4	(6.2±8.9)×10^4	<80

BMI: body mass index, WHR: waist-to-hip circumference ratio, body fat (%): percent of body fat, LDL: low density lipoprotein, CHO: cholesterol, TG: triglycerides, HDL: high density lipoprotein, Apo AI: apolipoprotein AI, Apo B: apolipoprotein B, ALT: alanine aminotransferase, AST: aspartate aminotransferase, GGT: gamma-glutamyltransferase, HCV RNA: hepatitis C virus ribonucleic acid.

Table 4 Comparisons of serum leptin levels between HCV-infected patients at different clinical stages and controls (mean±SD)

	Chronic hepatitis C	HCV-associated cirrhosis	HCV-associated HCC	Controls
No. (M/F)	17/13	6/4	2/0	18/12
Male	3.75±2.11	2.90±2.33	4.17±0.28	1.44±1.06
Female	9.25±3.61	8.77±4.07		6.83±3.23
Total	6.13±3.94[1]	5.25±4.21[2]	4.17±0.28[3]	3.59±3.44

[1]$P = 0.003$, [2]$P = 0.752$ and [3]$P = 0.822$ compared with controls, respectively. $F = 12.454$, $P = 0.002$, $F = 0.054$, $P = 0.823$ and $F = 6.365$, $P = 0.018$ when comparisons were performed between male and female patients with chronic hepatitis C, HCV-associated cirrhosis and controls.

with chronic HCV infection were analyzed. Multiple linear regression was performed using the leptin levels as a dependent variable and ALT, AST, CHO, HDL, TG, Apo AI, Apo B, LDL, HCV RNA, BMI, body fat, and WHR as independent variables. The results showed that the serum leptin levels were associated with body fat, BMI, and Apo B but not with liver function and serum HCV RNA levels (Table 5).

Table 5 Factors possibly associated with serum leptin levels in patients with chronic HCV infection

Dependent variable	Independent variables	Standardized coefficients (Beta model)	*P*
Leptin	Body fat (%)	1.630	<0.001
Leptin	BMI	1.050	0.003
Leptin	Apo B	0.342	0.008

Body fat (%): percent of body fat, BMI: body mass index, Apo B: apolipoprotein B.

The possibly-associated factors with serum leptin and ALT levels in patients with chronic HCV infection were also analyzed using the ALT levels as a dependent variable and CHO, HDL, TG, Apo AI, Apo B, LDL, HCV RNA, BMI, body fat, and WHR as independent variables. The results showed that serum leptin levels were positively-correlated with body fat ($r = 0.520$, $P = 0.003$) and ALT levels were positively-correlated with Apo B ($r = 0.400$, $P = 0.032$) and BMI ($r = 0.389$, $P = 0.034$). No correlation between serum leptin and ALT levels in patients with HCV-associated cirrhosis was found.

DISCUSSION

Hepatic steatosis is a common histopathologic feature in patients with chronic HCV infection[4,5]. HCV-core-protein expression can induce steatosis in transgenic mouse model[28]. The possible role of leptin in the pathogenesis of hepatic steatosis and fibrosis has been studied[29]. It was found that leptin has a close relationship with the hepatic steatosis in alcoholic steatohepatitis[30]. The role of leptin is also a focus of study due to the high incidence of hepatic steatosis in chronic hepatitis C patients. Leptin levels in patients with chronic HCV infection are increased, suggesting that HCV infection interferes with fat metabolism and leptin levels. However, it is not clear whether there are also some differences in leptin levels in chronic hepatitis C patients because of the difference in body composition and fat distribution between Chinese and Western people. Therefore, the serum leptin levels in Chinese patients with chronic HCV infection and normal healthy controls were determined and analyzed to address these issues in our study.

The subjects studied were strictly and accurately selected to rule out or minimize the possible influences of other factors, such as diabetes mellitus, alcohol, and antiviral therapy on leptin levels. Our results showed that the leptin levels in patients with chronic HCV infection were obviously increased as compared with normal controls. The serum leptin levels in both male and female patients with chronic HCV infection are increased as compared with controls although the leptin levels are generally higher in females than in males. Our results are in accordance with previous reports[31-35]. The precise mechanisms, by which chronic HCV infection causes elevated serum leptin levels, are not completely known. Factors such as inflammation, abnormal fat metabolism, and hepatic steatosis in patients with chronic HCV infection, might be involved.

Findings in this study may mainly represent the expression of reduced fat mass in cirrhotic patients[36] and the abnormalities of sexual hormone metabolism in male cirrhotic patients[37].

Our analyses showed that the serum leptin levels were correlated with body fat, BMI, and Apo B but not with liver function and serum HCV RNA levels. These results suggest that leptin levels in chronic HCV infection are preferentially affected by fat and lipid metabolisms. Giannini *et al*[38], demonstrated that serum leptin levels in nonalcoholic steatohepatitis (NASH) and chronic hepatitis C increase, although the differences are not statistically significant. Therefore, it seems that the extents of leptin elevation are closely related with the severity of abnormal fat metabolism and hepatic steatosis in chronic HCV-infected patients.

Our further analyses showed that ALT levels were positively correlated with BMI ($r = 0.410$, $P = 0.030$), body fat ($r = 0.520$, $P = 0.003$), Apo B ($r = 0.400$, $P = 0.032$) and BMI ($r = 0.389$, $P = 0.034$). However, the serum leptin and ALT levels in patients with HCV-associated cirrhosis had no correlation with any other variable. These results further demonstrate the close relationships between leptin levels and fat metabolism and between hepatic necroinflammation and lipid and fat metabolisms in patients with chronic hepatitis C. A possible link between leptin and decreased lipid levels and interaction between HCV and Apo B have been elucidated[39-41]. Disappearance of these correlations in patients with HCV-associated cirrhosis may be a reflection of reduced fat mass in cirrhotic patients[36,42] and the abnormalities of sexual hormone metabolism in male cirrhotic patients[37]. Taken together, serum leptin levels in patients with chronic HCV infection appear to be controlled by multiple factors such as body composition, gender, abnormalities of fat and lipid metabolism, and hepatic steatosis resulting from chronic HCV infection. The stages of liver diseases also affect leptin levels in patients with chronic HCV infection.

Another major focus of recent studies is the role of leptin in the modulation of immune response and inflammation. The increase in leptin production that occurs during infection and inflammation strongly suggests that leptin is a part of cytokine cascade, which regulates the innate immune response and host defense mechanisms although both proinflammatory and anti-inflammatory effects have been documented for leptin[43]. Leptin plays an important role in T-cell-mediated immune responses and stimulates proliferation of CD4+ T cells and promotes Th1 responses[44-46]. Moreover, congenital leptin deficiency in humans is found to be associated with a decreased number of circulating CD4+T cells, impaired T-cell proliferation and cytokine release, all of which could be reversed by administration of recombinant leptin[47]. Observations in alcoholics showed that circulating levels of leptin are associated with NK activity in humans, suggesting that abnormal *in vivo* concentrations of leptin may contribute to the decline of NK activity in alcoholics[48]. The results of experiments in animals showed that leptin represents a

functional link between endocrine and immune systems[49]. On the other hand, considerable evidence suggests that immune mechanisms are involved in the pathogenesis of HCV infection. Both humoral and cell-mediated immune responses are believed to participate in the host defense against HCV infection. In particular, cell-mediated response plays a role in the immunopathogenesis of chronic hepatitis C[50]. An enhanced Th2 response is present in HCV infection, which may be responsible for the chronicity of HCV infection[51]. Both class I-restricted CD8+T cell and class II-restricted CD4+T cell responses to viral antigens are an important pathway responsible for hepatocyte damage in hepatitis C[52]. Lack of correlation between intrahepatic HCV RNA level and microinflammation in chronic hepatitis C also suggests that HCV-associated liver damage is mostly immunomediated[53]. T cells infiltrate into the liver of patients with chronic hepatitis C, which is believed to play a crucial role in the immunopathogenesis of hepatic inflammation[54]. Therefore, whether the immunoregulatory functions of leptin have relevance to the immunopathogenesis of chronic HCV infection needs to be further investigated.

Studies and observations showed that in hypoleptinemic patients with extreme insulin resistance and lipodystrophy, leptin can ameliorate insulin resistance, hyperglycemia, hyperinsulinemia, dyslipidemia, and hepatic steatosis. In leptin-deficient states, leptin therapy can restore gonadotrophin secretion, luteinizing hormone, and thyroid-stimulating hormone pulsitility[55]. In addition, leptin has been suggested as a novel strategy for immune intervention in pathologic conditions[56]. Most of the above abnormal conditions exist in patients with chronic hepatitis or cirrhosis. Therefore, whether enhancing or inhibiting leptin's activities plays a therapeutic role in these conditions also needs to be investigated[57].

In conclusion, patients with chronic hepatitis C have increased serum leptin levels. However, serum leptin levels in HCV-associated cirrhotic patients have no significant difference compared with controls. Serum leptin levels in patients with chronic hepatitis C are positively-correlated with body fat, BMI, and Apo B. Serum ALT levels are closely-correlated with BMI. These findings suggest that HCV infection interferes with fat and lipid metabolism in patients with chronic HCV infection, and the serum leptin levels might be a reflection of the abnormalities in fat and lipid metabolism resulted from viral infection and related hepatic necroinflammation. Further studies are warranted to elucidate the possible immunoregulatory role and potential therapeutic role of leptin in chronic HCV infection.

ACKNOWLEDGMENTS

We thank Dr. Jian-Ming Qiu from Department of Molecular Microbiology and Immunology, School of Medicine, University of Missouri, Columbia for his support and helpful reading of the manuscript.

REFERENCES

1 **Ebeling F.** Epidemiology of the hepatitis C virus. *Vox Sang* 1998; **74 Suppl 2**: 143-146
2 **Memon MI,** Memon MA. Hepatitis C: an epidemiological review. *J Viral Hepat* 2002; **9**: 84-100
3 **Niederau C,** Lange S, Heintges T, Erhardt A, Buschkamp M, Hurter D, Nawrocki M, Kruska L, Hensel F, Petry W, Haussinger D. Prognosis of chronic hepatitis C: results of a large, prospective cohort study. *Hepatology* 1998; **28**: 1687-1695
4 **Goodman ZD,** Ishak KG. Histopathology of hepatitis C virus infection. *Semin Liver Dis* 1995; **15**: 70-81
5 **Fischer HP,** Willsch E, Bierhoff E, Pfeifer U. Histopathologic findings in chronic hepatitis C. *J Hepatol* 1996; **24**: 35-42
6 **Ramalho F.** Hepatitis C virus infection and liver steatosis. *Antiviral Res* 2003; **60**: 125-127
7 **Walsh MJ,** Vanags DM, Clouston AD, Richardson MM, Purdie DM, Jonsson JR, Powell EE. Steatosis and liver cell apoptosis in chronic hepatitis C: a mechanism for increased liver injury. *Hepatology* 2004; **39**: 1230-1238
8 **Serfaty L,** Andreani T, Giral P, Carbonell N, Chazouilleres O, Poupon R. Hepatitis C virus induced hypobetalipoproteinemia: a possible mechanism for steatosis in chronic hepatitis C. *J Hepatol* 2001; **34**: 428-434
9 **Sabile A,** Perlemuter G, Bono F, Kohara K, Demaugre F, Kohara M, Matsuura Y, Miyamura T, Brechot C, Barba G. Hepatitis C virus core protein binds to apolipoprotein AII and its secretion is modulated by fibrates. *Hepatology* 1999; **30**: 1064-1076
10 **Czaja AJ,** Carpenter HA, Santrach PJ, Moore SB. Host and disease-specific factors affecting steatosis in chronic hepatitis C. *J Hepatol* 1998; **29**: 198-206
11 **Adinolfi LE,** Gambardella M, Andreana A, Tripodi MF, Utili R, Ruggiero G. Steatosis accelerates the progression of liver damage of chronic hepatitis C patients and correlates with specific HCV genotype and visceral obesity. *Hepatology* 2001; **33**: 1358-1364
12 **Ong JP,** Younossi ZM, Speer C, Olano A, Gramlich T, Boparai N. Chronic hepatitis C and superimposed nonalcoholic fatty liver disease. *Liver* 2001; **21**: 266-271
13 **Hourigan LF,** Macdonald GA, Purdie D, Whitehall VH, Shorthouse C, Clouston A, Powell EE. Fibrosis in chronic hepatitis C correlates significantly with body mass index and steatosis. *Hepatology* 1999; **29**: 1215-1219
14 **Potter JJ,** Womack L, Mezey E, Anania FA. Transdifferentiation of rat hepatic stellate cells results in leptin expression. *Biochem Biophys Res Commun* 1998; **244**: 178-182
15 **Romero-Gomez M,** Castellano-Megias VM, Grande L, Irles JA, Cruz M, Nogales MC, Alcon JC, Robles A. Serum leptin levels correlate with hepatic steatosis in chronic hepatitis C. *Am J Gastroenterol* 2003; **98**: 1135-1141
16 **Piche T,** Vandenbos F, Abakar-Mahamat A, Vanbiervliet G, Barjoan EM, Calle G, Giudicelli J, Ferrua B, Laffont C, Benzaken S, Tran A. The severity of liver fibrosis is associated with high leptin levels in chronic hepatitis C. *J Viral Hepat* 2004; **11**: 91-96
17 **Piche T,** Gelsi E, Schneider SM, Hebuterne X, Giudicelli J, Ferrua B, Laffont C, Benzaken S, Hastier P, Montoya ML, Longo F, Rampal P, Tran A. Fatigue is associated with high circulating leptin levels in chronic hepatitis C. *Gut* 2002; **51**: 434-439
18 **Kaser S,** Kaser A, Vogel W, Patsch JR, Tilg H. Interferon-alpha suppresses leptin levels: studies in interferon-alpha treated patients with hepatitis C virus infection and murine adipocytes. *Eur Cytokine Netw* 2002; **13**: 225-229
19 **Widjaja A,** Wedemeyer H, Tillmann HL, Horn R, Ockenga J, Jaeckel E, von zur Muhlen A, Manns MP, Brabant G. Hepatitis C and the leptin system: bound leptin levels are elevated in patients with hepatitis C and decrease during antiviral therapy. *Scand J Gastroenterol* 2001; **36**: 426-431
20 **Crespo J,** Rivero M, Fabrega E, Cayon A, Amado JA, Garcia-Unzeta MT, Pons-Romero F. Plasma leptin and TNF-alpha levels in chronic hepatitis C patients and their relationship to hepatic fibrosis. *Dig Dis Sci* 2002; **47**: 1604-1610
21 **Giannini E,** Ceppa P, Botta F, Mastracci L, Romagnoli P, Comino I, Pasini A, Risso D, Lantieri PB, Icardi G, Barreca T, Testa R. Leptin has no role in determining severity of steatosis and fibrosis in patients with chronic hepatitis C. *Am J Gastroenterol* 2000; **95**: 3211-3217

22 **Gurrici S,** Hartriyanti Y, Hautvast JG, Deurenberg P. Differences in the relationship between body fat and body mass index between two different Indonesian ethnic groups: the effect of body build. *Eur J Clin Nutr* 1999; **53**: 468-472

23 **Wang J,** Thornton JC, Russell M, Burastero S, Heymsfield S, Pierson RN. Asians have lower body mass index (BMI) but higher percent body fat than do whites: comparisons of anthropometric measurements. *Am J Clin Nutr* 1994; **60**: 23-28

24 **Nagy TR,** Gower BA, Trowbridge CA, Dezenberg C, Shewchuk RM, Goran MI. Effects of gender, ethnicity, body composition, and fat distribution on serum leptin concentrations in children. *J Clin Endocrinol Metab* 1997; **82**: 2148-2152

25 **Perez-Bravo F,** Albala C, Santos JL, Yanez M, Carrasco E. Leptin levels distribution and ethnic background in two populations from Chile: Caucasian and Mapuche groups. *Int J Obes Relat Metab Disord* 1998; **22**: 943-948

26 **Ellis KJ,** Nicolson M. Leptin levels and body fatness in children: effects of gender, ethnicity, and sexual development. *Pediatr Res* 1997; **42**: 484-488

27 **He Q,** Horlick M, Thornton J, Wang J, Pierson RN, Heshka S, Gallagher D. Sex and race differences in fat distribution among Asian, African-American, and Caucasian prepubertal children. *J Clin Endocrinol Metab* 2002; **87**: 2164-2170

28 **Moriya K,** Yotsuyanagi H, Shintani Y, Fujie H, Ishibashi K, Matsuura Y, Miyamura T, Koike K. Hepatitis C virus core protein induces hepatic steatosis in transgenic mice. *J Gen Virol* 1997; **78**(Pt 7): 1527-1531

29 **Yin CH,** Wang BE, Ma H, Jia JD, Shen FJ. Leptin and liver fibrosis. *Zhonghua Ganzangbing Zazhi* 2003; **11**: 60-61

30 **Uygun A,** Kadayifci A, Yesilova Z, Erdil A, Yaman H, Saka M, Deveci MS, Bagci S, Gulsen M, Karaeren N, Dagalp K. Serum leptin levels in patients with nonalcoholic steatohepatitis. *Am J Gastroenterol* 2000; **95**: 3584-3589

31 **Rosenbaum M,** Nicolson M, Hirsch J, Heymsfield SB, Gallagher D, Chu F, Leibel RL. Effects of gender, body composition, and menopause on plasma concentrations of leptin. *J Clin Endocrinol Metab* 1996; **81**: 3424-3427

32 **Nagy TR,** Gower BA, Trowbridge CA, Dezenberg C, Shewchuk RM, Goran MI. Effects of gender, ethnicity, body composition, and fat distribution on serum leptin concentrations in children. *J Clin Endocrinol Metab* 1997; **82**: 2148-2152

33 **Ostlund RE,** Yang JW, Klein S, Gingerich R. Relation between plasma leptin concentration and body fat, gender, diet, age, and metabolic covariates. *J Clin Endocrinol Metab* 1996; **81**: 3909-3913

34 **Havel PJ,** Kasim-Karakas S, Dubuc GR, Mueller W, Phinney SD. Gender differences in plasma leptin concentrations. *Nat Med* 1996; **2**: 949-950

35 **Saad MF,** Damani S, Gingerich RL, Riad-Gabriel MG, Khan A, Boyadjian R, Jinagouda SD, el-Tawil K, Rude RK, Kamdar V. Sexual dimorphism in plasma leptin concentration. *J Clin Endocrinol Metab* 1997; **82**: 579-584

36 **Testa R,** Franceschini R, Giannini E, Cataldi A, Botta F, Fasoli A, Tenerelli P, Rolandi E, Barreca T. Serum leptin levels in patients with viral chronic hepatitis or liver cirrhosis. *J Hepatol* 2000; **33**: 33-37

37 **Wang YJ,** Wu JC, Lee SD, Tsai YT, Lo KJ. Gonadal dysfunction and changes in sex hormones in postnecrotic cirrhotic men: a matched study with alcoholic cirrhotic men. *Hepatogastroenterology* 1991; **38**: 531-534

38 **Giannini E,** Botta F, Cataldi A, Tenconi GL, Ceppa P, Barreca T, Testa R. Leptin levels in nonalcoholic steatohepatitis and chronic hepatitis C. *Hepatogastroenterology* 1999; **46**: 2422-2425

39 **Kalaivanisailaja J,** Manju V, Nalini N. Lipid profile in mice fed a high-fat diet after exogenous leptin administration. *Pol J Pharmacol* 2003; **55**: 763-769

40 **Schettler V,** Monazahian M, Wieland E, Ramadori G, Grunewald RW, Thomssen R, Muller GA. Reduction of hepatitis C virus load by H.E.L.P.-LDL apheresis. *Eur J Clin Invest* 2001; **31**: 154-155

41 **Enjoji M,** Nakamuta M, Kinukawa N, Sugimoto R, Noguchi K, Tsuruta S, Iwao M, Kotoh K, Iwamoto H, Nawata H. Beta-lipoproteins influence the serum level of hepatitis C virus. *Med Sci Monit* 2000; **6**: 841-844

42 **Greco AV,** Mingrone G, Favuzzi A, Capristo E, Gniuli D, Addolorato G, Brunani A, Cavagnin F, Gasbarrini G. Serum leptin levels in post-hepatitis liver cirrhosis. *J Hepatol* 2000; **33**: 38-42

43 **Faggioni R,** Feingold KR, Grunfeld C. Leptin regulation of the immune response and the immunodeficiency of malnutrition. *FASEB J* 2001; **15**: 2565-2571

44 **Lord GM,** Matarese G, Howard JK, Baker RJ, Bloom SR, Lechler RI. Leptin modulates the T-cell immune response and reverses starvation-induced immunosuppression. *Nature* 1998; **394**: 897-901

45 **Faggioni R,** Jones-Carson J, Reed DA, Dinarello CA, Feingold KR, Grunfeld C, Fantuzzi G. Leptin-deficient (ob/ob) mice are protected from T cell-mediated hepatotoxicity: role of tumor necrosis factor alpha and IL-18. *Proc Natl Acad Sci USA* 2000; **97**: 2367-2372

46 **Martin-Romero C,** Santos-Alvarez J, Goberna R, Sanchez-Margalet V. Human leptin enhances activation and proliferation of human circulating T lymphocytes. *Cell Immunol* 2000; **199**: 15-24

47 **Farooqi IS,** Matarese G, Lord GM, Keogh JM, Lawrence E, Agwu C, Sanna V, Jebb SA, Perna F, Fontana S, Lechler RI, DePaoli AM, O'Rahilly S. Beneficial effects of leptin on obesity, T cell hyporesponsiveness, and neuroendocrine/metabolic dysfunction of human congenital leptin deficiency. *J Clin Invest* 2002; **110**: 1093-1103

48 **Motivala SJ,** Dang J, Obradovic T, Meadows GG, Butch AW, Irwin MR. Leptin and cellular and innate immunity in abstinent alcoholics and controls. *Alcohol Clin Exp Res* 2003; **27**: 1819-1824

49 **Siegmund B,** Lehr HA, Fantuzzi G. Leptin: a pivotal mediator of intestinal inflammation in mice. *Gastroenterology* 2002; **122**: 2011-2025

50 **Jacobson Brown PM,** Neuman MG. Immunopathogenesis of hepatitis C viral infection: Th1/Th2 responses and the role of cytokines. *Clin Biochem* 2001; **34**: 167-171

51 **Fan X,** Liu W, Li C. Determination of serum cytokines in individuals with HCV infection. *Zhonghua Shiyan He Linchuang Bingduxue Zazhi* 2000; **14**: 145-147

52 **Tsai SL,** Huang SN. T cell mechanisms in the immunopathogenesis of viral hepatitis B and C. *J Gastroenterol Hepatol* 1997; **12**: S227-S235

53 **Negro F,** Krawczynski K, Quadri R, Rubbia-Brandt L, Mondelli M, Zarski JP, Hadengue A. Detection of genomic and minus-strand of hepatitis C virus RNA in the liver of chronic hepatitis C patients by strand-specific semiquantitative reverse-transcriptase polymerase chain reaction. *Hepatology* 1999; **29**: 536-542

54 **Umemura T,** Yoshizawa K, Ota M, Katsuyama Y, Inada H, Tanaka E, Kiyosawa K. Analysis of T cell repertoire in the liver of patients with chronic hepatitis C. *Clin Exp Immunol* 2000; **121**: 120-126

55 **Gorden P,** Gavrilova O. The clinical uses of leptin. *Curr Opin Pharmacol* 2003; **3**: 655-659

56 **Matarese G,** Sanna V, Fontana S, Zappacosta S. Leptin as a novel therapeutic target for immune intervention. *Curr Drug Targets Inflamm Allergy* 2002; **1**: 13-22

57 **Huang L,** Li C. Leptin: a multifunctional hormone. *Cell Res* 2000; **10**: 81-92

Science Editor Wang XL and Guo SY **Language Editor** Elsevier HK

PO Box 2345, Beijing 100023, China
www.wjgnet.com
wjg@wjgnet.com

ELSEVIER

World J Gastroenterol 2005;11(22):3363-3367
World Journal of Gastroenterology ISSN 1007-9327

Expression and immunoreactivity of an epitope of HCV in a foreign epitope presenting system

Mei Peng, Chang-Bai Dai, Yuan-Ding Chen

Mei Peng, Chang-Bai Dai, Yuan-Ding Chen, Department of Molecular Biology, Institute of Medical Biology, Chinese Academy of Medical Sciences/Peking Union Medical College, Kunming 650118, Yunnan Province, China
Supported by the Natural Science Fund of Yunnan Province, No. 2003C0076M
Correspondence to: Mei Peng, PhD, Department of Molecular Biology, Institute of Medical Biology, Chinese Academy of Medical Sciences/Peking Union Medical College, 379 Jiaoling Road, Kunming 650118, Yunnang Province, China. mpjpm@public.km.yn.cn
Telephone: +86-871-8334401 Fax: +86-871-8334483
Received: 2004-05-27 Accepted: 2004-07-11

Abstract

AIM: To construct and highly express an epitope of hepatitis C virus (HCV) in a foreign epitope presenting vector based on an insect virus, and to study the antigenicity of the epitope.

METHODS: The HCV epitope sequence (amino acid residues 315 to 328: EGHRMAWDMMMNWS) of the E1 region was constructed at different positions of a foreign epitope presenting vector based on an insect virus, flock house virus (FHV) capsid protein encoding gene as a vector, and expressed in *E. coli* cells. Western blotting and ELISA were used to detect the immunoreactivity of these recombinant proteins.

RESULTS: The gene encoding of the concerned B-cell epitope of HCV E1 envelope protein was expressed on FHV capsid carrier protein at positions I1 (aa 106), I2 (aa 153) and I3 (aa 305), respectively, on the surface of FHV capsid protein. The recombinant proteins in this system could be highly expressed in more than 40% of total cell protein of *E. coli* BL21. All the expressed recombinant proteins were in inclusion body form, and showed obvious immunoreactivity by Western blotting. Further purified recombinant proteins were detected by indirect ELISA as coating antigen respectively. All recombinant proteins could still show immunoreactivity.

CONCLUSION: The epitope of HCV E1 envelope protein can be highly expressed in FHV carrier system as a chimeric protein with high immunoreactivity. This system has multiple entry sites conferring many possible conformations closer to the native one for a given sequence.

Key words: Immunoreactivity; Epitope; HCV; Epitope presenting system

Peng M, Dai CB, Chen YD. Expression and immunoreactivity of an epitope of HCV in a foreign epitope presenting system. *World J Gastroenterol* 2005; 11(22): 3363-3367
http://www.wjgnet.com/1007-9327/11/3363.asp

INTRODUCTION

Hepatitis C virus is the major etiological agent for non-A, non-B hepatitis[1-3]. There are 1.7 hundred million infected patients all over the world[4], and chronic infection is established in about 50-90% of patients[5]. HCV-infected patients develop a heterogeneous immune response. The initial worldwide screening of blood for antibodies against HCV was carried out with a polyprotein (c100-3) from the NS3-NS4 region[6], but the specificity and sensitivity of this region are not sufficient[7,8]. Recent studies have identified several epitopes in the envelope protein[9-12].

The characterization of the sequences recognized by antibodies and their reactivity has been performed mainly with the use of synthetic peptides[13,14]. However, recent studies have provided evidence that there are severe limitations in the use of synthetic peptides bound to the solid phase for the detection of antibodies against conformational epitopes[15,16]. A new epitope presenting system, based on the capsid protein of the flock house virus (FHV), has been successfully used in the presentation of several conformational epitopes of human immunodeficiency virus type 1[17]. Therefore, we inserted the FHV capsid protein in three portions of an epitope of HCV envelope protein, and studied the immunogenicity of these chimeric proteins.

MATERIALS AND METHODS

Serum samples

HCV patient serum samples were kindly provided by Kunming Infectious Diseases Hospital. Antisera from HCV-Eb chimeric protein (spanning hole HCV E1 envelope protein without FHV capsid carrier protein) immunized guinea pigs were prepared in our laboratory.

Epitope of HCV envelope E1 and coding gene

The studied epitope was the E1 region of HCV comprised of 14 amino acids, EGHRMAWDMMMNWS, from the residues 315-328. These residues had the highest conservation in E1 region. Two primers coding this epitope were synthesized by Sangon Company: primers Ps (5'-tgagggtc-accgtatggcttgggacatgatgatgaactggtctcc-3') and Pas (3'-

cccagtggcataccgaaccctgtcctactacttgaccagaggagt-5').

Annealing and kinasing of the epitope primers

The annealing reaction mixture containing 4 μL primer Ps (≈100 ng), 4 μL primer Pas (≈100 ng), 5 μL buffer (10×) and 12 μL H_2O was incubated at 65 ℃ for 5 min, then cooled down to 37 ℃ for 45 min in 37 ℃ water bath. The annealed mixture was added with 2 μL ATP (25 mol/L), 2 μL kinase (10 U/μL) and 3 μL buffer (10×), and incubated in a 37 ℃ water bath for 1 h.

Construction of expression plasmids

FHV capsid gene RNA2 was genetically modified, having a restriction endoenzyme site Bsu36I at different positions of the molecule. The FHV-RNA2 was constructed onto the plasmid pET-3, and the product was designated as pET-RNA2.

After digestion with Bsu 36I (purchased from Biolabs), pET-RNA2 as a vector was ligated with kinased HCV epitope primers (double stranded), and transformed in *E.coli* DH5α competent cells. The positive recombinant plasmids were identified by digestion with proper restriction endoenzymes respectively, and finally sequenced by the dideoxy chain determination method with T7 DNA polymerase (T7 sequencing™, Pharmacia Biotech Inc., USA). Then correct plasmids was identified, designated as pET-RNA2-E1, and used for recombinant epitope (chimeric proteins) expression.

Expression of recombinant proteins in E.coli

Competent BL21 (DE3) was transformed with the recombinant plasmid pET-RNA2-E1, and incubated in LB medium. After transformation and incubation, 3 mL fresh culture was transferred into 250 mL fresh TB-P medium (phosphate-rich medium, containing 200 μg/mL ampicillin), and incubated overnight. The cells were then gathered by low-speed centrifugation and resuspended in 50 mL of sonication buffer. After sonication lysis and centrifugation, the recombinant epitope/chimeric protein was obtained in inclusion body form. The expressed proteins were detected in 120 g/L SDS-PAGE gels.

Western blot analysis of recombinant proteins

Total cell lysates were run on SDS-PAGE gels and transferred electrophoretically to nitrocellulose membrane for 2 h at the voltage of 100 V. The membrane was then incubated in blocking solution (50 g/L nonfat milk in Tris-buffered saline, TBS) for 1 h at room temperature at 80 r/min followed by incubation at room temperature for 2 h in the HCV positive sera prediluted to 1:100 with blocking solution. The membrane was washed thrice with TBS/T (1 g/L Tween-20 in TBS) for 10 min, and horseradish peroxidase-labeled goat anti-human IgG antibodies (purchased from Sigma) diluted in TBS/T (1:2 000) were exposed to the membrane at room temperature for 1 h. The membrane was visualized with a substrate solution of DAB (purchased from Sigma) and $NiCl_2$ after washing thrice for 10 min with TBS/T.

Enzyme linked immunoadsorbent assay (ELISA)

ELISA for recombinant protein of HCV E1 epitope and peptide of the E1 epitope was done in 96-well, flat-bottomed vinyl assay plates. Microplates were coated with purified recombinant protein or synthetic HCV E1 peptide in 0.05 mol/L sodium carbonate buffer (pH 9.6) for 2 h at 37 ℃ and overnight at 4 ℃. The recombinant protein was diluted to 0.5 μg/mL for ELISA, and the peptide was diluted to 5 μg/mL. Plates were washed 4 times with PBS containing 0.5 g/L Tween 20 and blocked with blocking buffer (0.5 g/L Tween 20, 2.5 g/L bovine serum albumin and 0.5 g/L NaN_3 in PBS) for 2 h at 37 ℃. Antisera against HCV-Eb (1:1 000) were applied for 30 min at 37 ℃. A peroxidase-conjugated goat anti-guinea pig IgG used as secondary antibody was incubated for 30 min at 37 ℃. Wells were washed four times with PBS/T between each step and visualized with o-phenyl-diamine-2HCL (50 mg/L in PBS, pH 5.0). The reaction was stopped with 50 μL of 2 mol/L H_2SO_4. Absorption was measured at A_{495}.

RESULTS

Construction and identification of recombinant plasmids

The recombinant plasmids were identified by digestion with proper restriction endoenzymes, respectively. A 410 bp (including 45 bp E1 epitope gene) fragment was obtained when pET-RNA-I1-E1 was digested with *Spe*I/*Mlu*I, a 365 bp fragment was obtained when pET-RNA-I1-wt digested with the same endoenzymes; A 472 bp (including 45 bp E1 epitope gene) fragment was obtained when pET-RNA-I2-E1 digested with *Spe*I/*Nco*I, a 427 bp fragment was obtained when pET-RNA-I2-wt digested with *Spe*I/*Nco*I; A 302 bp (including 45 bp E1 epitope gene) fragment was obtained when pET-RNA-I3-E1 digested with *Nsi*I/*Nco*I, a 257 bp fragment was obtained when pET-RNA-I3-wt digested with the same endoenzymes; agarose gel electrophoresis showed that the HCV epitope gene was cloned into three positions of the pET-RNA2 vector with correct size, (Figures 1 and 3). The nucleotide sequence of inserted fragments were identified by sequence analysis (Figure 2). The recombinant protein expressed by pET vector had a FHV RNA2 fusion protein.

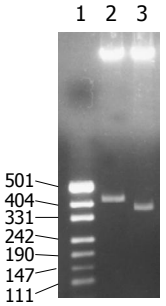

Figure 1 Restriction analysis of recombinant plasmids pET-RNA-I1. Lane 1: DNA molecular weight markers pUC19 DNA/Msp I (Hpa II); lane 2: pET-RNA-I1-E1 digested with *SpeI*/*MluI* (410 bp); lane 3: pET-RNA-I1- wt digested with *SpeI*/*MluI* (365 bp).

Expression of recombinant proteins in E.coli

Three recombinant plasmids pETRNA2-I_1E_1, pETRNA2-

I_2E_1, pETRNA2-I_3E_1, were carrying the HCV E1 epitope gene, expressed in *E. coli* BL21 (DE3). The yield of recombinant proteins was as high as 40% of the total cell proteins (Figure 4A). The recombinant proteins RNA-I_1E_1, RNA-I_2E_1, RNA-I_3E_1, were HCV E1 epitopes inserted in positions I1 (aa106), I2 (aa153), I3 (aa305) of the FHV capsid protein respectively. Better expression was found in pETRNA2-I_1E_1 and pETRNA2-I_2E_1.

Western blotting analysis

Three recombinant proteins were separated by SDS-PAGE and transferred electrophoretically to nitrocellulose for immunoblotting as shown in Figure 4B. The three proteins showed immunoreactivity. RNA2-I_1E_1, RNA2-I_3E_1 had strong reactivity with HCV positive sera, and the reactivity of pETRNA2-I_2E_1 was relatively weaker.

ELISA of recombinant proteins of HCV epitope

Three chimeric antigen proteins were further purified. After purification by Q-FF/HP negative ion-exchange and superdex 75 gel chromatography, the purity of these three chimeric proteins was higher than 90%. These chimeric antigens were coated respectively to microplates in 50 ng each well. Other wells were coated with synthetic HCV E1 peptide 5 μg/mL (500 ng/100 μL/well) in sodium carbonate buffer (pH 9.6) overnight. Antisera against HCV Eb and negative sera were used in ELISA. The results showed that the reactivities of two recombinant proteins (RNA2-I_1E_1, RNA2-I_3E_1) were greater than those of synthetic peptide (Figure 5).

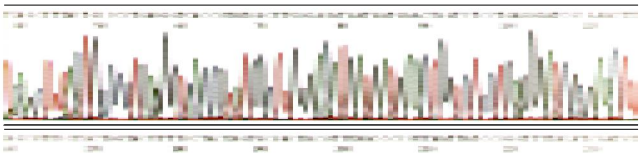

Figure 2 Sequence analysis of pET-RNA-I1-E1.

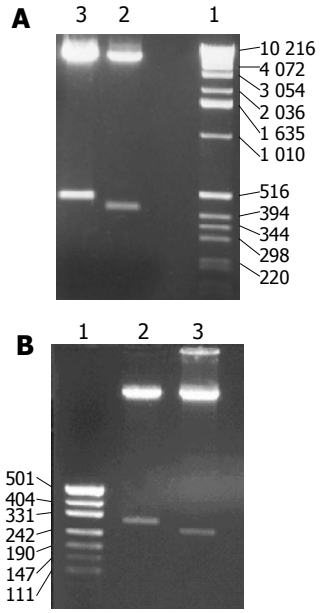

Figure 3 Restriction analysis of recombinant plasmid pET-RNA-I2 (**A**) and pET-RNA-I3 (**B**). **A**: Restriction analysis of recombinant plasmid pET-RNA-I2. Lane 1: DNA molecular weight markers (1 kb); lane 2: pET-RNA-I2- wt digested with *SpeI*/ *Nco*I (427bp); lane 3: pET-RNA-I2-E1 digested with *SpeI*/*Nco*I (472bp); **B**: Restriction analysis of recombinant plasmid pET-RNA-I3. Lane 1: DNA molecular weight markers pUC19 DNA/*Msp*I (*Hpa*II); lane 2: pET-RNA-I3-E1 digested with *NsiI*/*Nco*I (302 bp); lane 3: pET-RNA-I3- wt digested with *NsiI*/*Nco*I (257 bp).

DISCUSSION

It is well known that the immunogenicity of a peptide depends not only on its sequence, but also on the mode of presentation to the immune system. Attempts to increase the immunogenicity of these antigens used as vaccines have led to the development of a number of antigen presentation systems. Many of these are designed to present the antigen as a polyvalent particulate structure. Various types of particles have been used to present foreign epitopes: core antigen (HbcAg) and surface antigen (HBsAg) from HBV, capsid proteins from polio virus[18,19]. Using a human rhinovirus capsid sequence as a guest peptide and particles formed by HbcAg as a carrier, show that the internal location of the foreign sequence improves immunogenicity of that epitope by 10 to 50-fold when compared to the amino terminus location[20]. Furthermore, both constructs

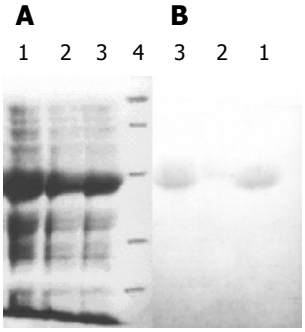

Figure 4 SDS-PAGE of inclusion body of RNA-E1 (**A**) and Western blot of chimeric antigen protein RNA-E1(**B**). **A**: SDS-PAGE of inclusion body of RNA-E1. Lane 1: Inclusion bodies of RNA-I1-E1; lane 2: Inclusion bodies of RNA-I2-E1; lane 3: Inclusion bodies of RNA-I3-E1; lane 4: M: Protein molecular weight standard (middle range); **B**: Western blot of chimeric antigen protein RNA-E1 Lane 1: RNA-I1-E1; lane 2: RNA-I2-E1; lane 3: RNA-I3-E1.

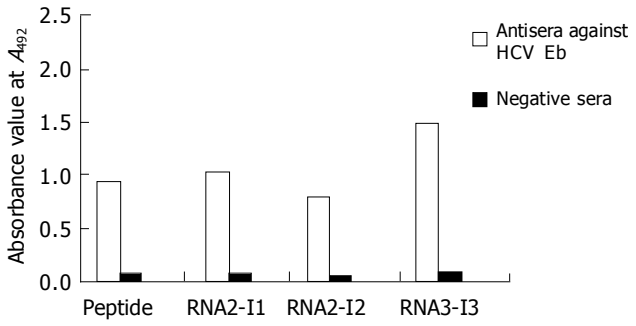

Figure 5 ELISA of E1 peptide and RNA-E1 chimeric antigen displaying epitope at three different positions.

present the epitope more efficiently to the mAbs, than the free peptide. Since the properties of a given epitope might be influenced by its conformation, it should have a carrier system with multiple entry sites conferring many possible conformations. We developed a new protein carrier (FHV capsid protein) based on the structure known at atomic level for the location of foreign eptitopes.

Studies of the HCV antigenic structure have allowed construction of diagnostic systems with improved assay specificity and sensitivity[21,22]. HCV infection is generally detected using recombinant antigens from the conserved capsid, NS3 and NS4 regions[23], but the specificity and sensitivity of some regions are not sufficient. Recent studies have identified several epitopes in the envelope protein. Research in epitopes of envelope protein will help develop diagnostic reagents and recombinant vaccines for HCV. Since the nucleotide mutation rate in envelope E1 (35%) is higher than in core (8%) of HCV, we studied the expression and immunogenicity of a highly conserved B-cell epitope of E1 among different HCV genotypes. Reactivity of this epitope to synthetic peptide was observed in 10 of 11 sera from HCV-infected humans and 11 of 15 sera from chimpanzee[9].

The conserved B-cell epitope gene of HCV E1 was synthesized and inserted into the three portions of the RNA2 encoding the FHV capsid protein as the vector.

The three chimeric genes were cloned to prokaryotic expression vector pET-3 and expressed in *E. coli* BL21 (DE3). To improve the yield, we used the TB-P medium (the phosphate-rich medium).

All the hybrid proteins reacted with antiserum of HCV positive patients in Western blot test, but RNA2-I_1E_1 and RNA2-I_3E_1 had a stronger reactivity with HCV positive sera than pETRNA2-I_2E_1, suggesting that the same epitope inserted into different positions of FHV capsid protein surface may have different conformations. In this way, the inserted epitope is placed on the exterior surface of the protein. Therefore, the epitope is predominantly recognized by HCV-positive sera. These antigens are extremely useful in studying the influence of the stereochemistry of the presenting molecule in the recognition of a short heterologous amino acid sequence by human immune system.

The reactivity of RNA2-I_1E_1, RNA2-I_3E_1 is much higher than that of synthetic peptide, and the synthetic peptides are presented in 10-fold molar than recombinant proteins, suggesting that antigenicity of HCV E1 epitope can be greatly enhanced by inserting the epitope in positions of FHV capsid protein surface. The same results are observed using a human rhinovirus capsid sequence as a guest peptide and particles formed by HBcAg as a carrier. Both constructs (the epitopes inserted in two different positions) present the epitopes more efficiently to the mAbs than the free peptide[20], indicating that the region is highly immunogenic. This is probably due to the fact that the peptide in solution, unlike in the solid phase or the epitope inserted in the carrier protein, can exist in several metastable conformations[24], some of which are more likely to acquire the native structure.

The results obtained in this study suggest that the FHV capsomer system has the potential and flexibility for presentation of conformational epitopes.

REFERENCES

1 **Itoh K,** Suzuki K, Ishiwata S, Tezuka T, Mizugaki M, Suzuki T. Application of a recombinant Fab fragment from a phage display library for sensitive detection of a target antigen by an inhibition ELISA system. *J Immunol Methods* 1999; **223**: 107-114

2 **Choo QL,** Kuo G, Weiner AJ, Overby LR, Bradley DW, Houghton M. Isolation of a cDNA clone derived from a blood-borne non-A, non-B viral hepatitis genome. *Science* 1989; **244**: 359-362

3 **Choo QL,** Weiner AJ, Overby LR, Kuo G, Houghton M, Bradley DW. Hepatitis C virus: the major causative agent of viral non-A, non-B hepatitis. *Br Med Bull* 1990; **46**: 423-441

4 **Ramsay ME,** Balogun MA, Teo CG, Mortimer PP. Accuracy of perceptions of hepatitis B and C status. Injecting drug users need vaccination against hepatitis *B. BMJ* 2000; **320**: 512; author reply 513

5 **Lopez-Labrador FX,** Ampurdanes S, Gimenez-Barcons M, Guilera M, Costa J, Jimenez de Anta MT, Sanchez-Tapias JM, Rodes J, Saiz JC. Relationship of the genomic complexity of hepatitis C virus with liver disease severity and response to interferon in patients with chronic HCV genotype 1b infection [correction of interferon]. *Hepatology* 1999; **29**: 897-903

6 **Kuo G,** Choo QL, Alter HJ, Gitnick GL, Redeker AG, Purcell RH, Miyamura T, Dienstag JL, Alter MJ, Stevens CE. An assay for circulating antibodies to a major etiologic virus of human non-A, non-B hepatitis. *Science* 1989; **244**: 362-364

7 **Miyamura T,** Saito I, Katayama T, Kikuchi S, Tateda A, Houghton M, Choo QL, Kuo G. Detection of antibody against antigen expressed by molecularly cloned hepatitis C virus cDNA: application to diagnosis and blood screening for posttransfusion hepatitis. *Proc Natl Acad Sci USA* 1990; **87**: 983-987

8 **Saito M,** Hasegawa A, Kashiwakuma T, Kohara M, Sugi M, Miki K, Yamamoto T, Mori H, Ohta Y, Tanaka E. Performance of an enzyme-linked immunosorbent assay system for antibodies to hepatitis C virus with two new antigens (c11/c7). *Clin Chem* 1992; **38**: 2434-2439

9 **Wang YF,** Brotman B, Andrus L, Prince AM. Immune response to epitopes of hepatitis C virus (HCV) structural proteins in HCV-infected humans and chimpanzees. *J Infect Dis* 1996; **173**: 808-821

10 **Ishida C,** Matsumoto K, Fukada K, Matsushita K, Shiraki H, Maeda Y. Detection of antibodies to hepatitis C virus (HCV) structural proteins in anti-HCV-positive sera by an enzyme-linked immunosorbent assay using synthetic peptides as antigens. *J Clin Microbiol* 1993; **31**: 936-940

11 **Ray R,** Khanna A, Lagging LM, Meyer K, Choo QL, Ralston R, Houghton M, Becherer PR. Peptide immunogen mimicry of putative E1 glycoprotein-specific epitopes in hepatitis C virus. *J Virol* 1994; **68**: 4420-4426

12 **Okamoto H,** Kurai K, Okada S, Yamamoto K, Lizuka H, Tanaka T, Fukuda S, Tsuda F, Mishiro S. Full-length sequence of a hepatitis C virus genome having poor homology to reported isolates: comparative study of four distinct genotypes. *Virology* 1992; **188**: 331-341

13 **Ching WM,** Wychowski C, Beach MJ, Wang H, Davies CL, Carl M, Bradley DW, Alter HJ, Feinstone SM, Shih JW. Interaction of immune sera with synthetic peptides corresponding to the structural protein region of hepatitis C virus. *Proc Natl Acad Sci USA* 1992; **89**: 3190-3194

14 **Ferroni P,** Mascolo G, Zaninetti M, Colzani D, Pregliasco F, Pirisi M, Barbone F, Gasparini V. Identification of four epitopes in hepatitis C virus core protein. *J Clin Microbiol* 1993; **31**: 1586-1591

15 **Moore JP,** Cao Y, Conley AJ, Wyatt R, Robinson J, Gorny MK, Zolla-Pazner S, Ho DD, Koup RA. Studies with monoclonal antibodies to the V3 region of HIV-1 gp120 reveal limitations to the utility of solid-phase peptide binding assays. *J Acquir Immune Defic Syndr* 1994; **7**: 332-339

16 **Schutten M,** Langedijk JP, Andeweg AC, Huisman RC, Meloen RH, Osterhaus AD. Characterization of a V3 domain-

specific neutralizing human monoclonal antibody that preferentially recognizes non-syncytium-inducing human immunodeficiency virus type 1 strains. *J Gen Virol* 1995; **76**(Pt 7): 1665-1673

17 **Scodeller EA,** Tisminetzky SG, Porro F, Schiappacassi M, De Rossi A, Chiecco-Bianchi L, Baralle FE. A new epitope presenting system displays a HIV-1 V3 loop sequence and induces neutralizing antibodies. *Vaccine* 1995; **13**: 1233-1239

18 **Clarke BE,** Newton SE, Carroll AR, Francis MJ, Appleyard G, Syred AD, Highfield PE, Rowlands DJ, Brown F. Improved immunogenicity of a peptide epitope after fusion to hepatitis B core protein. *Nature* 1987; **330**: 381-384

19 **Burke KL,** Dunn G, Ferguson M, Minor PD, Almond JW. Antigen chimaeras of poliovirus as potential new vaccines. *Nature* 1988; **332**: 81-82

20 **Brown AL,** Francis MJ, Hastings GZ, Parry NR, Barnett PV, Rowlands DJ, Clarke BE. Foreign epitopes in immunodominant regions of hepatitis B core particles are highly immunogenic and conformationally restricted. *Vaccine* 1991; **9**: 595-601

21 **Krajden M.** Molecular detection of hepatitis C virus: impact of detection methodology on clinical and laboratory correlations. *Crit Rev Clin Lab Sci* 1995; **32**: 41-66

22 **Roggendorf M,** Lu M, Meisel H, Riffelmann M, Schreier E, Viazov S. Rational use of diagnostic tools in hepatitis C. *J Hepatol* 1996; **24**: 26-34

23 **Chien DY,** Choo QL, Tabrizi A, Kuo C, McFarland J, Berger K, Lee C, Shuster JR, Nguyen T, Moyer DL. Diagnosis of hepatitis C virus (HCV) infection using an immunodominant chimeric polyprotein to capture circulating antibodies: re-evaluation of the role of HCV in liver disease. *Proc Natl Acad Sci USA* 1992; **89**: 10011-10015

24 **Moore JP.** The reactivities of HIV-1+ human sera with solid-phase V3 loop peptides can be poor predictors of their reactivities with V3 loops on native gp120 molecules. *AIDS Res Hum Retroviruses* 1993; **9**: 209-219

Science Editor Wang XL **Language Editor** Elsevier HK

PO Box 2345, Beijing 100023, China
www.wjgnet.com
wjg@wjgnet.com

ELSEVIER

World J Gastroenterol 2005;11(22):3368-3374
World Journal of Gastroenterology ISSN 1007-9327

• *BASIC RESEARCH* •

Green tea polyphenol epigallocatechin-3-gallate blocks PDGF-induced proliferation and migration of rat pancreatic stellate cells

Atsushi Masamune, Kazuhiro Kikuta, Masahiro Satoh, Noriaki Suzuki, Tooru Shimosegawa

Atsushi Masamune, Kazuhiro Kikuta, Masahiro Satoh, Noriaki Suzuki, Tooru Shimosegawa, Division of Gastroenterology, Tohoku University Graduate School of Medicine, Sendai, Japan
Supported by the Grant-in-Aid for Encouragement of Young Scientists from Japan Society for the Promotion of Science, No. 16590572, Pancreas Research Foundation of Japan, No. 01-01, and the Kanae Foundation for Life and Socio-Medical Science
Correspondence to: Dr. Atsushi Masamune, Division of Gastroenterology, Tohoku University Graduate School of Medicine, 1-1 Seiryo-cyo, Aoba-ku, Sendai 980-8574, Japan. amasamune@int3.med.tohoku.ac.jp
Telephone: +81-22-717-7171 Fax: +81-22-717-7177
Received: 2004-10-14 Accepted: 2004-11-19

Abstract

AIM: To clarify the effects of epigallocatechin-3-gallate (EGCG) on the platelet-derived growth factor (PDGF)-BB-induced proliferation and migration of pancreatic stellate cells (PSCs).

METHODS: PSCs were isolated from rat pancreas tissue and used in their culture-activated, myofibroblast-like phenotype. Cell proliferation was assessed by measuring the incorporation of 5-bromo-2′-deoxyuridine. Cell migration was assessed using modified Boyden chambers. Cyclin D1, $p21^{Waf1}$, and $p27^{Kip1}$ expression and phosphorylation of PDGF β-receptor, extracellular signal-regulated kinase, and Akt were examined by Western blotting. Activation of phosphatidylinositol 3-kinase was examined by kinase assay using phosphatidylinositol as a substrate. Cell cycle was assessed by flow cytometry after staining with propidium iodide.

RESULTS: EGCG at non-cytotoxic concentrations inhibited PDGF-induced proliferation and migration. This effect was associated with the inhibition of cell cycle progression beyond the G_1 phase, decreased cyclin D1 and increased $p27^{Kip1}$ expression. EGCG inhibited tyrosine phosphorylation of PDGF β-receptor and downstream activation of extracellular signal-regulated kinase and phosphatidylinositol 3-kinase/Akt pathways.

CONCLUSION: EGCG inhibited PDGF-BB-induced proliferation and migration of PSCs through the inhibition of PDGF-mediated signaling pathways.

Key words: Pancreatitis; Pancreatic fibrosis; Pancreatic stellate cells; Epigallocatechin-3-gallate; Green tea; Platelet-derived growth factor; Proliferation; Migration

Masamune A, Kikuta K, Satoh M, Suzuki N, Shimosegawa T. Green tea polyphenol epigallocatechin-3-gallate blocks PDGF-induced proliferation and migration of rat pancreatic stellate cells. *World J Gastroenterol* 2005; 11(22): 3368-3374
http://www.wjgnet.com/1007-9327/11/3368.asp

INTRODUCTION

In 1998, star-shaped cells in the pancreas, namely pancreatic stellate cells (PSCs), were identified and characterized[1,2]. In normal pancreas, stellate cells are quiescent and can be identified by the presence of vitamin A-containing lipid droplets in the cytoplasm. In response to pancreatic injury or inflammation, they are transformed ("activated") from their quiescent phenotype into myofibroblast-like cells, which actively proliferate, express the cytoskeletal protein α-smooth muscle actin, and produce extracellular matrix components. Many of the morphological and metabolic changes associated with the activation of PSCs in animal models of fibrosis also occur when these cells are grown in serum-containing medium in culture on plastic. There is accumulating evidence that activated PSCs play a pivotal role in the development of pancreatic fibrosis[1-4]. In addition, PSCs may participate in the pathogenesis of acute pancreatitis[3,5]. The activation of signaling pathways such as p38 mitogen-activated protein (MAP) kinase[6], Rho-Rho kinase[7], and c-Jun N-terminal kinase[8] is likely to play a role in PSC activation.

Stellate cell proliferation and expansion of their pool are the fundamental features of pancreatic fibrosis[3]. Platelet-derived growth factor (PDGF)-BB has been shown to be one of the most potent mitogen of PSCs, and is likely to be an important mediator of the increased proliferation of PSCs both *in vivo* and *in vitro*[9,10]. Accumulation of PSCs may also result from PSC migration, and recent studies have shown that PDGF-BB induced migration of PSCs[11,12]. Binding of PDGF to the receptors leads to dimerization of receptor subunits, phosphorylates the receptor on tyrosines (known as "autophosphorylation"), changes its cytoplasmic conformation, activates endogenous tyrosine kinases, and initiates intracellular signaling[13,14]. For downstream of PDGF receptor, there are at least two major signaling pathways: phosphatidylinositol 3-kinase (PI3-kinase)/Akt and c-Raf/MAP kinase kinase/extracellular signal-regulated kinase (ERK) pathways[13,14]. We and others have shown that ERK pathway contributes mainly to cell proliferation whereas PI3-kinase/Akt pathway contributes to cell migration[11,15]. Regulation of PSC proliferation and migration would serve as a therapeutic target for pancreatic fibrosis and inflammation.

Natural antioxidants, such as polyphenols from green

tea extracts, have attracted considerable attention for the prevention of oxidative stress-related diseases including cancer, cardiovascular diseases, and degenerative diseases[16,17]. Of the polyphenols purified from green tea, (-)-epigallocatechin-3-gallate (EGCG) is a major constituent and the most potent antioxidant[18]. The antioxidant potential of EGCG is far greater than that of vitamin E and/or C[19]. Previous studies have demonstrated that EGCG possesses antioxidant[20], anti-inflammatory[21], anti-proliferative[22], and anti-cancer activities[23-26]. EGCG inhibited lipopolysaccharide-induced nitric oxide production and inducible nitric oxide synthase gene expression in isolated peritoneal macrophages by decreasing the activation of nuclear factor κB[21]. EGCG inhibited PDGF-induced proliferation of vascular smooth muscle cells[22]. EGCG induced apoptosis more readily in cancer cells than their natural counterparts[23]. EGCG inhibited tumor growth, metastasis, and angiogenesis *in vivo*[24-26]. But no previous studies have addressed the effects of EGCG on cell functions of PSCs. We here report that EGCG inhibited PDGF-induced proliferation and migration of PSCs through the inhibition of PDGF-mediated signaling.

MATERIALS AND METHODS

Materials

EGCG was dissolved in H_2O and stocked at 10 mmol/L. 3-(4, 5-dimethylthiazole-2-yl)-2, 5-diphenyltetrazolium bromide (MTT) was obtained from Dojindo (Kumamoto, Japan). Rat recombinant PDGF-BB was purchased from R&D Systems (Minneapolis, MN). Rabbit antibodies against ERK (phosphorylated and total) and Akt (phosphorylated and total) were purchased from Cell Technologies, Inc. (Beverly, MA). Rabbit antibodies against PDGF β-receptor, cyclin D1, $p21^{Waf1}$, and $p27^{Kip1}$ were from Santa Cruz Biotechnology (Santa Cruz, CA). Rabbit antibody against glyceraldehyde-3-phosphate dehydrogenase (GAPDH) was obtained from Trevigen (Gaithersburg, MD). Rabbit antibody against phosphorylated PDGF β-receptor and mouse anti-phosphotyrosine antibody were obtained from Upstate Biotechnology Inc. (Lake Placid, NY). All other reagents were purchased from Sigma-Aldrich (St. Louis, MO) unless specifically described.

Cell culture

All animal procedures were performed in accordance with the National Institutes of Health Animal Care and Use Guidelines. Rat PSCs were prepared from the pancreas tissues of male Wistar rats (Japan SLC Inc., Hamamatsu, Japan) weighting 200-250 g using the Nycodenz solution (Nycomed Pharma, Oslo, Norway) after perfusion with 0.3 g/L collagenase P as previously described[11]. The cells were resuspended in Ham's F-12 medium containing 100 mL/L heat-inactivated fetal bovine serum (MP Biomedicals, Irvine, CA), penicillin sodium, and streptomycin sulfate. Cell purity was always more than 90% as assessed by a typical star-like configuration and by detecting vitamin A autofluorescence. All experiments were performed using cells between passages two and five. We incubated PSCs in serum-free medium for 24 h before the addition of experimental reagents. EGCG was added to the culture medium 1 h before the addition of PDGF-BB.

Cell viability assay

Cell viability was assessed by the MTT assay as previously described[27]. After the treatment with EGCG at the indicated concentrations for 72 h, MTT solution was added to the cells at a final concentration of 500 mg/L, and the incubation continued at 37 ℃ for 4 h. After the incubation period, the medium was aspirated and the formazan product was solubilized with dimethylsulfoxide. Cell viability was determined by $A_{570\text{-}690}$.

Cell proliferation assay

Serum-starved PSCs (approximately 80% density) were treated with PDGF-BB (at 25 μg/L) in the presence of EGCG at the indicated concentrations. Cell proliferation was assessed using a commercial kit (Cell proliferation ELISA, BrdU; Roche Diagnostics, Mannheim, Germany) according to the manufacturer's instruction. This is a colorimetric immunoassay based on the measurement of 5-bromo-2'-deoxyuridine (BrdU) incorporation during DNA synthesis. After 24-h incubation with experimental reagents, cells were labeled with BrdU for 3 h at 37 ℃. Cells were fixed, and incubated with peroxidase-conjugated anti-BrdU antibody. Then the peroxidase substrate 3,3',5,5'-tetramethylbenzidine was added, and BrdU incorporation was quantitated by $A_{370\text{-}492}$.

Cell migration assay

Cell migration was assessed as previously described[11]. Serum-starved PSCs were trypsinized, and resuspended at the concentration of 3×10^8 cells/L in serum-free medium containing EGCG at the indicated concentrations. For the assay, we used modified Boyden chambers with 8-μm-pore filters (Iwaki glass Co. Ltd., Funabashi, Japan) coated with rat-tail type I collagen. PDGF-BB (at 25 μg/L) was added to the lower chamber, and 250 μL of cell suspension was added to the upper chamber. The chambers were then incubated at 37 ℃ for 24 h. At the end of the incubation, the cell suspension in the upper chamber was aspirated, and the upper part of the filter was cleaned with cotton plugs. The cells migrated to the underside of the filter were stained with Difquick (Sysmex, Kobe, Japan), viewed, and counted at 200× magnification.

Cell cycle analysis

The cell cycle of PSCs was analyzed by flow cytometry as previously described[28]. Briefly, serum-deprived PSCs (approximately 60-70% density) were treated with PDGF-BB in the absence or presence of EGCG (at 25 μmol/L). After 24 h, cells were harvested and washed twice with phosphate-buffered saline. Cells were suspended in phosphate-buffered saline solution containing 40 mg/L propidium iodide, 0.2 mL/L Triton X-100, and 50 mg/L ribonuclease A. Samples were incubated in the dark at room temperature for 30 min and stored at 4 ℃ until the analysis. Cell fluorescence was measured by FACSCaliber flow cytometer (Becton Dickinson Co. Ltd, Tokyo, Japan), and analyzed using ModFit LT software (Verity Software House, Topsham, ME) to determine the distribution of cells in the various phases of the cell cycle.

Western blotting

The level of activated, phosphorylated ERK was determined by Western blotting as previously described[29]. Cells were lysed in sodium dodecyl sulfate buffer. Cellular proteins (approximately 100 μg) were fractionated on a 100 g/L sodium dodecyl sulfate-polyacrylamide gel. They were transferred to a nitrocellulose membrane (Bio-Rad, Hercules, CA), and the membrane was incubated overnight at 4 ℃ with rabbit anti-phosphospecific ERK antibody. After incubation with peroxidase-conjugated goat anti-rabbit IgG antibody for 1 h, proteins were visualized using an ECL kit (Amersham Biosciences UK Ltd). Levels of total ERK, Akt (phosphorylated at Ser^{473} and total), PDGF β-receptor (phosphorylated at Tyr^{716} and total), cyclin D1, $p21^{Waf1}$, $p27^{Kip1}$, and GAPDH were determined in a similar manner.

PI3-kinase assay

Serum-starved PSCs were treated with EGCG at the indicated concentrations in the absence or presence of PDGF-BB. After 5-min incubation, the monolayer was lysed in modified radioimmunoprecipitation assay buffer (50 mmol/L Tris-HCl at pH 7.4, 10 mL/L Nonidet P-40, 150 mmol/L NaCl, 1 mmol/L EDTA, 1 mmol/L activated sodium orthovanadate, 1 μmol/L phenylmethylsulfonyl fluoride, and 1 mg/L of each aprotinin, leupeptin, and pepstatin). The samples were centrifuged at 12 000 *g* for 5 min to remove insoluble cell debris. The protein concentration in the supernatant was determined using the BCA protein assay (Pierce, Rockford, IL). Cell lysates (approximately 250 μg) were incubated with the anti-phosphotyrosine antibody overnight at 4 ℃. The immune complex was absorbed to protein A-agarose beads (Upstate Biotechnology Inc.) for 2 h at 4 ℃. PI3-kinase activity was determined using PI as a substrate as previously described [30]. The product, PI3-phosphate, was resolved by thin layer chromatography in chloroform:methanol:water: 300 g/L ammonium hydroxide (60:47:11.3:2, v/v) as a solvent. After drying, the plates were autoradiographed. Unlabeled PI3-phosphate was run in parallel to determine its position.

Statistical analysis

The results were expressed as mean±SD. Luminograms and autoradiograms are representative of at least three experiments. Differences between the groups were evaluated by ANOVA, followed by Fisher's test for post hoc analysis. A *P*-value less than 0.05 was considered statistically significant.

RESULTS

EGCG was cytotoxic at higher concentrations

We first examined the effect of EGCG on the cell viability of PSCs. PSCs were incubated with increasing concentrations of EGCG in serum-free medium for 72 h, and the cell viability was assessed by MTT assay (Figure 1). EGCG up to 25 μmol/L did not alter the cell viability, but at higher concentrations, EGCG was cytotoxic to PSCs (Figure 2). The results were also confirmed by trypan blue dye exclusion test (data not shown). Based on these results, we used EGCG up to 25 μmol/L in the subsequent experiments.

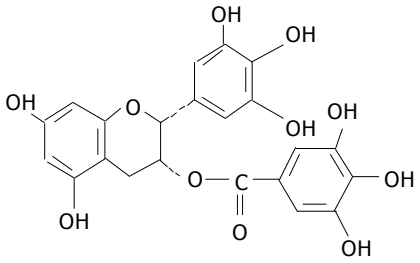

Figure 1 Chemical structure of EGCG.

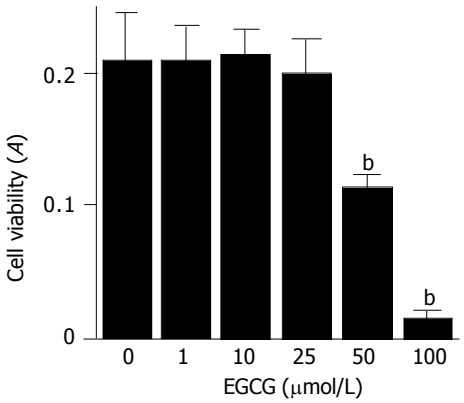

Figure 2 EGCG was cytotoxic at higher concentrations. PSCs were treated with EGCG at the indicated concentrations (μmol/L) in serum-free medium for 72 h. Cell viability was determined by the MTT assay, and the absorbance at 570-690 nm ("*A*") of the sample is shown. Data are shown as mean±SD (n = 6). $^{b}P<0.01$ *vs* EGCG at 0 μmol/L. *A*: optical density.

EGCG inhibited PDGF-induced proliferation and migration of PSCs

In agreement with the previous studies showing that PDGF-BB is a potent mitogen of PSCs *in vitro*[9,10], PDGF-BB significantly increased proliferation of PSCs (Figure 3A). PDGF-induced proliferation was inhibited by EGCG in a dose-dependent manner. The inhibitory effect was significant at as low as 1 μmol/L.

Accumulation of PSCs in fibrotic pancreas may also result from PSC migration, and PDGF-BB has been shown to be a potent inducer of PSC migration[11,12]. We examined whether EGCG affected PDGF-induced migration of PSCs. EGCG inhibited PDGF-BB-induced PSC migration in a dose-dependent manner (Figure 3B).

EGCG inhibited cell cycle progression beyond G_1 phase

We analyzed the cell cycle in PSCs in the presence or absence of EGCG. Exposure to PDGF was associated with a marked decrease in the percentage of cells in the G_0/G_1 phase together with an increase in the number of cells in the S phase (Figure 4A). The addition of the EGCG before PDGF reduced the number of cells in the S phase, and the percentage of cells in the G_0/G_1 phase was similar to the percentage observed in untreated cells. Thus, the addition of EGCG inhibited PDGF-induced progression of the cell cycle beyond the G_1 phase.

We examined the effects of PDGF and EGCG treatment on cell cycle-related molecules. The level of cyclin D1 expression in serum-starved cells was low, but PDGF increased the expression (Figure 4B). EGCG reduced the PDGF-induced cyclin D1

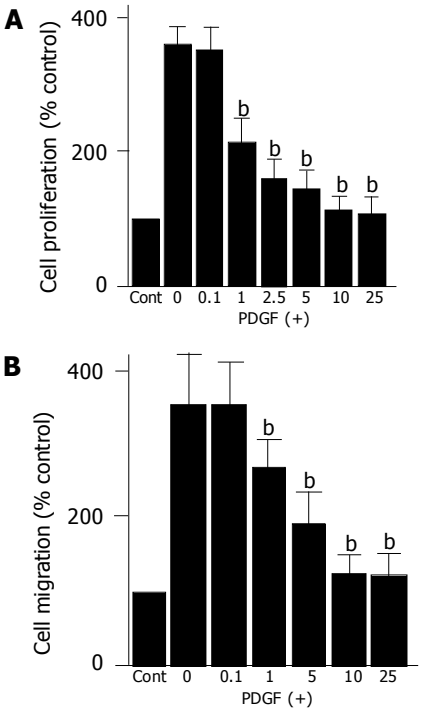

Figure 3 EGCG inhibited PDGF-induced proliferation and migration. **A:** Serum-starved PSCs were left untreated ("Cont") or treated with PDGF-BB (at 25 μg/L) in the presence or absence of EGCG at the indicated concentrations (μmol/L). After 24-h incubation, DNA synthesis was assessed by BrdU incorporation enzyme-linked immunosorbent assay. Data are shown as mean±SD (% of the control, n = 6). ^bP<0.01 *vs* PDGF only; **B:** cell migration was assessed using modified Boyden chambers with 8-μm pore filters. Serum-starved PSCs were left untreated ("Cont") or were treated with PDGF-BB (at 25 μg/L) in the lower chamber in the absence or presence of EGCG at the indicated concentrations (μmol/L). After 24-h incubation with PDGF, the cells migrated to the underside of the filter were stained, and counted. Data are shown as mean±SD (% of the control, n = 6). ^bP<0.01 *vs* PDGF only.

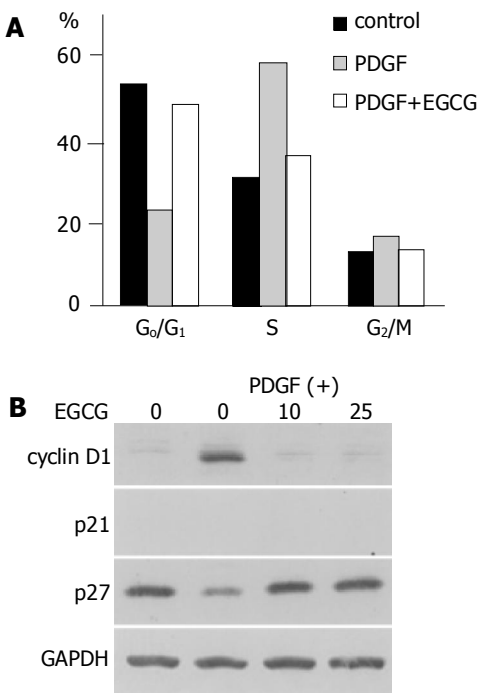

Figure 4 EGCG inhibited cell cycle progression beyond G_1 phase. **A:** PSCs were treated with PDGF-BB (at 25 μg/L) in the absence or presence of EGCG at 25 μmol/L. After 24-h incubation, cells were harvested, and cell cycle analysis was performed by flow cytometry after staining with propidium iodide. Data show the percentage of cells in each phase of the cell cycle in a representative experiment; **B:** PSCs were treated with PDGF-BB (at 25 μg/L) in the absence or presence of EGCG at the indicated concentrations (μmol/L). After 24-h incubation, cells were harvested, and total cell lysates were prepared. The levels of cyclin D1, $p21^{Waf1}$, $p27^{Kip1}$, and GAPDH were determined by Western blotting.

expression. In contrast, the level of $p27^{Kip1}$ expression was decreased by PDGF treatment, and EGCG increased the expression. $p21^{Waf1}$ could not be detected in our experimental system.

EGCG inhibited PDGF-induced phosphorylation of PDGF β-receptor, ERK, and Akt

We then attempted to clarify the molecular mechanisms responsible for EGCG's inhibitory effects on PSCs. PDGF-BB induced tyrosine phosphorylation of the PDGF β-receptor in a time-dependent manner (Figure 5A). EGCG inhibited PDGF-induced phosphorylation of PDGF β-receptor without affecting the protein expression of PDGF β-receptor.

Previous studies have shown that activation of c-Raf/MAP kinase kinase/ERK and PI3-kinase/Akt pathways plays key roles for PDGF-induced proliferation and migration, respectively[11,15]. EGCG inhibited PDGF-BB-induced phosphorylation of ERK and Akt in a dose-dependent manner (Figure 5A). In addition, EGCG inhibited PDGF-induced activation of PI3-kinase (Figure 5B). Thus, EGCG inhibited PDGF-induced tyrosine phosphorylation of PDGF β-receptor and downstream activation of ERK and PI3-kinase/Akt pathways.

EGCG did not alter the expression of total PDGF β-receptor

It has been shown in hepatic stellate cells that EGCG inhibited cell proliferation by blocking the tyrosine phosphorylation and by reducing the gene expression of PDGF β-receptor[31]. We examined whether EGCG altered the expression of total PDGF β-receptor. EGCG did not alter the expression of total PDGF β-receptor regardless of absence or presence of PDGF (Figure 6).

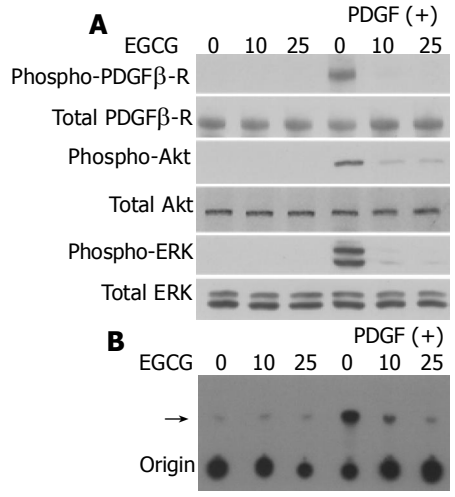

Figure 5 EGCG inhibited phosphorylation of PDGF β-receptor, ERK, and Akt. PSCs were incubated in the absence or presence of EGCG at the indicated concentrations for 1 h, and then treated with PDGF-BB (at 25 μg/L) for 5 min. **A:** total cell lysates were prepared, and the total and phosphorylated levels of PDGF β-receptor, Akt, and ERK were determined by Western blotting; **B:** total cell lysates were prepared and immunoprecipitated with anti-phosphotyrosine antibody. PI3-kinase activity was assessed using PI as a substrate. The arrow denotes the product, PI3-phosphate, resolved by thin layer chromatography.

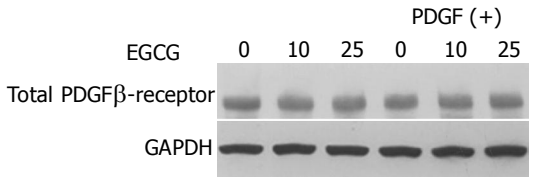

Figure 6 EGCG did not alter the expression of total PDGF β-receptor. PSCs were incubated with EGCG at the indicated concentrations in the absence or presence of PDGF-BB (at 25 μg/L). After 24 h, total cell lysates (approximately 100 μg) were prepared, and the levels of total PDGF β-receptor and GAPDH were determined by Western blotting.

DISCUSSION

The present study demonstrated that EGCG at non-cytotoxic concentrations inhibited PDGF-induced proliferation and migration. These inhibitory effects appeared through inhibiting tyrosine phosphorylation of PDGF β-receptor and downstream activation of ERK and PI3-kinase/Akt pathways. This is in agreement with the previous study showing that green tea catechins containing a galloyl group in the third position of the catechin structure interfered with PDGF-BB-induced mitogenic signaling in vascular smooth muscle cells by inhibiting tyrosine phosphorylation of the PDGF β-receptor[22]. The effects of EGCG were not mediated by its non-specific cytotoxicity because the levels of PDGF β-receptor and GAPDH were not decreased. In this study, EGCG was cytotoxic to PSCs above 25 μmol/L. This is relatively low compared to hepatic stellate cells where EGCG was not cytotoxic up to 100 μmol/L[31]. This may reflect differences in experimental conditions, including differences in cell types. Indeed, Chen and Zhang[31] treated hepatic stellate cells with EGCG in the presence of 100 mL/L fetal bovine serum whereas we treated PSCs with EGCG in serum-free medium.

We showed here that EGCG inhibited tyrosine phosphorylation of PDGF β-receptor. Tyrosine phosphorylation of PDGF β-receptor serves as a critical link between extracellular PDGF stimulation and intracellular signaling[13,14]. It has been shown that EGCG inhibited receptor-type protein tyrosine kinases (epidermal growth factor receptor, PDGF receptor, and fibroblast growth factor receptor) whereas EGCG scarcely inhibited serine- and threonine-specific protein kinases such as protein kinases A and C [32]. Like tyrphostin AG1296 [33], EGCG may induce conformational changes at the ATP-binding site of the PDGF β-receptor, thereby inhibiting its tyrosine phosphorylation. Other types of polyphenolic compounds (namely, genistein and quercetin) inhibit receptor tyrosine kinases via this mechanism[34]. On the other hand, it has been suggested that decreased tyrosine phosphorylation of PDGF receptor might be attributed to decreased binding of PDGF to the receptor. EGCG, as in the case of other flavanols, can form complexes with biologic macromolecule such as lipids, carbohydrates, proteins, and nucleic acids[35]. Suzuki *et al*[36], demonstrated that PDGF-BB was captured by EGCG immobilized on agarose gel. Weber *et al*[37], showed that EGCG was incorporated into different cellular components including cell surface membranes, which leads to a trapping of PDGF to non-receptor binding sites and reduced PDGF-BB binding to the respective receptors. Thus, EGCG incorporated into plasma membrane or soluble EGCG might directly interact with PDGF-BB, thereby preventing specific receptor binding.

It should be noted that EGCG here did not affect the total PDGF β-receptor expression. This is in contrast to hepatic stellate cells where EGCG inhibited cell proliferation by blocking the tyrosine phosphorylation and by reducing the gene expression of PDGF β-receptor[31]. In hepatic stellate cells, EGCG blocked the activation of activator protein-1 and nuclear factor κB, which, in turn, resulted in a marked reduction in the promoter activity and gene expression of the PDGF β-receptor[31]. Because EGCG did not alter the amount of PDGF β-receptor, different mechanisms might be involved. We here showed that EGCG inhibited the activation of ERK and PI3-kinase/Akt pathways. Because EGCG inhibited phosphorylation of PDGF β-receptor, it would be logical to assume that the reduction in activity of kinases downstream of PDGF receptor was solely due to the reduction in PDGF receptor activity. However, recent cell-free study showed that EGCG could directly inhibit ERK and Akt activation in response to epidermal growth factor[38]. Thus, activation of ERK and Akt might be inhibited in the cell by dual effects of EGCG: the suppression of incoming PDGF-associated stimulation and direct inhibition of these kinases. Further studies are required to elucidate the complexity of the regulation.

During tissue repair and inflammatory processes in the pancreas, PDGF is secreted by various cells including platelets, mononuclear cells, and activated macrophages[39]. Exposure of PSCs to PDGF *in vivo* is likely to occur in conditions of pancreatic inflammation characterized by the presence of platelets and activated macrophages[2,10]. PDGF-induced effects on PSCs *in vivo* may be further aided by the up-regulation of PDGF receptors on the surface of PSCs. In this regard, it should be noted that in a rat model of pancreatic fibrosis, immunostaining for PDGF β-receptor was found to be notably increased in association with areas of fibrosis, and the expression of the PDGF β-receptor, but not of the PDGF α-receptor, was closely associated with desmin staining, suggesting that PSCs expressed the PDGF β-receptor[3]. Codistribution of PDGF with cells expressing its receptor confirms a functional role of PDGF in the development of pancreatic fibrosis.

We showed here that PDGF-BB, which is one of the most potent mitogen for PSCs, induced the expression of cyclin D1 whereas $p27^{Kip1}$ expression was down-regulated. The effects of PDGF-BB on these cell cycle-related molecules were blocked by EGCG treatment, resulting in the inhibition of cell cycle progression beyond the G_1 phase. The D-group cyclin proteins play critical roles in the progression of cells through the G_1 phase of the cell cycle[40,41]. It has been reported that overexpression of cyclin D1 in cultured cells shortened G_1 phase and caused more rapid entry into S phase[40]. Conversely, microinjection of antisense cyclin D1 oligonucleotide or cyclin D1 antibody arrested the cells at G_1 phase[41]. Although regulation of cell cycle progression in PSCs remains largely unknown, our results suggested for the first time that induction of cyclin D1 and decreased $p27^{Kip1}$ might be a prerequisite for PSC proliferation. Because

PSCs were treated with EGCG in the presence of PDGF-BB, down-regulation of cyclin D1 and upregulation of $p27^{Kip1}$ might merely result from decreased tyrosine phosphorylation of PDGF β-receptor. It should be noted that EGCG by itself inhibited cyclin-dependent kinases 2 and 4 activities but induced $p21^{Waf1}$ and $p27^{Kip1}$ expression during growth arrest of human breast carcinoma cells[42].

We have recently shown that 4-hydroxy-2,3-nonenal, an aldehydic end-product of lipid peroxidation, induced type I collagen production in PSCs, suggesting a role of oxidative stress in the regulation of cell functions of PSCs. Although little is known about the effective EGCG concentrations required to modulate PDGF-mediated signaling pathways *in vivo*, it would be of interest to see whether EGCG inhibits the development of pancreatic fibrosis *in vivo*. In addition to its inhibitory effects on PDGF-induced cell functions, we have found that EGCG inhibited cytokine-induced production of monocyte chemoattractant protein-1 (Masamune *et al*, manuscript in preparation). The pharmacokinetics of the green tea polyphenols in humans have been examined in detail[43,44], and the maximum achievable EGCG concentration *in vivo* is less than the concentrations used in the current study. For example, 1 cup (240 mL) of green tea contains 200 mg of EGCG [43] and a single 200-mg dose of EGCG produces a plasma EGCG concentration of ~0.1 μmol/L[44]. However, the consumption of pharmaceutically prepared formulations of green tea polyphenols produces plasma EGCG concentrations approaching 2 μmol/L[44]. EGCG has been shown to protect against carbon tetrachloride-induced hepatotoxicity in mice[45], and endotoxin-induced lethal shock[46]. Its potent antioxidant capability and long history as beverage without adverse health effects make it a candidate for the treatment of pancreatic fibrosis. Experiments designed to test this hypothesis are under way in our laboratory.

REFERENCES

1 **Apte MV,** Haber PS, Applegate TL, Norton ID, McCaughan GW, Korsten MA, Pirola RC, Wilson JS. Periacinar stellate shaped cells in rat pancreas: identification, isolation, and culture. *Gut* 1998; **43**: 128-133

2 **Bachem MG,** Schneider E, Gross H, Weidenbach H, Schmid RM, Menke A, Siech M, Beger H, Grunert A, Adler G. Identification, culture, and characterization of pancreatic stellate cells in rats and humans. *Gastroenterology* 1998; **115**: 421-432

3 **Haber PS,** Keogh GW, Apte MV, Moran CS, Stewart NL, Crawford DH, Pirola RC, McCaughan GW, Ramm GA, Wilson JS. Activation of pancreatic stellate cells in human and experimental pancreatic fibrosis. *Am J Pathol* 1999; **155**: 1087-1095

4 **Masamune A,** Kikuta K, Satoh M, Sakai Y, Satoh A, Shimosegawa T. Ligands of peroxisome proliferator-activated receptor-gamma block activation of pancreatic stellate cells. *J Biol Chem* 2002; **277**: 141-147

5 **Masamune A,** Sakai Y, Kikuta K, Satoh M, Satoh A, Shimosegawa T. Activated rat pancreatic stellate cells express intercellular adhesion molecule-1 (ICAM-1) *in vitro*. *Pancreas* 2002; **25**: 78-85

6 **Masamune A,** Satoh M, Kikuta K, Sakai Y, Satoh A, Shimosegawa T. Inhibition of p38 mitogen-activated protein kinase blocks activation of rat pancreatic stellate cells. *J Pharmacol Exp Ther* 2003; **304**: 8-14

7 **Masamune A,** Kikuta K, Satoh M, Satoh K, Shimosegawa T. Rho kinase inhibitors block activation of pancreatic stellate cells. *Br J Pharmacol* 2003; **140**: 1292-1302

8 **Masamune A,** Kikuta K, Suzuki N, Satoh M, Satoh K, Shimosegawa T. A c-Jun NH2-terminal kinase inhibitor SP600125 (anthra[1,9-cd]pyrazole-6 (2H)-one) blocks activation of pancreatic stellate cells. *J Pharmacol Exp Ther* 2004; **310**: 520-527

9 **Apte MV,** Haber PS, Darby SJ, Rodgers SC, McCaughan GW, Korsten MA, Pirola RC, Wilson JS. Pancreatic stellate cells are activated by proinflammatory cytokines: implications for pancreatic fibrogenesis. *Gut* 1999; **44**: 534-541

10 **Luttenberger T,** Schmid-Kotsas A, Menke A, Siech M, Beger H, Adler G, Grunert A, Bachem MG. Platelet-derived growth factors stimulate proliferation and extracellular matrix synthesis of pancreatic stellate cells: implications in pathogenesis of pancreas fibrosis. *Lab Invest* 2000; **80**: 47-55

11 **Masamune A,** Kikuta K, Satoh M, Kume K, Shimosegawa T. Differential roles of signaling pathways for proliferation and migration of rat pancreatic stellate cells. *Tohoku J Exp Med* 2003; **199**: 69-84

12 **Phillips PA,** Wu MJ, Kumar RK, Doherty E, McCarroll JA, Park S, Pirola RC, Wilson JS, Apte MV. Cell migration: a novel aspect of pancreatic stellate cell biology. *Gut* 2003; **52**: 677-682

13 **Williams LT.** Signal transduction by the platelet-derived growth factor receptor. *Science* 1989; **243**: 1564-1570

14 **Claesson-Welsh L.** Platelet-derived growth factor receptor signals. *J Biol Chem* 1994; **269**: 32023-32026

15 **Jaster R,** Sparmann G, Emmrich J, Liebe S. Extracellular signal regulated kinases are key mediators of mitogenic signals in rat pancreatic stellate cells. *Gut* 2002; **51**: 579-584

16 **Trevisanato SI,** Kim YI. Tea and health. *Nutr Rev* 2000; **58**: 1-10

17 **Yang CS,** Wang ZY. Tea and cancer. *J Natl Cancer Inst* 1993; **85**: 1038-1049

18 **Ahmad N,** Mukhtar H. Green tea polyphenols and cancer: biologic mechanisms and practical implications. *Nutr Rev* 1999; **57**: 78-83

19 **Rice-Evans C.** Implications of the mechanisms of action of tea polyphenols as antioxidants *in vitro* for chemoprevention in humans. *Proc Soc Exp Biol Med* 1999; **220**: 262-266

20 **Katiyar SK,** Elmets CA. Green tea polyphenolic antioxidants and skin photoprotection (Review). *Int J Oncol* 2001; **18**: 1307-1313

21 **Lin YL,** Lin JK. (-)-Epigallocatechin-3-gallate blocks the induction of nitric oxide synthase by down-regulating lipopolysaccharide-induced activity of transcription factor nuclear factor-kappaB. *Mol Pharmacol* 1997; **52**: 465-472

22 **Sachinidis A,** Skach RA, Seul C, Ko Y, Hescheler J, Ahn HY, Fingerle J. Inhibition of the PDGF beta-receptor tyrosine phosphorylation and its downstream intracellular signal transduction pathway in rat and human vascular smooth muscle cells by different catechins. *FASEB J* 2002; **16**: 893-895

23 **Mukhtar H,** Ahmad N. Tea polyphenols: prevention of cancer and optimizing health. *Am J Clin Nutr* 2000; **71**: 1698S-1702S; discussion 1703S-1704S

24 **Wang ZY,** Huang MT, Ho CT, Chang R, Ma W, Ferraro T, Reuhl KR, Yang CS, Conney AH. Inhibitory effect of green tea on the growth of established skin papillomas in mice. *Cancer Res* 1992; **52**: 6657-6665

25 **Sazuka M,** Murakami S, Isemura M, Satoh K, Nukiwa T. Inhibitory effects of green tea infusion on *in vitro* invasion and *in vivo* metastasis of mouse lung carcinoma cells. *Cancer Lett* 1995; **98**: 27-31

26 **Cao Y,** Cao R. Angiogenesis inhibited by drinking tea. *Nature* 1999; **398**: 381

27 **Mosmann T.** Rapid colorimetric assay for cellular growth and survival: application to proliferation and cytotoxicity assays. *J Immunol Methods* 1983; **65**: 55-63

28 **Masamune A,** Sakai Y, Satoh A, Fujita M, Yoshida M, Shimosegawa T. Lysophosphatidylcholine induces apoptosis in AR42J cells. *Pancreas* 2001; **22**: 75-83

29 Masamune A, Satoh K, Sakai Y, Yoshida M, Satoh A, Shimosegawa T. Ligands of peroxisome proliferator-activated

receptor-gamma induce apoptosis in AR42J cells. *Pancreas* 2002; **24**: 130-138

30 **Choudhury GG,** Wang LM, Pierce J, Harvey SA, Sakaguchi AY. A mutational analysis of phosphatidylinositol-3-kinase activation by human colony-stimulating factor-1 receptor. *J Biol Chem* 1991; **266**: 8068-8072

31 **Chen A,** Zhang L. The antioxidant (-)-epigallocatechin-3-gallate inhibits rat hepatic stellate cell proliferation *in vitro* by blocking the tyrosine phosphorylation and reducing the gene expression of platelet-derived growth factor-beta receptor. *J Biol Chem* 2003; **278**: 23381-23389

32 **Liang YC,** Lin-shiau SY, Chen CF, Lin JK. Suppression of extracellular signals and cell proliferation through EGF receptor binding by (-)-epigallocatechin gallate in human A431 epidermoid carcinoma cells. *J Cell Biochem* 1997; **67**: 55-65

33 **Kovalenko M,** Ronnstrand L, Heldin CH, Loubtchenkov M, Gazit A, Levitzki A, Bohmer FD. Phosphorylation site-specific inhibition of platelet-derived growth factor beta-receptor autophosphorylation by the receptor blocking tyrphostin AG1296. *Biochemistry* 1997; **36**: 6260-6269

34 **Masuda M,** Suzui M, Lim JT, Weinstein IB. Epigallocatechin-3-gallate inhibits activation of HER-2/neu and downstream signaling pathways in human head and neck and breast carcinoma cells. *Clin Cancer Res* 2003; **9**: 3486-3491

35 **Yang CS,** Wang ZY. Tea and cancer. *J Natl Cancer Inst* 1993; **85**: 1038–1049

36 **Suzuki Y,** Hattori S, Isemura M. Epigallocatechin-3-O-gallate inhibits fibroblast contraction of floating collagen gel: interaction between epigallocatechin-3-O-gallate and platelet derived growth factor. *Biosci Biotechnol Biochem* 2004; **68**: 1817–1820

37 **Weber AA,** Neuhaus T, Skach RA, Hescheler J, Ahn HY, Schror K, Ko Y, Sachinidis A. Mechanisms of the inhibitory effects of epigallocatechin-3 gallate on platelet-derived growth factor-BB-induced cell signaling and mitogenesis. *FASEB J* 2004; **18**: 128-130

38 **Sah JF,** Balasubramanian S, Eckert RL, Rorke EA. Epigallocatechin-3-gallate inhibits epidermal growth factor receptor signaling pathway. Evidence for direct inhibition of ERK1/2 and AKT kinases. *J Biol Chem* 2004; **279**: 12755-12762

39 **Ross R.** Platelet-derived growth factor. *Lancet* 1989; **1**: 1179-1182

40 **Jiang W,** Kahn SM, Zhou P, Zhang YJ, Cacace AM, Infante AS, Doi S, Santella RM, Weinstein IB. Overexpression of cyclin D1 in rat fibroblasts causes abnormalities in growth control, cell cycle progression and gene expression. *Oncogene* 1993; **8**: 3447-3457

41 **Baldin V,** Lukas J, Marcote MJ, Pagano M, Draetta G. Cyclin D1 is a nuclear protein required for cell cycle progression in G1. *Genes Dev* 1993; **7**: 812-821

42 **Liang YC,** Lin-Shiau SY, Chen CF, Lin JK. Inhibition of cyclin-dependent kinases 2 and 4 activities as well as induction of Cdk inhibitors p21 and p27 during growth arrest of human breast carcinoma cells by (-)-epigallocatechin-3-gallate. *J Cell Biochem* 1999; **75**: 1-12

43 **Lakenbrink C,** Lapczynski S, Maiwald B, Engelhardt UH. Flavonoids and other polyphenols in consumer brews of tea and other caffeinated beverages. *J Agric Food Chem* 2000; **48**: 2848-2852

44 **Chow HH,** Cai Y, Hakim IA, Crowell JA, Shahi F, Brooks CA, Dorr RT, Hara Y, Alberts DS. Pharmacokinetics and safety of green tea polyphenols after multiple-dose administration of epigallocatechin gallate and polyphenon E in healthy individuals. *Clin Cancer Res* 2003; **9**: 3312–3319

45 **Chen JH,** Tipoe GL, Liong EC, So HS, Leung KM, Tom WM, Fung PC, Nanji AA. Green tea polyphenols prevent toxin-induced hepatotoxicity in mice by down-regulating inducible nitric oxide-derived prooxidants. *Am J Clin Nutr* 2004; **80**: 742–751

46 **Yang F,** de Villiers WJ, McClain CJ, Varilek GW. Green tea polyphenols block endotoxin-induced tumor necrosis factor-production and lethality in a murine model. *J Nutr* 1998; **128**: 2334-2340

Science Editor Li WZ **Language Editor** Elsevier HK

PO Box 2345, Beijing 100023, China
www.wjgnet.com
wjg@wjgnet.com

ELSEVIER

World J Gastroenterol 2005;11(22):3375-3384
World Journal of Gastroenterology ISSN 1007-9327

• *BASIC RESEARCH* •

Different cytokine response of primary colonic epithelial cells to commensal bacteria

Jing-Gang Lan, Sheena Margaret Cruickshank, Joy Carmelina Indira Singh, Mark Farrar, James Peter Alan Lodge, Peter John Felsburg, Simon Richard Carding

Jing-Gang Lan, Sheena Margaret Cruickshank, Joy Carmelina Indira Singh, Mark Farrar, Simon Richard Carding, School of Biochemistry and Microbiology, The University of Leeds, Leeds LS2 9JT, United Kingdom
James Peter Alan Lodge, General Surgery, Medicine and Anaesthesia, School of Medicine, The University of Leeds, Leeds LS2 9JT, United Kingdom
Peter John Felsburg, Department of Clinical Studies, University of Pennsylvania, Philadelphia, PA 19104, United States
Supported by the USA Public Health Service grants AI-41562 and PO1 RR12211 (SRC and PF), the Ann Gloag Fellowship of the Royal College of Surgeons Edinburgh and The Rays of Hope Charitable Trust (JS)
Correspondence to: Professor Simon Richard Carding, School of Biochemistry and Microbiology, The University of Leeds, Leeds LS2 9JT, United Kingdom. s.r.carding@leeds.ac.uk
Telephone: +44-113-3431404 Fax: +44-113-3431421
Received: 2004-07-31 Accepted: 2004-12-01

Abstract

AIM: To determine if primary murine colonic epithelial cells (CEC) respond to commensal bacteria and discriminate between different types of bacteria.

METHODS: A novel CEC: bacteria co-culture system was used to compare the ability of the colonic commensal bacteria, *Bacteroides ovatus*, *E. coli* (SLF) and *Lactobacillus rhamnosus* (LGG) to modulate production of different cytokines (n = 15) by primary CEC. Antibody staining and flow cytometry were used to investigate Toll-like receptor (TLR) expression by CEC directly *ex vivo* and TLR responsiveness was determined by examining the ability of TLR ligands to influence CEC cytokine production.

RESULTS: Primary CEC constitutively expressed functional TLR2 and TLR4. Cultured in complete medium alone, CEC secreted IL-6, MCP-1 and IP-10 the levels of which were significantly increased upon addition of the TLR ligands peptidoglycan (PGN) and lipopolysaccharide (LPS). Exposure to the commensal bacteria induced or up-regulated different patterns of cytokine production and secretion. *E. coli* induced production of MIP-1α/β and β defensin3 whereas *B. ovatus* and *L. rhamnosus* exclusively induced MCP-1 and MIP-2α expression, respectively. TNFα, RANTES and MEC were induced or up-regulated in response to some but not all of the bacteria whereas ENA78 and IP-10 were up-regulated in response to all bacteria. Evidence of bacterial interference and suppression of cytokine production was obtained from mixed bacterial: CEC co-cultures. Probiotic LGG suppressed *E. coli*- and *B. ovatus*-induced cytokine mRNA accumulation and protein secretion.

CONCLUSION: These observations demonstrate the ability of primary CEC to respond to and discriminate between different strains of commensal bacteria and identify a mechanism by which probiotic bacteria (LGG) may exert anti-inflammatory effects *in vivo*.

Key words: Epithelial cells; Colon; Commensal bacteria; Cytokines; Chemokines

Lan JG, Cruickshank SM, Singh JCI, Farrar M, Lodge JPA, Felsburg PJ, Carding SR. Different cytokine response of primary colonic epithelial cells to commensal bacteria. *World J Gastroenterol* 2005; 11(22): 3375-3384
http://www.wjgnet.com/1007-9327/11/3375.asp

INTRODUCTION

Intestinal mucosal surfaces are in continuous contact with heterogeneous populations of commensal microorganisms, which collectively make up the intestinal microbiota. Historically, the barrier function of intestinal epithelial cells (IEC) has been considered to be important in preventing the interaction of non-invasive microbes and protein antigens from making contact with, and activating the mucosal immune system and maintaining immune tolerance[1]. Indeed, breach of the epithelial barrier is a feature of chronic inflammatory disorders such as inflammatory bowel disease (IBD), and the virulence of enteric pathogens such as enterohemorrhagic *E. coli*, is in large part attributable to their ability to disrupt the epithelial barrier[2]. More recent studies suggest that IEC play a more active role in preventing or limiting host responses to harmless self-antigens. Studies using immortalized lines have shown that IEC selectively lack expression of pattern recognition receptors (PRRs) such as Toll-like receptors (TLR), or PRR-associated signal transduction complexes that mediate recognition of signature molecules of microorganisms (microbe-associated molecular patterns; MAMPs) including lipopolysaccharide (LPS) and peptidoglycan (PGN)[3]. The results of studies of TLR expression by IEC *in vivo* are however, ambiguous with some providing no evidence of TLR 2 or TLR4 expression in the normal intestinal mucosa whereas others have detected low levels of expression[4-6].

The host response to commensal bacteria *in vivo* has been investigated by profiling ileal tissue mRNA of germfree mice following conventionalization with commensal bacteria[7]. Although this study did not include an analysis of host immune response genes, it demonstrated that commensal bacteria could modulate expression of genes in ileal tissue and laser-capture microdissected epithelial cells that are involved in mucosal barrier integrity, xenobiotic metabolism, nutrient absorption, angiogenesis and postnatal intestinal maturation. Evidence that the host can distinguish between different commensal bacteria has been obtained by comparing the levels of mRNA encoding proteins involved in toxin metabolism (*mdr1a*), barrier function (*sprr2a*) and lipid metabolism (colipase), which showed quantitative differences in levels of ileal tissue mRNA in mice colonized by three different commensal bacteria. Since the bulk of these studies were carried out on intact ileal tissue samples, it was not possible to exclude non-epithelial cell contributions to the mRNA profile, and any indirect effects of other mucosal cells on epithelial cell responses to bacterial challenge *in vivo*. One way in which the molecular nature of IEC responses to commensal bacteria has been addressed is through the use of defined intestinal epithelial cell lines.

Studies using IEC lines have suggested that commensal bacteria may "programme" IEC to prevent or down-modulate pro-inflammatory responses to non-pathogenic bacteria by interfering with TLR expression[8] or NF-κB activation[9]. The involvement or requirement of NF-κB activation in IEC inflammatory responses is however questioned by *in vivo* studies, demonstrating that this transcription factor is primarily involved in IEC homeostasis and that NF-κB activation is associated with suppression of CEC proliferation[10]. Other studies using IEC lines have implied that there may be qualitative and/or quantitative differences in the response of IEC to harmless versus harmful microbes[9,11]. Thus, it is not clear if or how IEC normally respond to commensal bacteria. To address this issue we have used a novel CEC:bacteria co-culture system and three representative strains of commensal bacteria including a probiotic bacterium, to determine what effect non-pathogenic bacteria have on CEC cytokine production. Our results provide evidence for the ability of primary CEC to respond to and distinguish between different types of commensal bacteria.

MATERIALS AND METHODS

Animals

Specific pathogen free (SPF) C57BL/6 mice (Harlan, UK) were housed under SPF conditions at The University of Leeds and used between four and six weeks of age.

CEC isolation

CEC isolation, culture and characterization were extensively described previously[12,13]. CEC viability was routinely >95% and comprised >98% cytokeratin$^+$ cells as determined by antibody staining and flow cytometry. CEC preparations with <90% viability, or >10% cytokeratin$^-$ cells were discarded. Cells were initially cultured for up to 72 h in complete medium MEM (Sigma, Poole, Dorset, UK), 20% heat-inactivated fetal bovine serum (Harlan, UK), 2% Luria broth and 2 mmol/L *L*-glutamine to obtain a semi-confluent monolayer of polarized CEC. The medium was changed after 24 h to remove dead and non-adherent cells. These culture conditions were not ideal for hematopoietic cell growth and the absence of contaminating hematopoietic (CD45$^+$) cells was confirmed by antibody staining, flow cytometry, and RT-PCR using primers specific for CD45. Contamination by mesenchymal cells was evaluated by assaying the presence of vimentin mRNA by RT-PCR.

CEC:bacteria co-culture

CEC were cultured for 1-5 h at 37 ℃ in 50 mL/L CO_2 in complete media alone or in media containing three representative members of the murine and human colonic microbiota[14]. A human colonic isolate of *Bacteroides ovatus* (V975) was provided by Dr. T Whitehead (Peoria, IL), a murine intestinal isolate of *E. coli* (slow lactose fermenting; SLF) was provided by Dr. J Cebra (Philadelphia, PA), and *Lactobacillus rhamnosus* (*Lactobacillus* GG; LGG) was originally isolated from human feces (ATCC, catalog number 53103). CEC and bacteria were cultured at a ratio of 10 bacteria: 1 CEC and the number of bacteria and CEC were determined at the beginning and end of the culture. In some experiments viable or non-viable (heat killed) *L. rhamnosus* was added to an equal number of *E. coli* or *B. ovatus* immediately prior to culture with CEC such that the total number of bacteria was the same as that in single bacteria:CEC co-culture. In additional experiments, CEC were cultured with 10 μg/mL LPS (Sigma, Poole, UK) or 1 μg/mL PGN (Sigma) for 8 h prior to analysis of TLR expression and levels of the active form of ERK kinase. Conditioned media from CEC: bacteria co-culture were harvested and stored at -80 ℃ until analyzed by ELISA and CEC were extensively washed prior to processing for RNA isolation.

RT-PCR analysis

Total cellular RNA was isolated from cultured CEC by lysis in 4 mol/L guanidinium isothiocyanate and CsCl density gradient centrifugation followed by acidic phenol extraction and ethanol precipitation. One to two micrograms of RNA was reverse transcribed into cDNA and amplified by capillary PCR (Idaho Technology, Idaho Falls, ID) using specific oligonucleotide primers (Table 1). Wherever possible primer pairs spanning an intron were used wherever possible. Optimal amplification conditions for each primer pair were determined empirically using cloned cDNAs or mRNA/cDNAs obtained from primary or established cell lines that expressed the gene of interest. Quantitative scanning densitometry of EtBr-stained gels was used to compare levels of PCR products obtained under different culture conditions.

Flow cytometric analysis of TLR expression

Highly purified (>98% cytokeratin$^+$) preparations of freshly isolated CEC were stained with FITC-anti-TLR2 (clone 6C2, Hycult Biotechnology BV, Uden, The Netherlands) or TLR4 (Biocarta, Oxford, UK) antibodies followed by goat anti-rat-biotin (Caltag) and finally streptavidin-PE

Table 1 PCR primer sequences

Gene	Forward 5′→3′	Reverse 5′→3′
Cytokines		
IL-1β	GAGATTGAGCTGTCTGCTCA	AAGGAGAACCAAGCAACGAC
IL-6	GATGCTACCAAACTGGATATAATC	GGTCCTTAGCCACTCCTTCTGTG
IL-18	ACTGTACAACCGCAGTAATACGG	AGTGAACATTACAGATTTATCCC
TNFα	TGGGAGTAGACAAGGTACAACCC	CATCTTCTCAAAATTCGAGTGACAA
ENA78 (CXCL5)	CTTCCTCAGTCATAGCCGCAAC	ATCCGTGGGTGGAGAGAATCAG
IP-10 (CXCL10)	TTTCTGCCTCATCCTGCTGG	GGAGCCCTTTTAGACCTTTTTTGG
MIP-1α (CCL3)	GCCCTTGCTGTTCTTCTCTGT	GGCATTCAGTTCCAGGTCAGT
MIP-1β (CCL4)	ACACCATGAAGCTCTGCGT	CGCTGGAGCTGCTCAGTTC
MIP-2α (CXCL2)	CAAAGGCAAGGCTAACTG	TGTTCTACTCTCCTCGGT
MIP-3α (CCL-20)	GCAGAAGCAGCAAGCAACTACG	GAGGTTCACAGCCCTTTTCACC
MCP-1 (CCL2)	CTCACCTGCTGCTACTCATTC	GCTTGAGGTGGTTGTGGAAAA
MCP-3 (CCL7)	TGTGCCTGAACAGAAACCAACC	AAAAATGGGGAAAGGGGGAG
KC (GRO)	GTCCTTTGAACGTCTCTGTC	GCTGGCTTCTGACAACACTA
RANTES (CCL5)	CAAGGAGTATTTCTACACCAGCAGC	ATGCCGATTTTCCCAGGACC
MEC (CCL-28)	GCTGTGTGTGTGGCTTTTCAAAC	TTCTGTCCTTCCTGCTGGGTTG
TLR- signaling		
MyD88	ACCCCACTCGCAGTTTGTTGGATG	TGGTGATGCCTCCCAGTTCCTTTG
TIRAP	CAATCTACCTGGAATCGGCTGTC	GCATCTTCTTGGGCTTCTTCAAC
IRAK	TGCCGCTTCTACAAAGTGATGGACG	AATGGGTCTGGGAGCCTGGAAAAG
Caspase-1	ATTACTGCTATGGACAAGGCACGG	CCCTCGGAGAAAGATGTTGAAACTC
TRAF-6	AATGGAAGCACAGCAGTGTAACGGG	AAGGCAAGCAGTTCTGGTTTGGCG
IKKβ	TGGAGCCTGGGAAATGAAAGAACG	TCTAAGAGCCGATGCGATGTCACTC
IKKα	AGCCATTCCTCACTTACCAGTCCG	CAGCAGTCTCTTCCACAGAAAACCC
Others		
CD45	CTTCAGAGCCTCGTACCAGC	TGTGTCCAGAAGGGCAAATC
β-actin	GCTTCTTTGCAGCTCCTTCGTTG	TTCTCCATGTCGTCCCAGTTGG
Vimentin	CTGTGTCCTCGTCCTCCTACC	GCAGTTCTACCTTCTCGTTGG
β-defensin3	GCATTTGAGGAAAGGAACTCCACAAC	GTCTCCACCTGCAGCTTTTAGCAA
Angiogenin4	CTCTGGCTCAGAATGTAAGGTACGA	GAAATCTTTAAAGGCTCGGTACCC
SAA-1	GTAATTGGGGTCTTTGCC	TTCTGCTCCCTGCTCCTG

(Caltag). Samples were analyzed by flow cytometry. Appropriate isotype matched control antibodies were also used.

Cytokine ELISAs

Commercial preparations of paired antibodies for measurement of murine IL-1β, IL-6, TNFα, MCP-1, KC (Becton Dickinson Biosciences, Oxford, UK), MIP-1α, MIP-1β, and IP-10 (R&D Systems, Abingdon, UK) were used to develop ELISA according to the manufacturer's instructions. Individual samples were tested in triplicate and the concentration of cytokines was determined using known amounts of recombinant protein. The amounts of cytokine detected in CEC:bacteria co-culture were normalized according to the number of CEC in each culture.

Statistical analysis

Cytokine concentrations were expressed as mean±SD and evaluated using the Student's *t* test. $P<0.05$ was considered statistically significant.

RESULTS

Primary CEC expressed functional TLRs

To ascertain whether CEC had the potential to respond to commensal bacteria, we first examined CEC directly *ex vivo* for expression of TLR2 and TLR4 by antibody staining and flow cytometry. Examination of cellular levels of TLR2 and TLR4 protein showed that freshly isolated CEC expressed detectable levels of both TLR2 and TLR4 (Figure 1B). TLR2 and TLR4 expression by CEC were evaluated by determining the influence of TLR2 and four ligands PGN and LPS on cytokine production by CEC *in vitro*. For these experiments cultured CEC comprising crypts, enterocytes and goblet cells[12,13] were used. Contaminating hematopoietic ($CD45^+$) cells were not detected in any of these cultures using a RT-PCR assay capable of detecting less than 2% contaminating $CD45^+$ cells (Figure 1A). Vimentin antibody staining (data not shown) and RT-PCR analysis (Figure 1A) showed that $vimentin^+$ cells including fibroblasts, were also absent from these cultures. CEC were cultured *in vitro* in the presence of PGN or LPS for 12 h, then the conditioned medium was assayed in the presence of the cytokines IL-6 and MCP-1, which are known to be produced by CEC both *in vivo* and *in vitro*[15]. As seen in Figure 1C, CEC constitutively secreted high levels of MCP-1 (>1 000 pg/mL) and comparatively lower levels of IL-6 (<400 pg/mL). In response to LPS the levels of secretion of both cytokines were significantly increased ($P<0.002$ for

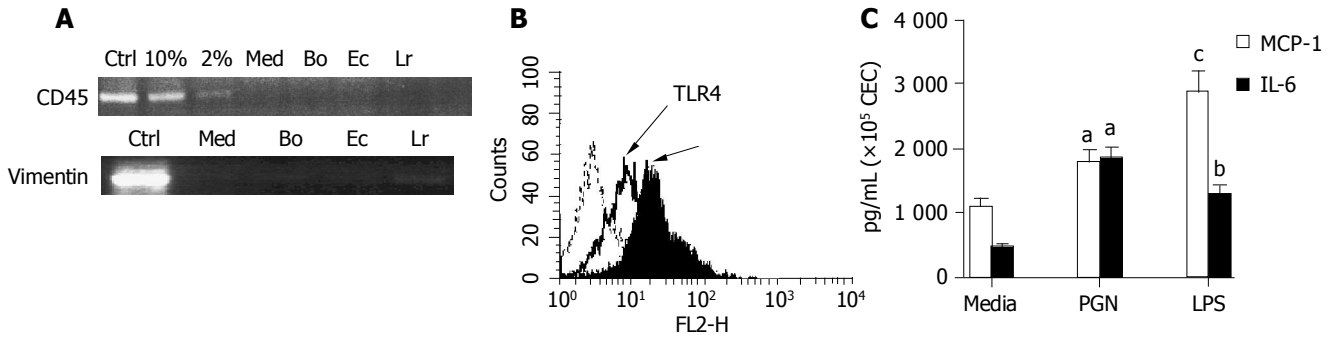

Figure 1 Evaluation of the purity and response of cultured murine CEC. **A**: CEC from 4-6 wk old C57BL/6 mice were cultured for 72 h in medium alone (M) or in medium containing *Bacteroides ovatus* (Bo), *E. coli* (Ec) or *Lactobacillus rhamnosus* (Lr) after which CEC RNA was extracted, reverse transcribed and cDNA amplified by RT-PCR using primers specific for CD45 or vimentin. PCR products were separated by gel electrophoresis and EtBr-stained amplicons visualized and digitally recorded under UV illumination. The sensitivity of CD45 detection was determined by adding spleen cells to highly purified CECs so that they comprised 2% or 10% of the total cell population prior to RNA extraction and RT-PCR analysis. Control samples (Ctrl) were spleen cells (+Ctrl) and no cDNA (-Ctrl) for CD45 RT-PCR and fibroblasts for vimentin RT-PCR assay. The results are representative of more than 10 independent experiments; **B**: TLR2 and TLR4 expression by CEC. The dashed line on the histogram plots represents staining with control antibody, the bold line represents staining profile of anti-TLR4 and the filled in histogram plot represents anti-TLR2 antibody staining; **C**: Responsiveness of TLR expressed by CEC. Supernatants from 4 h cultures of CEC in medium alone (Med) or in medium containing LPS (10 μg/mL) or PGN (1 μg/mL) were assayed for the presence of IL-6 and MCP-1 by ELISA. The results shown were collated from three independent experiments. The error bars represent SEM. $^{a}P<0.05$ LPS *vs* medium values, $^{b}P<0.01$ PGN *vs* medium values, $^{c}P<0.002$ LPS *vs* medium values.

MCP-1 and $P<0.05$ for IL-6). PGN also significantly increased the level of MCP-1 ($P<0.01$) and IL-6 ($P<0.01$) production when compared to cells cultured in medium alone. TLR4 expression by CEC was also confirmed by immunoblot analysis of the active and phosphorylated form of the MAP kinase, ERK 1/2, which showed that levels of the phosphorylated form of p42 and p44 isoforms of ERK were up-regulated in response to LPS and PGN (data not shown). Collectively, these data demonstrated that primary CEC could express functional TLR2 and TLR4.

Bacteria:CEC co-culture

CEC from 2-3 healthy adult C57BL/6 mice were pooled and cultured *in vitro* for up to 72 h to establish a semi-confluent monolayer of polarized epithelial cells prior to the addition of either *B. ovatus*, *E. coli* or LGG that were in logarithmic growth phase. The number of bacterial strains used was limited to three in order to facilitate screening of a large panel of genes ($n = 18$) encoding cytokines, acute phase proteins and antimicrobial proteins (Table 1). The choice of bacteria was based upon their prominence in the mouse and human colon[16,17], expression of antigens known to modulate immune (lymphocyte) cell activity[18-21], their availability and ability to sustain their normal growth activity under the conditions used to maintain CEC. *L. rhamnosus* (LGG) was also chosen as it is a widely used probiotic bacterium[22]. After co-culture supernatants were harvested for cytokine and chemokine analysis by ELISA and CEC were harvested for RNA isolation and RT-PCR analysis.

The duration of CEC:bacteria co-culture was restricted as short as possible in order to detect a response yet preventing bacterial overgrowth and any indirect effects on CEC as a result of changes in the culture media (e.g., pH, nutrient depletion). A ratio of 10 bacteria:1 CEC was found to be optimal for detecting changes in CEC gene expression without adversely affecting the composition of the culture medium and CEC viability (Lan and Carding, unpublished data). Approximately 2×10^5 CEC were cultured with different numbers of bacteria for 4-5 h, then the number of CEC and bacteria was determined. During a 4 h period the number of *E. coli* and *L. rhamnosus* bacteria increased approximately 4-fold (Figure 2A) whereas the number of viable CEC did not significantly change (Figure 2A). Although regarded as an anaerobe, *B. ovatus* is aerotolerant and over a 4 h period the viability and growth rate of *B. ovatus* were similar when cultured in CEC media under aerobic conditions (MEM 10% FCS, 100 mL/L CO_2) or in bacterial culture media (RGM) under anaerobic conditions (Figure 2A). By seeding CEC cultures with a slightly higher density of *B. ovatus,* the total number of bacteria after 4 h of culture was equivalent to the number of *E. coli* and *L. rhamnosus* recovered from CEC co-culture after 4 h (Figure 2A). The optimal time for detecting changes in CEC gene expression was determined by co-culturing bacteria with CEC and harvesting CEC at hourly intervals for RT-PCR analysis of expression of representative cytokine genes. For MIP-1α and TNFα as well as the majority of genes analyzed (Table 1), the highest levels of mRNA were detected after 4 h (Figure 2B). A ratio of 10 bacteria:1 CEC and a 4 h co-culture period were therefore used for all subsequent experiments.

Different regulation of cytokine gene expression by CEC in response to different bacteria

Activation of signal transduction pathways by TLRs led to the induction of various genes including inflammatory cytokines and chemokines that function in host defence. The ability of primary CEC to respond differently to different commensal bacteria at the level of cytokine mRNA expression was therefore assessed using semi-quantitative RT-PCR. Genes encoding 15 cytokines and three anti-microbial proteins (Tables 1 and 2) were chosen for this analysis on the basis of their constitutive or inducible production by cultured human or rodent IEC lines, or by IEC in healthy or inflamed colon of experimental animals or IBD patients[15,23-25].

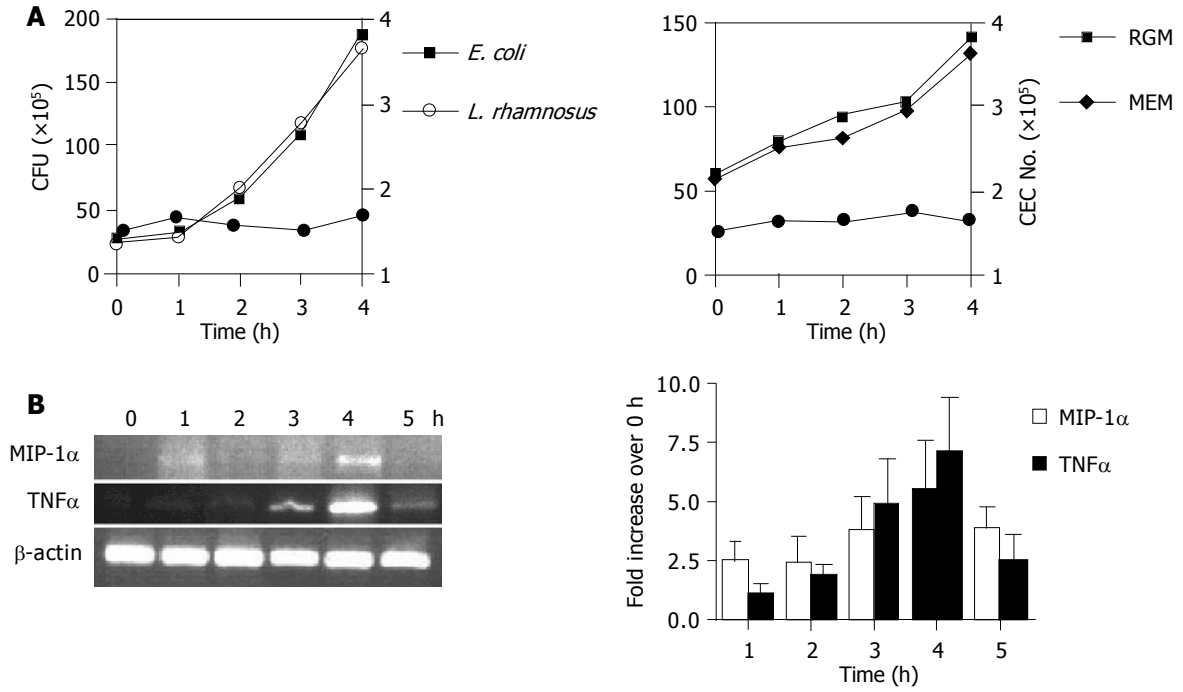

Figure 2 Bacterial growth (**A**) and kinetics of CEC cytokine gene expression (**B**) in CEC:bacteria co-cultures. **A**: Determination of bacterial (*L. rhamnosus and E. coli*) CFU by harvesting cells from CEC:bacteria co-cultures at hourly intervals up to 4 h by extensive washing of adherent CEC and plating serial dilutions onto agar plates and counting bacterial colonies 24 h later (left-hand panel). *B. ovatus* were cultured either alone under anaerobic conditions in RGM media or with CEC in 50 mL/L CO_2 and complete MEM (right-hand panel). CEC numbers (solid circle on both graphs) were determined by counting the number of cells recovered from co-cultures at the indicated times using a counting chamber; **B**: CEC cultured in the presence of *E. coli* for up to 5 h. CECs were processed for RNA isolation and RT-PCR analysis using primers specific for the housekeeping gene β-actin, and MIP-1α and TNFα as described in Materials and Methods. Quantitative densitometry was carried out on EtBr-stained gels and the results from three independent experiments were compiled to produce the data shown. Error bars indicate 95% confidence limits.

Table 2 Semi-quantitative assessment of bacteria-induced CEC gene expression

Gene	Medium	+*B. ovatus*	+*E. coli*	+*L. rhamnosus*
IL-1β	-[1]	1[2]	1	3
TNFα	-	0	2	1
IL-6	+	4	2	0
IL-18	-	0	0	0
ENA-78 (CXCL5)	+	1	1	1
IP-10 (CXCL10)	+	1	2	1
MIP-1α (CCL3)	-	0	3	0
MIP-1β (CCL4)	-	0	4	0
MIP-3α (CCL-20)	-	1	3	1
MCP-1 (CCL2)	+	2	4	4
MCP-3 (CCL5)	+	1	2	2
KC (GRO)	+	1	4	2
MIP-2α (CXCL2)	+	0	0	2
RANTES (CCL5)	-	0	2	1
MEC (CCL-28)	-	0	2	1
β-Defensin3	-	0	4	0
SAA-1	-	0	0	0
Angiogenin4	-	0	0	0

[1]Absence (–) or presence (+) of EtBr-stained PCR amplicons in CECs cultured in media alone. [2]Relative intensity of amplicons expressed by CEC cultured in presence of bacteria compared to cultured in media alone as determined by scanning densitometry. 0 = No change, 1 = <2-fold higher, 2 = 2- to 3-fold higher, 3 = 3- to 4-fold higher, 4 = >4-fold higher.

Cultured CEC constitutively expressed detectable levels of mRNAs encoding IL-6, ENA78, MCP-1, MCP-3, IP-10, KC and MIP-2α (Figure 3 and Table 2). By contrast, it was not possible to detect constitutive expression of transcripts encoding the cytokines IL-18, IL-1β, TNFα (Figure 2B), MIP-1α, MIP-1β, MIP-3α and MEC, the acute phase protein serum amyloid A (SAA-1), or the anti-microbial proteins angiogenin 4 (*Ang4*) and β-defensin 3 (Figure 3 and Table 2).

The addition of bacteria resulted in different profiles of cytokine gene expression by CEC (Figure 3 and Table 2). The levels of expression of some cytokines (IL-18), acute phase (SAA-1) and anti-microbial proteins (*Ang4)* remained the same as that seen in CEC cultured in media alone. Changes in cytokine mRNA levels were seen in response to a single strain of bacteria. Induction of MIP-1α, MIP-1β and β-defensin 3 mRNA expression was only evident in response to *E. coli*, whereas induction of MIP-2α was only seen in response to *L. rhamnosus*. Some cytokine mRNAs (IL-6, TNFα RANTES and MEC) increased in response to 2/3 of the bacteria. ENA78, KC, MCP-1, MCP-3 and IP-10 mRNA levels were up-regulated to some extent in response to the three strains of bacteria. To substantiate these findings we determined if the changes seen in cytokine mRNA reflected changes in the level of secreted proteins.

Changes in cytokine secretion by CEC in response to different bacteria

A total of eight cytokines were used for this study, the choice of which was based upon those that were analyzed by RT-PCR, and necessarily restricted by the availability of suitable reagents (paired antibodies). Six of the eight cytokines (TNFα, IL-1β, IL-6, MCP-1, IP-10 and KC) analyzed were

in good concordance with the profile of mRNA expression (Figure 3 and Table 2) and protein secretion (Figures 4 and 5) in CEC:bacteria co-culture. Consistent with the profile of constitutive expression of MCP-1, IP-10 and IL-6 mRNA by cultured CEC, it was also possible to demonstrate the constitutive secretion of these cytokines by CEC.

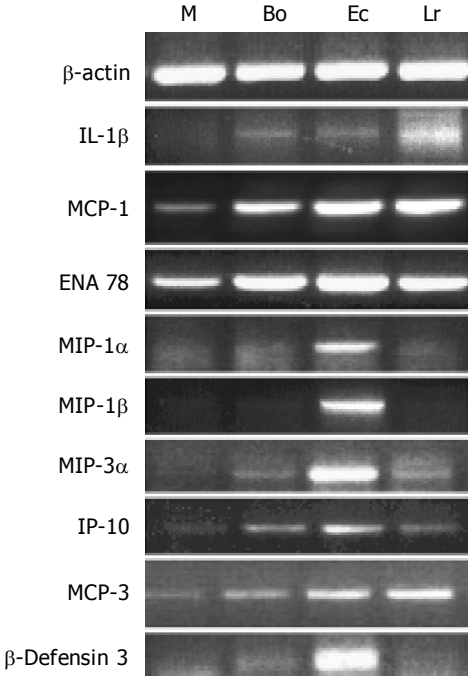

Figure 3 Changes in expression of cytokine genes in CEC in response to commensal bacteria. CECs were cultured for 4 h in complete medium alone (M) or in medium containing *Bacteroides ovatus* (Bo), *E. coli* (Ec) or *Lactobacillus rhamnosus* (Lr) after which RNA was extracted from CECs and processed for RT-PCR analysis using primers for β-actin and genes encoding cytokines and the anti-microbial peptide, β-defensin3 as described in the Materials and methods section. The results shown are typical of those obtained from a total of six independent experiments.

The selectivity of CEC cytokine responses to different bacteria seen at the level of mRNA expression was also seen in TNFα, IL-1β and IP-10 secretion induced or up-regulated by one and/or two but not all three strains of bacteria. The differences in levels of individual cytokines secreted by CEC, which could be seen by comparing levels of TNF-α and IL-1β with KC and IP-10 secretion, varied by almost two orders of magnitude. Clearly, CEC produced some cytokines (e.g., KC and IP-10) at much higher levels than others. In general however, the amounts of cytokine produced by CEC in response to commensal bacteria were lower than those produced by hematopoietic cells. In cases where individual commensal bacteria induced or up-regulated cytokine production by CEC, the same bacteria induced higher levels of production of the same cytokine by splenic macrophages. For example, splenic macrophages produced 5-10-fold higher levels of MIP-1α and IL-6 and 50-80-fold higher levels of MIP-1β, TNF-α and IL-1β. Whereas for other cytokines such as IP-10 and MCP-1, splenic macrophages produced only 2-3-fold higher levels of cytokine (data not shown).

Discrepancies in CEC cytokine mRNA and protein profiles were evident between MIP-1α and MIP-1β. Most striking was MIP-1α for which a single yet different bacterium was identified inducing mRNA accumulation (*E. coli*) and protein secretion (*L. rhamnosus*). Interestingly, MCP-1 protein analysis indicated that the probiotic bacterium *L. rhamnosus* significantly ($P<0.01$) suppressed constitutive cytokine secretion by CEC for which there was no compelling case from the mRNA analysis (Table 2 and Figure 3). Although there was some overlap in MIP-1β mRNA and protein expression by CEC with *E. coli* up-regulating both, this was not the case for *L. rhamnosus* which up-regulated protein secretion in the absence of any influence on mRNA expression.

Probiotic bacterium, L. rhamnosus (LGG), interfered with E. coli- and B. ovatus-induced cytokine production by CEC

Although probiotic therapy has been associated with anti-inflammatory effects in specific groups of IBD patients, the mechanism of action of probiotic bacteria is not clear[26]. Since the probiotic bacterium *L. rhamnosus* (LGG) had a less potent effect on modulating cytokine production by CEC in comparison to *E. coli* and *B. ovatus* (Figure 4 and Table 2), we determined if *L. rhamnosus* could modulate or interfere with CEC cytokine production induced by other bacteria. CEC were therefore cultured with individual bacteria alone or with an equal number of two of the bacteria such that all co-cultures had the same number of bacteria. Combining two different bacteria species had no obvious effect on bacterial viability or growth during the 4 h culture period with the total number of viable bacteria recovered being indistinguishable from co-cultures containing the individual bacteria species alone (Lan and Carding, unpublished data). KC and IL-6 were the cytokines of choice for these experiments since they were produced at high levels by CEC in response to either *E. coli* (KC) or *B. ovatus* (IL-6). These cytokines are also major pro-inflammatory cytokines and they or their human homologs (murine KC and human IL-8) have been associated with inflammation[27,28].

The inclusion of LGG in *E. coli*:CEC cultures effectively reduced the level of KC secreted by CEC by more than 6-fold in response to *E. coli* to that seen in control cultures containing media or LGG alone (Figure 6A). This suppressive effect was dependent upon viable bacteria since non-viable and heat killed *L. rhamnosus* had no effect on *E. coli*-induced KC production (data not shown) and was mediated at the level of KC mRNA transcription or accumulation since the addition of LGG to *E. coli*:CEC co-cultures reduced the amount of KC mRNA expression to levels seen in cultures containing LGG alone (Figure 6A). This suppressive effect was not seen using *B. ovatus* which had no (negative) impact on the amount of KC produced by CEC, in response to *E. coli* in mixed bacteria:CEC co-cultures (Figure 6A). Since *B. ovatus* had little effect on KC production by CEC it was not possible to determine if the suppressive effect of LGG extended to *B. ovatus*. It was however possible to investigate this by analyzing IL-6 production by CEC since *B. ovatus* induced high levels of IL-6 production whereas *E. coli* and LGG had little or no effect on IL-6 production (Figure 4). The addition of LGG to *B. ovatus*:CEC co-cultures effectively neutralized the ability of *B. ovatus* to increase

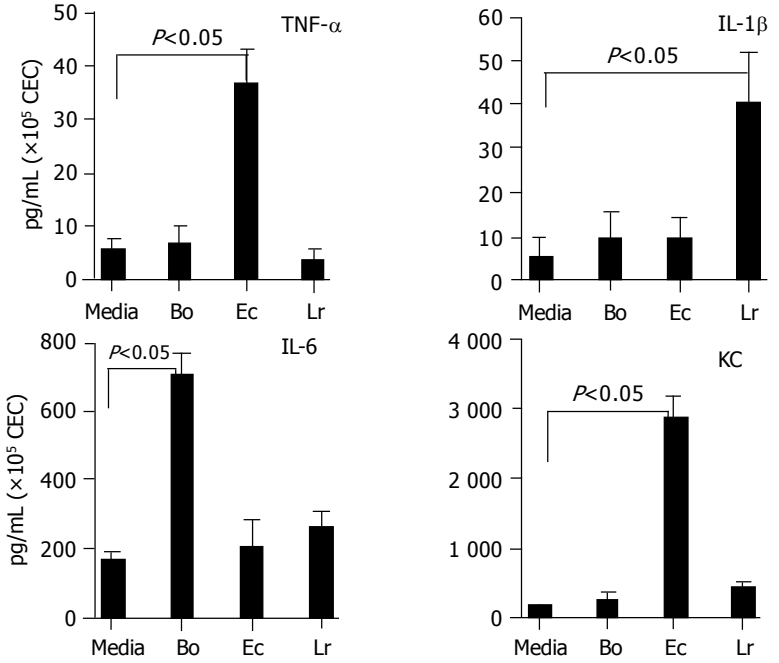

Figure 4 Profile of cytokines secreted by CEC in response to commensal bacteria. CECs were cultured for 4 h in complete medium alone (M) or in medium containing *Bacteroides ovatus* (Bo), *E. coli* (Ec) or *Lactobacillus rhamnosus* (Lr) after which conditioned medium was assayed for the presence of IL-6, TNF-α, IL-1β and KC. The amount of cytokine present was determined by reference to a standard curve generated using known amounts of recombinant protein. The limit of detection of each assay was ~5 pg/mL. The results shown were obtained by combining the data sets from a minimum of three independent experiments. Error bars designate 95% confidence limits.

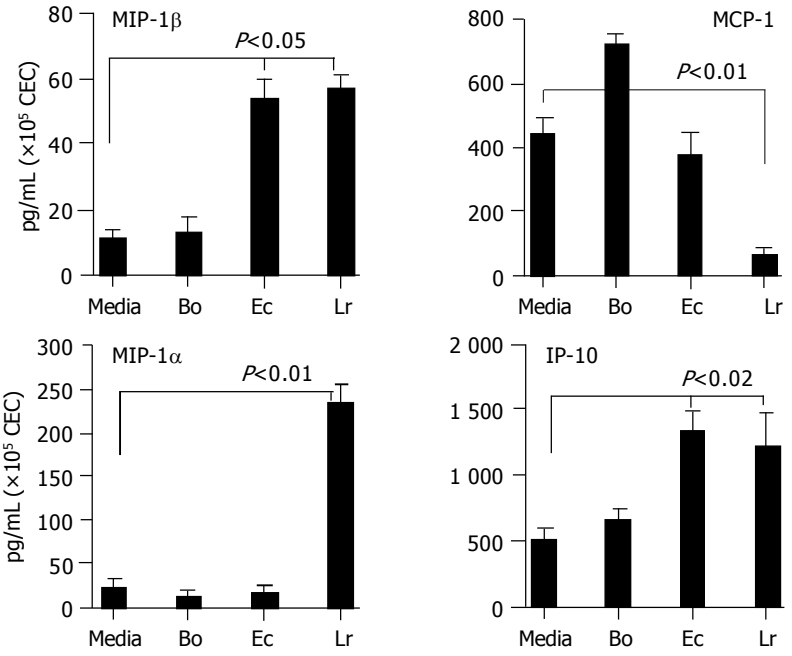

Figure 5 Chemokines secreted by CEC in response to commensal bacteria. CECs were cultured for 4 h in complete medium alone (M) or in medium containing *Bacteroides ovatus* (Bo), *E. coli* (Ec) or *Lactobacillus rhamnosus* (Lr) after which conditioned medium was assayed for the presence of MIP-1α, MIP-1β, IP-10 and MCP-1. The amount of chemokine present was determined by reference to a standard curve generated using known amounts of recombinant protein. The limit of detection of each assay was ~10 pg/mL. The results shown were obtained by combining the data sets from at least three independent experiments. Error bars designate 95% confidence limits.

the level of IL-6 produced by CEC (Figure 6B). As seen for KC production, the effect of LGG on *B. ovatus*-induced IL-6 production appeared to be at the level of gene transcription and/or mRNA turnover. Whereas *B. ovatus* alone dramatically increased the levels of IL-6 mRNA expressed by CEC, in cultures containing both *B. ovatus* and

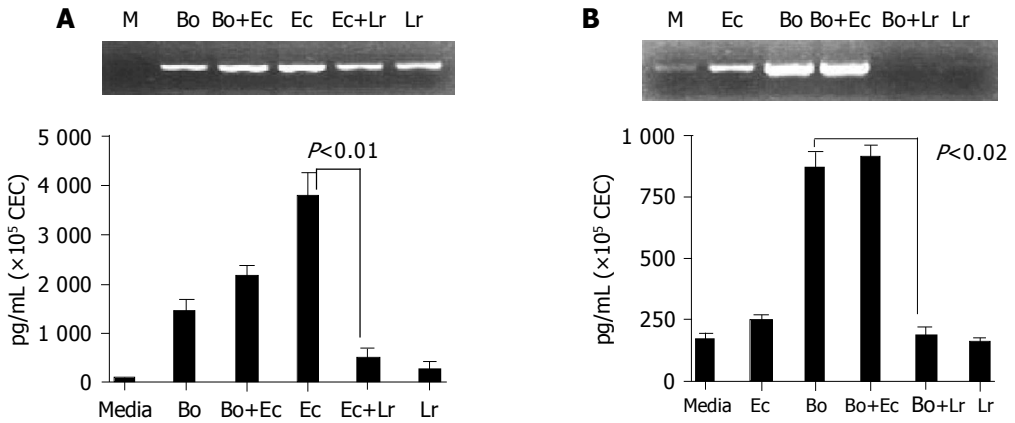

Figure 6 *L. rhamnosus* (LGG) interferes with *E. coli*- and *B. ovatus*-induced cytokine production by CEC. CEC were cultured for 4 h with individual bacteria alone or with a mixture of equal numbers of two different bacteria (*B. ovatus*+ *E. coli* or *E. coli*+*L. rhamnosus*) such that the total number of bacteria in each culture was the same. **A**: KC mRNA and protein expression by RT-PCE and ELISA; **B**: IL-6 mRNA and protein expression by RT-PCR and ELISA. ELISA data was obtained by combining the data sets from three independent experiments. Error bars designate 95% confidence limits.

LGG it was not possible to detect any IL-6 mRNA, which was also undetectable in cultures containing LGG alone (Figure 6B). This suppressive effect on IL-6 production was not seen with *E. coli* which was unable to exert a similar effect on *B. ovatus*-induced IL-6 mRNA or protein production (Figure 6B). These findings demonstrated that the probiotic bacteria LGG could influence and interfere with the interaction of other unrelated commensal bacteria with CEC.

DISCUSSION

This study represents one of the first attempts to investigate the interaction between isolated primary CEC and individual members of the commensal microbiota. A similar and complimentary *in vivo* study using conventionalized germfree mice has previously shown that commensal bacteria can modulate the expression of various (non-immune) genes in ileal IEC *in vivo*[7]. Our study although limited in the number and types of investigated commensal bacteria has focused on the ability of commensal bacteria to modulate expression of immune response-related genes and their products in isolated CEC. By studying CEC in isolation, any indirect effects of other mucosal cells that might occur *in vivo* have effectively been excluded. Our findings demonstrate that CEC have the potential to respond to commensal bacteria and that based upon differences in the cytokines they produce can at least discriminate between the three different bacteria used in this study. The ability of the probiotic bacterium LGG to interfere with the ability of other bacteria to modulate CEC cytokine production was unexpected and may have some relevance to the action of these probiotic bacteria *in vivo*.

Although the CEC:bacteria co-culture system described here provides a controlled *in vitro* accessible system for investigating host-microbe interactions, it is important to acknowledge its limitations. Similar to studies using immortalized IEC lines, our system cannot take into account the possibility that the behavior and response of CEC may normally be influenced directly or indirectly by other mucosal cell populations *in vivo* that are absent or underrepresented in our culture system. Our culture system by its design also cannot account for the complexity of bacterial populations that exist in the colon and as complex biofilms at mucosal epithelial surfaces, the constituents of which remain to be identified and may be uncultivable[14,16]. It should be noted however, that the species of bacteria we have used are major populations in the colon of laboratory rodents and collectively number 3-11×10^{10} organisms per gram of tissue[14,16]. Our culture system also cannot account for any interactions that might occur between different bacteria *in vivo* that might have an impact on the activity of individual bacteria and most likely the host response to them. As we have demonstrated here however, it is possible to compare IEC interactions with individual bacteria alone and in combination with other bacteria. While acknowledging these limitations, we believe our culture system represents an advance in the development of more physiologically relevant *in vitro* systems for investigating the nature of bacteria-IEC interactions. As complimenting existing methodologies can be used its *in vitro* accessibility is an advantage over more indirect and more expensive *in vivo* studies that use conventionalized gnotobiotic animals[29].

The significance of different cytokine responses by CEC to different commensal bacteria *in vitro* is not clear. In considering the limitations and somewhat artificial nature of our experimental system, the data should be interpreted cautiously. Since none of the bacteria used in this study is invasive, it is unlikely to be due to differences in the ability of the bacteria to "infect" CEC. It is possible that the cytokine-inducing activity of different bacteria may be dependent upon them reaching certain and perhaps different concentration thresholds. It may also be related to qualitative or quantitative differences in the MAMPs expressed by the different bacteria. For example, the *E. coli* strain used in this study produced a LPS that has been shown to elicit potent and persistent mucosal immune responses in germfree mice[18]. By contrast the MAMPs expressed by *B. ovatus* are poorly characterized, although the presence of antibodies to *B. ovatus* in the serum of IBD patients[19] suggests that they may not be entirely inert.

The biological significance of probiotic LGG-mediated modulation of cytokine production by CEC is not yet clear,

although its ability to suppress MCP-1 production by CEC could have beneficial effects on limiting or preventing the recruitment to the colonic mucosa of inflammatory cells including granulocytes and activated T cells capable of responding to MCP-1. The ability of LGG to indirectly affect CEC immune responses by interfering with the ability of other commensal bacteria to induce or upregulate cytokine production by CEC identifies CEC as a cellular target for probiotoic bacteria *in vivo*. The ability of probiotic bacteria to down-modulate proinflammatory cytokine (TNF-α and IL-6) production has been demonstrated previously *in vivo*[30] and *ex vivo* in tissue explant:bacteria co-cultures[31]. However, the identity of cells affected by the bacteria and the cellular source(s) of cytokines were not established in these studies. Although the mechanisms of action of probiotics remain unclear[32], their ability to alter the composition of the colonic or fecal microbiota has been associated with beneficial effects in certain groups of IBD patients and infants[26]. In addition, *Lactobacillus* sp. can also prevent the development of intestinal inflammation in animal models of IBD[21,33]. Our findings suggest a mechanism by which non-pathogenic or probitoic bacteria might suppress or limit the ability of other "pathogenic" bacteria to promote or sustain inflammatory responses. How LGG interferes with the ability of *E. coli* or *B. ovatus* to induce cytokine production by CEC was not established in this study. It may include the production of antimicrobial peptides (bacteriocins), expression of MAMPs of higher density, affinity for LGG, induction of TLR anatagonistic signaling pathways or molecules such as phosphoinositide 3-kinase[34], suppressor of cytokine signaling-1[35,36], single immunoglobulin interleukin-1 receptor related molecule[37], or NOD2[38] by LGG in CECs. The CEC:bacteria co-culture system described here may be of value in investigating these potential mechanisms in more detail.

In summary, the results presented in this study provide evidence for the ability of primary CEC to respond to and discriminate between three different strains of commensal bacteria and new insights into the interaction of different commensal bacteria with the host.

ACKNOWLEDGMENTS

The authors thank Dr. John Cebra and Terry Whitehead for providing *E. coli* and *B. ovatus* bacteria.

REFERENCES

1 **Baumgart DC,** Dignass AU. Intestinal barrier function. *Curr Opin Clin Nutr Metab Care* 2002; **5**: 685-694
2 **Hecht G.** Microbes and microbial toxins: paradigms for microbial-mucosal interactions. VII. Enteropathogenic Escherichia coli: physiological alterations from an extracellular position. *Am J Physiol Gastrointest Liver Physiol* 2001; **281**: G1-G7
3 **Melmed G,** Thomas LS, Lee N, Tesfay SY, Lukasek K, Michelsen KS, Zhou Y, Hu B, Arditi M, Abreu MT. Human intestinal epithelial cells are broadly unresponsive to Toll-like receptor 2-dependent bacterial ligands: implications for host-microbial interactions in the gut. *J Immunol* 2003; **170**: 1406-1415
4 **Cario E,** Podolsky DK. Differential alteration in intestinal epithelial cell expression of toll-like receptor 3 (TLR3) and TLR4 in inflammatory bowel disease. *Infect Immun* 2000; **68**: 7010-7017
5 **Fusunyan RD,** Nanthakumar NN, Baldeon ME, Walker WA. Evidence for an innate immune response in the immature human intestine: toll-like receptors on fetal enterocytes. *Pediatr Res* 2001; **49**: 589-593
6 **Hausmann M,** Kiessling S, Mestermann S, Webb G, Spottl T, Andus T, Scholmerich J, Herfarth H, Ray K, Falk W, Rogler G. Toll-like receptors 2 and 4 are up-regulated during intestinal inflammation. *Gastroenterology* 2002; **122**: 1987-2000
7 **Hooper LV,** Wong MH, Thelin A, Hansson L, Falk PG, Gordon JI. Molecular analysis of commensal host-microbial relationships in the intestine. *Science* 2001; **291**: 881-884
8 **Abreu MT,** Vora P, Faure E, Thomas LS, Arnold ET, Arditi M. Decreased expression of Toll-like receptor-4 and MD-2 correlates with intestinal epithelial cell protection against dysregulated proinflammatory gene expression in response to bacterial lipopolysaccharide. *J Immunol* 2001; **167**: 1609-1616
9 **Neish AS,** Gewirtz AT, Zeng H, Young AN, Hobert ME, Karmali V, Rao AS, Madara JL. Prokaryotic regulation of epithelial responses by inhibition of IkappaB-alpha ubiquitination. *Science* 2000; **289**: 1560-1563
10 **Inan MS,** Tolmacheva V, Wang QS, Rosenberg DW, Giardina C. Transcription factor NF-kappaB participates in regulation of epithelial cell turnover in the colon. *Am J Physiol Gastrointest Liver Physiol* 2000; **279**: G1282-G1291
11 **Haller D,** Bode C, Hammes WP, Pfeifer AM, Schiffrin EJ, Blum S. Non-pathogenic bacteria elicit a differential cytokine response by intestinal epithelial cell/leucocyte co-cultures. *Gut* 2000; **47**: 79-87
12 **Baumgart DC,** Olivier WA, Reya T, Peritt D, Rombeau JL, Carding SR. Mechanisms of intestinal epithelial cell injury and colitis in interleukin 2 (IL2)-deficient mice. *Cell Immunol* 1998; **187**: 52-66
13 **Telega GW,** Baumgart DC, Carding SR. Uptake and presentation of antigen to T cells by primary colonic epithelial cells in normal and diseased states. *Gastroenterology* 2000; **119**: 1548-1559
14 **Savage DC.** Microbial ecology of the gastrointestinal tract. *Annu Rev Microbiol* 1977; **31**: 107-133
15 **McGee D.** Inflammation and mucosal cytokine production In: Ogra P, Mestecky J, lamm ME, Strober W, Bienenstock J, McGhee JR, eds. Mucosal Immunology. *San Diego*: *Academic Press* 1999: 559-573
16 **Savage DC.** Gastrointestinal microflora of rodents In: Ruitenberg EJ, Peters PWJ, eds. Handbook on Animal Production. VolC2. *Amsterdam*: *Elsevier* 1985: 85-117
17 **Ahrne S,** Nobaek S, Jeppsson B, Adlerberth I, Wold AE, Molin G. The normal Lactobacillus flora of healthy human rectal and oral mucosa. *J Appl Microbiol* 1998; **85**: 88-94
18 **Moreau MC,** Ducluzeau R, Guy-Grand D, Muller MC. Increase in the population of duodenal immunoglobulin A plasmocytes in axenic mice associated with different living or dead bacterial strains of intestinal origin. *Infect Immun* 1978; **21**: 532-539
19 **Saitoh S,** Noda S, Aiba Y, Takagi A, Sakamoto M, Benno Y, Koga Y. Bacteroides ovatus as the predominant commensal intestinal microbe causing a systemic antibody response in inflammatory bowel disease. *Clin Diagn Lab Immunol* 2002; **9**: 54-59
20 **Cebra J,** Cebra E, Shahin R. Perturbations in specific B cell subsets following deliberate contamination in germfree or natural colonization of mice by intestinal flora In: Ryc C, Franek J, eds. Bacteria and the host. *Prague*: *Avicenum* 1986: 303-307
21 **Madsen KL,** Doyle JS, Jewell LD, Tavernini MM, Fedorak RN. Lactobacillus species prevents colitis in interleukin 10 gene-deficient mice. *Gastroenterology* 1999; **116**: 1107-1114
22 **Holzapfel WH,** Haberer P, Snel J, Schillinger U, Huis in't Veld JH. Overview of gut flora and probiotics. *Int J Food Microbiol* 1998; **41**: 85-101

23 **Ajuebor MN,** Swain MG. Role of chemokines and chemokine receptors in the gastrointestinal tract. *Immunology* 2002; **105**: 137-143
24 **Dwinell MB,** Johanesen PA, Smith JM. Immunobiology of epithelial chemokines in the intestinal mucosa. *Surgery* 2003; **133**: 601-607
25 **Banks C,** Bateman A, Payne R, Johnson P, Sheron N. Chemokine expression in IBD. Mucosal chemokine expression is unselectively increased in both ulcerative colitis and Crohn's disease. *J Pathol* 2003; **199**: 28-35
26 **Vaarala O.** Immunological effects of probiotics with special reference to lactobacilli. *Clin Exp Allergy* 2003; **33**: 1634-1640
27 **Bozic CR,** Kolakowski LF, Gerard NP, Garcia-Rodriguez C, von Uexkull-Guldenband C, Conklyn MJ, Breslow R, Showell HJ, Gerard C. Expression and biologic characterization of the murine chemokine KC. *J Immunol* 1995; **154**: 6048-6057
28 **Boisvert WA,** Curtiss LK, Terkeltaub RA. Interleukin-8 and its receptor CXCR2 in atherosclerosis. *Immunol Res* 2000; **21**: 129-137
29 **Gordon HA,** Pesti L. The gnotobiotic animal as a tool in the study of host microbial relationships. *Bacteriol Rev* 1971; **35**: 390-429
30 **Schultz M,** Linde HJ, Lehn N, Zimmermann K, Grossmann J, Falk W, Scholmerich J. Immunomodulatory consequences of oral administration of Lactobacillus rhamnosus strain GG in healthy volunteers. *J Dairy Res* 2003; **70**: 165-173
31 **Borruel N,** Carol M, Casellas F, Antolin M, de Lara F, Espin E, Naval J, Guarner F, Malagelada JR. Increased mucosal tumour necrosis factor alpha production in Crohn's disease can be downregulated *ex vivo* by probiotic bacteria. *Gut* 2002; **51**: 659-664
32 **Ghosh S,** van Heel D, Playford RJ. Probiotics in inflammatory bowel disease: is it all gut flora modulation? *Gut* 2004; **53**: 620-622
33 **Mao Y,** Nobaek S, Kasravi B, Adawi D, Stenram U, Molin G, Jeppsson B. The effects of *Lactobacillus* strains and oat fiber on methotrexate-induced enterocolitis in rats. *Gastroenterology* 1996; **111**: 334-344
34 **Fukao T,** Koyasu S. PI3K and negative regulation of TLR signaling. *Trends Immunol* 2003; **24**: 358-363
35 **Nakagawa R,** Naka T, Tsutsui H, Fujimoto M, Kimura A, Abe T, Seki E, Sato S, Takeuchi O, Takeda K, Akira S, Yamanishi K, Kawase I, Nakanishi K, Kishimoto T. SOCS-1 participates in negative regulation of LPS responses. *Immunity* 2002; **17**: 677-687
36 **Kinjyo I,** Hanada T, Inagaki-Ohara K, Mori H, Aki D, Ohishi M, Yoshida H, Kubo M, Yoshimura A. SOCS1/JAB is a negative regulator of LPS-induced macrophage activation. *Immunity* 2002; **17**: 583-591
37 **Wald D,** Qin J, Zhao Z, Qian Y, Naramura M, Tian L, Towne J, Sims JE, Stark GR, Li X. SIGIRR, a negative regulator of Toll-like receptor-interleukin 1 receptor signaling. *Nat Immunol* 2003; **4**: 920-927
38 **Watanabe T,** Kitani A, Murray PJ, Strober W. NOD2 is a negative regulator of Toll-like receptor 2-mediated T helper type 1 responses. *Nat Immunol* 2004; **5**: 800-808

Science Editor Wang XL and Guo SY **Language Editor** Elsevier HK

PO Box 2345, Beijing 100023, China
www.wjgnet.com
wjg@wjgnet.com

ELSEVIER

World J Gastroenterol 2005;11(22):3385-3391
World Journal of Gastroenterology ISSN 1007-9327

• *BASIC RESEARCH* •

Activation of JAK-STAT pathway is required for platelet-derived growth factor-induced proliferation of pancreatic stellate cells

Atsushi Masamune, Masahiro Satoh, Kazuhiro Kikuta, Noriaki Suzuki, Tooru Shimosegawa

Atsushi Masamune, Masahiro Satoh, Kazuhiro Kikuta, Noriaki Suzuki, Tooru Shimosegawa, Division of Gastroenterology, Tohoku University Graduate School of Medicine, Sendai, Japan
Supported by the grant-in-aid of Encouragement of Young Scientists from Japan Society for the Promotion of Science, No. 16590572, Pancreas Research Foundation of Japan No. 01-01, and the Kanae Foundation for Life and Socio-Medical Science
Correspondence to: Dr. Atsushi Masamune, Division of Gastroenterology, Tohoku University Graduate School of Medicine, 1-1 Seiryo-cyo, Aoba-ku, Sendai 980-8574, Japan. amasamune@int3.med.tohoku.ac.jp
Telephone: +81-22-717-7171 Fax: +81-22-717-7177
Received: 2004-08-26 Accepted: 2004-08-27

Abstract

AIM: To clarify the role of Janus kinase-signal transducers and activators of transcription (JAK-STAT) pathway in platelet-derived growth factor (PDGF) induced proliferation in activated pancreatic stellate cells (PSCs).

METHODS: PSCs were isolated from rat pancreas tissue, and used in their culture-activated, myofibroblast-like phenotype. STAT-specific binding activity was assessed by electrophoretic mobility shift assay. Activation of Src, JAK2, STAT1, STAT3, and ERK was determined by Western blotting using anti-phosphospecific antibodies. Cell proliferation was assessed by measuring the incorporation of 5-bromo-2′-deoxyuridine.

RESULTS: PDGF-BB induced STAT-specific binding activity, and activation of Src, JAK2, STAT1, STAT3, and ERK. Ethanol and acetaldehyde at clinically relevant concentrations decreased basal activation of JAK2 and STAT3. PDGF-induced activation of STAT1 and STAT3 was inhibited by a Src inhibitor PP1 and a JAK2 inhibitor AG490, whereas PDGF-induced activation of ERK was inhibited by PP1, and not by AG490. PDGF-induced proliferation was inhibited by PP1 and AG490 as well as by STAT3 antisense oligonucleotide.

CONCLUSION: PDGF-BB activated JAK2-STAT pathway via Src-dependent mechanism. Activation of JAK2-STAT3 pathway, in addition to ERK, may play a role in PDGF-induced proliferation of PSCs.

Key words: Pancreatitis; Pancreatic fibrosis; Pancreatic stellate cells; Platelet-derived growth factor; Janus kinase; Signal transducers and activators of transcription

Masamune A, Satoh M, Kikuta K, Suzuki N, Shimosegawa T. Activation of JAK-STAT pathway is required for platelet-derived growth factor-induced proliferation of pancreatic stellate cells. *World J Gastroenterol* 2005; 11(22): 3385-3391
http://www.wjgnet.com/1007-9327/11/3385.asp

INTRODUCTION

In 1998, star-shaped cells in the pancreas, namely pancreatic stellate cells (PSCs), were identified and characterized[1,2]. In normal pancreas, stellate cells are quiescent and can be identified by the presence of vitamin A-containing lipid droplets in the cytoplasm. In response to pancreatic injury or inflammation, they are transformed ("activated") from their quiescent phenotype into myofibroblast-like cells which actively proliferate, express α-smooth muscle actin, and produce type I collagen and other extracellular matrix components. There is accumulating evidence that activated PSCs play a pivotal role in the development of pancreatic fibrosis[1-4]. It has also been suggested that PSCs may participate in the pathogenesis of acute pancreatitis[3,5]. The molecular mechanisms responsible for PSC activation remain to be elucidated, but the activation of signaling pathways such as p38 mitogen-activated protein (MAP) kinase[6], Rho-Rho kinase pathway[7], and c-Jun N-terminal kinase[8] is likely to play a role. However, intracellular signaling pathways in PSCs remain largely unknown.

Stellate cell proliferation and expansion of their pool are a fundamental feature of pancreatic fibrosis[3]. Platelet-derived growth factor (PDGF) is one of the most potent mitogen of PSCs, and is likely to be an important mediator of the increased proliferation of the cells both *in vivo* and *in vitro*[9,10]. PDGF is a polypeptide growth factor that exists as a disulfide-linked homodimer (PDGF-AA or -BB) or a heterodimer (PDGF-AB) of two chains, A or B[11,12]. Two PDGF receptor subtypes bind to the three isoforms of PDGF differentially; PDGF β-receptor can interact only with B-chain containing isoforms whereas PDGF α-receptor can bind to all three isoforms. Binding of the ligands to the receptors leads to dimerization of receptor subunits, phosphorylates itself on tyrosines (known as "autophosphorylation"), changes its cytoplasmic conformation, activates endogenous tyrosine phosphorylating activity, and initiates intracellular signaling[11,12]. It has been shown that activation of extracellular signal-regulated kinase (ERK) plays a critical role in PDGF-induced proliferation of PSCs[13,14]. But, the fact that activation of ERK was required though not sufficient for PSC proliferation[15] suggests that other signaling pathways might be involved. Janus-activated kinases (JAKs) are a group

of non-receptor tyrosine kinases that, via phosphorylation, modulate the activities of a group of transcription factors, viz. signal transducers and activators of transcription (STAT)[16,17]. The STAT proteins exist in a latent form in the cytoplasm, and, upon receptor activation by cytokines and growth factors, become phosphorylated on tyrosine residues[16,17]. This phosphorylation results in translocation of the STATs to the nucleus, where they bind to sequence-specific DNA elements[16]. Recent studies have shown that activation of JAK2-STAT3 pathway mediates PDGF-induced proliferation in several types of cells such as NIH3T3 fibroblasts[18], human airway smooth muscle cells[19], and rat vascular smooth muscle cells[20]. But, possible regulation of cell functions by JAK-STAT pathway in PSCs is unknown.

In this study, we examined the role of JAK-STAT pathway in PSC proliferation in response to PDGF-BB. We report here that PDGF-BB activated JAK2-STAT3 pathway via Src-dependent mechanism, and that activation of this pathway is required for PDGF-induced PSC proliferation.

MATERIALS AND METHODS

Materials

Poly(dI.dC)-poly(dI.dC) and [γ-^{32}P]ATP were purchased from Amersham Biosciences UK, Ltd. (Buckinghamshire, UK). Rat recombinant PDGF-BB was obtained from R&D Systems (Minneapolis, MN, USA). Rabbit antibodies against phosphorylated Src, phosphorylated JAK2, STAT1 (phosphorylated at Tyr^{701} and total), STAT3 (phosphorylated at Tyr^{705} and total), and ERK (phosphorylated and total) were purchased from Cell Signaling Technology Inc. (Beverly, MA). Rabbit antibody against glyceraldehyde-3-phosphate dehydrogenase (GAPDH) was obtained from Trevigen (Gaithersburg, MD). AG490 and U0126 were purchased from Calbiochem (La Jolla, CA). PP1 and rabbit antibody against phosphorylated PDGF β-receptor were obtained from Upstate Biotechnology Inc. (Lake Placid, NY). All other reagents were purchased from Sigma-Aldrich (St. Louis, MO) unless specifically described.

Cell culture

All animal procedures were performed in accordance with the National Institutes of Health Animal Care and Use Guidelines. Rat PSCs were prepared from the pancreas tissues of male Wistar rats (Japan SLC Inc., Hamamatsu, Japan) weighing 200-250 g as previously described using the Nycodenz solution (Nycomed Pharma, Oslo, Norway) after perfusion with 0.3 g/L collagenase P[14]. The cells were resuspended in Ham's F-12 containing 100 mL/L heat-inactivated fetal bovine serum (ICN Biomedicals, Aurora, OH), penicillin sodium, and streptomycin sulfate. Cell purity was always more than 90% as assessed by a typical star-like configuration and by detecting vitamin A autofluorescence. All experiments were performed using cells between passages two and five. Unless specifically described, we incubated PSCs in serum-free medium for 24 h before the addition of experimental reagents.

Immunostaining

Serum-starved PSCs were grown directly on slides, and immunostaining for PDGF β-receptor was performed as previously described using a streptavidin-biotin-peroxidase complex detection kit (Histofine Kit; Nichirei, Tokyo, Japan). Briefly, cells were fixed with 1 000 mL/L methanol for 10 min at -20 ℃, and then endogenous peroxidase activity was blocked by incubation in methanol with 3 mL/L hydrogen peroxide for 5 min. After immersion in normal goat serum for 1 h, the slides were incubated with rabbit anti-PDGF β-receptor antibody overnight at 4 ℃. The slides were incubated with biotinylated goat anti-rabbit Ig antibody for 45 min, followed by peroxidase-conjugated streptavidin for 30 min. Finally, color was developed by incubating the slides for several min with diaminobenzidine (Dojindo, Kumamoto, Japan). For a negative control, the primary antibody was replaced with non-immune rabbit IgG.

Western blotting

Western blotting was performed as previously described[21]. Cells were treated with PDGF-BB and lysed in sodium dodecyl sulfate (SDS) buffer. Cellular proteins (approximately 100 μg) were fractionated on a 100 g/L SDS-polyacrylamide gel, and transferred to a nitrocellulose membrane (Bio-Rad, Hercules, CA). The level of activated, phosphorylated STAT3 was determined by Western blotting using anti-phosphospecific STAT3 antibody. The antibody recognizes only phosphorylated form of STAT3, thus allowing the assessment of activation of the kinase. After incubation with a secondary antibody (goat anti-rabbit, horseradish peroxidase conjugated), proteins were visualized by using an ECL kit (Amersham Biosciences UK, Ltd.). The levels of total STAT3, phosphorylated PDGF β-receptor, phosphorylated Src, phosphorylated JAK2, STAT1 (phosphorylated and total), ERK (phosphorylated and total), and GAPDH were also determined in a similar manner.

Nuclear extracts preparation and electrophoretic mobility shift assay

Nuclear extracts were prepared after 15 min treatment, and electrophoretic mobility shift assay was performed as previously described[22]. Double-stranded STAT consensus oligonucleotide probe m67 (5'-CATTTCCCGTAAATC-3') was endlabeled with [γ-^{32}P]ATP. m67 is a high-affinity mutant of the sis-inducible element of the human c-*fos* gene, and binds to STAT1 and STAT3[23]. Nuclear extracts (approximately 5 μg) were incubated with the labeled oligonucleotide probe for 20 min at 22 ℃, and electrophoresed through a 40 g/L polyacrylamide gel. Gels were dried, and autoradiographed at -80 ℃ overnight. A 100-fold excess of unlabeled oligonucleotide was incubated with nuclear extracts for 10 min prior to the addition of the radiolabeled probe in the competition experiments. For super shift assays, nuclear extracts were incubated for 1 h at 4 ℃ with antibodies against STAT1 or STAT3 before incubation with the radiolabeled probe.

Cell proliferation assay

Cell proliferation was assessed using a commercial kit (Cell proliferation ELISA, BrdU; Roche Diagnostics, Mannheim, Germany) according to the manufacturer's instruction. This is a colorimetric immunoassay based on the measurement of 5-bromo-2'-deoxyuridine (BrdU) incorporation during

DNA synthesis. After 24-h incubation with experimental reagents, cells were labeled with BrdU for 3 h at 37 ℃. Cells were then fixed, and incubated with peroxidase-conjugated anti-BrdU antibody. Then the peroxidase substrate 3,3',5,5'-tetramethylbenzidine was added, and BrdU incorporation was quantitated by $A_{370\text{-}492}$.

Antisense oligonucleotide transfection

The antisense, phosphorothioated 21-mer oligonucleotides directed against the translation start site (AUG codon) and surrounding nucleotides of the rat STAT1 gene and STAT3 genes were synthesized by SigmaGenosys, Ishikari, Japan. The STAT1 antisense oligonucleotide sequence was 5'-CCACTGCGACATCCTCTTTAA-3' and the corresponding sense oligonucleotide sequence was 5'-TTAAAGAGGAT-GTCGCAGTGG-3'. The STAT3 antisense oligonucleotide sequence was 5'-CCACTGAGCCATCCTGCCGCA-3' and the corresponding sense oligonucleotide sequence was 5'-TGCGGCAGGAYGGCTCAGTGG-3'. Serum-starved PSCs were treated with sense, antisense, or scramble oligonucleotides (5'-CAAATGGGCTCCGACGTCGGT-3') in the presence of FUGENE6 (Roche Diagnostics). After 24 h, cells were stimulated with PDGF-BB (at 25 ng/mL) for another 24 h, and proliferation was assessed by the incorporation of BrdU as described before.

Statistical analysis

The results were expressed as mean±SD. Luminograms and photographs are representative of at least three experiments. Differences between the groups were evaluated by ANOVA, followed by Fisher's test for post hoc analysis. A *P*-value less than 0.05 was considered statistically significant.

RESULTS

Activated PSCs expressed PDGF-receptor

We first examined the expression of PDGF-receptor in PSCs by immunostaining. Culture-activated PSCs expressed PDGF β-receptor (Figure 1A). Negative control using non-immune rabbit IgG in place of the specific antibody gave little staining (data not shown). The PDGF receptors dimerize, and become autophosphorylated on tyrosine residues upon binding to their ligands[12]. Indeed, PDGF-BB induced tyrosine phosphorylation of the PDGF β-receptor in a time-dependent manner (Figure 1B). In this study, the isoform PDGF-BB was selected for use because the previous study reported that PDGF-AA had little effect on PSC proliferation[9].

PDGF-BB activated STAT1 and STAT3

We examined whether PDGF-BB activated STAT pathway. PDGF-BB increased STAT-specific DNA binding activity as assessed by electrophoretic mobility shift assay (Figure 2A). The specificity of the DNA binding activity was demonstrated by the addition of a 100-fold molar excess of unlabeled STAT oligonucleotide, and not by unrelated Oct-1 oligonucleotide in competition assays (Figure 2A, data not shown). Specific antibodies against STAT1 and STAT3 retarded the DNA–protein complex, indicating that the complex consisted of STAT1 and STAT3. We also examined whether PDGF-BB activated STAT1 and STAT3 by Western blotting using anti-phosphospecific antibodies. PDGF-BB activated STAT1 and STAT3 in a time-dependent manner, with peaking around 5-15 min (Figure 2B).

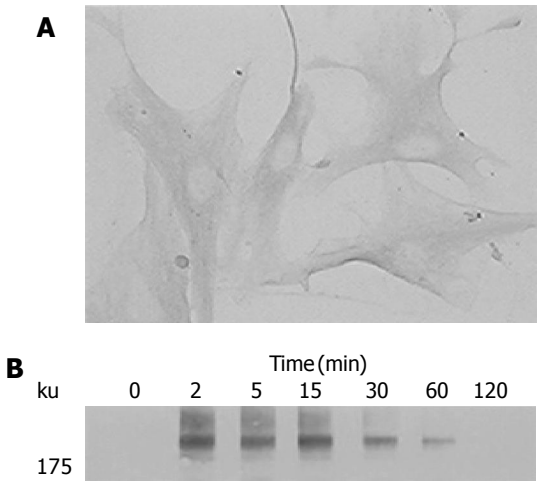

Figure 1 Activated PSCs expressed PDGF β-receptor. **A:** Serum-starved, culture-activated PSCs were grown directly on slides. Immunostaining for PDGF β-receptor was performed using a streptavidin-biotin-peroxidase complex detection kit. Original magnification: ×20 objective; **B:** Serum-starved PSCs were treated with PDGF-BB (at 25 ng/mL) for the indicated time. Total cell lysates were prepared, and separated by 70 g/L SDS-polyacrylamide gel electrophoresis. The phosphorylation of PDGF β-receptor was examined by Western blotting.

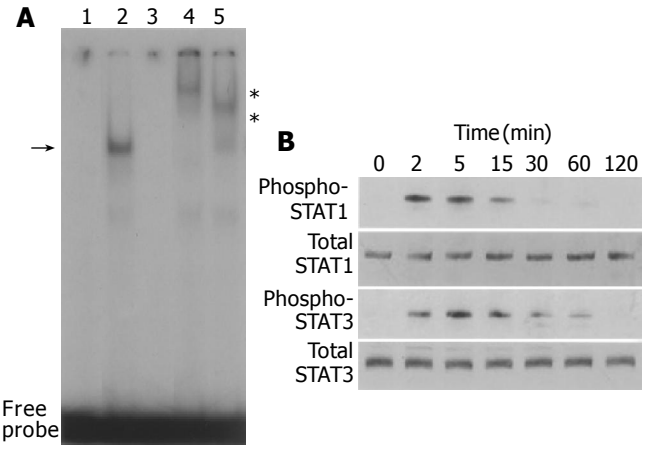

Figure 2 PDGF activated STAT1 and STAT3. **A:** PSCs were treated with PDGF-BB (at 25 ng/mL, lane 2) in serum-free medium for 15 min. Nuclear extracts were prepared and subjected to electrophoretic mobility shift assay using STAT consensus oligonucleotide probe m67. Arrow denotes specific inducible complex competitive with cold double-stranded oligonucleotide probe (lane 3). For super shift assays, nuclear extracts were incubated with antibodies against STAT1 (lane 4) or STAT3 (lane 5) before incubation with the radiolabeled probe. *: super shifts. Lane 1: control (serum-free medium only); **B:** PSCs were treated with PDGF-BB (at 25 ng/mL) for the indicated time. Total cell lysates (approximately 100 μg) were prepared, and separated by 100 g/L SDS-polyacrylamide gel electrophoresis. The activation of STAT1 and STAT3 was examined by Western blotting using anti-phosphospecific antibodies. The levels of total STAT1 and STAT3 were also determined.

Src and JAK2 mediate activation of STAT1 and STAT3

The mechanism of growth factor-induced activation of STAT is not fully elucidated; JAK, Src, and receptor tyrosine kinases might all be involved[24]. PDGF-BB induced phosphorylation

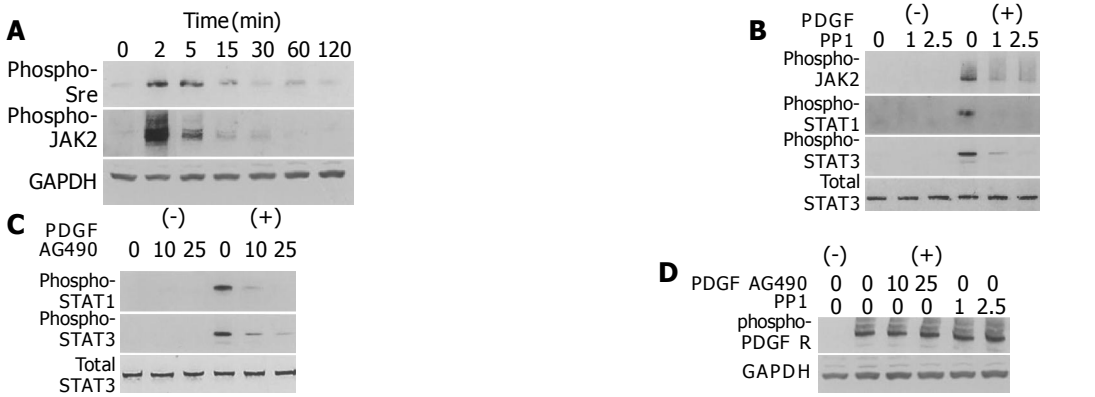

Figure 3 Src and JAK2 mediate the activation of STAT1 and STAT3. **A:** PSCs were treated with PDGF-BB (at 25 ng/mL) for the indicated time. Total cell lysates (approximately 100 μg) were prepared, and separated by 100 g/L SDS-polyacrylamide gel electrophoresis. The activation of Src and JAK2 was examined by Western blotting using anti-phosphospecific antibodies. The level of GAPDH was also determined; **B-D:** PSCs were treated with a Src inhibitor PP1 (at 1 or 2.5 μmol/L) or a JAK2 inhibitor AG490 (at 10 or 25 μmol/L) in the absence or presence of PDGF-BB (at 25 ng/mL) for 5 min. Total cell lysates (approximately 100 μg) were prepared, and the levels of phosphorylated JAK2, STAT1, STAT3, and PDGF β-receptor were determined by Western blotting. The levels of total STAT3 and GAPDH were also determined.

of Src and JAK2 in a time-dependent manner (Figure 3A). To determine which kinase(s) mediates PDGF-induced activation of STAT1 and STAT3, we employed specific inhibitors of Src and JAK2. Pretreatment of PSCs with a specific Src inhibitor PP1[25] inhibited STAT1 and STAT3 activation as well as that of JAK2 (Figure 3B). Pretreatment of PSCs with AG490, a specific JAK2 kinase inhibitor[26], also blocked PDGF-BB-induced STAT1 and STAT3 activation (Figure 3C). These inhibitory effects were not due to the cytotoxicity, because these reagents did not affect the viability assessed by trypan blue dye exclusion test (data not shown). Neither AG490 nor PP1 inhibited autophosphorylation of the PDGF β-receptor (Figure 3D). Thus, the activation of STAT1 and STAT3 by PDGF-BB required the activation of both JAK and Src, and Src was located upstream of JAK for PDGF signaling in PSCs.

Ethanol and acetaldehyde decreased basal activation of JAK2 and STAT3

We have previously shown that ethanol and acetaldehyde at clinically relevant concentrations activated ERK, but did not induce proliferation of PSCs[15]. We examined whether ethanol and acetaldehyde activated JAK-STAT pathway. Ethanol and acetaldehyde at clinically relevant concentrations (50 mmol/L and 200 mmol/L, respectively) decreased basal activation of JAK2 and STAT3 in a time-dependent manner (Figure 4). The basal activation of STAT1 could not be detected even after long exposure.

Activation of Src, JAK2, and STAT3 is required for PDGF-BB-induced proliferation

In agreement with the previous studies showing that PDGF-BB is a potent mitogen for PSCs[9,10], PDGF-BB increased PSCs proliferation as assessed by BrdU incorporation (Figure 5A). This increase in BrdU incorporation was inhibited by AG490 and PP1, suggesting that JAK2 and Src kinases are required for proliferation.

To clarify the role of STAT1 and STAT3 in PDGF-BB-induced proliferation we employed STAT1 and STAT3 antisense oligonucleotides. STAT1 and STAT3 antisense

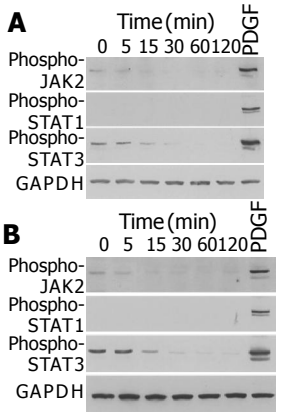

Figure 4 Ethanol and acetaldehyde decreased basal activation of JAK2 and STAT3. PSCs were treated with ethanol (at 50 mmol/L, panel **A**) or acetaldehyde (at 200 mmol/L, panel **B**) for the indicated time, or with PDGF-BB (at 25 ng/mL) for 5 min. Total cell lysates (approximately 100 μg) were prepared, and separated by 100 g/L SDS-polyacrylamide gel electrophoresis. The activation of JAK2, STAT1, and STAT3 was examined by Western blotting using anti-phosphospecific antibodies. The level of GAPDH was also determined.

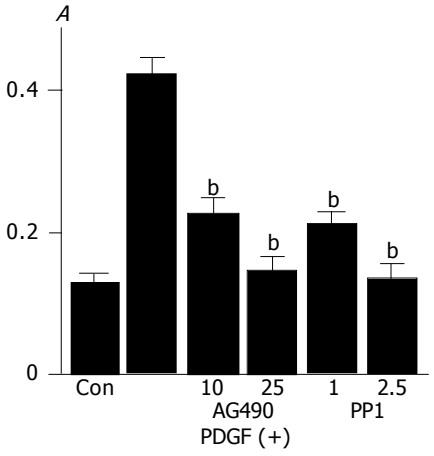

Figure 5 Activation of Src and JAK2 is required for PDGF-induced proliferation and serum-starved PSCs were treated with PDGF-BB (at 25 ng/mL) in the presence or absence of AG490 (at 10 or 25 μmol/L) or PP1 (at 1 or 2.5 μmol/L). After 24-h incubation, DNA synthesis was assessed by BrdU incorporation ELISA. Data are shown as mean±SD (n = 6). $^bP<0.01$ versus PDGF-BB only. Con: control (serum-free medium only), *A*: optical density.

oligonucleotides directed against their translation initiation sites prevented the synthesis of STAT1 and STAT3, respectively (Figure 6A). PDGF-induced proliferation was abolished by the transfection of STAT3 antisense oligonucleotide, and not of STAT1 antisense oligonucleotide (Figure 6B).

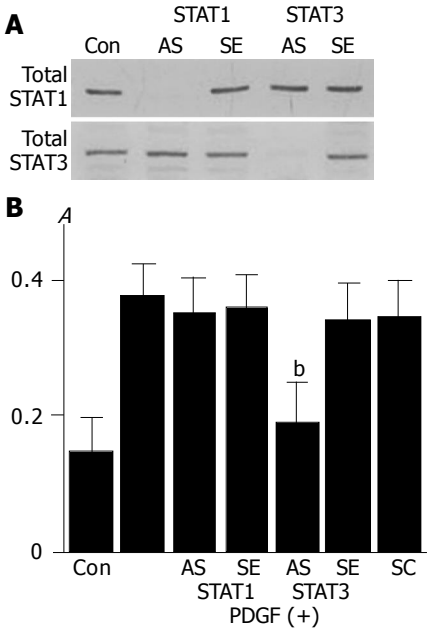

Figure 6 Activation of STAT3, and not STAT1, is required for PDGF-induced proliferation. **A:** PSCs were treated with antisense ("AS") or sense ("SE") oligonucleotides for STAT1 or STAT3 for 24 h. The expression of total STAT1 and STAT3 was examined by Western blotting; **B:** PSCs were treated with sense, antisense, or scramble ("SC") oligonucleotides. After 24 h, cells were stimulated with PDGF-BB (at 25 ng/mL) for another 24 h, and DNA synthesis was assessed by BrdU incorporation enzyme-linked immunosorbent assay. Data are shown as mean±SD (% of the control, n = 6). $^bP<0.01$ *vs* PDGF-BB only. Con: control (serum-free medium only), *A*: optical density.

Src, not JAK2, is located upstream of ERK

It has been reported that activation of ERK pathway plays critical roles in PDGF-induced proliferation of PSCs[13,14]. We examined whether PP1 and AG490 inhibited PSC proliferation through the inhibition of ERK activation. AG490 did not affect PDGF-BB-induced activation of ERK (Figure 7A). PP1, however, did inhibit PDGF-BB-induced activation of ERK (Figure 7B). On the other hand, U0126, an inhibitor of MAP kinase kinase and consequent ERK activation[27], did not affect the activation of STAT1, and STAT3 (Figure 7C). Thus, ERK and JAK2-STAT3 pathways exert independent regulatory effects on PDGF-induced proliferation in PSCs.

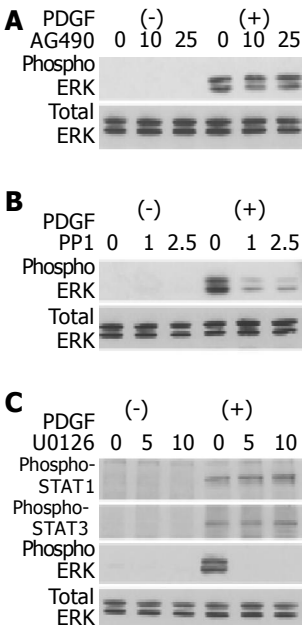

Figure 7 Src, not JAK2, is located upstream of ERK. PSCs were treated with a JAK2 inhibitor AG490 (**A**) (at 10 or 25 μmol/L), a Src inhibitor PP1 (**B**) (at 1 or 2.5 μol/L), or a MAP kinase kinase inhibitor U0126 (**C**) (at 5 or 10 μmol/L) in the absence or presence of PDGF-BB (at 25 ng/mL) for 5 min. Total cell lysates were prepared, and the levels of phosphorylated ERK, STAT1, and STAT3 were determined by Western blotting. The level of total ERK was also determined.

DISCUSSION

Stellate cell proliferation and expansion of their pool are a fundamental feature of pancreatic fibrosis[3]. PDGF-BB has been shown to be one of the most potent mitogens of PSCs *in vitro*[9,10]. It has been reported that activation of ERK pathway plays a critical role in PDGF-induced proliferation of PSCs[13,14]. On the other hand, we have previously reported that ethanol and acetaldehyde at clinically relevant concentrations activated ERK, but failed to induce proliferation in PSCs[15], suggesting that other signaling pathways might be involved in this process as well. In this study, we examined the role of JAK-STAT pathway in PDGF-induced proliferation of PSCs. We showed here that PDGF induced the activation of Src, JAK2, STAT1, and STAT3 in PSCs. JAK proteins phosphorylate STAT proteins at tyrosine residues and activate them, although other mechanisms might be involved[28,29]. In PSCs, the activation of STAT1 and STAT3 was inhibited by a Src kinase inhibitor PP1 and a JAK2 kinase inhibitor AG490, suggesting that the activation of STAT was dependent on Src and JAK2. PDGF-induced proliferation was inhibited by PP1, AG490, and STAT3 antisense oligonucleotide, and not by STAT1 antisense oligonucleotide. Thus, activation of Src-JAK2-STAT3 pathway plays a role in PDGF-induced proliferation in PSCs. Although STAT pathway has been shown to play a role in proliferative responses in some cell types[18-20], no previous studies have examined whether STAT pathway is activated and it regulates cell functions in PSCs. Detailing STAT signaling in PSCs is important because regulation and functions of STATs differ greatly depending on the cell type. Our results are in agreement with the previous studies showing a role of this pathway in the regulation of cell growth in several cell types including NIH3T3 fibroblasts[18], human airway smooth muscle cells[19], and rat vascular smooth muscle cells[20].

We showed here that culture-activated PSCs expressed PDGF β-receptor. During tissue repair and inflammatory processes in the pancreas, PDGF is secreted by various cells including platelets, mononuclear cells, and activated macrophages[30]. Exposure of PSCs to PDGF *in vivo* is likely to occur in conditions of pancreatic inflammation characterized by the presence of platelets and activated macrophages[2,10]. PDGF-induced effects on PSCs *in vivo* may be further aided

by the upregulation of PDGF receptors in PSCs. In this regard, it is of interest to note that in a rat model of pancreatic fibrosis, immunostaining for PDGF β-receptor was found to be increased in activated PSCs in the area of fibrosis[3]. Codistribution of PDGF with cells expressing its receptor confirms a functional role of PDGF in the development of pancreatic fibrosis.

In addition to ERK[13,14], this study indicates that the Src-JAK2-STAT3 pathway is also required for proliferation in PSCs. The STAT pathway has been shown to interact with MAP kinase pathway in different cellular context. For example, the STAT transcription factors are a potential convergence site for the MAP kinase and JAK kinase pathways; JAKs phosphorylate STATs on tyrosine, leading to dimerization and nuclear localization, whereas MAP kinase phosphorylates STAT1 and STAT3 on serine, leading to maximal transcriptional activation[17,31]. Considering that PDGF activates multiple signaling pathways, including phosphatidylinositol 3-kinase and the MAP kinase pathway in PSCs[13,14], it is possible that Src-JAK2-STAT3 pathway cooperates with these signaling pathways in mediating the proliferative response in PSCs. Inhibition of Src by PP1 blocked the activation of ERK as well as of JAK2-STAT3, suggesting that Src is located upstream of ERK. This is consistent with the previous report that Src kinase is upstream of ERK activation and can participate in Raf activation[32]. Although AG490 was effective in blocking STAT3 activation and proliferation, it did not have any apparent effect on PDGF-induced ERK activation. On the other hand, inhibition of ERK by U0126 abolished PDGF-induced proliferation, but not the activation of JAK2 and STAT3. Collectively, Src is a potential convergence site for the MAP kinase and JAK-STAT pathway, and each pathway may exert independent regulatory effects on PDGF-induced proliferation in PSCs (Figure 8).

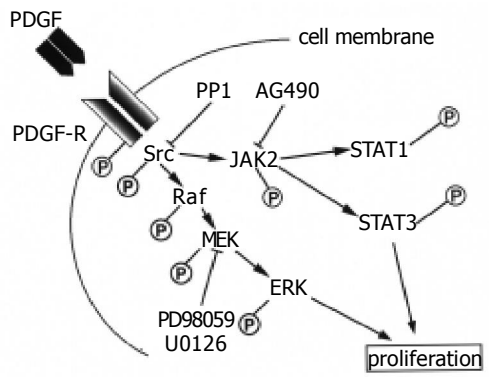

Figure 8 Signaling pathways for PDGF-induced proliferation in PSCs.

Although it has been shown that PDGF activates STAT1 in hepatic stellate cells[33], no previous studies have addressed the role of JAK-STAT pathway in the proliferative response in PSCs or hepatic stellate cells. We showed here that PDGF activated STAT1 and STAT3 in PSCs. Although STAT3 appears to play a role in proliferation in PSCs, the responsible mechanisms for STAT3-mediated proliferation remain obscure. Potential STAT target genes for mediating PDGF-induced proliferation of PSCs include the immediate-early gene c-*myc*, the cell cycle regulatory gene cyclin D_1, and the anti-apoptotic genes Bcl-2 and Bcl-x[34]. In vascular smooth muscle cells, it has been recently shown that induction of cytosolic phospholipase A_2 expression and arachidonic acid release are involved in PDGF-BB-stimulated cell growth and that these events are mediated by JAK2-dependent STAT3 activation[20]. Along this line, PDGF-induced PSC proliferation was blocked by AACOCF3, an inhibitor of cytosolic phospholipase A_2 (Masamune *et al*, unpublished observation).

We have previously shown that ethanol and acetaldehyde at clinically relevant concentrations activated ERK, but did not induce proliferation of PSCs[15]. We showed here that, unlike PDGF, ethanol and acetaldehyde did not induce the activation of JAK-STAT pathway. Interestingly, ethanol and acetaldehyde decreased basal activation of JAK2 and STAT3 in PSCs. This is in agreement with the previous study showing that ethanol inhibited the activation of STAT3 in rat hepatocytes[35]. It is possible that failure of proliferation induction by ethanol and acetaldehyde may be attributable to the failure of JAK-STAT pathway activation. Obviously, further studies are required to test this hypothesis.

It remains unknown as to the role of STAT1 in the cell functions of PSCs. In addition to its roles in cell immunity, proliferation, apoptosis, and transformation, recent studies have suggested that STAT1 participates in the development of fibrosis. For example, STAT1 mediates transforming growth factor-β and fibronectin synthesis in response to high glucose in glomerular mesangial cells[36]. STAT1 as well as STAT3 mediate thrombin-induced upregulation of tissue type inhibitor metalloproteinase-1 in human glomerular mesangial cells[37]. Interestingly, Weiskirchen *et al*, reported that LIM-domain protein cysteine- and glycine-rich protein 2 (CRP2) is a potential new factor in the JAK-STAT pathway in hepatic stellate cells[38]. The protein inhibitor of activated STAT1 was shown to be selectively associated with the C-terminal LIM domain of CRP2, and the suppression of CRP2 might be a prerequisite for the myofibroblastic transition of hepatic stellate cells. Further studies are necessary to clarify the role of altered expression of STAT1 and CRP2 in the activation process of PSCs.

In summary, we have shown that PDGF activated STAT1 and STAT3, and that the activation of JAK2-STAT3 pathway plays a role in the PDGF-induced proliferation of PSCs. A better understanding of the molecular mechanisms of PSC proliferation may provide more rational targets for the treatment of patients with pancreatic fibrosis and inflammation.

REFERENCES

1 **Apte MV,** Haber PS, Applegate TL, Norton ID, McCaughan GW, Korsten MA, Pirola RC, Wilson JS. Periacinar stellate shaped cells in rat pancreas: identification, isolation and culture. *Gut* 1998; **43**: 128-133

2 **Bachem MG,** Schneider E, Gross H, Weidenbach H, Schmid RM, Menke A, Siech M, Beger H, Grunert A, Adler G. Identification, culture, and characterization of pancreatic stellate cells in rats and humans. *Gastroenterology* 1998; **115**: 421-432

3 **Haber PS,** Keogh GW, Apte MV, Moran CS, Stewart NL, Crawford DH, Pirola RC, McCaughan GW, Ramm GA, Wilson JS. Activation of pancreatic stellate cells in human

and experimental pancreatic fibrosis. *Am J Pathol* 1999; **155**: 1087-1095

4 **Masamune A,** Kikuta K, Satoh M, Sakai Y, Satoh A, Shimosegawa T. Ligands of peroxisome proliferator-activated receptor-gamma block activation of pancreatic stellate cells. *J Biol Chem* 2002; **277**: 141-147

5 **Masamune A,** Sakai Y, Kikuta K, Satoh M, Satoh A, Shimosegawa T. Activated rat pancreatic stellate cells express intercellular adhesion molecule-1(ICAM-1) *in vitro*. *Pancreas* 2002; **25**: 78-85

6 **Masamune A,** Satoh M, Kikuta K, Sakai Y, Satoh A, Shimosegawa T. Inhibition of p38 mitogen-activated protein kinase blocks activation of rat pancreatic stellate cells. *J Pharmacol Exp Ther* 2003; **304**: 8-14

7 **Masamune A,** Kikuta K, Satoh M, Satoh K, Shimosegawa T. Rho kinase inhibitors block activation of pancreatic stellate cells. *Br J Pharmacol* 2003; **140**: 1292-1302

8 **Masamune A,** Kikuta K, Suzuki N, Satoh M, Satoh K, Shimosegawa T. A c-Jun NH2-terminal kinase inhibitor SP600125 (anthra[1,9-cd]pyrazole-6 (2H)-one) blocks activation of pancreatic stellate cells. *J Pharmacol Exp Ther* 2004; **310**: 520-527

9 **Apte MV,** Haber PS, Darby SJ, Rodgers SC, McCaughan GW, Korsten MA, Pirola RC, Wilson JS. Pancreatic stellate cells are activated by proinflammatory cytokines: implications for pancreatic fibrogenesis. *Gut* 1999; **44**: 534-541

10 **Luttenberger T,** Schmid-Kotsas A, Menke A, Siech M, Beger H, Adler G, Grunert A, Bachem MG. Platelet-derived growth factors stimulate proliferation and extracellular matrix synthesis of pancreatic stellate cells: implications in pathogenesis of pancreas fibrosis. *Lab Invest* 2000; **80**: 47-55

11 **Williams LT.** Signal transduction by the platelet-derived growth factor receptor. *Science* 1989; **243**: 1564-1570

12 **Claesson-Welsh L.** Platelet-derived growth factor receptor signals. *J Biol Chem* 1994; **269**: 32023-32026

13 **Jaster R,** Sparmann G, Emmrich J, Liebe S. Extracellular signal regulated kinases are key mediators of mitogenic signals in rat pancreatic stellate cells. *Gut* 2002; **51**: 579-584

14 **Masamune A,** Kikuta K, Satoh M, Kume K, Shimosegawa T. Differential roles of signaling pathways for proliferation and migration of rat pancreatic stellate cells. *Tohoku J Exp Med* 2003; **199**: 69-84

15 **Masamune A,** Kikuta K, Satoh M, Satoh A, Shimosegawa T. Alcohol activates activator protein-1 and mitogen-activated protein kinases in rat pancreatic stellate cells. *J Pharmacol Exp Ther* 2002; **302**: 36-42

16 **Darnell JE.** STATs and gene regulation. *Science* 1997; **277**: 1630-1635

17 **Imada K,** Leonard WJ. The Jak-STAT pathway. *Mol Immunol* 2000; **37**: 1-11

18 **Bowman T,** Broome MA, Sinibaldi D, Wharton W, Pledger WJ, Sedivy JM, Irby R, Yeatman T, Courtneidge SA, Jove R. Stat3-mediated Myc expression is required for Src transformation and PDGF-induced mitogenesis. *Proc Natl Acad Sci USA* 2001; **98**: 7319-7324

19 **Simon AR,** Takahashi S, Severgnini M, Fanburg BL, Cochran BH. Role of the JAK-STAT pathway in PDGF-stimulated proliferation of human airway smooth muscle cells. *Am J Physiol Lung Cell Mol Physiol* 2002; **282**: L1296-L1304

20 **Yellaturu CR,** Rao GN. Cytosolic phospholipase A2 is an effector of Jak/STAT signaling and is involved in platelet-derived growth factor BB-induced growth in vascular smooth muscle cells. *J Biol Chem* 2003; **278**: 9986-9992

21 **Masamune A,** Satoh K, Sakai Y, Yoshida M, Satoh A, Shimosegawa T. Ligands of peroxisome proliferator-activated receptor-gamma induce apoptosis in AR42J cells. *Pancreas* 2002; **24**: 130-138

22 **Masamune A,** Igarashi Y, Hakomori S. Regulatory role of ceramide in interleukin(IL)-1 beta-induced E-selectin expression in human umbilical vein endothelial cells. Ceramide enhances IL-1 beta action, but is not sufficient for E-selectin expression. *J Biol Chem* 1996; **271**: 9368-9375

23 **Ward AC,** Hermans MH, Smith L, van Aesch YM, Schelen AM, Antonissen C, Touw IP. Tyrosine-dependent and -independent mechanisms of STAT3 activation by the human granulocyte colony-stimulating factor (G-CSF) receptor are differentially utilized depending on G-CSF concentration. *Blood* 1999; **93**: 113-124

24 **Vignais ML,** Sadowski HB, Watling D, Rogers NC, Gilman M. Platelet-derived growth factor induces phosphorylation of multiple JAK family kinases and STAT proteins. *Mol Cell Biol* 1996; **16**: 1759-1769

25 **Amoui M,** Draber P, Draberova L. Src family-selective tyrosine kinase inhibitor, PP1, inhibits both Fc epsilonRI- and Thy-1-mediated activation of rat basophilic leukemia cells. *Eur J Immunol* 1997; **27**: 1881-1886

26 **Meydan N,** Grunberger T, Dadi H, Shahar M, Arpaia E, Lapidot Z, Leeder JS, Freedman M, Cohen A, Gazit A, Levitzki A, Roifman CM. Inhibition of acute lymphoblastic leukaemia by a Jak-2 inhibitor. *Nature* 1996; **379**: 645-648

27 **Favata MF,** Horiuchi KY, Manos EJ, Daulerio AJ, Stradley DA, Feeser WS, Van Dyk DE, Pitts WJ, Earl RA, Hobbs F, Copeland RA, Magolda RL, Scherle PA, Trzaskos JM. Identification of a novel inhibitor of mitogen-activated protein kinase kinase. *J Biol Chem* 1998; **273**: 18623-18632

28 **Nguyen H,** Ramana CV, Bayes J, Stark GR. Roles of phosphatidylinositol 3-kinase in interferon-gamma-dependent phosphorylation of STAT1 on serine 727 and activation of gene expression. *J Biol Chem* 2001; **276**: 33361-33368

29 **Sachsenmaier C,** Sadowski HB, Cooper JA. STAT activation by the PDGF receptor requires juxtamembrane phosphorylation sites but not Src tyrosine kinase activation. *Oncogene* 1999; **18**: 3583-3592

30 **Ross R.** Platelet-derived growth factor. *Lancet* 1989; **1**: 1179-1182

31 **Finbloom DS,** Larner AC. Regulation of the Jak/STAT signalling pathway. *Cell Signal* 1995; **7**: 739-745

32 **Goi T,** Shipitsin M, Lu Z, Foster DA, Klinz SG, Feig LA. An EGF receptor/Ral-GTPase signaling cascade regulates c-Src activity and substrate specificity. *EMBO J* 2000; **19**: 623-630

33 **Kawada N,** Uoya M, Seki S, Kuroki T, Kobayashi K. Regulation by cAMP of STAT1 activation in hepatic stellate cells. *Biochem Biophys Res Commun* 1997; **233**: 464-469

34 **Stephanou A,** Latchman DS. STAT-1: a novel regulator of apoptosis. *Int J Exp Pathol* 2003; **84**: 239-244

35 **Chen J,** Kunos G, Gao B. Ethanol rapidly inhibits IL-6-activated STAT3 and C/EBP mRNA expression in freshly isolated rat hepatocytes. *FEBS Lett* 1999; **457**: 162-168

36 **Wang X,** Shaw S, Amiri F, Eaton DC, Marrero MB. Inhibition of the Jak/STAT signaling pathway prevents the high glucose-induced increase in tgf-beta and fibronectin synthesis in mesangial cells. *Diabetes* 2002; **51**: 3505-3509

37 **Chen X,** Liu W, Wang J, Wang X, Yu Z. STAT1 and STAT3 mediate thrombin-induced expression of TIMP-1 in human glomerular mesangial cells. *Kidney Int* 2002; **61**: 1377-1382

38 **Weiskirchen R,** Moser M, Weiskirchen S, Erdel M, Dahmen S, Buettner R, Gressner AM. LIM-domain protein cysteine- and glycine-rich protein 2 (CRP2) is a novel marker of hepatic stellate cells and binding partner of the protein inhibitor of activated STAT1. *Biochem J* 2001; **359**: 485-496

Science Editor Li WZ **Language Editor** Elsevier HK

PO Box 2345, Beijing 100023, China
www.wjgnet.com
wjg@wjgnet.com

ELSEVIER

World J Gastroenterol 2005;11(22):3392-3397
World Journal of Gastroenterology ISSN 1007-9327

• *BASIC RESEARCH* •

Establishment and characterization of an opisthorchiasis-associated cholangiocarcinoma cell line (KKU-100)

Banchob Sripa, Saman Leungwattanawanit, Takayuki Nitta, Chaisiri Wongkham, Vajarabhongsa Bhudhisawasdi, Anucha Puapairoj, Chongrak Sripa, Masanao Miwa

Banchob Sripa, Saman Leungwattanawanit, Anucha Puapairoj, Chongrak Sripa, Department of Pathology, Faculty of Medicine, Khon Kaen University, Khon Kaen 40002, Thailand
Takayuki Nitta, Masanao Miwa, Institute of Basic Medical Science, University of Tsukuba, Ibaraki 305-8575, Tsukuba, Japan
Chaisiri Wongkham, Department of Biochemistry, Faculty of Medicine, Khon Kaen University, Khon Kaen 40002, Thailand
Vajarabhongsa Bhudhisawasdi, Department of Surgery, Faculty of Medicine, Khon Kaen University, Khon Kaen 40002, Thailand
Banchob Sripa, Chaisiri Wongkham, Vajarabhongsa Bhudhisawasdi, Anucha Puapairoj, Liver Fluke and Cholangiocarcinoma Research Center, Khon Kaen University, Khon Kaen 40002, Thailand
Supported by the Faculty of Medicine, Khon Kaen University, Thailand
Correspondence to: Dr. Banchob Sripa, Department of Pathology, Faculty of Medicine, Khon Kaen University, Khon Kaen, 40002, Thailand. banchob@kku.ac.th
Telephone: +66-43-202024 Fax: +66-43-348375
Received: 2004-06-30 Accepted: 2004-08-02

Abstract

AIM: To establish and characterize a new cholangiocarcinoma cell line from a patient living in the *Opisthorchis viverrini* (*O. viverrini*) endemic area of Northeast Thailand.

METHODS: Fresh liver biopsy and bile specimens were obtained from a 65-year-old Thai woman with cholangiocarcinoma of the *porta hepatis*. After digestion, the cells were cultured in Ham's F12 media. The established cell line was then characterized for growth kinetics, cell morphology, immunocytochemistry and cytogenetics. Tumorigenicity of the cell line was determined by heterotransplanting in nude mice.

RESULTS: The primary tumor was a poorly differentiated tubular adenocarcinoma. Examination of the bile revealed malignant cells with *O. viverrini* eggs. The cholangiocarcinoma cell line KKU-100 was established 4 mo after the primary culture-population doubling time was 72 h. KKU-100 possesses compact and polygonal-shaped epithelial cells. Immunocytochemically, this cell line exhibited cytokeratin, EMA, CEA, and CA125, but not α-fetoprotein (AFP), CA19-9, desmin, c-met, or p53. Such protein expressions parallel those of the primary tumor. Cytogenetic analysis identified aneuploidy karyotypes with a modal chromosome number of 78 and marked chromosomal structural changes. Inoculation of KKU-100 cells into nude mice produced a transplantable, poorly differentiated aden-ocarcinoma, similar to the original tumor.

CONCLUSION: KKU-100 is the first egg-proven, *Opisthorchis*-associated cholangiocarcinoma cell line, which should prove useful for further investigations of the tumor biology of this cancer.

Key words: Cholangiocarcinoma; Cell line; Establishment; Characterization; Opisthorchiasis

Sripa B, Leungwattanawanit S, Nitta T, Wongkham C, Bhudhisawasdi V, Puapairoj A, Sripa C, Miwa M. Establishment and characterization of an opisthorchiasis-associated cholangiocarcinoma cell line (KKU-100). *World J Gastroenterol* 2005; 11(22): 3392-3397
http://www.wjgnet.com/1007-9327/11/3392.asp

INTRODUCTION

Cholangiocarcinoma is rare but its prevalence in Northeast Thailand makes the region the area of highest incidence in the world[1]. Coincidentally, Thailand has a high prevalence of infection of the liver fluke, *Opisthorchis viverrini*, and an estimated six million people are infected[2]. Both experimental and epidemiological evidence implicate opisthorchiasis in the etiology of cholangiocarcinoma in this endemic area[3,4]. Cumulative data suggest that the pathogenesis of this bile duct cancer in this region is different from that observed in Western countries with different etiologies[4]. However, the detailed mechanisms of the cellular and molecular pathogenesis of *Opisthorchis*-associated cholangiocarcinoma and its biology are unclear.

Human solid tumor cell lines are important sources for studies of tumor biology including tumor cell growth, differentiation, metastasis, molecular pathogenesis, and susceptibility to drugs. A small number of reports, compared to other cancers, describing cholangiocarcinoma cell lines have been published, most from extrahepatic cholangiocarcinoma[5-9] and a few from intrahepatic cholangiocarcinoma[9,10-13]. Only one cholangiocarcinoma cell line was developed from a Thai[14]. We therefore aimed to establish more cholangiocarcinoma cell lines from patients living in Northeast Thailand. Our report describes the establishment and characterization of an egg-proven, *Opisthorchis*-associated cholangiocarcinoma cell line, developed in our laboratory and designated as KKU-100.

MATERIALS AND METHODS

Patient

A 65-year old Thai woman was admitted to the Faculty of

Medicine, Srinagarind Hospital, Khon Kaen University, Thailand. She arrived with nausea, progressive jaundice and itching. She was previously diagnosed by ultrasonography at a provincial hospital as having cholangiocarcinoma. Significant laboratory investigations at admission showed elevated alkaline phosphatase (ALP) (266 U/mL, normal 42-120 U/mL), total bilirubin (23.1 mg/mL, normal 0.25-1.5 mg/mL), carcinoembryonic antigens (CEA) (44.6 ng/mL, normal <2.5 ng/mL), while the serum α-fetoprotein (AFP) (2.8 U/mL, normal <10 U/mL), HBsAg and HBsAg were negative. The stool examination revealed *O. viverrini* eggs. The serum counterpart was positive for the parasite-specific antibody using ELISA.

The diagnosis of cholangiocarcinoma was confirmed by ultrasonography, computer tomography, and endoscopic retrograde cholangiopancreatography (ERCP). Operative findings revealed skipped tumor lesions at the *porta hepatis* with bile duct obstruction and ascites (approximately 1 000 mL). The cul-de-sac, peritoneum and bowel wall were tumor free. A bilateral peripheral hepatojejunostomy (Roux-en-Y) with cystojejunostomy was the palliative treatment performed. Liver biopsy of the tumor mass was taken, the histopathology indicated a poorly differentiated tubular adenocarcinoma. Biliary cytology revealed clusters of tumor cells with *O. viverrini* eggs. The patient developed sepsis and died two follow-ups after surgery. Informed consent was obtained from the patient.

Establishment of tumor cell line

The liver biopsy was transported to the Department of Pathology immediately after surgery and used for cell culture. The tumor tissue was aseptically washed in Ham's F12 media (Seromed, Berlin, Germany) containing penicillin (200 U/mL) and streptomycin (200 μg/mL), minced, then digested with 0.25% trypsin-EDTA (Gibco/BRL, Grand Island, MA) for 1 h at 37 ℃. After dissociation, the tissue fragments were force-filtered through a 100-μm pore mesh and the cell suspension was washed in the media 2-3 times to remove any residual blood. The washed cells were then cultured in Ham's F12 containing penicillin (100 U/mL) and streptomycin (100 μg/mL) with 20% fetal bovine serum (Gibco/ BRL) at 37 ℃ with 50 mL/L CO_2, the media were changed twice, weekly. Cultured tumor cells were observed daily under a phase-contrast microscope (Olympus, Tokyo, Japan). Contaminating fibroblasts were periodically removed with a cell scraper (Costar, Cambridge, MA) and by differential trypsinization.

Growth kinetics

After establishment, growth kinetics of the tumor cells was obtained by seeding the cells at 2×10^5 cells/well in duplicate in a 24-well plate (Nunc, Roskilde, Denmark). After seeding, the media were changed every two days. The cells were detached from the wells with trypsin-EDTA and the average number of viable cells was counted every 24 h in a hemacytochamber in the presence of trypan-blue dye. Cells were counted for up to 12 d. The doubling time of the cell population was estimated during the logarithmic growth phase.

Morphology

Tissue culture flasks were routinely monitored for cell morphology under a phase-contrast microscope.

Heterotransplantation

Four- to six-week-old athymic nude mice (BALB/cAnNCrj-nu/nu) were used for heterotransplantation. The mice were injected subcutaneously with KKU-100 cells (1×10^7 cells) suspended in culture medium and kept under specific pathogen-free conditions. The tumor was observed every week and when it reached a diameter of ⩾1.5 cm, the mice were killed. The tumor was minced and transplanted again to other nude mice for serial transplantation. A portion of tumor was fixed in 10% buffered formalin, routinely processed for histopathology and immunocytochemistry.

Immunocytochemistry

To characterize the expression of cytokeratin, tumor markers and some gene products, the cells were grown as a confluent monolayer, washed in cold PBS, then scraped. After centrifugation, the cell pellet was fixed in buffered formalin and routinely processed in a cell block. Paraffin sections were cut and immunostained for cytokeratin, CEA, AFP, CA125, CA19-9, c-met and p53 using the standard avidin-biotin peroxidase method[15]. Details of the antibodies are shown in Table 1. Mouse monoclonal antibody to pancytokeratins (Dako, Denmark, clone MNF 116) reacts with cytokeratins 5, 6, 8, 17, and probably 19 as shown in the specification sheet of the manufacturer. Primary and heterotransplanted tumors were similarly immunostained.

Cytogenetics

After 20 passages, the established tumor cells at the exponential phase were subjected to chromosomal analysis by treating them with 0.1 μg/mL colcemid (Gibco/BRL). The cells were treated with a KCl/HEPES/EDTA hypotonic solution and harvested according to standard cytogenetic procedures. Slides of fixed cells were trypsin-Giemsa-banded to identify individual metaphase chromosomes. Representative chromosome sets were photographed and karyotyped. The modal chromosome number was determined from 100 cells.

Mycoplasma detection

Direct agar incubation of spent medium using a mycoplasma agar plate (Gibco/BRL) was routinely performed to detect any mycoplasma contamination.

RESULTS

Establishment of KKU-100 cell line

A few days after the primary culture, a few single colonies of epithelial-like round cells and fibroblasts attached to the 25 mL culture flask. The colonies were inactive and stable for several weeks while fibroblasts grew faster. Fibroblasts were periodically removed by scraping. Three months after the cell culture was initiated, the epithelial-like cells became active and propagated as monolayer cells. The colonies were then subcultured with trypsin-EDTA. Contaminating fibroblasts were removed by scraping and differential trypsinization. After four successive passages, a pure tumor cell line with continuous, stabilized multiplication was established and designated as KKU-100. The cell line KKU-100 was

maintained in our laboratory in >100 passages over the past 5 years.

Growth kinetics

KKU-100 cells followed a typical growth curve, including lag, logarithmic and stationary phases during the 12-d culture. By the tenth passage, the population doubling time in Ham's F12 with 10% fetal bovine serum, was approximately 72 h.

Morphology of KKU-100

Under a phase-contrast microscope, KKU-100 exhibited compact, monotonous polygonal to spindle cells. The cells were 'floating' or 'clumping' in a confluent monolayer that could be shaken free, mixed into the medium and transferred to another flask (Figure 1). Individual KKU-100 cells had a large nucleus containing 2-5 nucleoli and a clear cytoplasm.

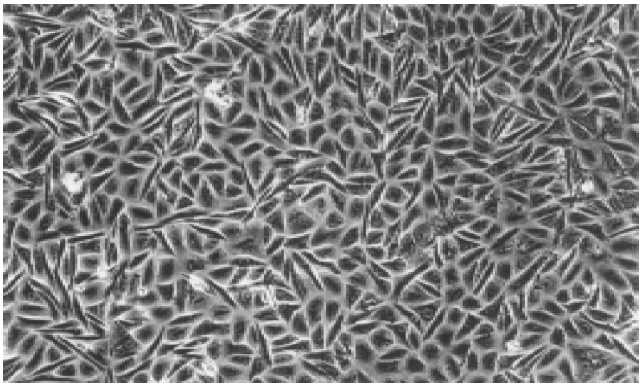

Figure 1 A confluent monolayer of KKU-100 cells shows compact polygonal to spindle cells. (Phase-contrast, original magnification, ×100).

Heterotransplantation

Tumor nodules were developed in the nude mice three weeks after inoculation of KKU-100 cells and reached their greatest dimension of 1.6 cm in 10 wk. Serial transplantations into other nude mice had a shorter induction time for tumor nodules and grew larger. The second generation of transplanted tumors developed one week post inoculation and reached a maximum size of 4.4 cm in 10 wk. Histologically, the transplanted tumor was a poorly differentiated adenocarcinoma, similar to the primary tumor (Figures 2A and B).

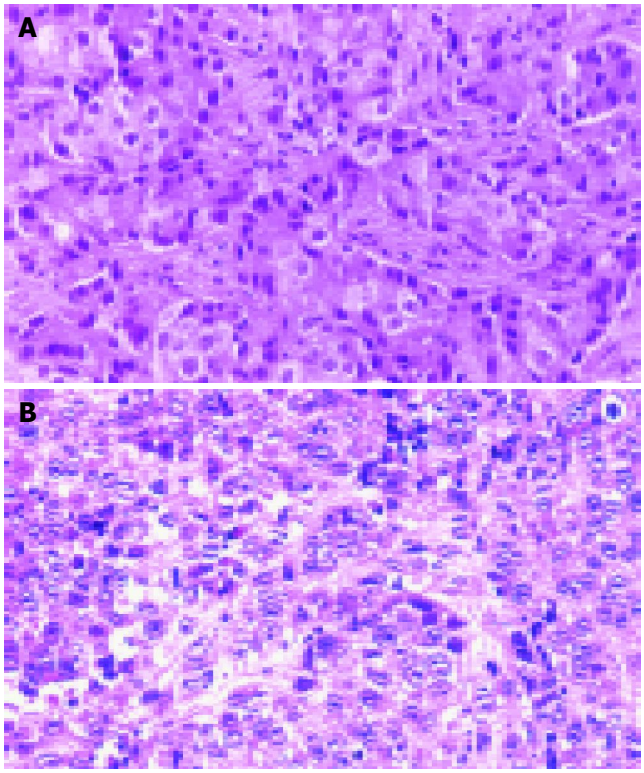

Figure 2 Histopathology of the primary tumor (**A**) and KKU-100 heterotransplanted tumors (**B**) in nude mice. (hematoxylin and eosin, original magnification ×200).

Immunocytochemistry

Expression and grading of cellular antigens, tumor markers and cancer gene products of the original tumor and KKU-100 cells are shown in Table 1. KKU-100 cells expressed cytokeratin, EMA, CEA, and CA125 but not AFP, CA19-9, desmin, c-met and p53. These protein expressions were similar to those of the primary tumor. However, heterotransplanted tumors in nude mice retained only EMA protein (Figures 3A-D and Table 1).

Chromosomal analysis

A cytogenetics study revealed a number of chromosomes ranging between 56 and 92 with a modal chromosome number of 78. The G-banded analysis demonstrated aneuploidy karyotype with marked chromosomal structural abnormalities. Several marker chromosomes were noted. Example of the karyotype is shown in Figure 4.

Table 1 Details of antibodies used and their expression in primary tumor, KKU-100 cells and heterotransplanted tumors

Antibodies	Sources	Primary tumor[1]	KKU-100 cells[1]	Heterotrans-planted tumor[1]
Cytokeratin (clone MNF116)	Dako, Denmark	+++	++	-
EMA (clone E29)	Dako, Denmark	++	++	+++
Desmin (clone D33)	Dako, Denmark	-	-	-
CEA (polyclonal)	Dako, Denmark	+++	+	-
AFP (polyclonal)	Dako, Denmark			
CA19-9 (clone 116-NS-19-9)	Dako, Denmark	-	-	-
CA125 (clone Ov185:1)	Novocastra, UK	+++	+	-
c-Met (polyclonal)	Santa Cruz, USA	-	-	-
p53 (clone DO-7)	Dako, Denmark	-	-	-

[1]Grading: - = negative, + = <25% tumor cell stained, ++ = 25-50% tumor cell stained, +++ = >50% tumor cell stained.

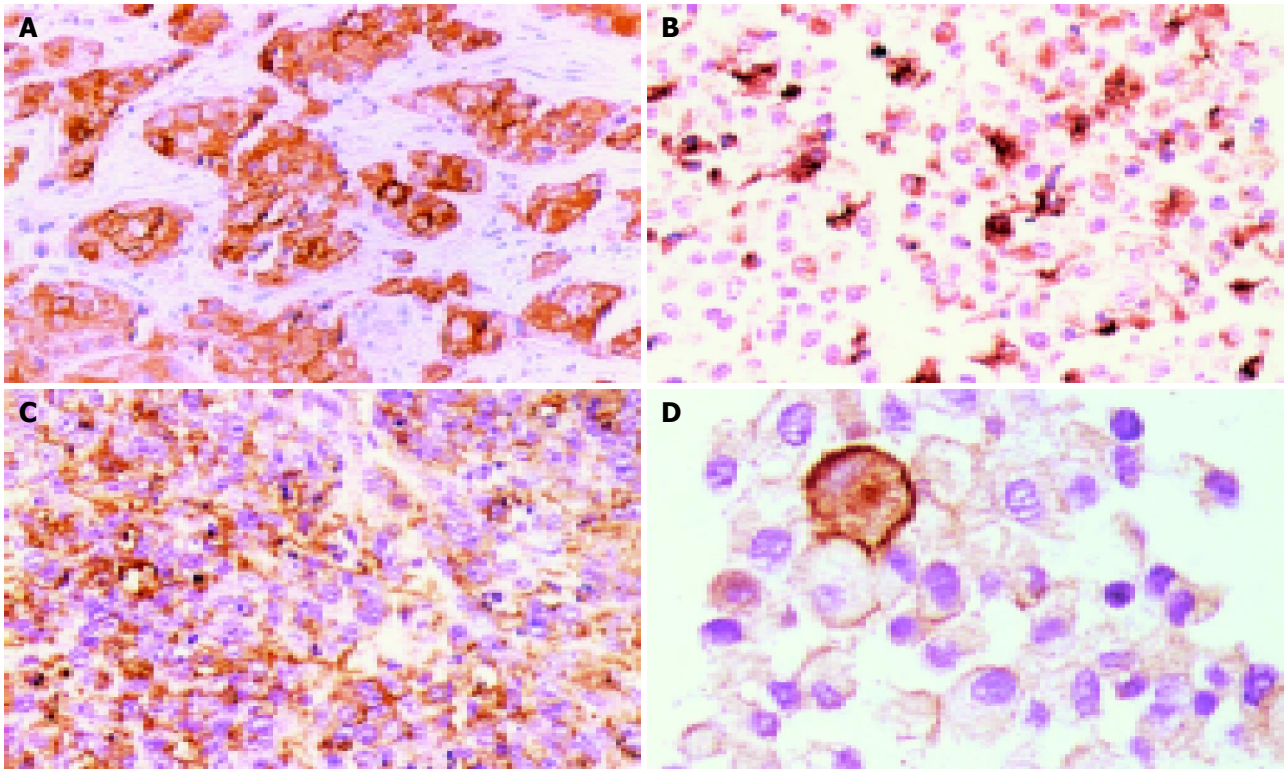

Figure 3 Immunocytochemistry of the primary tumor and KKU-100 cells. **A:** the primary tumor showing strong expression of cytokeratin; **B:** strong expression of KKU-100 cell line; **C:** EMA expression in both heterotransplanted tumor cells; **D:** EMA expression in KKU-100 cells (immunoperoxidase, original magnification ×200).

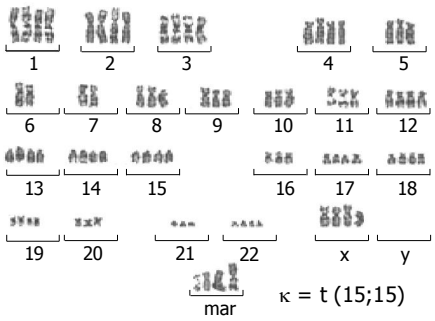

Figure 4 Representative G-banded karyotype of KKU-100 at passage 20 showing chromosomal abnormalities and marker chromosome (mar) : 84, +XX, +1, +2, +3, +4, +5, +8, +9, 10, +11, +12, +13, +14, +der(15)t(15;15), +16, +17, +18, +19, +20, +21, +22, +mar.

Mycoplasma detection

Mycoplasmas were not detected in the spent medium during cell culturing.

DISCUSSION

A small number of cholangiocarcinoma cell lines are available for cancer research and little is known about this bile duct cancer. To date, approximately eight cell lines have been developed from intrahepatic bile duct cancer, namely HChol-Y1[5], SNU-1079[9], HuCC-T1[11], PCI:SG231[12], CC-SW-1 and CC-LP-1[13], HuCCA-1[14], KMC-1[16]. There is no cell line, to our knowledge, developed from porta hepatis, though tumors at this site are lethal and account for about two-thirds of all cholangiocarcinomas[17,18]. This is probably due to the difficulty of tumor resection and obtaining specimens[19]. KKU-100 may probably be the first porta hepatic-derived and egg-proven *Opisthorchis*-associated cholangiocarcinoma cell line. A previous cholangiocarcinoma cell line associated with opisthorchiasis, detected by ELISA, was isolated from a Thai patient[14]. Our cell line is the second cell line developed in the area endemic for opisthorchiasis and cholangiocarcinoma in Thailand.

KKU-100 was derived from poorly differentiated tubular adenocarcinoma, the common histologic type of cholangiocarcinoma reported in Thailand[20]. It possesses some characteristics of carcinoma in nature as evidenced by the expression of cytokeratin and EMA but not desmin. An electron microscopic study revealed microvilli and junctional complexes, the distinguishing ultrastructural features of adenocarcinoma (data not shown). Heterotransplantation of the KKU-100 cells into nude mice retained its histological features of the primary tumor. This is similar to several other cholangiocarcinoma cell lines that produce a similar histologic type in heterotransplanted animals[8,10,12,13]. However, some immunocytochemical characteristics of the cell line were lost such as cytokeratin, CEA and CA125 upon transplantation. This may be due to the natural selection and adaptation of the cells to survive under culture condition or nude mouse microenvironment[21,22].

Immunocytochemical analysis of tumor markers revealed that KKU-100 was positive for CEA, CA125 but not AFP and CA19-9-corresponding to the original tumor. The expression of CEA but not AFP in the primary tumor tissue and cells correlated with a marked elevation of serum CEA (44.6 ng/mL) and negative for AFP in this patient (data not

shown). This is common in pure cholangiocarcinoma, where elevated levels of serum CEA occur in ≤80% of cases[23,24], whereas AFP is almost negative. However, the expression of CEA and CA 125 in KKU-100 cells was less than the primary tumor. This is similar to most established cholangiocarcinoma cell lines that show minimal or no CEA expression[6,8,13]. The lowering or loss of some protein expression may be from the natural selection and adaptation of the cells to environment as previously mentioned. Only one cholangiocarcinoma cell line, HuCCA-1, exhibits CA 125[14], our cell line is the second. In contrast, several cholangiocarcinoma cell lines can express or secrete CA19-9, such as HChol-Y1[10], HuCC-T1[11], KMBC[8] and KMC-1[16]. Other tumor markers secreted/expressed by KKU-100 will be investigated for use in diagnostics and early detection in endemic areas.

Alterations of oncogenes and tumor suppressor genes are involved in the malignant transformation and progression of nearly all tumors. For cholangiocarcinoma, however, little is known about its molecular carcinogenesis. The p53 tumor suppressor gene, a common genetic alteration in various cancers, is over-expressed in up to 78.5% of cholangiocarcinomas[25-27], while mutations of exon 5-8 range between 5% and 37.5%[28-30]. Overexpression of c-met oncogene products has been described in about 60% of human cholangiocarcinomas[31] and in furan-induced cholangiocarcinomas in rats[32]. However, KKU-100 cells show no expression of these two gene products. Besides the two genes studied, several other gene alterations may occur in KKU-100 because there are marked chromosomal abnormalities in both number and structures. Detailed studies are in progress.

Cholangiocarcinoma is a major concern in Northeast Thailand because it is a fatal, malignant neoplasm with no curative treatment, neither chemotherapy nor radiation[18]. At present, only surgical excision of the detectable tumor is associated with any improved survival[18]. Since most patients have already advanced stage cancer when they arrive, palliative treatment is all that can be offered[4]. Further study on the various aspects of cholangiocarcinoma, such as tumor biology, cellular and molecular carcinogenesis, biomarkers for early diagnosis and drug responses to new therapeutic agents, is needed. KKU-100 cells should prove a valuable aid to such research and applicable management of cholangiocarcinoma.

ACKNOWLEDGMENTS

The authors thank Ratana Thatarporn, Erika Kuroichi and Suvit Balthaisong for technical assistance, and Mr. Bryan Roderick Hamman for helping with the English-language presentation.

REFERENCES

1 **Vatanasapt V,** Uttaravichien T, Mairiang EO, Pairojkul C, Chartbanchachai W, Haswell-Elkins M. Cholangiocarcinoma in north-east Thailand. *Lancet* 1990; **335**: 116-117
2 **Jongsuksuntigul P,** Imsomboon T. Opisthorchiasis control in Thailand. *Acta Trop* 2003; **88**: 229-232
3 **Infection with liver flukes (*Opisthorchis viverrini*, *Opisthorchis felineus* and *Clonorchis sinensis*).** *IARC Monogr Eval Carcinog Risks Hum* 1994; **61**: 121-175
4 **Vatanasapt V,** Sripa B, Sithithaworn P, Mairiang P. Liver flukes and liver cancer. *Cancer Surv* 1999; **33**: 313-343
5 **Hudd C,** Euhus DM, LaRegina MC, Herbold DR, Palmer DC, Johnson FE. Effect of cholecystokinin on human cholangiocarcinoma xenografted into nude mice. *Cancer Res* 1985; **45**:1372-1377
6 **Knuth A,** Gabbert H, Dippold W, Klein O, Sachsse W, Bitter-Suermann D, Prellwitz W, Meyer zum Buschenfelde KH. Biliary adenocarcinoma. Characterisation of three new human tumor cell lines. *J Hepatol* 1985; **1**: 579-596
7 **Katoh H,** Shinbo T, Otagiri H, Saitoh M, Saitoh T, Ishizawa S, Shimizu T, Satoh A, Tazawa K, Fujimaki M. [Character of a human cholangiocarcinoma CHGS, serially transplanted to nude mice. *Hum Cell* 1988; **1**: 101-105
8 **Yano H,** Maruiwa M, Iemura A, Mizoguchi A, Kojiro M. Establishment and characterization of a new human extrahepatic bile duct carcinoma cell line (KMBC). *Cancer* 1992; **69**: 1664-1673
9 **Ku JL,** Yoon KA, Kim IJ, Kim WH, Jang JY, Suh KS, Kim SW, Park YH, Hwang JH, Yoon YB, Park JG. Establishment and characterisation of six human biliary tract cancer cell lines. *Br J Cancer* 2002; **87**: 187-193
10 **Yamaguchi N,** Morioka H, Ohkura H, Hirohashi S, Kawai K. Establishment and characterization of the human cholangiocarcinoma cell line HChol-Y1 in a serum-free, chemically defined medium. *J Natl Cancer Inst* 1985; **75**: 29-35
11 **Miyagiwa M,** Ichida T, Tokiwa T, Sato J, Sasaki H. A new human cholangiocellular carcinoma cell line (HuCC-T1) producing carbohydrate antigen 19/9 in serum-free medium. *In Vitro Cell Dev Biol* 1989; **25**: 503-510
12 **Storto PD,** Saidman SL, Demetris AJ, Letessier E, Whiteside TL, Gollin SM. Chromosomal breakpoints in cholangiocarcinoma cell lines. *Genes Chromosomes Cancer* 1990; **2**: 300-310
13 **Shimizu Y,** Demetris AJ, Gollin SM, Storto PD, Bedford HM, Altarac S, Iwatsuki S, Herberman RB, Whiteside TL. Two new human cholangiocarcinoma cell lines and their cytogenetics and responses to growth factors, hormones, cytokines or immunologic effector cells. *Int J Cancer* 1992; **52**: 252-260
14 **Sirisinha S,** Tengchaisri T, Boonpucknavig S, Prempracha N, Ratanarapee S, Pausawasdi A. Establishment and characterization of a cholangiocarcinoma cell line from a Thai patient with intrahepatic bile duct cancer. *Asian Pac J Allergy Immunol* 1991; **9**: 153-157
15 **Hsu SM,** Raine L, Fanger H. Use of avidin-biotin-peroxidase complex (ABC) in immunoperoxidase techniques: a comparison between ABC and unlabeled antibody (PAP) procedures. *J Histochem Cytochem* 1981; **29**: 577-580
16 **Iemura A,** Maruiwa M, Yano H, Kojiro M. A new human cholangiocellular carcinoma cell line (KMC-1). *J Hepatol* 1992; **15**: 288-298
17 **Uttaravichen T,** Buddhisawasdi V, Pairojkul C. Bile duct cancer and the liver fluke. Pathology, presentation and surgical management. *Asian J Surg* 1996; **19**: 267-270
18 **de Groen PC,** Gores GJ, LaRusso NF, Gunderson LL, Nagorney DM. Biliary tract cancers. *N Engl J Med* 1999; **341**: 1368-1378
19 **Ahrendt SA,** Cameron JL, Pitt HA. Current management of patients with perihilar cholangiocarcinoma. *Adv Surg* 1996; **30**: 427-452
20 **Sinawat P,** Hemsrichart V. A histopathologic study of 61 cases of peripheral intrahepatic cholangiocarcinoma. *J Med Assoc Thai* 1991; **74**: 448-453
21 **Fogh J.** Human tumor lines for cancer research. *Cancer Invest* 1986; **4**: 157-184
22 **Rubin H.** Selected cell and selective microenvironment in neoplastic development. *Cancer Res* 2001; **61**: 799-807
23 **Bates SE,** Longo DL. Use of serum tumor markers in cancer diagnosis and management. *Semin Oncol* 1987; **14**: 102-138
24 **Jalanko H,** Kuusela P, Roberts P, Sipponen P, Haglund CA, Makela O. Comparison of a new tumour marker, CA 19-9, with alpha-fetoprotein and carcinoembryonic antigen in patients with upper gastrointestinal diseases. *J Clin Pathol* 1984; **37**: 218-222

25 **Ohashi K,** Nakajima Y, Kanehiro H, Tsutsumi M, Taki J, Aomatsu Y, Yoshimura A, Ko S, Kin T, Yagura K. Ki-ras mutations and p53 protein expressions in intrahepatic cholangiocarcinomas: relation to gross tumor morphology. *Gastroenterology* 1995; **109**: 1612-1617

26 **Rizzi PM,** Ryder SD, Portmann B, Ramage JK, Naoumov NV, Williams R. p53 Protein overexpression in cholangiocarcinoma arising in primary sclerosing cholangitis. *Gut* 1996; **38**: 265-268

27 **Terada T,** Nakanuma Y. Expression of apoptosis, proliferating cell nuclear antigen, and apoptosis-related antigens (bcl-2, c-myc, Fas, Lewis(y) and p53) in human cholangiocarcinomas and hepatocellular carcinomas. *Pathol Int* 1996; **46**: 764-770

28 **Kiba T,** Tsuda H, Pairojkul C, Inoue S, Sugimura T, Hirohashi S. Mutations of the p53 tumor suppressor gene and the ras gene family in intrahepatic cholangiocellular carcinomas in Japan and Thailand. *Mol Carcinog* 1993; **8**: 312-318

29 **Sturm PD,** Baas IO, Clement MJ, Nakeeb A, Johan G, Offerhaus A, Hruban RH, Pitt HA. Alterations of the p53 tumor-suppressor gene and K-ras oncogene in perihilar cholangiocarcinomas from a high-incidence area. *Int J Cancer* 1998; **78**: 695-698

30 **Petmitr S,** Pinlaor S, Thousungnoen A, Karalak A, Migasena P. K-ras oncogene and p53 gene mutations in cholangiocarcinoma from Thai patients. *Southeast Asian J Trop Med Public Health* 1998; **29**: 71-75

31 **Terada T,** Nakanuma Y, Sirica AE. Immunohistochemical demonstration of MET overexpression in human intrahepatic cholangiocarcinoma and in hepatolithiasis. *Hum Pathol* 1998; **29**: 175-180

32 **Radaeva S,** Ferreira-Gonzalez A, Sirica AE. Overexpression of C-NEU and C-MET during rat liver cholangiocarcinogenesis: A link between biliary intestinal metaplasia and mucin-producing cholangiocarcinoma. *Hepatology* 1999; **29**: 1453-1462

Science Editor Wang XL **Language Editor** Elsevier HK

PO Box 2345, Beijing 100023, China
www.wjgnet.com
wjg@wjgnet.com

ELSEVIER

World J Gastroenterol 2005;11(22):3398-3404
World Journal of Gastroenterology ISSN 1007-9327

• *BASIC RESEARCH* •

Lethal effect and apoptotic DNA fragmentation in response of D-GalN-treated mice to bacterial LPS can be suppressed by pre-exposure to minute amount of bacterial LPS: Dual role of TNF receptor 1

Bing-Rong Zhou, Marina Gumenscheimer, Marina A. Freudenberg, Chris Galanos

Bing-Rong Zhou, Department of Microbiology, Second Military Medical University, Shanghai 200433, China
Marina Gumenscheimer, Marina A. Freudenberg, Chris Galanos, Max-Planck-Institut für Immunbiologie Stübeweg 51 D-79108 Freiburg in Br. Germany
Supported by a fellowship (to Zhou B) from Max-Planck-Society, Germany, and partially supported by the National Key Basic Research and Development Program (973 Program) of China, No. 2002CB513006 (to Zhou B)
Correspondence to: Dr. Chris Galanos, Max-Planck-Institut für Immunbiologie Stübeweg 51 D-79108 Freiburg in Br. Germany. galanos@immunbio.mpg.de
Telephone: +49-761-5108400 Fax: +49-761-5108403
Received: 2004-03-15 Accepted: 2004-04-29

Abstract

AIM: To investigate whether induction of tolerance of mice to lipopolysaccharide (LPS) was able to inhibit apoptotic reaction in terms of characteristic DNA fragmentation and protect mice from lethal effect.

METHODS: Experimental groups of mice were pretreated with non-lethal amount of LPS (0.05 μg). Both control and experimental groups simultaneously were challenged with LPS plus D-GalN for 6-7 h. The evaluations of both DNA fragmentations from the livers and the protection efficacy against lethality to mice through induction of tolerance to LPS were conducted.

RESULTS: In the naive mice challenge with LPS plus D-GalN resulted in complete death in 24 h, whereas a characteristic apoptotic DNA fragmentation was exclusively seen in the livers of mice receiving LPS in combination with D-GalN. The mortality in the affected mice was closely correlated to the onset of DNA fragmentation. By contrast, in the mice pre-exposed to LPS, both lethal effect and apoptotic DNA fragmentation were suppressed when challenged with LPS/D-GalN. In addition to LPS, the induction of mouse tolerance to TNF also enabled mice to cross-react against death and apoptotic DNA fragmentation when challenged with TNF and/or LPS in the presence of D-GalN. Moreover, this protection effect by LPS could last up to 24 h. TNFR1 rather than TNFR2 played a dual role in signaling pathway of either induction of tolerance to LPS for the protection of mice from mortality or inducing morbidity leading to the death of mice.

CONCLUSION: The mortality of D-GalN-treated mice in response to LPS was exceedingly correlated to the onset of apoptosis in the liver, which can be effectively suppressed by brief exposure of mice to a minute amount of LPS. The induced tolerance status was mediated not only by LPS but also by TNF. The developed tolerance to either LPS or TNF can be reciprocally cross-reacted between LPS and TNF challenges, whereas the signaling of induction of tolerance and promotion of apoptosis was through TNFR1, rather than TNFR2.

Key words: LPS tolerance; DNA fragmentation; Apoptosis; TNF receptor

Zhou BR, Gumenscheimer M, Freudenberg MA, Galanos C. Lethal effect and apoptotic DNA fragmentation in response of D-GalN-treated mice to bacterial LPS can be suppressed by pre-exposure to minute amount of bacterial LPS: Dual role of TNF receptor 1. *World J Gastroenterol* 2005; 11 (22): 3398-3404
http://www.wjgnet.com/1007-9327/11/3398.asp

INTRODUCTION

Bacterial lipopolysaccharide (LPS), also known as endotoxin, is an integral component of outer membrane located in the cell wall of Gram-negative bacteria, and is one of the main causative agents of septic shock in the duration of Gram-negative bacterial infection in humans[1]. It has been found *in vivo* that the pathogenic role of LPS is not directly through LPS molecule itself, but rather mediated by a group of endogenous mediators including TNF[1-3], IL-6[1,3], and IL-12[1,2], which, when in excess, leads to serious systemic disorders with a high mortality rate[1]. Among these, TNFα is regarded as a reputed agent involved in the development of LPS pathogenesis[1], it binds to corresponding surface receptors exerting its biological effects. These receptors are termed as TNFR1 and TNFR2[5-9], respectively.

However, increasing evidence showed that by prior exposure of animals like mice to a minor amount of LPS (even a non-lethal dose of LPS was applied), a hypo-responsiveness or refractoriness to subsequent challenge of LPS was developed[10-15]. This phenomenon has been described as tolerance of host to LPS[10-15]. LPS tolerance can be observed with a decreased febrile response and escape from death as well as a reduced production of inflammatory endogenous cytokines in response to a secondary stimulation with LPS[10-15]. In this case, tolerant mice towards LPS actually protect themselves

from lethality due to pretreatment with LPS. Furthermore, it has also been found that the tolerant mice to LPS are cross-reaction towards the pathogenic role of TNF[10,12,13] in terms of protection of host. In some reports[11,12], tolerance of mice to TNF was also able to alleviate and counteract deadly suffering in the affected mice while challenged with a lethal combination of TNF and D-GalN[13].

Apoptotic reaction has been extensively studied in cell models and/or in special animal models. Cells undergoing apoptosis exhibit specific morphological changes[17,19,24], including membrane blebbing, cytoplasmic and chromatin condensation, nuclear breakdown, DNA fragmentation, assemble of membrane-enclosed vesicles termed apoptotic bodies. All these are eventually subjected to phagocytosis. Among these, DNA fragmentation has been regarded as a classic mark[16-24]. We have found that a characteristic apoptotic DNA fragmentation in the liver of the affected mice was intimately correlated to lethality in mice that were challenged with a tremendously low amount of LPS (0.05 μg) in combination with D-GalN[27]. In this study, we addressed that whether the tolerance of mice to LPS would inhibit the apoptotic DNA fragmentation, and which TNF receptors were involved in the induction of lethality and tolerant status formation.

MATERIALS AND METHODS

Chemicals

Recombinant human tumor necrosis factor (rhTNFα) was provided by the BASF Company (Ludwigshafen, Germany), the activity was 5×10^6 U/mg protein. LPS was prepared from *Salmonella abortus equi* as described previously[28]. D-GalN hydrochloride was purchased from C. Roth Karlsruhe, Germany.

Mice

Mouse strains were kept under specific pathogen-free conditions in the animal facilities. In this study, C57BL10 ScSn (ScSn) and TNFR1-/-, and TNFR2-/- (genotypic background BL6´129sv) were used, respectively. Ten-week-old mice weighing approximately 22-25 g of both sexes were housed in stainless steel wire cages with free access to food and water. There was no difference in either male or female mice. After about a 1-wk equilibration period, the animals were randomly divided into different experimental groups according to the protocol. Mice were handled and cared for in accordance with the Guide for the Care and Use of Laboratory Animals in Germany, as legally required. The experimental protocol was carried out in compliance with German regulations and local ethical committee guidelines for animal research.

Experimental design

All reagents used in these experiments included D-GalN, LPS, and TNFα. They were first dissolved in pyrogen-free phosphate-buffered saline (PBS, pH 7.2). Combination of LPS and/or TNFα with D-GalN (each dose of reagent used was indicated in the figure legend) in a total volume of 200 μL was injected into the mice. This volume was also used throughout the study. Injections were usually performed intravenously (i.v.) in the lateral tail vein of the mice.

Induction of tolerance and lethal test[29]

For the induction of tolerance, mice were pretreated with LPS (usually a concentration of 0.05 μg) or TNFα (usually a concentration of 2 μg) for different time lengths, thereafter the mice were challenged with the required reagent in combination with D-GalN for indicated time periods (usually for 6-7 h). As controls, mice received LPS and/or TNF in combination with D-GalN for an indicated time length. At certain time point, the livers were removed under ether anesthesia and DNA extraction was carried out immediately. Blood was collected under ether anesthesia by puncturing the axillary vessels, plasma was prepared and stored at -80 ℃ until use. For the lethal effect of the mice after challenged with the indicated reagent, usually the mice were observed for 24 h.

Removal of organs from mice and homogenization[27,30]

Organs of interest (livers either from experimental mice or from control mice) were removed under ether anesthesia of the animals, and placed in 1 mL lysis buffer solution (10 mmoL Tris-HCl, pH 7.5, 100 mmoL EDTA, 0.5% SDS, proteinase K 100 μg/mL, proteinase K was added shortly before use) and immediately pressed with the flat end of a sterile syringe piston through a metal mesh placed on ice. Alternatively, the organs were placed in a glass homogenizer containing 1 mL of lysis buffer, and homogenized at a high-speed vortexing (3 000 r/min) for 5 min on ice. The resulting suspensions were kept at -40 ℃ until extraction of DNA.

Extraction and preparation of RNA-free DNA

Usually 0.4 mL of the homogenized tissue suspension as described above was used for DNA extraction. The extraction procedure used was basically the same as described previously[27,30]. DNA from each sample was extracted twice with phenol, once with phenol-chloroform-isoamyl alcohol (PCI, 25:24:1; V:V:V) and once with chloroform. The procedure was detailed as follows. An equal volume of phenol (0.4 mL) was added to 0.4 mL suspension of homogenized tissues, and mixed well by vortexing vigorously for 5 min. After centrifugation at 17 300 *g* at 4 ℃ for 10 min, the supernatant (aqueous phase) containing DNA was pipetted into a clean microcentrifuge tube. To this an equal volume of phenol was added and extraction was repeated as described above. The resulting supernatant was extracted once with PCI and once with chloroform to remove residual phenol. After centrifugation at 17 300 *g* at 4 ℃ for 10 min, the supernatant was transferred to a clean tube and DNA was precipitated by adding 2.5 volumes of absolute ethanol and sodium acetate to a final concentration of 0.3 mol/L and kept at -20 ℃ for 30 min (or overnight). Next it was spun by centrifugation (17 300 *g* at 4 ℃ for 10 min) and pellet was dissolved in TE buffer (Tris-HCL 10 mmol/L, pH 7.4, ethylene diaminotetraacetic acid 1 mmol/L, pH 8.0) containing RNase (0.1 mg/L) at 37 ℃ for 1 h. Subsequently, the suspension was re-extracted with phenol, PCI and chloroform, and precipitated as described above. Finally, the concentration of DNA was measured by a spectrophotometer (PM6, Zeiss, Jena, Germany).

Analysis of DNA ladder by agarose gel electrophoresis[20,23,27,30]

Before electrophoresis, the DNA concentration of the samples

was adjusted to approximately equivalent concentration. About 2-3 μg of DNA sample was mixed with loading buffer (40% sucrose, 0.25% xylene cyanol, 0.25% bromophenol blue) and placed in the wells of agarose gel. The agarose gel (15 mL/L) in electrophoresis buffer TBE (0.5×) was run at 100 V until the purple tracer marker migrated to approximately 2 cm before the end of the gel. The gels were photographed under UV light using a Mitrubishi video copy processor (Gibcol BRL, Heidelberg, Germany), graphs were stored in a magnetic disc. Alternatively photos were printed out directly for immediate analysis of results.

TNFα bioassay

TNFα in plasma was measured in a cytotoxicity test using a TNF-sensitive L929 cell line in the presence of actinomycin D as described previously[31]. The detection limit of the assay was 50 pg TNF/mL plasma.

RESULTS

Pre-exposure to LPS effectively suppressed apoptotic DNA fragmentation

We found that the mortality in mice when challenged with LPS at the dose of 0.05 μg and in the presence of D-GalN (20 mg) was paralleled well to the characteristic apoptotic hallmark, DNA fragmentation in the liver of the affected mice, which was also shown elsewhere[27]. We further explored whether pre-exposure of mice (ScSn) to LPS (0.05 μg) was able to inhibit the onset of apoptotic DNA fragmentation and protect host mice from lethal challenge as well as which receptor signaling pathway in the mice was pre-exposed to a minute dose of LPS.

The results showed that when mice were pre-exposed to LPS for as long as 75 min and then challenged with a combination of LPS (0.05 μg) in the presence of D-GalN (20 mg) for 6 h, the distinctive apoptotic DNA fragmentation was suppressed (Figure 1, lanes 2 and 3). In contrast, in the naïve mice that had no pre-exposure to LPS, the apoptotic DNA fragmentation from the homogenate liver of mice was clearly seen in agarose gel electrophoresis (Figure 1, lane 1 and Figure 2, lanes 8 and 9). Therefore, pre-exposure of mice to LPS was able to suppress the onset of apoptotic DNA fragmentation.

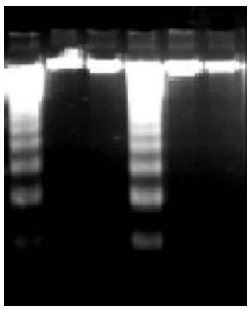

Lanes	1	2	3	4	5	6
Pre-LPS	-	+	+	-	+	+
LPS/GaIN	+	+	+	-	-	-
TNF/GIaN	-	-	-	+	+	+

Figure 1 Suppression of LPS and/or TNF-induced apoptotic DNA fragmentation in D-GalN-treated mice by pre-exposure to LPS.

Moreover, in mice pre-exposed to TNF (2 μg) instead of LPS for 3 h, the same results as those in the mice pre-exposed to LPS were shown and that it effectively suppressed apoptotic DNA fragmentation when mice were challenged with TNF (1 μg) plus D-GlaN (20 mg) for 6 h (Figure 2, lanes 1 and 2). However, in the control mice receiving TNF (1 μg) and D-GalN (20 mg), DNA fragmentation occurred (Figure 1, lane 4 and Figure 2, lanes 5-7). As a result, pre-exposure to either TNF was both able to inhibit the characteristic apoptotic DNA fragmentation when challenged with TNF in the presence of D-GalN.

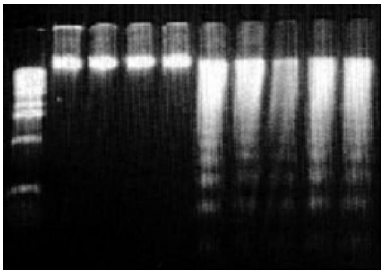

Lanes	M	1	2	3	4	5	6	7	8	9
Pre-TNF		+	+	+	+	-	-	-	-	-
TNF-GaIN		+	+	-	-	+	+	+	-	-
LPS-GaIN		-	-	+	+	-	-	-	+	+

Figure 2 Inhibition of LPS and/or TNF-induced DNA fragmentation in D-GalN-treated mice by pre-exposure to TNF, M: DNA marker.

Cross-reaction in the suppression of apoptotic DNA fragmentation

In addition to the suppression of apoptotic DNA fragmentation by pre-exposure of the corresponding homogenous agents and then challenge with LPS and/or TNF in the presence of D-GalN, DNA fragmentation could also be suppressed by the corresponding heterogeneous agents. In this study, we found that when pre-exposure to LPS (0.05 μg) for 75 min, apoptotic DNA fragmentation was dramatically suppressed in mice when challenged with TNF (1 μg) in the presence of D-GalN (20 mg) (Figure 1, lanes 5 and 6). Furthermore, this also took place in the mice that were pre-exposed to TNF (2 μg) instead of LPS for 3 h and subsequently challenged with LPS (0.05 μg) other than TNF, in the presence of D-GalN. Therefore, the suppression of characteristic apoptotic DNA fragmentation seemed to be a cross-reaction (Figure 2, lanes 3 and 4).

Induction of LPS tolerance and onset of apoptotic DNA fragmentation

Biological roles of LPS were mediated by endogenous TNF molecules produced from macrophage cells and other cell types[1-2,9]. TNF molecules must bind to the cognated TNF receptors responsible for signals in the biological roles of TNF molecules[5,8,9]. Here, we used the mice that were knocked out of corresponding TNF receptor genes. These mice were directly challenged with LPS and D-GlaN under the same experimental conditions as those performed in ScSn mice aforementioned. The results showed that administration of LPS (0.05 μg) and D-GalN (20 mg) resulted in apoptotic

DNA fragmentation only in the livers of TNFR2-/-mice (Figure 3, lanes 1 and 3), while the DNA fragmentation was absent in the livers of TNFR1-/-mice (Figure 3, lanes 5 and 7). In addition, in the same experimental situation, the DNA fragmentation in the spleens from TNFR1-/- and TNFR2-/- mice, respectively, was also examined. The results showed that neither in the spleens of TNFR1-/-mice (Figure 3, lanes 6 and 8) nor in those of TNFR2-/-mice (Figure 3, lanes 2 and 4), apoptotic DNA fragmentation was detectable. These results depicted in Figure 3 strongly suggested that the induction of apoptotic DNA fragmentation in mice by LPS was mediated by TNFR1 rather than TNFR2. TNFR2 did not seem to be involved in the induction of apoptotic DNA fragmentation by LPS, since its absence in TNFR2-/-mice had no influence on the development of apoptotic DNA fragmentation. Still in this situation, the host liver, not the spleen, was a target organ when challenged with LPS in the presence of D-GalN.

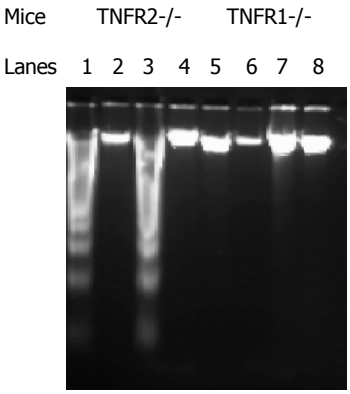

Figure 3 Requirements of TNFR1 for the induction of DNA fragmentation by LPS in D-GlaN-treated mice.

In the following experiments, we still investigated the role of TNFR1 in the induction of tolerance to LPS. The TNFR2-/-mice were pretreated with LPS (0.1 μg) for 75 min, the property was retained that is the tolerance to the induction of apoptotic DNA fragmentation by a challenge with LPS (0.05 μg) in the presence of D-GalN (20 mg) (Figure 4, lanes 1-3). In contrast, the control mice that had no pretreatment with LPS (Figure 4, lanes 4-6) and were directly challenged with LPS (0.05 μg) in the presence of D-GalN, exhibited the expected DNA fragmentation. These data indicated that the development of tolerance to LPS could lead to the inhibition of DNA fragmentation in the livers of affected mice when challenged with LPS and involved TNFR1 only.

Suppression of apoptotic DNA fragmentation activity in the liver of mice pre-exposed to LPS

We found that the ScSn mice pre-exposed to LPS (0.05 μg) for 75 min were able to suppress the apoptotic DNA fragmentation when challenged with LPS (0.05 μg) plus D-GlaN (20 mg) (Figure 1). In the following experiments, we studied the time course of development and duration of tolerance induced by LPS pretreatment and the apoptotic

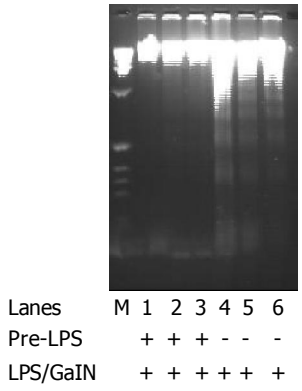

Figure 4 Induction of tolerance to the apoptotic activity by LPS in TNFR2-/-mice, M: DNA marker.

effect of LPS on D-GalN-treated mice. When pretreated with LPS (0.1 μg) for different time periods (Figure 5), the TNFR2-/-mice were challenged with a lethal combination of LPS (0.05 μg) and D-GalN (20 mg). Seven hours after challenge, the livers were removed under ether anesthesia and DNA was extracted and analyzed for the presence of fragmentation (Figures 4, 5 and Table 1). The results showed that the suppressive effect on the onset of apoptotic DNA fragmentation was detectable after preexposure of mice to LPS for 75 min (Figures 1 and 4) and this effect was maintained for up to 24 h (Figure 5 and Table 1).

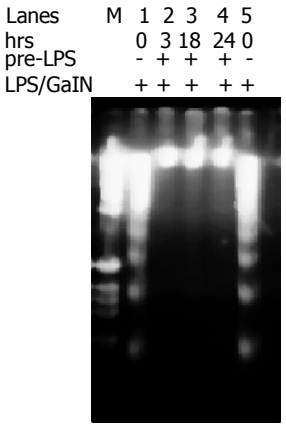

Figure 5 Time course of DNA fragmentation inhibition pretreated by LPS in TNFR2-/-mice, M: DNA marker.

Table 1 Effect of LPS pretreatment on the lethality and DNA fragmentation induced by LPS/D-GalN in TNFR2-/- mice

LPS pretreatment (0.1 μg) before challenge (h)	Challenge: LPS (0.05 μg) + D-GalN (20 mg)	
	Lethality (dead/total)	DNA fragmentation
None	5/5	+
24	0/5	-
18	0/5	-
3	0/5	-
1.25	0/5	-

+, fragmentation present; -, fragmentation absent.

Lethal effects of LPS on D-GlaN-treated mice correlated with characteristic apoptotic DNA fragmentation

In the following experiments, we investigated whether a correlation existed between the apoptotic DNA fragmentation in the livers of affected mice and lethal outcome. Mouse strains of TNFR2-/- were pretreated with 0.1 μg of LPS for different time periods, and then challenged with LPS (0.05 μg) in the presence of D-GalN. Mice with no pretreatment served as controls. The results indicated that DNA fragmentation in the liver of affected mice was highly correlated with the mortality of mice, which was due to the onset of apoptosis in the liver of affected mice (Table 1). Likewise a similar correlation between suppression of DNA fragmentation and suppression of mouse death was also seen in mice after pretreatment with TNFα and challenged with TNFα in combination with D-GalN (data not shown).

DISCUSSION

LPS, as a very important pathogenic agent released from Gram-negative bacteria[1], exerts dual biological roles in animals and humans. In the experimental animal model, if the mice were administrated with a high dose of purified LPS, a commonly lethal effect on mice would ensue and severe injuries would occur in some vital organs documented as multi-organ failure. On the contrary, if the animals were pre-exposed to a minute amount of LPS, or to detoxified LPS[1,32,33], and/or derivatives of LPS, monophosphoryl lipid A[32], a hypo-reaction would develop, protecting the affected mice from later challenge with a lethal amount of LPS and even live bacteria[34]. These distinctively paradoxical effects[7, 35,36] induced by LPS are attributed to the pre-exposure of mice to LPS, therefore alternating the potential reactivity of mice to bacterial component LPS.

In the present study, pre-exposure of animals to a minute amount of LPS leading to the suppression of both apoptotic DNA fragmentation and lethality against the later lethal challenge of LPS in the presence of D-GalN, to some extent, might reflect the role of hosts in terms of instinctive protection of themselves[7,10, 12-14]. This phenomenon in mice and other relevant host animal models has been widely documented, particularly in the field of study on tolerance of hosts to lethal toxicity of LPS[10-14]. However, the actual mechanism underlying the tolerance of hosts to LPS still seems obscure.

The exploration of mechanism responsible for cell apoptosis and anti-apoptosis (suppression of apoptosis[7,18,25]) has become a hot spot. Appropriate pretreatment with LPS resulting in a prolonged survival when challenged with a high dose of LPS and others including a lethal combination of LPS (or TNF) and D-GalN, which is a special case in studying mechanisms of how a given host responds to LPS, has been so far reported to be ascribed to the inhibition of apoptosis[16,19,38]. Hence, the onset of apoptosis challenged by exposure to LPS and induction of tolerance through pre-exposure of host and/or cells to LPS leading to suppression of apoptosis consists of the interaction between the protection role in host cells and detrimental effect of causative agents from bacteria. The similarity between the tolerance to the lethal toxicity of LPS, and the suppression of apoptosis has greatly intrigued us to further explore the mechanism, which might be due to the existence of a common signaling pathway[7,26,38].

The results of this study showed that, by a brief pre-exposure to a minute amount of LPS alone, induction of apoptosis in terms of the characteristic apoptotic hallmark, DNA fragmentation[17-19,24] and lethal effect of LPS were effectively suppressed. The pre-exposure to LPS was able to prevent mice from the predestined death when challenged with a lethal combination of LPS and D-GalN. Moreover, this protective effect on lethality and apoptosis by pre-exposure to a causative agent other than LPS, even by TNF, was also quite apparent. The results of the present study indicated that this protection role in suppression of both apoptotic reaction and lethal effect was seemingly related to the action of either LPS or TNF. In fact, whether endogenous TNF production induced by LPS or recombinant human TNF, they were able to converge signals through TNFR1[4,8], which functions in signaling to apoptotic reaction, and induction of tolerance to LPS. In view of this, TNF is still a key molecule outside of cells.

TNF, as one of the most putative mediators[1-2,10-15] in the pathogenesis of LPS and Gram-negative bacterial infection, has been widely proved. However, in the present study, TNF activity in plasma was not detectable (data not shown). The possible reason might be the concentration (0.05 μg only) of LPS used was too low to induce a large amount of free TNF molecules released into blood circulation. However, in order to study the action of TNF, we used TNFR2-/- mice. When challenged with LPS (0.05 μg) plus D-GalN, the lethality and apoptotic DNA fragmentation and suppression of both in TNFR2-/- mice could be seen as those in ScSn mice. This clearly indicated that the TNF molecules produced by such a low amount of LPS were in action. On the other hand, the free TNF molecules in plasma were not detectable, this could not exclude the role of membrane-type TNF[8,9,43] despite that we did not detect the membrane-type TNF in the present study. However, membrane TNF binds to the cytoplasmic membrane carrying out its functions like free-type TNF molecules through local cell-cell interaction. Therefore, in inducing apoptotic reaction in the liver and lethality in mice, the membrane-type TNF might exert its biological role.

However, signaling in inducing apoptotic reaction and lethality is through TNFR1[5,6,8], the signaling in which the induction of tolerance to LPS in mice leads to suppression of apoptotic effect and lethality is also through TNFR1[4,6,8,9]. The results in Figures 4 and 5 clearly indicated that induction of tolerance to apoptotic reaction and lethality involved only TNFR1. Therefore, TNFR1 plays a dual signaling role in inducing apoptotic reaction and lethality as well as host protection in terms of suppression of apoptotic reaction and lethality. Regarding the duality[7,38-42] of TNFR1 in signaling of either induction of apoptotic reaction or induction of suppression of apoptotic reaction due to tolerance, the latest progress of TNFR1 in signaling of cells still involves a complicated signaling circuit in post-receptors. The bifurcation and divergence point[26,38-42] in signaling is seemingly dependent upon the turn of the activation of signaling molecules tending to die (e.g., Caspase 8, Caspase 3 and others[17-19,21-24]) and to survive (e.g., activated NFκB and others[25,37-42] could protect cells).

The role and function of TNFR2 in the induction of apoptotic reaction and lethality are less clear and not as evidenced as TNFR1. Some studies reported that TNFR2 possessed the ability to pass TNF ligand[4] to TNFR1 leading to a relatively local high concentration of TNF in the vicinity of TNFR1 that accepts TNF ligand from TNFR2 and is then activated, signaling the TNFR1 apoptotic machinery. In the present study, the results showed that TNFR2 did not directly take part in the induction of apoptotic reaction. Despite that we used recombinant human TNF instead of mouse TNF, it was reported that in mice only TNFR1 could bind to human TNF molecules[8]. This also implicated that induction of apoptotic DNA fragmentation and lethality as well as suppression of both involved TNFR1[4-6,8,9] rather than TNFR2.

The fragmentation of DNA in an ongoing apoptotic reaction of host cells has been regarded as a gold standard[17,19,23,24]. In necrosis, DNA is degraded showing a smear in electrophoresis gel. However, in this study, when a combination of LPS and D-GalN was administered, a fragmented DNA pattern was distinguishable. In the control mice receiving LPS (0.05 μg), TNF (2 μg) and D-GalN (20 mg) respectively, DNA molecules were intact. The characteristic DNA fragmentation in the mice challenged with LPS plus D-GalN might involve a set of endogenous deoxyribonucleases, which have been described as a killer and/or executor [21] in ongoing apoptotic reaction in cells. Up to now, some of them have been characterized, such as DNase[17-19,21-24], Caspases family[21] and Caspase-activated DNase (CAD/DFF40)[18,19,23], which are activated and executed to degrade the corresponding substrates, ultimately leading to cell death. In fact, the degradation of nucleosomal DNA as one of the parameters in apoptotic reaction is based upon endogenous DNase that could recognize and cleave the special nucleic acid sequence between chromosomes[23-24] during apoptosis. However, it is not yet completely clear whether the inhibition of lethality and DNA fragmentation in response of D-GalN-treated mice to LPS (or TNFα) resulted from down-regulated endogenous DNase activity by unknown mechanism in the mice tolerant either to LPS or to TNFα.

The data obtained in this study suggested that the experimental sequence of D-GalN *vs* LPS or TNFα was a crucial factor, which could determine the death or survival of the affected mice. For instance, if mice were exposed to LPS (or TNFα) before D-GalN, they subsequently developed tolerance to lethality and DNA fragmentation. However, if exposure of mice to D-GalN was before exposure to LPS (or TNFα), it resulted in lethality in mice and apoptotic DNA fragmentation in the liver.

D-GlaN was originally identified as a hepatotoxic agent[29]. The underlying mechanism of its toxicity was shown to involve a strong depletion of uridine triphosphate in hepatocytes[29], which leads to an inhibition of synthesis of macromolecules, including RNA, membrane glycoproteins and glycogen. Inhibition of RNA synthesis induced by D-GalN could lead to a further decrease in protein synthesis[37]. Therefore, the crucial consequence of D-GalN action on the liver is an arrest of vital protein synthesis[37] at the transcriptional level. Although D-GalN could increase the sensitization of mice or cultured cells to LPS (or TNF), mice tolerant to LPS or TNFα could still effectively antagonize the lethality and apoptotic activity in the liver, suggesting that D-GalN is not able to alter or reverse this tolerant status to LPS or TNFα in mice. The role of D-GalN was reported to arrest transcription. However, more detailed experiments are needed to elucidate its mechanism.

In conclusion, pre-exposure of mice to a minute amount of LPS and/or TNFα can effectively suppress both apoptotic reaction and lethality. Induction as well as suppression of apoptotic reaction involves TNFR1. Thereby, mice will protect themselves from the detrimental effect even the lethal challenge with a high dose of LPS and bacteria.

ACKNOWLEDGMENTS

We are grateful to Hella Stübig and Nadja Goos for their excellent technical assistance and to Dr. Thomas Merlin for helpful discussions.

REFERENCES

1 **Galanos C,** Freudenberg MA, Katschinski T, Salomão R, Mossmann H, Kumazawa Y. Tumor Necrosis Factor and Host Response to Endotoxin. In: Ryan J, Morrison DC, eds. Bacterial Endotoxic Lipopolysaccharides. Vol II–Immunopharmacology and Pathophysiology. New York: Marcel Dekker, CRC Press, 1992: 75-104

2 **Zentella A,** Manogue K, Cerami A. The role of cachectin/TNF and other cytokines in sepsis. *Prog Clin Biol Res* 1991; **367**: 9-24

3 **Pallua N,** von Heimburg D. Pathogenic role of interleukin-6 in the development of sepsis. Part I: Study in a standardized contact burn murine model. *Crit Care Med* 2003; **31**: 1490-1494

4 **Tartaglia LA,** Pennica D, Goeddel DV. Ligand passing: the 75-kDa tumor necrosis factor (TNF) receptor recruits TNF for signaling by the 55-kDa TNF receptor. *J Biol Chem* 1993; **268**: 18542-18548

5 **Chen G,** Goeddel DV. TNF-R1 signaling: a beautiful pathway. *Science* 2002; **296**: 1634-1635

6 **Tartaglia LA,** Rothe M, Hu YF, Goeddel DV. Tumor necrosis factor's cytotoxic activity is signaled by the p55 TNF receptor. *Cell* 1993; **73**: 213-216

7 **Wallach D.** Cell death induction by TNF: a matter of self-control. *Trends Biochem Sci* 1997; **22**: 107-109

8 **MacEwan DJ.** TNF ligands and receptors-a matter of life and death. *Br J Pharmacol* 2002; **135**: 855-875

9 **Nowak M,** Gaines GC, Rosenberg J, Minter R, Bahjat FR, Rectenwald J, MacKay SL, Edwards CK, Moldawer LL. LPS-induced liver injury in D-galactosamine-sensitized mice requires secreted TNF-alpha and the TNF-p55 receptor. *Am J Physiol Regul Integr Comp Physiol* 2000; **278**: R1202-R1209

10 **Cross AS.** Endotoxin tolerance-current concepts in historical perspective. *J Endotoxin Res* 2002; **8**: 83-98

11 **Ferlito M,** Romanenko OG, Ashton S, Squadrito F, Halushka PV, Cook JA. Effect of cross-tolerance between endotoxin and TNF-alpha or IL-1beta on cellular signaling and mediator production. *J Leukoc Biol* 2001; **70**: 821-829

12 **Murphey ED,** Traber DL. Protective effect of tumor necrosis factor-alpha against subsequent endotoxemia in mice is mediated, in part, by interleukin-10. *Crit Care Med* 2001; **29**: 1761-1766

13 **Tanamoto K.** Induction of lethal shock and tolerance by Porphyromonas gingivalis lipopolysaccharide in D-galactosamine-sensitized C3H/HeJ mice. *Infect Immun* 1999; **67**: 3399-3402

14 **West MA,** Heagy W. Endotoxin tolerance: A review. *Crit Care Med* 2002; **30**: S64-S73

15 **Ziegler-Heitbrock HW.** Molecular mechanism in tolerance to lipopolysaccharide. *J Inflamm* 1995; **45**: 13-26
16 **Rich T,** Allen RL, Wyllie AH. Defying death after DNA damage. *Nature* 2000; **407**: 777-783
17 **Wyllie AH.** Apoptosis: an overview. *Br Med Bull* 1997; **53**: 451-465
18 **Widlak P.** The DFF40/CAD endonuclease and its role in apoptosis. *Acta Biochim Pol* 2000; **47**: 1037-1044
19 **Nagata S,** Nagase H, Kawane K, Mukae N, Fukuyama H. Degradation of chromosomal DNA during apoptosis. *Cell Death Differ* 2003; **10**: 108-116
20 **Mignon A,** Rouquet N, Fabre M, Martin S, Pagès JC, Dhainaut JF, Kahn A, Briand P, Joulin V. LPS challenge in D-galactosamine-sensitized mice accounts for caspase-dependent fulminant hepatitis, not for septic shock. *Am J Respir Crit Care Med* 1999; **159**: 1308-1315
21 **Nicholson DW,** Thornberry NA. Caspases: killer proteases. *Trends Biochem Sci* 1997; **22**: 299-306
22 **Tanuma S,** Shiokawa D. An endonuclease responsible for apoptosis. *Prog Mol Subcell Biol* 1996; **16**: 1-12
23 **Sakahira H,** Enari M, Nagata S. Cleavage of CAD inhibitor in CAD activation and DNA degradation during apoptosis. *Nature* 1998; **391**: 96-99
24 **Schwartzman RA,** Cidlowski JA. Apoptosis: the biochemistry and molecular biology of programmed cell death. *Endocr Rev* 1993; **14**: 133-151
25 **Wang CY,** Mayo MW, Baldwin AS. TNF- and cancer therapy-induced apoptosis: potentiation by inhibition of NF-kappaB. *Science* 1996; **274**: 784-787
26 **Ruckdeschel K,** Mannel O, Schrottner P. Divergence of apoptosis-inducing and preventing signals in bacteria-faced macrophages through myeloid differentiation factor 88 and IL-1 receptor-associated kinase members. *J Immunol* 2002; **168**: 4601-4611
27 **Zhou BR,** Gumenscheimer M, Freudenberg M, Galanos C. A striking correlation between lethal activity and apoptotic DNA fragmentation of liver in response of D-galactosamine sensitized mice to a non-lethal amount of lipopolysaccharide. *Acta Pharmacol Sin* 2003; **24**: 193-198
28 **Galanos C,** Luderitz O, Westphal O. Preparation and properties of a standardized lipopolysaccharide from salmonella abortus equi (Novo-Pyrexal). *Zentralbl Bakteriol Orig A* 1979; **243**: 226-244
29 **Galanos C,** Freudenberg MA, Reutter W. Galactosamine-induced sensitization to the lethal effects of endotoxin. *Proc Natl Acad Sci USA* 1979; **76**: 5939-5943
30 **Wang SD,** Huang KJ, Lin YS, Lei HY. Sepsis-induced apoptosis of the thymocytes in mice. *J Immunol* 1994; **152**: 5014-5021
31 **Merlin T,** Gumenscheimer M, Galanos C, Freudenberg MA. TNF-alpha hyper-responses to Gram-negative and Gram-positive bacteria in Propionibacterium acnes primed or Salmonella typhimurium infected mice. *J Endotoxin Res* 2001; **7**: 157-163
32 **Toyoda T,** Kwan AL, Bavbek M, Kassell NF, Wanebo JE, Lee KS. Enhanced endogenous antioxidant activity and inhibition of cerebral vasospasm in rabbits by pretreatment with a non-toxic endotoxin analog, monophosphoryl lipid A. *J Neurosurg* 1998; **88**: 1082-1087
33 **Madonna GS,** Peterson JE, Ribi EE, Vogel SN. Early-phase endotoxin tolerance: induction by a detoxified lipid A derivative, monophosphoryl lipid A. *Infect Immun* 1986; **52**: 6-11
34 **Ruckdeschel K,** Richter K. Lipopolysaccharide desensitization of macrophages provides protection against Yersinia enterocolitica-induced apoptosis. *Infect Immun* 2002; **70**: 5259-5264
35 **Kasner L,** Chan CC, Whitcup SM, Gery I. The paradoxical effect of tumor necrosis factor alpha (TNF-alpha) in endotoxin-induced uveitis. *Invest Ophthalmol Vis Sci* 1993; **34**: 2911-2917
36 **Liu AH.** Endotoxin exposure in allergy and asthma: reconciling a paradox. *J Allergy Clin Immunol* 2002; **109**: 379-392
37 **Leist M,** Gantner F, Bohlinger I, Germann PG, Tiegs G, Wendel A. Murine hepatocyte apoptosis induced *in vitro* and *in vivo* by TNF-alpha requires transcriptional arrest. *J Immunol* 1994; **153**: 1778-1788
38 **Wallach D,** Kovalenko AV, Varfolomeev EE, Boldin MP. Death-inducing functions of ligands of the tumor necrosis factor family: a Sanhedrin verdict. *Curr Opin Immunol* 1998; **10**: 279-288
39 **Roy S,** Nicholson DW. Cross-talk in cell death signaling. *J Exp Med* 2000; **192**: F21-F25
40 **Wallach D,** Holtmann H, Engelmann H, Nophar Y. Sensitization and desensitization to lethal effects of tumor necrosis factor and IL-1. *J Immunol* 1988; **140**: 2994-2999
41 **Beg AA,** Baltimore D. An essential role for NF-kappaB in preventing TNF-alpha-induced cell death. *Science* 1996; **274**: 782-784
42 **Mayo MW,** Wang CY, Cogswell PC, Rogers-Graham KS, Lowe SW, Der CJ, Baldwin AS. Requirement of NF-kappaB activation to suppress p53-independent apoptosis induced by oncogenic Ras. *Science* 1997; **278**: 1812-1815
43 **Grell M,** Zimmermann G, Gottfried E, Chen CM, Grunwald U, Huang DC, Wu Lee YH, Durkop H, Engelmann H, Scheurich P, Wajant H, Strasser A. Induction of cell death by tumour necrosis factor (TNF) receptor 2, CD40 and CD30: a role for TNF-R1 activation by endogenous membrane-anchored TNF. *EMBO J* 1999; **18**: 3034-3043

Science Editor Wang XL and Zhu LH **Language Editor** Elsevier HK

PO Box 2345, Beijing 100023, China
www.wjgnet.com
wjg@wjgnet.com

ELSEVIER

World J Gastroenterol 2005;11(22):3405-3410
World Journal of Gastroenterology ISSN 1007-9327

• *BASIC RESEARCH* •

Cholecystokinin octapeptide improves cardiac function by activating cholecystokinin octapeptide receptor in endotoxic shock rats

Xiao-Yun Zhao, Yi-Ling Ling, Yu-Guang Li, Ai-Hong Meng, Han-Ying Xing

Xiao-Yun Zhao, Yu-Guang Li, The First Affiliated Hospital of Shantou University Medical College, Shantou 515031, Guangdong Province, China
Xiao-Yun Zhao, Hebei Provincial Geriatric Key Laboratory, Shijiazhuang 050051, Hebei Province, China
Yi-Ling Ling, Ai-Hong Meng, Han-Ying Xing, Department of Pathophysiology of Hebei Medical University, Shijiazhuang 050017, Hebei Province, China
Supported by the projects of Health Committee and Education Committee of Hebei Province, No. 2K002, and No. 200122
Correspondence to: Dr. Xiao-Yun Zhao, The First Affiliated Hospital of Shantou University Medical College, Shantou 515031, Guangdong Province, China. xiaoyunzh@hotmail.com
Telephone: +86-754-8230260 Fax: +86-754-8259850
Received: 2004-03-20 Accepted: 2004-04-05

Abstract

AIM: To explore the effect of sulfated cholecystokinin octapeptide (sCCK-8) on cardiac functions and its receptor mechanism in endotoxic shock (ES) rats.

METHODS: The changes of the mean arterial pressure (MAP), heart rate (HR), the left ventricular pressure (LVP) and the maximal/minimum rate of LVP ($\pm LVdp/dt_{max}$) were measured by using physiological record instrument in eight groups of rats. The expression of cholecystokinin-A receptor (CCK-AR) and cholecystokinin-B receptor (CCK-BR) mRNA of myocardium in ES rats was examined by reverse transcription polymerase chain reaction (RT-PCR).

RESULTS: (1) Low doses of sCCK-8 (0.4 μg/kg) caused tachycardia (441±27, normal control 391±22 s/min) and slight increase in MAP, LVP and $\pm LVdp/dt_{max}$ (16.96±1.79, 18.21±1.69 and +768.85±31.28/-565.04±27.71 kPa, respectively, all $P<0.01$), while medium doses (4.0 μg/kg) and high doses of sCCK-8 (40 μg/kg) elicited bradycardia and marked increase in MAP, LVP and $\pm LVdp/dt_{max}$ (17.29±1.63, 19.46±2.57 and +831.46±22.57/-606.08 ±31.32; 17.46±1.08, 19.83±2.91 and +914.52±35.95/ -639.15±30.23 kPa, respectively, all $P<0.01$). Proglumide (1.0 mg/kg), a nonselective antagonist of CCK-receptor (CCK-R), significantly inhibited the pressor effects of sCCK-8 (15.96±1.38, 17.36±0.66 and +748.18±19.29/-512.12±14.39 kPa, respectively, all $P<0.01$), whilst reversing the bradycardiac responses. (2) High doses of LPS (8 mg/kg) elicited marked decrease in MAP, LVP and $\pm LVdp/dt_{max}$. (7.16±0.59, 7.6±0.68 and +298.01±25.52/ -166.96±19.25 kPa, respectively, all $P<0.01$). Pretreatment with sCCK-8 (40 μg/kg) could reverse the decline of cardiac functions (10.71±0.45, 11.7±1.26 and +446.04±67.18/ -347.90±36.98 kPa, respectively, all $P<0.01$), while proglumide could cause further decline of cardiac function in ES rats (4.71±0.67, 5.58±1.25 and +226.48±15.84/ -142.83±20.23 kPa, respectively, all $P<0.01$). (3) CCK-A/BR mRNAs were expressed in myocardium of control rats. Gene expression of CCK-AR and CCK-BR significantly increased in myocardium of ES rats. The increase of CCK-AR mRNA induced by LPS began at 0.5 h, peaked at 2 h, kept a high level at 6 h and declined at 12 h, respectively. Similar to CCK-AR mRNA, the expression of CCK-BR mRNA peaked at 2 h and kept a high level at 6 h, but it did not change at the first 0.5 h and was stable at a high level at 12 h.

CONCLUSION: The above results indicate that endogenous and exogenous sCCK-8 may significantly improve cardiac function and intractable hypotension of ES rats, which was likely related to high expression of CCK-A/BR in myocardium induced by LPS.

Key words: Sulfated cholecystokinin octapeptide; Endotoxic shock

Zhao XY, Ling YL, Li YG, Meng AH, Xing HY. Cholecystokinin octapeptide improves cardiac function by activating cholecystokinin octapeptide receptor in endotoxic shock rats. *World J Gastroenterol* 2005; 11(22): 3405-3410
http://www.wjgnet.com/1007-9327/11/3405.asp

INTRODUCTION

Lipopolysaccharide (LPS), the main component of bacterial endotoxin, can induce endotoxic shock (ES), which is very critical in clinic and leads to high mortality. ES is associated with cardiac dysfunction and intractable low arterial pressure[1]. We have shown previously that endogenous and exogenous cholecystokinin octapeptide (CCK-8) had anti-ES effect, such as reversing the fall in mean arterial pressure (MAP), preventing pulmonary artery hypertension (PAH), attenuating pathomorphological changes of main organs, and decreasing mortality[2,3]. In contrast, pretreatment with proglumide, the nonselective CCK-receptor (CCK-R) antagonist, could delay the recovery of blood pressure and increase mortality of ES rats[2,3]. However, the effect of CCK-8 on cardiac function and its mechanism remains unclear. Recently, our study showed that CCK-8 might

enhance cardiac function in a dose- dependent manner, which was likely induced by directly activating CCK-R in myocardium[4]. CCK-R was classified into two subtypes: CCK-AR and CCK-BR. CCK-AR was found predominantly in gastrointestinal tract and restricted areas of the brain, whereas CCK-BR was known to exist widely in brain and gastric glands[5]. At present, it is unknown whether sCCK-8 improves the cardiac function in ES rats and whether LPS induces the change of gene expression of CCK-R in myocardium. The aim of this study was to explore the effect of CCK-8 on cardiac function in ES rats and its receptor mechanism.

MATERIALS AND METHODS

Materials

LPS (*E.coli* 0111: B4), sulfated CCK-8 (sCCK-8) and proglumide were obtained from Sigma (St. Louis, MO). Total RNA isolation system and access RT-PCR system were purchased from Promega Inc., Beijing. All the other reagents used were of analytical grade, purchased from Chinese Chemicals Co., Male, specific pathogen-free Sprague-Dawley rats (weighing 220-260 g) were obtained from Experimental Animal Center of Hebei Province.

Animal preparation

Forty-eight rats were randomly assigned to eight groups ($n = 6$ in each) and different agents were administered: (1) low-dose sCCK-8 group: the rats were given sCCK-8 (0.4 μg/kg); (2) medium-dose sCCK-8 group: the rats were given sCCK-8 (4.0 μg/kg); (3) high-dose sCCK-8 group: the rats were given sCCK-8 (40 μg/kg); (4) proglumide plus sCCK-8 group: sCCK-8 (4.0 μg/kg) was given 10 min after administration of proglumide (1 mg/ kg); (5) ES group: the rats were given LPS (8 mg/kg); (6) ES plus sCCK-8 group: sCCK-8 (40 μg/kg) pretreatment 10 min before LPS (8 mg/kg); (7) proglumide plus LPS group: proglumide (1 mg/kg) pretreatment 10 min before LPS (8 mg/kg); (8) negative control animals received saline.

General operation

The animals were anesthetized with urethane (1.0 g/kg, ip). The right carotid artery was exposed and a catheter was inserted into the left ventricle (LV). The arterial cannula was connected to a pressure transducer (AP-601G) for measurement of LV systolic pressure (LVP). The signal of LVP was introduced by a differentiator Amp (ED-601G) to record the maximal/minimum rate of LVP ($\pm LVdp/dt_{max}$). HR was measured with an HR counter (AT-600G) triggered by left ventricular pressure pulse. Another catheter was inserted into the femoral artery and connected to a pressure transducer (AP-601G) for measurement of MAP. The changes in MAP, LVP and $\pm LVdp/dt_{max}$ were recorded on a polygraph (RM-6000G, Nihon Kohden). The caudal vein was cannulated for intravenous administration of various agents. All of the operations were finished in 40 min. Following a 15 min stabilization period, MAP, LVP and $\pm LVdp/dt_{max}$ were recorded as the control, and the agents were administered intravenous injection in a bolus dose. The rats were killed at 2 h.

Gene expression of CCK-R in cardiac tissue

Fifteen rats were divided into five groups ($n = 3$), (1) control group; (2)-(5) LPS groups, the rats were given 8 mg/kg LPS and were killed at 0.5, 2, 6, and 12 h. The kidney sections were used as positive control. Total RNA was extracted from both the myocardial and kidney samples by guanidinium thiocyanate method. The concentration of RNA was determined by absorbance at 260 nm. The primers for CCK-AR, CCK-BR and β-actin were constructed according to the report of Monstein[6] as follows: CCK-AR (630 bp), 5'-CTC GCT CGC CCA GAA CTC TAC CAA GGA ATC AAA TTT GAT GC-3' (sense) and 5'-CTG GTT CGG CCC ATG GAG CAG AGG TGC TCA TGT GGC TGT AG-3' (antisense); CCK-BR (320 bp), 5'-CTC GCT CGC CCA GAA CTC TAC CTA GGA CTC CAC TTT GA-3' (sense) and 5'-CTG GTT CGG CCC ACG CAC CAC CCG CTT CTT AGC CAG CA-3' (antisense); β-actin (420 bp), 5'-GAGACCTTCAACACCCAGCC-3; (sense) and 5'-GCGGGGCATCGGAACCGCTCA-3'(antisense). All the primers were synthesized by Sangon Corporation (Shanghai).

RT-PCR was performed in 25 μL reaction volume. Cycling parameters for amplifying RT products were as follows: at 48 ℃ for 45 min, one cycle; at 94 ℃ for 2 min, one cycle; at 94 ℃ for 1 min, 55 ℃ for 45 s, 72 ℃ for 45 s, five cycles; at 94 ℃ for 45 s, 55 ℃ for 45 s, 72 ℃ for 1 min, 35 cycles; at 72 ℃ for 10 min, one cycle. PCR products were electrophoresed on 1. Five percent agarose gel, stained with ethidium bromide (0.5 μg/mL), and analyzed by Gel-Pro analyzer version 3.1 software (Media Cybernetics). The ratio of arbitrary unit (AU, $D_{area} \cdot D_{density}$) of target genes over β-actin was used for expressing the relative level of mRNA expression.

Statistical analysis

All data were expressed as mean±SD. Statistical significance was performed by one-way ANOVA followed by the paired t test for within group comparisons and the unpaired t test for between group comparisons. Statistical significance was accepted when $P<0.05$.

RESULTS

Changes in cardiac function after administration of sCCK-8

Low dose of sCCK-8 caused a tachycardia in 30-50 s ($P<0.01$). The change of HR restored to baseline after 10-15 min. Both medium and high doses of sCCK-8 elicited a bradycardia in 30-50 s ($P<0.01$). The change of HR restored to baseline after 10-15 min. Either low or high dose of sCCK-8 produced a dose-dependent marked increase in MAP, LVP and $\pm LVdp/dt_{max}$ in 30-50 s ($P<0.01$). Similar to the change of HR, these changes of MAP, LVP and $\pm LVdp/dt_{max}$ restored to baseline after 10-15 min. Pretreatment with proglumide could reverse the bradycardia induced by moderate dose of sCCK-8 to a tachycardia. The increases in MAP, LVP, and $\pm LVdp/dt_{max}$ also could be inhibited by administration of proglumide ($P<0.01$, Table 1).

Changes in cardiac function after administration of sCCK-8 in ES rats

LPS caused a variation in heart rate (HR)-a bradycardia

Table 1 Comparison of the cardiac functions after administration of sCCK-8 and proglumide (mean±SD; n = 6)

		CCK(μg)			
	Pre-administration	0.4 μg /kg	4.0 μg/ kg	40 μg /kg	Proglumide +CCK4.0 μg /k g
HR/bmp	391±22	441±27[b]	353±18[b]	340±21[b]	427±36[b,d]
MAP/kPa	14.07±1.68	16.96±1.79[b]	17.29±1.63[b]	17.46±1.08[b]	15.96±1.38[b,d]
LVP/kPa	16.48±2.56	18.21±1.69[b]	19.46±2.57[b]	19.83±2.91[b]	17.36±0.66[b,d]
LV$dp/dt_{max}$(kPa.S) $^{-1}$	634.43±32.88	768.85±31.28[b]	831.46±22.57[b]	914.52±35.95[b]	748.18±19.29[b,d]
LV$dp/dt_{min}$(kPa.S) $^{-1}$	429.82±18.95	565.04±27.71[b]	606.08±31.32[b]	639.15±30.23[b]	512.12±14.39[b,d]

[b]P<0.01 *vs* preadministration; [d]P<0.01 *vs* medium dose of sCCK-8 group.

following a tachycardia and rapid decrease of MAP, LVP, and ±LV$dp/dt_{max}$ (P<0.01). MAP declined to two bottoms at 30 and 75 min, while LVP and ±LV$dp/dt_{max}$ declined to two bottoms at 30 and 105 min. The rapid variation of HR and decline of MAP, LVP, and ±LV$dp/dt_{max}$ could be reversed by pretreatment with sCCK-8 in ES rats. The decrease of MAP, LVP, and ±LV$dp/dt_{max}$ were not inhibited by pretreatment with sCCK-8 at first 20 min, however, they were restored rapidly after 20 min, then they remained higher than ES rats at 120 min (P<0.01), but could not return to normal. Pretreatment with proglumide resulted in a further decline of MAP, LVP, and ±LV$dp/dt_{max}$ (P<0.01) in ES rats (Figures 1-3).

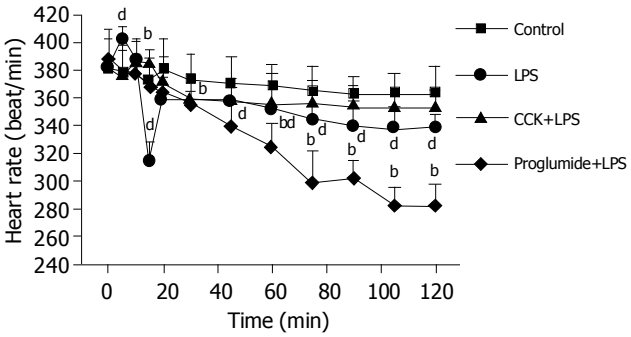

Figure 1 Changes of mean heart rate (HR) after intravenous injection of sCCK-8 or proglumide to ES rats. (mean±SD, n = 6). [b]P<0.01 *vs* control; [d]P<0.01 *vs* LPS group.

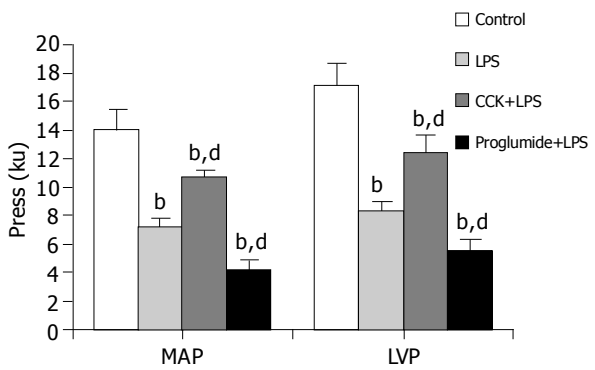

Figure 2 Changes in MAP and LVP after intravenous injection of sCCK-8 or proglumide to ES rats. (mean±SD, n = 6). [b]P<0.01 *vs* control; [d]P<0.01 *vs* LPS group.

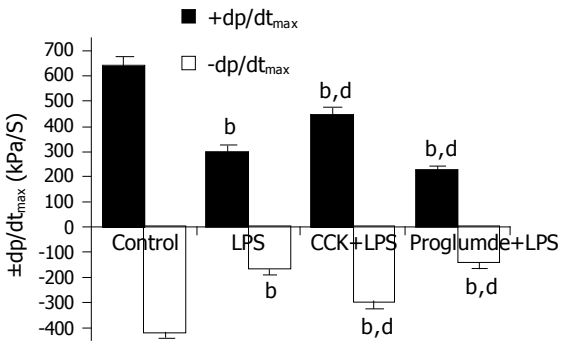

Figure 3 Changes in ±LV$dp/dt_{max}$ after intravenous injection of sCCK-8 or proglumide to ES rats. (mean±SD, n = 6) [b]P<0.01 *vs* control, [d]P<0.01 *vs* LPS.

Gene expression of CCK-R in myocardium of ES rats

Gene expression of CCK-A/ BR in myocardium of ES rats was up regulated by RT-PCR. The increase of CCK-AR mRNA induced by LPS began at 0.5 h, peaked at 2 h, kept a high level at 6 h and declined at 12 h, and they were 1.35, 2.23, 1.95, and 0.65 times that of control group, respectively. Similar to CCK-AR mRNA, the expression of CCK-BR mRNA peaked at 2 h and kept at a high level at 6 h, but it did not change at the first 0.5 h and was still at a high level at 12 h, and they were 0.944, 4.78, 2.79, and 2.67 times that of control group, respectively. The expression of housekeeping β-actin in different groups remained similar (Figure 4).

DISCUSSION

As a brain-gut peptide, cholecystokinin (CCK) exerts different physiological and pathophysiological actions[7]. Some previous studies suggested that sCCK-8, the predominant active form of endogenous CCK, might play an important role in adjusting the cardiac function and the effects were mediated by CCK-R. Marker *et al*[8], reported that CCK-8 added to the perfusion stream of isolated rat hearts produced an immediate bradycardia, which was abolished by using a CCK-R antagonist. Furthermore, Janssen *et al*[9], reported that CCK-8 elicited a dose-dependent increase in blood pressure and a variation in heart rate responses, that is, low doses of CCK-8 (0.5 μg/kg) caused tachycardia accompanied by renal, mesenteric and hindquarters vasoconstrictions, while high dose of CCK-8 (5 μg/kg) caused bradycardia accompanied by vasodilatation of the above arteries. To exclude the effect of central nervous system, a recent report by Gaw revealed that sCCK-8 caused

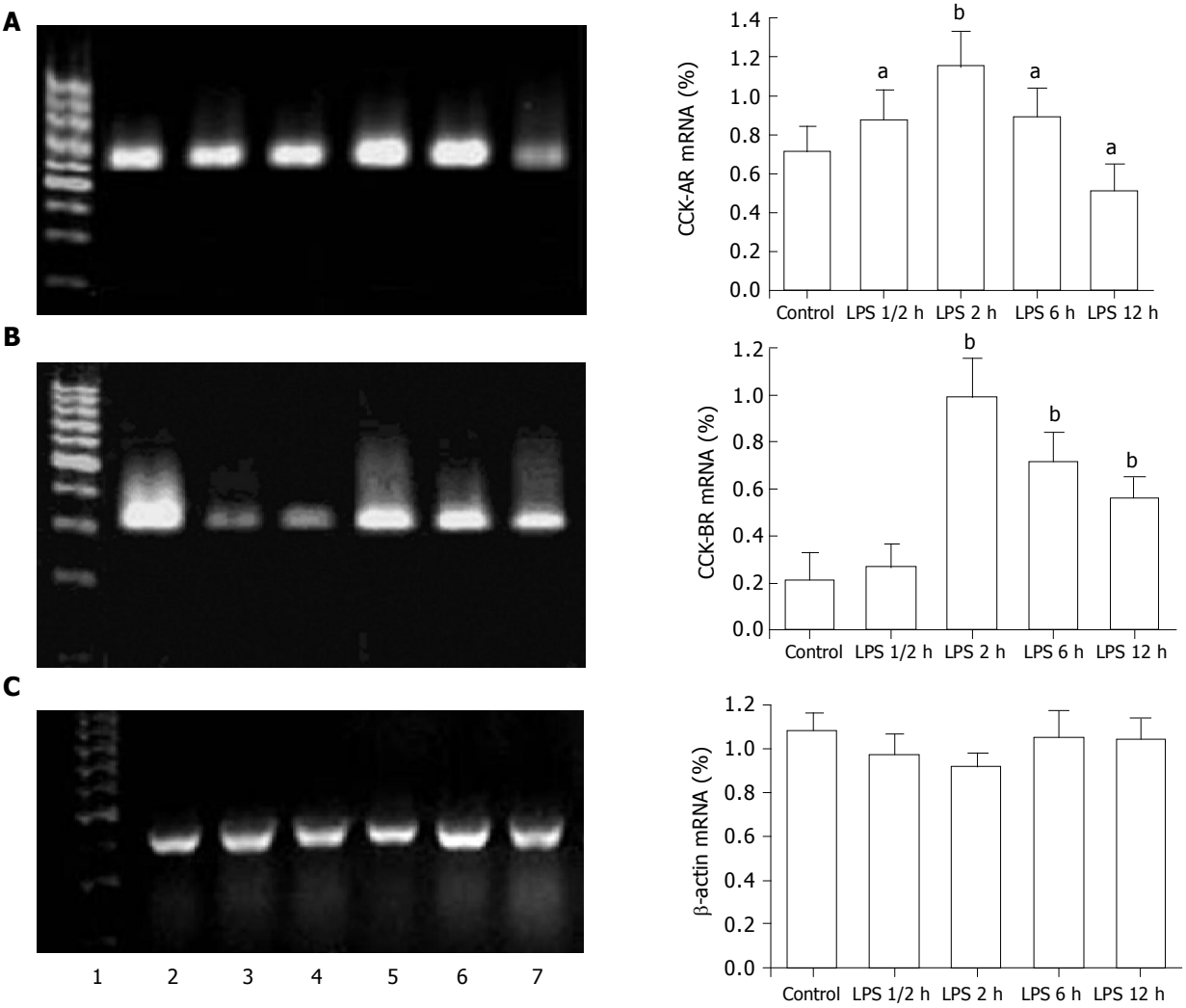

Figure 4 Expression of CCK-A/BR and β-actin mRNA of RT-PCR in the myocardium of ES rats. (mean±SD, n = 3) $^{a}P<0.05$ *vs* control, $^{b}P<0.01$ *vs* control. **A**: Representative pictures of CCK-AR (630 bp); **B**: representative pictures of CCK-BR (320 bp); **C**: representative pictures of β-actin (420 bp). Lane 1: DNA marker, lane 2: products expressed from kidney tissue as a positive control, lane 3: products expressed from control-saline-treated, lanes 4-7: products expressed from LPS-treated at 0.5, 2, 6, and 12 h, respectively.

a dose-dependent bradycardia and increase in MAP in pithed rats. Both the pressor response and bradycardia elicited by CCK-8 were reduced by selective CCK-AR antagonists, while the selective CCK-BR antagonists did not inhibit the effects of CCK-8[10]. Many other evidences for the involvement of CCK-AR in the effects of sCCK-8 in cardiovascular regulation[9,10]. In our experiment, administration of sCCK-8 resulted in a dose-dependent increase of cardiac function, leading to increase of MAP. The bradycardia was induced by medium and high doses of sCCK-8, while low dose of sCCK-8 caused a tachycardia. The effects of CCK-8 on cardiac functions were significantly inhibited by nonselective CCK-R antagonist - proglumide. Another study on single cardiomyocyte showed that sCCK-8 could increase [Ca(2+)](i) via activating the receptor-operated Ca(2+) channel and eliciting the influx of Ca(2+) in isolated guinea-pig cardiomyocyte[11]. The above results provided further evidence that the effect of CCK-8 on cardiovascular system might be mediated by the activation of CCK-R in myocardium.

Previous studies indicated the sustained improvement of the cardiovascular function induced by injection of sCCK-8 into rats bled to invariably fatal hemorrhagic shock[12]. Riepl's report that the level of sCCK-8 in serum was increased in endotoxemia of rats attracted our great interest[13]. The study in our department showed that endogenous and exogenous sCCK-8 had anti-ES effect, and that sCCK-8 had the ability to reverse the fall in mean arterial pressure, which was related with decreased clearance of sCCK-8 by lung in ES[14]. Recently, our study indicated that administration of sCCK-8 prevented increase of TNF-α gene and protein expression induced by LPS in spleen and lung, and decreased the levels of TNF-α, IL-1β, and IL-6 in serum, lung and spleen in ES rats. The study about its upstream signal mechanisms demonstrated that sCCK-8 inhibited LPS-induced NF-κB activity, I-κB degradation, TNF-α release and gene expression in PIMs, which was abrogated by proglumide[16]. Furthermore, CD14 on PIMs which was induced by LPS and its receptor could be downregulated by sCCK-8 *in vitro*[17]. These results suggested that sCCK-8 had anti-inflammatory effect to some extent, and sCCK-8 could clearly lessen the inflammatory lesions in lung, spleen and liver tissues in ES rats[2,14]. Our study

showed that sCCK-8 could remit the variation of HR and increase of both MAP and contractility of myocardium, then exert anti-ES effect, which were likely related to activation of CCK-R on myocardium.

CCK receptors have been pharmacologically classified into two subtypes: CCK-A receptor (CCK-AR) and CCK-B receptor (CCK-BR) according to their affinity for the peptide agonists CCK and gastrin[5]. CCK-AR is highly selective for sulfated analogs of CCK and the antagonist L-364 718, whereas CCK-BR has similarly high affinity to both sulfated and nonsulfated peptide analogs of CCK/gastrin peptides and the antagonist L-365 260[5]. CCK-AR is found principally in gastrointestinal tract and selective areas of the CNS, while CCK-BR is found principally in CNS and selective areas of the gastrointestinal tract, on pancreatic acinar cells and parietal cells[17,18]. CCK binds to CCK-AR present in a variety of gastrointestinal target tissues including pancreatic acini, islets, gastric mucosa and gallbladder to induce pancreatic enzyme secretion, insulin secretion, release of pepsinogen and gallbladder contraction[19]. CCK-BR in CNS regulates feeding, anxiety and memory, *etc*.[17]. CCK-AR and CCK-BR are also expressed in neoplastic cells such as pancreatic cancer cells[20,21], gastric cancer cells[23,24], colonic cancer cells[24] and small cell lung cancer cells[25-27] where they may stimulate cell growth. In addition, CCK-R is also related with brain injury[28], cortical infarct[29] and gastric ulceration[30]. We first detected CCK-AR and CCK-BR mRNA expression successfully not only in lung tissue, but also in heart tissue of rats[4]. Our data also demonstrated, for the first time that the expression of CCK-AR and CCK-BR mRNA were increased when induced by LPS, while other researchers found the expression level of CCK-AR was related to CCK-8 itself[31]. These data suggested that both CCK-AR and CCK-BR were widely distributed in various kinds of tissues and their presence provided the structural basis for CCK to exert a broad array of physiological action, including improving cardiac function by CCK-8 in ES rats.

In summary, the above results indicate that endogenous and exogenous sCCK-8 may markedly improve the cardiac function and hypotension of ES rats, which is likely related to high expression of CCK-A/BR on myocardium induced by LPS.

REFERENCES

1 **Forfia PR,** Zhang X, Ochoa F, Ochoa M, Xu X, Bernstein R, Sehgal PB, Ferreri NR, Hintze TH. Relationship between plasma NOx and cardiac and vascular dysfunction after LPS injection in anesthetized dogs. *Am J Physiol* 1998; **274**: H193-H201

2 **Ling YL,** Huang SS, Wang LF, Zhang JL, Wan M, Hao RL. Cholecystokinin-octapeptide (CCK-8) reverses experimental endotoxin shock. *ShengLi XueBao* 1996; **48**: 390-394

3 **Ling YL,** Cong B, Gu ZY, Li SJ, Zhou XH. Inhibitory effect of cholecystokinin octapeptide on pulmonary arterial hypertension during endotoxic shock. *Zhongguo Xueshu Qikan Wenzhai* 2000; **6**: 890-892

4 **Zhao XY,** Ling YL, Meng AH, Shan BE, Zhang JL. Effects of cholecystokinin octapeptide on rat cardiac function and the receptor mechanism. *ShengLi XueBao* 2002; **54**: 239-243

5 **Wank SA.** Cholecystokinin receptors. *Am J Physiol* 1995; **269**: G628-G646

6 **Monstein HJ,** Nylander AG, Salehi A, Chen D, Lundquist I, Hakanson R. Cholecystokinin-A and cholecystokinin-B/gastrin receptor mRNA expression in the gastrointestinal tract and pancreas of the rat and man. A polymerase chain reaction study. *Scand J Gastroenterol* 1996; **31**: 383-390

7 **Crawley JN,** Corwin RL. Biological actions of cholecystokinin. *Peptides* 1994; **15**: 731-755

8 **Marker JD,** Roberts ML. Chronotropic actions of cholecystokinin octapeptide on the rat heart. *Regul Pept* 1988; **20**: 251-259

9 **Janssen PJ,** Gardiner SM, Compton AM, Bennett T. Mechanisms contributing to the differential haemodynamic effects of bombesin and cholecystokinin in conscious, Long Evans rats. *Br J Pharmacol* 1991; **102**: 123-134

10 **Gaw AJ,** Hills DM, Spraggs CF. Characterization of the receptors and mechanisms involved in the cardiovascular actions of sCCK-8 in the pithed rat. *Br J Pharmacol* 1995; **115**: 660-664

11 **Zhao XY,** Ling YL, Shang ZL, Li Q, Yin JX, Tan GJ. Cholecystokinin octapeptide increases free intracellular calcium of guinea pig cardiomyocytes through activation of Ca2+ channel and tyrosine kinase. *Shengli Xuebao* 2004; **56**: 31-35

12 **Guarini S,** Bazzani C, Leo L, Bertolini A. Haematological changes induced by the intravenous injection of CCK-8 in rats subjected to haemorrhagic shock. *Neuropeptides* 1988; **11**: 69-72

13 **Wang LF,** Ling YL, Huang SS, Zhang JL, Wan M, Hao RL, Ding XY, Zuo JL. Clearance of cholecystokinin by lung duringnormal and endotoric shock. *Zhongguo Bingli Shengli Zazhi* 1996; **12**: 571-574

14 **Riepl R,** Jenssen TG, Revhaug A, Burhol PG, Gierchksky KE, Lehnert P. Increase of plasma cholecystokinin by Escherichia coli endotoxin-induced shock in swine. *Z Gastroenterol* 1986; **24**: 691-699

15 **Cong B,** Ling YL, Gu ZY, Wan JX, Yao YX. Effect of cholecystokinin octapeptide on lipopolysaccharide- induced increase of NF-κB activity in rat lung tissues (Abstract). *Zhongguo Bingli Shengli Zazhi* 2000; **16**: 991

16 **Li SJ,** Cong B, Yan YL, Yao YX, Ma CL, Ling YL. Cholecystokinin octapeptide inhibits the *in vitro* expression of CD14 in rat pulmonary interstitial macrophages induced by lipopolysaccharide. *Chin Med J* 2002; **1159**: 276-279

17 **Noble F,** Roques BP. CCK-B receptor:chemistry,molecular biology,biochemistry and pharmacology. *Prog Neurobiol* 1999; **58**: 349-379

18 **Kulaksiz H,** Arnold R, Goke B, Maronde E, Meyer M, Fahrenholz F, Forssmann WG, Eissele R. Expression and cell-specific localization of the cholecystokinin B/gastrin receptor in the human stomach. *Cell Tissue Res* 2000; **299**: 289-298

19 **Wank SA.** G protein-coupled receptors in gastrointestinal physiology I. CCK receptors: an exemplary family. *Am J Physiol* 1998; **274**: G607-G613

20 **Monstein HJ,** Ohlsson B, Axelson J. Differential expression of gastrin, cholecystokinin-A and cholecystokinin-B receptor mRNA in human pancreatic cancer cell lines. *Scand J Gastroenterol* 2001; **36**: 738-743

21 **Clerc P,** Leung-Theung-Long S, Wang TC, Dockray GJ, Bouisson M, Delisle MB, Vaysse N, Pradayrol L, Fourmy D, Dufresne M. Expression of CCK2 receptors in the murine pancreas: proliferation,transdifferentiation of acinar cells, and neoplasia. *Gastroenterology* 2002; **122**: 428-437

22 **Pagliocca A,** Wroblewski LE, Ashcroft FJ, Noble PJ, Dockray GJ, Varro A. Stimulation of the gastrin-cholecystokinin(B) receptor promotes branching morphogenesis in gastric AGS cells. *Am J Physiol Gastrointest Liver Physiol* 2002; **283**: G292-G299

23 **Okada N,** Kubota A, Imamura T, Suwa H, Kawaguchi Y, Ohshio G, Seino Y, Imamura M. Evaluation of cholecystokinin, gastrin, CCK-A receptor, and CCK-B/gastrin receptor gene expressions in gastric cancer. *Cancer Lett* 1996; **106**: 257-262

24 **Fontana MG,** Moneghini D, Villanacci V, Donato F, Rindi G. Effect of cholecystokinin-B gastrin receptor blockade on chemically induced colon carcinogenesis in mice:follow-up at 52

weeks. *Digestion* 2002; **65**: 35-40
25 **Reubi JC,** Schaer JC, Waser B. Cholecystokinin(CCK)-A and CCK-B/gastrin receptors in human tumors. *Cancer Res* 1997; **57**: 1377-1386
26 **Matsumori Y,** Katakami N, Ito M, Taniguchi T, Iwata N, Takaishi T, Chihara K, Matsui T. Cholecystokinin-B/gastrin receptor: a novel molecular probe for human small cell lung cancer. *Cancer Res* 1995; **55**: 276-279
27 **Behr TM,** Jenner N, Radetzky S, Behe M, Gratz S, Yucekent S, Raue F, Becker W. Targeting of cholecystokinin-B/gastrin receptors *in vivo*: preclinical and initial clinical evaluation of the diagnostic and therapeutic potential of radiolabelled gastrin. *Eur J Nucl Med* 1998; **25**: 424-430
28 **Zhu CQ,** Wang GH, Tang CR. Alteration of the concentration of both preprocholecystokinin and preproenkephalin mRNA after brain injury in rat: *in situ* hybridization study. *Acta Academiae Medicinae Shanghai* 1995; **22**: 266-268
29 **Van Bree L,** Zhang F, Schiffmann SN, Halleux P, Mailleux P, Vanderhaeghen JJ. Homolateral cerebrocortical changes in neuropeptide and receptor expression after minimal cortical infarction. *Neuroscience* 1995; **69**: 847-858
30 **Konturek SJ,** Konturek PC, Plonka A, Duda A, Sito E, Zuchowicz M, Hahn EG. Implication of gastrin in cyclooxygenase-2 expression in *Helicobacter pylori* infected gastric ulceration. *Prostaglandins Other Lipid Mediat* 2001; **66**: 39-51
31 **Brzozowski T,** Konturek PC, Konturek SJ, Pajdo R, Drozdowicz D, Kwiecien S, Hahn EG. Acceleration of ulcer healing by cholecystokinin (CCK): role of CCK-A receptors, somatostatin, nitric oxide and sensory nerves. *Regul Pept* 1999; **82**: 19-33

Science Editor Zhu LH **Language Editor** Elsevier HK

PO Box 2345, Beijing 100023, China
www.wjgnet.com
wjg@wjgnet.com

ELSEVIER

World J Gastroenterol 2005;11(22):3411-3418
World Journal of Gastroenterology ISSN 1007-9327

• *BASIC RESEARCH* •

Construction of a novel *Shigella* live-vector strain co-expressing CS3 and LTB/STm of enterotoxigenic *E.coli*

Ji-Ping Zheng, Zhao-Shan Zhang, Shu-Qin Li, Xiang-Xin Liu, Sheng-Ling Yuan, Peng Wang, De-Wen Zhan, Ling-Chun Wang, Cui-Fen Huang

Ji-Ping Zheng, Zhao-Shan Zhang, Shu-Qin Li, Xiang-Xin Liu, Sheng-Ling Yuan, Peng Wang, De-Wen Zhan, Ling-Chun Wang, Cui-Fen Huang, Beijing Institute of Biotechnology, Beijing 100071, China
Supported by the National High Technology Research and Development Program of China (863 Program), No. 2001AA215211, and the Military Basic Research Foundation, No. 01Z026
Correspondence to: Zhao-Shan Zhang, Beijing Institute of Biotechnology, 20 Dongdajie Street, Fengtai District, Beijing 100071, China. zhangzs@nic.bmi.ac.cn
Telephone: +86-10-63834140 Fax: +86-10-63833521
Received: 2004-09-13 Accepted: 2004-12-09

Abstract

AIM: To construct and evaluate a polyvalent recombinant vaccine strain *Shigella flexneri* 2a T32 against enterotoxigenic *E.coli* (ETEC).

METHODS: By using a host-plasmid balanced lethal system based on *asd* gene, a polyvalent recombinant strain was constructed to highly express CS3 and regularly express fusion enterotoxin of LTB subunit and mutant ST (LTB/STm) in a vaccine strain *Shigella flexneri* 2a T32 with specific deletion of *asd* gene. Fimbria CS3 was observed by immunofluorescence and electron microscopy assay. The security of LTB/STm was examined by ileal loop assay and suckling mouse assay. To evaluate this new candidate vaccine, it was compared with a previous vaccine strain in plasmid and protein level, growth assay and immunogenicity in Balb/c mice.

RESULTS: The newly constructed vaccine expressed CS3 and grew better than the previously constructed vaccine except for the lower expression of LTB/STm. Serum IgG and mucosal IgA against CS3, LTB, ST, and host lipopolysaccharide (LPS) were produced after immunization of Balb/c mice by oral route with the new strain. The titers were not significantly different from the Balb/c mice with the previous strain.

CONCLUSION: This novel candidate diarrheal vaccine can effectively induce serum and mucosal antibody responses against ETEC and *Shigella*.

Key words: ETEC; *Shigella flexneri*; CS3; LTB; ST; Vector vaccine; Immunogenicity

Zheng JP, Zhang ZS, Li SQ, Liu XX, Yuan SL, Wang P, Zhan DW, Wang LC, Huang CF. Construction of a novel *Shigella* live-vector strain co-expressing CS3 and LTB/STm of enterotoxigenic *E.coli*. *World J Gastroenterol* 2005; 11(22): 3411-3418

http://www.wjgnet.com/1007-9327/11/3411.asp

INTRODUCTION

Enterotoxigenic *E.coli* (ETEC) and *Shigella* are responsible for the high morbidity and mortality caused by diarrheal diseases suffered by infants and children in developing countries, as well as the prevalent causes of diarrhea in travelers from industrialized countries traveling to high risk areas of the world. Infections of these bacteria sometimes are concomitant with some serious complications. Every year more than one million children under the age of five die of diarrhea caused by the pathogens[1,2]. The death rate is much higher under unconventional circumstances such as calamities and wars, which threaten human life and health greatly. It is imperative to develop a safe and effective vaccine against ETEC and *Shigella*. Colonization factor antigens (CFAs) and enterotoxins are two important factors for ETEC diarrhea, a vaccine containing both types of these antigens together would prevent the ETEC diarrhea effectively. In this research, a main common fimbrial antigen CS3 and two kinds of enterotoxin LT and ST were constructed in FWL01, a *Shigella flexneri* 2a vaccine T32 without the *asd* gene. Multi-copy plasmid with strong promoters was used to obtain high expression and significant immune responses.

MATERIALS AND METHODS

Bacterial strains and plasmids

E.coli strains and plasmids used in this research are listed in Table 1. *Shigella* strain FWL01, an engineered *asd* mutant of attenuated strain 2a T32 from wild type strain 2457T, and *E. coli* X6097 were used as the host strain for Asd^+ plasmid[3]. Wild type strain 2457T was used for challenge experiments.

Enzymes and chemicals

Restriction enzymes, bacterial alkaline phosphatase, T4 DNA polymerase, and T4 DNA ligase were products of TaKaRa Co., Ltd (Kyoto, Japan) or England Biolabs (Beverly, MA). Other chemicals were purchased from Sigma (St. Louis, MO).

Table 1 Bacteria and plasmids used in this research

Strains and plasmids	Characteristics	Reference or source
E.coli		
E44815	CS3, LT, ST	NICPBP
X6097	*asd*$^-$	Dr. Roy CurissIII
S. flexneri		
2457T		Dr. Wang
FWL01	(*ipa-virg*)$^-$, *sm*^{R}, *asd*$^-$*ctxB*$^+$	Dr. Wang[3]
Plasmids		
pASD21	*amp*^{R}, *asd*	Dr. Wang [4]
pXZL01	*amp*^{R}, LTB/STm	This lab[5]
pHCSIII	*asd*, CS3	This lab[5]
pZHY22	*asd*, LTB/STm,CS3	This lab[6]
pZCS02	*asd*, LTB/STm, CS3	This study

Bacterial culture conditions

E.coli strains were routinely incubated in Luria-Bertani (LB) medium supplemented with appropriate antibiotics. The strains carrying CS3 were grown on colonization factor antigen (CFA) agar plates (1% casamino acid, 0.15% yeast extract, 2% agar, 0.04 mmol/L $MnCl_2$, and 0.4 mmol/L $MgSO_4$, pH 7.4) at 37 ℃ for 16 h to express fimbrieal CS3. Toxin medium (20 g/L casamino acids, 10 g/L yeast extract, 5 g/L NaCl, 15 g/L K_2HPO_4, 2 mg/L $MgSO_4 \cdot 7H_2O$, 2 mg/L $FeCl_3$, 1 mg/L $CoCl_2 \cdot 6H_2O$, 5 g/L glucose, 90 mg/L lincomycin, pH 7.4) was used to incubate wild strain E44815 or recombinant strains for elaboration of enterotoxins.

Antigens and antisera

LTB and polyclonal rabbit anti-serum of LTB were kindly obtained from Meguro-Ku Institute (Tokyo, Japan). Monoclonal antibodies against CS3 and ST were kindly obtained from Ann-Mari Svenneriholm (Sweden).

To prepare recombinant ST fusion protein with glutathione s-transferase (GST), nontoxic mutant ST precursor gene (proximate 200 bp) was cloned into plasmid pGEX-4T-2 of BL21(DE3). Fusion protein was expressed inductively at 37 ℃ for 2 h and purified with glutathione-linked agarose beads according to the pGEX vector protocol (Phamacia Biotech).

Animals

Japanese white rabbits (2-2.5 g), adult guinea pigs, female Balb/c mice at the age of six weeks and three days, respectively were obtained from the Experiment Animal Center of Military Academy of Medical Sciences (Beijing, China). All the animals were maintained in pathogen-free conditions. The mice were randomly divided into two groups of five. Group A was inoculated with the strain FWL01(pZCS02), group B was inoculated with the strain FWL01(pZHY22). The guinea pigs were inoculated with the recombinant strain FWL01(pZCS02) or wild type *Shigella flexneri* 2a strain 2457T into the conjunctival sac of one eye.

Construction of plasmid co-expressing CS3 and LTB/STm

pOMP, the plasmid used for expression of the ETEC antigens in *Shigella*, was derived from plasmid pUC18 by inserting a *asd* gene and deleting *amp*^{r} gene, and then adding a 138bp *Eco*RI-*Sac*I synthesized promoter *PompC* containing multiple cloning sites (*Xho*I, *Apa*I, *Eco*T14I, *Mlu*I and *Sac*I I) (Figure1). The o*mpC* promoter was selectively activated by

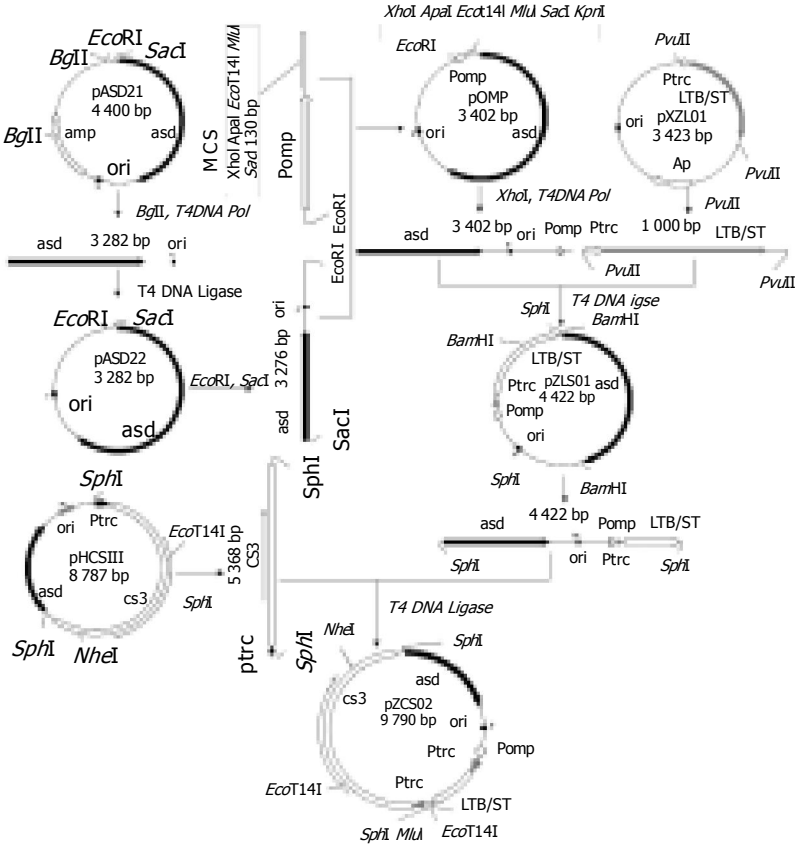

Figure 1 Construction of plasmid pZCS02.

increased osmolarity. To highly express fusion enterotoxin, the fusion gene LTB/STm with promoter *trc* was cloned as a proximate 1 kbp *Pvu*II- *Pvu*II fragment from plasmid pXZL01 into pOMP downstream of the promoter *ompC* digested with *Pvu*II, the operon encoding LTB/STm was expressed under promoters *trc* and *ompC*. Finally, the 5 368 bp CS3 gene with promoter *trc* was inserted into this vector from plasmid pHCSIII by *Sph*I digestion. This plasmid co-expressing CS3 and fusion enterotoxin LTB/STm was named pZCS02.

Transformation

Competent cells of *S.flexneri* FWL01 were prepared by growing the bacteria in LB broth to an optical density at 600 nm (A_{600}) of 0.4-0.6. The cells were centrifuged, washed twice with cold H_2O and once with 10% cold glycerol, and resuspended in the latter at 1/100 of the original volume. A mixture of 50 μL of cells and plasmid DNA was electroporated in 0.2-cm-path cuvette in a gene Pulser (Bio-Rad Laboratories, Hercules, CA) at 2.5 kV, 200 Ω, and 25 uF. Transformants were selected on LB plates containing streptomycin.

Preparation of CS3 extraction

The bacteria grown on CFA agar plates at 37 ℃ for 16 h were harvested and resuspended in PBS. The cells were heated at 60 ℃ for 30 min and violently vortexed for 1 min[7], then the suspension was sequentially centrifuged at 4 ℃, 15 000 *g* for 20 min and at 4 ℃, 65 000 *g* for 1.5 h. The precipitate containing CS3 was washed twice in 1% SDS, then dissolved in 0.1 mol/L PB and stored at -20 ℃.

Preparation of fusion enterotoxin

The bacteria were grown in CAYE with lincomycin for 16-18 h under conditions of vigorous aeration and agitation. The cells of culture broth were collected and resuspended in 0.1 mol/L PB at 1/20 of the original volume, then lysed by sonication. The crude lysate was clarified by centrifugation and precipitated with sequential ammonium sulfate precipitation (35% and 55% saturation). The precipitate containing LTB/STm was then harvested and dialyzed extensively against 50 mmol/L PB[8], the protein was stored at -20 ℃.

SDS-PAGE and Western blot analysis

Bacterial broth cultures were diluted to a same A_{600} of 1.0 and one of 1 mL culture was centrifuged and resuspended in 100 μL sample buffer and boiled for 5 min. Aliquots of 5 μL of each sample were electrophoresed on SDS-15% polyacrylamide gels. Gel was transferred to pyroxylin membranes. The membranes were blocked by incubation in PBS-0.05% Tween 20 (PBS-T) containing 5% defatted milk for 2 h, incubated with primary absorbed polyclonal rabbit anti-sera or monoclonal anti-sera antibodies specific for each antigen for 1 h and washed thrice in PBS-T. Then the membranes were incubated in goat anti-rabbit or anti-mouse IgG labeled with horseradish peroxidase specific for primary antibodies at the appropriate concentration for 1 h and washed thrice with PBS-T. The membranes were developed with 3,3'-diaminobenzidine (DAB) and hydrogen peroxide[9].

Immunofluorescence microscopy

CS3 fimbria expressed on *Shigella* was detected by indirect immunofluorescence according to the procedure described previously[10]. The cells were harvested, washed, and resuspended in PBS in a 0.5 mL tube at 1.0 of A_{600} from CFA plates after 16 h growth, then blocked by PBS-T containing 3% BSA for 30 min, stained with monoclonal antibody of CS3 fimbria diluted to 1∶500 for 1 h and with fluorescein isothiocyanate (FITC)-labeled goat anti-mouse immunoglobulins (China) diluted to 1∶10 for an additional hour. At last, a drop of stained bacteria was added on glass slides and examined under an Olympus BX50 fluorescence microscope (Olympus Optical Co.) equipped with epi-illumination and interference filters for FITC.

Electron microscopy

The cells were harvested from CFA plates, resuspended in PBS and placed onto 200-mesh copper grids coated with carbon formvar for 2 min. The grids were then stained for 10 s with 2% phosphotungstic acid (pH 7.2) and examined under a Philips TECHNAI 10 transmission electron microscope at 80 kV[11].

Stability assay

Fresh single colony from LB plate of *Shigella* containing the recombinant plasmid was inoculated and incubated for 12 h in LB broth at 37 ℃ and shaken at 200 r/min. A 10^{-2} dilution of overnight cultures was added to 5.0 mL fresh LB broth with or without 50 μg/mL diaminopimelic acid (DAP) and incubated at 37 ℃. After 10 generations (approximately 12 h), the cultures were diluted and the procedure was continued for 100 generations in the same type of media. Then samples of the cultures were diluted to $1/10^6$ into fresh LB broth and spread on LB plates containing DAP. One hundred colonies selected randomly were inoculated on fresh LB plates and recorded the number of new colonies the next day. Ten new colonies were randomly selected for detecting the maintenance of plasmid with CS3 slide agglutination test. Each stability test was performed twice[12].

Growth assay

A single colony of recombinant *Shigella* was inoculated and incubated in LB medium for 24 h, the A_{600} of the bacterial culture was recorded every 2 h, then growth curves were drawn.

Security assay

Security of the recombinant strain was measured by ileal loop assay to detect LT activity. Suckling mouse assay was used to detect ST activity and Sereny keratoconjunctivitis test was performed to detect *Shigella* activity. The method of ileal loop assay of LT was performed as follows. After being fasted for 48 h, six ileal loops of approximately 10 cm in length were made in an adult Japanese white rabbit. One milliliter of culture filtrates of ETEC-*Shigella* derivatives was inoculated into each loop as described previously[13]. After 18 h, rabbits were killed and the loops were examined for fluid accumulation. E44815 and FWL01 served as positive and negative control. The result was expressed as

milliliters of fluid accumulation per centimeter of loop. Suckling mouse assay of ST was performed as follows. A total of 0.1 mL aliquot of each culture supernatant [FWL01 (pZCS02), E44815, and FWL01] was directly delivered to the stomach of infant mice (three days old) via a flexible plastic tube. Three hours later, each mouse was weighed. The intestine was removed from the mice and weighed, the ratio of gut weight to remaining carcass weight (G/C ratio) was calculated. A G/C ratio of ⩾0.083 corresponded to unambiguous accumulation of fluid in the gut lumen and considered as a positive result for ST[14]. To detect the host strain security, recombinant strain was harvested from CFA plates and 10 μL of it was inoculated into the conjunctival sac of one eye of guinea pigs. Inflammatory responses of the inoculated eyes were observed for 5 d. Wild type *S. flexneri* 2a 2457T served as positive control[15].

Immunization and sample collection

Overnight cultures of the immunizing strains were harvested from CFA plates without any antibiotics and suspended in PBS to a concentration of 10^{10} CFU/mL. Before immunization, the mice were deprived of food and water for 4 h. The mice were incubated with feeding needles for intragastrical delivery of 100 μL of saturated NaHCO3. After 30 min, the mice were administered 200 μL bacterial suspensions and fasted for an additional 30 min. The mice were immunized on d 0, 14, and 28. Blood and fecal samples were collected from mice at pre-immunization and two weeks following each immunization, and serum was obtained by puncturing eyes. The blood was allowed to clot for 30 min at room temperature, centrifuged at 5 000 r/min for 10 min, and the serum was collected and stored at -20 ℃. Approximately 4 g of feces was added into 1 mL buffer. The fecal pellets were soaked in ice water for 15 min, and vigorously vortexed for 1 min, and the supernatants were stored at -20 ℃. To collect intestinal secretions, after the last collection of serum and fecal samples, whole small intestine from the duodenum to the ileocecal junction was excised and broken into pieces, then 3 mL buffer (PBS, 0.01 mol/L EDTA) was added to vortex vigorously for 1 min. After centrifugation at 13 000 *g* for 30 min at 4 ℃, supernatants were stored at -20 ℃.

ELISA

Antibodies against CS3, LTB, ST and lipopolysaccharide (LPS) were determined by ELISA[16,17]. Two-fold serially diluted immune serum was added to antigen-coated wells followed by goat anti-serum IgG and IgA. The absorbance was read at 492 nm, Endpoint titers were recorded as the reciprocal of the highest serial dilution of immune serum at which the OD was at least twice that of the non-immune control serum (non-immunized mice) and A_{492} of the immune serum was at least 0.2. Fecal and intestinal samples were diluted at 1:20 and 1:50. The absorbance at 492 nm represented the antibody response of each sample.

RESULTS

Construction of plasmid encoding ETEC antigens

We previously demonstrated the ability of *S. flexneri* 2a T32 vaccine derivative strain FWL01 to express the ETEC antigens CFA/I, CS3, CS6, LTB, and ST, and to elicit serum IgG and mucosal IgA responses to both ETEC and O antigens of the *Shigella* vector following intragastric immunization of Balb/c mice[6,18]. The plasmid pZHY22 expressing CS3 and fusion LTB/STm[6] previously constructed was of high molecule (12 kb) which means the low stability and poor growth of strain, although robust immune responses were induced using this recombinant plasmid[6]. To improve the expression system of the plasmid, much lower molecular weight plasmid pZCS02 (9 790 bp) was constructed without any antibiotic gene. Promoter *trc* was engineered into the upstream of CS3 operon and two promoters, *ompC,* and *trc*, were cloned into the upstream of fusion enterotoxin gene, in order to enhance the expression of CS3 and fusion enterotoxin. Moreover, the additional multi-cloning site allowed to clone more genes encoding ETEC antigens of interest. This new generation kept the *asd* gene and colE1 *ori* for multiple copies in previous plasmid pZHY22. As the *asd* gene was deleted in the vector strain FWL01, this plasmid-host balanced lethal system by *asd* has been constructed to minimize plasmid loss from actively growing bacteria without any antibiotic[4-6].

Expression of CS3 in shigella

Following electrophoresis with FWL01 (pZCS02) extracts, CS3 fimbria production was detected by Western immunoblotting assay (Figure 2A). The results indicated that the cloned CS3 operon in pZCS02 of FWL01 encoding a 17.5-ku protein corresponded to the CS3 fimbrial structural subunit. To compare the expression of CS3 in pZCS02 and pZHY22, the whole cell extracts of the two *Shigella* strains containing one of these plasmids prepared under the same condition were electrophoresed in one gel (Figure 2B). The results showed that the CS3 expression was boosted by promoter *trc* in plasmid pZCS02.

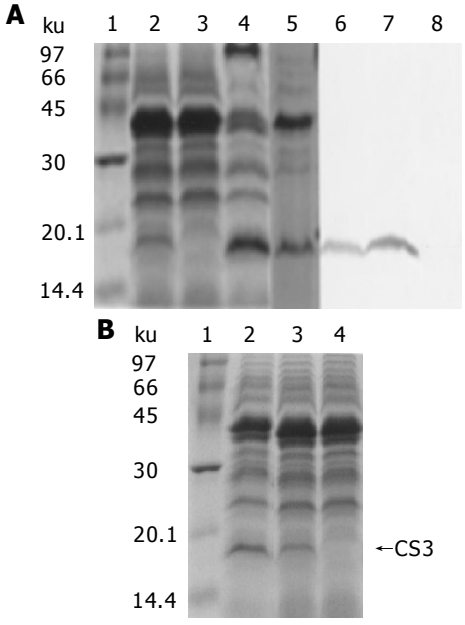

Figure 2 Expression of CS3 in *S. flexneri* FWL01(pZCS02) (**A**) and FWL01 (pZHY22) (**B**): Lane 1: Protein marker; lane 2: Extraction of FWL01(pZCS02); lane 3: Extraction of FWL01(**A**) and FWL01(pZHY22) (**B**); lane 4: Extraction of E 44815 (**A**) and FWL01(**B**); lane 5: Purified CS3 extraction of FWL01(pZCS02); lane 6: purified CS3 extraction of FWL01(pZCS02); lane 7: Purified CS3 fimbriae; lane 8: Extraction of FWL01.

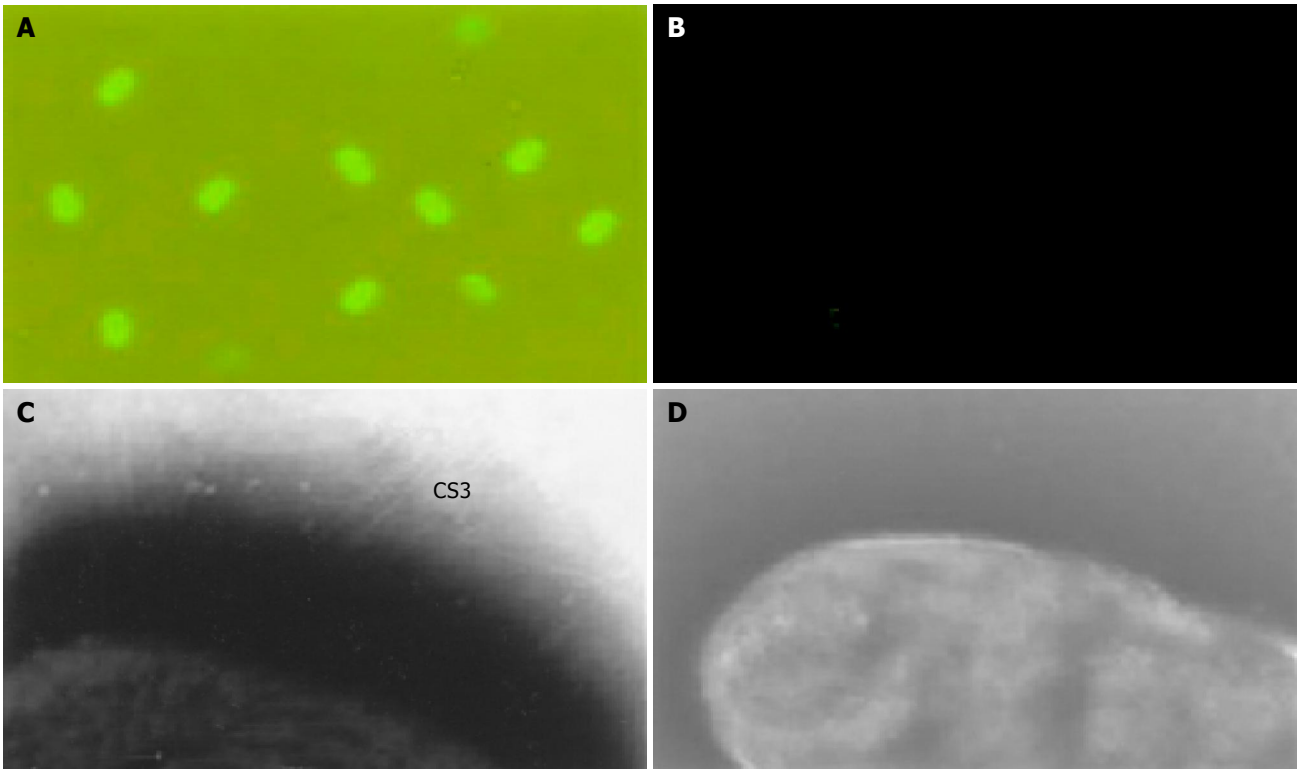

Figure 3 Immunofluorescence microscopy of FWL01(pZCS02) with primary anti-CS3 serum and followed FITC-labeled goat anti-mouse IgG (**A**) and with primary PBS and followed FITC-labeled goat anti-mouse IgG (**B**), electron microscopy of fimbrial CS3 on surface of FWL01(pZCS02) (**C**) and vector strain *S. flexneri* FWL01 (**D**).

Since ETEC strains could colonize the small-bowel mucosa by means of surface fimbrial antigens and induce antibody responses against these fimbriae to provide protection against ETEC disease, the expression of functional fimbrial CS3 is required for vaccine to inhibit attachment of the ETEC. CS3 expression and typical fimbrial morphology on the surface of vector *Shigella* strain were detected and confirmed by immunofluorescence and electron microscopy (Figure 3).

Expression of LTB/STm and safety assay of recombinant Shigella

The fusion gene LTB with mutant precursor form of ST at downstream of promoters *ompC* and *trc* was designed to expect high expression of this fusion enteroxin by regulation of osmolarity. This mutant ST had two amino acid substitutions at positions 12 and 14 of mature toxin which dramatically diminished the activity (GDP ribosylating) of the toxin and rendered it virtually nontoxic. Therefore the expression of this fusion enterotoxin was driven from the osmotically responsive *ompC* promoter and *trc*. Western blot assay indicated the LTB/STm protein was about 18.4 ku (Figure 4A) and had lower expression in plasmid pZCS02 than in vector pZHY22 in *Shigella* (Figure 4B). The results might be caused by *ompC* of osmoregulation. The ileal loop and suckling mouse assays (Table 2) exhibited the fusion enterotoxin was safe without LT and ST activities. Sereny keratoconjunctivitis test suggested that all the eyes attacked with FWL01 (pZCS02) were not infected, while negative-control animals exhibited full-blown keratoconjunctivitis within three days following conjunctiva challenged with wild type *S. flexneri* 2a.

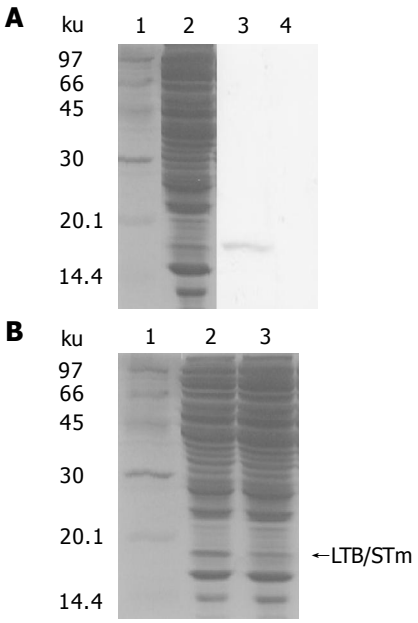

Figure 4 Expression of fusion protein LTB/STm of FWL01 (pZCS02). **A**: SDS-PAGE and Western blotting of fusion protein LTB/STm of FWL01 (pZCS02). Lane 1: Protein marker; lane 2: Lysate of the whole cell of FWL01 (pZCS02); lane 3: Lysate of the whole cell of FWL01 (pZCS02); lane 4: Lysate of FWL01; **B**: Comparison of the expression of LTB/STm between FWL01 (pZCS02) and FWL01 (pZHY22) under the same conditions. Lane 1: Protein marker; lane 2: Lysate of the whole cell of FWL01 (pZCS02); lane 3: Lysate of the whole cell of FWL01 (pZHY22).

Stability assay of plasmid

To determine whether the module of *asd* host-plasmid

Table 2 Suckling mouse assay of ST

Strain	G/C	Positive(+) Negative(–)	Suckling mice
ETEC 44815	0.126±0.04	+	5
FWL01	0.067±0.04	–	5
FWL01(pZCS02)	0.065±0.03	–	5

G/C is the ratio of gut weight to remaining carcass weight. A G/C ratio of ⩾0.083 is positive.

Table 3 ELISA detection (A_{492}) of intestinal sIgA

Intestinal sIgA	Anti-CS3	Anti-LTB	Anti-ST	Anti-LPS
Negative control	0.109±0.001	0.144±0.004	0.077±0.003	0.121±0.005
FWL01(pZHY22)	0.972±0.191	0.570±0.270	0.172±0.023	0.558±0.121
FWL01(pZCS02)	0.741±0.153	0.803±0.371	0.259±0.088	0.384±0.082

Samples were diluted at 1:50.

balanced lethal system was efficient, plasmid-containing colonies were grown in LB medium with or without DAP. After 100 generations, all colonies tested in cultures without DAP showed that the plasmid was present in 100% of the cells, whereas only 60% of the cells cultured with DAP contained the plasmid. All the randomly selected colonies were agglutinated with CS3 fimbrial anti-serum. The results suggested that the *asd* host-plasmid balanced lethal system was an efficient module to stabilize plasmid. The 24 h growth curves showed that the growth of FWL01 (pZCS02) was faster than that of FWL01 (pZHY22) and nearly identical to the carrier FWL01. The results indicated that low molecular pZCS02 and expression of LTB/STm in pZCS02 by osmoregulation reduced the negative influence on FWL01.

Immunogenicity of FWL01(pZCS02)

To assess the immunogenicity of the *S. flexneri* vaccine derivative strain FWL01 containing pZCS02, we studied whether the immune responses to each of the represented antigens from the vaccine were as equivalent as or higher than those elicited by the previously constructed strain FWL01(pZHY22). Balb/c mice were immunized with the strains FWL01(pZCS02) and FWL01(pZHY22), respectively. The results of the immunogenicity study are summarized in Figure 5 and Table 3. Both groups responded to ETEC antigens and *Shigella* vector itself with both serum IgG and mucosal antibodies against CS3, LTB, ST, and LPS. Each response observed following the primary immunization was boosted to higher levels following the second immunization. Moreover, the two groups elicited approximately equivalent antibody responses following each immunization. However, the mucosal responses to CS3 of group A immunized with FWL01 (pZCS02) were somewhat lower than those of group B immunized with FWL01 (pZHY22), though the difference was less than two-fold and not statistically significant.

DISCUSSION

In human ETEC diarrheal infection, fimbria-mediated attachment to enterocytes of the proximal small intestine and enterotoxin production are involved in the pathogenesis and offer targets for immunoprophylaxis. Approximately 35% of enterotoxins express LT and ST, and about 35% express only ST and the rest express only LT of the ETEC strain[19]. Twenty different colonization factor antigens of CFAs in human ETEC have been described[19]. Epidemiological studies carried out in many geographical areas have shown that the occurrence of different CFAs of human ETEC varies[20]. But the most prevalent antigenic CFA/I and the complex of CS1-CS6 have been found in 50-80% of clinical human ETEC isolates[21]. These seven fimbrial types are considered essential in future ETEC vaccine to elicit broad-spectrum protection. CFAs have been shown to cooperate synergistically with ETEC toxin antigen in providing protection against ETEC[22]. Effective ETEC vaccine should be given orally and evoke both anticolonization and antitoxic immune responses in the intestine.

Shigellae cause diseases by invading the colonic epithelium through specialized M cells and then spread from cell to cell with inflammatory responses, leading to cell death and dysentery[23]. There are four species of *Shigellae*. *S. dysenteriae* (group A), *S. flexneri* (group B), *S. boydii* (group C) and *S. sonner* (group D). *S. flexneri* serotypes are the most common agents of endemic shigellosis in developing countries[24]. Protective immunity against *Shigella* is serogroup and largely serotype-specific, as it is targeted against epitopes residing within the O polysaccharide of LPS. Live, oral, attenuated vaccine strains are safe and effective in eliciting protective immunity.

Attenuated *Shigella* vaccine strain exhibits as a live vector

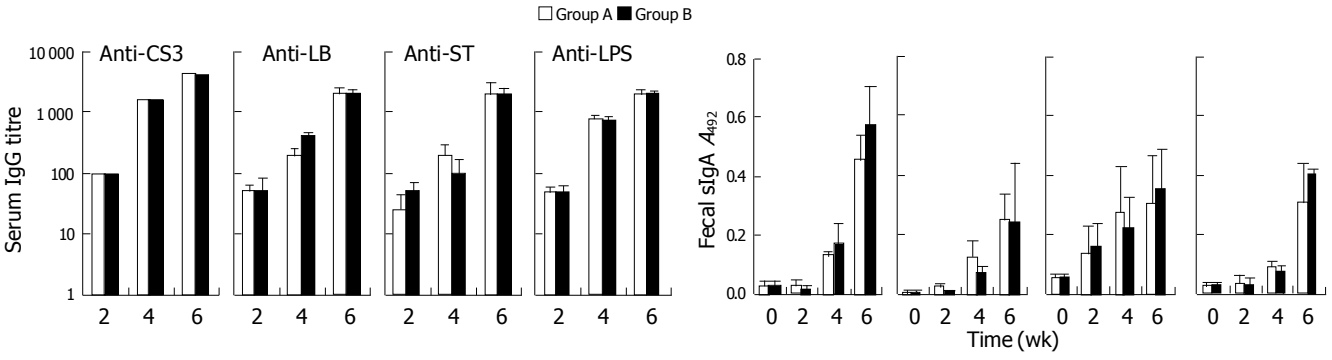

Figure 5 Antibody responses to ETEC antigens and *Shigella* 2a in orally immunized Balb/c mice.

for ETEC antigens within the gut-associated lymphoid tissue. In order to create a multivalent vaccine against both *Shigella* and ETEC, we used live attenuated strains of *S. flexneri* 2a as a vector for expression of CFA/I, CS6, CS3, and fusion enterotoxin LTB/STm. These live vector constructs are able to elicit both serum and mucosal immune responses against O antigens of the *Shigella* vector and the ETEC antigens following intragastric immunization in the Balb/c mice model. We have previously engineered both CS3 and nontoxic fusion enterotoxin LTB/STm with promoter *trc* into derivative plasmid pBR322 to construct pZHY22 in FWL01. The low level of CS3 expression and poor growth of the ETEC-*Shigella* strain were up to our expectation, though each ETEC antigen had high immunogenicity[6].

In this study we constructed pZCS02, a novel plasmid carrying the genetic determinants encoding CS3 and fusion LTB/STm derivate from pUC18. There is evidence that the expression level of CS3 is higher in pUC18 than in pBR322[18]. Based on the previous plasmid pZHY22, we cloned a *trc* promoter into the upstream of CS3 and an *ompC* promoter into the upstream of *trc* promoter and fusion enterotoxin LTB/STm into pZCS02. Thus this plasmid (9 790 bp) is smaller than pZHY22 (12 000 bp). In theory, Promoter can enhance expression of the downstream gene. The results showed that the expression of CS3 in pZCS02 was higher than that in pZHY22. Moreover, the growth of *Shigella* containing pZCS02 was much better than that of *Shigella* containing pZHY22. These advantages are required for ETEC vaccine. But the expression of LTB/STm was unexpectedly lower than that of pZHY22, which may be caused by the *ompC* activity of osmoregulation.

It was also demonstrated in our work that immunization with FWL01 (pZCS02) elicited immune responses not only to CS3, LTB and ST, but also *Shigella* O antigen. Specific serum and mucosal antibody responses were generated against ETEC antigens. Moreover, these responses were approximately similar to those elicited by immunization with live vector FWL01 carrying pZHY22. The immune responses against CS3 even decreased slightly. One reasonable explanation is the lower expression of LTB/STm. LTB like CTB, is a potent adjuvant, which influences the immune response against CS3.

In theory, surface expression of ETEC fimbrial antigens and elaboration of ETEC enterotoxins can alter the immunogenicity and safety of the *shigella* vector. However, the two groups of Balb/c mice immunized with this *Shigella* live vector expressing both ETEC fimbrial and enterotoxic antigens had high serum and mucosal responses. Guinea pigs challenged with this vaccine containing ETEC antigens had no inflammatory response compared to 100% keratoconjunctivis after inoculation of wild type *shigella*.

It should be noted that the *asd* system not only stably maintains the *asd*+ plasmid in *asd* mutant vector FWL01, but also eliminates the need of drug resistance markers, thus avoiding use of antibiotics during fermentation of vaccine. FWL01 is a derivate of *S. flexneri* 2a vaccine T32 without *asd*. Every year, 62.8-77.3% of shigellosis are caused by *S. flexneri* in China[25]. We have engineered CFA/I and CS6 in FWL01 and obtained satisfactory immune responses to the two antigens in a Balb/c mice model[26]. This novel vector vaccine may play an important role in preventing diarrheal diseases caused by ETEC and *S. flexneri* 2a.

ACKNOWLEDGMENTS

We thank Professor Yang Xiao and Ms. Yu-Chuan Li for immunofluorescence and electron microscopy facilities.

REFERENCES

1 **Gilligan PH.** *Escherichia coli*. EAEC, EHEC, EIEC, ETEC. *Clin Lab Med* 1999; **19**: 505-521
2 **Lindberg AA,** Pal T. Strategies for development of potential candidate *Shigella* vaccines. *Vaccine* 1993; **11**: 168-179
3 **Wang HL,** Feng EL, Lin Y, Liao X, Su GF. Construction of △ *asd* mutant of *Shigella flexneri* 2a strain T32. *Junshi Yixue Kexueyuan Yuankan* 2000; **24**: 81-87
4 **Wang HL,** Feng EL, Lin Y, Su GF. Coloning and sequencing of *shigella flexneri* 2a asd gene. *Weishengwuxue Yu Mianyixue Jinzhan* 2000; **28**: 15-19
5 **Xu B,** Zhang ZS, Li SQ, Shu D, Yu SY, Huang CF. Construction of the attenuated Salmonella typhimurium strain expressing Escherichia coli LT-B/ST fusion antigens. *Junshi Yixue Kexueyuan Yuankan* 1999; **23**: 172-174
6 **Liu TT,** Li SQ, Zhang ZS, Zheng JP, Liu XL, Luo G, Huang CF. Simultaneous expression of CS3 colonization factor antigen and LT-B/ST fusion enterotoxin antigen of enterotoxigenic *Escherichia coli* by attenuated *shigella flexneri* 2a. *Shengwu Huaxue Yu Shengwu Wuli Xuebao* 2003; **35**: 49-54
7 **Levine MM,** Ristaino P, Marley G, Smyth C, Knutton S, Boedeker E, Black R, Young C, Clements ML, Cheney C. Coli surface antigens 1 and 3 of colonization factor antigen II-positive enterotoxigenic *Escherichia coli*: morphology, purification, and immune responses in humans. *Infect Immun* 1984; **44**: 409-420
8 **Zhang ZS,** Li SQ, Dong ZZ, Huang CF. Fusion of genes enterotoxigenic *Escherichia coli* heat-liable and heat-stable enterotoxins. *Zhonghua Weishengwuxue He Mianyixue Zazhi* 1994; **14**: 219-222
9 **Sambrook J,** Fritsch EF, Maniatis T. Molecular Cloning: A Laboratory Manual, 2nd ed. New York: *Cold Spring Harbor Laboratory Press* 1989: 880-898
10 **Francisco JA,** Campbell R, Iverson BL, Georgiou G. Production and fluorescence-activated cell sorting of *Escherichia coli* expressing a functional antibody fragment on the external surface. *Proc Natl Acad Sci USA* 1993; **90**: 10444-10448
11 **Meacock PA,** Cohen SN. Partitioning of bacterial plasmids during cell division: a cis-acting locus that accomplishes stable plasmid inheritance. *Cell* 1980; **20**: 529-542
12 **Nakayama K,** Kelly SM, Curtiss R 3rd. Construction of an ASD^+ expression-cloning vector: stable maintenance and high level expression of cloned genes in a *salmonella* vaccine strain. *Biol Technol* 1988; **6**: 693-697
13 **Aitken R,** Hirst TR. Recombinant enterotoxins as vaccines against *Escherichia coli*-mediated diarrhoea. *Vaccine* 1993; **11**: 227-233
14 **Giannella RA.** Suckling mouse model for detection of heat-stable *Escherichia coli* enterotoxin: characteristics of the model. *Infect Immun* 1976; **14**: 95-99
15 **Sereny B.** Experimental keratoconjunctivitis *shigellosa*. *Acta Microbiol Acad Sci Hung* 1957; **4**: 367-376
16 **Li SQ,** Zhang ZS, Chen TM, Huang CF. Detection of colonization factor antigen I of enterotoxigenic *Escherichia coli* through ELISA. *Jiefangjun Yixue Zazhi* 1988; **13**: 271-273
17 **Ahren C,** Wenneras C, Holmgren J, Svennerholm AM. Intestinal antibody response after oral immunization with a prototype cholera B subunit-colonization factor antigen enterotoxigenic *Escherichia coli* vaccine. *Vaccine* 1993; **11**: 929-934
18 **Dong ZZ,** Zhang ZS, LI SQ, Zhang BN, Huang CF. Clonging and expression of the gene encoding CS3 fimbriae antigen of

enterotoxigenic *Escherichia coli*. *Zhonghua Weishengwuxue He Mianyixue Zazhi* 1994; **14**: 84-88

19 **Gaastra W,** Svennerholm AM. Colonization factors of human enterotoxigenic Escherichia coli (ETEC). *Trends Microbiol* 1996; **4**: 444-452

20 **Sommerfelt H,** Steinsland H, Grewal HM, Viboud GI, Bhandari N, Gaastra W, Svennerholm AM, Bhan MK. Colonization factors of enterotoxigenic *Escherichia coli* isolated from children in north India. *J Infect Dis* 1996; **174**: 768-776

21 **Giron JA,** Xu JG, Gonzalez CR, Hone D, Kaper JB, Levine MM. Simultaneous expression of CFA/I and CS3 colonization factor antigens of enterotoxigenic *Escherichia coli* by delta aroC, delta aroD Salmonella typhi vaccine strain CVD 908. *Vaccine* 1995; **13**: 939-946

22 **Kaper JB,** Levine MM. Progress towards a vaccine against enterotoxigenic *Escherichia coli*. *Vaccine* 1988; **6**: 197-199

23 **Sansonetti PJ.** Microbes and microbial toxins: paradigms for microbial-mucosal interactions III. Shigellosis: from symptoms to molecular pathogenesis. *Am J Physiol Gastrointest Liver Physiol* 2001; **280**: G319-G323

24 **Kotloff KL,** Winickoff JP, Ivanoff B, Clemens JD, Swerdlow DL, Sansonetti PJ, Adak GK, Levine MM. Global burden of Shigella infections: implications for vaccine development and implementation of control strategies. *Bull World Health Organ* 1999; **77**: 651-666

25 **Pan SW.** Epidemic *Shiga* bacillus dysentery in China. *Zhonghua Liuxingbingxue Zazhi* 1988; **9**: 59-62

26 **Zheng JP,** Wang LC, Luo G, Li SQ, Duan HQ, Huang CF, Zhang ZS. Co-expression of CFA/I and CS6 of enterotoxingenic *Escherichia coli* (ETEC) in Shigella flexneri 2a T32 derivative strain FWL01. *Shengwu Huaxue Yu Shengwu Wuli Xuebao* 2003; **35**: 1005-1010

Science Editor Wang XL and Guo SY **Language Editor** Elsevier HK

PO Box 2345, Beijing 100023, China
www.wjgnet.com
wjg@wjgnet.com

ELSEVIER

World J Gastroenterol 2005;11(22):3419-3425
World Journal of Gastroenterology ISSN 1007-9327

• *BASIC RESEARCH* •

Intravenous acid fibroblast growth factor protects intestinal mucosal cells against ischemia-reperfusion injury via regulating Bcl-2/Bax expression

Wei Chen, Xiao-Bing Fu, Shi-Li Ge, Tong-Zhu Sun, Gang Zhou, Bing Han, Yi-Ri Du, Hai-Hong Li, Zhi-Yong Sheng

Wei Chen, Xiao-Bing Fu, Tong-Zhu Sun, Gang Zhou, Bing Han, Yi-Ri Du, Hai-Hong Li, Zhi-Yong Sheng, Wound Healing and Cell Biology Laboratory, Burns Institute, 304th Hospital, Trauma Center of Postgraduate Medical College, Beijing 100037, China
Shi-Li Ge, Institute of Radiation Medicine, Academy of Military Medical Sciences, Beijing 100850, China
Supported by the National Basic Science and Development Programme, No. G1999054204; the National Natural Science Foundation of China, No. 30170966, 30230370
Correspondence to: Professor Xiao-Bing Fu, MD, Wound Healing and Cell Biology Laboratory, 304th Hospital, Burns Institute, Trauma Center of Postgraduate Medical College, 51 Fu Cheng Road, Beijing 100037, China. fuxb@cgw.net.cn
Telephone: +86-10-66867396 Fax: +86-10-88416390
Received: 2004-05-27 Accepted: 2004-06-24

Abstract

AIM: To detect the effect of acid fibroblast growth factor (aFGF) on apoptosis and gene expression of bax and bcl-2 gene in rat intestine after ischemia/reperfusion (I/R) injury, and to explore the protective mechanisms of aFGF.

METHODS: One hundred and eight Wistar rats were randomly divided into sham-operated control group (C) (n = 6), intestinal ischemia group (I) (n = 6), aFGF treatment group (A) (n = 48) and intestinal ischemia-reperfusion group (R) (n = 48). In group I, the animals were killed after 45 min of superior mesenteric artery (SMA) occlusion, while in groups R and A, the rats sustained 45 min of SMA occlusion and were then treated with normal saline and aFGF, respectively, sustained 15 min, 30 min, 1, 2, 6, 12, 24, or 48 h of reperfusion, respectively. In group C, SMA was separated, but without occlusion. Apoptosis in intestinal villus was determined with terminal deoxynucleotidyl transferase mediated dUTP-biotin nick-end labeling technique (TUNEL). Intestinal tissue samples were taken not only for detection of bax and bcl-2 gene expression by RT-PCR, but also for detection of bax and bcl-2 protein expression and distribution by immunohistochemical analysis.

RESULTS: The rat survival rates in aFGF treated group were higher than group R (P<0.05) and the improvement of intestinal histological structures was observed at 2, 6, and 12 h after the reperfusion in group A compared with group R. The apoptotic rates were (41.17±3.49)%, (42.83±5.23)% and (53.33±6.92)% at 2, 6 and 12 h after reperfusion, respectively in group A, apparently less than those of group R at matched time points (50.67±6.95, 54.17±7.86, 64.33±6.47, respectively) (P<0.05). The bax gene transcription and translation were significantly decreased in group A *vs* group R, while mRNA and protein contents of Bcl-2 in group A were obviously higher than those in group R during 2-12 h period after reperfusion.

CONCLUSION: The changes in histological structure and the increment of apoptotic rate indicated that the intestinal barrier was damaged after intestinal I/R injury, whilst intravenous aFGF could alleviate apoptosis induced by ischemia and reperfusion in rat intestinal tissues, in which genes of bax and bcl-2 might play important roles.

Key words: Acid fibroblast growth; Ischemia; Reperfusion; Bcl-2 gene; Bax gene

Chen W, Fu XB, Ge SL, Sun TZ, Zhou G, Han B, Du YR, Li HH, Sheng ZY. Intravenous acid fibroblast growth factor protects intestinal mucosal cells against ischemia-reperfusion injury via regulating Bcl-2/Bax expression. *World J Gastroenterol* 2005; 11(22): 3419-3425
http://www.wjgnet.com/1007-9327/11/3419.asp

INTRODUCTION

aFGF belongs to a family of at least 20 related growth factors that bind to varying extents to four different cell surface receptors and their splicing variants. aFGF and basic FGF(bFGF) are the prototypic members of the family, and share a similar broad spectrum of biological activities. These two growth factors are mitogens *in vitro* for most of the ectodermal- and mesodermal-derived cell lines. In addition, these proteins show a wide range of endocrine-like activities[1-4]. Previous studies have shown that intravenous administration of exogenous bFGF could improve the physiological functions of intestine after I/R injury[5,6]. However, the protective mechanisms of aFGF on intestinal I/R injury remain unknown.

Apoptosis, a form of death characterized by cell shrinkage, plasma membrane blebbing, chromatin condensation and genomic DNA fragmentation, is essential for development and maintenance of tissue homeostasis[6,7]. On the other hand, apoptosis has been implicated in many diseases such as intestinal ischemic and reperfusion insult. I/R induced apoptosis in the jejunum and ileum[8]. However, little investigation has been conducted to determine whether the protective effect afforded

by aFGF relates to reduction in apoptosis during ischemia/reperfusion. The objective of this study was therefore to determine whether aFGF could protect the rat intestinal mucosa against ischemia/reperfusion-induced apoptosis. Since bcl-2 family of proteins plays a major role in determining the ultimate sensitivity or resistance of cells to myriad stimulus and insults that induce apoptosis[9-11], we also examined the effects of aFGF on gene expression of bcl-2 family underlying the protective mechanisms of aFGF on intestinal ischemia injury.

MATERIALS AND METHODS

Animal model and experimental design

One hundred and eight healthy male Wistar rats weighing 220±20 g (Animal Center, Chinese Academy of Military Medical Science, Beijing) were used in this study. Animals were housed in wire-bottomed cages placed in a room illuminated from 08:00 to 20:00 (12:12 h light-dark cycle) and maintained at (21±1) ℃. Rats were allowed free access to water and chow ad libitum. After the animals received anesthesia by 3% sodium pentobarbital (40 mg/kg), a laparotomy was performed. The superior mesenteric artery (SMA) was identified and freed by blunt dissection. A micro-bulldog clamp was placed at the root of SMA to cause complete cessation of blood flow for 45 min, and thereafter the clamp was loosened to form reperfusion injury. The animals were randomly divided into sham-operated control group (C) (n = 6), intestinal ischemia group (I) (n = 6), aFGF treatment group (A) (n = 48) and intestinal ischemia-reperfusion group (R) (n = 48). According to the different periods after reperfusion, groups R and A were further divided into 0.25, 0.5, 1, 2, 6, 12, 24, and 48 h subgroups, respectively (n = 6, each subgroup). In group I, the animals were killed after 45 min of SMA occlusion, while in groups R and A, the rats sustained 45 min of SMA occlusion and were treated with 0.15 mL normal saline and 0.15 mL saline plus 20 μg/kg aFGF (R&D Systems, Inc.) injected from tail vein, respectively, then sustained 15, 30 min, 1, 2, 6, 12, 24, or 48 h of reperfusion, respectively. In group C, SMA was separated, but without occlusion, and samples were taken after exposure of SMA for 45 min. In groups R and A, rats were killed at different time points after reperfusion, and intestinal tissue biopsies were taken. A small piece of tissue sample was fixed with 10% neutral buffered formalin for immunohistochemical detection of intestinal epithelial apoptosis, and protein expression of bax and bcl-2. The rest of tissue samples were placed in liquid nitrogen for detection of bax and bcl-2 gene expression by RT-PCR.

Histological staining

Formalin fixed, paraffin embedded intestinal samples were cut into 5-μm-thick sections, deparaffinized in xylene, rehydrated in graded ethanol, and then stained with hematoxylin-eosine (HE) for histological observation under light microscope.

In situ detection of cell death

The apoptotic cells in intestinal tissues were detected with the terminal deoxynucleotidyl transferase (TdT)-mediated dUDP-biotin nick end labeling (TUNEL) method. Specimens were dewaxed and immersed in phosphate-buffered saline containing 0.3% hydrogen peroxide for 10 min at room temperature and then incubated with 20 μg/mL proteinase K for 15 min. Seventy-five microliters of equilibration buffer were applied directly onto the specimens for 10 min at room temperature, followed by 55 μL of TdT enzyme and then at 37 ℃ for 1 h. The reaction was terminated by transferring the slides to prewarmed stop/wash buffer for 30 min at 37 ℃. The specimens were covered with a few drops of rabbit serum and incubated for 20 min at room temperature and then covered with 55 μL of anti-digoxigenin peroxidase and incubated for 30 min at room temperature. Specimens were then soaked in Tris buffer containing 0.02% diaminobenzidine and 0.02% hydrogen peroxide for 1 min to achieve color development. Finally, the specimens were counterstained by immersion in hematoxylin. The cells with clear nuclear labeling were defined as TUNEL-positive cells.

Immunohistochemistry

Immunostaining for bax and bcl-2 proteins was performed on paraffin sections with a high-temperature antigen-unmasking method in citrate buffer and ABC peroxidase, using monoclonal mouse antibodies against antigens (Santa Cruz Co., 1:100 in PBS), a goat anti-mouse secondary antibody (Santa Cruz Co., 1:100) and DAB substrate kit (Santa Cruz Co.). Sections of 5 μm thickness were cut and mounted onto slides coated with 3-triethoxysilylpropylamide. They were rehydrated and submerged in 3% hydrogen peroxide for 10 min, washed in PBS for 5 min, then blocked with 5% normal swine serum in PBS for 30 min at room temperature, followed by incubation with primary antibodies at a concentration of 5 μg/mL (diluted in PBS containing 5% swine serum) overnight at 4 ℃. Control slides were incubated with PBS without primary antibodies. Tissue sections were then washed in PBS and incubated for 60 min at room temperature with biotinylated secondary antibody and PBS. After washing in PBS, the sections were exposed to acidin-biotin complex for 60 min at room temperature and again washed in PBS. The sections were reacted with 0.5 mL/L DAB in 50 mmol/L Tris-HCl (pH 7.4), with 1 mL/L hydrogen peroxide for 5 min and counte-rstained with hematoxylin. The results of positive staining cells and their distribution were observed under a microscope of 400 magnification. Fifty intestinal villi were required for counting, and then the ratio of positive cells were calculated and analyzed.

RNA extraction and RT-PCR analysis

Total RNA was extracted using TRIzol reagent (Gibco BRL, USA), and then was serially diluted with water pretreated with diethylpyrocarbonate containing one unit RNase inhibitor per μL and 3 mmol/L dithiothreitol. RNA 1 μL, oligo (dT_{12-18}) 1 μL, avian myeloblastosis virus reverse transcriptase (AMV-RT) 1 μL, 10 mmol/L deoxynucleoside triphosphate (dNTP) 2 μL, 0.1 mol/L DTT 2 μL, 5× buffer 4 μL, and sterilized distilled water up to a total volume of 20 μL were incubated at 37 ℃ for 60 min. After reverse transcription, samples were heated at 95 ℃ for 5 min to denature the AMV-RT and stored at -20 ℃ for PCR. Subsequently, 2 μL of each reaction product was amplified in 50 μL of a PCR mixture. Then 29 cycles were performed with a Perkin-Elmer Cetus/DNA thermal cycler (Takara Shuzo Co.,

Table 1 Oligonucleotide primers for RT-PCR detection of bax, bcl-2 and β-actin mRNA transcripts

Genes	Upper primers	Lower primers
bax	5′-AGGTCTTTTTCCGAGTGGCAGC-3′	5′-CCCGGAGGAAGTCCAATGTCC-3′
bcl-2	5′-GACTTCGCCGAGATGTCCAG-3′	5′-GTGCAGGTGCCGGTTCAGG-3′
β-actin	5′-AGCCATGTACGTAGCCATCC-3′	5′-GCCATCTCTTGCTCGAAGTC-3′

Tokyo, Japan) at 94 ℃ for 1 min, 50 ℃ for 1 min, 72 ℃ for 1 min, and then at 72 ℃ for 10 min at the end of the procedure. Table 1 shows the synthesized oligonucleotide primers used for RT-PCR for genes of bax and bcl-2. In this study, β-actin, which is ubiquitously expressed, was used as a positive control in a pilot study before formal experimentation, and PCR reactions for each primer set were repeated four times to verify reproducibility of results. After PCR, 5 μL sample aliquots were electrophoresed on a 2% agarose gel for 30 min, stained with ethidium bromide and photographed. Densitometry was done with a Bechman densitometer. The level of gene expression was expressed as the ratio of the gray density of the objective gene over the gray density of β-actin.

Statistical analysis

All values were expressed as mean±SD. Differences in mean values were compared using SPSS 11.0 by one-way ANOVA and Student-Newman-Keul (SNK) test. $P<0.05$ was considered as statistically significant.

RESULTS

Change of morphological appearance

The histological evaluations revealed that damage to the small intestine in the 45-min ischemia group was small, with slightly edematous villus tips just after the ischemic period, while the partial loss of the mucosa could be observed at 2 h after reperfusion. During 6-12 h after reperfusion, the damage of intestinal epithelial cells, hemorrhage and necrosis could be found, accompanied by inflammatory cell infiltration into the intestinal wall. In the period of 24-48 h after reperfusion, the mucosal integrity was partially restored. Histological structure of the intestinal mucosa was markedly improved after administration of aFGF. The protective function of aFGF on intestinal mucosa was most effective during 2-12 h after reperfusion.

Change of cellular apoptotic rates

Apoptosis was measured and quantified by TUNEL assay in serial sections prepared from the middle quarter of the small intestine (jejunum). The time at which the animals were killed after a 45 min SMA occlusion followed by reperfusion was varied to further define the apoptotic response. Statistically significant increases in TUNEL-positive cells were not detectable until 1 h after reperfusion and were maximal at 12 h. The cellular apoptotic rate in intestinal mucosa after reperfusion for 12 h was 3.3 times that in group C. After reperfusion for 24 and 48 h, the mucosal apoptotic rates were restored to the level in group C. Administration of aFGF produced statistically significant decreases in the apoptotic rates compared with group R during 2-12 h after reperfusion ($P<0.05$). No significant decreases in apoptosis were observed at 24 and 48 h after reperfusion (Table 2).

Table 2 Effect of aFGF on the apoptotic rates in intestinal mucosa after ischemia-reperfusion insult (n = 6, mean±SD, %)

Groups	Group R	Group A
Group C	19.67±3.50	19.67±3.50
Group I	27.67±9.63	27.67±9.63
15 min after reperfusion	29.50±5.61	25.17±6.43
30 min after reperfusion	31.00±5.02[a]	26.00±4.86
1 h after reperfusion	34.67±5.47[a]	32.83±7.08[a]
2 h after reperfusion	50.67±6.95[a]	41.17±3.49[ac]
6 h after reperfusion	54.17±7.86[a]	42.83±5.23[ac]
12 h after reperfusion	64.33±6.47[a]	53.33±6.92[ac]
24h after reperfusion	28.50±5.47	23.33±3.83
48 h after reperfusion	26.00±5.76	22.00±4.60

[a]$P<0.05$ *vs* group C;[c]$P<0.05$ *vs* group R at matched time points.

Expression characteristics of bax and bcl-2 proteins

Quantitative immunohistochemical results for bax protein and bcl-2 protein were evaluated in Table 3. Protein

Table 3 Effect of aFGF on protein contents of bax and bcl-2 in intestinal villus after ischemia-reperfusion (n = 6, mean±SD, %)

Groups	Bax protein		Bcl-2 protein	
	Group R	Group A	Group R	Group A
Group C	19.83±3.66	19.83±3.66	35.33±4.59	35.33±4.59
Group I	23.83±7.65	23.83±7.65	28.17±4.12	28.17±4.12
15 min after reperfusion	25.00±5.93	19.83±5.27	29.83±6.12	31.17±5.04
30 min after reperfusion	28.00±9.23	20.33±4.76	28.83±5.85	30.17±5.95
1 h after reperfusion	37.83±4.75[a]	24.17±4.49[c]	24.50±6.16[a]	26.00±5.10[a]
2 h after reperfusion	47.67±7.26[a]	37.50±7.01[a,c]	20.67±7.15[a]	29.67±4.84[c]
6 h after reperfusion	54.67±5.28[a]	47.00±3.52[a,c]	18.83±5.35[a]	27.83±2.72[c]
12 h after reperfusion	46.33±4.27[a]	37.67±3.83[a,c]	19.50±4.37[a]	25.67±4.03[ac]
24 h after reperfusion	29.00±4.43	25.00±4.34	28.67±2.94	29.33±6.02
48 h after reperfusion	26.17±3.49	22.83±3.19	29.00±3.74	30.50±4.89

[a]$P<0.05$ *vs* group C;[c]$P<0.05$ *vs* group R at matched time points.

expression of bax was weak in the sham-operated intestinal tissues and ischemic tissues. However, the positive cellular rate elevated with the increment of duration after reperfusion injury. In the period of 2-12 h after reperfusion, bax was expressed at a dramatically higher level in comparison with group C ($P<0.05$) and positive signals of bax were distributed in the whole structure of villus, including mucosa, submucosa, lamina propria and myometrium. At 24 h after reperfusion, the positive cellular rate was not substantially changed compared with group C. Treatment of aFGF could apparently inhibit the protein expression of Bax in intestinal mucosa during 2-12 h after reperfusion in comparison with group R at different matched times ($P<0.05$) (Figure 1). There was a negative correlation between positive expression levels and the intensities of bax and bcl-2. Bcl-2 was strongly expressed in the sham-operated intestinal tissues and positive particles of bcl-2 were mainly localized in the cytoplasm and nuclei of villus cells and in the nuclei of crypt cells (Figure 2). bcl-2 expression level in intestinal mucosa decreased with increasing reperfusion time, and the positive cellular rate was restored to the level of sham-operated tissues at 24 and 48 h after reperfusion. Compared with the normal saline treated group, the positive cellular rates of bcl-2 were significantly higher during the period from 2 to 12 h after reperfusion in aFGF treated group ($P<0.05$).

Expression characteristics of bax and bcl-2 mRNA

We investigated gene expression of bax and bcl-2 in differentially treated intestinal villus through RT-PCR analysis (Table 4). Figure 3 shows bax gene amplification product in villus of differentially treated groups, which was composed of 168 bp, had a remarkable and rapid increment in intestinal villus after ischemia and reperfusion, peaked at 1 h after reperfusion, and then decreased to the levels similar to that of sham-operated group. After aFGF administration, the levels of bax in villous cells were apparently lower than that in normal saline treated group, especially at 15 min, 1, 2 and 6 h after reperfusion ($P<0.05$). The length of RT-PCR products of bcl-2 was 228 bp (Figure 4). Bcl-2 gene was expressed at a remarkably lower level in villus compared with sham-operated group after reperfusion. After treatment with aFGF, although bcl-2 gene was weakly expressed during the period from 15 min to 6 h after reperfusion versus group C, the level of bcl-2 gene expression returned to the level of sham-operated group at 12-48 h after reperfusion. In group A, the amounts of bcl-2 mRNA transcript were markedly elevated in comparison with group R at matched times after reperfusion ($P<0.05$), except for at 15 min after reperfusion (Tabel 4). The length of RT-PCR products of β-actin was 294 bp (Figure 5). As RT-PCR positive control, the quantity of β-actin mRNA was relatively the same in all intestinal villi analyzed (Figure 5).

DISCUSSION

It is well known that the intestinal mucosa is highly sensitive

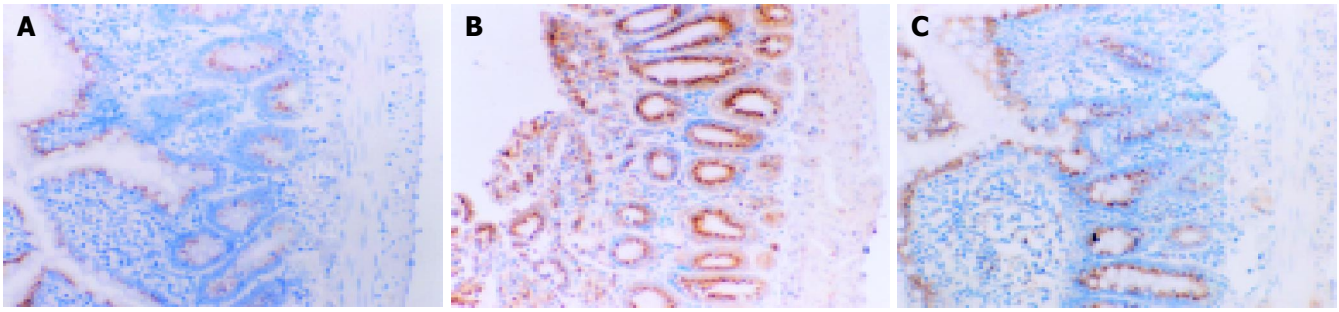

Figure 1 The expression of Bax protein in sham-operated control group (**A**), 6 h after ischemia-reperfusion in group R (**B**) and 6 h after ischemia-reperfusion in group A (**C**). Protein expression of Bax was weak in sham-operated control group. Bax was strongly expressed in villus at 6 h after reperfusion, and was mainly localized in the whole constitutive cells of villus. The positive stained cells decreased remarkably at 6 h after reperfusion in group A *vs* group R.

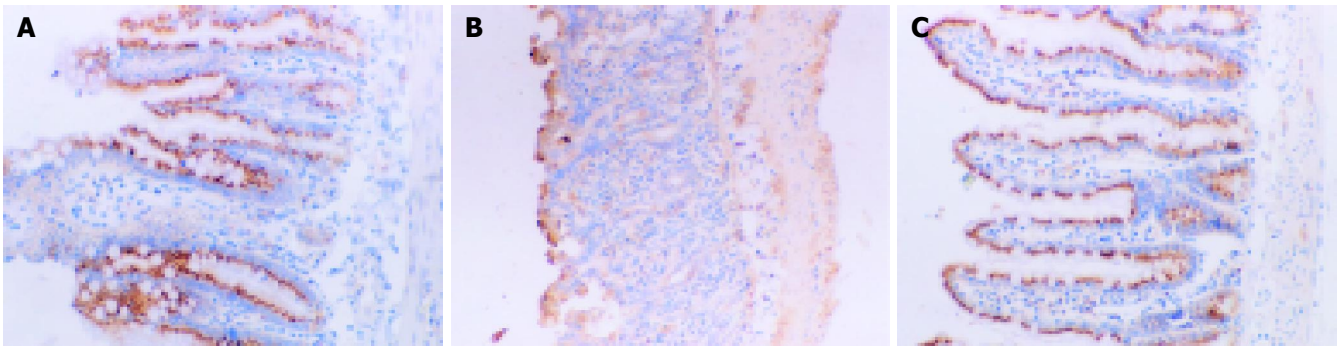

Figure 2 The expression of bcl-2 protein in sham-operated control group (**A**), 6 h after ischemia-reperfusion in group R (**B**) and 6 h after ischemia-reperfusion in group A (**C**) bcl-2 was strongly expressed in the sham-operated intestinal tissues and positive particles of bcl-2 were mainly localized in the lower half of the villus and in the cytoplasm and nuclei of villus cells. bcl-2 expression level decreased at 6 h after reperfusion in group R. Compared with group R, the positive cellular rates of bcl-2 were significantly higher at 6 h after reperfusion in group C.

Table 4 Effect of aFGF on gene expression of bax and bcl-2 in intestinal villus after ischemia-reperfusion (n = 6, mean±SD, %)

Groups	Bax gene		bcl-2 gene	
	Group R	Group A	Group R	Group A
Group C	80.956±8.141	85.729±7.523	24.614±3.175	27.803±3.347
Group I	105.961±8.880[a]	97.815±9.568[a]	11.221±2.752[a]	10.744±3.549[a]
15 min after Reperfusion	93.937±3.281[a]	83.928±6.659[c]	23.057±4.642	20.457±5.013[a]
30 min after Reperfusion	94.138±4.583[a]	94.288±3.707	12.921±3.059[a]	17.961±1.653[a,c]
1 h after Reperfusion	108.367±12.668[a]	76.063±6.337[c]	11.789±3.200[a]	20.529±2.200[a,c]
2 h after Reperfusion	90.176±6.630	76.723±6.153[c]	9.083±2.168[a]	20.655±1.544[a,c]
6 h after Reperfusion	85.837±6.037	62.415±3.535[ac]	6.512±2.477[a]	15.510±1.757[a,c]
12 h after Reperfusion	86.987±6.331	80.155±6.756	7.882±2.086[a]	27.349±3.592[c]
24 h after Reperfusion	85.230±9.132	90.479±5.137	15.898±2.393[a]	30.364±2.298[c]
48 h after Reperfusion	86.728±7.278	94.846±14.403	14.755±3.268[a]	23.937±2.726[c]

[a]P<0.05 *vs* group C; [c]P<0.05 *vs* group R at matched time points.

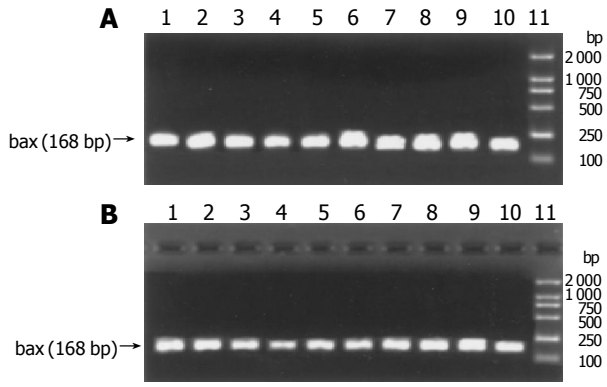

Figure 3 Expression of bax gene in normal saline treated (**A**) and aFGF treated (**B**) rat intestinal villus. Bar indicates the size of RT-PCR cDNA products. 1: 48 h after reperfusion, 2: 24 h after reperfusion, 3: 12 h after reperfusion, 4: 6 h after reperfusion, 5: 2 h after reperfusion, 6: 1 h after reperfusion, 7: 30 min after reperfusion, 8: 15 min after reperfusion, 9: ischemia group, 10: sham-operated control group, 11: DL2000 marker.

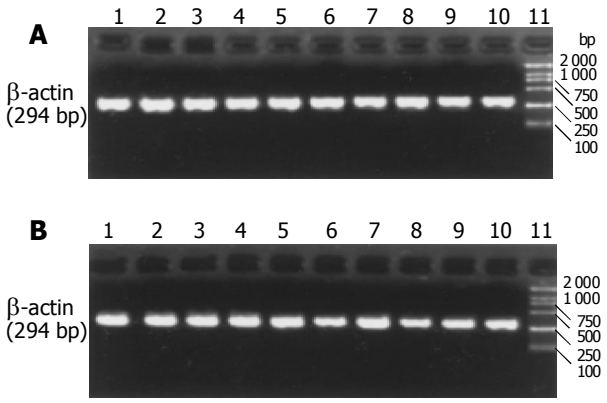

Figure 5 Expression of β-actin gene in normal saline treated (**A**) and aFGF treated (**B**) rat intestinal villus. Bar indicates the size of RT-PCR cDNA products. 1: 48 h after reperfusion, 2: 24 h after reperfusion, 3: 12 h after reperfusion, 4: 6 h after reperfusion, 5: 2 h after reperfusion, 6: 1 h after reperfusion, 7: 30min after reperfusion, 8: 15 min after reperfusion, 9: ischemia group, 10: sham-operated control group, 11: DL2000 marker.

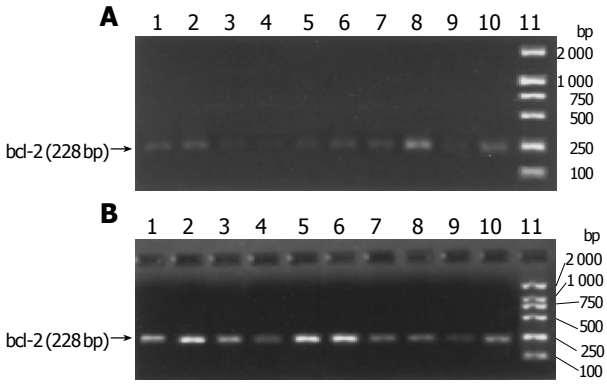

Figure 4 Expression of bax gene in normal saline treated (**A**) and aFGF treated (**B**) rat intestinal villus. Bar indicates the size of RT-PCR cDNA products. 1: 48 h after reperfusion, 2: 24 h after reperfusion, 3: 12 h after reperfusion, 4: 6 h after reperfusion, 5: 2 h after reperfusion, 6: 1 h after reperfusion, 7: 30 min after reperfusion, 8: 15 min after reperfusion, 9: ischemia group, 10: sham-operated control group, 11: DL2000 marker.

to I/R, which may cause release of bacteria and toxin from the gut into the host blood circulation and changes of inflammatory factors, cytokines and growth factors, resulting in damage to the intestinal barrier. In the current study, we found that I/R, following occlusion of the SMA, induced apoptosis in the intestinal villus. Results of TUNEL examination displayed that the apoptotic rate increased during ischemia and was maximal at 12 h after reperfusion. The location of apoptotic bodies was extended from villus tip in sham-operated rats to the whole structure of villus, including mucosa, submucosa, lamina propria and myometrium in rat insulted by I/R. The quantification of apoptosis was corroborated with histological examination using HE staining. We also found that administration of exogenous aFGF could reduce the intestinal injury caused by I/R insult. The antiapoptotic effect of aFGF was through regulation of expression of genes related to apoptosis. Previous experimental data showed that the change of gene expression of apoptosis-related genes played pivotal roles in alleviating cardiac, myocardial[12], cerebral[13,14], muscular[15], cutaneous[16] and adrenal cortex[17] apoptosis induced by I/R, which is in agreement with our results.

Apoptosis is governed by a number of regulatory genes mediated by apoptosis signals. Among them, the bcl-2 family of proteins constitutes a central checkpoint. The bcl-2 family consists of both cell death promoters and cell death preventers. Bax is one of proapoptotic proteins, whereas bcl-2 is one of anti-apoptotic proteins. The ratio of anti- to pro-apoptotic

molecules such as bcl-2/bax determines the response to a death signal[18-20]. Bcl-2 seems to prevent apoptosis induced by many stimuli, for example, irradiation, FasL[21], TRAIL[22] and deprivation of growth factor, and it has been shown to suppress cytochrome c (cyt.c) efflux from mitochondria, inhibit calcium release from the endoplasmic reticulum[23-25]. Bax, which normally resides in the cytosol, translocates to mitochondria when triggered by certain stimuli, and changes to its active configuration as a dimerized integral mitochondrial membrane protein[26]. Translocated bax has been shown to induce cyt.c release followed by caspase activation. Several studies have reported that increment of the ratio of bcl-2/bax protein can prevent the progression of apoptosis in myocardium after I/R[27,28]. In the present study, it was shown that apoptosis began to occur in rat intestinal villus subjected to 45 min of ischemia followed by 30 min of reperfusion. Although gene transcription and translation of bcl-2 were both inhibited after reperfusion, the expression of bax was apparently enhanced. It was suggested that the decreased ratio of bcl-2/bax by ischemia and reperfusion might play a pivotal role in induction of apoptosis. Our study also showed that the number of apoptotic cells in intestinal villus insulted by I/R was significantly decreased by aFGF administration. aFGF could inhibit bax gene expression and enhance bcl-2 gene expression in comparison with normal saline treatment. So the increment of the ratio of bcl-2/bax by administration of aFGF might be one of mechanisms attenuating I/R-induced apoptosis. These results are consistent with the result by Coopersmith *et al*[29] that transgenic rat expressing bcl-2 could suppress apoptosis induced by I/R.

Our study also found that apoptosis occurred at 30 min postreperfusion followed by a return to baseline levels by 24 h, suggesting that induction of intestinal apoptosis by I/R and mucosal recovery were rapid processes. The reason for this interesting kinetics of induction of mucosal cell death and restoration was unclear. There were two possible explanations. First, it may be that there is a time-dependent increase in apoptosis-promoting factors, including Bax, during ischemia and early phases of reperfusion, which rapidly decreases with prolonged reperfusion. Second, corresponding to the decline in apoptosis-promoting factors, there may be simultaneous induction of inhibitors of apoptosis, e.g., Bcl-2, during the later phase of reperfusion. The exact mechanism needs to be studied in depth.

In conclusion, the present study provides the preliminary evidence that the protective effects of aFGF against I/R in rat intestinal villus might be partially due to its ability to inhibit I/R-induced apoptosis. Furthermore, our data strongly suggest that aFGF exerts its antiapoptotic effect via regulating gene expression of bcl-2, bax and the ratio of bcl-2/bax proteins. The precise mechanism for the inhibition of intestinal I/R injury and attenuation of apoptosis afforded by aFGF requires further investigation.

REFERENCES

1 **Weng LX,** Fu XB, Li XX, Sun TZ, Zheng SY, Chen W. Effects of acidi fibroblast growth factor on hepatic and renal functions after intestinal ischemia/reperfusion injury. *Zhongguo Weizhongbing Jijiu Yixue* 2004; **16**: 19-21

2 **Cuevas P,** Carceller F, Martinez-Coso V, Asin-Cardiel E, Gimenez-Gallego G. Fibroblast growth factor cardioprotection against ischemia-reperfusion injury may involve K+ATP channels. *Eur J Med Res* 2000; **5**: 145-149

3 **Cuevas P,** Carceller F, Martinez-Coso V, Cuevas B, Fernandez-Ayerdi A, Reimers D, Asin-Cardiel E, Gimenez-Gallego G. Cardioprotection from ischemia by fibroblast growth factor: role of inducible nitric oxide synthase. *Eur J Med Res* 1999; **4**: 517-524

4 **Fu XB,** Yang YH, Sun XQ, Sun TZ, Gu XM, Sheng ZY. Protective effects of endogenous basic fibroblast growth factor activated by 2, 3 butanedion monocime on functional changes of ischemic intestine, liver and kidney in rats. *Zhongguo Weizhongbing Jijiu Yixue* 2000; **12**: 69-72

5 **Fu XB,** Yang YH, Sun TZ, Sun XQ, Gu XM, Chang GY, Sheng ZY. Effect of inhibition or anti-endogenous basic fibroblast growth factor on functional changes in intestine, liver and kidneys in rats after gut ischemia-reperfusion injury. *Zhongguo Weizhongbing Jijiu Yixue* 2000; **12**: 465-468

6 **Srinivasan A,** Li F, Wong A, Kodandapani L, Smidt R, Krebs JF, Fritz LC, Wu JC, Tomaselli KJ. Bcl-xL functions downstream of caspase-8 to inhibit Fas- and tumor necrosis factor receptor 1-induced apoptosis of MCF7 breast carcinoma cells. *J Biol Chem* 1998; **273**: 4523-4529

7 **Mills JC,** Lee VM, Pittman RN. Activation of a PP2A-like phosphatase and dephosphorylation of tau protein characterize onset of the execution phase of apoptosis. *J Cell Sci* 1998; **111 (Pt 5)**: 625-636

8 **Noda T,** Iwakiri R, Fujimoto K, Matsuo S, Aw TY. Programmed cell death induced by ischemia-reperfusion in rat intestinal mucosa. *Am J Physiol* 1998; **274**: G270-G276

9 **Chao DT,** Korsmeyer SJ. BCL-2 family: regulators of cell death. *Annu Rev Immunol* 1998; **16**: 395-419

10 **Cory S,** Huang DC, Adams JM. The Bcl-2 family: roles in cell survival and oncogenesis. *Oncogene* 2003; **22**: 8590-8607

11 **Rosse T,** Olivier R, Monney L, Rager M, Conus S, Fellay I, Jansen B, Borner C. Bcl-2 prolongs cell survival after Bax-induced release of cytochrome *c*. *Nature* 1998; **391**: 496-499

12 **Chang TH,** Liu XY, Zhang XH, Wang HL. Effects of *dl*-praeruptorin A on interleukin-6 level and Fas, bax, bcl-2 protein expression in ischemia-reperfusion myocardium. *Acta Pharmacol Sin* 2002; **23**: 769-774

13 **Zhou H,** Ma Y, Zhou Y, Liu Z, Wang K, Chen G. Effects of magnesium sulfate on neuron apoptosis and expression of caspase- 3, bax and bcl-2 after cerebral ischemia- reperfusion injury. *Chin Med J (Engl)* 2003; **116**: 1532-1534

14 **Wang Y,** Hayashi T, Chang CF, Chiang YH, Tsao LI, Su TP, Borlongan C, Lin SZ. Methamphetamine potentiates ischemia/reperfusion insults after transient middle cerebral artery ligation. *Stroke* 2001; **32**: 775-782

15 **Hatoko M,** Tanaka A, Kuwahara M, Yurugi S, Iioka H, Niitsuma K. Difference of molecular response to ischemia-reperfusion of rat skeletal muscle as a function of ischemic time: study of the expression of p53, p21(WAF-1), Bax protein, and apoptosis. *Ann Plast Surg* 2002; **48**: 68-74

16 **Hatoko M,** Tanaka A, Kuwahara M, Yurugi S. Molecular response to ischemia-reperfusion of rat skin: study of expression of p53, p21WAF-1, and Bax proteins, and apoptosis. *Ann Plast Surg* 2001; **47**: 425-430

17 **Baskin DS,** Ngo H, Didenko VV. Thimerosal induces DNA breaks, caspase-3 activation, membrane damage, and cell death in cultured human neurons and fibroblasts. *Toxicol Sci* 2003; **74**: 361-368

18 **Deng W,** Wang DA, Gosmanova E, Johnson LR, Tigyi G. LPA protects intestinal epithelial cells from apoptosis by inhibiting the mitochondrial pathway. *Am J Physiol Gastrointest Liver Physiol* 2003; **284**: G821-G829

19 **Chen W,** Fu XB, Sun TZ. Characteristics of Bax and Bcl-2 expression in ulcerative and normal skin and their effects on ulcer formation. *Modern Rehib* 2001; **5**: 54-55

20 **Chen W,** Fu XB, Sun TZ. Characteristica of Bax and Bcl-2 expression in hypertrophic scars and its biological significance. *J Trauma Surg* 2002; **4**: 276-278

21 **Chang YC,** Xu YH. Expression of Bcl-2 inhibited Fas-mediated apoptosis in human hepatocellular carcinoma BEL-7404 cells. *Cell Res* 2000; **10**: 233-242
22 **Guo BC,** Xu YH. Bcl-2 over-expression and activation of protein kinase C suppress the trail-induced apoptosis in Jurkat T cells. *Cell Res* 2001; **11**: 101-106
23 **Foyouzi-Youssefi R,** Arnaudeau S, Borner C, Kelley WL, Tschopp J, Lew DP, Demaurex N, Krause KH. Bcl-2 decreases the free Ca2+ concentration within the endoplasmic reticulum. *Proc Natl Acad Sci USA* 2000; **97**: 5723-5728
24 **Zhang M,** Zhang HQ, Xue SB. Effect of Bcl-2 and caspase-3 on calcium distribution in apoptosis of HL-60 cells. *Cell Res* 2000; **10**: 213-220
25 **Bogdanov MB,** Ferrante RJ, Mueller G, Ramos LE, Martinou JC, Beal MF. Oxidative stress is attenuated in mice overexpressing BCL-2. *Neurosci Lett* 1999; **262**: 33-36
26 **Gross A,** Pilcher K, Blachly-Dyson E, Basso E, Jockel J, Bassik MC, Korsmeyer SJ, Forte M. Biochemical and genetic analysis of the mitochondrial response of yeast to BAX and BCL-X (L). *Mol Cell Biol* 2000; **20**: 3125-3136
27 **Cui J,** Engelman RM, Maulik N, Das DK. Role of ceramide in ischemic preconditioning. *J Am Coll Surg* 2004; **198**: 770-777
28 **Nakamura M,** Wang NP, Zhao ZQ, Wilcox JN, Thourani V, Guyton RA, Vinten-Johansen J. Preconditioning decreases Bax expression, PMN accumulation and apoptosis in reperfused rat heart. *Cardiovasc Res* 2000; **45**: 661-670
29 **Coopersmith CM,** O'Donnell D, Gordon JI. Bcl-2 inhibits ischemia-reperfusion-induced apoptosis in the intestinal epithelium of transgenic mice. *Am J Physiol* 1999; **276**: G677-G686

Science Editor Zhu LH and Guo SY **Language Editor** Elsevier HK

PO Box 2345, Beijing 100023, China
www.wjgnet.com
wjg@wjgnet.com

ELSEVIER

World J Gastroenterol 2005;11(22):3426-3430
World Journal of Gastroenterology ISSN 1007-9327

• *BASIC RESEARCH* •

Adult islets cultured in collagen gel transdifferentiate into duct-like cells

Jin Lu, Ya-Peng Gu, Xia Xu, Mei-Lian Liu, Ping Xie, Hui-Ping Song

Jin Lu, Ya-Peng Gu, Xia Xu, Mei-Lian Liu, Ping Xie, Hui-Ping Song, Department of Biochemistry, Xiangya School of Medicine, Central South University, Changsha 410078, Hunan Province, China
Supported by the National Natural Science Foundation of China, No. 30200136
Correspondence to: Professor Hui-Ping Song, Department of Biochemistry, Xiangya School of Medicine, Central South University, Xiangya Road, Changsha 410078 Hunan Province, China. huiping_song@hotmail.com
Telephone: +86-731-2355115
Received: 2004-07-02 Accepted: 2004-09-09

Abstract

AIM: To establish a model of islet-ductal cell transdifferentiation to identify the transdifferentiated cells.

METHODS: Collagen was extracted from rat tail at first. Purified rat islets were divided into three groups, embedded in collagen gel and incubated respectively in DMEM/F12 alone (control group), DMEM/F12 plus epidermal growth factor (EGF), DMEM/F12 plus EGF and cholera toxin (CT). Transdifferentiation was proved by microscopy, RT-PCR, immunohistochemistry and RIA.

RESULTS: Islets embedded in collagen gel plus EGF and CT were cystically transformed and could express new gene cytokeratin 19 while still maintaining the expression of insulin and Pdx-1 genes. Immunohistochemistry demonstrated that the protein of cytokeratin 19 was only expressed in the third group. The insulin content secreted by islets in the third group decreased significantly during the transdifferentiation.

CONCLUSION: CT is a crucial factor for the islet-ductal cell transdifferentiation.

Key words: Islets of Langerhans; Ductal cell; Transdifferentiation

Lu J, Gu YP, Xu X, Liu ML, Xie P, Song HP. Adult islets cultured in collagen gel transdifferentiate into duct-like cells. *World J Gastroenterol* 2005; 11(22): 3426-3430
http://www.wjgnet.com/1007-9327/11/3426.asp

INTRODUCTION

Transdifferentiation is a process in which differentiated cells alter their identity to become other distinct cell types. This process has been proven by researches[1,2]. During pancreas development, both the exocrine and endocrine systems seem to originate from the ductal cells which are considered as a kind of pancreatic stem cells. This hypothesis is supported by the phenomenon that ductal cells have the ability to transdifferentiate into acinar cells and islets[3-5]. But this process is bilateral. On the contrary, acinar cells and islets can transdifferentiate into duct-like cells[6,7]. It has also been reported that islets in a long-term culture can transdifferentiate into exocrine and undifferentiated cells, which may be considered as pancreatic precursor cells[8]. The process of mature endocrine cells transdifferentiating into exocrine cells was also confirmed in our study. Our data show that, rat islets cultured in rat tail collagen gel plus EGF and CT can transdifferentiate into duct-like cells.

MATERIALS AND METHODS

Isolation and purification of islets

Male Sprague-Dawley (SD) rats, weighing 230-250 g, were obtained from Central South University Laboratory Animal Department. For each isolation, one rat was anesthetized with pentobarbital sodium (30 mg/kg) intraperitoneally. Isolation of pancreatic islets was performed as previously described[9]. Briefly, after the output site of the duct from pancreas to duodenum was clamped, the pancreas was distended maximally with 20 mL collagenase (type IV, 1.5 mg/mL, Invitrogen) using a pulsed infusion technique via the portal duct of pancreas. The whole pancreas was removed from male SD rats and placed in a stationary water bath at 37 ℃ for 25 min to allow it to digest enzymatically. Digestate was agitated gently for 1 min every 5 min during incubation. The digestion process was stopped by adding 30 mL of cold Hank's balanced salt solution (HBSS) supplemented with 5% fetal bovine serum (FBS). After having vortexed for 1 min to dissociate the islets from adherent acinar elements, the mixture was passed through a steel mesh filter with an aperture of 0.5 mm. The filtrate was subjected to the conventional method of histopaque density gradient centrifugation to separate islets from the digestion mixture.

DTZ staining and hand-picking

DTZ stock solution preparation Ten milligrams of DTZ were dissolved entirely in 5 mL of dimethyl sulfoxide (DMSO), then filtered through a 0.2-μm nylon filter and stored briefly at -20 ℃.

***In vitro* DTZ staining** Ten microliters of the stock solution was added to 1 mL of culture medium. The culture dishes were incubated at 37 ℃ for 15 min in the DTZ solution.

After the dishes were rinsed thrice with HBSS, clusters stained crimson red were identified as islets. These islets were hand-picked under a stereomicroscope. After hand-picking, the dishes were refilled with DMEM containing 10% FBS. The stain completely disappeared from the cells after 2 h.

Three-dimensional (3D) collagen gel matrix preparation and islet culture

Collagen preparation Collagen was extracted from rat tail tendons as previously described[10]. Tendons were excised from rat tails and sheared. Some connective tissues were removed carefully, washed twice with PBS and then soaked in 4 mmol/L acetic acid. After having stirred for two d at 4 ℃, collagen was extracted. The extracts were centrifuged for 30 min at 10 000 *g* and supernatant was collected into another distilled vessel for use. Protein concentration in the collagen was 1.0-1.5 mg/mL measured with an ultraviolet spectrophotometer.

Preparation of collagen gels Following sterile components (0.7 mL 10×DMEM/F12, 0.1 mL heat-inactivated low-endotoxin FCS, 0.1 mL 0.1 mol/L NaOH, 0.1 mL islet suspension) were carefully mixed to avoid bubbles. All components required to make collagen gels were placed on ice except for the islet suspension. Thus, the mixture resulted in a physiologic ionic strength and 1×DMEM/F12 in the final gel. The mixture was incubated at 37 ℃ in 50 mL/L CO_2 and then gelation was completed after 60 min.

Islet culture Islets embedded in collagen gel were divided into three groups and incubated under the following conditions.

3D culture alone (control group) DMEM/F12 (penicillin 100 U/mL, streptomycin 100 μg/mL, 10 mmol/L HEPES) +10% FCS+nicotinamide (10 mmol/L).

3D culture+EGF: DMEM/F12 (penicillin 100 U/ml, streptomycin 100 μg/mL, 10 mmol/L HEPES)+10% FCS +EGF (100 ng/mL)+nicotinamide (10 mmol/L).

3D culture + EGF + CT: DMEM/F12 (penicillin 100 U/mL, streptomycin 100 μg/mL, 10 mmol/L HEPES) +10% FCS+EGF (100 ng/mL)+CT (100 ng/mL) +nicotinamide (10 mmol/L).

Insulin content assay

Samples were taken at the 1st, 3rd, 5th, 16th, 28th, 40th, 52nd, 76th, 88th ,120th, 168th h. After old culture medium was piped out thoroughly, islets were rinsed twice and fresh medium was added. Culture media were sampled after 1 h and frozen at -20 ℃. Insulin content in samples was detected by radioimmunoassay (RIA).

Immunohistochemistry

Islets were hand-picked from slides pretreated with poly-L-lysine and fixed in 4% paraformaldehyde (PFA). Then the fixed islets were processed for routine histology and immunostained for insulin (mouse anti-insulin, Boster, Wuhan) and cytokeratin 19 (mouse anti-cytokeratin 19, Boster, Wuhan) using the streptavidin-biotin complex (SABC) method following the instructions of kit (Boster, Wuhan). For cytokeratin 19, islet cells were pretreated with 0.1% trypsin. The sections were incubated overnight at 4 ℃ with appropriate primary antibodies. Negative controls involved omission of the primary antibodies.

RNA extraction and RT-PCR analysis

The collagen matrix was dissolved in 0.25 mg/mL collagenase and islets were washed thrice. Total RNA was extracted from cultured rat islets using TRIzol (GIBCO BRL) and reverse-transcribed into cDNA with TaKaRa RNA PCR kit (AMV) Ver. 2.1 (TaKaRa, Japan) according to the standard procedure. cDNA samples were subjected to PCR amplification with specific primers. The cycling parameters were pre-denaturation at 94 ℃ for 2 min, denaturation at 94 ℃ for 30 s, annealing at 55 ℃ for 30 s, and elongation at 72 ℃ for 1 min (34 cycles). Table 1 summarizes the sequences of the PCR primers used in this study.

Table 1 Primers used in study

Targeted mRNA	Primer	Length
Rat Pdx-1	F: gaggacccgtacagcctaca R: cgttgtcccgctactacgtt	201 bp
Rat Insulin	F: ccgtcgtgaagtggagga R: cagttggtagagggagcagat	154 bp
Rat Cytokeratin 19	F: atccccaaagacacgagatg R: gtgagctacaaccgcagctt	200 bp
Rat β-actin	F: taaagagaagctgtgctatgttgc R: atgatcttgatcttcatggtgcta	354 bp

Statistical analysis

All data were expressed as mean±SD with $n = 3$ at each time point. The difference between time points with respect to insulin content was evaluated by one-way ANOVA. $P<0.05$ was considered statistically significant.

RESULTS

Microscopy

We used DTZ to identify islets which were stained crimson while acinar and ductal tissue failed to incorporate the stain. Islets were stained with DTZ and hand-picked after density gradient centrifugation. The stain completely disappeared from the cells after 2 h (Figure 1).

Islets embedded in collagen gel could retain their natural shape, while those in monolayer cultures could not (Figure 2).

The islets in groups 1 and 2 were not different in shape on d 1, 3 and 5. But some islets in group 3 continually enlarged in these days (Figure 3). The percentage of islets undergoing cystic transformation was increased over the time-course of the culture period in group 3.

Secreted insulin content

During the culture time, the abilities of islets to secrete insulin in three groups were all decreased. Five hours later, islets lost their secreting ability faster in group 3 than in groups 1 and 2 ($P<0.05$ or 0.01) (Figure 4).

Immunohistochemistry

Islets cultured for 1, 3, 5 d were insulin positive and cytokeratin 19 negative in groups 1 and 2.

In group 3, islets were insulin positive and cytokeratin 19 negative on d 1. There was a decrease in expression of insulin mainly in the center of islets and some islet cells around the cystic spaces began to express protein cytokeratin 19

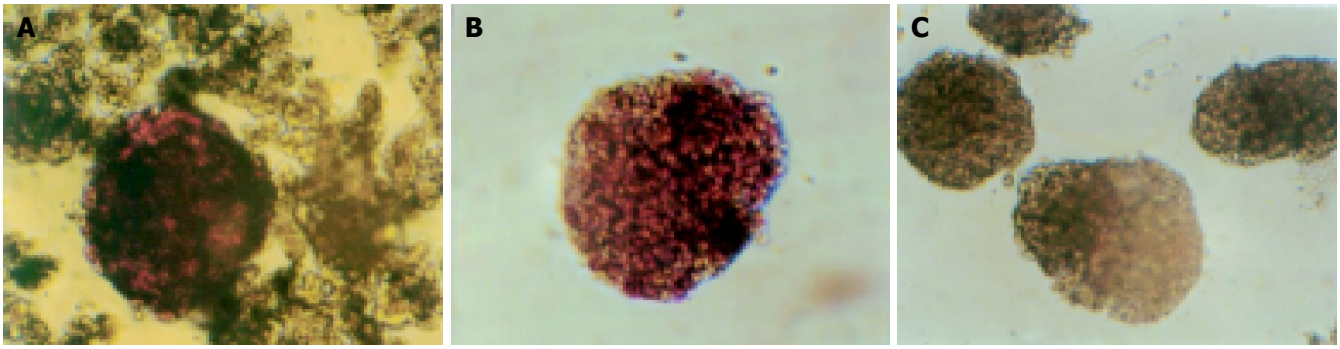

Figure 1 Islets stained crimson with DTZ (**A**), purified by density gradient separation and hand-picking (**B**), and loss of color 2 h after islet staining (**C**) (×100).

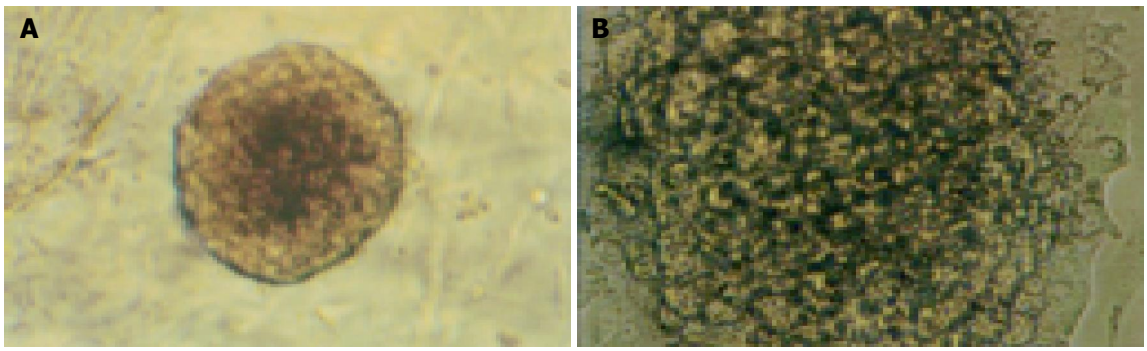

Figure 2 Shape of islets culture in collagen gel (**A** ×100) and in monolayer (**B** ×200).

Figure 3 Islets of group 3 cystic transformed gradually in the process of culture. **A:** d 1 in culture; **B:** d 3 in culture; **C:** d 5 in culture (inverted microscope ×100).

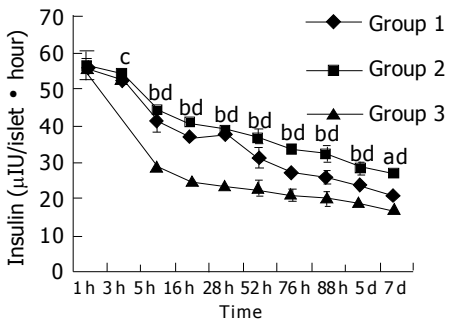

Figure 4 Insulin contents in culture media of three groups at different time points were detected using RIA. ($^{a}P<0.05$: group 1 *vs* group 3; $^{b}P<0.01$: group 1 *vs* group 3; $^{c}P<0.05$: group 2 *vs* group 3; $^{d}P<0.01$: group 2 *vs* group 3).

on d 3. Only a few cells in the islets expressed insulin continually on d 5, but most cells expressed cytokeratin 19 (Figures 5 and 6).

Reverse transcription and polymerase chain reaction

Freshly isolated islets expressed islet characteristic genes (pdx-1 and insulin) but did not express duct characteristic gene (cytokeratin 19) (Figure 7). After incubation for 7 d, islets in the three groups could express genes (insulin and pdx-1), but cytokeratin 19 was only expressed in group 3 (Figure 8).

DISCUSSION

Cells of both the exocrine (acinar cells) and endocrine systems (islet cells) seem to originate from the ductal cells. From

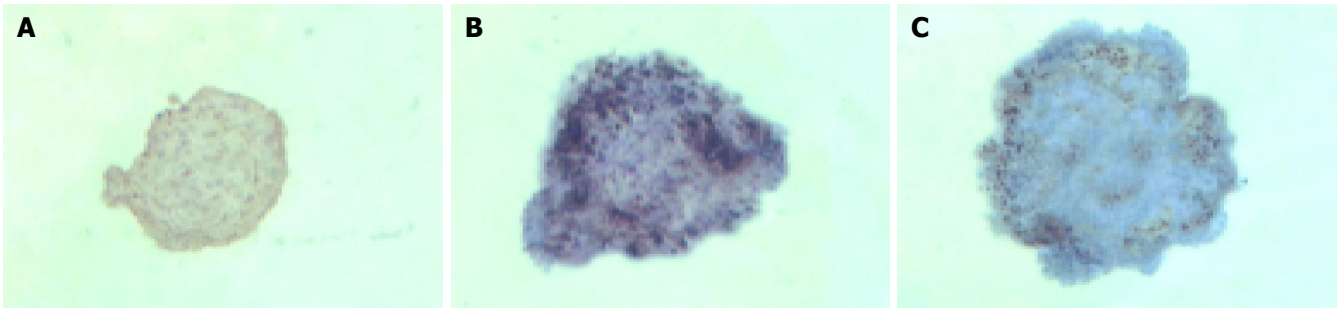

Figure 5 Islets of group 3 stained for insulin by immunocytochemistry. **A:** d 1 (strongly stain); **B:** d 3 (decreased stain); **C:** d 5 (lightly stain). (DAB stain and counterstained with hematine crystal ×100).

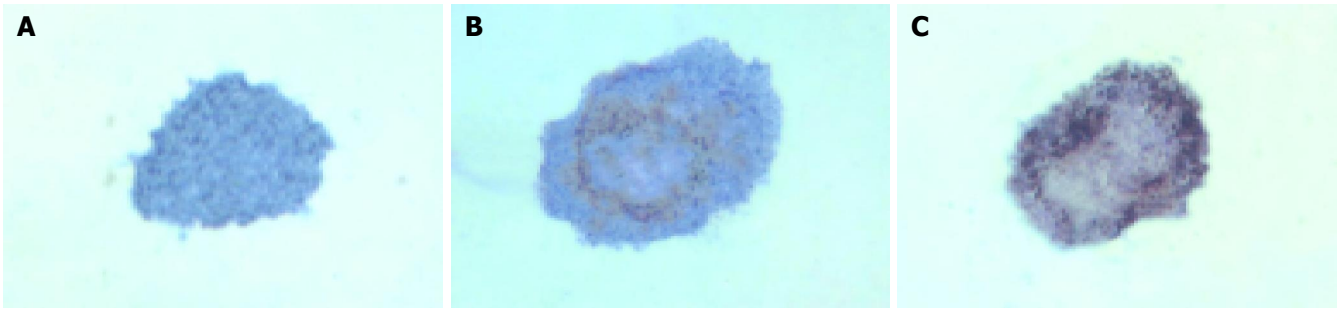

Figure 6 Islets of group 3 stain for cytokeratin 19. **A:** d 1 (did not stain); **B:** d 3 (lightly stain); **C**: d 5 (strongly stain).

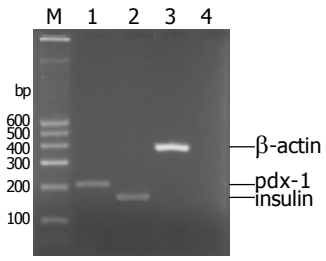

Figure 7 Pdx-1, insulin genes were expressed in freshly isolated islets, but cytokeratin 19 was not expressed (lane 1: Pdx-1; lane 2: Insulin; lane 3: β-actin; lane 4: cytokeratin 19).

experiments *in vitro* it is evident that during development, endocrine cells emerge from the pancreatic ducts and form aggregates that eventually form islets of Langerhans. Teitelman *et al*[11], removed pancreatic rudiments from E11 mouse embryos and maintained in culture, and found that pancreas (including exocrine and endocrine tissues) regenerates *in vitro* from E11 pancreatic ducts. Rosenberg *et al*[12], reported that partial obstruction of the pancreatic duct in adult hamsters leads to islet cell differentiation from cells in the interlobular ducts, followed by formation of new islets. More recently, Susan Bonner-Weir *et al*[5], cultivated human adult pancreatic duct cells *in vitro* and differentiated the duct cells into "cultivated human islet buds" (CHIBs) which have the ability to secrete glucose-response insulin.

On the other hand, islets can transdifferentiate into duct-like cells. Human and dog islets embedded in collagen gel and cultured in media plus EGF and CT for several days can transform and express duct cell marker CK-19[7,13]. In this study, we isolated rat islets and incubated them in the same conditions as above, and proved that rat islets could transdifferentiate into duct-like cells.

Extracellular matrix (ECM) is one of the most important components in creating cellular microenvironment. Among the ECM components, collagen can provide cells with a bio-

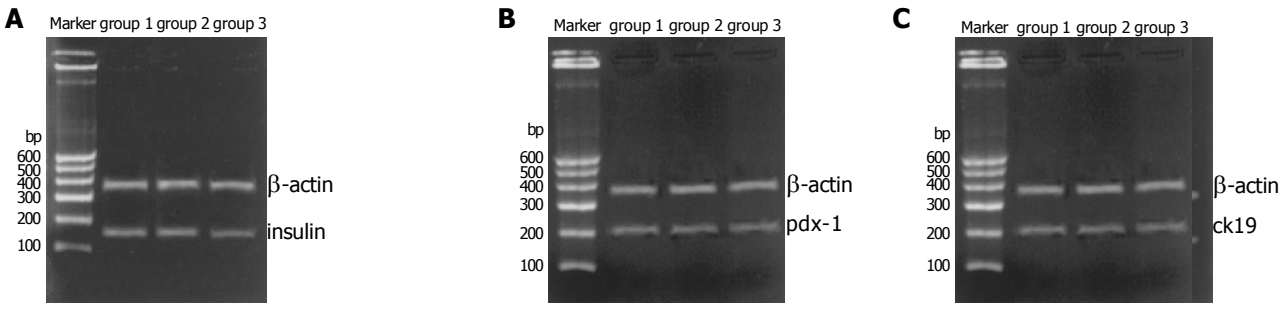

Figure 8 Gene's expression of islets of three groups cultured for 7 d; **A:** all of three groups expressed insulin; **B:** all of three groups expressed pdx-1; **C:** only group 3 expressed CK19 which group 1 and group 2 did not express.

mimic environment favorable for their reorganization, or maintenance of the three-dimensional structure. The use of collagen gel as an extracellular matrix material is an important part of the culture system in our study. Collagen gel matrix can help promote or maintain the differentiated state of cells in culture, such as liver cells[14] and mammary epithelial cells[15]. ECM may also promote the process of cell transdifferentiation[6,16]. Collagen plays an important role in the process. Islets cannot transdifferentiate in agarose gel[13]. ECM is the necessary condition for transdifferentiation. In our study, islets embedded in collagen gel without EGF and CT did not express CK-19, consistent with the report by Wang *et al*[13].

EGF can activate protein tyrosine kinase (PTK), protein kinase C and increase intracellular Ca^{2+} concentration after binding to EGF receptor[17]. CT can activate adenylate cyclase, and result in the increase of intracellular cAMP concentration[18]. It was reported that the process of cystic transformation requires both an elevation of intracellular cAMP and the presence of ECM proteins[13]. Both cAMP and Ca^{2+} are classic second messengers. Perhaps EGF and CT affect the signal transduction of islet cells in two ways by increasing the concentration of these messengers. In our study, we found that EGF alone had no ability to initiate islet cell transdifferentiation, but it could preserve islet's function. It is supported by the fact that both EGF and betacellulin are members of EGF-family of cytokines, and betacellulin is a kind of beta-cell growth factor, suggesting that EGF also can stimulate beta-cell growth.

In conclusion, the process of transdifferentiation is promoted by cooperation of collagen matrix, EGF and CT. But the exact mechanisms of interaction of these factors remain to be fully elucidated.

REFERENCES

1 **Ng YY,** Huang TP, Yang WC, Chen ZP, Yang AH, Mu W, Nikolic-Paterson DJ, Atkins RC, Lan HY. Tubular epithelial-myofibroblast transdifferentiation in progressive tubulointerstitial fibrosis in 5/6 nephrectomized rats. *Kidney Int* 1998; **54**: 864-876

2 **Badorff C,** Brandes RP, Popp R, Rupp S, Urbich C, Aicher A, Fleming I, Busse R, Zeiher AM, Dimmeler S. Transdifferentiation of blood-derived human adult endothelial progenitor cells into functionally active cardiomyocytes. *Circulation* 2003; **107**: 1024-1032

3 **Bonner-Weir S,** Baxter LA, Schuppin GT, Smith FE. A second pathway for regeneration of adult exocrine and endocrine pancreas. A possible recapitulation of embryonic development. *Diabetes* 1993; **42**: 1715-1720

4 **Walker NI,** Winterford CM, Kerr JF. Ultrastructure of the rat pancreas after experimental duct ligation. II. Duct and stromal cell proliferation, differentiation, and deletion. *Pancreas* 1992; **7**: 420-434

5 **Bonner-Weir S,** Taneja M, Weir GC, Tatarkiewicz K, Song KH, Sharma A, O'Neil JJ. *In vitro* cultivation of human islets from expanded ductal tissue. *Proc Natl Acad Sci USA* 2000; **97**: 7999-8004

6 **Arias AE,** Bendayan M. Differentiation of pancreatic acinar cells into duct-like cells *in vitro*. *Lab Invest* 1993; **69**: 518-530

7 **Yuan S,** Rosenberg L, Paraskevas S, Agapitos D, Duguid WP. Transdifferentiation of human islets to pancreatic ductal cells in collagen matrix culture. *Differentiation* 1996; **61**: 67-75

8 **Schmied BM,** Ulrich A, Matsuzaki H, Ding X, Ricordi C, Weide L, Moyer MP, Batra SK, Adrian TE, Pour PM. Transdifferentiation of human islet cells in a long-term culture. *Pancreas* 2001; **23**: 157-171

9 **Inoue K,** Gu Y, Shinohara S, Kogire M, Mitsuo M, Nakai I, Hayashi H, Uchida K, Maetani S, Ikada Y. Isolation of adult pig islet. *In vitro* assessment and xenotransplantation. *Int J Pancreatol* 1992; **12**: 173-180

10 **Mio T,** Adachi Y, Romberger DJ, Ertl RF, Rennard SI. Regulation of fibroblast proliferation in three-dimensional collagen gel matrix. *In Vitro Cell Dev Biol Anim* 1996; **32**: 427-433

11 **Teitelman G,** Lee J, Reis DJ. Differentiation of prospective mouse pancreatic islet cells during development *in vitro* and during regeneration. *Dev Biol* 1987; **120**: 425-433

12 **Rosenberg L,** Brown RA, Duguid WP. A new approach to the induction of duct epithelial hyperplasia and nesidioblastosis by cellophane wrapping of the hamster pancreas. *J Surg Res* 1983; **35**: 63-72

13 **Wang R,** Li J, Rosenberg L. Factors mediating the transdifferentiation of islets of Langerhans to duct epithelial-like structures. *J Endocrinol* 2001; **171**: 309-318

14 **Rubin K,** Hook M, Obrink B, Timpl R. Substrate adhesion of rat hepatocytes: mechanism of attachment to collagen substrates. *Cell* 1981; **24**: 463-470

15 **Yang J,** Larson L, Flynn D, Elias J, Nandi S. Serum-free primary culture of human normal mammary epithelial cells in collagen gel matrix. *Cell Biol Int Rep* 1982; **6**: 969-975

16 **Reh TA,** Nagy T, Gretton H. Retinal pigmented epithelial cells induced to transdifferentiate to neurons by laminin. *Nature* 1987; **330**: 68-71

17 **Boonstra J,** Rijken P, Humbel B, Cremers F, Verkleij A, van Bergen en Henegouwen P. The epidermal growth factor. *Cell Biol Int* 1995; **19**: 413-430

18 **Holmgren J.** Actions of cholera toxin and the prevention and treatment of cholera. *Nature* 1981; **292**: 413-417

Science Editor Wang XL and Guo SY **Language Editor** Elsevier HK

PO Box 2345, Beijing 100023, China
www.wjgnet.com
wjg@wjgnet.com

ELSEVIER

World J Gastroenterol 2005;11(22):3431-3440
World Journal of Gastroenterology ISSN 1007-9327

• *BASIC RESEARCH* •

Bone marrow-derived mesenchymal stem cells protect against experimental liver fibrosis in rats

Dong-Chang Zhao, Jun-Xia Lei, Rui Chen, Wei-Hua Yu, Xiu-Ming Zhang, Shu-Nong Li, Peng Xiang

Dong-Chang Zhao, Rui Chen, Wei-Hua Yu, Xiu-Ming Zhang, Shu-Nong Li, Peng Xiang, Center for Stem Cell Biology and Tissue Engineering, Sun Yat-Sen University, 74# Zhongshan Road II, Guangzhou 510080, Guangdong Province, China
Dong-Chang Zhao, Jun-Xia Lei, Wei-Hua Yu, Xiu-Ming Zhang, Shu-Nong Li, Department of Pathophysiology, Medical School of Sun Yat-Sen University, 74# Zhongshan Road II, Guangzhou 510080, Guangdong Province, China
Dong-Chang Zhao, Department of Pediatrics, Guangdong Province Maternal and Children's Hospital, 13# Guangyuan Xilu, Guangzhou 510010, Guangdong Province, China
Supported by the Major State Basic Research Development Program of China (973 Program), No. 2001CB509904, the Key Scientific and Technological Projects of Guangdong Province, No. 2003A3020103, the Key Scientific and Technological Projects of Guangzhou City, No. 2002U13E0011, and the National Natural Science Foundation of China, No. 30100188
Correspondence to: Dr. Peng Xiang, Center for Stem Cell Biology and Tissue Engineering, Sun Yat-Sen University, 74# Zhongshan Road II, Guangzhou 510080, Guangdong Province, China. pxiang@gzsums.edu.cn
Telephone: +86-20-87335822 Fax: +86-20-87335858
Received: 2004-12-20 Accepted: 2005-01-05

Abstract

AIM: Recent reports have shown the capacity of mesenchymal stem cells (MSCs) to differentiate into hepatocytes *in vitro* and *in vivo*. MSCs administration could repair injured liver, lung, or heart through reducing inflammation, collagen deposition, and remodeling. These results provide a clue to treatment of liver fibrosis. The aim of this study was to investigate the effect of infusion of bone marrow (BM)-derived MSCs on the experimental liver fibrosis in rats.

METHODS: MSCs isolated from BM in male Fischer 344 rats were infused to female Wistar rats induced with carbon tetrachloride (CCl_4) or dimethylnitrosamine (DMN). There were two random groups on the 42nd d of CCl_4: CCl_4/MSCs, to infuse a dose of MSCs alone; CCl_4/saline, to infuse the same volume of saline as control. There were another three random groups after exposure to DMN: DMN10/MSCs, to infuse the same dose of MSCs on d 10; DMN10/saline, to infuse the same volume of saline on d 10; DMN20/MSCs, to infuse the same dose of MSCs on d 20. The morphological and behavioral changes of rats were monitored everyday. After 4-6 wk of MSCs administration, all rats were killed and fibrosis index were assessed by histopathology and radioimmunoassay. Smooth muscle alpha-actin (alpha-SMA) of liver were tested by immunohistochemistry and quantified by IBAS 2.5 software. Male rats sex determination region on the Y chromosome (*sry*) gene were explored by PCR.

RESULTS: Compared to controls, infusion of MSCs reduced the mortality rates of incidence in CCl_4-induced model (10% *vs* 20%) and in DMN-induced model (20-40% *vs* 90%).The amount of collagen deposition and alpha-SMA staining was about 40-50% lower in liver of rats with MSCs than that of rats without MSCs. The similar results were observed in fibrosis index. And the effect of the inhibition of fibrogenesis was greater in DMN10/MSCs than in DMN20/MSCs. The *sry* gene was positive in the liver of rats with MSCs treatment by PCR.

CONCLUSION: MSCs treatment can protect against experimental liver fibrosis in CCl_4-induced or DMN-induced rats and the mechanisms of the anti-fibrosis by MSCs will be studied further.

Key words: Mesenchymal stem cells; Liver fibrosis; Rat; Therapy

Zhao DC, Lei JX, Chen R, Yu WH, Zhang XM, Li SN, Xiang P. Bone marrow-derived mesenchymal stem cells protect against experimental liver fibrosis in rats. *World J Gastroenterol* 2005; 11(22): 3431-3440
http://www.wjgnet.com/1007-9327/11/3431.asp

INTRODUCTION

Liver fibrosis is the wound-healing response of the liver to chronic injury[1]. Following repeated injury, the liver undergoes a tissue remodeling and forms fibrosis. It is characterized by excessive accumulation of extracellular matrix, with the formation of scar tissue encapsulating the area of injury. This results in many clinical manifestations, including ascites, variceal hemorrhage, and encephalopathy. The prognosis of patients with the disease is poor, although liver transplantation is a good alternative treatment. Moreover, there are limited available donor livers for hundreds of millions of patients worldwide[2,3]. So, it is very important to investigate appropriate therapies for the disease by different treatments.

We[4] and others[5-9] have established that BM-derived MSCs could engraft injured tissue, such as, bone marrow, lung, liver, heart or brain, and recover its function. These results indicate that MSCs is an attractive cell source for regenerative medicine. Recent reports have shown the

capacity of MSCs to differentiate into hepatocytes *in vitro*[10,11,] and *in vivo*[6,12,13]. Further, MSCs administration could repair injured lung, liver, or heart by reducing inflammation, collagen deposition and remodeling[5-7]. These imply that MSCs could not only have a possibility to repair acute damaged tissue but also have potentiality of reducing chronic fibrogenesis. Although Sakaida *et al*[14], and Fang *et al*[6], reported that BM or MSCs could reduce CCl_4-induced liver fibrosis in mice, the mechanism by which MSCs repair the fibrosis is unclear and their results seem controvertible. Fang *et al*[6], suggested that delaying MSCs administration by 1 wk after CCL_4 challenge did not prevent the disease progression, while Sakaida *et al*[14], found that BM treatment to 4 wk CCl_4-induced rats could get significantly reduced liver fibrosis. From the point of view of clinical practice, it is very important to select the model of liver fibrosis close to human disease for evaluating the effect of MSCs on the fibrosis. In the present study, we employed two models of fibrosis induced with CCL_4 or DMN to evaluate the effect of MSCs on the fibrosis. Our results showed that MSCs treatment could reduce mortality rates of rats and improve their fibrosis index, and earlier the MSCs were administrated, greater was the anti-fibrosis effect. We provide evidence here indicating that infusion of BM-derived MSCs should be therapeutic in liver fibrosis by blocking the fibrosis formation and progression.

MATERIALS AND METHODS

Preparing for BM-derived MSCs in rats

MSCs were prepared from rat bone marrow as described previously in our laboratory[15]. In brief, whole BM was flushed from the tibia and femur of Fischer 344 rats (6 wk old, male). MSCs preferentially attached to the polystyrene surface and were further purified by passages. MSCs were identified to express CD29 but not MHC class II antigens, costimulatory molecules CD80 and CD86 by flow cytometry[15]. The multiple differentiation potential of MSCs into neural cells, adipocyte and osteoblasts was also confirmed *in vitro*.

The multiple differentiation potential of MSCs into neural cells, adipocyte, and osteoblasts was also confirmed *in vitro*. In brief, to induce osteogenic differentiation, 8^{th}-10^{th}-passage cells were treated with osteogenic medium for 3 wk with medium changes twice weekly. Osteogenic medium consists of L-DMEM supplemented with 0.1 μmol/L dexamethasone (Sigma-Aldrich, St. Louis, MO, USA), 10 mmol/L β-glycerol phosphate (Sigma-Aldrich), and 0.2 mmol/L ascorbic acid (Sigma-Aldrich). Osteogenesis was assessed by Chinalizarin staining. To induce adipogenic differentiation, 8^{th}-10^{th}-passage cells were treated with adipogenic medium for 3 wk. Medium changes were performed twice weekly. Adipogenic medium consists of H-DMEM supplemented with 0.5 mmol/L 3-isobutyl-1-methylxanthine (Sigma-Aldrich), 1 μmol/L hydrocortisone (Sigma-Aldrich), 0.1 mmol/L indomethacin (Sigma-Aldrich), and 10% rabbit serum (Sigma-Aldrich). Adipogenesis was assessed by Oil Red O staining. To induce neurogenic differentiation, 8^{th}-10^{th}-passage cells were pretreated for 24 h with neurogenic medium, which consists of H-DMEM supplemented with 1 mmol/L β-mercaptoethanol (β-ME, Sigma-Aldrich). Then cells were treated with 5 mmol/L β-ME for 1 h. Neurogenesis was identified by antibody against neuron-specific enolase (NSE, SouthernBiotech, Birmingham, USA) staining.

Fischer 344 rats BM-MSCs in the $8\text{-}10^{th}$ passage were suspended in sterile saline and used for further experiments as described below.

CCl_4- or DMN-induced liver fibrosis and MSCs administration

Female Wistar rats were 6-wk old, weighing between 140 and 160 g. Rats were bred and maintained in an air-conditioned animal house with specific pathogen-free conditions, and were subjected to a 12:12-h daylight/darkness and allowed unlimited access to chow and water. The morphological and behavioral changes of rats were monitored everyday. Liver fibrosis was induced by CCl_4 or DMN administration as described[16]. The protocol was approved by Animal Care Committee of Sun Yat-Sen University.

CCl_4-induced model

On d 0, rats were injected by subcutaneous at a dose of 0.2 mL/100 g body weight of 40 mL/L CCl_4 (Guangzhou Chemical Factory, China) dissolved in paraffin oil (Guangzhou Chemical Factory, China). The injection was given twice a week for 6 wk. The same volume of paraffin oil alone was used as control. Liver fibrosis was determined by killing three to six rats with histopathology weekly. Twenty rats were randomly divided into two groups on d 42: CCl_4/MSCs, $n = 10$, to infuse a dose of MSCs 3×10^6 cells per rat by intravenous; CCl_4/saline, $n = 10$, to infuse the same volume of saline as a control. Blank control were designed, paraffin/saline, $n = 10$, to infuse the same volume of saline on d 42 after paraffin administration. On d 70, all rats were killed and venous blood was collected and liver tissue harvested for analysis.

DMN-induced model

On d 0, rats were injected intraperitoneally at a dose of 100 μL DMN (Sigma, USA) (diluted 1:100 with 0.15 mol/L sterile saline) per 100 g body weight. The injection was given on three consecutive days of each week for 6 wk. Control animals received the same volume of 0.15 mol/L sterile saline. Three or six treated animals were killed weekly with determination of establishment fibrosis by histopathology. Sixty rats were randomly divided into three groups in different time points of DMN-induced: DMN10/MSCs, $n = 10$, to infuse a dose of MSCs 3×10^6 cells per rat by intravenous on d 10; DMN20/MSCs, $n = 10$, to infuse the same dose MSCs on d 20; DMN10/saline, $n = 40$, to infuse the same volume of saline on d 10. We also designed saline, $n = 10$, to infuse the same volume of saline for blank control. On d 49, venous blood was collected and all rats were killed, and liver tissue harvested for analysis.

Analysis of liver histopathology and immunohistochemistry

Liver samples were collected into PBS and fixed overnight in 40 g/L paraformaldehyde in PBS at 4 ℃. Serial 5-μm sections of the right lobes of the livers were stained with hematoxylin and eosin (HE) and Masson Trichrome (MT)

as rules in our laboratory. Additional sections were tested with the antibody against α-SMA (1:200 dilutions, NeoMarkers) and immunoreactive materials were visualized by use of a streptavidin-biotin staining kit (UltraSensitive™ SP kit, Maixin-Bio, Fujian, China) and diaminobenzidine, as previously described[16]. MT and α-SMA staining was quantified using IBAS 2.5 software (Germany) and the data expressed as percentage of positive staining. The average of the score taken from five random fields was used to generate a single per slide.

Hydroxyproline (Hyp) content assay

A colorimetric assay was performed as described[16]. Briefly, lyopholized liver sections (0.5 g) were hydrolyzed for 20 h in 6 mol/L HCl at 100 ℃, redissolved in water, and centrifuged to remove any impurities. Samples were incubated for 10 min in 0.05 mol/L chloramine-T (Fisher, Fair Lawn, NJ, USA) at room temperature, followed by 15-min incubation in Ehrlich's-perchloric acid solution at 65 ℃. Sample absorbencies were assessed at 561 nm and resulting values compared to a Hyp standard curve. Each sample was assayed in duplicate. The Hyp content was expressed as micrograms per gram of wet liver.

Examination of the level of laminin (LN), hyaluronic acid (HA), alanine aminotransferase aspartate (ALT) and total bilirubin in serum (TBIL)

ALT and TBIL were assessed using our routine laboratory methods. Serum HA and LN were also measured with the kit (Navy Medical Institute, Shanghai, China) by radioimmunoassay.

PCR detection of male-derived MSCs

Genomic DNA was prepared from liver tissue of the rats in each group using genomic DNA purification kit (G&T Biotech, MD, USA). The presence or absence of sex determination region on the Y chromosome (*sry*) gene of liver in recipient female rats was assessed by PCR. The presence of DNA in all tissues was assessed by analysis of the "house-keeping" gene *β-actin*. Primer sequences for *sry* gene (forward 5'-catcgaagggttaaagtgcca-3', reverse 5'-atagtgtgtaggttgttgtcc-3') were obtained from published sequences[17,18] and amplify a product of 104 bp. *β-actin* primers (forward 5'-tgttgtccctgtatgcctct-3', reverse 5'-taatgtcacgcacgatttcc-3') were designed from GenBank (accession no. J00691) and amplify a product of 206 bp. The PCR conditions were as follows: incubation at 94 ℃ for 4 min; 35 cycles of incubation at 94 ℃ for 50 s, 60 ℃ for 30 s, and 72 ℃ for 1 min; with a final incubation at 72 ℃ for 10 min. PCR products were separated using 2% agarose gel electrophoresis, stained with ethidium bromide and imaged by Image Station 200R (Kodak, USA). Positive (male Fischer 344 rat genomic DNA) and negative (female Wistar rat genomic DNA) controls were included in each assay.

Statistical analysis

Data are expressed as mean±SD. Significant differences were determined by using ANOVA in SPSS 9.0. Results were considered significant when $P<0.05$.

RESULTS

Multiple differentiation potential of MSCs into neural-like cells, adipocyte, and osteoblasts

Figure 1 shows that BM-derived MSCs had differentiated into neural-like cells, adipocyte, and osteoblasts in different conditions (Figures 1A-C).

CCl_4 or DMN administration induced fibrogenesis in rats

Rats given CCl_4 showed slower weight gain than rats with paraffin oil alone (Figure 2A). The average weight of rats with CCl_4 for 6 wk was 50-70 g lower than rats with paraffin oil alone. The mortality rates of incidence were about 10% in rats with CCl_4 after 6 wk, while the paraffin oil-treated rats were all alive. Up to d 21 of exposure to CCl_4, the substantial fibrosis was not observed by histological examination. We found massive rearrangement of the hepatic architecture, including septal fibrosis, extensive bridging, inflammation and extensive fatty changes after 6 wk, while rats with only paraffin oil had normal liver architecture (Figures 4A1 and B1). These results were corresponding with previous findings[19].

We also established the other fibrosis model induced with DMN, because there were differences of hepatotoxicity between CCl_4 and DMN[20]. The body weight was obviously lower in rats with DMN for 3 wk than that in rats with

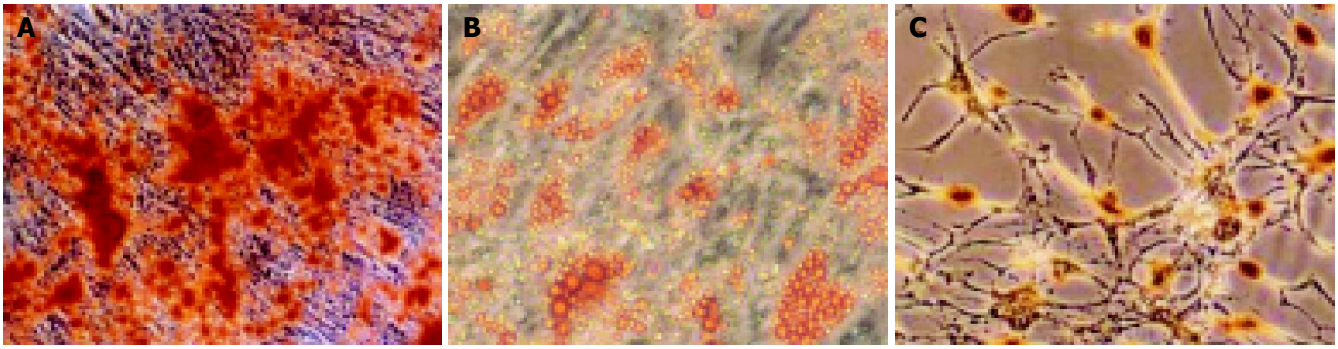

Figure 1 MSCs are induced to differentiate into osteoblasts and stained red color by Chinalizarin (**A**). Under adipogenic conditions, MSCs accumulate lipid vacuoles, which are positively stained by Oil Red O assay (**B**). Under neurogenic conditions, MSCs differentiate into neuronal-like cells and stained positively for NSE by immunocytochemical analysis (**C**). (Original magnification, ×200.)

only saline (Figure 2B). If the body weight fell to less than 100 g, the rat was likely to die soon. The first rat died on d 10 after DMN administration. By d 21, 20% of rats died. Histopathology showed centrilobular congestion and hemorrhagic necrosis liver of rats after 1 wk. Centrilobular necrosis and intense neutrophilic infiltration were observed on d 14. By d 21, collagen fiber deposition could be observed, together with severe centrilobular necrosis and bridging necrosis, with bile duct proliferation and fibrosis surrounding the central veins. These results were corresponding with previous findings[16,21].

To further verify fibrosis, we performed immunohistochemical staining of liver sections for α-SMA, and examined levels of LN, HA, ALT, and TBIL in serum and liver Hyp contents (Figure 4E and Table 1).

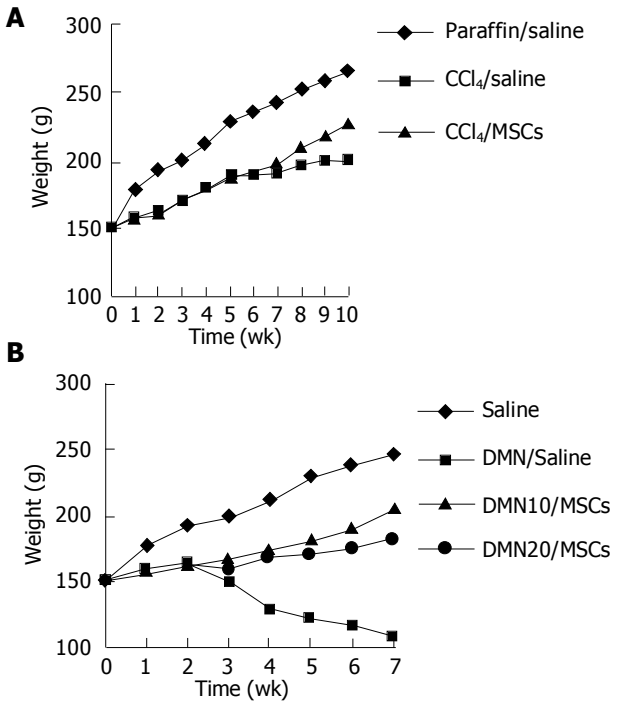

Figure 2 Average weekly weight of rats induced with CCl_4 (A) or DMN (B). **A**: Paraffin/saline, *n* = 10; CCl_4/saline, *n* = 10-8; CCl_4/MSCs, *n* = 10-9; **B**: saline, *n* = 10; DMN/saline, *n* = 40-4; DMN10/MSCs, *n* = 10-8; DMN20/MSCs, *n* = 10-6.

MSCs treatment improved the morphological and behavioral changes

On d 42 after CCl_4 treatment, rats were infused with MSCs or saline. We found that rats with MSCs had got good morphological and behavioral changes after 7th d, while rats with saline appeared extremely lethargic. Two rats with saline died before the completion of the protocol, while rats with MSCs were all alive. There was a slight lift of weight in CCl_4/MSCs compared with CCl_4/saline (Figure 2A). We also observed that some rats in CCl_4/saline had a large amount of ascites while being killed, which could be a reason for gain of weight while living.

There were dramatic changes of rats with MSCs after 7th d in DMN-induced model (Figure 2B). Rats exhibited grooming, but piloerection, their food and water intake were much increased and their weights increased faster. Rats without MSCs had bad good morphological and behavioral changes. Their weights gain stopped. Their eyes were pale and urines were yellow, and some animals had labored respiration. Thirty-six of forty rats in DMN/saline died of progressive liver fibrosis within 49th d after DMN administration. Life time of rats survived in DMN10/MSCs and DMN20/MSCs was significantly longer than that of rats in DMN/saline (Figure 3). Further, amounts of survival rats in DM10/MSCs were more than those in DMN20/MSCs.

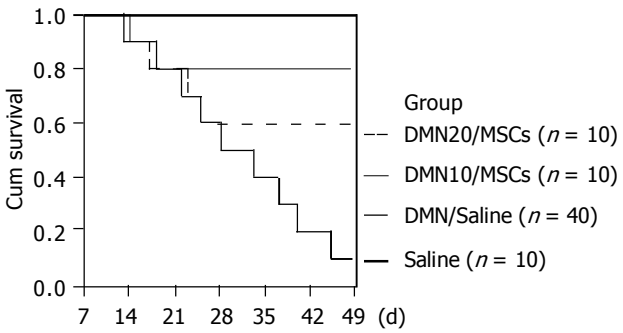

Figure 3 Survival of rats in control group and DMN-induced group with or without MSCs administration. Analysis of survival was conducted by a log-rank test based on the Kaplan–Meier method.

MSCs treatment decreased collagen deposition

We analyzed liver histology in rats with MSCs in two models by HE staining and MT staining. HE staining showed that architecture of liver got better in CCl_4/MSCs (Figure 4C1). Inflammation reduced and pseudolobules were resolved. Collagen accumulation and fatty degeneration were significantly lower in CCl_4/MSCs compared with CCl_4/saline (Figures 4C1, C2, D1, and D2). Quantification of MT staining demonstrated more than 40% decrease of collagen in liver of rats in CCl_4/MSCs compared to that of rats in CCl_4/saline (Figure 4E). Meanwhile, the liver histology also got improved in rats with MSCs treatment whether in DMN10/MSCs or in DMN20/MSCs (Figures 5C1 and D1). The

Table 1 Effect of MSCs on levels of fibrosis index of rats induced with CCl_4

Group	*n*	HA (μg/L)	LN (μg/L)	TBIL (mg/L)	ALT (U/L)	Hyp (μg/g)
Paraffin/saline	10	167.5±25.8[b]	54.2±13.2[b]	8.8±3.5[b]	46.8±7.9[b]	650±130[b]
CCl_4×6 wk	10	883.5±109.6	224.2±56.2	22.8±5.9	132.7±42.9	2 500±330
CCl_4/saline	8	783.5±89.6	215.8±61.9	21.6±5.5	110.1±58.3	2 100±430
CCl_4/MSCs	9	454.1±98.8[b]	85.2±43.9[b]	9.8±6.3[b]	51.3±11.9[b]	1 150±510[b]

[b]$P<0.01$ *vs* CCl_4/saline. Not significantly different between values of CCl_4/saline and CCl_4×6 wk.

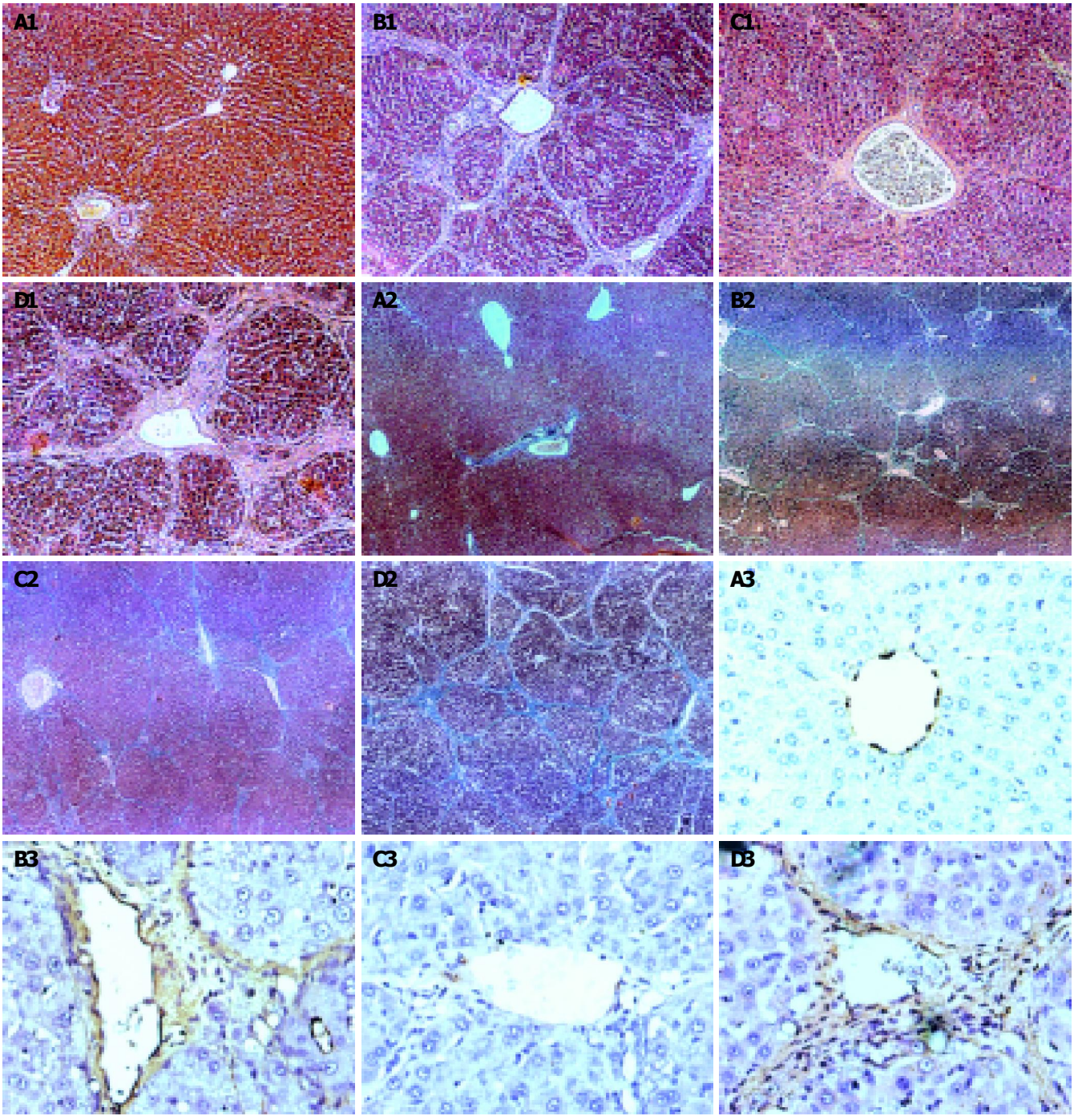

Figure 4 Analysis of liver histopathology and immunohistochemistry in rats induced with CCl_4. **A**: Paraffin/saline; **B**: CCl_4×6 wk; **C**: CCl_4/MSCs; **D**: CCl_4/saline; 1: HE staining, original magnification ×100; 2: MT staining, original magnification ×40; 3: immunohistochemistry for α-SMA, DAB staining, original magnification ×400; **E**: MT and α-SMA staining was quantified using IBAS 2.5 software. Data represent the fold-increase in positive staining *vs* paraffin/saline. Values are presented as mean±SD. $^bP<0.01$ *vs* CCl_4/saline. Not significantly different between values of CCl_4/saline and CCl_4×6 wk.

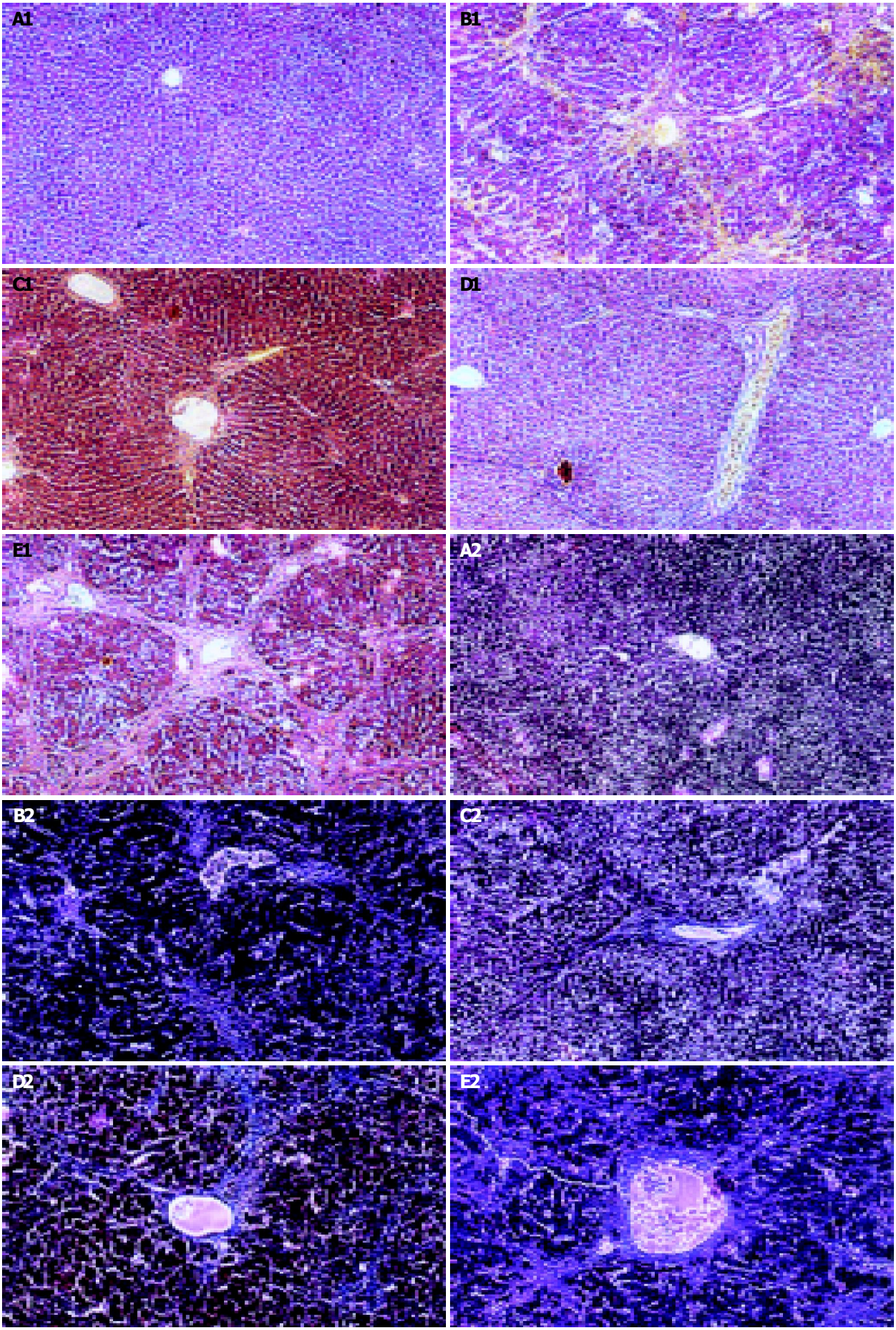
A1
B1
C1
D1
E1
A2
B2
C2
D2
E2

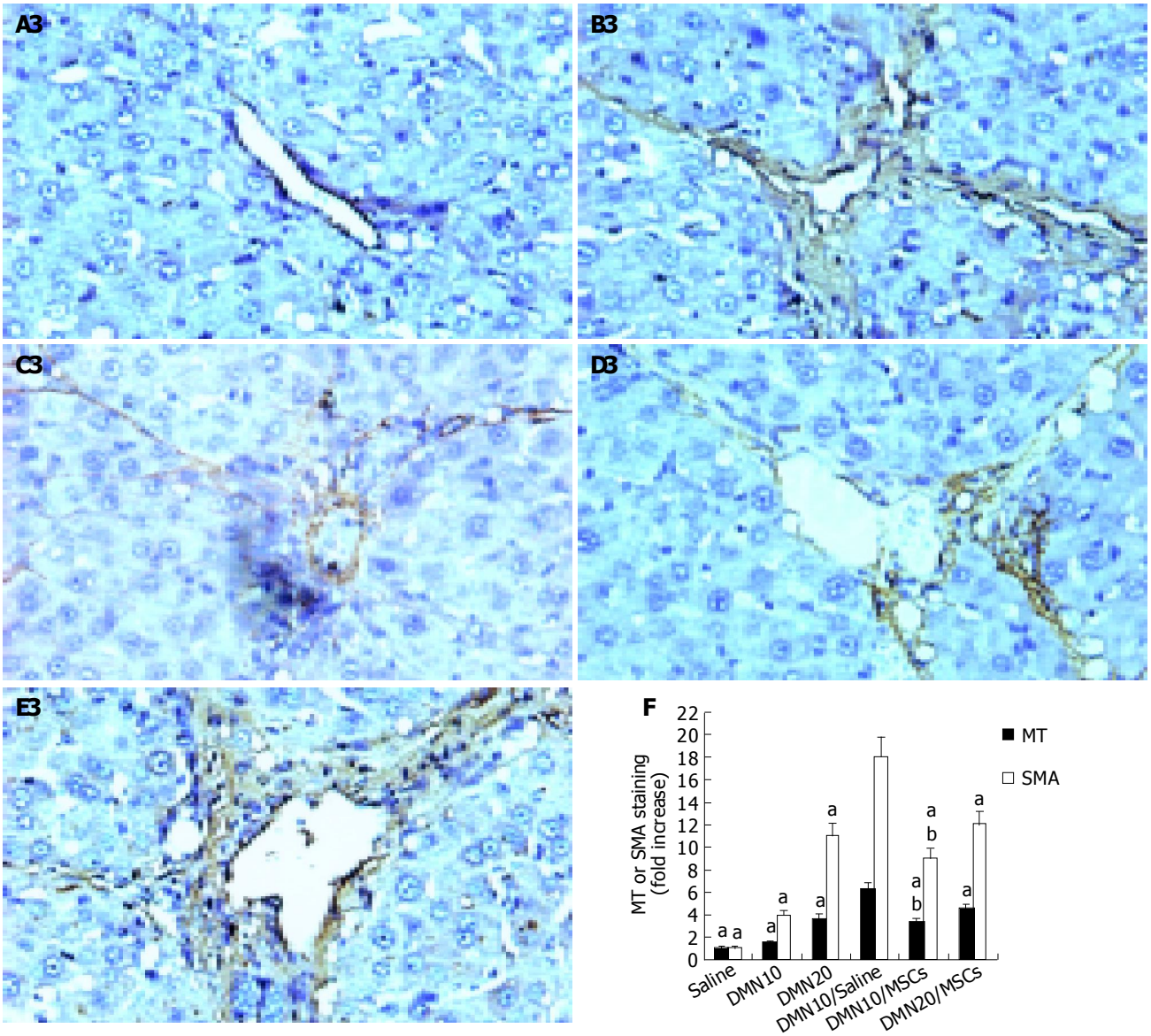

Figure 5 Analysis of liver histopathology and immunohistochemistry in rats induced with DMN. **A**: DMN10; **B**: DMN20; **C**: DMN10/MSCs; **D**: DMN20/MSCs; **E**: DMN10/saline; 1: HE staining, original magnification ×100; 2: MT staining, original magnification ×100; 3: immunohistochemistry for α-SMA, DAB staining, original magnification ×400; **F**: MT and α-SMA staining was quantified using IBAS 2.5 software. Data represent the fold-increase in positive staining *vs* saline. Values are presented as mean±SD. $^aP<0.05$ *vs* DMN20/MSCs, $^bP<0.01$ *vs* DMN10/saline respectively.

necrosis of hepatocyte was replaced by the regenerate. The thickened septal fibrosis became thinner or disappeared. Moreover, the degree of fibrosis was decreased in DMN10/MSCs than that in DMN20/MSCs by quantification of MT staining (Figure 5F). It implied that earlier the MSCs were treated, greater was the effect of MSCs on the inhibition of fibrosis.

We examined levels of HA and LN in serum and liver Hyp contents, which are biochemical markers of liver fibrosis. The result showed that the levels of markers significantly decreased in rats with MSCs than that in rats without MSCs in two models (Tables 1 and 2). And reduction of levels of Hyp and HA and LN was more obvious in DMN10/MSCs than that in DMN20/MSCs. These results

Table 2 Effect of MSCs on levels of fibrosis index of rats induced with DMN

Group	*n*	HA (μg/L)	LN (μg/L)	TBIL (mg/L)	ALT (U/L)	Hyp (μg/g)
Saline	10	142.3±18.9[a]	44.5±16.4[a]	5.1±1.5[a]	32.7±6.8[a]	450±110[a]
DMN10	10	338.7±60.3[a]	82.3±23.5[a]	8.7±1.8[a]	85.3±12.5[a]	760±210[a]
DMN20	10	583.5±59.6[a]	114.9±44.2[a]	10.8±3.5[a]	162.7±22.7[a]	1 250±450[a]
DMN10/saline	4	981.4±110.5	214.2±56.5	21.6±5.5	212.1±51.4	2 250±650
DMN10/MSCs	8	395.2±43.1[a,b]	83.1±43.1[a,b]	9.1±4.7[a,b]	67.7±32.9[a,b]	1 010±580[a,b]
DMN20/MSCs	6	517.8±82.6[a]	98.2±57.2[a]	11.1±6.2[a]	89.7±38.6[a]	1 150±750[a]

$^aP<0.05$ *vs* DMN20/MSCs, $^bP<0.01$ *vs* DMN10/saline respectively.

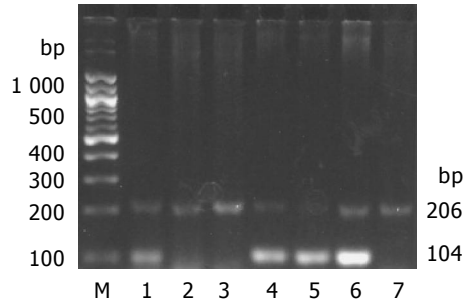

Figure 6 PCR signals of *sry* gene and *β-actin* gene in liver of rats. *sry*, 104 bp; *β-actin*, 206 bp; M: 100-bp DNA maker; lane 1: CCl_4/MSCs; lane 2: CCl_4×6 wk; lane 3: DMN10/saline; lane 4: DMN10/MSCs; lane 5: DMN20/MSCs; lane 6: a male Fischer rat 344 as positive control; lane 7: a female Wistar rat as negative control.

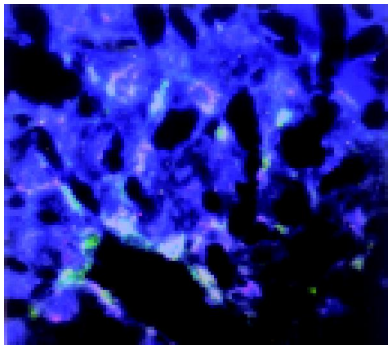

Figure 7 Signals of SRY by FISH with Rat 12/Y whole chromosome probes. Red color represent chromosome Y, green color represent chromosome 12, blue color represent nuclear. Original magnification ×40.

were consistent with the histology of liver.

We tested the level of ALT and TBIL in serum, which are primary indexes of liver function. Levels of these two indexes were closed to normal in CCl_4/MSCs, but stayed higher in CCl_4/saline. We also found that levels were lower in DMN10/MSCs and DMN20/MSCs than that in DMN/saline, although there were few high levels of ALT and TBIL in DMN20/MSCs.

MSCs administration resulted in decreased α-SMA expression

Immunohistochemistry of liver sections for α-SMA expression showed intense staining patterns in CCl_4/saline and DMN/saline (Figures 4B3, 4D3, 5A3, 5B3, and 5E3). However, the levels of α-SMA staining in CCl_4/MSCs, DMN10/MSCs, and DMN20/MSCs were significantly less (Figures 4C3, 5C3, and 5D3) compared to CCl_4/saline and DMN/saline. Quantification of levels of α-SMA staining of liver demonstrated more than 40-50% decrease in rats after MSCs administration in two experimental fibrosis models (Figure 5E). And there were higher levels of α-SMA staining in DMN20/MSCs than that in DMN10/MSCs. This result was consistent with liver histopathology in two models.

Expression of sry gene in livers of rats induced with CCl_4 or DMN

After 4 wk of MSCs treatment, the *sry* gene was positive by using PCR analysis in the liver of female recipient induced with CCl_4. And the similar result was seen in DMN10/MSCs and DMN20/MSCs after 29-39 d of MSCs treatment (Figure 6). These results suggested that BM-derived MSCs were capable of liver engraftment of rats induced with CCl_4 or DMN (Figures 7-9).

DISCUSSION

In the current study, BM-derived MSCs were isolated and expanded in adult rats and their multiple differentiation potential was also confirmed *in vitro*. We evaluated the anti-fibrosis effects of infusion of BM-derived MSCs to rats with CCl_4- or DMN-induced. The results showed that MSCs treatment could reduce mortality rates of rats and improve the fibrosis index.

CCl_4-induced liver fibrosis is a classical experimental fibrosis model. Although this model could undergo spontaneous resolution of fibrosis after stopping CCl_4 challenging in some reports[22], we here did not find recovery of liver fibrosis in CCl_4/saline within 4 wk of withdrawal of CCl_4. In contrast, collagen accumulation and fatty degeneration were significantly lower in CCl_4/MSCs compared with CCl_4/saline. Further, we also confirmed the anti-fibrosis effects of MSCs by DMN-induced liver fibrosis model. DMN is a hepatotoxin, carcinogen and mutagen, and can cause liver fibrosis. It provides a suitable

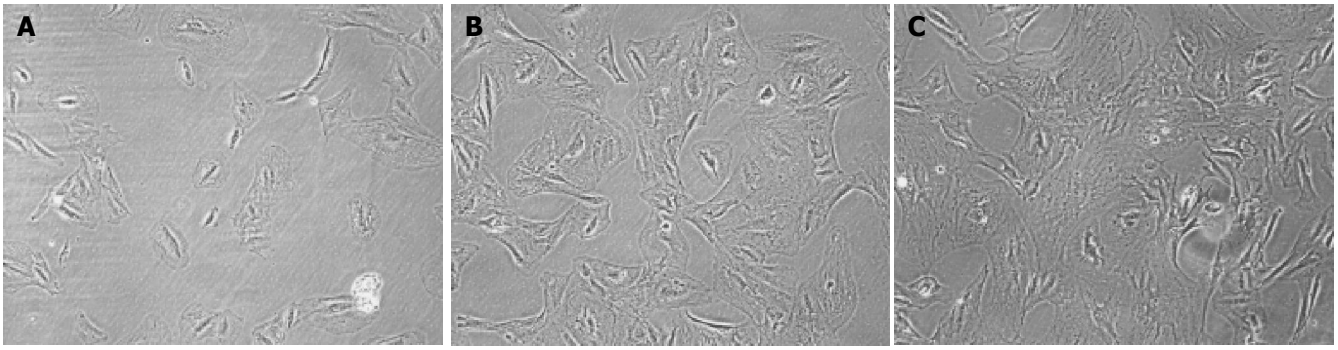

Figure 8 Morphology of hepatic stellate cells co-culture with or without mesenchymal stem cells by transwell *in vitro* for 72 h. **A**: Hepatic stellate cells co-culture with mesenchymal stem cells; **B**: hepatic stellate cells co-culture with hepatoceyte cells line; **C**: hepatic stellate cells only culture. Original magnification ×10.

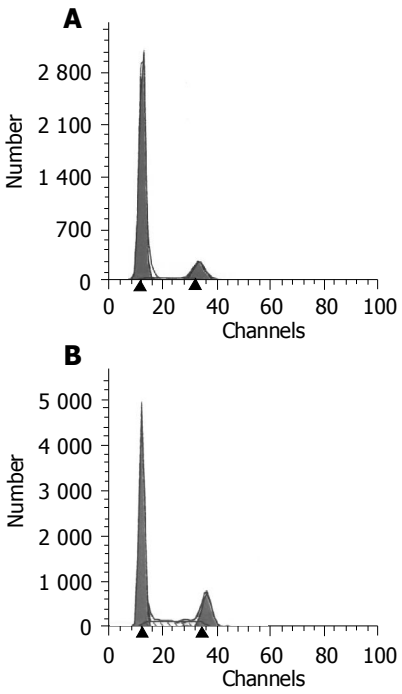

Figure 9 Analysis of hepatic stellate cells by FACS. **A**: Hepatic stellate cells co-culture with mesenchymal stem cells; **B**: hepatic stellate cells only culture.

rapid experimental fibrosis model as like in human liver fibrosis[21,23]. We investigated two groups with MSCs infusion in the different time of fibrosis development in this model. One group DMN10/MSCs was treated with MSCs on the 10th d after DMN administration, in which time it was in early stage of liver fibrogenesis. The other group DMN20/MSCs was infused to MSCs on the 20th d after DMN administration, in which time the fibrosis was forming. Our work demonstrated that infusion of MSCs administration can prolong the life time of rats and improve the liver function and reduce hemorrhagic necrosis collagen accumulation of liver in both groups. Moreover, fibrosis index got more improvement in DMN10/MSCs than that in DMN20/MSCs. These results suggest that infusion of MSCs could not only inhibit the fibrosis formation but also halt the progression of fibrosis in CCl_4- or DMN-treated rats.

We[15,24] and others[25] have showed that BM-derived MSCs did not express MHC class II antigens, costimulatory molecules CD80 and CD86. This phenotype is regarded as nonimmunogenic and suggests that MSCs might be effective in inducing tolerance. It was identified that allogeneic or xenogeneic MSCs could persist into hosts after infusion[26]. We here employ BM-derived MSCs from Fischer 344 rats to infuse Wistar rats with liver fibrosis and get a good result. It implies that infusion of allogeneic MSCs is a great value for liver fibrosis in clinical practice.

In the current study the male donor cells was confirmed in the injured liver of female recipients by PCR for the *sry* gene. However, the mechanism by which MSCs repair the fibrosis is unclear. Fang *et al*[6], found that although albumin-positive donor-derived cells were present at lower frequency in sections of CCl_4-induced liver tissues, infusion of $Flk1^+$ murine MSCs might ameliorate liver fibrosis. Ortiz *et al*[5], observed that MSCs administration reduced the degree of bleomycin-induced inflammation and collagen deposition within lung tissue, but male donor DNA accounted for 2.21×10^{-5}% of total lung DNA in female recipient mice with MSCs treatment. Kinnaird *et al*[27], and Silva *et al*[28], thought that MSCs could secrete a wide array of arteriogenic cytokines and contribute to reducing fibrosis through paracrine mechanisms. These results suggested that MSCs themselves could not functionally rescue the recipients by substituting the damaged cells directly[29]. Although one limitation of the current study is that the quality or quantity of MSCs engraftment in liver was not clear, the fact that MSCs have anti-fibrosis effects in injured liver was clearly proved. We suggest that MSCs may protect against CCl_4- or DMN-induced injury by altering the microenvironment of liver at sites of engraftment. In the present study, levels of α-SMA positive staining of liver sections have more than 50% decrease after MSCs administration in two models (Figures 4E and 5F). This is an exciting event because the expression of α-SMA in liver is an indicator of hepatic stellate cells (HSCs) activation, which is recognized as the key players in liver fibrogenesis[1]. For example, MSCs could secrete many cytokine and growth factors, such as hepatic growth factor[30], which shows anti-apoptotic activity in hepatocytes and plays an essential part in the regeneration of the liver[21] and nerve growth factor[9], which can induce apoptosis of cultured HSCs[31]. And recently, we have provided some evidences that *in vitro* coculture MSCs and HSCs can increase the number of HSCs in G_0 phase and reduce the number of HSCs in S phase (unpublished). Thus, MSCs may play a inhibition role in process of HSCs transition from the quiescent state to activated state.

In summary, this data reveals that infusion of BM-derived MSCs can protect against liver fibrosis and the mechanisms of the anti-fibrosis by MSCs will be studied further.

ACKNOWLEDGMENTS

The authors thank Professor Min Xiong and Professor Run-De Hu for help in histopathology, and the staff of Center for Stem Cell Biology and Tissue Engineering, Sun Yat-Sen University.

REFERENCES

1 **Friedman SL.** Liver fibrosis- from bench to bedside. *J Hepatol* 2003; **38** Suppl 1: S38-S53
2 **Iredale JP.** Cirrhosis: new research provides a basis for rational and targeted treatments. *BMJ* 2003; **327**: 143-147
3 **Lee DS,** Gil WH, Lee HH, Lee KW, Lee SK, Kim SJ, Choi SH, Heo JS, Hyon WS, Kim GS, Paik SW, Koh KC, Joh JW. Factors affecting graft survival after living donor liver transplantation. *Transplant Proc* 2004; **36**: 2255-2256
4 **Wen GM,** Li HW, Xiao QZ, Cheng ZG, Zhang XM, Li Y, Duan LN, Li SN. Studies on differentiation potential of human bone marrow mesenchymal stem cells into hematopoietic cells *in vivo*. *Zhongguo Bingli Shengli Zazhi* 2003; **19**: 157-162
5 **Ortiz LA,** Gambelli F, McBride C, Gaupp D, Baddoo M, Kaminski N, Phinney DG. Mesenchymal stem cell engraftment in lung is enhanced in response to bleomycin exposure and ameliorates its fibrotic effects. *Proc Natl Acad Sci USA* 2003; **100**: 8407-8411
6 **Fang B,** Shi M, Liao L, Yang S, Liu Y, Zhao RC. Systemic infusion of FLK1(+) mesenchymal stem cells ameliorate car-

bon tetrachloride-induced liver fibrosis in mice. *Transplantation* 2004; **78**: 83-88
7 **Mangi AA,** Noiseux N, Kong D, He H, Rezvani M, Ingwall JS, Dzau VJ. Mesenchymal stem cells modified with Akt prevent remodeling and restore performance of infarcted hearts. *Nat Med* 2003; **9**: 1195-1201
8 **Toma C,** Pittenger MF, Cahill KS, Byrne BJ, Kessler PD. Human mesenchymal stem cells differentiate to a cardiomyocyte phenotype in the adult murine heart. *Circulation* 2002; **105**: 93-98
9 **Li Y,** Chen J, Chen XG, Wang L, Gautam SC, Xu YX, Katakowski M, Zhang LJ, Lu M, Janakiraman N, Chopp M. Human marrow stromal cell therapy for stroke in rat: neurotrophins and functional recovery. *Neurology* 2002; **59**: 514-523
10 **Schwartz RE,** Reyes M, Koodie L, Jiang Y, Blackstad M, Lund T, Lenvik T, Johnson S, Hu WS, Verfaillie CM. Multipotent adult progenitor cells from bone marrow differentiate into functional hepatocyte-like cells. *J Clin Invest* 2002; **109**: 1291-1302
11 **Lee KD,** Kuo TK, Whang-Peng J, Chung YF, Lin CT, Chou SH, Chen JR, Chen YP, Lee OK. *In vitro* hepatic differentiation of human mesenchymal stem cells. *Hepatology* 2004; **40**: 1275-1284
12 **Devine SM,** Cobbs C, Jennings M, Bartholomew A, Hoffman R. Mesenchymal stem cells distribute to a wide range of tissues following systemic infusion into nonhuman primates. *Blood* 2003; **101**: 2999-3001
13 **Jiang Y,** Jahagirdar BN, Reinhardt RL, Schwartz RE, Keene CD, Ortiz-Gonzalez XR, Reyes M, Lenvik T, Lund T, Blackstad M, Du J, Aldrich S, Lisberg A, Low WC, Largaespada DA, Verfaillie CM. Pluripotency of mesenchymal stem cells derived from adult marrow. *Nature* 2002; **418**: 41-49
14 **Sakaida I,** Terai S, Yamamoto N, Aoyama K, Ishikawa T, Nishina H, Okita K. Transplantation of bone marrow cells reduces CCl_4-induced liver fibrosis in mice. *Hepatology* 2004; **40**: 1304-1311
15 **Xiao QZ,** Li HW, Wen GM, Liu JB, Zhang XM, Li Y, Li SN. Study on the biological characteristics of rat bone marrow mesenchymal stem cells. *Zhongguo Bingli Shengli Zazhi* 2004; **3**: 289-294
16 **Nakamura T,** Sakata R, Ueno T, Sata M, Ueno H. Inhibition of transforming growth factor beta prevents progression of liver fibrosis and enhances hepatocyte regeneration in dimethylnitrosamine-treated rats. *Hepatology* 2000; **32**: 247-255
17 **Wu GD,** Tuan TL, Bowdish ME, Jin YS, Starnes VA, Cramer DV, Barr ML. Evidence for recipient derived fibroblast recruitment and activation during the development of chronic cardiac allograft rejection. *Transplantation* 2003; **76**: 609-614
18 **An J,** Beauchemin N, Albanese J, Abney TO, Sullivan AK. Use of a rat cDNA probe specific for the Y chromosome to detect male-derived cells. *J Androl* 1997; **18**: 289-293
19 **Parsons CJ,** Bradford BU, Pan CQ, Cheung E, Schauer M, Knorr A, Krebs B, Kraft S, Zahn S, Brocks B, Feirt N, Mei B, Cho MS, Ramamoorthi R, Roldan G, Ng P, Lum P, Hirth-Dietrich C, Tomkinson A, Brenner DA. Antifibrotic effects of a tissue inhibitor of metalloproteinase-1 antibody on established liver fibrosis in rats. *Hepatology* 2004; **40**: 1106-1115
20 **Yasuda M,** Okabe T, Itoh J, Takekoshi S, Hasegawa H, Nagata H, Osamura RY, Watanabe K. Differentiation of necrotic cell death with or without lysosomal activation: application of acute liver injury models induced by carbon tetrachloride (CCL4) and dimethylnitrosamine (DMN). *J Histochem Cytochem* 2000; **48**: 1331-1339
21 **Ueki T,** Kaneda Y, Tsutsui H, Nakanishi K, Sawa Y, Morishita R, Matsumoto K, Nakamura T, Takahashi H, Okamoto E, Fujimoto J. Hepatocyte growth factor gene therapy of liver cirrhosis in rats. *Nat Med* 1999; **5**: 226-230
22 **Iredale JP,** Benyon RC, Pickering J, McCullen M, Northrop M, Pawley S, Hovell C, Arthur MJ. Mechanisms of spontaneous resolution of rat liver fibrosis. Hepatic stellate cell apoptosis and reduced hepatic expression of metalloproteinase inhibitors. *J Clin Invest* 1998; **102**: 538-549
23 **George J,** Rao KR, Stern R, Chandrakasan G. Dimethylnitrosamine-induced liver injury in rats: the early deposition of collagen. *Toxicology* 2001; **156**: 129-138
24 **Li HW,** Wen GM, Xiao QZ, Li HL, Duan LN, Xiang P, Zhang XM, Li SN. Effects of cotransplantation of donor-derived bone marrow mesenchymal stem cells on acute graft versus host disease. *Zhongguo Bingli Shengli Zazhi* 2003; **5**: 577-580
25 **Tse WT,** Pendleton JD, Beyer WM, Egalka MC, Guinan EC. Suppression of allogeneic T-cell proliferation by human marrow stromal cells: implications in transplantation. *Transplantation* 2003; **75**: 389-397
26 **Javazon EH,** Beggs KJ, Flake AW. Mesenchymal stem cells: paradoxes of passaging. *Exp Hematol* 2004; **32**: 414-425
27 **Kinnaird T,** Stabile E, Burnett MS, Shou M, Lee CW, Barr S, Fuchs S, Epstein SE. Local delivery of marrow-derived stromal cells augments collateral perfusion through paracrine mechanisms. *Circulation* 2004; **109**: 1543-1549
28 **Silva GV,** Litovsky S, Assad JA, Sousa AL, Martin BJ, Vela D, Coulter SC, Lin J, Ober J, Vaughn WK, Branco RV, Oliveira EM, He R, Geng YJ, Willerson JT, Perin EC. Mesenchymal stem cells differentiate into an endothelial phenotype, enhance vascular density, and improve heart function in a canine chronic ischemia model. *Circulation* 2005; **111**: 150-156
29 **Kanazawa Y,** Verma IM. Little evidence of bone marrow-derived hepatocytes in the replacement of injured liver. *Proc Natl Acad Sci USA* 2003; **100** Suppl 1: 11850-11853
30 **Matsuda-Hashii Y,** Takai K, Ohta H, Fujisaki H, Tokimasa S, Osugi Y, Ozono K, Matsumoto K, Nakamura T, Hara J. Hepatocyte growth factor plays roles in the induction and autocrine maintenance of bone marrow stromal cell IL-11, SDF-1 alpha, and stem cell factor. *Exp Hematol* 2004; **32**: 955-961
31 **Trim N,** Morgan S, Evans M, Issa R, Fine D, Afford S, Wilkins B, Iredale J. Hepatic stellate cells express the low affinity nerve growth factor receptor p75 and undergo apoptosis in response to nerve growth factor stimulation. *Am J Pathol* 2000; **156**: 1235-1243

Science Editor Guo SY **Language Editor** Elsevier HK

PO Box 2345, Beijing 100023, China
www.wjgnet.com
wjg@wjgnet.com

ELSEVIER

World J Gastroenterol 2005;11(22):3441-3445
World Journal of Gastroenterology ISSN 1007-9327

• *BASIC RESEARCH* •

Gender differences in hepatic ischemic reperfusion injury in rats are associated with endothelial cell nitric oxide synthase-derived nitric oxide

Ping Lü, Fang Liu, Chun-You Wang, Dao-Da Chen, Zhong Yao, Yuan Tian, Jing-Hui Zhang, Yi-Hua Wu

Ping Lü, Chun-You Wang, Dao-Da Chen, Department of General Surgery, Union Hospital, Tongji Medical College, Huazhong University of Science and Technology, Wuhan 430022, Hubei Province, China
Fang Liu, Department of Radiology, Union Hospital, Tongji Medical College, Huazhong University of Science and Technology, Wuhan 430022, Hubei Province, China
Zhong Yao, Cold Spring Harbor Laboratory, New York 11724, USA
Yuan Tian, Jing-Hui Zhang, Yi-Hua Wu, General Surgery Laboratory, Union Hospital, Tongji Medical College, Huazhong University of Science and Technology, Wuhan 430022, Hubei Province, China
Correspondence to: Dr. Ping Lü, Department of General Surgery, Union Hospital, Tongji Medical College, Huazhong University of Science and Technology, Wuhan 430022, Hubei Province, China. luliu@public.wh.hb.cn
Telephone: +86-27-85726273 Fax: +86-27-85726830
Received: 2004-06-08 Accepted: 2004-06-18

Abstract

AIM: This study was designed to examine the hypothesis that gender differences in I/R injury are associated with endothelial cell nitric oxide synthase (eNOS)-derived nitric oxide (NO).

METHODS: Wistar rats were randomized into seven experimental groups (12 animals per group). Except for the sham operated groups, all rats were subjected to total liver ischemia for 40 min followed by reperfusion. All experimental groups received different treatments 45 min before the laparotomy. For each group, half of the animals (six) were used to investigate the survival; blood samples and liver tissues were obtained in the remaining six animals after 3 h of reperfusion to assess serum NO, alanine aminotransferase (ALT) and TNF-α levels, liver tissue malondialdehyde (MDA) content, and severity of hepatic I/R injury.

RESULTS: Basal serum NO levels in female sham operated (FS) group were nearly 1.5-fold of male sham operated (MS) group (66.7±11.0 μmol/L *vs* 45.3±10.1 μmol/L, $P<0.01$). Although serum NO levels decreased significantly after hepatic I/R ($P<0.01$, *vs* sham operated groups), they were still significantly higher in female rat (F) group than in male rat (M) group (47.8±8.6 μmol/L *vs* 23.8±4.7 μmol/L, $P<0.01$). Serum ALT and TNF-α levels, and liver tissue MDA content were significantly lower in F group than in M group (370.5±46.4 U/L, 0.99±0.11 μg/L and 0.57±0.10 μmol/g *vs* 668.7±78.7 U/L, 1.71±0.18 μg/L and 0.86±0.11 μmol/g, respectively, $P<0.01$). I/R induced significant injury to the liver both in M and F groups ($P<0.01$ *vs* sham operated groups). But the degree of hepatocyte injury was significantly milder in F group than in M group ($P<0.05$ and $P<0.01$). The median survival time was six days in F group and one day in M group. The overall survival rate was significantly higher in F group than in M group ($P<0.05$). When compared with male rats pretreated with saline (M group), pretreatment of male rats with 17-β-estradiol (E_2) (M+E_2 group) significantly increased serum NO levels and significantly decreased serum ALT and TNF-α levels, and liver tissue MDA content after I/R ($P<0.01$). The degree of hepatocyte injury was significantly decreased and the overall survival rate was significantly improved in M+E_2 group than in M group ($P<0.01$ and $P<0.05$). The NOS inhibitor N^{ω}-nitro-L-arginine methyl ester (L-NAME) treatment could completely abolish the protective effects of estrogen in both male and female rats.

CONCLUSION: The protective effects afforded to female rats subjected to hepatic I/R are associated with eNOS-derived NO.

Key words: Gender identity; Liver; Reperfusion injury; Endothelial constitutive nitric oxide synthase

Lü P, Liu F, Wang CY, Chen DD, Yao Z, Tian Y, Zhang JH, Wu YH. Gender differences in hepatic ischemic reperfusion injury in rats are associated with endothelial cell nitric oxide synthase-derived nitric oxide. *World J Gastroenterol* 2005; 11(22): 3441-3445
http://www.wjgnet.com/1007-9327/11/3441.asp

INTRODUCTION

Hepatic ischemic reperfusion (I/R) injury is commonly seen in the field of hepatic surgery, such as in the course of hepatectomy, liver transplantation and resuscitation after shock. The injurious effect of I/R presents with a spectrum of clinical manifestations ranging from asymptomatic elevation of liver enzymes to acute liver failure and death. Although liver transplantation has become an accepted therapy for end-stage liver disease because of improved techniques, I/R injury resulting in primary liver graft dysfunction and failure continues to pose significant clinical problems[1].

An increasing body of evidence indicates that gender

differences exist in cardiovascular and immunologic responses to various adverse circulatory conditions, including vascular occlusive disease, hypertension, stroke, shock, and atherosclerosis[2-4]. In addition, clinical studies have shown that female patients survived better than males after liver transplantation or hepatocellular carcinoma resection[5,6]. The underlying mechanism of these gender differences remains to be elucidated.

It has been suggested that the response of the hepatic endothelium to I/R plays a key role in the development of injury[7,8]. Estrogen has been postulated as a "survival factor" for endothelial cells[9,10]. Both women and men have functional α and β estrogen receptors expressed in endothelial cells[11,12]. Estrogen not only can rapidly induce the release of endothelial cell nitric oxide synthase (eNOS)-derived nitric oxide (NO) via a nongenomic manner[13-15], but also can transcriptionally activate the expression of eNOS in endothelial cells via the more classical genomic mechanisms[16,17]. Because we have previously demonstrated that constitutive isoform of NO synthase (cNOS, also known as eNOS)-derived NO plays an important role in limiting hepatic I/R injury in a model of full-size liver I/R[18,19], we hypothesized that the protective mechanism observed in females subjected to hepatic I/R may also depend on eNOS-derived NO.

MATERIALS AND METHODS

Animals

Normal male and female Wistar rats weighing 290-350 g were purchased from the Center of Experimental Animal in Tongji Medical College, Huazhong University of Science and Technology. This project was approved by the Tongji Medical College, and the procedures were carried out according to the routine animal-care guidelines.

Reagents

N^{ω}-nitro-L-arginine methyl ester (L-NAME) and 17-β-estradiol (E_2) were purchased from Sigma Chemical Co., St. Louis, MO, USA.

Model of total hepatic I/R

A model of total hepatic I/R was used as described previously[18,19]. Briefly, rats were anesthetized with ether inhalation, and the midline laparotomy was performed to expose the liver. The total hepatic ischemia was achieved by occluding the hepatic arterial and portal venous blood by using a microaneurysm clip. Rats were then given an ip dose of heparin (200 U/kg) to prevent blood coagulation. After 40 min of ischemia, reperfusion was initiated by removal of the clip. Sham operated control rats were treated in an identical fashion but without vascular clamping. The abdominal cavity was closed, and the rats were allowed to recover with free access to food and water. Rats were then observed daily until d 7 postsurgery to assess survival or were killed after 3 h of reperfusion, and blood samples and liver tissues were obtained for analysis.

Blood and tissue analyses

Serum alanine aminotransferase (ALT) was measured by using standard techniques with a serum analyzer (HITACHI 7170A autoanalyzer, Japan). TNF-α concentration was determined with a commercial radioimmunoassay kit (East Asia Immunotechnology Institute, Beijing, China). Serum NO products nitrite/nitrate (NO_2^-/NO_3^-) were detected using a colorimetric NO detection kit (Nanjing Jiancheng Bioengineering Institute, Nanjing, China). The liver tissue malondialdehyde (MDA) concentration was determined using thiobarbituric acid test (assay kit was purchased from Nanjing Jiancheng Bioengineering Institute, Nanjing, China).

Morphometric assessment of I/R injury

Excised liver specimens were fixed in 40 g/L formaldehyde and embedded in paraffin. Hematoxylin-eosin-stained sections (5 μm) were evaluated at 200× magnification by a point-counting method for severity of hepatic injury by using an ordinal scale as follows[20]: grade 0, minimal or no evidence of injury; grade 1, mild injury consisting of cytoplasmic vacuolation and focal nuclear pyknosis; grade 2, moderate to severe injury with extensive nuclear pyknosis, cytoplasmic hypereosinophilia, loss of intercellular borders, and mild to moderate neutrophil infiltration; and grade 3, severe injury with disintegration of hepatic cords, hemorrhage, and severe polymorphonuclear cell infiltration. An average of 100 adjacent points on a 1-mm^2 grid was graded for each specimen (n = 4).

Experimental design

Rats were randomized into seven experimental groups (12 per group). Apart from the sham operated groups, all rats were subjected to I/R injury. Each group received different treatments 45 min before the laparotomy. The seven groups consisted of group 1, male sham operated rats, 2 mL saline given intravenously (MS group); group 2, female sham operated rats, 2 mL saline given intravenously (FS group); group 3, male rats, 2 mL saline given intravenously (M group); group 4, female rats, 2 mL saline given intravenously (F group); group 5, female rats, L-NAME (10 mg/kg) dissolved in 2 mL saline, given intravenously (F + L-NAME group); group 6, male rats, E_2 (4 000 μg/kg) dissolved in 2 mL saline, given intravenously (M+E_2 group); and group 7, male rats, E_2 (4 000 μg/kg)+L-NAME (10 mg/kg), dissolved in saline, given intravenously (M+E_2+L-NAME group). For each group, half of the rats (six) were used to investigate the survival, and blood samples and liver tissues were obtained in the remaining six rats for analysis after 3 h of reperfusion.

Statistic analysis

All values are expressed as mean±SD. Statistical significance between two groups of parametric data was evaluated by using an unpaired Student's t test. Survival was analyzed by using the Kaplan-Meier method, and the difference in overall survival rate was evaluated using the log rank test. Statistical significance was accepted at $P<0.05$.

RESULTS

Differences in serum NO, ALT and TNF-α levels, and liver tissue MDA content

There were no significant differences between MS and FS groups with respect to serum ALT (Figure 1) and TNF-α

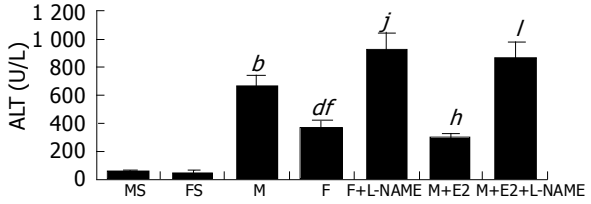

Figure 1 Serum ALT levels (n = 6, mean±SD). There were no significant differences between MS and FS groups with respect to serum ALT levels. Serum ALT levels increased significantly after hepatic I/R in M or F group *vs* MS or FS group (^bP<0.01 or ^dP<0.01, respectively), but they were significantly lower in F group *vs* M group rats (^fP<0.01). When compared with male rats pretreated with saline (M group), pretreatment of male rats with E_2 (M+E_2 group) significantly decreased serum ALT levels after hepatic I/R (^hP<0.01). Pretreatment with L-NAME in female rats or co-pretreatment with E_2 and L-NAME in male rats significantly increased serum ALT levels *vs* those in F or M+E_2 group rats, respectively, after hepatic I/R (^iP<0.01 or ^lP<0.01).

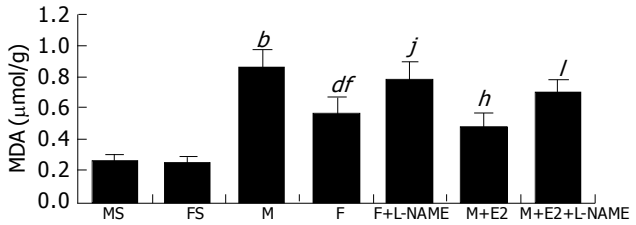

Figure 3 Liver tissue MDA content (n = 6, mean±SD). The differences of liver tissue MDA content between MS and FS groups were not significant. Liver tissue MDA content increased significantly after hepatic I/R in M or F group *vs* MS or FS group (^bP<0.01 or ^dP<0.01, respectively), but they were significantly lower in F group *vs* M group rats (^fP<0.01). When compared with male rats pretreated with saline (M group), pretreatment of male rats with E_2 (M+E_2 group) significantly decreased liver tissue MDA content after hepatic I/R (^hP<0.01). Pretreatment with L-NAME in female rats or co-pretreatment with E_2 and L-NAME in male rats significantly increased liver tissue MDA content *vs* that in F or M+E_2 group animals, respectively, after hepatic I/R (^iP<0.01 or ^lP<0.01).

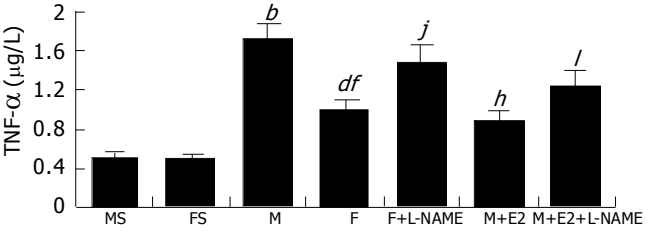

Figure 2 Serum TNF-α levels (n = 6, mean±SD). No significant differences existed between MS and FS groups with respect to serum TNF-α levels. Serum TNF-α levels increased significantly after hepatic I/R in M or F group *vs* MS or FS group (^bP<0.01 or ^dP<0.01, respectively), but they were significantly lower in F group *vs* M group rats (^fP<0.01). When compared with male rats pretreated with saline (M group), pretreatment of male rats with E_2 (M+E_2 group) significantly decreased serum TNF-α levels after hepatic I/R (^hP<0.01). Pretreatment with L-NAME in female rats or co-pretreatment with E_2 and L-NAME in male rats significantly increased serum TNF-α levels *vs* those in F or M+E_2 group animals, respectively, after hepatic I/R (^iP<0.01 or ^lP<0.01).

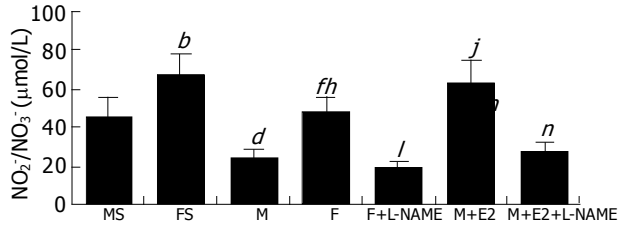

Figure 4 Serum NO_2^-/NO_3^- levels (n = 6, mean±SD). Basal serum NO levels were significantly higher in FS group than those in MS group (^bP<0.01). Although serum NO levels decreased significantly after hepatic I/R in M or F group *vs* MS or FS group (^dP<0.01 or ^fP<0.01, respectively), they were still significantly higher in F group than those in M group rats (^hP<0.01). When compared with male rats pretreated with saline (M group), pretreatment of male rats with E_2 (M+E_2 group) significantly increased serum NO levels after hepatic I/R (^iP<0.01). Pretreatment with L-NAME in female rats or co-pretreatment with E_2 and L-NAME in male rats significantly decreased serum NO levels *vs* those in F or M+E_2 group rats, respectively, after hepatic I/R (^lP<0.01 or ^nP<0.01).

levels (Figure 2), and liver tissue MDA (Figure 3) content. But serum NO levels were significantly higher in FS group than those in MS group (66.7±11.0 μmol/L *vs* 45.3±10.1 μmol/L, P<0.01, Figure 4). Serum ALT and TNF-α levels, and liver tissue MDA content increased significantly, whereas serum NO levels decreased significantly after hepatic I/R both in M and F groups (P<0.01 *vs* sham operated groups). As compared with M group, serum NO levels were significantly higher (47.8±8.6 μmol/L *vs* 23.8±4.7 μmol/L, P<0.01), but serum ALT and TNF-α levels, and liver tissue MDA content were significantly lower in F group (370.5±46.4 U/L, 0.99±0.11 μg/L and 0.57±0.10 μmol/g *vs*. 668.7±78.7 U/L, 1.71±0.18 μg/L and 0.86±0.11 μmol/g, respectively, P<0.01).

Differences in degree of hepatocyte injury

No significant differences in degree of hepatocyte injury between the MS and FS groups were noted (Table 1). Liver architecture was well conserved and liver cells were morphologically normal with a typical plate appearance. I/R induced significant injury to the liver both in M and F groups (P<0.01 *vs* sham operated groups). But the degree of hepatocyte injury was significantly milder in F group *vs* M group determined by a point-counting method with an ordinal scale (P<0.05 and P<0.01).

Differences in survival

A survival advantage was seen in F group *vs* M group. The median survival time was six days in F group *vs* one day in M group. The overall survival rate was significantly higher in F group *vs* M group (P<0.05).

Worsening of hepatic I/R injury of female rats by NOS inhibitor L-NAME

Significantly lower serum NO levels and significantly higher serum ALT and TNF-α levels, and liver tissue MDA content were documented after I/R in female rats pretreated with L-NAME (F+L-NAME group) compared with female rats pretreated with saline (F group) (P<0.01, Figures 1-4). The degree of hepatocyte injury was exacerbated (Table 1) and the overall survival rate was significantly decreased after hepatic I/R in F+L-NAME group rats compared with F group rats (P<0.01 and P<0.05). The median survival time decreased from six days in F group to one day in F+L-NAME group.

Table 1 Degree of hepatocyte injury (determined by a point-counting method with an ordinal scale) (n = 4, mean±SD)

	Grade 0 (%)	Grade 1 (%)	Grade 2 (%)	Grade 3 (%)
MS	99.4±0.1	0.6±0.1	0	0
FS	99.4±0.2	0.6±0.2	0	0
M	0.2±0.1[b]	8.6±1.7[b]	76.9±2.4[b]	14.4±7.2[b]
F	2.7±1.0[d,f]	37.2±3.7[d,f]	52.2±3.2[d,f]	7.9±1.4[d,a]
F+L-NAME	1.0±0.3[c]	16.0±4.6[h]	75.1±4.1[h]	8.0±1.0
M+E_2	4.0±1.2[f]	57.7±3.9[f]	32.9±5.3[f]	5.5±0.5[f]
M+E_2+L-NAME	1.6±0.6[e]	28.5±1.9[j]	62.3±3.1[j]	7.6±1.3[e]

There were no significant differences between MS and FS groups with respect to degree of hepatocyte injury. [b]P<0.01 *vs* MS group. [d]P<0.01 *vs* FS group. [a]P<0.05 *vs* M group, [f]P<0.01 *vs* M group. [c]P<0.05 *vs* F group, [h]P<0.01 *vs* F group. [e]P<0.05 *vs* M+E_2 group, [j]P<0.01 *vs* M+E_2 group.

Suppression of the protective effects of 17-β-estradiol (E_2) on hepatic I/R injury by L-NAME in male rats

When compared with male rats pretreated with saline (M group), pretreatment of male rats with E_2 (M+E_2 group) significantly increased serum NO levels and significantly decreased serum ALT and TNF-α levels, and liver tissue MDA content after I/R (P<0.01, Figures 1-4). The degree of hepatocyte injury was significantly decreased (Table 1) and the overall survival rate was significantly improved in M+E_2 group *vs* M group (P<0.01 and P<0.05). The median survival time increased from one day in M group to less than seven days in M+E_2 group. Significantly lower serum NO levels and significantly higher serum ALT and TNF-α levels, and liver tissue MDA content were shown after hepatic I/R in male rats pretreated with E_2 and L-NAME (M+E_2+L-NAME group) compared with male rats given E_2 alone (M+E_2 group) (P<0.01, Figures 1-4). The protection of E_2 on I/R injury of the liver was completely reverted by the co-administration of L-NAME in male rats. The degree of hepatocyte injury was exacerbated (Table 1) and the overall survival rate was significantly decreased after hepatic I/R in M+E_2+L-NAME group *vs* M+E_2 group rats (P<0.01 and P<0.05). The median survival time decreased from less than seven days in M+E_2 group to 1.5 d in M+E_2 + L-NAME group.

DISCUSSION

In the present study we found that female rats were protected to a much greater extent from the injurious effects of hepatic I/R than were male rats, and E_2 pretreatment could induce protection to male rats on hepatic I/R injury. We also found that the NOS inhibitor L-NAME could abolish these gender differences and revert protection induced by estrogen pretreatment on male rats. As we have previously proved that hepatic I/R does not induce the expression of inducible NOS (iNOS) in our model[19], the results of the current study clearly demonstrated that the protective effect afforded by estrogen was associated with eNOS-derived NO.

Estrogen may increase NO production from eNOS by genomic and/or nongenomic responses[13-17]. It was confirmed that estrogen might up-regulate eNOS gene expression to increase NO production in vascular endothelial cells as well as sinusoidal endothelial cells from liver[16,21]. Additionally, engagement of estrogen receptor-α for estrogen can mediate Ca^{2+} uptake and "activate" existing eNOS. It was demonstrated that this rapid nongenomic production of eNOS-derived NO involved a rapid, PI3-kinase-dependent activation of Akt and consequent serine phosphorylation of eNOS[14,22]. Consistent with these observations, we found that basal serum NO levels in female sham operated rats were nearly 1.5-fold of those in males. Although serum NO levels decreased significantly after hepatic I/R (P<0.01, *vs* sham operated groups), which was due to endothelial cell injury or dysfunction in our full size hepatic I/R model, they were still significantly higher in F group than those in M group rats (P<0.01). The precise mechanisms by which eNOS-derived NO protects female rats from the injurious effects of I/R remain to be identified. One possible mechanism may involve the antioxidant properties of eNOS-derived NO[23]. NO is known to inhibit reactive oxygen species (ROS)-mediated reactions and it has been suggested that the protective effects in a variety of conditions are due to the ability of NO to detoxify ROS such as O_2^-, OH^-, and/or ferryl hemoprotein[24]. This might be one of the main causes why liver tissue MDA content was significantly lower in F group than that in M group. Another mechanism by which eNOS-derived NO may exert protection in our model of I/R is vasodilation and enhanced perfusion of the postischemic tissue[14,25]. We have previously demonstrated that eNOS-derived NO may counteract the physiological effect of endothelin-1 (ET-1), a potent and long-lasting vasoconstrictive peptide[18,19]. Other mechanisms by which eNOS-derived NO may protect the liver from hepatic I/R-induced injury may be related to its inhibition of platelet aggregation and adhesion as well as attenuation of endothelium-leukocyte interactions, all of which may be beneficial to reduce hepatic I/R injury[26]. TNF-α has been shown to play a critical role in inflammatory responses during hepatic I/R[27]. We found in this study that serum TNF-α levels were significantly lower in F group than those in M group. It was postulated that the anti-inflammatory properties of estrogen might be due to its blockade of translocation of the transcription factor nuclear factor κB[28] and this might be via endogenous signal molecule NO or other signal molecules. It was also found that eNOS-derived NO may protect animals after hepatic I/R by protecting the liver from the injurious effects of TNF-α[29].

We also studied the protective effect of estrogen on I/R injury of the liver in male rats. In previous studies, administration of 4 000 μg/kg E_2 was found to increase plasma E_2 in mice comparable to levels seen in female mice in the proestrus state[30]. We found that male rats pretreated with 4 000 μg/kg E_2 were protected from the injurious

effects of hepatic I/R to an extent not less than that of female rats. The role of eNOS-derived NO as a crucial component for the protective effects afforded by estrogen was confirmed in studies using L-NAME-treated female and male rats. Since some of the protective effects of estrogen are NO-independent[31], it was puzzling that L-NAME treatment could completely abolish the protective effects of estrogen in both male and female rats in this study. We postulated that L-NAME treatment would aggravate endothelial cell injury or dysfunction in our full size hepatic I/R model, which might conceal the NO-independent protective effects of estrogen.

In conclusion, the results of this study demonstrate that the protective effects afforded to female rats subjected to hepatic I/R are associated with eNOS-derived NO. These results may have important implications for the design of novel strategies against ischemic reperfusion injury in the future.

REFERENCES

1 **Arranz J,** Soriano A, Garcia I, Garcia I, Concepcion MT, Navarro J, Arteaga A, Filella X, Gonzalez F, Fernandez C, Barrera M, Munoz L, Perera AJ, Pozo JL, Jimenez A, Macia M, Arteaga I. Association between anatomopathologic graft disorders during reperfusion and vena cava sIL-2r in orthotopic liver transplantation. *Transplant Proc* 2003; **35**: 1880-1883

2 **Shearman AM,** Cupples LA, Demissie S, Peter I, Schmid CH, Karas RH, Mendelsohn ME, Housman DE, Levy D. Association between estrogen receptor alpha gene variation and cardiovascular disease. *JAMA* 2003; **290**: 2263-2270

3 **Dubey RK,** Oparil S, Imthurn B, Jackson EK. Sex hormones and hypertension. *Cardiovasc Res* 2002; **53**: 688-708

4 **Hayward CS,** Kalnins WV, Kelly RP. Gender-related differences in left ventricular chamber function. *Cardiovasc Res* 2001; **49**: 340-350

5 **Jain A,** Reyes J, Kashyap R, Dodson SF, Demetris AJ, Ruppert K, Abu-Elmagd K, Marsh W, Madariaga J, Mazariegos G, Geller D, Bonham CA, Gayowski T, Cacciarelli T, Fontes P, Starzl TE, Fung JJ. Long-term survival after liver transplantation in 4,000 consecutive patients at a single center. *Ann Surg* 2000; **232**: 490-500

6 **Lee CC,** Chau GY, Lui WY, Tsay SH, King KL, Loong CC, Hshia CY, Wu CW. Better post-resectional survival in female cirrhotic patients with hepatocellular carcinoma. *Hepatogastroenterology* 2000; **47**: 446-449

7 **Sakamoto N,** Sun Z, Brengman ML, Maemura K, Ozaki M, Bulkley GB, Klein AS. Hepatic reticuloendothelial system dysfunction after ischemia-reperfusion: role of P-selectin-mediated neutrophil accumulation. *Liver Transpl* 2003; **9**: 940-948

8 **Khandoga A,** Biberthaler P, Enders G, Teupser D, Axmann S, Luchting B, Hutter J, Messmer K, Krombach F. P-selectin mediates platelet-endothelial cell interactions and reperfusion injury in the mouse liver *in vivo*. *Shock* 2002; **18**: 529-535

9 **Mendelsohn ME.** Genomic and nongenomic effects of estrogen in the vasculature. *Am J Cardiol* 2002; **90**: 3F-6F

10 **Spyridopoulos I,** Sullivan AB, Kearney M, Isner JM, Losordo DW. Estrogen-receptor-mediated inhibition of human endothelial cell apoptosis. Estradiol as a survival factor. *Circulation* 1997; **95**: 1505-1514

11 **Li L,** Haynes MP, Bender JR. Plasma membrane localization and function of the estrogen receptor alpha variant (ER46) in human endothelial cells. *Proc Natl Acad Sci USA* 2003; **100**: 4807-4812

12 **Hodges YK,** Tung L, Yan XD, Graham JD, Horwitz KB, Horwitz LD. Estrogen receptors alpha and beta: prevalence of estrogen receptor beta mRNA in human vascular smooth muscle and transcriptional effects. *Circulation* 2000; **101**: 1792-1798

13 **Simoncini T,** Genazzani AR, Liao JK. Nongenomic mechanisms of endothelial nitric oxide synthase activation by the selective estrogen receptor modulator raloxifene. *Circulation* 2002; **105**: 1368-1373

14 **Hisamoto K,** Ohmichi M, Kurachi H, Hayakawa J, Kanda Y, Nishio Y, Adachi K, Tasaka K, Miyoshi E, Fujiwara N, Taniguchi N, Murata Y. Estrogen induces the Akt-dependent activation of endothelial nitric-oxide synthase in vascular endothelial cells. *J Biol Chem* 2001; **276**: 3459-3467

15 **Mendelsohn ME.** Nongenomic, ER-mediated activation of endothelial nitric oxide synthase: how does it work? What does it mean? *Circ Res* 2000; **87**: 956-960

16 **Sakamoto M**, Uen T, Nakamura T, Hashimoto O, Sakata R, Kin M, Ogata R, Kawaguch T, Torimura T, Sata M. Estrogen upregulates nitric oxide synthase expression in cultured rat hepatic sinusoidal endothelial cells. *J Hepatol* 2001; **34**: 858-864

17 **Nuedling S,** Kahlert S, Loebbert K, Doevendans PA, Meyer R, Vetter H, Grohe C. 17 Beta-estradiol stimulates expression of endothelial and inducible NO synthase in rat myocardium *in-vitro* and *in-vivo*. *Cardiovasc Res* 1999; **43**: 666-674

18 **Lü P,** Chen D, Tian Y, Zhang J, Wu Y. The effect of nitric oxide/endothelins system on the hepatic ischemia/reperfusion injury. *J Huazhong Univ Sci Technolog Med Sci* 2002; **22**: 216-217, 227

19 **Lü P,** Chen DD, Tian Y, Zhang JH, Wu YH. The protection of the hepatic ischemic preconditioning is concerned with the NO/ET-1 system. *Zhongguo Bingli Shengli Zazhi* 2000; **16**: 901-905

20 **Camargo CA,** Madden JF, Gao W, Selvan RS, Clavien PA. Interleukin-6 protects liver against warm ischemia/reperfusion injury and promotes hepatocyte proliferation in the rodent. *Hepatology* 1997; **26**: 1513-1520

21 **Kleinert H,** Wallerath T, Euchenhofer C, Ihrig-Biedert I, Li H, Forstermann U. Estrogens increase transcription of the human endothelial NO synthase gene: analysis of the transcription factors involved. *Hypertension* 1998; **31**: 582-588

22 **Haynes MP,** Li L, Sinha D, Russell KS, Hisamoto K, Baron R, Collinge M, Sessa WC, Bender JR. Src kinase mediates phosphatidylinositol 3-kinase/Akt-dependent rapid endothelial nitric-oxide synthase activation by estrogen. *J Biol Chem* 2003; **278**: 2118-2123

23 **Wink DA,** Miranda KM, Espey MG, Pluta RM, Hewett SJ, Colton C, Vitek M, Feelisch M, Grisham MB. Mechanisms of the antioxidant effects of nitric oxide. *Antioxid Redox Signal* 2001; **3**: 203-213

24 **Grisham MB,** Jourd'Heuil D, Wink DA. Nitric oxide. I. Physiological chemistry of nitric oxide and its metabolites:implications in inflammation. *Am J Physiol* 1999; **276**: G315-G321

25 **Haynes MP,** Sinha D, Russell KS, Collinge M, Fulton D, Morales-Ruiz M, Sessa WC, Bender JR. Membrane estrogen receptor engagement activates endothelial nitric oxide synthase via the PI3-kinase-Akt pathway in human endothelial cells. *Circ Res* 2000; **87**: 677-682

26 **Huang PL.** Endothelial nitric oxide synthase and endothelial dysfunction. *Curr Hypertens Rep* 2003; **5**: 473-480

27 **Iwasaki Y,** Tagaya N, Hattori Y, Yamaguchi K, Kubota K. Protective effect of ischemic preconditioning against intermittent warm-ischemia-induced liver injury. *J Surg Res* 2002; **107**: 82-92

28 **Wen Y,** Yang S, Liu R, Perez E, Yi KD, Koulen P, Simpkins JW. Estrogen attenuates nuclear factor-kappa B activation induced by transient cerebral ischemia. *Brain Res* 2004; **1008**: 147-154

29 **Rai RM,** Lee FY, Rosen A, Yang SQ, Lin HZ, Koteish A, Liew FY, Zaragoza C, Lowenstein C, Diehl AM. Impaired liver regeneration in inducible nitric oxide synthasedeficient mice. *Proc Natl Acad Sci USA* 1998; **95**: 13829-13834

30 **Knoferl MW,** Diodato MD, Angele MK, Ayala A, Cioffi WG, Bland KI, Chaudry IH. Do female sex steroids adversely or beneficially affect the depressed immune responses in males after trauma-hemorrhage? *Arch Surg* 2000; **135**: 425-433

31 **Nascimento CA,** Kauser K, Rubanyi GM. Effect of 17beta-estradiol in hypercholesterolemic rabbits with severe endothelial dysfunction. *Am J Physiol* 1999; **276**: H1788-H1794

Science Editor Zhu LH **Language Editor** Elsevier HK

PO Box 2345, Beijing 100023, China
www.wjgnet.com
wjg@wjgnet.com

ELSEVIER

World J Gastroenterol 2005;11(22):3446-3450
World Journal of Gastroenterology ISSN 1007-9327

• *BRIEF REPORTS* •

Adenovirus-mediated FasL gene transfer into human gastric carcinoma

Shi-Ying Zheng, De-Chun Li, Zhi-De Zhang, Jun Zhao, Jin-Feng Ge

Shi-Ying Zheng, Jun Zhao, Jin-Feng Ge, Department of Cardiothoracic Surgery, The First Affiliated Hospital of Suzhou University, Suzhou 215006, Jiangsu Province, China
De-Chun Li, Zhi-De Zhang, Department of General Surgery, The First Affiliated Hospital of Suzhou University, Suzhou 215006, Jiangsu Province, China
Supported by the Medical Scientific Foundation of Jiangsu Province, No. H200147
Correspondence to: Dr. Shi-Ying Zheng, Department of Cardiothoracic Surgery, The First Affiliated Hospital of Suzhou University, Suzhou 215006, Jiangsu Province, China. syzheng88@sina.com
Telephone: +86-512-65263570
Received: 2004-06-19 Accepted: 2004-07-22

Abstract

AIM: To evaluate the possible value of FasL in gastric cancer gene therapy by investigating the effects of FasL expression on human gastric cancer cell line.

METHODS: An adenoviral vector encoding the full-length human FasL cDNA was constructed and used to infect a human gastric cancer (SGC-7901) cell line. FasL expression was confirmed by X-gal staining, flow cytometric analysis and RT-PCR. The effect of FasL on cell proliferation was determined by clonogenic assay, cytotoxicity was detected by MTT assay, and cell viability was measured by trypan blue exclusion. The therapeutic efficiency of Ad-FasL *in vivo* was investigated with a xenograft tumor model in nude mice.

RESULTS: SGC-7901 cells infected with Ad-FasL showed increased expression of FasL, resulting in significantly decreased cell growth and colony-forming activity when compared with control adenovirus-infected cells. The cytotoxicity of anti-Fas antibody (CH-11) in gastric cancer cells was stronger than that of ActD (91±8 *vs* 60±5, $P<0.01$), and the cytotoxicity of Ad-FasL was stronger than that of CH-11 (60±5 *vs* 50±2, $P<0.05$). In addition, G_1-phase arrest (67.75±0.39 *vs* 58.03±2.16, $P<0.05$) and apoptosis were observed in Ad-FasL-infected SGC-7901 cells, and the growth of SGC-7901 xenografts in nude mice was retarded after intra-tumoral injection with Ad-FasL (54% *vs* 0%, $P<0.0001$).

CONCLUSION: Infection of human gastric carcinoma cells with Ad-FasL induces apoptosis, indicating that this target gene might be of potential value in gene therapy for gastric cancer.

Key words: FasL gene; Gene transfer; Apoptosis; Carcinoma; Gastrocellular; Gene therapy

Zheng SY, Li DC, Zhang ZD, Zhao J, Ge JF. Adenovirus-mediated FasL gene transfer into human gastric carcinoma. *World J Gastroenterol* 2005; 11(22): 3446-3450
http://www.wjgnet.com/1007-9327/11/3446.asp

INTRODUCTION

Gastric cancer is one of the most common digestive tract cancers in China. Although an increasing number of gastric cancer patients have benefited from the development of modern tumor therapies, the prognosis of this disease is still relatively poor. Gastric cancer often resists various treatments, including immunotherapy, wherein deficient tumor-specific T-cell responses result in poor immune response.

In this context, apoptosis mediated by the Fas/FasL system is of great interest to researchers, as cytotoxic T-lymphocytes (CTLs) utilize the perforin/granzyme and Fas/FasL systems to kill cancer cells. Fas is a member of the tumor necrosis factor/nerve growth factor receptor family, whereas the Fas ligand (FasL) is a member of the tumor necrosis factor/nerve growth factor family[1-7]. The FasL is primarily expressed in active CTLs, and induces apoptosis of Fas-expressing tumor cells[2,6]. Since the Fas/FasL apoptosis pathway is a key mechanism for clearing tumor cells, researchers are currently seeking methods for triggering FasL expression in tumor cells via gene therapy, thus 'marking' them for Fas/FasL-mediated apoptosis[5,8]. Accordingly, we used adenoviral gene transfer to trigger high-level FasL expression in SGC-7901 (human gastric cancer) cells to investigate the possible use of FasL in gastric cancer gene therapy.

MATERIALS AND METHODS

Cell line

The human gastric cancer cell line SGC-7901 was obtained from the Shanghai Institute of Cell Biology at the Chinese Academy of Sciences (Shanghai, China). Cells were cultured in Medium 199 (Gibco) supplemented with 10% fetal bovine serum.

Recombinant retroviral vector construction

The recombinant FasL retroviral vector was constructed in our laboratory. The FasL gene expression cassette includes the CMV promoter, a full-length FasL cDNA (Jingmei

Company, Shenzheng, China) and the SV40 polyA signal sequences. This cassette was inserted into the E1 region of an adenoviral genome lacking the viral E1 and E3 sequences. Briefly, the FasL cDNA was inserted into the pAdCMV shuttle plasmid (kindly provided by Dr. Daru Lu) and co-transfected with pJM17 (Microbix Biosystems Inc., Canada) into human embryonic 293 cells (provided by Dr. Lu) using the Lipofectin reagent (Gibco). The FasL expression cassette was then transferred into the adenovirus genome by homologous recombination. The control virus Ad-LacZ was constructed in the same manner. Virus proliferation, purification and titering were performed as described by He *et al*[9].

Adenovirus transduction efficiency

Gastric carcinoma cells were infected with Ad-LacZ at various multiplicities of infection (MOIs). After 48 h, cells were fixed in 40 g/L formaldehyde for 6-8 h and then treated with X-gal solution (1 mg/mL X-gal in a solution of 0.1 mol/L PBS, 1.3 mmol/L $MgCl_2$, 3 mmol/L $K_3Fe(CN)_6$) for 2 h or overnight in a 37 ℃ incubator. The percentage of blue cells was then determined.

FasL gene transfection

Cells were passaged at a density of 10^5/well. For viral infection, cells were incubated with virus suspensions (at various MOIs) and 8 μg/mL polybrene (Sigma) for 2-3 h at 37 ℃, washed twice with fresh medium, and further incubated for 48 h. Then cells were passaged and incubated in medium containing 1 mg/mL G418 (Gibco) for selection of transfectants. The medium was changed every 3-4 d until anti-G418 cells appeared.

Detection of exogenous FasL expression

Cells were harvested, washed with PBS, and treated with FITC-conjugated FasL antibody (Jackson ImmunoResearch Lab) or control serum for 0.5-1 h at 4 ℃. Cells were once again washed with PBS, and FasL protein expression was confirmed by FCM analysis (Becton Dickinson, San Jose, CA). For FasL gene expression, RT-PCR was performed with the kit according to the manufacturer's instructions (Shanghai Shanggong Company, Shanghai, China). The primers were: forward 5'-CTGAATTCTGACTCACCA-GCTGCCATGC-3', reverse 5'-TACTCGAGCTATTAGA-GCTTATATAAGCCG-3'.

Clonogenic assay

SGC-7901 cells were infected with Ad-FasL or Ad-LacZ (100 MOI). After 24 h, the cells were seeded in 6-well plates at 500 cells/well. After being incubated for 2-3 wk, cells were stained with 0.1% crystal violet and counted under a microscope. Colonies of more than 50 cells were counted for all clonogenic assays.

Cell cycle and apoptosis assays

Cells infected with Ad-FasL or Ad-LacZ (more than 10^6 cells) in either suspension or adhesion were harvested and fixed in 70% ethanol for 3 h. Cells were then treated with 50 μg/mL RNase for 1 h at 37 ℃, and stained with 100 μg/mL PI for 20-30 min prior to FCM analysis.

MTT assay

SGC-7901 cells were treated with 100 ng/mL anti-Fas antibody (CH-11; PharMingen), 50 ng/mL actinomycin D (ActD; Sigma), and infected with Ad-FasL (100 MOI) or treated with anti-Fas antibody combined with Ad-FasL infection. Cytotoxicity was determined by MTT assay. About 10^{3-4} cells/well were plated in 96-well plates and incubated overnight in 100 μL of culture medium. After 2-3 d, 20 μL of MTT solution (5 mg/mL) was added to each culture well. After incubating for 4 h at 37 ℃, the MTT was removed and 200 μL of dimethyl sulfoxide (Sigma) was added and mixtures were shaken, the crystals were fully dissolved (about 10 min). The A value of each well was detected using a microculture plate reader (Huandong Cesium Electron Tube Company) with a test wavelength of 490 nm. Cell survival rate (SR) was expressed as the following equation: SR=(A in experimental group/A in control group)×100%. Results were expressed as mean±SD; the Student's t-test was used for statistical analysis.

Cell proliferation assay

SGC-7901 cells (2.5-3.0×10^3 cells/well) were plated in 24-well plates (3 wells for each test) and infected with various MOIs of Ad-LacZ or Ad-FasL for 24 h. Cells were harvested every 2 d, and the living cell rate (LR) was measured by trypan blue exclusion assay. LR was expressed as the following equation:

LR=number of living cells/(number of living cells+number of dead cells)×100%. Results were expressed as mean±SD; ANOVA was used for statistical analysis with SPSS 10.0 software. $P<0.05$ was considered statistically significant.

Animal model

BALB/c nude mice (The Shanghai Institute of Cancer Research) were subcutaneously injected with SGC-7901 cells at 1-5×10^7 cells/mouse. When tumors grew to 0.5 cm in diameter, the mice were randomly divided into treated and control groups (n = 5). Tumor volumes were calculated by [(1/2)×(longest diameter)×(shortest diameter)] as described previously. Tumors were measured every 5 d for 6 wk. Growth curves were drawn and the percentage of tumor inhibition was calculated (treated group/control group×100%).

RESULTS

FasL gene transfection

Anti-G418 colonies were obtained after screening for 2 wk. The selected clone containing the FasL gene was named as SGC-7901-FasL, and the control clone containing the blank vector was designated as SGC-7901-vect. There was no morphologic difference between cultures of these two cells.

Determination of FasL protein expression

FCM analysis revealed that SGC-7901-FasL cells expressed FasL on their surface, whereas SGC-7901-vect did not (Figure 1).

Determination of FasL mRNA expression

Total RNA was extracted from the test and control cells,

and FasL-specific primers were used for amplification by RT-PCR. The expected 231-bp fragment was amplified from SGC-7901-FasL cells, but not from SCG-7901-vect cells (Figure 2).

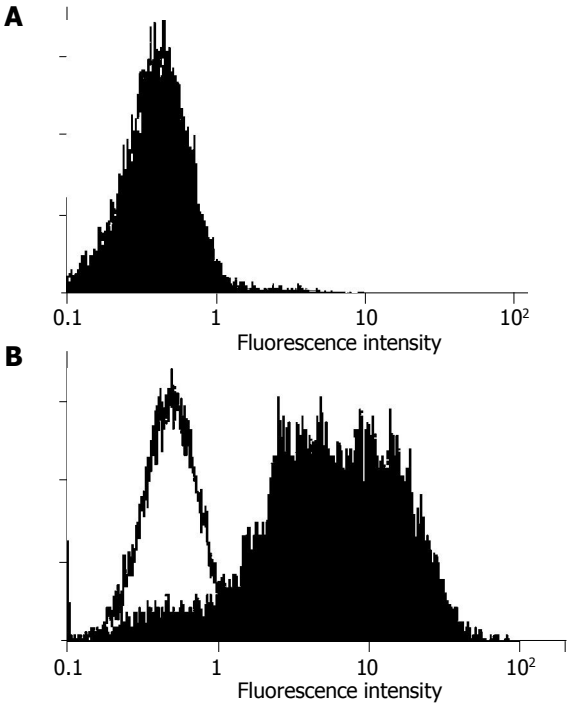

Figure 1 FasL expression on the surface of adenovirus infected SGC-7901 cells. **A**: Ad-LacZ (titer 4.0×10^5 CFU/mL); **B**: Ad-FasL (titer 2.8×10^5 CFU/mL).

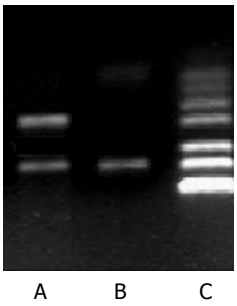

Figure 2 FasL expression as examined by RT-PCR. A: SGC-7901-Fas-L (the FasL amplicon has a size of 231 bp); B: SGC-7901-vect (negative control); C: DNA marker.

Inhibition of SGC-7901 cell growth by exogenous FasL

Two days after infection, SGC-7901-FasL cells were smaller and became more round in shape. Over the next 4 d, the plasma membranes of these cells blebbed, the cytoplasm and nuclei condensed, and the cells ultimately lysed into membrane-bound apoptotic bodies. Cytotoxicity was determined by MTT 4 d after infection. Ad-FasL cultures showed 84% fewer viable cells than Ad-LacZ infected cultures, suggesting that Ad-FasL was cytotoxic to gastric cancer cells. Clonogenic assay showed that SGC-7901 cells infected with Ad-FasL (100 MOI) did not form colonies, whereas Ad-LacZ cultures formed numerous colonies, demonstrating that expression of FasL significantly decreased colony formation.

Cell cycle and apoptosis in Ad-FasL-infected gastric cancer cells

As shown in Table 1, Ad-FasL-infected cultures showed fewer cells in S or G_2M phase, and more cells in G_1 phase, indicating that FasL could inhibit amplification of gastric tumor cells. A sub-G_1 peak (apoptosis peak; Table 1) appeared 4 d after infection of Ad-FasL, indicating that the FasL gene not only induced G_1 phase arrest, but also induced apoptosis of SGC-7901 cells.

Table 1 Influence of FasL expression on cell cycle (FCM analysis) (mean±SD)

Cell lines	G_1/G_0 (%)	S (%)	G_2M (%)
SGC-7901	58.03±2.16	29.72±1.36	9.16±0.92
SGC-7901-vect	61.12±2.24	30.95±1.22	11.02±0.18
SGC-7901-FasL	67.75±0.39[a]	26.56±0.59[c]	5.69±1.12[e]

[a]$P<0.05$, [c]$P<0.05$, [e]$P<0.05$, SGC-7901-FasL *vs* SGC-7901 or SGC-7901-vect.

Cytotoxicity of FasL to SGC-7901 cells

To further evaluate the possibility of gastric cancer gene therapy with Ad-FasL, SGC-7901 cells were infected with Ad-FasL or treated with anti-Fas antibody, and the resulting cytotoxicity was compared with that of ActD, a RNA synthesis inhibitor known as cytotoxin. The cytotoxicity of the anti-Fas antibody (CH-11) to gastric cancer cells was stronger than that of ActD, and the cytotoxicity of Ad-FasL was stronger than that of CH-11 (Table 2).

Table 2 Relative *in vitro* cytotoxicities of various treatments (mean±SD)

Cell line	Treatment group			
	ActD	Ad-LacZ	CH-11	Ad-FasL
SGC-7901	91±8	68±2	60±5[a]	50±2[b]

[a]$P<0.05$ *vs* CH-11 or (compared with CH-11 or anti-Fas antibody+ActD), [b]$P<0.01$ *vs* ActD (compared with ActD).

Inhibition of Ad-FasL on tumor growth in animal model

Nude mice were subcutaneously injected with SGC-7901 cells, then intratumoral injections of Ad-FasL were administered. The growth of tumor infected with Ad-FasL was inhibited by 54%, suggesting that Ad-FasL was a viable gene therapy candidate (Figure 3).

DISCUSSION

Although a growing number of tumor patients have benefited from modern oncotherapeutic methods, there is still a need to improve therapies for malignant tumors. Gene therapy is expected to join surgical, radiological and chemotherapeutic strategies in future methods of integrated oncotherapy. Pre-clinical studies have confirmed that adenovirus-mediated high level expression of carcinoma-inhibiting genes (such as p53) can inhibit tumor growth, induce apoptosis and increase

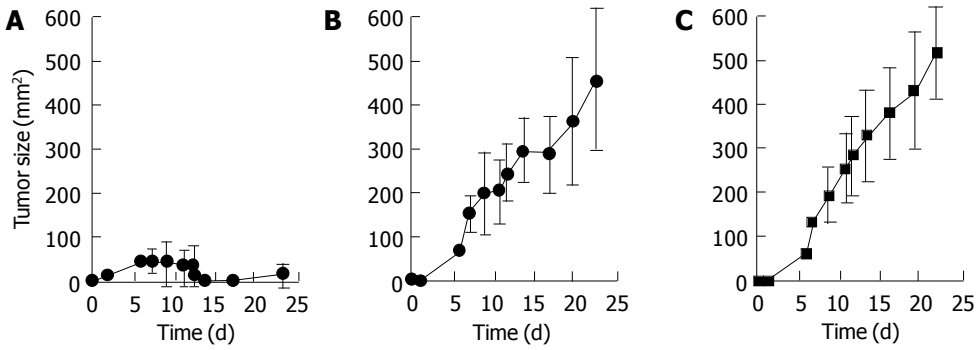

Figure 3 Treatment of SGC-7901 tumor-bearing mice with SGC-7901+FasL cells. **A**: Mice were injected with SGC-7901 cells (5×10^5), followed by treatment with FasL (n = 8); **B**: mice were injected with SGC-7901 cells (5×10^5); **C**: mice were injected with SGC-7901 cells (5×10^5), followed by treatment with PBS (n = 8). Tumor incidence is presented at each time point in Figure. P<0.0001.

tumor tissue sensitivity to radio- and chemotherapy[10-14]. Recent clinical studies in China and abroad have indicated that adenoviral gene therapy is safe and applicable[12-15]. Here, we used this vector to express FasL in cultured human gastric cancer cells. The FasL gene expression cassette includes the CMV promoter, a full-length FasL cDNA, and SV40 polyA signal sequences. A transduction efficiency test using a similarly constructed Ad-LacZ vector illustrated that the adenoviral construct possessed high transduction efficiency. FCM and RT-PCR were used to detect high-level FasL expression in target cells, confirming that the adenovirus vector effectively transfers the FasL gene into tumor cells.

Previous studies[16,17] indicated that binding between FasL and Fas induces receptor trimerization, and apoptosis of Fas-expressing cells. Current theory holds that the signaling responsible for this apoptosis occurs in one of the following three ways: between T cells and target cells, among target cells; or between T cells[18-23]. Fas expression is markedly higher in gastric cancer cells than in normal gastric mucosal cells, implying that Fas participates in the genesis of gastric carcinoma. Fas activation can induce gastric carcinoma cell apoptosis, indicating that the Fas/FasL system might be a good target for gene therapy. In this study, we attempted to induce direct apoptosis of target cells (cis-type apoptosis) by transfecting a highly efficient Ad-FasL expression vector into gastric carcinoma cells (SGC-7901). Expression of FasL inhibited the apoptosis of SGC-7901 cells up to 84%, and significantly inhibited the ability of SGC-7901 cells to form colonies. These results have not been reported in China.

FasL is thought to engage with Fas by inducing receptor trimerization, which then transfers signals to the Fas intracellular death domains (DD). Then, the Fas-associated death domain dimerizes with the DD to transfer an apoptotic signal to Caspase-8, instigating a caspase cascade leading to cell apoptosis[24-26]. In our study, FCM analysis showed that SGC-7901 cells infected with Ad-FasL quickly arrested in the G_1 phase, which was subsequently followed by tumor cell apoptosis. Taken together, these *in vitro* results suggest that FasL gene transfer is capable of inducing gastric tumor cell apoptosis and that it may be a viable candidate for tumor gene therapy.

In our study, an *in vitro* cytotoxicity assay showed that Ad-FasL could significantly inhibit the growth of gastric cancer cells. The inhibition was much stronger than the cytotoxicity conferred by CH-11 treatment, indicating that the Fas/FasL system plays an important role in gastric cancer cell apoptosis[27-29]. In contrast, a SGC-7901 tumor model in nude mice showed only 54% inhibition of tumor growth in response to Ad-FasL infection. This difference between the *in vivo* and *in vitro* response rates might be caused by poor distribution of the recombinant adenovirus in the solid tumor, resulting in lack of target gene transfer to all the tumor cells. Thus, future Fas/FasL gene therapy experiments *in vivo* should focus on stabilizing vectors, increasing transfection efficiency, repeating administration and combining interventional therapy and gene therapy, thereby improving the therapeutic efficacy.

REFERENCES

1 **Sharma K,** Wang RX, Zhang LY, Yin DL, Luo XY, Solomon JC, Jiang RF, Markos K, Davidson W, Scott DW, Shi YF. Death the Fas way: regulation and pathophysiology of CD95 and its ligand. *Pharmacol Ther* 2000; **88**: 333-347
2 **Sapi E,** Brown WD, Aschkenazi S, Lim C Munoz A, Kacinski BM, Rutherford T, Mor G. Regulation of Fas ligand expression by estrogen in normal ovary. *J Soc Gynecol Investig* 2002; **9**: 243-250
3 **Gniadecki R.** Depletion of membrane cholesterol causes ligand-independent activation of Fas and apoptosis. *Biochem Biophys Res Commun* 2004; **320**: 165–169
4 **Walczak H,** Krammer PH. The CD95 (APO-1/Fas) and the TRAIL (APO-2L) apoptosis systems. *Exp Cell Res* 2000; **256**: 58-66
5 **Li-Weber M,** Krammer PH. Function and regulation of the CD95 (APO-1/Fas) ligand in the immune system. *Semin Immunol* 2003; **15**: 145–157
6 **Reichmann E.** The biological role of the Fas/FasL system during tumor formation and progression. *Semin Cancer Biol* 2002; **12**: 309–315
7 **Gu XH,** Li QF, Wang YM. Expression of hepatocyte apoptosis and Fas/FasL, in liver tissues of patients with hepatitis D. *Shijie Huaren Xiaohua Zazhi* 2000; **8**: 35-38
8 **Aoki K,** Akyürek LM, San H, Leung K, Parmacek MS, Nabel EG, Nabel GJ. Restricted expression of an adenoviral vector encoding Fas ligand (CD95L) enhances safety for cancer gene therapy. *Mol Ther* 2000; **1**: 555-565
9 **He TC,** Zhou S, da Costa LT, Yu J, Kinzler KW, Vogelstein B. A simplified system for generating recombinant adenoviruses. *Proc Natl Acad Sci USA* 1998; **95**: 2509-2514
10 **Dunkern T,** Roos W, Kaina B. Apoptosis induced by MNNG in human TK6 lymphoblastoid cells is p53 and Fas/CD95/Apo-1 related. *Mutat Res* 2003; **544**: 167–172

11 **Juang SH,** Pan WY, Kuo CC, Liou JP, Hung YM, Chen LT, Hsieh HP, Chang JY. A novel bis-benzylidenecyclopentanone derivative, BPR0Y007, inducing a rapid caspase activation involving upregulation of Fas (CD95/APO-1) and wild-type p53 in human oral epidermoid carcinoma cells. *Biochem Pharmacol* 2004; **68**: 293–303

12 **Rubinchik S,** Wang D, Yu H, Fan F, Luo M, Norris JS, Dong JY. A complex adenovirus vector that delivers FASL-GFP with combined prostate-specific and tetracycline-regulated expression. *Mol Ther* 2001; **4**: 416-426

13 **Xu GW,** Sun ZT, Forrester K, Wang XW, Coursen J, Harris CC. Tissue-specific growth suppression and chemosensitivity promotion in human hepatocellular carcinoma cells by retroviral-mediated transfer of the wild-type p53 gene. *Hepatology* 1996; **24**: 1264–1268

14 **Habib NA,** Hodgson HJ, Lemoine N, Pignatelli M. A phase I/II study of hepatic artery infusion with wtp53-CMV-Ad in metastatic malignant liver tumours. *Hum Gene Ther* 1999; **10**: 2019–2034

15 **Schuler M,** Rochlitz C, Horowitz JA, Schlegel J, Perruchoud AP, Kommoss F, Bolliger CT, Kauczor HU, Dalquen P, Fritz MA, Swanson S, Herrmann R, Huber C. A phase I study of adenovirus-mediated wild-type p53 gene transfer in patients with advanced non-small cell lung cancer. *Hum Gene Ther* 1998; **9**: 2075–2082

16 **Miura Y,** Thoburn CJ, Bright EC, Hess AD. Cytolytic effector mechanisms and gene expression in autologous graft-versus-host disease: distinct roles of perforin and Fas ligand. *Biol Blood Marrow Transplant* 2004; **10**: 156-170

17 **Webb SD,** Sherratt JA, Fish RG. Cells behaving badly: a theoretical model for the Fas/FasL system in tumour immunology. *Math Biosci* 2002; **179**: 113–129

18 **Wang LS,** Liu HJ, Zhang JH, Wu CT. Purging effect of dibutyl phthalate on leukemia cells involves fas independent activation of caspase-3/CPP32 protease. *Cancer Lett* 2002; **186**: 177–182

19 **Chun YJ,** Park S, Yang SA. Activation of Fas receptor modulates cytochrome P450 3A4 expression in human colon carcinoma cells. *Toxicol Lett* 2003; **146**: 75–81

20 **Modiano JF,** Sun J, Lang J, Vacano G, Patterson D, Chan D, Franzusoff A, Gianani R, Meech SJ, Duke R, Bellgrau D. Fas ligand-dependent suppression of autoimmunity via recruitment and subsequent termination of activated T cells. *Clin Immunol* 2004; **112**: 54–65

21 **Granville DJ,** Jiang H, McManus BM, Hunt DW. Fas ligand and TRAIL augment the effect of photodynamic therapy on the induction of apoptosis in JURKAT cells. *Int Immunopharmacol* 2001; **1**: 1831–1840

22 **Webb SD,** Sherratt JA. A perturbation problem arising from the modelling of soluble Fas ligand in tumour immunology. *Mathem Comp Modell* 2003; **37**: 323-331

23 **Kase H,** Aoki Y, Tanaka K. Fas ligand expression in cervical adenocarcinoma: relevance to lymph node metastasis and tumor progression. *Gynecol Oncol* 2003; **90**: 70–74

24 **Wiener Z,** Ontsouka EC, Jakob S, Torgler R, Falus A, Mueller C, Brunner T. Synergistic induction of the Fas (CD95) ligand promoter by Max and NFkappaB in human non-small lung cancer cells. *Exp Cell Res* 2004; **299**: 227–235

25 **Chatterjee D,** Schmitz I, Krueger A, Yeung K, Kirchhoff S, Krammer PH, Peter ME, Wyche JH, Pantazis P. Induction of apoptosis in 9-nitrocamptothecin-treated DU145 human prostate carcinoma cells correlates with de novo synthesis of CD95 and CD95 ligand and down-regulation of c-FLIP(short). *Cancer Res* 2001; **61**: 7148-7154

26 **Liu HF,** Liu WW, Fang DC. Effect of combined anti Fas mAb and IFN-γ on the induction of apoptosis in human gastric carcinoma cell line SGC-7901. *Shijie Huaren Xiaohua Zazhi* 2000; **8**: 1361-1364

27 **Kim KB,** Choi YH, Kim IK, Chung CW, Kim BJ, Park YM, Jung YK. Potentiation of Fas- and TRAIL-mediated apoptosis by IFN-gamma in A549 lung epithelial cells: enhancement of caspase-8 expression through IFN-response element. *Cytokine* 2002; **20**: 283–288

28 **Gonzalez-Cuadrado S,** Lopez-Armada MJ, Gomez-Guerrero C, Subira D, Garcia-Sahuquillo A, Ortiz-Gonzalez A, Neilson EG, Egido J, Ortiz A. Anti-Fas antibodies induce cytolysis and apoptosis in cultured human mesangial cells. *Kidney Int* 1996; **49**: 1064-1070

29 **Schmitz I,** Krueger A, Baumann S, Kirchhoff S, Krammer PH. Specificity of anti-human CD95 (APO-1/Fas) antibodies. *Biochem Biophys Res Commun* 2002; **297**: 459–462

Science Editor Wang XL and Guo SY **Language Editor** Elsevier HK

PO Box 2345, Beijing 100023, China
www.wjgnet.com
wjg@wjgnet.com

ELSEVIER

World J Gastroenterol 2005;11(22):3451-3456
World Journal of Gastroenterology ISSN 1007-9327

• *BRIEF REPORTS* •

Cell cycle arrest and apoptotic cell death in cultured human gastric carcinoma cells mediated by arsenic trioxide

Qin-Shu Shao, Zai-Yuan Ye, Zhi-Qiang Ling, Jin-Jing Ke

Qin-Shu Shao, Zai-Yuan Ye, Jin-Jing Ke, Zhejiang Provincial People's Hospital, Hangzhou 310014, Zhejiang Province, China
Zhi-Qiang Ling, Zhejiang Academy of Medical Sciences, Hangzhou 310013, Zhejiang Province, China
Supported by the Zhejiang Province Science and Technology Fund for excellent returnee; 2001-275
Correspondence to: Dr. Zhi-Qiang Ling, Zhejiang Academy of Medical Sciences, Hangzhou 310013, Zhejiang Province, China. lingzq@hotmail.com
Telephone: +86-571-88862228 Fax: +86-571-88075447
Received: 2004-07-28 Accepted: 2004-09-24

Abstract

AIM: To investigate the effect of arsenic trioxide on human gastric cancer cell line MKN45 with respect to both cytotoxicity and induction of apoptosis *in vitro*.

METHODS: MKN45 cells were treated with arsenic trioxide (As_2O_3) at the concentration of 1, 5, and 10 μmol/L, respectively, for three successive days. Cell growth and proliferation were observed by cell counting and trypan blue exclusion. Cytotoxicity of As_2O_3 was determined by MTT assay. Morphologic changes were studied with light microscopy. Flow cytometry was used to assay cell DNA distribution and apoptotic cells were confirmed with terminal deoxynucleotidyl transferase-mediated dUTP nick-end labeling (TUNEL) and DNA electrophoresis.

RESULTS: The growth of MKN45 cells was significantly inhibited by As_2O_3 which was confirmed by colony-forming assay. After 7 d of culture with various concentrations of As_2O_3, colony-forming capacity of MKN45 cells decreased with As_2O_3 increment in comparison with that of control group. The inhibitory rate of colony-formation was 38.5%, 99.1%, and 99.5% when the concentration of As_2O_3 was 1, 5, and 10 μmol/L in culture medium, respectively. The cell number of a single colony in drug treatment groups was less than that of control group. The cell-killing rate of As_2O_3 to MKN45 cells was both dose- and time-dependent with an IC^{50} of (11.05±0.25) μmol/L. After incubation in 10 μmol/L As_2O_3 for 24 h, the cell-killing rate was 27.1%, and it was close to 50% after 48 h. The results showed that As_2O_3 induced time- and dose-dependent apoptosis in MKN45 cells, blocked at G_2/M phase. The apoptotic peak (sub-G_1 phase) appeared and cell apoptotic rate in MKN45 cells was 18.3-32.5% after treatment by 10 μmol/L As_2O_3 for 48 h. The percentage of G_2/M cell of the experimental groups was 2.0-5.0 times than that of the control group. Gel electrophoresis of DNA from cells treated with each concentration of As_2O_3 for 48 h revealed a "ladder" pattern, indicating preferential DNA degradation at the internucleosomal, linker DNA sections. TUNEL also demonstrated strand breaks in DNA of MKN45 cells treated with As_2O_3, while control cells showed negative labeling.

CONCLUSION: As_2O_3 can induce apoptosis of human gastric carcinoma cells MKN45, which is the basis of its effectiveness. It shows great potential in the treatment of gastric carcinoma.

Key words: Arsenic trioxide; Gastric carcinoma; Cell cycle; Apoptosis

Shao QS, Ye ZY, Ling ZQ, Ke JJ. Cell cycle arrest and apoptotic cell death in cultured human gastric carcinoma cells mediated by arsenic trioxide. *World J Gastroenterol* 2005; 11(22): 3451-3456
http://www.wjgnet.com/1007-9327/11/3451.asp

INTRODUCTION

Arsenic trioxide (As_2O_3) is a major ingredient of traditional Chinese medicine (TCM). It is derived from Pi'shi by sublimation. In the practice of TCM, it is used externally to cure hemorrhoids, acute ulcerative gingivitis, and asthma, *etc.* Its anti-tumor activity was discovered by a group of Chinese doctors in 1970s[1-6]. Since then, the effect of As_2O_3 in treating cancers has been extensively studied. The first use of As_2O_3 in cancer therapy was to treat acute promyelocytic leukemia (APL). Both the results of *in vitro* and clinical trials showed that As_2O_3 was effective in inhibiting the growth of APL. Because of the significant anti-cancer effect of As_2O_3, studies were carried out on its potential use in cancer treatment of non-APL such as myeloid leukemia, hepatocellular carcinoma, neuroblastoma, esophageal carcinoma as well as head and neck cancers. Reports showed that As_2O_3 was also effective in inhibiting the growth of these cancers[7-11,13].

Gastric cancer is one of the most common malignant tumors in China. Evidences have demonstrated that gastric cancer is a disease caused not only by excessive cellular proliferation and poor differentiation, but also by decrease in apoptosis of gastric cells[12,14-19]. Though the disease in its early stage can be treated by surgical resection, in advanced stage its response to conventional chemotherapy or radiotherapy is usually not satisfactory. Moreover, surgical resection and radiotherapy are carried out provided that

the cancer is restricted to a particular region. However, cancer may metastasize to other regions at the later stage of cancer development. For chemotherapy, side effects like toxic hepatitis and heart damage may result. Moreover, prolonged treatment with anticancer drugs may give rise to multidrug-resistant cancer cells, which in turn, poses great obstacle in cancer therapy. Therefore, discovery of new drugs for the treatment of gastric cancer is urgent. Apoptosis is an important mode of cell death that occurs in response to a variety of agents including ionizing radiation or anticancer chemotherapeutic drugs[20-24].

In the present study, the effects of As_2O_3 on human gastric cancer cell line, MKN45, was investigated by *in vitro* study.

MATERIALS AND METHODS

Cell culture and drug treatment

Poorly differentiated human gastric adenocarcinoma cell line, MKN45, was grown in RPMI 1640 (Gibco BRL, Life Technologies, Inc., Rockville, MD, USA) supplemented with 2 mol/L L-glutamine, 10% heat-inactivated fetal bovine serum (FBS, Gibco BRL, Life Technologies, Inc.) and 5% mixture of 100 U/mL penicillin, 100 μg/mL streptomycin, 0.25 μg/mL amphotericin B (Antibiotic-Antimycotic, Gibco BRL, Life Technologies, Inc.). After being subcultured for 24 h, exponentially growing cell suspensions were distributed into 25-cm^2 cell culture flasks at a density of 5×10 000 cells/mL (5 mL medium). Cells were passaged twice weekly, routinely examined for mycoplasma contamination, maintained in 37 ℃ incubator in a humidified atmosphere consisting of 50 mL/L CO_2 in air.

As_2O_3 (Sigma Chemical, St. Louis, MO, USA) was dissolved in PBS at 1 mol/L as a stock solution, stored at 4 ℃. For *in vitro* use, the stock solution was diluted to the appropriate concentration in growth medium without FBS. Exponentially growing cells were treated with As_2O_3 at a final concentration of 1, 5,10 μmol/L respectively. Control cultures were treated with distilled PBS at a final concentration of 0.1% in culture medium. All experiments were performed in triplicate.

Cell growth and proliferation assay

The proliferation of MKN45 cells during the period of experiments was monitored by counting cell number, IC_{50} and mitotic indices. Cell suspension was mixed with equal volume of 0.08% trypan blue solution (Sigma Chemical Co., Ltd, St. Louis, MO, USA). The mixture was then transferred to the hemacytometer. Only viable cells (unstained cells) were counted.

Inhibition rate of cell growth (%) = [viable control cells-viable treated cells]/viable control cells×100%.

To avoid possible influence of cell density on cell growth and survival, cells were maintained at less than 1×10^5/mL with daily adjustment by addition of fresh culture medium containing the corresponding concentration of As_2O_3.

Colony-forming assays

To assess effects of As_2O_3 on MKN45 cell lines, exponentially growing cells at a density of 5×10 000 cells/mL (5 mL medium) were mixed with RPMI 1640 supplemented with 2 mol/L L-glutamine, 20% heat-inactivated fetal bovine serum and 5% mixture of 100 U/mL penicillin, 100 μg/mL streptomycin, 0.25 μg/mL amphotericin B. One microliter of liquid culture was plated in a 35-mm plastic culture plate in the presence of various concentrations of As_2O_3, and maintained in 37 ℃ incubator in a humidified atmosphere containing 50 mL/L CO_2 in air. After 7 d, more than 40 colony formation in methylcellulose was assessed by inverted phase-contrast microscopy. All experiments were performed in triplicate.

MTT cytotoxicity assay

In vitro growth inhibition effect of As_2O_3 on MKN45 cells was determined by measuring MTT (3-[4,5-dimethylthiazol-2-yl]-2,5-diphenyltetrazolium bromide) dye absorbance of living cells. Briefly, cells (1×10^5 cells per well) were seeded in 96-well microtiter plates (Nunc, Roskilde, Denmark). After exposure to various As_2O_3 for 48 and 72 h respectively, 100 μL (1 g/L) MTT (Sigma) solution was added to each well and the plates were incubated for an additional 4 h at 37 ℃. MTT solution in medium was aspirated. To achieve solubilization of the formazan crystal formed in viable cells, 100 μL DMSO was added to each well before absorbance at 570 nm was measured. Each concentration treatment was done in triplicate wells. The cytotoxicity rates were measured by the formula:

the cytotoxicity rate=[1-A_{570} test/A_{570} control]×100%.

Morphologic assessment of apoptosis by light microscopy and DAPI staining

Following exposure to As_2O_3, cells were obtained, washed with PBS, cytospun onto slides, and stained with Wright-Giemsa for morphologic assessment of apoptosis by light microscopy. Evidence of apoptosis was indicated by the presence of cell shrinkage, membrane blebbing, fragmentation of nuclei, and formation of apoptotic bodies. Apoptosis was also detected by DAPI (Sigma) as previously described, and the percentages of cells in interphase, mitosis, and apoptosis were quantified.

Cell cycle analysis

Cell cycle and apoptotic cells were detected by flow cytometry which was performed as described previously. After drug treatment, about 1×10^6 cells at each time point were collected by trypsin digestion and centrifugation, then fixed in 70% ethanol/PBS for at least 12 h at 4 ℃. After 100 μL (1 g/L) RNase treatment, cells were stained with 50 mg/L propidium iodide. Cells were examined by flow cytometry using an FACScan (FACS-420, USA). Also, in cell cycle analysis, cells were considered to be in apoptosis if they exhibited sub-G_1 DNA fluorescence and a forward angle light scatter, the same as or slightly lower than that of cells in G_1. The results were analyzed with Lysis II software (FACS-420, USA).

DNA gel electrophoresis

A total of 10^6 cells with or without As_2O_3 treatment were gently scraped from the dishes and washed twice in cold PBS. The pellets were collected by centrifugation and

resuspended in 1 mL of buffer containing 150 mol/L NaCl, 10 mol/L Tris-HCl pH 8.0, 20 mol/L EDTA pH 8.0, and 0.5% SDS. After thorough mixing, 20 μL of proteinase K (10 mg/mL) was added and incubated at 50 ℃ for 2 h and cooled to 0 ℃, 2 mL of ethanol (at -20 ℃) was added to precipitate DNA, which was collected by centrifugation (1 200 r/min, 20 min), dried in air and dissolved in 50 μL of 10 mol/L Tris, 1 mol/L EDTA at pH 8.0 (TE buffer). Each DNA preparation was mixed with 2 mL RNase (10 mg/mL) and 6 μL of loading buffer (30% glycerol, 0.1% bromophenol blue) and electrophoresed for approximately 3.5 h (2 V/cm gradient). A marker was obtained from Boehringer Mannhiem, Penzberg, Germany. The gels were stained with ethidium bromide, and the DNA bands were visualized under ultraviolet light and photographed.

Terminal deoxynucleotidyl transferase-mediated dUTP nick-end labeling (TUNEL) assay

TUNEL assay was used to monitor the extent of DNA fragmentation due to apoptosis. The assay was performed according to the recommendations of the manufacturer (Boehringer, Mannheim, Germany). In brief, following exposure to As_2O_3, cells were obtained, washed with PBS, cytospun onto slides, and dried in air. The cells were fixed with a freshly prepared paraformaldehyde solution (4% in PBS, pH 7.4) for 30 min at room temperature. The slides were rinsed with PBS and incubated in permeabilization solution (0.1% Triton® X-100, 0.1%[s1] sodium citrate) for 2 min on ice. They were then rinsed twice with PBS and the area around the samples was dried. Fifty microliters of TUNEL reaction mixture were placed on the sample, and the slides incubated in a humidified chamber for 60 min at 37 ℃ in the dark. After rinsing of the slides thrice with PBS, samples were analyzed under a fluorescence microscope (Zeiss, Jena, Germany). The percentage of fluorescence-positive apoptotic cells was calculated out of more than 500 cells on each slide.

Statistical analysis

Most experiments were performed in triplicate, and the results from separate experiments are expressed as mean±standard deviation (mean±SD). The $P<0.05$ was taken as a significant difference between groups as determined by χ^2-test.

RESULTS

Inhibitory effect of As2O3 on growth of MKN45 cell line

After exposure of exponentially growing MKN45 cells to As_2O_3 for 72 h, the inhibitory effect of As_2O_3 on cell growth was significant as revealed by cell counting, and was both dose- and time-dependent (Table 1). There were significant differences between each concentration and control group ($P<0.01$) respectively. The IC_{50} of As_2O_3 on MKN45 was 11.05±0.25 μmol/L.

Table 1 The effects of As_2O_3 on the growth of MKN45 cells at different times and concentrations

Groups		Cell number (1×10^5/mL)		
		24 h	48 h	72 h
PBS control		7.15±1.08	9.18±0.99	13.34±0.54
As_2O_3 (μmol/L)	1	2.47±0.99	3.34±1.02	2.73±1.38
	5	2.51±0.63	2.84±1.12	1.75±1.12
	10.0	2.09±0.67	1.34±0.51	0.25±0.24

Effect of As_2O_3 on colony formation of MKN45 cells

The growth of MKN45 cells was significantly inhibited by As_2O_3 which was confirmed by colony-forming assay. After 7 d of culture with various concentrations of As_2O_3, colony-forming capacity of MKN45 cells decreased with As_2O_3 increment in comparison with that of control group. The inhibitory rate of colony forming was 38.5%, 99.1%, and 99.5% when the concentration of As_2O_3 was 1, 5, and 10 μmol/L in culture medium, respectively. The cell number of a single colony in drug treatment groups was less than that of control group.

Effect of As_2O_3 on MKN45 cells

The cell-killing rate of As_2O_3 on MKN45 cells was significant as revealed by MTT, and was both dose- and time-dependent. After incubation in 1 μmol/L As_2O_3 for 24 h, the cell-killing rate was 11.5%, and after treatment with 10 μmol/L As_2O_3 for 48 h, the cell-killing rate was close to 50% (Table 2). These results indicated that the cytotoxic effect of As_2O_3 was strong.

Morphologic changes of MKN45 cells

By inverted phase-contrast microscopy, we found that the attaching ability of MKN45 cells to the flask treated with 1, 5, and 10 μmol/L As_2O_3 was weaker as compared with that of controls, and cell growth markedly inhibited.

MKN45 cells treated with As_2O_3 underwent significant changes as seen under microscope, the nucleocytoplasmic ratio enlarged, with indentation of nuclei. The nucleocytoplasmic ratio in MKN45 cells treated with 1 μmol/L As_2O_3 was much smaller than that in controls, and the nuclei appeared round, with loss of nuclear indentation, but with well-differentiated organelles in the cytoplasm. When treated with As_2O_3 at 5 and 10 μmol/L for three successive days, one could find intact cell membrane, nuclear condensation and apoptotic body formation, but much less than in 1 μmol/L As_2O_3 group.

Effect of As_2O_3 on cell cycle of MKN45 cells

The effect of As_2O_3 on MKN45 cells showed remarkable cell cycle specificity. There was no significant change in cell cycle after 1-10 μmol/L treatment for 24 h, being similar to control group. The fraction of G_0/G_1 was decreased from 55.6%, 57.1%, 55.2% to 37.2%, 19.9%, 13.1% after 1, 5, 10 μmol/L treatment for 48 h, respectively, while the

Table 2 Cytotoxic effect of As_2O_3 on MKN45 cells (%)

		Treatment time (t/h)		
		24 h	48 h	72 h
As_2O_3(μmol/L)	1	11.5±5.2	18.9±5.6	34.8±6.8
	5	19.1±3.8	34.3±3.7	46.9±7.6
	10.0	23.9±7.3	48.8±8.2	69.5±10.6

fraction of G_2/M phase was increased from 16.3%, 16.7%, 17.5% to 22.6%, 41.5%, 69.0%, respectively.

The results showed that As_2O_3 induced time- and dose-dependent apoptosis in MKN45 cells, blocked at G_2/M phase. The apoptotic peak (sub-G_1 phase) appeared and cell apoptotic rate was 18.3-32.5% after being treated by 10 μmol/L As_2O_3 for 48 h (Tables 3 and 4). The percentage of G_2/M cells of the experimental groups was 2.0-5.0 times that of the control group. It demonstrated that As_2O_3 arrested cell cycle at G_2/M phase, inhibited cell proliferation and induced apoptosis at G_1 phase.

Table 3 Effect of As_2O_3 on apoptosis of MKN45 cells

Groups		Apoptosis (%)		
		24 h	48 h	72 h
Control		0.5±0.1	0.4±0.3	0.5±0.2
As_2O_3 (μmol/L)	1	2.7±2.1[a]	7.2±2.5[a]	12.3±3.6[a]
	5	7.3±5.7[a]	17.3±5.7[a]	21.1±5.6[a]
	10.0	11.6±3.4[a]	25.4±7.1[a]	35.8±8.1[a]

[a]P<0.05 *vs* control.

Gel electrophoresis

Gel electrophoresis of DNA from cells treated with each concentration of As_2O_3 for 48 h revealed a "ladder" pattern, indicating preferential DNA degradation at the internucleosomal, linker DNA sections.

TUNEL assay

TUNEL assay also demonstrated strand breaks in DNA of MKN45 cells treated with As_2O_3, while control cells showed negative labeling.

DISCUSSION

The medicinal effect of As_2O_3 is of great significance, though it is also well known for its toxicity. As_2O_3 has been used as medicine for thousands of years in both the Chinese and Western societies. However, its use in cancer treatment was not discovered until 1970s[1-5,8]. Since then, As_2O_3 has been found to be an effective anticancer drug in APL as well as non-APL leukemia[9-11,16-18]. Recently, studies were carried out to expand the use of As_2O_3 in the treatment of solid tumors. The present study explored its effect on human gastric cancer cell line.

As_2O_3 has been used in clinical trials of APL for years and 10 mg/d of As_2O_3 was shown to be effective in inducing complete remission of both the newly diagnosed and relapsed APL patients. The action mechanism of As_2O_3 is complicated. In APL, it has been reported that As_2O_3 exerted its effect by degradation of the fusion protein, PML/RARα, in turn, inducing differentiation and triggering apoptosis. This was supported by clinical trials. However, some studies showed that As_2O_3 mediated its effect in a PML/RARα independent manner. This suggested that the effect of PML/RARα is not restricted to cancers which express PML/RARα[24-27,33]. In fact, apoptosis is one of the key pathways of As_2O_3, regardless of cell types. Studies showed that caspase-3 is activated upon As_2O_3 treatment. Caspases can be considered as the central trigger of apoptosis because they bring about most of the visible changes that characterize apoptotic cell death. Among various caspases, caspase-3 is one of the most crucial caspases[28-32,34].

Mitochondria play an important role in apoptosis. As_2O_3 causes the collapse of mitochondrial membrane potential, indicating that mitochondria participate in As_2O_3-induced apoptosis. Disruption of the mitochondrial membrane potential and release of cytochrome *c* to the cytosol can be considered as the major event through which mitochondria participate in the induction of apoptosis. The change in the mitochondrial membrane potential upon As_2O_3 treatment was examined by flow cytometry, while the release of cytochrome *c* to the cytosol was detected by Western analysis. As_2O_3 recruits a number of pathways but the whole picture of its action mechanism is not fully understood[35-39].

The present study showed that As_2O_3 exhibited strong anticancer activity on MKN45 cells via inhibition of proliferation and induction of apoptosis, which was both dose- and time-dependent in a certain range of dose with an IC^{50} of (11.05±0.25) μmol/L. The apoptosis rate was increased 3.5 times when the concentration of As_2O_3 increased from 1 to 10 μmol/L. Gel electrophoresis of DNA and TUNEL demonstrated existence of apoptotic cells. Flow cytometry analysis showed that the apoptotic peak (sub-G_1 phase) changed considerably with the increase of concentration of As_2O_3 and, cell were blocked at G_2/M phase. The effect of As_2O_3 on cell cycle was obvious, while no distinct changes occurred in cell cycle treatment by different concentrations of As_2O_3 for 24 h being similar to control group. However, the cell cycle changed markedly after drug treatment for 48 h, G_0/G_1 phase decreased from 55.6%, 57.1%, 55.2% to 37.2%, 19.9%, 13.1% and the G_2/M phase increased from 16.3%, 16.7%, 17.5% to 22.6%, 41.5%, 69.0% in 1, 5, 10 μmol/L As_2O_3 treatment groups, respectively. The arrest of G_2/M phase become more

Table 4 Effect of As_2O_3 on cell cycle of MKN45 cells

Group		Cell cycle (%)								
		24 h			48 h			72 h		
		G_1/G_0	S	G_2/M	G_1/G_0	S	G_2/M	G_1/G_0	S	G_2/M
Control		54.5	25.8	19.7	56.7	30.1	13.2	55.5	28.1	16.4
As_2O_3 (μmol/L)	1	55.6	28.1	16.3	37.2	40.2	22.6[a]	35.1	36.8	28.1[a]
	5	57.1	26.2	16.7	19.9	38.6	41.5[a]	18.4	35.2	46.4[a]
	10.0	55.2	27.3	17.5	13.1	17.9	69.0[a]	10.9	15.2	73.9[a]

[a]P<0.05 *vs* control.

apparent after treatment with As_2O_3 for 72 h, its proportion increased with the increase of concentration of As_2O_3 in a dose- and time-dependent manner. The proportion of cells in G_2/M phase was 2.0-5.0 times that of untreated cells after treatment with As_2O_3 for 48 h, demonstrating that the anticancer effect of As_2O_3 on MKN45 cells was attributed to the inhibition of cell proliferation, arrest of cell cycle and induction of apoptosis.

In conclusion, our study demonstrates the proliferation inhibition and apoptosis induction effects of As_2O_3 at the concentrations of 1, 5, and 10 μmol/L on human gastric cancer cell line MKN45. These results shed light on the use of As_2O_3 in treating human gastric cancer. To fully utilize As_2O_3 in cancer treatment, however, much more efforts should be made on the study of its action mechanism, pharmacokinetic characteristics, dosing schedules as well as potential adverse effects.

REFERENCES

1 **Evens AM,** Tallman MS, Gartenhaus RB. The potential of arsenic trioxide in the treatment of malignant disease: past, present, and future. *Leuk Res* 2004; **28**: 891-900
2 **Candoni A,** Silvestri F, Buonamici S, Li D, Reddy P, Galili N, Nucifora G, Raza A. Targeted therapies in myelodysplastic syndromes: ASH 2003 review. *Semin Hematol* 2004; **41**: 13-20
3 **Sun Y,** Kim SH, Zhou DC, Ding W, Paietta E, Guidez F, Zelent A, Ramesh KH, Cannizzaro L, Warrell RP, Gallagher RE. Acute promyelocytic leukemia cell line AP-1060 established as a cytokine-dependent culture from a patient clinically resistant to all-trans retinoic acid and arsenic trioxide. *Leukemia* 2004; **18**: 1258-1269
4 **Hayakawa F,** Privalsky ML. Phosphorylation of PML by mitogen-activated protein kinases plays a key role in arsenic trioxide-mediated apoptosis. *Cancer Cell* 2004; **5**: 389-401
5 **Gao F,** Yi J, Yuan JQ, Shi GY, Tang XM. The cell cycle related apoptotic susceptibility to arsenic trioxide is associated with the level of reactive oxygen species. *Cell Res* 2004; **14**: 81-85
6 **Rousselot P,** Larghero J, Labaume S, Poupon J, Chopin M, Dosquet C, Marolleau JP, Janin A, Brouet JC, Fermand JP. Arsenic trioxide is effective in the treatment of multiple myeloma in SCID mice. *Eur J Haematol* 2004; **72**: 166-171
7 **Park WH,** Seol JG, Kim ES, Hyun JM, Jung CW, Lee CC, Kim BK, Lee YY. Arsenic trioxide-mediated growth inhibition in MC/CAR myeloma cells via cell cycle arrest in association with induction of cyclin-dependent kinase inhibitor, p21, and apoptosis. *Cancer Res* 2000; **60**: 3065–3071
8 **Miller WH,** Schipper HM, Lee JS, Singer J, Waxman S. Mechanisms of action of arsenic trioxide. *Cancer Res* 2002; **62**: 3893–3903
9 **Kogan SC,** Brown DE, Shultz DB, Truong BT, Lallemand-Breitenbach V, Guillemin MC, Lagasse E, Weissman IL, Bishop JM. BCL-2 cooperates with promyelocytic leukemia retinoic acid receptor alpha chimeric protein (PMLRARalpha) to block neutrophil differentiation and initiate acute leukemia. *J Exp Med* 2001; **193**: 531-543
10 **Iwama K,** Nakajo S, Aiuchi T, Nakaya K. Apoptosis induced by arsenic trioxide in leukemia U937 cells is dependent on activation of p38, inactivation of ERK and the Ca^{2+}-dependent production of superoxide. *Int J Cancer* 2001; **92**: 518–526
11 **Maeda H,** Hori S, Nishitoh H, Ichijo H, Ogawa O, Kakehi Y, Kakizuka A. Tumor growth inhibition by arsenic trioxide (As2O3) in the orthotopic metastasis model of androgen-independent prostate cancer. *Cancer Res* 2001; **61**: 5432–5440
12 **Hyun Park W,** Hee Cho Y, Won Jung C, Oh Park J, Kim K, Hyuck Im Y, Lee MH, Ki Kang W, Park K. Arsenic trioxide inhibits the growth of A498 renal cell carcinoma cells via cell cycle arrest or apoptosis. *Biochem Biophys Res Commun* 2003; **300**: 230-235
13 **Seol JG,** Park WH, Kim ES, Jung CW, Hyun JM, Lee YY, Kim BK. Potential role of caspase-3 and -9 in arsenic trioxide-mediated apoptosis in PCI-1 head and neck cancer cells. *Int J Oncol* 2001; **18**: 249–255
14 **Davison K,** Mann KK, Waxman S, Miller WH. JNK activation is a mediator of arsenic trioxide-induced apoptosis in acute promyelocytic leukemia cells. *Blood* 2004; **103**: 3496-3502
15 **Liang XQ,** Cao EH, Zhang Y, Qin JF. P53-induced gene 11 (PIG11) involved in arsenic trioxide-induced apoptosis in human gastric cancer MGC-803 cells. *Oncol Rep* 2003; **10**: 1265-1269
16 **Kang YJ.** New understanding in cardiotoxicity. *Curr Opin Drug Discov Devel* 2003; **6**: 110-116
17 **Zhou Y,** Hileman EO, Plunkett W, Keating MJ, Huang P. Free radical stress in chronic lymphocytic leukemia cells and its role in cellular sensitivity to ROS-generating anticancer agents. *Blood* 2003; **101**: 4098-4104
18 **Feng CQ,** Ma WL, Zheng WL. Research advances on effect of arsenic trioxide on tumor. *Aizheng* 2002; **21**: 1386-1389
19 **Huang SG,** Kong BH, Ma YY, Jiang S. Impact of arsenic trioxide on proliferation and metastasis of drug-resistant human ovarian carcinoma cell line. *Aizheng* 2002; **21**: 863 –867
20 **Miller WH Jr,** Schipper HM, Lee JS, Singer J, Waxman S. Mechanisms of action of arsenic trioxide. *Cancer Res* 2002; **62**: 3893-3903
21 **Tsimberidou AM,** Estey E, Whitman GJ, Dryden MJ, Ratnam S, Pierce S, Faderl S, Giles F, Kantarjian HM, Garcia-Manero G. Extramedullary relapse in a patient with acute promyelocytic leukemia: successful treatment with arsenic trioxide, all-trans retinoic acid and gemtuzumab ozogamicin therapies. *Leuk Res* 2004; **28**: 991-994
22 **Shen ZX,** Shi ZZ, Fang J, Gu BW, Li JM, Zhu YM, Shi JY, Zheng PZ, Yan H, Liu YF, Chen Y, Shen Y, Wu W, Tang W, Waxman S, De The H, Wang ZY, Chen SJ, Chen Z. All-trans retinoic acid/As2O3 combination yields a high quality remission and survival in newly diagnosed acute promyelocytic leukemia. *Proc Natl Acad Sci USA* 2004; **101**: 5328-5335
23 **Lu D,** Bai XC, Gui L, Su YC, Deng F, Liu B, Li XM, Zeng WS, Cheng BL, Luo SQ. Hydrogen peroxide in the Burkitt's lymphoma cell line Raji provides protection against arsenic trioxide-induced apoptosis via the phosphoinositide-3 kinase signalling pathway. *Br J Haematol* 2004; **125**: 512-520
24 **Karlsson J,** ORa I, Porn-Ares I, Pahlman S. Arsenic trioxide-induced death of neuroblastoma cells involves activation of Bax and does not require p53. *Clin Cancer Res* 2004; **10**: 3179-3188
25 **Chelbi-alix MK,** Bobe P, Benoit G, Canova A, Pine R. Arsenic enhances the activation of Stat1 by interferon gamma leading to synergistic expression of IRF-1. *Oncogene* 2003; **22**: 9121-9130
26 **Li X,** Ding X, Adrian TE. Arsenic trioxide induces apoptosis in pancreatic cancer cells via changes in cell cycle, caspase activation, and GADD expression. *Pancreas* 2003; **27**: 174-179
27 **Kang SH,** Song JH, Kang HK, Kang JH, Kim SJ, Kang HW, Lee YK, Park DB. Arsenic trioxide-induced apoptosis is independent of stress-responsive signaling pathways but sensitive to inhibition of inducible nitric oxide synthase in HepG2 cells. *Exp Mol Med* 2003; **35**: 83-90
28 **Hu XM,** Hirano T, Oka K. Arsenic trioxide induces apoptosis in cells of MOLT-4 and its daunorubicin-resistant cell line via depletion of intracellular glutathione, disruption of mitochondrial membrane potential and activation of caspase-3. *Cancer Chemother Pharmacol* 2003; **52**: 47-58
29 **Jia P,** Chen G, Huang X, Cai X, Yang J, Wang L, Zhou Y, Shen Y, Zhou L, Yu Y, Chen S, Zhang X, Wang Z. Arsenic trioxide induces multiple myeloma cell apoptosis via disruption of mitochondrial transmembrane potentials and activation of caspase-3. *Chin Med J (Engl)* 2001; **114**: 19-24
30 **Akay C,** Thomas C, Gazitt Y. Arsenic trioxide and paclitaxel induce apoptosis by different mechanisms. *Cell Cycle* 2004; **3**: 324-334
31 **Zheng Y,** Shi Y, Tian C, Jiang C, Jin H, Chen J, Almasan A,

Tang H, Chen Q. Essential role of the voltage-dependent anion channel (VDAC) in mitochondrial permeability transition pore opening and cytochrome c release induced by arsenic trioxide. *Oncogene* 2004; **23**: 1239-1247

32 **McCafferty-Grad J,** Bahlis NJ, Krett N, Aguilar TM, Reis I, Lee KP, Boise LH. Arsenic trioxide uses caspase-dependent and caspase-independent death pathways in myeloma cells. *Mol Cancer Ther* 2003; **2**: 1155-1164

33 **Akay C,** Gazitt Y. Arsenic trioxide selectively induces early and extensive apoptosis via the APO2/caspase-8 pathway engaging the mitochondrial pathway in myeloma cells with mutant p53. *Cell Cycle* 2003; **2**: 358-368

34 **Lecureur V,** Le Thiec A, Le Meur A, Amiot L, Drenou B, Bernard M, Lamy T, Fauchet R, Fardel O. Potassium antimonyl tartrate induces caspase- and reactive oxygen species-dependent apoptosis in lymphoid tumoral cells. *Br J Haematol* 2002; **119**: 608-615

35 **Gupta S,** Yel L, Kim D, Kim C, Chiplunkar S, Gollapudi S. Arsenic trioxide induces apoptosis in peripheral blood T lymphocyte subsets by inducing oxidative stress: a role of Bcl-2. *Mol Cancer Ther* 2003; **2**: 711-719

36 **Dvorakova K,** Payne CM, Tome ME, Briehl MM, Vasquez MA, Waltmire CN, Coon A, Dorr RT. Molecular and cellular characterization of imexon-resistant RPMI8226/I myeloma cells. *Mol Cancer Ther* 2002; **1**: 185-195

37 **Michel L,** Dupuy A, Jean-Louis F, Sors A, Poupon J, Viguier M, Musette P, Dubertret L, Degos L, Dombret H, Bachelez H. Arsenic trioxide induces apoptosis of cutaneous T cell lymphoma cells: evidence for a partially caspase-independent pathway and potentiation by ascorbic acid (vitamin C). *J Invest Dermatol* 2003; **121**: 881-893

38 **Choi YJ,** Park JW, Suh SI, Mun KC, Bae JH, Song DK, Kim SP, Kwon TK. Arsenic trioxide-induced apoptosis in U937 cells involve generation of reactive oxygen species and inhibition of Akt. *Int J Oncol* 2002; **21**: 603-610

39 **Sordet O,** Rebe C, Leroy I, Bruey JM, Garrido C, Miguet C, Lizard G, Plenchette S, Corcos L, Solary E. Mitochondria-targeting drugs arsenic trioxide and lonidamine bypass the resistance of TPA-differentiated leukemic cells to apoptosis. *Blood* 2001; **97**: 3931-3940

Science Editor Zhu LH and Guo SY **Language Editor** Elsevier HK

PO Box 2345, Beijing 100023, China
www.wjgnet.com
wjg@wjgnet.com

ELSEVIER

World J Gastroenterol 2005;11(22):3457-3460
World Journal of Gastroenterology ISSN 1007-9327

• *BRIEF REPORTS* •

Applications of gray relational analysis in gastroenterology

Xue-Rui Tan, Yu-Guang Li, Ming-Zhe Chen

Xue-Rui Tan, Yu-Guang Li, First Affiliated Hospital of Shantou University Medical College, Shantou 510041, Guangdong Province, China
Ming-Zhe Chen, Medical School of Tsinghua University, Beijing 100083, China
Supported by the National Natural Science Foundation of China, No. 30271158
Correspondence to: Xue-Rui Tan, MD, PhD, First Affiliated Hospital of Shantou University Medical College, Shantou 510041, Guangdong Province, China. tanxuerui@vip.sina.com
Telephone: +86-754-8552841 Fax: +86-754-8611690
Received: 2004-02-02 Accepted: 2004-02-21

Abstract

AIM: To introduce the basic methods of gray relational analysis (GRA) and to illustrate its applications in gastroenterology.

METHODS: With the essential formulae of GRA and several typically practical examples, the procedure of GRA was introduced. Examples were drawn from the gastroenterological studies. Thus the trait of GRA could be demonstrated.

RESULTS: The superiority of GRA in gastroenterological study was proved by the examples.

CONCLUSION: GRA can be applied mechanically or flexibly in gastroenterology.

Key words: Gray relational analysis; Gastroenterology

Tan XR, Li YG, Chen MZ. Applications of gray relational analysis in gastroenterology. *World J Gastroenterol* 2005; 11(22): 3457-3460
http://www.wjgnet.com/1007-9327/11/3457.asp

INTRODUCTION

Gray relational analysis (GRA) was initiated by Professor Ju-Long Deng, the famous scientist and founder of gray system theory, Huazhong University of Science and Technology[1]. Previous applications of GRA in medical researches were mostly in cardiology[2-7]. In our viewpoint, it is very useful to introduce GRA to gastroenterologists.

MATERIALS AND METHODS

Essential formulae of GRA

Let X be the gray relational factor set, $x_0 \in X$ be the consulting sequence, $x_i \in X$ (i = 1, 2,…, m; $m \geqslant 2$, as the comparative factors) be the comparative sequence, x_0 and x_i are named factor sequences. The $x_0(k)$ and $x_i(k)$ are the values of x_0 and x_i at k point (k = 1, 2,…, n; $n \geqslant 3$). Thus, the formulae of gray relational coefficient $\gamma(x_0(k), x_i(k))$ and gray relational grade $\gamma(x_0,x_i)$ are the following:

$$\gamma(x_0(k),x_i(k))=\frac{\min\limits_i\min\limits_k|x_0(k)-x_i(k)|+\zeta\max\limits_i\max\limits_k|x_0(k)-x_i(k)|}{|x_0(k)-x_i(k)|+\zeta\max\limits_i\max\limits_k|x_0(k)-x_i(k)|} \quad \text{and} \quad \gamma(x_0,x_i)=\frac{1}{n}\sum_{k=1}^{n}\gamma(x_0(k),x_i(k))$$

The gray relational order, based on the gray relational grade $\gamma(x_0,x_i)$ which represents the strength of relationship between x_0 and x_i, can be constructed. In the formula, $\min\limits_i\min\limits_k|x_0(k)-x_i(k)|$ and $\max\limits_i\max\limits_k|x_0(k)-x_i(k)|$ are the absolute values of the minimum and maximum from the differences between $x_i(k)$ and $x_0(k)$. $x_i(k)$ and $x_0(k)$ are the values at point k in the x_0 and x_i, the sequences without dimension. Here, ζ = 0.5.

Dis-dimension method Let $x=(x(1), x(2),…, x(n))$ be the sequence with dimension. Thus, $f: x \rightarrow \chi$,

$$f(x(k))=\frac{x(k)}{x^*}=\chi(k),\ k=1,2,k\ldots,n;\ \chi(k)\in s(1) \quad \text{where } x^*\in\left\{x(1),\max_k x(k),\min_k x(k),\frac{1}{n}\sum_{k=1}^{n}x(k)\right\};$$

Consider parameter sequence $x_i=(x_i(1),x_i(2), …,x(n))$, where i=1, 2,…,N;

$$\begin{aligned} y_{(1)} &= (x_1(1),x_2(1),\cdots,x_N(1));\\ y_{(2)} &= (x_1(2),x_2(2),\cdots,x_N(2));\\ &\cdots\cdots\\ y_{(n)} &= (x_1(n),x_2(n),\cdots,x_N(n)); \end{aligned}$$

Thus, $f: x_i \rightarrow \chi_i$, $f(x_i(k))=\dfrac{x_i(k)-\min y(k)}{\max y(k)-\min y(k)}=\chi_i(k),\chi_i(k)\in s(1).$

Here, $\max y(k)=\max\limits_i x_i(k),\ \min y(k)=\min\limits_i x_i(k),\ k\in K, K=1,2,k\ldots,n.$

Evaluation matrix of GRA Suppose $x_{0j} \in x_0$ be a group of the consulting factors, j = 1, 2,…, e. Thus, there is the gray relational matrix R about x_0 and x_i as the following:

$$\mathrm{R}(x_0,x_i)=\begin{bmatrix} \gamma(x_{01},x_1) & \gamma(x_{02},x_1) & \cdots & \gamma(x_{0e},x_1) \\ \gamma(x01_1,x_2) & \gamma(x0_2,x_2) & \cdots & \gamma(x_{0e},x_2) \\ \cdots & \cdots & \cdots & \cdots \\ \gamma(x_{0_1},x_m) & \gamma(x0_2,x_m) & \cdots & \gamma(x_{0_e},x_m) \end{bmatrix}\begin{matrix}\gamma(x_{0j},x_1)\\ \gamma(x_{0_j},x_2)\\ \cdots\\ \gamma(x_{0_j},x_m)\end{matrix}$$

GRA model of clinical trial Let $x_i \in X$, $x_i=(x_i(1), x_i(2), …, x_i(n))$ be the observing parameter sequences of group i or case i; i=1, 2,…, m, $m \geqslant 2$, as the number of trial group or trial case.

Let $x_0 \in X$, $x_0 = (x_0(1), x_0(2),…, x_0(n))$ be the ideal parameter sequence of trial, the ideal values used to construct x_0 are chosen from x_i. Here, k=1, 2,…, n, $n \geqslant 3$, as the number of parameters in the sequences. Hence, the gray relational grade $g(x_0,x_i)$ acts as the reflection of approaching the ideal effects. Then, the formulae:

$$\gamma(x_i(k),x(k))=\frac{\min\limits_i\min\limits_k|x_i(k)-x(k)|+\zeta\max\limits_i\max\limits_k|x_i(k)-x(k)|}{|x_i(k)-x(k)|+\zeta\max\limits_i\max\limits_k|x_i(k)-x(k)|} \quad \text{and} \quad \gamma(x_0,x_i)=\frac{1}{n}\sum_{k=1}^{n}\gamma(x_0(k),x_i(k))$$

are called GRA model of clinical trial.

Table 1 Baseline values in four patients before treatment

No. (k)	Age (yr) (x_1)	Course of jaundice (mo) (x_2)	Toughness degree of liver (x_3)	Liver below costal arch (cm) (x_4)	Liver below xiphoid (cm) (x_5)	Splenomegaly (cm) (x_6)
1	55	5.0	3	3	6	0
2	43	2.0	2	3	7	1
3	27	0.7	2	6	4	4
4	48	1.0	3	2	0	2

Table 2 Hepatic functions in four patients before and after albendazole treatment

No. (k)	Bilirubin (μmol/L) (x_7)		One minute bilirubin (μmol/L) (x_8)		ALP (IU) (x_9)		GOT (x_{10})		A/G (g/L) (x_{11})	
	Before	After	Before	After	Before	After	Before	After	Before	After
1	89.2	14.2	11.3	2.1	176.6	28.4	30.0	30.0	45.5/37.5	44.2/27.5
2	60.2	8.9	8.0	0.5	58.0	51.0	76.0	30.0	41.0/56.0	45.1/33.9
3	62.0	8.9	23.4	0.9	481.0	10.6	72.0	63.0	28.0/54.0	48.0/36.0
4	212.9	17.0	129.2	1.9	463.0	247.0	135.0	30.0	33.0/45.0	45.0/27.0

Examples

GRA on small sample data background The objective of this study was to evaluate the relationship between the baseline condition of patients with alveococcosis and the therapeutic effects by using albendazole regularly. Four patients with complete data who were diagnosed clinically and complicated by obstructive jaundice were enrolled in this study. Albendazole was orally given twice daily for over 1 year with a dosage of 20 mg/kg each day in all cases. Baseline values of the observation parameters are shown in Table 1. The effects of albendazole on hepatic functions are shown in Table 2.

Analysis Step 1: To calculate the improved ratio of hepatic functions. The improved ratio was calculated by using the formula:

$$r = \frac{|a - b|}{a}$$

Here, r = improved ratio, a = parameter value before treatment, b = parameter value after treatment.

The calculated values of the improved ratio are listed in Table 3.

Step 2: Correlation analysis Let x_7-x_{11} be the dependent variables, let x_1-x_6 be the independent variables, correlation analysis was performed using the statistical analysis system (version 6.12). The results of correlation analysis are shown in Table 4, indicating that the correlation between dependent variables and independent variables was not significant.

Step 3: GRA Let $x_{0j} \in x_0$ be a group of the consulting factors, j = 7, 8, 9, 10, 11 as the consulting factors, let x_1-$x_6 \in x_i$, i = 1, 2, 3, 4, 5, 6 be the comparative factors. GRA was operated by using GRA program that we edited in the statistical analysis system (version 6.12). Dis-dimension process was the averaging method. Thus, the gray relational matrix R about x_0 and x_i is as follows:

Table 3 Improved ratio of hepatic functions after treatment

k	x_7	x_8	x_9	x_{10}	x_{11}
1	0.84081	0.81416	0.83902	0.00000	0.32468
2	0.85216	0.93750	0.12069	0.60526	0.81711
3	0.98074	0.96154	0.97796	0.12500	1.57141
4	0.92015	0.98529	0.46652	0.77778	1.27274

$$R(x0_j,xi)= \begin{array}{c} \\ \gamma(x0_j,x1) \\ \gamma(x0_j,x2) \\ \gamma(x0_j,x3) \\ \gamma(x0_j,x4) \\ \gamma(x0_j,x5) \\ \gamma(x0_j,x6) \\ \\ \end{array} \begin{array}{c} \begin{array}{ccccc} \gamma(x7,xi) & \gamma(x8,xi) & \gamma(x9,xi) & \gamma(x10,xi) & \gamma(x11,xi) \end{array} \\ \begin{bmatrix} 0.83086 & 0.84450 & 0.68009 & 0.59362 & 0.68935 \\ 0.65564 & 0.63919 & 0.58232 & 0.57313 & 0.56608 \\ 0.82607 & 0.82195 & 0.68418 & 0.56399 & 0.75575 \\ 0.75198 & 0.78167 & 0.75162 & 0.49046 & 0.77538 \\ 0.66376 & 0.67106 & 0.64311 & 0.58631 & 0.52690 \\ 0.65423 & 0.65564 & 0.62717 & 0.59336 & 0.76081 \end{bmatrix} \\ \begin{array}{ccccc} 0.73042 & 0.73567 & 0.66217 & 0.56681 & 0.67905 \end{array} \end{array} \begin{array}{c} \\ 0.72768 \\ 0.60327 \\ 0.73039 \\ 0.71112 \\ 0.61823 \\ 0.65824 \\ \\ \end{array}$$

The GRA results revealed in the gray relational factor set that the superior consulting factors were x_7 and x_8, the superior comparative factors were x_1, x_3 and x_4.

GRA for four therapeutic strategies of duodenal ulcer related to Helicobacter pylori

Background The purpose of this project was to evaluate the effects of four therapeutic strategies on duodenal ulcer (DU) related to *Helicobacter pylori* (*H pylori*). Forty-nine male and nine female patients with DU were complicated by *H pylori*-positivities proved by endoscopic examination and *H pylori* test, and had no gastric or complex ulcer. Their ages were 24-62 years (average 37.1±6.5 years). All the subjects had no obvious complications or other systemic disorders. They did not take antibiotics, bismuth agents or restrain acids/antacids for 2 wk preceding the study.

Table 4 Results of correlation analysis

	x_7	x_8	x_9	x_{10}	x_{11}
x_1	−0.81774	−0.59309	−0.27907	0.10911	−0.77759
	0.1823	0.4069	0.7209	0.8909	0.2224
x_2	−0.78666	−0.98054	0.15755	−0.56181	−0.98954
	0.2133	0.0195	0.8425	0.4382	0.0105
x_3	−0.31909	−0.37737	0.15463	0.06341	−0.45498
	0.6809	0.6226	0.8454	0.9366	0.5450
x_4	0.66573	0.12652	0.63044	−0.59213	0.40379
	0.3343	0.8735	0.3696	0.4079	0.5962
x_5	−0.56410	−0.60064	−0.11905	−0.52589	−0.57561
	0.4359	0.3994	0.8810	0.4741	0.4244
x_6	0.97814	0.72219	0.38317	0.03476	0.90090
	0.0219	0.2778	0.6168	0.9652	0.0991

Note: The upper numbers are the correlation coefficients between corresponding variables and the lower numbers are the P values.

Table 5 Raw data in four groups

Group (i) / k	n	n	Disappearance of symptoms		Eradication of *H pylori*		Active mucitis fading		Ulcer cure	
			Rate (%) (1)	Time (d) (2)	n	Rate (%) (3)	n	Rate (%) (4)	n	Rate (%) (5)
A (x_1)	14	14	100	3.8	11	78.6	9/13	69.2	12	85.7
B (x_2)	15	15	100	3.6	10	66.7	9/13	69.2	11	73.3
C (x_3)	14	10	71.4[a]	6.8	11	78.6	9/12	75	9	64.3
D (x_4)	15	15	100	3.7	2	13.3[b]	3/12	25	9	60
Ideal (x_0)			100	3.6		78.6		75		85.7

[a]$P<0.05$, [b]$P<0.01$ *vs* other groups; i=A, B, C, D=1, 2, 3, 4; k=1, 2, 3, 4, 5.

Table 6 Gray relational coefficients between ideals (x_0) and other groups (x_i)

Group (i) / k	Disappearance of symptoms		Eradication of *H pylori*	Active mucitis fading	Ulcer cure
	Rate (%) (1)	Time (d) (2)	Rate (%) (3)	Rate (%) (4)	Rate (%) (5)
A (1)	1	0.9175	1	0.8481	1
B (2)	1	1	0.7328	0.8481	0.7547
C (3)	0.6302	0.4099	1	1	0.6407
D (4)	1	0.9569	0.3333	0.3932	0.6013

Materials

Step 1: Data collection Grouping and therapeutic strategies: All the subjects were randomly divided into four groups. Group A had 14 cases that were treated with a triple therapeutic strategy of tinidazole (Livzon), Lizhu Dele/colloidal bismuth subcitrate (Livzon Pharmaceutical Factory, Zhuhai) and omeprazole (Sanye Pharm). Group B had 14 cases that were treated with a triple therapeutic strategy of metronidazole (Tongji Meiji), amoxicillin (Baiyunshan, Guangzhou) and omeprazole (Sanye Pharm). Group C had 14 cases that were treated with a triple therapeutic strategy of metronidazole (Tongji Meiji), amoxicillin (Baiyunshan, Guangzhou) and De-Nol/colloidal bismuth subcitrate (Yamanouchi Europe). Group D had 15 cases that were treated with a single therapeutic strategy of omeprazole (Sanye Pharm). There were no significant differences between groups in age or sex distribution. The dose of tinidazole was 1.0 mg b.i.d, Lizhu Dele/colloidal bismuth subcitrate 110 mg q.i.d, omeprazole 20 mg q.d, amoxicillin 0.5 mg q.i.d, metronidazole 0.2 mg t.i.d, De-Nol/colloidal bismuth subcitrate 120 mg q.i.d. Lizhu Dele/colloidal bismuth subcitrate and De-Nol/colloidal bismuth subcitrate were taken orally 30 min ante cibum or before sleep. The others were taken orally 30 min post cibum. Lizhu Dele/colloidal bismuth subcitrate, De-Nol/colloidal bismuth subcitrate and omeprazole were given for 2 wk and the others for 1 wk.

Endoscopic examination and *H pylori* test All the subjects underwent endoscopic examination and *H pylori* test. After pharynx local anesthesia, gastroduodenal endoscopy was performed in all subjects taking a left lateral position by Q30 electronic endoscope system. Images were screened and rinsed, washing-cell specimen muter representatives were taken from the site of ulcer lesion during endoscopy. At normal temperature, the specimen muter representatives were put in the *H pylori* fast test box containing reagents (the PLA Higher Medical School, Lanzhou, China). After 24 h, the reagents that appeared in rose were defined as positive, and those that remained unchanged in color were defined as negative.

Estimation criteria All patients were asked to return for a check-up in a month after treatment. They were evaluated under four aspects: (1) Disappearance of symptoms (all baseline symptoms including pyrosis, epigastric pain, abdominal distension, acid suffusion and belching of gas, etc. disappeared). (2) Eradication of *H pylori* (the specimen muter representatives in *H pylori* test double boxes became negative, and one of them being positive was thought that eradication of *H pylori* infection was not achieved). (3) Active mucitis fading (the original hyperemia, erosion, edema in the duodenal mucosa were not seen endoscopically). (4) Ulcer cure (the duodenal ulcer vanished or pitted, and abated, dilated or unchanged ulcers in the ulcer area were defined as uncured).

Step 2: Raw data of four groups are listed in Table 5.

Step 3: GRA Let the ideal sequence x_0, $x_0(k) \in x_0$, $k = 1, 2, 3, 4, 5$, be the consulting factor sequences. Let x_i, $x_i(k) \in x_i$, $i = 1, 2, 3, 4, 5, 6$, be the comparative factor sequences. GRA was operated using GRA program that we edited in the statistical analysis system (version 6.12). Thus, the gray relational coefficients between x_0 and x_i are as follows (Table 6).

The gray relational grades to ideals of four groups were: γ_{0A}, i.e., $\gamma_{01} = 0.95312$; γ_{0B}, i.e., $\gamma_{02} = 0.86712$; γ_{0C}, i.e., $\gamma_{03} = 0.73616$; γ_{0D}, i.e., $\gamma_{04} = 0.65694$.

Thus the gray relational order was $x_1 > x_2 > x_3 > x_4$; i.e., strategy A $\succ$ strategy B $\succ$ strategy C $\succ$ strategy D.

GRA on serum markers of liver fibrosis

Background Serum procollagen type III (PC III), prolidase (PLD), and hyaluronic acid (HA), are of diagnostic significance in liver fibrosis. To find out the markers with early diagnostic value of liver fibrosis via GRA, 100 patients with chronic liver diseases including 28 patients with chronic persistent hepatitis (CPH), 21 patients with chronic active hepatitis (CAH), and 51 patients with liver cirrhosis (LC), were studied. Thirty HBVM-negative subjects with normal liver biochemical test served as controls. The clinical materials of the subjects are listed in Table 7.

Table 7 Clinical materials of the subjects (mean±SD)

Groups	Number of subjects	Age (yr)	Number of males
Controls	30	31.7±7.2	19
CPH	28	35.2±9.1	20
CAH	21	34.9±6.9	16
LC	51	45.1±11.4	41

Clinical materials Examination of PC III, PLD and HA PC III was assayed by using a commercially available radioimmunoassay (Chongqing Institute of Phymatosis, Chongqing). The activity of PLD was assayed by using a commercially available ultraviolet spectrophotometry (Third Military Medical University, Chongqing). Serum HA was assayed by using a commercially available radioimmunoassay (Shanghai Institute of Navy Medicine, Shanghai). PC III, PLD and HA in controls were regarded as the normal upper limits, and the sensitivity of each marker was calculated. The results are shown in Table 8.

Table 8 Sensitivity of serum PC III, PLD and HA

Marker	CPH	CAH	LC
PCIII	28.6	100.0	88.2
PLD	0.0	57.1	90.2
HA	7.1	76.2	94.2

GRA Step 1: To construct the ideal sequence The ideal sequence was constructed according to the pathological changes of liver diseases. There was no liver fibrosis in CPH, and so the sensitivity of an ideal marker value for the diagnosis of CPH should be zero. Whereas there was early liver fibrosis in CAH, and so the sensitivity of an ideal marker value for CAH should be 100%. The average value of the sensitivity of PC III, PLD and HA in LC was 90.9%, which can be chosen as the sensitivity of an ideal marker value for LC. So, the ideal sequence was x_0 = (0, 100, 90.9).

Step 2: To identify the comparative sequences The observed parameter sequences of i (i = 1, 2, 3 = sensitivity of PC III, sensitivity of PLD and sensitivity of HA) were x_i, x_1, x_2, $x_3 \in x_i$. Thus, the parameter sequences were x_1 = (28.6, 100, 88.2), x_2 = (0, 57.1, 90.2), x_3 = (7.1, 76.2, 94.2), which served as the comparative sequences. x_0, $x_i \in X$, was the GAR factor set.

Step 3: GRA operation GRA was performed using the GRA program that we edited in the statistical analysis system (version 6.12). The results were: $\gamma(x_0,x_1) = 0.7733$, $\gamma(x_0,x_2) = 0.7667$, $\gamma(x_0,x_3) = 0.7$. So the gray relational order was: $\gamma(x_0,x_1)>\gamma(x_0,x_2)>\gamma(x_0,x_3)$; i.e., $x_1 \succ x_2 \succ x_3$.

In conclusion, The GRA showing superiority to statistical methods in some cases can be applied mechanically or flexibly in gastroenterology.

DISCUSSION

Through GRA, serum PC III was identified as the marker with early diagnostic value of liver fibrosis. This example provides a new insight into the study of liver diseases and illustrates a practical application of GRA.

Since the discovery of *H pylori* in 1983, a wealth of data about DU related to *H pylori* has been accumulated, and the therapeutic strategies of duodenal ulcer have been changed. There is evidence that ulcer cure and reduction of recurrence could be achieved by effective antibiotic therapy. Such colloidal bismuth subcitrates as Lizhu Dele or De-Nol can form a protective bismuth-protein membrane which can promote healing of the ulcer and prevent recurrence of ulcer. The results of GRA showed that the gray relational order of the comprehensive effects in terms of the symptom disappearance, eradication of *H pylori*, active mucitis fading and ulcer cure is strategy A $\succ$ strategy B $\succ$ strategy C $\succ$ strategy D, and strategy A is the best of four strategies which showed no differences from the previous reports.

Alveococcosis is as harmful as a malignant tumor. Untreated cases had a 5-year mortality rate of 70% and 10-year of 93%. The severity is related to jaundice. Patients with alveococcosis had a low diagnostic and hospitalization rate. There is a shortage of clinical samples, and not suitable for statistical analysis. The first time report on alveococcosis had no statistical analysis. The GRA results indicated that jaundice parameter bilirubin and 1-min bilirubin were the superior consulting factors, which suggest the main effect of albendazole on alveococcosis. The relevant factors with severity of the disease such as age, degree of liver toughness and liver below costal arch were the superior comparative factors, which suggest that the effects of albendazole on alveococcosis were partially restricted by the baseline conditions of patients. This example provides objective evidence and demonstrates that GRA is superior to statistical analysis for small sample data.

REFERENCES

1 **Deng JL**. Introduction to grey system theory. *J Grey System* 1989; **1**: 1-24

2 **Huang WD,** Shi HR, Tan XR. A grey relational study on determination of stroke volume with D and M echocardiography. *J Grey System* 1994; **6**: 203-211

3 **Tan XR,** Deng JL, Huang WD, Wang ZL. GRA on plasma ET-1, PAP, PaO_2 and $PaCO_2$ in the elderly patients with PHD. In: Liu SF, Xu ZX. *Huise Xitong Yanjiu Jinzhan Huazhong Li Gong Daxue Chubanshe Wuhan China* 1996: 133-135

4 **Xu YC,** Tan XR. Grey relational analysis of a trial of trental *vs* antiaggregants. *J Grey System* 1997; **9**: 365-370

5 **Tan XR,** Yang YH, Deng JL. Grey relational analysing factors in hypertensive with cardiac insufficiency. *J Grey System* 1998; **10**: 75-80

6 **Tan XR,** Deng JL, Chu YJ. Grey relational analysis of circadian variation of plasma renin activity, angiotensin Ⅱ and blood pressure in hypertensives. *J Grey System* 1999; **11**: 41-46

7 **Tan XR,** Yang HS, Chu YJ. Superior grey relational analysis on cardiac structure and function with blood pressure in systolic hypertension. *International Symposium on Hypertension and Related Diseases Chinese Hypertension League Chinese Society of Cardiology & Chinese Academy of Medical Science Beijing-Langfang China* 1999: **135**

Science Editor Zhu LH, Wang XL and Li WZ **Language Editor** Elsevier HK

PO Box 2345, Beijing 100023, China
www.wjgnet.com
wjg@wjgnet.com

ELSEVIER

World J Gastroenterol 2005;11(22):3461-3464
World Journal of Gastroenterology ISSN 1007-9327

• *BRIEF REPORTS* •

Quality of gastric ulcer healing evaluated by endoscopic ultrasonography

Jian-Min Si, Qian Cao, Jia-Guo Wu

Jian-Min Si, Qian Cao, Jia-Guo Wu, Gastroenterology Laboratory, Institute of Clinical Medicine, Sir Run Run Shaw Hospital, School of Medicine, Zhejiang University, Hangzhou 310006, Zhejiang Province, China
Supported by the Grant from the Eisai Human Health Care Company
Correspondence to: Professor Jian-Min Si, Gastroenterology Laboratory, Institute of Clinical Medicine, Sir Run Run Shaw Hospital, School of Medicine, Zhejiang University, Hangzhou 310006, Zhejiang Province, China. sijm@163.net
Telephone: +86-571-87217002 Fax: +86-571-87217044
Received: 2004-08-26 Accepted: 2004-11-04

Abstract

AIM: To evaluate the quality of gastric ulcer healing after different antiulcer treatment by endoscopic ultrasonography (EUS).

METHODS: The patients were divided into three groups, and received lansoprazole, amoxicillin and clarithromycin for 1 wk. Then group A took lansoprazole combined with tepreton for 5 wk, group B took lansoprazole and group C took tepreton for 5 wk. Endoscopy and EUS were performed before and 6 wk after medication.

RESULTS: There was no significant difference in cumulative healing rate to S stage between the groups (89%, 82% *vs* 83%, $P>0.05$). The rate of white scar formation was significantly higher in group A than in groups B and C (67%, 36%, 50%, $P<0.05$). The average contraction rates of the width of ulcer crater, length of disrupted muscularis propria layer and hypoechoic area were higher in group A than in groups B and C (0.792±0.090, 0.660±0.105 *vs* 0.668±0.143, $P<0.05$). The hypoechoic area disappeared in four cases of group A, one of group B and two of group C. The percentage of hypoechoic area disappearance was higher in group A than in the other two groups (44%, 9% *vs* 17%, $P<0.05$). Gastric ulcer healing was better in group A.

CONCLUSION: The combined administration of proton-pump inhibitors and mucosal protective agent can improve gastric ulcer healing.

Key words: Quality of ulcer healing; Endoscopic ultrasonography; Gastric ulcer

Si JM, Cao Q, Wu JG. Quality of gastric ulcer healing evaluated by endoscopic ultrasonography. *World J Gastroenterol* 2005; 11(22): 3461-3464
http://www.wjgnet.com/1007-9327/11/3461.asp

INTRODUCTION

With the introduction of antiulcer agents, the peptic ulcer healing rate has increased considerably, but the high recurrence rate after treatment is a major concern for primary care physicians. Infection with *Helicobacter pylori* (*H pylori*) is the main reason; however, ulcer recurrence may be attributed to other factors such as gastric acid rebound and the persistent presence of mucosal aggravating factors. In 1991, Tarnawski *et al*[1], put forward a new concept of quality of ulcer healing (QOUH). A growing number of reports indicate that low recurrence rate occurs after high QOUH is achieved. Therefore, attentions have been focused on making a good choice of antiulcer agents to promote the QOUH. Although healing of gastric ulcer has been studied radiologically, endoscopically, and by other techniques, these studies were not able to obtain an objective estimate of the transmural histological changes accompanying the healing process within the ulcer[2]. Such changes could only be estimated from superficial changes during ulcer healing. The techniques of endoscopic ultrasonography (EUS) make it possible to observe the ulcer vertically as the cross-sectional image. The present study was designed to evaluate the quality of gastric ulcer healing in 32 patients by EUS and endoscopy. Quality of gastric ulcer healing could be improved after 6-wk treatment, whether high quality of gastric ulcer healing could be achieved by administration of proton-pump inhibitors (PPIs) in combination with mucosal protective agent, difference in quality of gastric ulcer healing between using PPIs or mucosal protective agent alone as a maintenance therapy.

MATERIALS AND METHODS

Patients

Thirty-two patients were enrolled from June 2001 to May 2002. All patients aged 18-70 years had an endoscopic and ultrasonographic diagnosis of deep gastric ulcer (ulcer that completely disrupts the muscularis propria layer[3]) in active stage 1 or 2 (A_1 or A_2), regardless of gender and status of *H pylori* infection. Subjects did not take antiulcer agents and all gastrointestine related medications were stopped 3 d prior to study. The patients with major organ diseases (heart, liver, lung, kidney, *etc.*), malignant ulcer, NSAID-induced ulcer, Zollinger-Ellison syndrome, and pregnancy were excluded

in the study. The background factors of patients are shown in Table 1.

Administration of medications

Subjects were randomly divided into three groups using the envelope method. All the patients received lansoprazole (takeprone, 30 mg b.i.d.), amoxicillin (1 000 mg b.i.d.) and clarithromycin (klacid, 500 mg b.i.d.) for 1 wk as a routine *H pylori* eradication triple therapy[4]. Then group A took lansoprazole (takeprone, 30 mg q.i.d.) combined with tepreton (selbex, 50 mg t.i.d.) for 5 wk. Group B took lansoprazole (takeprone, 30 mg q.d.) for 5 wk. Group C took tepreton (selbex, 50 mg t.i.d.) for 5 wk.

Endoscopy and EUS observation

Endoscopy and EUS were performed immediately before medication and 6 wk after medication. The same physician performed all EUS procedures with no knowledge of the patients' treatment regimen. The endoscopic equipment used was an Olympus GIF-240 and EUS equipment was a FUJINON SP-701 radial scanning ultrasound endoscopic diagnostic device with a frequency of 12 MHz, air was removed and water was injected to produce the image.

The stages of ulcer were classified according to the method of Sakita and Miwa[5], white scars were classified as S_2 while red scars as S_1. Layers of the gastric wall were determined by EUS according to the report of Aibe *et al*[6]. Examination of the depth of open ulcer and ulcer scars by EUS was in accordance with Murakami's classification[7,8]. Open ulcers consisted of three components: an ulcer crater, a hyperechoic layer at the floor of the crater, and an internal hypoechoic area.

Assessment of Helicobacter pylori infection

During endoscopic examination before and after treatment, two biopsy specimens were taken with a sterilized biopsy forceps from an area of intact mucosa 1 cm from an ulcer crater or a healed ulcer. One specimen was stained with Giemsa to show *H pylori*, the other was for rapid urease test to show *H pylori* infection. Patients were regarded as having *H pylori* infection if either one of the tests was positive but both tests needed to be negative to rule out *H pylori* infection.

Observation parameters[9]

Endoscopic observation parameters included ulcer location (body/angulus/antrum), cumulative healing rates at S stage (including S_1 and S_2 stages) and S_2 stage. EUS observation parameters include width (W) of ulcer crater before (W_1) and 6 wk after medication (W_2), length (L) of disrupted muscularis propria layer before (L_1) and 6 wk after administration (L_2), hypoechoic area (A) of the ulcer base before (A_1) and 6 wk after administration (A_2), condition of the hypoechoic area disappearance 6 wk after drug administration. The quality of gastric ulcer healing was estimated by the contraction rates of W, L, A and the disappearance rate of hypoechoic area.

Statistical analysis

Results were expressed as mean±SD. Data were analyzed using Student's *t* test and χ^2 test. $P<0.05$ was considered statistically significant.

RESULTS

Background factors

The background factors of the 32 patients are shown in Table 1. There were no significant differences in the three groups.

Table 1 Background factors of 32 patients (mean±SD)

	Group A	Group B	Group C
Number of cases	9	11	12
Gender (M/F)	2:7	3:8	4:8
Age (yr)	43.3±22.4	47.1±19.8	53.3±20.2
Ulcer location (antrum/angulus/body)	3:4:2	5:3:3	4:5:3
H pylori (pretreatment)	8	9	9
H pylori (after treatment)	0	0	1
W_1 (mm)	8.43±2.40	9.08±2.51	9.52±2.34
L_1 (mm)	16.30±3.41	14.38±3.29	16.19±3.49
A_1 (mm)	402.76±94.89	394.85±74.82	424.56±65.61

Endoscopic findings

Figure 1 shows the gastric ulcer healing rates at S_2 and S stage. The cumulative healing rate at S_2 and S stage was 67% and 89% respectively in group A, 36% and 82% respectively in group B, 50% and 83% respectively in group C. There was no significant difference in the healing rate at S stage among the three groups ($P>0.05$). However, the rate of white scar formation was significantly higher in group A than in groups B and C ($P<0.05$). The results indicated that the healing time was not shortened by administration of PPIs in combination with mucosal protective agents. In other words, they could improve the quality of healing by promoting white scar formation rather than by shortening the time of healing.

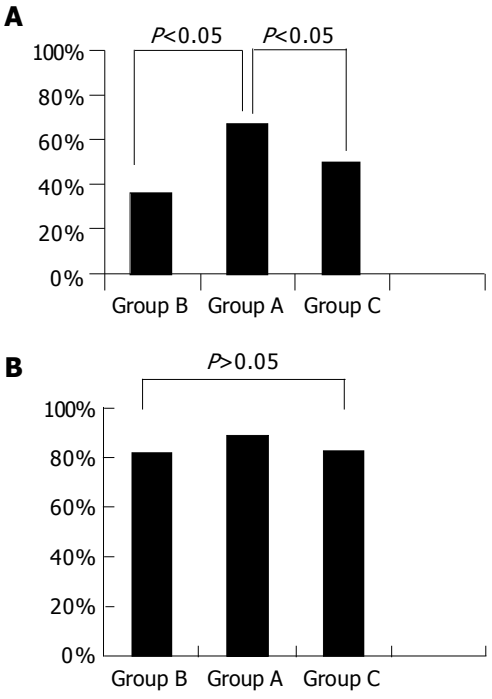

Figure 1 Cumulative healing rate at S_2 stage (**A**) and at S stage (**B**).

EUS findings

We observed the width (W) of ulcer craters, length (L) of disrupted muscularis propria layer, and hypoechoic area (A) before and 6 wk after therapy. We calculated the contraction rates of W, L, and A. The average rates were higher in group A than in groups B and C ($P<0.05$). There was no significant difference between groups B and C (Table 2).

We also observed the conditions of hypoechoic area disappearance 6 wk after drug administration. The hypoechoic area disappeared in four cases of group A, one of group B and two of group C. The percentage of hypoechoic area disappearance was higher in group A than in the other two groups ($P<0.05$). There was no significant difference between groups B and C ($P>0.05$) (Figure 2).

In terms of the contraction rates of W, L, and A as well as the condition of hypoechoic area disappearance, the quality of gastric ulcer healing tended to be better in group A, suggesting that administration of PPIs in combination with mucosal protective agents could improve the quality of gastric ulcer healing.

Table 2 Average contraction rates of W, L, and A in three groups (mean±SD)

	Group A	Group B	Group C
Contraction rates of W	0.623±0.067	0.537±0.098	0.585±0.123
Contraction rates of L	0.496±0.052	0.391±0.073	0.407±0.083
Contraction rates of A	0.792±0.090	0.660±0.105	0.668±0.143

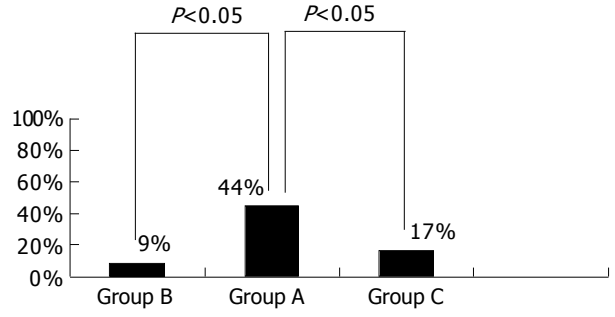

Figure 2 Percentage of hypoechoic area disappearance.

DISCUSSION

Since the advent of antiulcer agents in clinical practice, the healing rate of peptic ulcer has reached more than 95%. But the high recurrence rate is greatly concerned.

Ulcer recurrence may be attributable to other factors, such as gastric acid rebound, persistent presence of mucosal aggravating factors, and impairment of local protective mechanisms. It has been reported that recurrence is common when gastric ulcers form a red scar with red regenerative epithelium, whereas ulcers that form a white scar with an epithelium similar to the normal surrounding mucosa show a low rate of recurrence[10].

Based on a visual examination, the ulceration process includes three stages, namely stage A (active stage), stage H (healing stage) and stage S (scar stage), the ulcer scars are classified by color as S_1 (red) or S_2 (white). Histologically, the healing of ulcer is accomplished by filling mucosal defect with epithelial cells and connective tissue to reconstruct mucosa. Epithelial cells at the ulcer margin dedifferentiate and proliferate, supplying cells for re-epithelialization of the mucosal scar surface and reconstruction of glandular structures. Granulation tissue at the ulcer base supplies connective tissue cells to restore the lamina propria and endothelial cells and microvessels for mucosal microvasculature reconstruction. The final outcome of healing reflects a dynamic interaction between "epithelial" component from the ulcer margin and connective tissue component containing microvessels originating from granulation tissue. The ulcer healing process is influenced by gastric acid, pepsin and growth factors such as epidermal growth factor, transforming growth factor (TGF alpha) and fibroblast growth factor, *etc*. It has long been postulated that mucosa in areas of grossly 'healed' gastric or duodenal ulcers returns to normal, either spontaneously or after treatment[11]. This assumption is based almost entirely upon visual examination by endoscopy. Histological and ultrastructural studies can examine the deeper mucosa in areas of grossly healed ulcers, the gastric mucosa of grossly 'healed' ulcers show re-epithelialization of the mucosal surface, but showed prominent abnormalities present in the subepithelial mucosa including reduced height, marked dilation of gastric glands, poor differentiation and/or degenerative changes in glandular cells, increased connective tissue, and disorganized microvascular network. These abnormalities could interfere with oxygenation, nutrient supply, and mucosal resistance and defense, thus becoming the factors for ulcer recurrence. These observations indicate that the quality of mucosal structural restoration rather than the speed of ulcer healing is the most important factor in determining risk of ulcer recurrence[1,11]. In 1991, Tarnawski *et al*[1], put forward a new concept of QOUH. Since then, EUS has been used to estimate the ulcer healing process and attentions have been focused on the correlation between QOUH and effective ulcer treatment.

Kimura *et al*[12], reported that the QOUH can be classified into high, fair and poor quality. High quality healing recognized on EUS is complete disappearance of a low echo mass and subsidence of the wall thickness. They studied 79 patients with gastric ulcer by EUS for a year, found that the incidence of high quality healing was 21.2% (11 of 52 ulcer scars) in the S_1 stage group, which remarkably increased up to 70.4% (19 of 27) in the S_2 group ($P<0.01$). The cumulative relapse rate at 12 mo during maintenance therapy with H2 blocker was found to be 4.5% in the group with high quality healing on EUS, 40.9% in the group with fair quality healing, and 75% in the group with poor quality healing. Hence the aim of antiulcer treatment is to promote the QOUH and reduce the recurrence rate. The primary care physicians are looking for a good choice of antiulcer agents to achieve high quality of healing. Caution should be taken for indiscriminate and long-term administration of antiulcer medications.

Most studies based on visual examination (by endoscopy in patients, or the evaluation of ulcer size in experimental

studies) have shown the efficacy of new antiulcer drugs on healing of gastric ulcers, but few were based on EUS[13]. We designed the present study to objectively establish a relationship between the efficacy of antiulcer drugs and quality of gastric ulcer healing by EUS and endoscopy.

Taking group A for example, although the cumulative healing rate at S_2 stage was 67%, the high quality of gastric ulcer healing was 44%. The grossly 'healed' ulcer did not represent true healing completely. EUS may provide a reliable and objective assessment of the quality of gastric ulcer healing.

The routine course of gastric ulcer treatment is 6 wk, but after evaluating the quality of gastric ulcer healing by EUS in 32 patients, we found that administration of drugs for 6 wk was not enough to achieve high quality of gastric ulcer healing (the highest rate was only 44%). An insufficient time period of treatment may be another reason for ulcer recurrence. We need further studies to establish an effective course of gastric ulcer treatment.

After evaluating the quality of gastric ulcer healing by EUS in 32 patients, we also conclude that combined treatment of PPIs with mucosal protective agents gave a desirable result in terms of promoting the quality of gastric ulcer healing. Using PPIs or mucosal protective agent alone as a maintenance therapy for gastric ulcer showed no significant difference after 5 wk. PPIs can inhibit the secretion of gastric acid, defense factors and impair tissue regeneration. The mucosal protective agents such as teprenone can increase phospholipid and glycoprotein macromolecules in gastric mucosa and stimulate gastric mucosal blood circulation and increase prostaglandins in mucosa. They also stimulate secretion of growth factors. Tarnawski *et al*[14], also found that inhibition of acid secretion significantly accelerates ulcer healing, but acid reducers used alone cannot improve the quality of healing. Both sucralfate and omeprazole treatment can improve the quality of gastric ulcer healing. Stimulating actions of sucralfate on growth factors may be the basis for improving the QOUH. PPIs and mucosal protective agents may be used in maintenance therapy.

REFERENCES

1 **Tarnawski A,** Stachura J, Krause WJ, Douglass TG, Gergely H. Quality of gastric ulcer healing: a new, emerging concept. *J Clin Gastroenterol* 1991; **13** Suppl 1: S42-S47

2 **Imaizumi H,** Koizumi W, Nakai H, Tanabe S, Ohida M, Saigenji K. Effects of *Helicobacter pylori* eradication therapy on the healing process of peptic ulcers. *Nihon Rinsho* 1999; **57**: 167-172

3 **Okai T,** Sawabu N, Songur Y, Motoo Y, Watanabe H. Comparison of lansoprazole and famotidine for gastric ulcer by endoscopic ultrasonography: a preliminary trial. *J Clin Gastroenterol* 1995; **20** Suppl 2: S32-S35

4 **Asaka M,** Satoh K, Sugano K, Sugiyama T, Takahashi S, Fukuda Y, Ota H, Murakami K, Kimura K, Shimoyama T. Guidelines in the management of Helicobacter pylori infection in Japan. *Helicobacter* 2001; **6**: 177-186

5 **Takemoto T,** Sasaki N, Tada M, Yanai H, Okita K. Evaluation of peptic ulcer healing with a highly magnifying endoscope: potential prognostic and therapeutic implications. *J Clin Gastroenterol* 1991; **13** Suppl 1: S125-S128

6 **Aibe T,** Fuji T, Okita K, Takemoto T. A fundamental study of normal layer structure of the gastrointestinal wall visualized by endoscopic ultrasonography. *Scand J Gastroenterol Suppl* 1986; **123**: 6-15

7 **Yamanaka T,** Nakazawa S, Segawa K, Yoshino J. An analysis of the structure of gastric ulcer by endoscopic ultrasonography. *Nihon Shokakibyo Gakkai Zasshi* 1987; **84**: 187-198

8 **Murakami T,** Suzuki T. Pathology of gastric and duodenal ulcers, 1st edition. Nankodo: Tokyo, 1971: 79-102

9 **Tanaka M,** Maruoka A, Chijiiwa Y, Tanaka M, Nawata H. Endoscopic ultrasonographic evaluation of gastric ulcer healing on treatment with proton pump inhibitors versus H2-receptor antagonists. *Scand J Gastroenterol* 1994; **29**: 1140-1144

10 **Nebiki H,** Arakawa T, Higuchi K, Kobayashi K. Quality of ulcer healing influences the relapse of gastric ulcers in humans. *J Gastroenterol Hepatol* 1997; **12**: 109-114

11 **Tarnawski A,** Douglass TG, Stachura J, Krause WJ. Quality of gastric ulcer healing: histological and ultrastructural assessment. *Aliment Pharmacol Ther* 1991; **5** Suppl 1: 79-90

12 **Kimura K,** Yoshida Y, Kihira K, Kasano T, Ido K. Endoscopic ultrasonographic (EUS) evaluation of the quality of gastric ulcer healing. *Gastroenterol Jpn* 1993; **28** Suppl 5: 178-185

13 **Yang XS,** Li YN. The quality of ulcer healing. *Chinese J Internal Medicine* 1995; **34**: 274-276

14 **Tarnawski A,** Santos AM, Hanke S, Stachura J, Douglass TG, Sarfeh IJ. Quality of gastric ulcer healing. Is it influenced by antiulcer drugs? *Scand J Gastroenterol* 1995; **208** (Suppl): 9-13

Science Editor Wang XL and Guo SY **Language Editor** Elsevier HK

PO Box 2345, Beijing 100023, China
www.wjgnet.com
wjg@wjgnet.com

ELSEVIER

World J Gastroenterol 2005;11(22):3465-3467
World Journal of Gastroenterology ISSN 1007-9327

• *BRIEF REPORTS* •

CT perfusion at early stage of hepatic diffuse disease

Sheng Guan, Wei-Dong Zhao, Kang-Rong Zhou, Wei-Jun Peng, Jian Mao, Feng Tang

Sheng Guan, Wei-Dong Zhao, Kang-Rong Zhou, Department of Radiology, Zhongshan Hospital, Fudan University, Shanghai 200032, China
Wei-Jun Peng, Jian Mao, Feng Tang, Department of Radiology, Tumor Hospital, Fudan University, Shanghai 200032, China
Supported by a Grant from the Ministry of Public Health of China, No. 20011420
Correspondence to: Dr. Kang-Rong Zhou, Shanghai Medical Imaging Research Institute, 180 Fenglin Road, Shanghai 200032, China. gsradio@yahoo.com.cn
Telephone: +86-21-54230281
Received: 2004-07-26 Accepted: 2004-11-29

Abstract

AIM: To determine the validity of the non-invasive method of CT perfusion (CTP) in rat model of hepatic diffuse disease.

METHODS: Twenty-eight Wistar rats were divided into two groups. Liver diffuse lesions were induced by diethylnitrosamine in 14 rats of test group. Rats in control group were bred with pure water. From the 1st to 12th wk after the test group was intervened, both groups were studied every week with CTP. CTP parameters of liver parenchyma in different periods and pathologic changes in two groups were compared and analyzed.

RESULTS: The process of hepatic diffuse lesions in test groups was classified into three stages or periods according to the pathologic alterations, namely hepatitis, hepatic fibrosis, and cirrhosis. During this period, hepatic artery flow (HAF) of control group declined slightly, mean transit time (MTT), blood flow (BF) and volume (BV) increased, but there were no significant differences between different periods. In test group, HAF tended to increase gradually, MTT prolonged obviously, BV and BF decreased at the same time. The results of statistical analysis revealed that the difference in the HAF ratio of test group to control group was significant. The ratio of BV and BF in test group to control group in stage of hepatitis and hepatic cirrhosis, hepatic fibrosis and early stage of hepatic cirrhosis was significantly different, but there was no significant difference between hepatitis and hepatic fibrosis. The main pathological changes in stage of hepatitis were swelling of hepatic cells, while sinusoid capillarization and deposition of collagen aggravated gradually in the extravascular Disse's spaces in stage of fibrosis and early stage of cirrhosis.

CONCLUSION: The technique could reflect some early changes of hepatic blood perfusion in rat with liver diffuse disease and is valuable for their early diagnosis.

Key words: Experimental animal; Hepatitis; Hepatic fibrosis; Hepatic cirrhosis; Computed tomography; Perfusion

Guan S, Zhao WD, Zhou KR, Peng WJ, Mao J, Tang F. CT perfusion at early stage of hepatic diffuse disease. *World J Gastroenterol* 2005; 11(22):3465-3467
http://www.wjgnet.com/1007-9327/11/3465.asp

INTRODUCTION

The imaging diagnosis of hepatitis, hepatic fibrosis and early-stage hepatic cirrhosis is still very difficult because they lack morphological changes. However, some hemodynamic changes of these diseases have been found[1]. Invasive and non-invasive methods[2-4] are employed to detect these alterations. At present, blood perfusion data of liver tissues and lesions can be obtained by non-invasive method of CT perfusion (CTP) scan using rapid scan technique and analytic software. Clinical observations have shown its feasibility[5-7]. But there are few studies on the blood changes in hepatitis, hepatic fibrosis and cirrhosis at early stage[8]. This study was to investigate the validity of CTP in rat model of hepatic diffuse disease.

MATERIALS AND METHODS

Animals

Twenty-eight male Wistar rats, 6 wk old, were divided into test and control groups (14 each group). Three days were given to get themselves adapted to the environment in independent ventilating cabinets. Test group was continually intervened every day by adding diethylnitrosamine (DEN, 0.01%, Sigma, 0.99 mg/mL) into their drinking water. Control group drank pure water at the same time. The rats in both groups were scanned by spiral CT once a week for 12 wk after the intervention in test group. Rats of both groups were killed 24 h after CT scan and liver parenchyma tissue of corresponding part was collected and stained with hematoxylin and eosin for pathological examination.

CT imaging

All examinations were completed on a spiral CT scanner. Plain scan was performed to select a slice in which the liver, aorta and portal vein were clearly visualized. Then single section sequential dynamic contrast enhancement CT scan was done according to the protocol of 0.6 s scan time, 0.4 s cycle time, 50 s total scan time; 120 kV, 80 mA; 5-mm slice, 512×512 matrix, 12 cm FOV. An ionic contrast agent (60% angiografin, 1 mL/kg) with diluted concentration of 33% was injected into the tail vein after 5-10 slices were scanned.

Tissue analysis

Within 24 h after CT imaging, the rats were killed and livers were removed at autopsy. DEN-induced liver injury was assessed by standard hematoxylin-eosin staining and electron microscopy, and compared to the normal livers.

Data analysis

All images were transmitted to a workstation (SPARC; Volume Viewer) for data analysis using GE AW4.2. Four of the six parameters were calculated by this software, including blood flow (BF), blood volume (BV), mean transit time (MTT), hepatic arterial flow (HAF). The other two parameters devised for tumor lesion were not included in this test. Three regions of interest (ROI) were drawn in the abdominal aorta, portal vein and right lobe of the liver respectively to obtain satisfactory time-density curves. Hepatic artery was substituted by abdominal aorta because of its small caliber. The ROI of liver parenchyma was as large as possible and avoided large blood vessels.

Statistical analysis

Data were expressed as mean±SD. The Student-Newman-Keuls was used for comparison between two groups in different periods. Considering the changes of perfusion parameters in normal group, ratios of the relative data between test group and normal group were compared. $P<0.05$ was considered statistically significant.

RESULTS

Pathology

Hepatic lesions in test group were proved to be the main pathologic changes manifested as swelling of hepatocytes 1-4 wk after intervention. Fibrotic changes were found at 5-8 wk. Hepatic lesions developed into cirrhosis at 9-14 wk and were characterized by many cirrhosis nodules. Diffuse lesions in different lobes were at different levels. Left lobe and/or left segment of right lobe developed into cirrhosis earlier and more serious than others.

CT results

No obvious morphologic changes were seen in both groups during the experiment.

Time-density curves (Figure 1) of CTP were satisfactory and all hepatic blood perfusion data (Table 1) could be obtained. From the 1st to 12th wk after the test group was treated with DEN, HAF increased gradually, MTT prolonged obviously, BV and BF decreased at the same time. While HAF of control group declined slightly, MTT, BF and BV increased. Statistical analysis (Figure 2) showed that the differences in the HAF ratios of test group to control group at different stages were significant ($P<0.05$). The BV and BF ratios at stage of hepatitis and hepatic cirrhosis, hepatic fibrosis and early stage of hepatic cirrhosis were significantly different ($P<0.05$), but no significant difference was found between hepatitis and hepatic fibrosis.

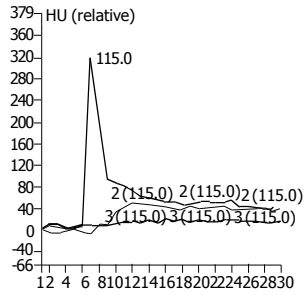

Figure 1 Time-density curves for abdominal aorta (curve 1), portal vein (curve 2) and liver parenchyma (curve 3).

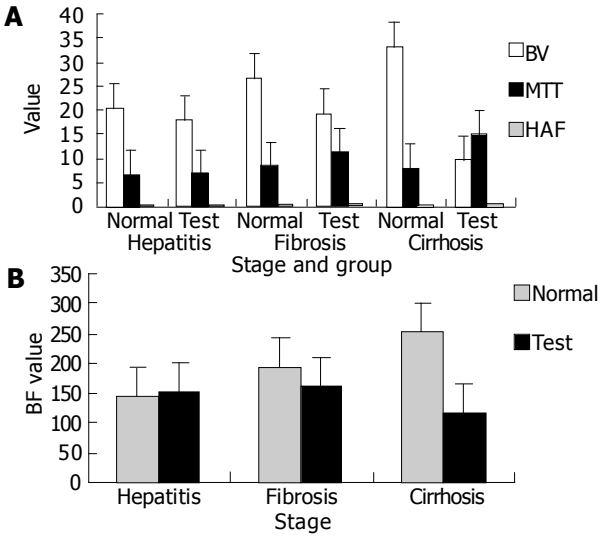

Figure 2 Histogram of BV, MTT, HAF (**A**) and BF (**B**) at different stages in two groups.

DISCUSSION

At present, the diagnosis of hepatitis, hepatic fibrosis and early hepatic cirrhosis in clinic mainly depends on blood examination and the history of patients. Hepatic biopsy has to be considered in order to determine the degree of lesion but is not always exact. Hemodynamic change is important in determining the function of liver. The blood volume of liver accounting for 1/4 of cardiac output is important in maintaining hepatic function. Decrease of blood perfusion

Table 1 CTP data at different stages of test group and control group (mean±SD)

	Hepatitis (1-4 wk)		Fibrosis (5-8 wk)		Cirrhosis (9-12 wk)	
	Test	Normal	Test	Normal	Test	Normal
HAF (%)	0.33±0.23	0.25±0.17	0.55±0.13	0.22±0.16	0.7±0.24	0.19±0.17
BV (mL/100 g/min)	18.05±3.27	20.54±2.35	19.35±3.96	26.65±6.67	9.51±3.61	33.06±4.45
BF (mL/100 g)	152.84±59.12	143.43±26.65	161.77±56.64	192.44±79.98	117.59±78.66	251.67±73.50
MTT (s)	6.6±2.39	6.57±3.28	11.41±3.92	8.3±2.75	15.02±5.21	7.88±2.06

in liver will impair its function by reducing the exchange of blood and hepatocytes. Therefore, the investigation of perfusion parameters of liver is of great value in clinical diagnosis and treatment of liver disease.

Non-invasive techniques used in clinic to estimate hepatic perfusion include hepatic clearance of sorbitol, SPECT, PET, Doppler, *etc*. However, there are some shortcomings of these methods. For example, the method of hepatic clearance of sorbitol is affected severely by some enzymes and transit mechanism when applied in patients with severe liver diffuse disease. Nuclear medicine techniques are hampered by their limited spatial and temporal resolution in differentiating the overlapping parts of hepatic artery and portal vein perfusion in liver, and can barely reflect a large area of liver and can be affected easily by abdominal aorta, inferior vena cava and right kidney when hepatic artery perfusion is measured quantitatively[3]. Doppler and color Doppler can only measure the velocity of large blood vessels and could not directly evaluate the blood amount of hepatic parenchyma[9]. The applications of invasive methods including angiography, CTA, CTAP, *etc*., do not play an important role in routine clinical practice.

Studies of Miles *et al*[10], reported that it is possible to analyze hepatic perfusion using single slice dynamic CE CT scan. According to its achievements in brain diseases[11], this technique may be a promising way to detect hepatic blood perfusion. To date, there are few reports about its application in liver diseases[12,13].

Our results showed that HAF in control group declined slightly and MTT, BF and BV increased gradually from the 1st to 12th wk after the test group was treated, but there were no significant differences. The explanation may be because the experimental rats were growing and hepatic perfusion data would change with the growth. In test group, HAF tended to increase, MTT prolonged obviously, BV and BF decreased at the same time. Considering the changes of perfusion parameters in control group, the ratios of the counterpart data in test group and control group were compared. The results of statistical analysis demonstrated that the differences in HAF and MTT at different stages of test group were significant ($P<0.05$), and the differences in BV and BF between hepatitis and hepatic cirrhosis, hepatic fibrosis and early stage of hepatic cirrhosis were significant ($P<0.05$), suggesting that single slice dynamic CE CT scan can estimate the changes of hepatic blood perfusion related with liver diffuse disease. There was no significant difference in BV and BF between hepatitis and hepatic fibrosis. The explanation may be that liver at this stage can still compensate for its blood perfusion by increasing hepatic arterial volume or the pressure of portal vein. The perfusion data of early stage of hepatic cirrhosis changed a lot compared to those at stage of hepatitis. Pathologic analysis showed that transformation of the fenestrated sinusoids into continuous capillaries and deposition of collagen in the extravascular spaces were the key factors. This kind of alterations may increase the interstitial pressure and obstruct hepatic blood perfusion. Shunts between hepatic artery and portal vein disturb hepatic perfusion in hepatic cirrhosis, but this phenomenon was not obvious in our animal models.

MR perfusion in liver has been studied recently. However, there is no good analytic software because of its complexity compared to CT. Furthermore, the theory and manipulation of MR perfusion are not as simple as CTP in liver examination. Therefore, CTP is more feasible than MR at present.

ACKNOWLEDGMENTS

We thank Hong Ao for the establishment of rat model; Guang Cao, Fei Sun, Wei Sun for the MR scan; Zhong-Wei Chen for the pathologic analysis.

REFERENCES

1 **Orrego H,** Blendis LM, Crossley IR, Medline A, Macdonald A, Ritchie S, Israel Y. Correlation of intrahepatic pressure with collagen in the Disse space and hepatomegaly in humans and in the rat. *Gastroenterology* 1981; **80**: 546-556
2 **Nakao N,** Miura K, Takahashi H, Miura T, Ashida H, Ishikawa Y, Utsunomiya J. Hepatic perfusion in cavernous transformation of the portal vein: evaluation by using CT angiography. *AJR Am J Roentgenol* 1989; **152**: 985-986
3 **O'Connor MK,** Krom RF, Carton EG, Sanchez-Urdazpal L, Juni JE, Ferguson DM, Wiesner RF. Ratio of hepatic arterial-to-portal venous blood flow-validation of radionuclide techniques in an animal model. *J Nucl Med* 1992; **33**: 239-245
4 **Annet L,** Materne R, Danse E, Jamart J, Horsmans Y, Van Beers BE. Hepatic flow parameters measured with MR imaging and Doppler US: correlations with degree of cirrhosis and portal hypertension. *Radiology* 2003; **229**: 409-414
5 **Leggett DA,** Kelley BB, Bunce IH, Miles KA. Colorectal cancer: diagnostic potential of CT measurements of hepatic perfusion and implications for contrast enhancement protocols. *Radiology* 1997; **205**: 716-720
6 **Bader TR,** Herneth AM, Blaicher W, Steininger R, Muhlbacher F, Lechner G, Grabenwoger F. Hepatic perfusion after liver transplantation: noninvasive measurement with dynamic single-section CT. *Radiology* 1998; **209**: 129-134
7 **Arita T,** Matsunaga N, Takano K, Hara A, Fujita T, Honjo K. Hepatic perfusion abnormalities in acute pancreatitis: CT appearance and clinical importance. *Abdom Imaging* 1999; **24**: 157-162
8 **Van Beers BE,** Leconte I, Materne R, Smith AM, Jamart J, Horsmans Y. Hepatic perfusion parameters in chronic liver disease: dynamic CT measurements correlated with disease severity. *AJR Am J Roentgenol* 2001; **176**: 667-673
9 **Kok T,** Slooff MJ, Peeters PM, Zwaveling JH, Bijleveld CM, Gi-van Loon CE, Klompmaker IJ, Haagsma EB. Changes in portal hemodynamics and acute rejection in the first 2 weeks after orthotopic liver transplantation. A prospective Doppler ultrasound study. *Invest Radiol* 1996; **31**: 774-780
10 **Miles KA,** Hayball MP, Dixon AK. Functional images of hepatic perfusion obtained with dynamic CT. *Radiology* 1993; **188**: 405-411
11 **Wintermark M,** Smith WS, Ko NU, Quist M, Schnyder P, Dillon WP. Dynamic perfusion CT: optimizing the temporal resolution and contrast volume for calculation of perfusion CT parameters in stroke patients. *AJNR Am J Neuroradiol* 2004; **25**: 720-729
12 **Tsushima Y,** Funabasama S, Sanada S, Aoki J, Endo K. Perfusion changes of hepatic parenchyma due to infectious hepatobiliary disease: demonstration by perfusion CT. *Comput Med Imaging Graph* 2003; **27**: 289-291
13 **Shi LJ,** Tian JM, Wang PJ, Bi YM, Tian J, Li SP, Li YL. Pilot study on clinical application of hepatic perfusion with multi-slice spiral CT. *Zhonghua Ganzangbing Zazhi* 2003; **11**: 522-525

Science Editor Wang XL **Language Editor** Elsevier HK

PO Box 2345, Beijing 100023, China
www.wjgnet.com
wjg@wjgnet.com

ELSEVIER

World J Gastroenterol 2005;11(22):3468-3472
World Journal of Gastroenterology ISSN 1007-9327

• *BRIEF REPORTS* •

α-catenin expression is decreased in patients with gastric carcinoma

Yong-Ning Zhou, Cai-Pu Xu, Yu Chen, Biao Han, Shi-Ming Yang, Dian-Chun Fang

Yong-Ning Zhou, Biao Han, Department of Gastroenterology, First Hospital, Lanzhou University, Lanzhou 730000, Gansu Province, China
Cai-Pu Xu, Shi-Ming Yang, Dian-Chun Fang, Department of Gastroenterology, Southwest Hospital, Third Military Medical University, Chongqing 400038, China
Yu Chen, Institute of Burn Research, Southwest Hospital, Third Military Medical University, Chongqing 400038, China
Supported by the Scientific Foundation of Gansu Province, No. QS022-C33-029
Correspondence to: Dr. Yong-Ning Zhou, Department of Gastroenterology, First Teaching Hospital, Lanzhou Medical College, Lanzhou 730000, Gansu Province, China. yongningzhou@sina.com.cn
Telephone: +86-931-8625400
Received: 2004-05-27 Accepted: 2004-06-28

Abstract

AIM: To assess the expression of α-catenin in gastric carcinoma and to determine the role of α-catenin expression in gastric carcinogenesis.

METHODS: α-catenin expression was assessed by semi-quantitative reverse transcriptase-polymerase chain reaction and immunohistochemical staining in 49 gastric carcinomas, 26 adjacent non-cancerous mucosae, and gastric biopsy specimens from 11 healthy controls.

RESULTS: mRNA levels of α-catenin were reduced or absent in 34 of 49 (69%) gastric carcinoma tissues and in 5 of 26 (19%) tumor-free gastric mucosae of carcinoma patients, respectively. Of the carcinoma samples with altered α-catenin mRNA levels, α-catenin expression was negative in 20 and decreased in 14 cases. Up to 69% of tumors were stained abnormally for α-catenin. Of the 34 cases whose mRNA expression of α-catenin was reduced, 32 (94%) showed abnormal immunostaining patterns, while only 2 showed a normal α-catenin expression. The frequency of reduced expression of α-catenin mRNA was 14% in well-differentiated carcinomas, higher than that in poorly differentiated carcinomas (86%). A significant correlation was not shown between α-catenin expression and both depth of invasion and lymph node metastasis. Moreover, there was no statistical difference between loss or down-regulation of α-catenin mRNA and *Helicobacter pylori* (*H pylori*) infection.

CONCLUSION: Downregulation of α-catenin expression is common in gastric carcinoma, and α-catenin expression may be used as a differentiation marker. Downregulation of α-catenin expression may be an early event in tumorigenesis. Reduced α-catenin expression is not correlated with *H pylori* infection.

Key words: α-catenin; Gastric carcinoma; Gastric carcinogenesis

Zhou YN, Xu CP, Chen Y, Han B, Yang SM, Fang DC. α-catenin expression is decreased in patients with gastric carcinoma. *World J Gastroenterol* 2005; 11(22): 3468-3472
http://www.wjgnet.com/1007-9327/11/3468.asp

INTRODUCTION

Gastric carcinoma is the second most common malignancy worldwide, and one of the leading causes of death in countries such as Japan, China, and Chile. Even in the developed Western countries, the 5-year survival rate of gastric carcinoma patients is only 10-19%[1]. In China, gastric carcinoma is the most common malignancy annually diagnosed, with a cancer-related mortality of 23%[2]. Lanzhou, a city of northwest China, is one of the highly prevalent geographic areas of gastric carcinoma with a cancer-related mortality of 48%[2]. It is currently unknown what factors contribute to the develo-pment, progression, and metastasis of gastric cancers. Many investigations attribute this high incidence to dietary and genetic factors, as well as *Helicobacter pylori* (*H pylori*) infection[3].

Development of malignant tumors is in part characterized by the ability of tumor cells to break away from cell-cell adhesion and to invade surrounding tissues. E-cadherin is the main adhesion molecule of epithelia, and has been implicated in carcinogenesis because it is frequently lost in human epithelial carcinomas[4]. Formation of strong intercellular adhesion requires a linkage between transmembranous E-cadherin and actin filaments in the cytoskeleton. The extracellular domain of E-cadherin regulates homophilic interaction. The amino acid sequences of cytoplasmic domain, on the other hand, are highly conserved among the family members and indispensable to bind to actin filaments. At least two cytoplasmic proteins, called α-catenin and β-catenin, are closely associated with this domain[5,6]. When the carboxyl-terminal region of the cytoplasmic domain of E-cadherin is deleted, the truncated E-cadherin cannot act as adhesion molecules[5,7,8]. Thus, catenins play an important role in E-cadherin function.

α-catenin is believed to be important in linking E-cadherin to the actin cytoskeleton. Biochemical evidence suggests that α-catenin does not bind to E-cadherin directly but rather mediates the interaction of E-cadherin-β-catenin complex with the actin cytoskeleton, whereas β-catenin binds directly

to the cytoplasmic domain of E-cadherin. However, cells lacking α-catenin are unable to form stable adhesions junction, despite normal E-cadherin and β-catenin expression[6,9].

The important role of E-cadherin-catenin complex in mediating epithelial cell-cell adhesion is reflected by many studies showing that its abnormal expression and dysfunction are correlated to cancer cell dedifferentiation, invasion, and metastasis[10-13]. We have previously shown that abnormal expression of E-cadherin and β-catenin occurs in a considerable proportion of gastric carcinomas. In this study, we examined α-catenin expression in gastric carcinoma by reverse transcriptase-polymerase chain reaction (RT-PCR) and immunohistochemical analysis to assess the possible role of α-catenin in the process of gastric carcinogenesis. The possible relationship between α-catenin expression and tumor clinicopathology was also discussed.

MATERIALS AND METHODS

Materials

Specimens of gastric cancers were obtained from 49 consecutive patients who underwent gastrectomy at the Department of Surgery (First Teaching Hospital, Lanzhou Medical College, Lanzhou, China), from January to August 2002. There were 39 males and 10 females, with a median age of 54 years (range, 38-72 years). None of the patients received chemotherapy or radiotherapy before surgery. Clinicopathological information was obtained from hospital records. Samples were taken from the representative cancerous lesions as well as adjacent non-cancerous mucosae. Immediately after removal, all specimens were placed in liquid nitrogen and stored at -80 ℃ until use. In addition, mucosal biopsy specimens from nine healthy controls were examined. Sections were stained with Warthin-Starry staining for detection of *H pylori*.

Tumor staging and classification

Tumors were staged at the time of surgery by the standard criteria for TNM staging using the unified international gastric cancer staging classification[14] and the following morphological details were recorded: depth of invasion (pT category), lymph node involvement (pN category). According to the criteria of the Japanese Research Society for Gastric Cancer[15], tumors were classified into well or poorly differentiated (including undifferentiated or signet ring) carcinomas. Pathological data are summarized in Table 1.

Table 1 Relationship between expression of α-catenin mRNA and histopathological features in gastric carcinoma

	No	α-catenin mRNA expression		*P*
		+ (%)	-or ± (%)	
All case	49	15 (30.6)	34 (69.4)	
pT category				
T_1/T_2	17	7 (41.2)	10 (58.8)	1.36
T_3/T_4	32	8 (25.0)	24 (75.0)	NS
pN category				
N-negative	26	10 (38.5)	16 (61.5)	1.60
N-positive	23	5 (21.7)	18 (78.3)	NS
Tumor grade				
Differentiated	20	11 (55.0)	9 (45.0)	9.46
Undifferentiated	29	4 (13.8)	25 (86.2)	<0.01

+, positive; ±, faint band; -, negative.

RT-PCR assay

Total RNA was extracted by Tripure method (TakaRa, Japan). One microgram of total RNA was reverse transcripted in 20 μL volume of reaction mixture using the SuperScript Preamplification system (TakaRa) according to its instruction. A pair of primers was designed to amplify the coding region of α-catenin mRNA. A sense primer, Pr-1 (5'-TCGCCCA-GCTAGCCGCAGAAATG-3'), and an antisense primer, Pr-2 (5'-TCAGCAACCGGGTAAACAGCAGAGA-3'), were used and the expected PCR product was 437 bp. PCR was carried out in 25 μL total reaction mixture. Reaction mixture was incubated for 5 min at 94 ℃. Samples were denatured at 94 ℃ for 30 s, annealed at 62 ℃ for 30 s, and extended at 72 ℃ for 30 s. After 35 cycles there was a final elongation for 5 min at 72 ℃, 10 μL of the PCR product was then electrophoresed on 1.5% agarose gel together with size markers.

Semiquantitative analysis

Levels of α-catenin mRNA were quantified using semiquantitative RT-PCR as previously described. GAPDH was used as an internal standard to confirm the equal loading in each experiment and amplified from the same cDNAs. The level of PCR-amplified products was analyzed densitometrically from the agarose gel and standardized to the respective GAPDH mRNA level. The α-catenin/GAPDH ratio was calculated and analyzed using the *t* test.

Immunohistochemical staining

The following items were purchased from Maxim Biotech Inc. (South San Francisco, CA, USA): mouse mAbs against human α-catenin, UltraSensitive S-P Kit, and peroxidase-conjugated streptavidin. Diaminobenzidine tetrahydrochloride (DAB) and other routine chemicals were obtained from Sigma-Aldrich Corp. (St. Louis, MO, USA).

To detect the presence and patterns of α-catenin, we utilized the peroxidase-conjugated streptavidin immunostaining technique, as previously described by others[13]. Briefly, 4-μm-thick tissue sections were dewaxed and rehydrated through changes of xylene and graded alcohol. Endogenous peroxidase activity was blocked by incubating the sections with 0.6% hydrogen peroxide for 10 min. Heat-mediated antigen retrieval was performed by heating the sections (immersed in 0.01 mol/L citrate buffer, pH 6.0) in a microwave oven (750 W) for 20 min. The slides were then washed with PBS before they were exposed to 10% normal goat serum for 10 min to block the non-specific background reaction. The slides were then incubated with respective primary antibody overnight at 4 ℃. Following the wash with PBS, the slides were incubated for 15 min with the secondary antibody and biotinylated goat anti-mouse IgG. The slides were further washed for 3 min×10 min in PBS, followed by incubation with peroxidase-conjugated streptavidin for 10 min. The peroxidase reaction was developed in PBS using hydrogen peroxide as a substrate and DAB as a chromogen. Sections were counter-stained with hematoxylin, dehydrated, and evaluated under a light microscope.

Interpretation of immunostaining

Slides were independently examined by two experienced pathologists who were blinded to the stage of the tumor and

to the initial score of the other observer, and a high level of concordance (90%) was achieved. In case of disagreement, the slides were reviewed and a consensus view was achieved. Staining intensity was graded semiquantitatively from 0 to 3, as previously described[16,17]: 0: negative staining; 1: cytoplasmic staining; 2: heterogeneous staining (tumors composing of both normal and abnormal staining areas); and 3: a normal membranous staining. Because the staining pattern sometimes varied within the same tumor particularly when the differentiation status varied, the final score was based on the dominant pattern. For the ease of data analysis, all tumors with loss of membranous expression were classified as abnormal which included those with absent, heterogeneous or cytoplasmic staining patterns.

Statistical analysis

The χ^2 test was used for correlation between α-catenin expression and clinicopathologic indices. The correlation between α-catenin mRNA expression and α-catenin immunostaining was analyzed by Spearman's rank correlation coefficient. $P<0.05$ was considered statistically significant.

RESULTS

Expression of α-catenin mRNA in gastric carcinoma

All gastric biopsies obtained from healthy control subjects exhibited α-catenin mRNA. In contrast, in 34 of 49 tumor samples, α-catenin mRNA levels altered. Thus, of the 49 gastric tumor tissues, expression of α-catenin was completely lost in 12 (41%) and decreased in 8 (28%) compared with normal issue (Figure 1). In total, 34 (69%) tumor specimens exhibited low or absent α-catenin expression, whereas in the tumor-free locations (26 cases) absent α-catenin expression was observed in only 5 cases.

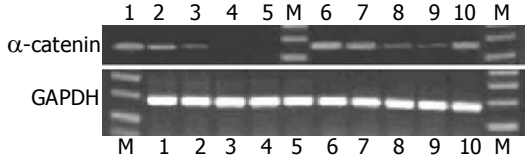

Figure 1 RT-PCR analysis of α-catenin mRNA in gastric tissues. Amplification of GAPDH mRNA was performed to ensure equal loading. Lanes 1 and 10: healthy controls; lane 6: tumor free; lanes 2-5, 7-9: tumor; M: marker.

The relationship between α-catenin expression and clinicopathological features is shown in Table 1. The frequency of decreased α-catenin expression was higher in poorly differentiated carcinomas (25 [86%] of 29 cases) than in well-differentiated carcinomas (9 [45%] of 20 cases). Thus, the expression of α-catenin was significantly correlated with differentiation ($P<0.01$). A significant correlation was not shown between α-catenin expression and depth of invasion (pT category), with loss or absent expression in 10 of 17 (59%) tumors with T_1/T_2 and 24 of 32 (75%) tumors with T_3/T_4 ($P>0.05$). In comparing the lymph node metastasis (pN category) with loss or absent expression of α-catenin, α-catenin was reduced in 62% (16/26) of tumors with N_0 and 78% (18/23) of tumors with N_1 ($P>0.05$).

α-catenin immunostaining in gastric carcinoma

Without exception, all normal mucosal specimens showed distinct, evenly distributed immunostaining for α-catenin along the intercellular borders. Of the 49 gastric tumor cases, 35 (71%) showed an abnormal α-catenin expression, and 14 (29%) showed a normal expression. Furthermore, of the 34 cases whose mRNA expression of α-catenin was reduced, 32 (94%) showed an abnormal immunostaining pattern, while only 2 showed a normal α-catenin expression (Figure 2). Using Spearman's rank correlation coefficient, there was an apparent association between reduced expression of α-catenin mRNA and abnormal α-catenin immunostaining ($r_s = 0.867$, $P = 0.001$). Comparison of α-catenin immunostaining with clinicopathological features revealed that abnormal α-catenin expression correlated with differentiation ($P<0.01$), but not with pT category or pN category.

Correlation of α-catenin expression with H pylori infection

A total of 49 gastric carcinomas were examined for *H pylori* infection using Warthin-Starry staining. *H pylori* infection and mRNA expression of α-catenin were studied. Twenty-two of 31 tissue specimens with *H pylori* infection exhibited a reduced α-catenin expression, whereas in 18 tissue specimens with no *H pylori* infection 12 exhibited a low or no α-catenin expression. A statistically significant correlation was not observed between reduced expression of α-catenin mRNA and *H pylori* infection ($P>0.05$).

DISCUSSION

Functional cell-cell contacts play a critical role in the organization

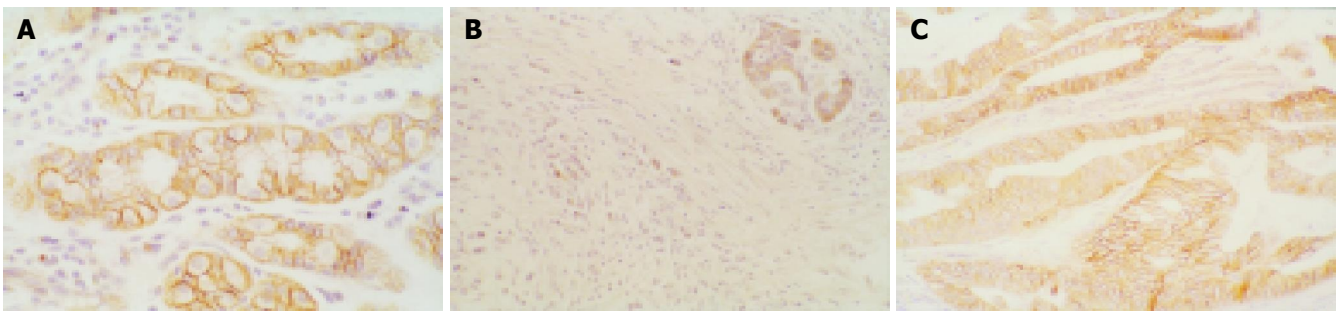

Figure 2 Immunoreactivity of α-catenin in gastric carcinoma. **A:** Normal membranous staining pattern (SP ×400). **B:** Poorly differentiated tumors with complete loss of membranous staining in the majority of cells. Membranous staining can be seen in a few cells retaining gastric gland (SP ×200). **C:** Moderately differentiated tumors showing membranous staining pattern (SP ×200).

of differentiated epithelial tissues. It is predominantly regulated by E-cadherin, a calcium-dependent cell adhesion molecule that binds to other E-cadherin molecules on adjacent cells and is located at the adheren junction of epithelial cells[5,18]. It has become now apparent that loss of E-cadherin-mediated cell-cell adhesion is associated with the progression of many carcinomas, known to act as an "invasion suppressor system" in cancer cells[4,19,20]. In cultured cell lines, loss of E-cadherin function caused a reduction in cell-cell adhesiveness and acquisition of an invasive capacity[21,22]. Also, the reduced expression of E-cadherin has been correlated with differentiation, tumor invasion, and metastasis in various cancerous tissues[4,10]. Loss of E-cadherin/catenin-dependent cell-cell adhesion was often caused by mutations of the *E-cadherin* or the α-*catenin* gene[9,23-26]. Approximately 50% of sporadic diffuse gastric carcinomas demonstrated somatic mutations that could inactivate E-cadherin[27,28]. A germline mutation in E-cadherin associated with familial gastric carcinoma was recently reported in a New Zealand kindred[24,29]. Another mechanism of altered cell-cell adhesion is the downregulation of *E-cadherin* gene expression, for instance by modified methylation patterns of a 5'CpG island in the E-cadherin promoter[30-32]. Moreover, catenins (α-, β-) play an important role in E-cadherin function. Mutant E-cadherin molecules lacking the catenin-binding sites failed to interact with the actin filaments[7,8], indicating that interactions between E-cadherin and cytoskeletal proteins through catenins could confer stability on the cell–cell adheren junctions. Recently, several studies[16,33-35] have shown that expression of E-cadherin and catenins is frequently downregulated in gastric carcinoma. We have previously demonstrated that abnormal expression of E-cadherin and β-catenin occurs in a considerable proportion of gastric carcinomas, and there is a significant relationship between abnormal E-cadherin or β-catenin expression and tumor clinicopathology.

α-catenin, a protein associated with E-cadherin, could bind to the cytoplasmic domain of E-cadherin, form a linkage to actin filaments, and regulate E-cadherin function[5,6]. PC9 lung carcinoma cells, which do not have the α-catenin protein, could not bind tightly to each other despite the fact that they possess E-cadherin. Transfection of the α-catenin gene could restore their intercellular adhesion[26]. As no methylation around the promoter region CpG island has been documented in the α-catenin gene[4,36], gene deletions might be involved in reduced expression of α-catenin. In addition, post-transcriptional mechanisms may be important in the regulation of α-catenin function. E-cadherin might stabilize α-catenin protein through their specific binding to α-catenin[37,38], or might increase the translation level of this molecule by decreasing the concentration of free α-catenin protein[39]. In our study, we found loss of membranous α-catenin immunostaining in a subgroup of gastric carcinomas, and these results were in agreement with those of previous reports[16,17,34,40]. However, these studies were based on immunohistochemical analyses and alteration of α-catenin expression was defined as abnormal non-membranous immunostaining in gastric carcinoma cells. In the present study, using a different approach, we found that mRNA expression of α-catenin was lost or downregulated, compared with the adjacent normal gastric mucosa or normal gastric tissues from healthy subjects. Of the 49 cases studied, α-catenin expression was found to be downregulated or lost in 69% of gastric carcinomas. These results suggest that alteration of α-catenin occurs at the transcription level. We found that reduced α-catenin expression did not correlate with pT category or pN category, but correlated strongly with poor differentiation grade. Thus, our results suggest that α-catenin expression may be used as a differentiation marker. Moreover, our findings of reduced α-catenin mRNA expression in 5 of 26 tumor-free gastric mucosae suggest that changes in α-catenin expression may be an early event in gastric carcinoma.

It has been accepted that patients infected with *H pylori* undergo up to ninefold greater risk of developing gastric carcinoma and several groups have reported that *H pylori* infection leads to enhanced cell proliferation and diminished apoptosis of the gastric mucosa and both these features are common in the process of malignant transformation. Terres *et al*[41], reported that *H pylori*-infected individuals exhibited downregulation of E-cadherin expression. Furthermore, Yu *et al*[42], have previously shown that loss or downregulation of α-catenin mRNA in the gastric mucosa is associated with *H pylori* infection. However, in this study, there was no statistically significant correlation between α-catenin expression and *H pylori* infection. Since the number of carcinoma cases in this study was small, further investigations are required.

In conclusion, loss or absence of α-catenin expression is common in gastric carcinoma, and may be an early event in gastric carcinoma. α-catenin expression may be used as a differentiation marker. Reduced α-catenin expression does not correlate with *H pylori* infection.

REFERENCES

1 **Hansson LE,** Sparen P, Nyren O. Survival in stomach cancer is improving: results of a nationwide population-based Swedish study. *Ann Surg* 1999; **230**: 162-169
2 **Sun X,** Mu R, Zhou Y, Dai X, Qiao Y, Zhang S, Huangfu X, Sun J, Li L, Lu F. 1990-1992 mortality of stomach cancer in China. *Zhonghua Zhongliu Zazhi* 2002; **24**: 4-8
3 An international association between *Helicobacter pylori* infection and gastric cancer. The EUROGAST Study Group. *Lancet* 1993; **341**: 1359-1362
4 **Hirohashi S**. Inactivation of the E-cadherin-mediated cell adhesion system in human cancers. *Am J Pathol* 1998; **153**: 333-339
5 **Hinck L,** Nathke IS, Papkoff J, Nelson WJ. Dynamics of cadherin/catenin complex formation: novel protein interactions and pathways of complex assembly. *J Cell Biol* 1994; **125**: 1327-1340
6 **Kintner C.** Regulation of embryonic cell adhesion by the cadherin cytoplasmic domain. *Cell* 1992; **69**: 225-236
7 **Takeichi M.** Cadherin cell adhesion receptors as a morphogenetic regulator. *Science* 1991; **251**: 1451-1455
8 **Jawhari A,** Farthing M, Pignatelli M. The importance of the E-cadherin-catenin complex in the maintenance of intestinal epithelial homoeostasis: more than intercellular glue? *Gut* 1997; **41**: 581-584
9 **Berx G,** Van Roy F. The E-cadherin/catenin complex: an important gatekeeper in breast cancer tumorigenesis and malignant progression. *Breast Cancer Res* 2001; **3**: 289-293
10 **Shiozaki H,** Oka H, Inoue M, Tamura S, Monden M. E-cadherin mediated adhesion system in cancer cells. *Cancer* 1996; **77**: 1605-1613
11 **Krishnadath KK,** Tilanus HW, van Blankenstein M, Hop WC, Kremers ED, Dinjens WN, Bosman FT. Reduced expres-

sion of the cadherin-catenin complex in oesophageal adenocarcinoma correlates with poor prognosis. *J Pathol* 1997; **182**: 331-338
12 **Chan AO,** Lam SK, Chu KM, Lam CM, Kwok E, Leung SY, Yuen ST, Law SY, Hui WM, Lai KC, Wong CY, Hu HC, Lai CL, Wong J. Soluble E-cadherin is a valid prognostic marker in gastric carcinoma. *Gut* 2001; **48**: 808-811
13 **Popov Z,** Gil-Diez de Medina S, Lefrere-Belda MA, Hoznek A, Bastuji-Garin S, Abbou CC, Thiery JP, Radvanyi F, Chopin DK. Low E-cadherin expression in bladder cancer at the transcriptional and protein level provides prognostic information. *Br J Cancer* 2000; **83**: 209-214
14 **Kennedy BJ.** The unified international gastric cancer staging classification. *Scand J Gastroenterol* 1987; **22**: 11-13
15 **Kajitani T.** The general rules for the gastric cancer study in surgery and pathology. Part I. Clinical classification. *Jpn J Surg* 1981; **11**: 127-139
16 **Jawhari A,** Jordan S, Poole S, Browne P, Pignatelli M, Farthing MJ. Abnormal immunoreactivity of the E-cadherin-catenin complex in gastric carcinoma: relationship with patient survival. *Gastroenterology* 1997; **112**: 46-54
17 **Ohene-Abuakwa Y,** Noda M, Perenyi M, Kobayashi N, Kashima K, Hattori T, Pignatelli M. Expression of the E-cadherin/catenin (alpha-, beta-, and gamma-) complex correlates with the macroscopic appearance of early gastric cancer. *J Pathol* 2000; **192**: 433-439
18 **Pignatelli M,** Vessey CJ. Adhesion molecules: novel molecular tools in tumor pathology. *Hum Pathol* 1994; **25**: 849-856
19 **Lee JH,** Koh JT, Shin BA, Ahn KY, Roh JH, Kim YJ, Kim KK. Comparative study of angiostatic and anti-invasive gene expressions as prognostic factors in gastric cancer. *Int J Oncol* 2001; **18**: 355-361
20 **Machado JC,** Soares P, Carneiro F, Rocha A, Beck S, Blin N, Berx G, Sobrinho-Simoes M. E-cadherin gene mutations provide a genetic basis for the phenotypic divergence of mixed gastric carcinomas. *Lab Invest* 1999; **79**: 459-465
21 **Frixen UH,** Behrens J, Sachs M, Eberle G, Voss B, Warda A, Lochner D, Birchmeier W. E-cadherin-mediated cell-cell adhesion prevents invasiveness of human carcinoma cells. *J Cell Biol* 1991; **113**: 173-185
22 **Vleminckx K,** Vakaet L, Mareel M, Fiers W, van Roy F. Genetic manipulation of E-cadherin expression by epithelial tumor cells reveals an invasion suppressor role. *Cell* 1991; **66**: 107-119
23 **Fukudome Y,** Yanagihara K, Takeichi M, Ito F, Shibamoto S. Characterization of a mutant E-cadherin protein encoded by a mutant gene frequently seen in diffuse-type human gastric carcinoma. *Int J Cancer* 2000; **88**: 579-583
24 **Chun YS,** Lindor NM, Smyrk TC, Petersen BT, Burgart LJ, Guilford PJ, Donohue JH. Germline E-cadherin gene mutations: is prophylactic total gastrectomy indicated? *Cancer* 2001; **92**: 181-187
25 **Zheng ZH,** Sun XJ, Qiu GR, Liu YH, Wang MX, Sun KL. E-cadherin gene mutation in precancerous condition, early and advanced stages of gastric cancer. *Shijie Huaren Xiaohua Zazhi* 2002; **10**: 153-156
26 **Shimoyama Y,** Nagafuchi A, Fujita S, Gotoh M, Takeichi M, Tsukita S, Hirohashi S. Cadherin dysfunction in a human cancer cell line: possible involvement of loss of alpha-catenin expression in reduced cell-cell adhesiveness. *Cancer Res* 1992; **52**: 5770-5774
27 **Becker KF,** Atkinson MJ, Reich U, Becker I, Nekarda H, Siewert JR, Hofler H. E-cadherin gene mutations provide clues to diffuse type gastric carcinomas. *Cancer Res* 1994; **54**: 3845-3852
28 **Machado J,** Carneiro F, Sobrinho-Simoes M. E-cadherin mutations in gastric carcinoma. *J Pathol* 2000; **191**: 466-468
29 **Guilford P,** Hopkins J, Harraway J, McLeod M, McLeod N, Harawira P, Taite H, Scoular R, Miller A, Reeve AE. E-cadherin germline mutations in familial gastric cancer. *Nature* 1998; **392**: 402-405
30 **Tamura G,** Yin J, Wang S, Fleisher AS, Zou T, Abraham JM, Kong D, Smolinski KN, Wilson KT, James SP, Silverberg SG, Nishizuka S, Terashima M, Motoyama T, Meltzer SJ. E-Cadherin gene promoter hypermethylation in primary human gastric carcinomas. *J Natl Cancer Inst* 2000; **92**: 569-573
31 **Leung WK,** Yu J, Ng EK, To KF, Ma PK, Lee TL, Go MY, Chung SC, Sung JJ. Concurrent hypermethylation of multiple tumor-related genes in gastric carcinoma and adjacent normal tissues. *Cancer* 2001; **91**: 2294-2301
32 **Rountree MR,** Bachman KE, Baylin SB. DNMT1 binds HDAC2 and a new co-repressor, DMAP1, to form a complex at replication foci. *Nat Genet* 2000; **25**: 269-277
33 **Karatzas G,** Karayiannakis AJ, Syrigos KN, Chatzigianni E, Papanikolaou S, Simatos G, Papanikolaou D, Bogris S. Expression patterns of the E-cadherin-catenin cell-cell adhesion complex in gastric cancer. *Hepatogastroenterology* 2000; **47**: 1465-1469
34 **Joo YE,** Rew JS, Kim HS, Choi SH, Park CS, Kim SJ. Changes in the E-cadherin-catenin complex expression in early and advanced gastric cancers. *Digestion* 2001; **64**: 111-119
35 **Blok P,** Craanen ME, Dekker W, Tytgat GN. Loss of E-cadherin expression in early gastric cancer. *Histopathology* 1999; **34**: 410-415
36 **Jubb AM,** Bell SM, Quirke P. Methylation and colorectal cancer. *J Pathol* 2001; **195**: 111-134
37 **Watabe M,** Nagafuchi A, Tsukita S, Takeichi M. Induction of polarized cell-cell association and retardation of growth by activation of the E-cadherin-catenin adhesion system in a dispersed carcinoma line. *J Cell Biol* 1994; **127**: 247-256
38 **Nagafuchi A,** Takeichi M, Tsukita S. The 102 kd cadherin-associated protein: similarity to vinculin and posttranscriptional regulation of expression. *Cell* 1991; **65**: 849-857
39 **Oda T,** Kanai Y, Oyama T, Yoshiura K, Shimoyama Y, Birchmeier W, Sugimura T, Hirohashi S. E-cadherin gene mutations in human gastric carcinoma cell lines. *Proc Natl Acad Sci USA* 1994; **91**: 1858-1862
40 **Shun CT,** Wu MS, Lin MT, Chang MC, Lin JT, Chuang SM. Immunohistochemical evaluation of cadherin and catenin expression in early gastric carcinomas: correlation with clinicopathologic characteristics and *Helicobacter pylori* infection. *Oncology* 2001; **60**: 339-345
41 **Terres AM,** Pajares JM, O'Toole D, Ahern S, Kelleher D. *H pylori* infection is associated with downregulation of E-cadherin, a molecule involved in epithelial cell adhesion and proliferation control. *J Clin Pathol* 1998; **51**: 410-412
42 **Yu J,** Ebert MP, Miehlke S, Rost H, Lendeckel U, Leodolter A, Stolte M, Bayerdorffer E, Malfertheiner P. alpha-catenin expression is decreased in human gastric cancers and in the gastric mucosa of first degree relatives. *Gut* 2000; **46**: 639-644

Science Editor Wang XL and Li WZ **Language Editor** Elsevier HK

PO Box 2345, Beijing 100023, China
www.wjgnet.com
wjg@wjgnet.com

ELSEVIER

World J Gastroenterol 2005;11(22):3473-3478
World Journal of Gastroenterology ISSN 1007-9327

• *BRIEF REPORTS* •

Molecular epidemiological study on pre-X region of hepatitis B virus and identification of hepatocyte proteins interacting with whole-X protein by yeast two-hybrid

Qian Yang, Jun Cheng, Jing Dong, Jian Zhang, Shu-Lin Zhang

Qian Yang, Shu-Lin Zhang, Department of Infectious Diseases, The Second Hospital of Xi'an Jiaotong University, Xi'an 710004, Shaanxi Province, China
Jun Cheng, Jing Dong, Jian Zhang, Gene Therapy Research Center, Institute of Infectious Diseases, the 302 Hospital of PLA, 100 Xisihuanzhong Road, Beijing 100039, China
Supported by the grants from the National Natural Science Foundation, No. C03011402, No. C30070690; and the 9.5 Research and Technique Foundation of PLA, No. 98D063; and the Launching Foundation for Student Studying Abroad of PLA, No. 98H038; and the 10.5 Youth Research and Technique Foundation of PLA, No. 01Q138 and No. 01MB135
Correspondence to: Dr. Jun Cheng, Gene Therapy Research Center, Institute of Infectious Diseases, the 302 Hospital of PLA, 100 Xisihuanzhong Road, Beijing 100039, China. cj@genetherapy.com.cn
Telephone: +86-10-66933391 Fax: +86-10-63801283
Received: 2004-07-12 Accepted: 2004-08-30

Abstract

AIM: To identify the pre-X region in hepatitis B virus (HBV) genome and to study the relationship between the genotype and the pre-X region. To investigate the biological function of whole-X (pre-X plus X) protein, we performed yeast two-hybrid to screen proteins in liver interacting with whole-X protein.

METHODS: The pre-X region of HBV was amplified by polymerase chain reaction (PCR) method, and was cloned to pGEM Teasy vector. After the target region was sequenced, Vector 8.0 software was used to analyze the sequences. The whole-X bait plasmid was constructed by using yeast two-hybrid system 3. Yeast strain AH109 was transformed. After expression of the whole-X protein in AH109 yeast strains was proved, yeast two-hybrid screening was performed by mating AH109 with Y187 containing liver cDNA library plasmid. The mated yeast was plated on quadruple dropout medium and assayed for α-gal activity. The interaction between whole-X protein and the protein obtained from positive colonies was further confirmed by repeating yeast two-hybrid. After extracting and sequencing of plasmid from blue colonies, we carried out analysis by bioinformatics.

RESULTS: After sequencing, 27 of 45 clones (60%) were found encoding the pre-X peptide. Eighteen of twenty-seven clones (66.7%) of pre-X coding sequences were found from genotype C. Five positive colonies that interacted with whole-X protein were obtained and sequenced; namely, fetuin B, UDP glycosyltransferase 1 family-polypeptide A9, mannose-P-dolichol utilization defect 1, fibrinogen-B beta polypeptide, transmembrane 4 superfamily member 4-CD81 (TM4SF4).

CONCLUSION: The pre-X gene exists in HBV genome. Genes of proteins interacting with whole-X protein in hepatocytes were successfully cloned. These results brought some new clues for studying the biological functions of whole-X protein.

Key words: Pre-X; Hepatitis B virus; Molecular epidemiology; Yeast two-hybrid

Yang Q, Cheng J, Dong J, Zhang J, Zhang SL. Molecular epidemiological study on pre-X region of hepatitis B virus and identification of hepatocyte proteins interacting with whole-X protein by yeast two-hybrid. *World J Gastroenterol* 2005; 11(22): 3473-3478
http://www.wjgnet.com/1007-9327/11/3473.asp

INTRODUCTION

Hepatitis B virus (HBV) predominantly infects host hepatocytes and causes a spectrum of pathological processes, ranging from occult infection to the later development of primary liver cancer[1,2]. HBV genomes have a compact genetic organization with four open reading frames (ORFs) as P, X, S, and C corresponding to the polymerase, the X protein, the S including pre-S, and the nucleocapsid/HBeAg proteins, respectively. The P gene covers more than 70% of the complete genome and overlaps the entire pre-S and S-genes and the X and core genes partially[3,4]. pX is likely to be an important regulatory protein since its sequence is conserved among the mammalian hepadnaviridae members. pX increases HBV transcription by trans-activating the viral enhancer-I via the sequence named the E-element. HBx deregulates cell cycle checkpoints and stimulates DNA synthesis, leading to the proliferation of quiescent fibroblasts. Importantly, HBx is a moderate but broad-acting transcriptional transactivator and activates a variety of cellular and viral genes, including proto-oncogenes, such as *c-myc*, *c-fos*, and *c-jun*. However, little is known about the exact role of HBx in tumorigenesis[5-7].

Some of the reported HBV sequences have an additional in-frame initiation codon, ATG, 56 nucleotide triplets upstream of X gene's ATG. In our study on molecular epidemiological features of HBV genome, the ORF named pre-X region was found[8,9]. The pre-X gene can be translated with X gene in

frame. The pre-X plus X gene, named whole-X gene, is 630 bp long and the whole-X polypeptide encoded by this gene comprises 210 amino acids. In order to further reveal the biological roles of whole-X protein, we therefore tried to identify its associated proteins in the present study by the GAL4-based yeast two-hybrid system using the full-length whole-X cDNA as a bait to screen the human fetal liver cDNA library.

MATERIALS AND METHODS

Yeast strains

Matchmaker GAL4 two-hybrid system 3 and vector pACT2 containing the human liver cDNA library were obtained from Clontech Co., USA. Yeast strain AH109 (MATa, trp 1-901, leu2-3, 112, ura 3-52, his3-200, gal4, gal80, LYS2::GAL1UAS-GAL1TATA-HIS3, GAL2UAS-GAL2TATA-ADE2 URA3::MEL1TATA-lacZ MEL1) contains pGBKT7-53, coding for DNA-BD/mouse p53 fusing protein. Yeast strain Y187Y187 (MATa ura3-52, his3-200, Ade2-101, trp1-901, leu2-3, 112, gal4, gal80, met-, URA3::GAL1UAS-GAL1TATA-lacZ MEL1) contains pTD1-1, in which pACT2 coding for AD/SV40 large T antigen fusing protein. AH109 was used for cloning of bait plasmids and Y187 was used for cloning of library plasmids. Yeast-*Escherichia coli* shuttle plasmids, pGBKT7 DNA-BD cloning plasmid, pGADT7 AD cloning plasmid, pGBKT7-53 control plasmid, pGADT7, pGBKT7-Lam control plasmid, pCL1 plasmid were obtained from Clontech Ltd Co. (K1612-1).

Chemical agents and cultural media

Taq DNA polymerase was purchased from Promega Co. T4 DNA ligase, *Eco*RI and *Bam*HI restriction endonuclease were purchased from Takara Co. *c-Myc* mAb secreted by 1-9E10.2 hybridoma (ATCC), goat anti-mouse IgG conjugated with horseradish peroxidase were from Zhongshan Company, China. Tryptone and yeast extracts from OXOID. X-a-Gal and cultural media: YPDA, SD/-Trp SD/-Leu, SD/-Trp/-Leu, SD/-Trp/-Leu/-His, SD/-Trp/-Leu/-His/-Ade from Clontech Ltd Co.

Amplification and sequences of the pre-X region of HBV

DNA was extracted from serum of 17 patients with chronic hepatitis B. The extracted DNA was mixed with polymerase chain reaction (PCR) mixture containing the primers: sense 5'- CCA AGT GTT TGC TGA CGC AAC C', antisense 5'-GGA TCC AGT TGG CAG CAC ACC-3'. The PCR product was cloned with pGEM-T vector (Promega Co.). The primary structure of insert was confirmed by direct sequencing[10,11].

Plasmid constructs

The full-length whole-X gene of HBV was cloned into the yeast two-hybrid BD vector using a *Bam*HI and *Eco*RI, which could facilitate expression of DNA binding domain, *c-myc* and whole-X fusion protein. The construction was verified by restriction digestion and sequencing (Figure 1).

```
31                                                                                                  130

F296-1 C        ATGGGGCTTGGCCATTGGCCATCAGCGCATGCGTGGAACCTTTGTGGCTCCTCTGCCGATCCATACTGCGGAACTCC
                TTGCAGCTTGTTTTGCTCGCAGC
F296-4 C        ----------------------------------------------------------------------------------------
F296-5 C        ----------------------------------------------------------------------------------------
F298-1 C        C---------------------------------------------------------------------------------------
F298-2 C        ----------------------------------------------------------------------------------------
F298-3 C        ----------------------------------------------------------------------------------------
F298-5 C        ----------------------------------------------------------------------------------------
F299-1 C        C---------------------------------------------------------------------------------------
F299-2 C        C---------------------------------------------------------------------------------------
F300-1 B/C      C---------------------------------------------------------------------------------------
F300-2 B/C      C---------------------------------------------------------------------------------------
F300-4 B/C      C---------------------------------------------------------------------------------------
F325-2 B        T---------------------------------------------------------------------------------------
F325-3 B        T---------------------------------------------------------------------------------------
F325-4 B        T---------------------------------------------------------------------------------------
F325-6 B        T---------------------------------------------------------------------------------------
F326-1 C        ----------------------------------------------------------------------------------------
F326-2 C        ----------------------------------------------------------------------------------------
F326-4 C        ----------------------------------------------------------------------------------------
F326-6 C        ----------------------------------------------------------------------------------------
F327-1 C        T---------------------------------------------------------------------------------------
F327-2 C        T---------------------------------------------------------------------------------------
Y931-2 B        ----------------------------------------------------------------------------------------
Y931-3 B        ----------------------------------------------------------------------------------------
Y933-1 B        T---------------------------------------------------------------------------------------
Y933-2 B        T---------------------------------------------------------------------------------------
Y940-4 C        ----------------------------------------------------------------------------------------
Y942-3 C        ----------------------------------------------------------------------------------------
```

```
Y943-1 A        T----------------------------------------------------------------------------------------
Y947-2 C        ----------------------------------------------------------------------------------------
Y947-3 C        ----------------------------------------------------------------------------------------
Y949-2 C        ----------------------------------------------------------------------------------------
Y949-3 C        ----------------------------------------------------------------------------------------
Y949-4 C        ----------------------------------------------------------------------------------------
Y949-5 C        ----------------------------------------------------------------------------------------
Y982-1 B/C      ----------------------------------------------------------------------------------------
Y982-3 B/C      ----------------------------------------------------------------------------------------
Y982-4 B/C      ----------------------------------------------------------------------------------------
Y982-5 B/C      ----------------------------------------------------------------------------------------
Y982-6 B/C      ----------------------------------------------------------------------------------------
Y983-2 B/C      ----------------------------------------------------------------------------------------
Y983-3 B/C      ----------------------------------------------------------------------------------------
Y985-2 C        ----------------------------------------------------------------------------------------
Y985-3 C        ---------------------------------------------------------------------------------------
Y985-6 C        ---------------------------------------------------------------------------------------
Consensus       ATGGGGCTTGGCCATAGGCCATCGGCGCATGCGTGGAACCTTTGTGGCTCCTCTGCCGATCCATACTGCGGAACTCC
                TAGCAGCTTGTTTTGCTCGCAGC

                131                                                                        198
F296-1 C        CGGTCTGGGGCAAACCTTATCGGAACTGACAACTCTGTTGTCCTCTCTCGGAAATACACCTCCTTTCC
F296-4 C        ----------------------------------------T---------------------------
F296-5 C        ----------------------------------------T---------------------------
F298-1 C        ----------------------------------------CGA-------------------------
F298-2 C        ----------------------------------------------------------------------
F298-3 C        ----------------------------------------------------------------------
F298-5 C        ----------------------------------------------------------------------
F299-1 C        ----------------------------------------------------------------------
F299-2 C        ----------------------------------------------------------------------
F300-1 B/C      ------------------------T---------------------------------------------
F300-2 B/C      ------------------------T---------------------------------------------
F300-4 B/C      ------------------------T---------------------------------------------
F325-2 B        -------------------------T--------------------------------------------
F325-3 B        -------------------------T--------------------------------------------
F325-4 B        -------------------------T--------------------------------------------
F325-6 B        -------------------------T--------------------------------------------
F326-1 C        ----------------------------------------------------------------------
F326-2 C        ----------------------------------------------------------------------
F326-4 C        ----------------------------------------------------------------------
F326-6 C        ----------------------------------------------------------------------
F327-1 C        ----------------------------------------------------------------------
F327-2 C        ----------------------------------------------------------------------
Y931-2 B        ----------------------------------------------------------------------
Y931-3 B        ----------------------------------------------------------------------
Y933-1 B        -------------------------T--------------------------------------------
Y933-2 B        -------------------------T--------------------------------------------
Y940-4 C        ----------------------------------------------------------------------
Y942-3 C        ----------------------------------------------------------------------
Y943-1 A        -------------------------T--------------------------------------------
Y947-2 C        ----------------------------------------------------------------------
Y947-3 C        ----------------------------------------------------------------------
Y949-2 C        ----------------------------------------------------------------------
Y949-3 C        ----------------------------------------------------------------------
Y949-4 C        ----------------------------------------------------------------------
Y949-5 C        ----------------------------------------------------------------------
Y982-1 B/C      ----------------------------------------------------------------------
Y982-3 B/C      ----------------------------------------------------------------------
Y982-4 B/C      ----------------------------------------------------------------------
```

```
Y982-5 B/C  ----------
Y982-6 B/C  ----------
Y983-2 B/C  ----------
Y983-3 B/C  ----------
Y985-2 C    ----------
Y985-3 C    ----------
Y985-6 C    ----------

Consensus  CGGTCTGGAGCAAAACTTATCGG ACCGACAACTCTGTTGTCCTCTCTCGGAAATACACCTCCTTTCC
```

Figure 1 Nucleotide sequence of the pre-X gene.

Western blot analysis

Denatured cell extracts were subjected to electrophoresis using 4-12% SDS-polyacrylamide gels and transferred to nitrocellulose membranes[14]. The membranes were blocked with 5% non-fat dry milk for 1 h and then incubated with monoclonal anti-*c-myc* antibody (Santa Cruz Biotechnology Inc., Santa Cruz, CA) for 2 h and with HRP-conjugated secondary antibody for another 1 h prior to detection of antibody reactive proteins with chemiluminescence reagent (ECL, Amersham Pharmacia Biotech).

Yeast two-hybrid screen

The screening protocol was detailed previously[12]. Yeast transformants were plated and selected on media lacking leucine, tryptophan, histidine, and adenine. After 6-18 d, the yeast colonies were transferred onto the plates containing X-a-Gal to check for expression of the MEL1 reporter gene (blue colonies).

Isolating plasmid DNA from putatively positive yeast clones and confirming the true interaction in yeast

Yeast plasmid was isolated with the lyticase method (provided by Clontech Co.) and transformed into *E. coli* strain DH5α and amplified in bacteria. Plasmids isolated from bacteria were reintroduced into yeast strain Y187, then mating experiments were carried out by mating with yeast strain AH109 containing pGBKT7-whole-X or pGBKT7-Lam. The diploid yeast was plated on media lacking leucine, tryptophan, histidine, and adenine with X-α-Gal.

Bioinformatic analysis

After the positive colonies were sequenced, the sequences were blasted with GenBank to analyze the function of the genes.

RESULTS

The pre-X gene sequencing

After sequencing, 27 of 45 clones (60%) were found encoding the pre-X peptide. Eighteen of twenty-seven clones (66.7%) of pre-X coding sequences were found from genotype C. Three types of replacement mutation led to pre-mature coding of pre-X gene. The mutation in pre-X peptide had the feature of individual mutation (Figure 1).

Expression of whole-X protein

Yeast strain AH109 transformed with pGBKT7-whole-X could stably express the fusion protein at higher level and could only grow on SD/-Trp medium (Figure 2).

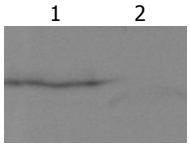

Figure 2 Expression of whole-X protein in yeast demonstrated by Western blotting. Lane 1: whole-X protein, lane 2: negative control.

Yeast two-hybrid cloning of proteins interacting with whole-X protein

The whole-X protein was used as the bait for screening a human liver yeast two-hybrid library. One hundred and twenty-six clones grew in the absence of tryptophan, leucine, histidine, adenine. The clones were processed for β-galactosidase assay, and blue colonies were picked. pACT2/cDNA plasmids were isolated and eliminated by *Eco*RI digestion (Figure 3). After elimination, 14 positive clones were further tested for specificity of β-galactosidase expression (Figure 4). After confirmation of the true interaction with whole-X protein in yeast, five independent positive clones were identified and sequenced (Figure 4).

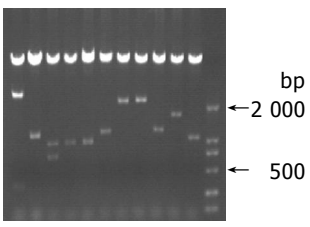

Figure 3 Colonies cut by *Eco*RI on 0.9% agarose/EtBr gel.

Analysis of coding sequence of positive clones

The nucleotide sequences of five clones from this cDNA library were analyzed[24], the full length sequences were obtained with Vector NTI 6 and by searching BLAST database (http://www.ncbi.nlm.nih.gov/). Some genes coding proteins were involved in cell cycle regulation, and apoptosis, signal transduction pathway and tumor development (Table 1).

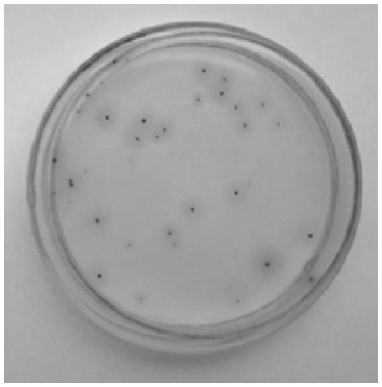

Figure 4 Positive clones interactive with the whole-X protein growing on media containing X-α-Gal and lacking leucine, tryptophan, histidine and adenine.

Table 1 Sequence analysis of five clones interacted with whole-X protein

Known genes	Number of clones	Homologous (%)
Fetuin B	4	100
UDP glycosyltransferase 1 family, polypeptide A9	2	99
Mannose-P-dolichol utilization defect 1 (MPDU1)	3	100
Fibrinogen, B beta polypeptide (FGB)	2	100
Transmembrane 4 superfamily member 4 (TM4SF4)	2	100

DISCUSSION

HBV belongs to the family of hepadnaviruses. It has a 3 200 bp partially double-stranded DNA genome from which four major classes of transcripts are synthesized. The 3.5 kb pregenomic RNA not only serves as template for reverse transcription, but also contains coding regions for nucleocapsid protein and reverse transcriptase. A subclass of this transcript with a slightly longer 59 end codes for the precore protein, which, after processing, is secreted as HBV e antigen (HBeAg). The 2.4 kb RNA encompasses the preS1 ORF that encodes the large surface (L) protein. The 2.1 kb RNA contains the preS2 and S ORFs that encode the middle (M) and small (s) surface proteins, respectively. The smallest transcript (approximately 0.9 kb) codes for the X protein. Mutations and deletions in the HBV genome have frequently been detected during persistent viral infection[13,14].

Takahashi *et al*[15], in an infected serum, have identified a protein that is coded for by the X gene of HBV, and found a polypeptide that was weakly bound with an anti-X-mAb. This result is hard to re-confirm with different sera. They sequenced the upstream region of the gene of HBV DNA from the initial sample and found that there is a pre-X ORF of 56 codons, the pre-X variant is frequently detected in chronic liver disease, but seldom in asymptomatic carriers. Another characteristic of the pre-X variant is the cancellation of in-frame stop codon, suggesting that pre-X and X are linearly translated in this variant. Loncarevic *et al*[17], reported an HBV genome that possesses an intact pre-X ORF.

In our study, 17 samples were collected. One was genotype A, 3 were genotype B, 10 were genotype C and 3 were B/C genotype mixture. After sequencing, 27 of 45 clones (60%) were found encoding the pre-X peptide. Eighteen of twenty-seven clones (66.7%) pre-X coding sequences were found from genotype C. Three types of replacement mutation lead to pre-mature coding of pre-X gene. The mutation in pre-X peptide had the feature of individual mutation, suggesting that coding of the pre-X gene is popular in HBV genome.

The pre-X mutations may have some effect on expression of the X gene. Loncarevic *et al*[17], reported that all the five HBV DNA clones derived from hepatocellular carcinoma had intact pre-X ORF. Protein–protein interactions play an important role in almost all events that takes place in cells. The two-hybrid screen is a promising experimental approach to identify whole-X protein interacting proteins.

The yeast two-hybrid system is a better choice of detecting protein-protein interactions. Yeast two-hybrid system 3 based on the system is commercially available from Clontech Co.[18-20]. In this system, the promoters controlling *HIS3, ADE2*, and *MEL1* expression in AH109 have significantly fewer false positives and the simple mating protocol significantly reduces the labor and time involved in performing a two-hybrid library screening and improves the chances of finding rare protein-protein interactions and leads to more reproducible results[21,22]. On screening a human liver cDNA library, five putative clones are identified as associated proteins, namely fetuin B, UDP glycosyltransferase 1 family-polypeptide A9, MPDU1, FGB, transmembrane 4 superfamily member 4-CD81 (TM4SF4). Mammalian transmembrane 4 superfamily (TM4SF) proteins (also known as tetraspans or tetraspanins) include at least 16 core members and a number of additional proteins with sequence similarities. Almost all mammalian cells contain one or more TM4SF proteins[23]. TM4SF protein CD81 may function in cell migration, proliferation and tumor cell metastasis. Most TM4SF proteins can be found on plasma membrane, and several are located in cell lamellipodia and lopodia, consistent with their role in cell motility. TM4SF proteins including CD81 are also found in various intracellular granules and vesicles. A specific subset of TM4SF proteins may recruit PI 4-kinase to specific membrane locations, and thereby influence phosphoinositide-dependent signaling[24]. Fetuin B is a liver-produced negative acute phase protein. Multiple physiological roles of the protein have been suggested, including ability to bind to hydroxyapatite crystals and to specifically inhibit the tyrosine kinase activity of the insulin receptor. It is mainly a fetal protein, in the sense that the highest concentrations are found in serum and body fluids of embryos and fetuses[25]. Fetuin might be involved in cell differentiation and tissue transformation during the initial histogenesis[26]. The result of this study shows that the whole-X protein may modulate signal transduction pathway by protein-protein binding and carcinoma formation.

REFERENCES

1 **Bertoletti A,** Ferrari C. Kinetics of the immune response during HBV and HCV infection. *Hepatology* 2003; **38**: 4-13

2 **Besisik F,** Karaca C, Akyuz F, Horosanli S, Onel D, Badur S, Sever MS, Danalioglu A, Demir K, Kaymakoglu S, Cakaloglu Y, Okten A. Occult HBV infection and YMDD variants in hemodialysis patients with chronic HCV infection. *J Hepatol* 2003; **38**: 506-510

3 **Bock CT,** Schwinn S, Locarnini S, Fyfe J, Manns MP, Trautwein C, Zentgraf H. Structural organization of the hepatitis B virus

minichromosome. *J Mol Biol* 2001; **307**: 183-196
4 **Sterneck M,** Kalinina T, Gunther S, Fischer L, Santantonio T, Greten H, Will H. Functional analysis of HBV genomes from patients with fulminant hepatitis. *Hepatology* 1998; **28**: 1390-1397
5 **Kim KH,** Seong BL. Pro-apoptotic function of HBV X protein is mediated by interaction with c-FLIP and enhancement of death-inducing signal. *EMBO J* 2003; **22**: 2104-2116
6 **Lee MO,** Choi YH, Shin EC, Kang HJ, Kim YM, Jeong SY, Seong JK, Yu DY, Cho H, Park JH, Kim SJ. Hepatitis B virus X protein induced expression of interleukin 18 (IL-18): a potential mechanism for liver injury caused by hepatitis B virus (HBV) infection. *J Hepatol* 2002; **37**: 380-386
7 **Hoare J,** Henkler F, Dowling JJ, Errington W, Goldin RD, Fish D, McGarvey MJ. Subcellular localisation of the X protein in HBV infected hepatocytes. *J Med Virol* 2001; **64**: 419-426
8 **Dong J,** Cheng J. Study on definition of pre-X region in hepatitis B virus genome. *Shijie Huaren Xiaohua Zazhi* 2003; **11**: 1097-1101
9 **Dong J,** Cheng J, Wang QH, Liu Y, Wang G, Shi SS, Xia XB, Shao Q, Si CW. The preliminary study on hepatitis B virus (HBV) quasispecies in patients with chronic HBV infection. *Zhonghua Chuanranbing Zazhi* 2001; **19**: 199-203
10 **Yang Q,** Dong J, Cheng J, Liu Y, Hong Y. Definition of pre-X promoter sequence from hepatitis B virus genome and characterization of it's transcription activity. *JiefangJun YiXue Zazhi* 2003; **28**: 763-765
11 **Li K,** Wang L, Cheng J, Lu YY, Zhang LX, Li L, Liu Y, Duan HJ. Expression of NS2 gene of hepatitis C virus from yeast two hybrid'Bait' vector in yeast. *Shijie Huaren Xiaohua Zazhi* 2002; **10**: 129-132
12 **Yang Q,** Cheng J, Liu Y, Hong Y, Wang JJ, Zhang SL. Cloning and analysis of genes transactivated by NS5A-TP4 protein by suppression subtractive hybridization. *Zhongxiyi Jiehe Ganbing Zazhi* 2003; **13**: 325-335
13 **Locarnini S.** Molecular virology of hepatitis B virus. *Semin Liver Dis* 2004; **24 Suppl 1**: 3-10
14 **Arad U,** Axelrod J, Ben-nun-Shaul O, Oppenheim A, Galun E. Hepatitis B virus enhances transduction of human hepatocytes by SV40-based vectors. *J Hepatol* 2004; **40**: 520-526
15 **Takahashi K,** Kishimoto S, Ohori K, Yoshizawa H, Akahane Y, Okamoto H, Mishiro S. A unique set of mutations in the "preX" region of hepatitis B virus DNA frequently found in patients but not in asymptomatic carriers: implication for a novel variant. *Int Hepatol Commun* 1995; **3**: 131-138
16 **Takahashi K,** Akahane Y, Hino K, Ohta Y, Mishiro S. Hepatitis B virus genomic sequence in the circulation of hepatocellular carcinoma patients: comparative analysis of 40 full-length isolates. *Arch Virol* 1998; **143**: 2313-2326
17 **Loncarevic IF,** Zentgraf H, Schroder CH. Sequence of a replication competent hepatitis B virus genome with a preX open reading frame. *Nucleic Acids Res* 1990; **18**: 4940
18 **Fields S,** Song O. A novel genetic system to detect protein-protein interactions. *Nature* 1989; **340**: 245-246
19 **Evangelista C,** Lockshon D, Fields S. The yeast two-hybrid system: prospects for protein linkage maps. *Trends Cell Biol* 1996; **6**: 196-199
20 **Kharel Y,** Takahashi S, Yamashita S, Koyama T. *In vivo* interaction between the human dehydrodolichyl diphosphate synthase and the Niemann-Pick C2 protein revealed by a yeast two-hybrid system. *Biochem Biophys Res Commun* 2004; **318**: 198-203
21 **Vidalain PO,** Boxem M, Ge H, Li S, Vidal M. Increasing specificity in high-throughput yeast two-hybrid experiments. *Methods* 2004; **32**: 363-370
22 **von Mering C,** Krause R, Snel B, Cornell M, Oliver SG, Fields S, Bork P. Comparative assessment of large-scale data sets of protein-protein interactions. *Nature* 2002; **417**: 399-403
23 **Fan J,** Hooker CW, McManus DP, Brindley PJ. A new member of the transmembrane 4 superfamily (TM4SF) of proteins from schistosomes, expressed by larval and adult Schistosoma japonicum. *Biochim Biophys Acta* 1997; **1329**: 18-25
24 **Hashida H,** Takabayashi A, Tokuhara T, Hattori N, Taki T, Hasegawa H, Satoh S, Kobayashi N, Yamaoka Y, Miyake M. Clinical significance of transmembrane 4 superfamily in colon cancer. *Br J Cancer* 2003; **89**: 158-167
25 **Denecke B,** Graber S, Schafer C, Heiss A, Woltje M, Jahnen-Dechent W. Tissue distribution and activity testing suggest a similar but not identical function of fetuin-B and fetuin-A. *Biochem J* 2003; **376**: 135-145
26 **Leite-Browning ML,** McCawley LJ, Choi OH, Matrisian LM, Ochieng J. Interactions of alpha2-HS-glycoprotein (fetuin) with MMP-3 and murine squamous cell carcinoma cells. *Int J Oncol* 2002; **21**: 965-971

Science Editor Wang XL and Guo SY **Language Editor** Elsevier HK

PO Box 2345, Beijing 100023, China
www.wjgnet.com
wjg@wjgnet.com

ELSEVIER

World J Gastroenterol 2005;11(22):3479-3484
World Journal of Gastroenterology ISSN 1007-9327

• *BRIEF REPORTS* •

Rat bone marrow mesenchymal stem cells differentiate into hepatocytes *in vitro*

Xin-Qin Kang, Wei-Jin Zang, Tu-Sheng Song, Xiao-Li Xu, Xiao-Jiang Yu, Dong-Ling Li, Ke-Wei Meng, Sheng-Li Wu, Zhi-Ying Zhao

Xin-Qin Kang, Wei-Jin Zang, Xiao-Li Xu, Xiao-Jiang Yu, Dong-Ling Li, Division of Cardiovascular Physiology and Pharmacology, Medical School of Xi'an Jiaotong University, Xi'an 710061, Shaanxi Province, China
Wei-Jin Zang, The Key Laboratory of Biomedical Information Engineering of Ministry of Education, School of Life Science and Technology, Xi'an Jiaotong University, Xi'an 710061, Shaanxi Province, China
Xin-Qin Kang, Tu-Sheng Song, Department of Biology, Medical School of Xi'an Jiaotong University, Xi'an 710061, Shaanxi Province, China
Ke-Wei Meng, Sheng-Li Wu, Department of Hepatobiliary Surgery, First Hospital of Xi'an Jiaotong University, Xi'an 710061, Shaanxi Province, China
Zhi-Ying Zhao, Department of Anatomy, Medical School of Xi'an Jiaotong University, Xi'an 710061, Shaanxi Province, China
Supported by the National Natural Science Foundation of China, No. 30270554 and the Doctoral Foundation of Xi'an Jiaotong University, No. DFXJTU2002-16
Correspondence to: Wei-Jin Zang, Box 77, Division of Cardiovascular Physiology and Pharmacology, Medical School of Xi'an Jiaotong University, Xi'an 710061, Shaanxi Province, China. zwj@mail.xjtu.edu.cn
Telephone: +86-29-82655003 Fax: +86-29-82655190
Received: 2004-06-29 Accepted: 2004-08-05

Abstract

AIM: To investigate the mechanism and regulation of differentiation from bone marrow mesenchymal stem cells (MSCs) into hepatocytes and to find a new source of cell types for therapies of hepatic diseases.

METHODS: MSCs were isolated by combining gradient density centrifugation with plastic adherence. The cells were cultured in osteogenic or adipogenic differentiation medium and determined by histochemical staining. MSCs were plated in plastic culture flasks that were not coated with components of extracellular matrix (ECM). When MSCs reached 70% confluence, they were cultured in low glucose Dulbecco's modified Eagle's medium supplemented with 10 mL/L fetal bovine serum, 20 ng/mL hepatocyte growth factor (HGF) and 10 ng/mL fibroblast growth factor-4 (FGF-4). The medium was changed every 3 d and stored for albumin, alpha-fetoprotein (AFP) and urea assay. Glycogen store of hepatocytes was determined by periodic acid-Schiff staining.

RESULTS: By combining gradient density centrifugation with plastic adherence, we isolated a homogeneous population of cells from rat bone marrow and differentiated them into osteocytes and adipocytes. When MSCs were cultured with FGF-4 and HGF, approximately 56.6% of cells became small round and epithelioid on d 24 by morphology. Compared with the control, levels of AFP increased significantly from d 12 to 15.5±1.4 μg/L (t = 2.31, P<0.05) in MSCs cultured with FGF-4 and HGF, and were higher (46.2±1.5 μg/L) on d 21 (t = 41.926, P<0.01), then decreased to 24.8±2.2 μg/L on d 24 (t = 10.345, P<0.01). Albumin increased significantly on d 21 (t = 3.325, P<0.01) to 1.4±0.2 μg/mL, and to 2.1±0.7 μg/mL on d 24 (t = 3.646, P<0.01). Urea (2.3±0.4 mmol/L) was first detected on d 21 (t = 6.739, P<0.01), and continued to increase to 2.6±0.9 mmol/L on d 24 (t = 4.753, P<0.01). Glycogen storage was first seen on d 21.

CONCLUSION: The method combining gradient density centrifugation with plastic adherence can isolate MSCs. Rat MSCs may be differentiated into hepatocytes by FGF-4 and HGF. Cytokines may play a more important role in differentiation from rat MSCs into hepatocytes.

Key words: Mesenchymal stem cell; Differentiation; Hepatocyte

Kang XQ, Zang WJ, Song TS, Xu XL, Yu XJ, Li DL, Meng KW, Wu SL, Zhao ZY. Rat bone marrow mesenchymal stem cells differentiate into hepatocytes *in vitro*. *World J Gastroenterol* 2005; 11(22): 3479-3484
http://www.wjgnet.com/1007-9327/11/3479.asp

INTRODUCTION

Liver transplant may be the only way to treat patients with a heavily damaged liver. However, enough livers are not available. Moreover, rejection is another problem to be solved. The characteristics and potentials of mesenchymal stem cells (MSCs) suggest that MSCs may be a better way to solve the problems. Bone marrow is a complex tissue containing two kinds of stems cells: hematopoietic stem cells (HSCs) and MSCs. MSCs are nonhematopoietic cells and serve as hematopoietic tissues. It was reported that MSCs could differentiate into mesoderm cells lineage such as osteoblasts[1-3], adipocytes[4-6], neuron and brain cells[7-10], and cardiomyocytes[11-13] *in vivo* and *in vitro*. Recent work has convincingly demonstrated that adult bone marrow contains cells capable of differentiating into liver epithelial cells *in vivo*[14-17]. As far as differentiation from MSCs into hepatocytes

in vitro is concerned, Schwartz *et al*[18], have reported that multipotent adult progenitor cells cultured on matrigel or fibronectin could differentiate into functional hepatocyte-like cells. Fiegel *et al*[19], cultured HSC on collagen matrix and differentiated them into hepatocytic cells *in vitro*. Matrigel, fibronectin, and collagen matrix are components of extracellular matrix (ECM).

Up to now, the mechanism of stem cell differentiation is unclear. Most researchers believe that microenvironment play an important role in differentiation of stem cells[20,21]. The differentiation of stem cells is regulated by microenvironment, stem cells have reciprocity with neighboring cells, ECM and cytokines. They have effects on the progress of differentiation of stem cells. It is unknown whether MSCs cultured in plastic culture flasks not coated by ECM can differentiate into hepatocytes *in vitro*.

Although there are many methods to isolate MSCs from the bone marrow, no optimal method is available. In our experiment, we used a relatively simple method, combining gradient density centrifugation with adherence, to isolate rat MSCs and cultured them in plastic culture flasks not treated by ECM. By induction of acid fibroblast growth factor-4 (FGF-4) and hepatocyte growth factor (HGF), rat MSCs could differentiate into hepatocytes *in vitro*.

MATERIALS AND METHODS

Animals and reagents

Sprague-Dawley (SD) rats were obtained from Laboratory Animal Center of Xi'an Jiaotong University. Fetal bovine serum (FBS) was purchased from Hangzhou Sijiqing Biological Engineering Material Co. Ltd. Albumin RIA kit and alpha-fetoprotein RIA kit were purchased from Beijing Atom High-tech Co. Ltd. Low glucose Dulbecco's modified Eagle's medium containing 1 g/L glucose (DMEM-LG) was purchased from GIBCO. Bovine insulin, 1-methyl-3-isobutylxamthine, indomethacin, dexamethasone and ascorbic acid-2-phosphate were purchased from Sigma-Aldrich. β-Glycerophosphate was purchased from Fulke. Acid FGF-4 and HGF were purchased from R&D Systems, Inc. Plastic cell culture flasks (25 cm^2) were purchased from Corning Incorporated (Coster®, USA).

Isolation and culture of mesenchymal stem cells from rat bone marrow

SD rats were killed by knocking at their heads, then put into 750 mL/L alcohol for 15 min. We took the femur, tibia ulna, a total of four bones from one rat. Muscles on the bones were taken out as clean as possible. Medullary cavities of bones were washed with DMEM-LG. The DMEM-LG containing cells were layered over an equal volume of Percoll solution (1.073 g/mL). Mononuclear cells (MNCs) were recovered from the gradient interface and washed with PBS after centrifugation at 900 r/min for 30 min. The MNCs were suspended in 5 mL DMEM-LG supplemented with 100 mL/L FBS, 100 U/mL penicillin, 100 U/mL streptomycin, at last plated in 25-cm^2 plastic cell culture flasks at the density of 10^6/mL. The cells were maintained at 37 ℃ in 50 mL/L CO_2 in fully humidified air. In the following 3 d, the medium was changed every day and then every 3 or 4 d.

Induction of multilineage differentiation

Cultured cells were harvested from the culture bottles with 0.25 g/L trypsin. Cultured cells at passage 2 were seeded in six-well cell culture clusters. When the cells grew at 70% confluence, they were still cultured in DMEM-LG supplemented with 100 mL/L FBS (as a control) or treated in osteogenic differentiation medium or adipogenic differentiation medium, respectively. Osteogenic differentiation medium: DMEM-LG supplemented with 100 mL/L FBS, 50 μg/mL ascorbate acid-2-phosphate, 10^{-8} mol/L dexamethasone and 10 mmol/L β-glycerophosphate. Adipogenic differentiation medium: DMEM-LG supplemented with 10 mL/L FBS, 1 μmol/L dexamethasone, 10 μg/mL bovine insulin, 0.25 mmol/L 1-methyl-3-isobutylxamthine and 100 μmol/L indomethacin. The medium was changed every 4 d, and cells were used for histochemical staining after the completion of differentiation identified by morphology.

Hepatocyte differentiation

The cultured cells at passage 2 were seeded in the plastic culture flasks at 5×10^5/bottle. When the cells grew at 70% confluence, the control group was continuously cultured in DMEM-LG supplemented with 10 mL/L FBS, 100 U/mL penicillin, 100 U/mL streptomycin. The hepatocyte differentiation group was cultured in DMEM-LG supplemented with 10 mL/L FBS, 20 ng/mL HGF, 10 ng/mL FGF-4, 100 U/mL penicillin and 100 U/mL streptomycin. Each flask was added with 5 mL medium, and changed every 3 d. The medium was stored at -20 ℃ for albumin, alpha-fetoprotein (AFP) and urea assay.

Radioimmunoassay

Concentrations of AFP and albumin in the changed medium were determined by radioimmunoassay on d 3, 6, 9, 12, 15, 18, 21, and 24. It was considered that there might be a very small amount of AFP and albumin in the changed medium. So we condensed the medium five times before radioimmunoassay.

Urea assay

Urea concentrations were determined by colorimetric assay. The control group was used as a negative control, which was cultured in DMEM-LG supplemented with 10 mL/L FBS, 100 U/mL penicillin and 100 U/mL streptomycin. The method could detect the urea at least 10 mmol/L.

Periodic acid-Schiff treatment for glycogen

In the hepatocyte differentiation group, on days 18, 21, and 24, we took out the medium from the flasks, rinsed cells with PBS thrice, fixed them with 100 mL/L formaldehyde for 30 min. The cells were oxidized in 10 g/L periodic acid for 10 min and rinsed thrice in dH_2O. Afterwards, cells were treated with Schiff's reagent for 10 min, rinsed in dH_2O for 10 min, stained with hematoxylin for 2 min, differentiated by 1% alcohol-HCl, and rinsed in dH_2O again, observed under an invert microscope.

Statistical analysis

The data of AFP, albumin and urea were expressed as

mean±SE. The results were analyzed by *t*-test. $P<0.05$ was considered statistically significant.

RESULTS

Isolation and culture of mesenchymal stem cells from rat bone marrow

The cells isolated by gradient density centrifugation showed heterogeneity during the first 3 d. The adherent cells were observed on d 1-2. The spindle-shaped cells appeared at the bottom of culture flasks. Many round cells were suspended in the medium. By continuous changes of medium, the suspending cells became less and less. When the medium was changed thrice, the suspending cells were completely removed from the medium. The adhered cells were fibroblast-like and grew as a whirlpool. The sub-cultured cells were much pure and fibroblast-like (Figure 1A). The primary culture cells reached confluence 10-12 d later, the cells sub-cultured at a ratio of 1:3 reached confluence 8-10 d later.

Induction of multilineage differentiation

The cells at passage 2 were cultured in DMEM-LG supplemented with 10 mL/L FBS. When the cells grew at 70% confluence, they were treated with or without (control) 50 μg/mL of ascorbate-2 phosphate, 10^{-8} mol/L of dexamethasone, and 10 mmol/L of β-glycerophosphate. Osteogenic differentiation was attained on d 21 following the treatment. Under the influence of these reagents, approximately 37.5% of the cells formed alkaline phosphatase-positive aggregates (Figure 1B) or von Kossa stain-positive nodules, while the controls did not, suggesting that rat MSCs differentiated into osteocytes. Under the influence of 1 μmol/L dexamethasone, 10 μg/mL bovine insulin, and 0.25 mmol/L 1-methyl-3-isobutylxamthine, the isolated mesenchymal cells formed oil red-O-positive cells on the 3rd d after treatment, while the controls did not. If the lipid droplet appeared in cytoplasm of adipocytes, oil red O would specifically stain them. Six days after treatment, approximately 90.33% of the cells induced adipocytes and reached confluence (Figure 1C).

Mesenchymal stem cells became small round and epithelioid when cultured with FGF-4 and HGF

When the cultured cells reached 70% confluence, they were treated with hepatocyte differentiation medium. The medium contained DMEM-LG supplemented with 10 mL/L FBS, 20 ng/mL HGF, and 10 ng/mL FGF-4, 100 U/mL penicillin and 100 U/mL streptomycin. Before the 6-d treatment they did not show any changes compared with the controls. After treatment, the small round cells appeared in the treatment group, epithelioid cells were also observed. The diameter of the cells was 10-16 μm. On d 24, approximately 56.6% of cells were small round and epithelioid. The control cells were still fibroblast-like, the density of cells was increased. The cells were overlapped in some regions.

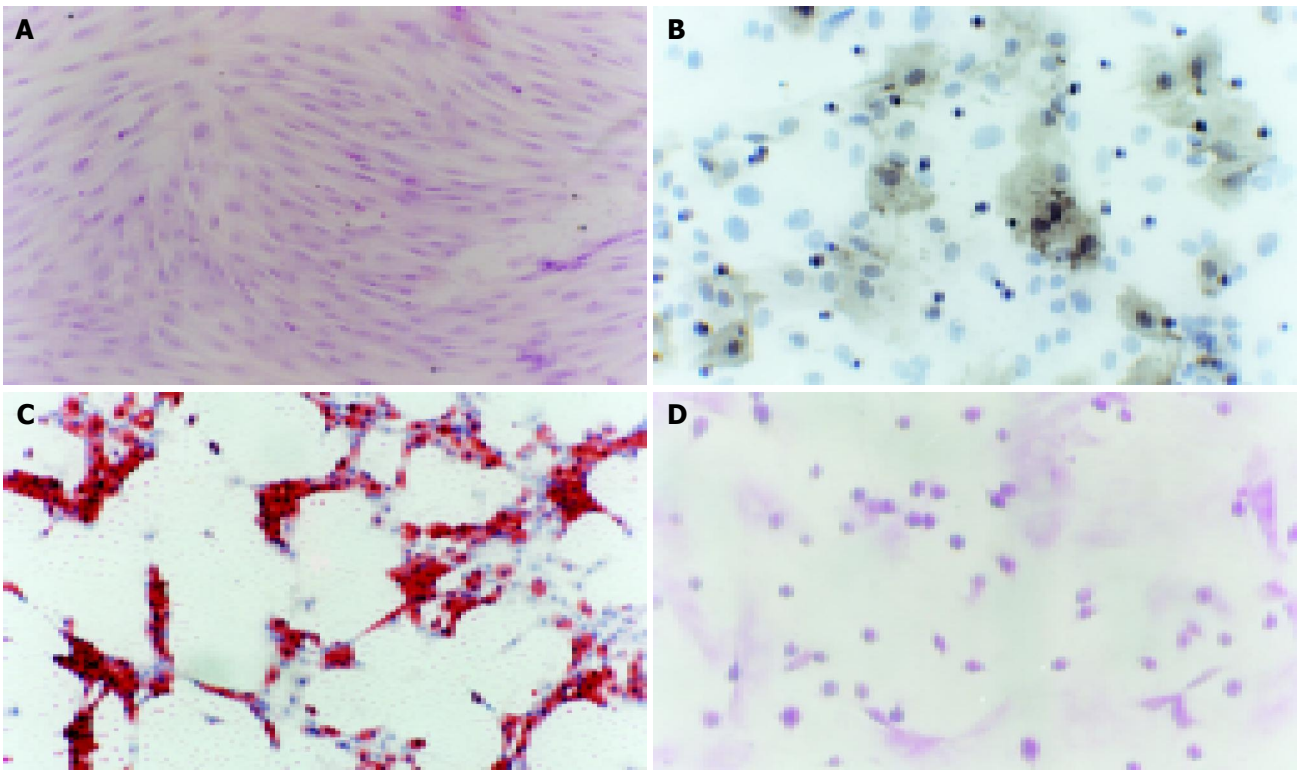

Figure 1 Different morphology and differentiation of rat MSCs. **A**: Morphology of rat MSCs stained with HE. The cells were fibroblast-like and grew as a whirlpool (×100); **B**: Appearance of osteocytes 21 d after induction. The positive cells were observed by stain for alkaline phosphatase. The gray parts were cytoplasm stained for alkaline phosphatase. The cells differentiated MSCs into osteocytes. The blue ones were nuclei stained with hematoxylin (×400); **C**: Oil red-O positive cells 6 d after adipogenic differentiation of rat MSCs. The red parts were lipid-rich vacuoles, the blue ones were nuclei stained with hematoxylin (×100); **D**: Cells stained by PAS. Glycogen storage was seen as accumulated magenta staining. The small round cells and epithelioid cells had magenta staining in the region (×200).

Radioimmunoassay

By radioimmunoassay, albumin and AFP production was measured at various time points throughout the differentiation. On undifferentiated rat MSCs we could detect low levels of AFP, but not albumin. However, there was a small amount of albumin in the medium. It was hardly detected by albumin RIA assay. Compared with controls, the levels of AFP increased significantly from d 12 with a concentration of 15.5±1.4 μg/L (P<0.05) in MSCs cultured with FGF-4, and HGF continued to increase and was higher on d 21 (P<0.01) with a concentration of 46.2±1.5 μg/L, then decreased to 24.8±2.2 μg/L on d 24 (P<0.01). The level of albumin could not be detected by radioimmunoassay before d 12, albumin increased significantly on d 21 with a concentration of 1.4±0.2 μg/mL (P<0.01), and 2.1±0.7 μg/mL on day 24 (P<0.01). According to the data, increasing time points were different between AFP and albumin (Table 1).

Urea assay

Urea production and secretion by hepatocytes were detected at various time points throughout differentiation. Following treatment with FGF-4 and HGF, urea produced by MSCs was detected with a concentration of 2.3±0.4 mmol/L on d 21, and 2.6±0.9 mmol/L on d 24 (Table 1).

Periodic acid-Schiff treatment for glycogen

We analyzed the levels of glycogen storage by periodic acid-Schiff (PAS) staining of FGF-4 and HGF induced MSCs on d 18, 21, and 24. Glycogen storage was first seen on d 21, positively stained for PAS (Figure 1D).

DISCUSSION

In our present study, we used the method combining gradient density centrifugation with plastic adherence to isolate MSCs from rat bone marrow. By the primary induction of multilineage differentiation, the isolated cells satisfied the characteristics of MSCs. Moreover, we cultured rat MSCs in culture flasks not treated by ECM and differentiated them into hepatocytes by induction of HGF and FGF-4, suggesting that cytokines played a most important role in differentiation from rat MSCs into hepatocytes.

There are many methods to isolate bone marrow MSCs from bone marrow, including plastic adherence[22], gradient density centrifugation[23] and immunomagnetic selection[19,24]. Different methods have different defects and virtues. For example, plastic adherence can easily get stem cells on the basis of stem cell plastic adherence characteristics, but it is difficult to get pure stem cells. Gradient density centrifugation depends on the density of MNCs to separate MSCs. Immunomagnetic selection uses the receptors and antigens of MSC. Other methods have also been used to isolate MSCs[25-28], but no one is optimal. In this study we used the Percoll (1.073 g/mL) to isolate MSCs from the bone marrow. After centrifugation, we found many suspended cells in the medium for 72 h. It might be due to the density of cells which was slightly changed in DMEM-LG. So we combined the gradient density centrifugation with plastic adherence and changed the medium thrice to purify MSCs after gradient density centrifugation. According to the results, this method is relatively simple, and can easily get pure MSCs.

MSCs have many differentiating potentials *in vivo* and *in vitro*. In order to prove what we have isolated from bone marrow was MSCs, we made the isolated cells differentiate into osteoblasts and adioblasts by induction of reagents. The isolated cells had the characteristics of MSCs, suggesting that the method combining gradient density centrifugation with plastic adherence is an ideal way to isolate rat MSCs.

During the 24 d of differentiation, FGF-4 and HGF induced MSCs into cells with morphological and functional characteristics of hepatocytes. In our study, the cells that were differentiated into hepatocyte-like cells could produce urea, secrete albumin and AFP, and store glycogens. Urea production was characterized by hepatocyte activity, although kidney tubular epithelium also produced urea. In contrast, albumin and AFP production is a specific test for the presence and metabolic activity of hepatocytes. Only hepatocytes can generate and store glycogens. In our research, we found that AFP could be detected throughout the differentiation, because the medium contained a low level of AFP. From d 12, the level of AFP increased significantly compared with controls, suggesting that MSCs began to secrete AFP. It was reported that AFP was produced by immature hepatocytes. That is to say, the hepatocytes were immature on d 12 and 15. Before d 12, the concentration of albumin could not be measured by radioimmunoassay because there was a much small amount of albumin in the medium. When MSCs differentiated, albumin was significantly

Table 1 Concentration of AFP, albumin and urea in the medium at different time points (mean±SE)

Group	3 d	6 d	9 d	12 d	15 d	18 d	21 d	24 d
AFP (μg/L)								
Differentiation	12.1±1.2	11.7±0.8	14.4±2.1	15.5±1.4[a]	24.5±2.9[b]	25.9±3.0[b]	46.2±1.5[b]	24.8±2.2[b]
Control	11.5±0.9	11.6±1.2	12.6±2.4	13.4±1.9	12.8±1.5	14.0±0.7	12.9±1.3	11.1±2.4
Albumin (μg/mL)								
Differentiation	–	–	–	–	0.5±0.4	0.8±0.6	1.4±0.2[b]	2.1±0.7[b]
Control	–	–	–	–	–	0.7±0.6	0.6±0.5	0.6±0.7
Urea (mmol/L)								
Differentiation	–	–	–	–	–	–	2.3±0.4[b]	2.6±0.9[b]
Control	–	–	–	–	–	–	0.6±0.5	0.5±0.5

[a]P<0.05 *vs* control, [b]P<0.01 *vs* control, – stands for what could not detected, n = 6.

secreted by MSCs from d 21, and urea was also significantly secreted from d 21. By PAS staining, the differentiated cells could store glycogens. The data suggest that rat MSCs can be differentiated into hepatocytes by induction of FGF-4 and HGF.

Some researchers believe that microenvironment played an important role in differentiation of stem cells[20,21]. The differentiation of stem cells is controlled under microenvironment. Stem cells have reciprocity with adjacent cells, ECM and cytokines. They also have effects on differentiation of stem cells. Schwartz *et al*[18], and Fiegel *et al*[19], plated marrow stem cells on matrigel, fibronectin or collagen matrix and differentiated them into hepatocyte-like cells. Matrigel consists of a mixture of ECM components. Fibronectin and collagen matrix are two of ECM components. But in our experiment, we cultured MSCs in plastic culture flasks not treated with matrigel or fibronectin. However, MSCs still differentiated into hepatocytes, suggesting that it is not important to culture MSCs on whatever materials *in vitro*. Maybe, cytokines play a most important role in differentiating rat MSCs into hepatocytes. It seemed that the ECM could potentially modulate the local concentration of cytokines and cytokines could regulate stem cell proliferation and differentiation. After being cultured with HGF, adult human MSCs could also differentiate into hepatocytes *in vitro*[19]. HGF was first identified as a blood-derived mitogen for hepatocytes. HGF and its receptor c-Met are the key factors for liver growth and function. FGF-4 is mitogenic for fibroblasts and endothelial cells. Mouse embryonic stem cells grown in medium supplemented with FGF-4 could differentiate into cells expressing hepatocyte-specific genes and antigens[29]. By co-operation of HGF and FGF, the differentiation of MSCs was triggered and MSCs developed into hepatocytes.

MSCs could be isolated, expanded, and maintained *in vitro* in an undifferentiated state for more than 100 population doublings[30], and differentiate into hepatocytes. The finding may make MSCs as ideal cells for *in vivo* therapy of genetic or acquired disorders of the liver and for use in bioartificial liver devices. Moreover, MSCs might be used as a new potential therapeutic modality for severe acute pancreatitis. We hope that marrow MSCs will play a more important role in therapy of liver diseases in the future.

REFERENCES

1 **Chen TL,** Shen WJ, Kraemer FB. Human BMP-7/OP-1 induces the growth and differentiation of adipocytes and osteoblasts in bone marrow stromal cell cultures. *J Cell Biochem* 2001; **82**: 187-199

2 **Ahdjoudj S,** Lasmoles F, Oyajobi BO, Lomri A, Delannoy P, Marie PJ. Reciprocal control of osteoblast/chondroblast and osteoblast/adipocyte differentiation of multipotential clonal human marrow stromal F/STRO-1(+) cells. *J Cell Biochem* 2001; **81**: 23-38

3 **Atmani H,** Chappard D, Basle MF. Proliferation and differentiation of osteoblasts and adipocytes in rat bone marrow stromal cell cultures: effects of dexamethasone and calcitriol. *J Cell Biochem* 2003; **89**: 364-372

4 **Allan EH,** Ho PW, Umezawa A, Hata J, Makishima F, Gillespie MT, Martin TJ. Differentiation potential of a mouse bone marrow stromal cell line. *J Cell Biochem* 2003; **90**: 158-169

5 **Atmani H,** Audrain C, Mercier L, Chappard D, Basle MF. Phenotypic effects of continuous or discontinuous treatment with dexamethasone and/or calcitriol on osteoblasts differentiated from rat bone marrow stromal cells. *J Cell Biochem* 2002; **85**: 640-650

6 **Porter RM,** Huckle WR, Goldstein AS. Effect of dexamethasone withdrawal on osteoblastic differentiation of bone marrow stromal cells. *J Cell Biochem* 2003; **90**: 13-22

7 **Wislet-Gendebien S,** Leprince P, Moonen G, Rogister B. Regulation of neural markers nestin and GFAP expression by cultivated bone marrow stromal cells. *J Cell Sci* 2003; **116**: 3295-3302

8 **Song S,** Kamath S, Mosquera D, Zigova T, Sanberg P, Vesely DL, Sanchez-Ramos J. Expression of brain natriuretic peptide by human bone marrow stromal cells. *Exp Neurol* 2004; **185**: 191-197

9 **Rismanchi N,** Floyd CL, Berman RF, Lyeth BG. Cell death and long-term maintenance of neuron-like state after differentiation of rat bone marrow stromal cells: a comparison of protocols. *Brain Res* 2003; **991**: 46-55

10 **Lou Sj,** Gu P, Chen F, He C, Wang Mw, Lu Cl. The effect of bone marrow stromal cells on neuronal differentiation of mesencephalic neural stem cells in Sprague-Dawley rats. *Brain Res* 2003; **1**: 114-121

11 **Orlic D,** Kajstura J, Chimenti S, Jakoniuk I, Anderson SM, Li B, Pickel J, McKay R, Nadal-Ginard B, Bodine DM, Leri A, Anversa P. Bone marrow cells regenerate infarcted myocardium. *Nature* 2001; **410**: 701–705

12 **Orlic D.** Adult bone marrow stem cells regenerate myocardium in ischemic heart disease. *Ann N Y Acad Sci* 2003; **996**: 152-157

13 **Jackson KA,** Majka SM, Wang H, Pocius J, Hartley CJ, Majesky MW, Entman ML, Michael LH, Hirschi KK, Goodell MA. Regeneration of ischemic cardiac muscle and vascular endothelium by adult stem cells. *J Clin Invest* 2001; **107**: 1395-1402

14 **Krause DS,** Theise ND, Collector MI, Henegariu O, Hwang S, Gardner R, Neutzel S, Sharkis SJ. Multi-organ, multi-lineage engraftment by a single bone marrow-derived stem cell. *Cell* 2001; **105**: 369-377

15 **Lagasse E,** Connors H, Al-Dhalimy M, Reitsma M, Dohse M, Osborne L, Wang X, Finegold M, Weissman IL, Grompe M. Purified hematopoietic stem cells can differentiate into hepatocytes *in vivo*. *Nat Med* 2000; **6**: 1229-1234

16 **Wang X,** Montini E, Al-Dhalimy M, Lagasse E, Finegold M, Grompe M. Kinetics of liver repopulation after bone marrow transplantation. *Am J Pathol* 2002; **161**: 565-574

17 **Mallet VO,** Mitchell C, Mezey E, Fabre M, Guidotti JE, Renia L, Coulombel L, Kahn A, Gilgenkrantz H. Bone marrow transplantation in mice leads to a minor population of hepatocytes that can be selectively amplified *in vivo*. *Hepatology* 2002; **35**: 799-804

18 **Schwartz RE,** Reyes M, Koodie L, Jiang Y, Blackstad M, Lund T, Lenvik T, Johnson S, Hu WS, Verfaillie CM. Multipotent adult progenitor cells from bone marrow differentiate into functional hepatocyte-like cells. *J Clin Invest* 2002; **109**: 1291-1302

19 **Fiegel HC,** Lioznov MV, Cortes-Dericks L, Lange C, Kluth D, Fehse B, Zander AR. Liver-specific gene expression in cultured human hematopoietic stem cells. *Stem Cells* 2003; **21**: 98-104

20 **Watt FM,** Hogan BL. Out of Eden: stem cells and their niches. *Science* 2000; **287**: 1427-1430

21 **Tosh D,** Slack JM. How cells change their phenotype. *Nat Rev Mol Cell Biol* 2002; **3**: 187-194

22 **Meirelles Lda S,** Nardi NB. Murine marrow-derived mesenchymal stem cell: isolation, *in vitro* expansion, and characterization. *Br J Haematol* 2003; **123**: 702-711

23 **Sheng XG,** Feng JZ, Wu S, Jin LJ, Yu XY, Zhang B. Differentiation of rabbit bone marrow mesenchymal stem cells into myogenic cells *in vitro* and expression of vascular endothelial growth factor gene after transfection. *Diyi Junyi Daxue Xuebao* 2004; **24**: 290-294

24 **Locatelli F,** Corti S, Donadoni C, Guglieri M, Capra F, Strazzer S, Salani S, Del Bo R, Fortunato F, Bordoni A, Comi GP. Neuronal differentiation of murine bone marrow Thy-1- and Sca-1-positive cells. *J Hematother Stem Cell Res* 2003; **12**: 727-734

25 **Stamm C,** Kleine HD, Westphal B, Petzsch M, Kittner C, Nienaber CA, Freund M, Steinhoff G. CABG and bone marrow stem cell transplantation after myocardial infarction. *Thorac Cardiovasc Surg* 2004; **52**: 152-158

26 **Sun S,** Guo Z, Xiao X, Liu B, Liu X, Tang PH, Mao N. Isolation of mouse marrow mesenchymal progenitors by a novel and reliable method. *Stem Cells* 2003; **21**: 527-535

27 **Hung SC,** Chen NJ, Hsieh SL, Li H, Ma HL, Lo WH. Isolation and characterization of size-sieved stem cells from human bone marrow. *Stem Cells* 2002; **20**: 249-258

28 **Quirici N,** Soligo D, Bossolasco P, Servida F, Lumini C, Deliliers GL. Isolation of bone marrow mesenchymal stem cells by anti-nerve growth factor receptor antibodies. *Exp Hematol* 2002; **30**: 783-791

29 **Ruhnke M,** Ungefroren H, Zehle G, Bader M, Kremer B, Fandrich F. Long-term culture and differentiation of rat embryonic stem cell-like cells into neuronal, glial, endothelial, and hepatic lineages. *Stem Cells* 2003; **21**: 428-436

30 **Jiang Y,** Jahagirdar BN, Reinhardt RL, Schwartz RE, Keene CD, Ortiz-Gonzalez XR, Reyes M, Lenvik T, Lund T, Blackstad M, Du J, Aldrich S, Lisberg A, Low WC, Largaespada DA, Verfaillie CM. Pluripotency of mesenchymal stem cells derived from adult marrow. *Nature* 2002; **418**: 41-49

Science Editor Wang XL and Guo SY **Language Editor** Elsevier HK

PO Box 2345, Beijing 100023, China
www.wjgnet.com
wjg@wjgnet.com

ELSEVIER

World J Gastroenterol 2005;11(22):3485-3489
World Journal of Gastroenterology ISSN 1007-9327

• *BRIEF REPORTS* •

Comparative proteome analysis of untreated and *Helicobacter pylori*-treated HepG2

Yan Zhang, Xue-Gong Fan, Ren Chen, Zhi-Qiang Xiao, Xue-Ping Feng, Xue-Fei Tian, Zhao-Hui Chen

Yan Zhang, Xue-Gong Fan, Ren Chen, Xue-Fei Tian, Department of Infectious Diseases, Xiangya Hospital, Central South University, Changsha 410008, Hunan Province, China
Zhi-Qiang Xiao, Xue-Ping Feng, Zhao-Hui Chen, Medical Research Center, Xiangya Hospital, Central South University, Changsha 410008, Hunan Province, China
Correspondence to: Xue-Gong Fan, Department of Infectious Diseases, Xiangya Hospital, Central South University, Changsha 410008, Hunan Province, China. xgfan@hotmail.com
Telephone: +86-731-4327392 Fax: +86-731-4327332
Received: 2004-07-02 Accepted: 2004-09-30

Abstract

AIM: To investigate the pathological effect of *Helicobacter pylori* (*H pylori*) on human hepatic cells, proteomic methods were used to find and to identify proteins that were overexpressed in HepG2 cells treated by *H pylori*.

METHODS: *H pylori* was co-cultured with HepG2 for 6 h. Two-dimensional gel electrophoresis was used to gain the protein expression pattern of untreated and *H pylori*-treated HepG2. After staining and image analysis, spots of interest were isolated and subjected to mass spectrometry.

RESULTS: Seven proteins, which were up-regulated in *H pylori*-treated HepG2 cells, were identified. These proteins included integrin beta-1, protein kinase C alpha, LIM/homeobox protein Lhx1, eIF-2-beta, MAP kinase kinase 3, PINCH protein and Ras-related protein Rab-37, which involved in transcription regulation, signal transduction, metabolism and so on.

CONCLUSION: *H pylori* may exert the pathological effect on HepG2 cells by up-regulating the expression of some proteins.

Key words: *H pylori*; HepG2 cells

Zhang Y, Fan XG, Chen R, Xiao ZQ, Feng XP, Tian XF, Chen ZH. Comparative proteome analysis of untreated and *Helicobacter pylori*-treated HepG2. *World J Gastroenterol* 2005; 11(22): 3485-3489
http://www.wjgnet.com/1007-9327/11/3485.asp

INTRODUCTION

Helicobacter pylori (*H pylori*) is highly associated with active and chronic gastritis as well as peptic ulcer diseases. *H pylori* is also considered to be a class I carcinogen because of its role in the development of gastric carcinoma and gastric mucosa-associated lymphoid tissue lymphoma. In addition to gastric *Helicobacter*s, *Helicobacter* species have been isolated from the intestinal tract, liver and bile ducts of animals, and they have also been found to play a pathological role in enterohepatic diseases in animals[1]. Recently, several separate research groups have detected such *Helicobacter* DNA as *H pylori*, *H bilis, Flexispira rappini* and *H pullorum* in bile, gall bladder or liver tissue obtained from patients with chronic cholecystitis, primary sclerosing cholangitis (PSC), primary biliary cirrhosis (PBC), or primary liver carcinoma[2-12]. Our previous study showed that *Helicobacter* species DNA could be found in liver tissue from 52.6% to 60% patients with primary liver carcinoma by polymerase chain reaction (PCR) using 16S rRNA primers, while none was found in control group. PCR amplicons were identified by Southern blot and sequenced, and the homology similarity was 99-100% with 16S rRNA of *H pylori*[13-15]. These reports suggested that *Helicobacter* organisms, including *H pylori*, may play a pathogenic role in the development of hepatobiliary diseases in humans. Whether *Helicobacter* spp. is an innocent bystander, cofactor or culprit, it is still under review[16].

Proteome is a new word that was proposed by Wilkins[17] to define all the different proteins occurring in an organism in space and time. Proteomics is an emerging area of research of the post-genomic era which is based on three technological platforms, high-resolution two-dimensional gel electrophoresis (2-DE), highly sensitive biological mass spectrometry (MS), and the rapidly growing protein and DNA databases. During the past few years, proteomics has been extensively applied to several fields of medicine to better understand normal physiology, to define the pathophysiology of diseases, and to identify novel biomarkers and new therapeutic targets[18]. In order to further explore the pathological effect of *H pylori* on human hepatic cells, we have employed high-throughput and high-resolution 2-DE analysis of human HepG2 cell extracts to examine protein expression patterns between untreated and *H pylori*-treated HepG2 cells, and certain differential expression proteins were identified by matrix-assisted laser desorption/ionization time of flight mass spectrometry (MALDI-TOF-MS) and database analysis. The results presented here will no doubt provide clues to study further the molecular mechanisms of pathological effect of *H pylori* on hepatic cells.

MATERIALS AND METHODS

Chemicals and materials

Immobilized pH gradient (IPG) strips as well as ImageMaster

2D Elite 3.01 software were purchased from Amersham Pharmacia Biotechnology (Uppsala, Sweden). Acrylamide and other reagents for the polyacrylamide gel preparation were from Amresco (OH, USA); urea, CHAPS, thiourea, DTT, iodoacetamide, proteomics grade trypsin, CCA and antibiotics were from Sigma (St. Louis, MO, USA); medium and fetal bovine serum (FBS) for cell culture were from Gibco-BRL (Grand Island, NY, USA).

Methods

Cell line and cell culture The human hepatic cell line HepG2 was purchased from Cell Bank of Shanghai Academy of Science. The cells were cultured in Dulbecco's Modified Eagle's medium (DMEM) supplemented with 100 mL/L FBS, 100 U/mL penicillin G, and 100 μg/mL streptomycin sulfate in an atmosphere of 50 mL/L CO_2 at 37 ℃. The cells were maintained in the logarithmic growth phase for stimulation experiment.

H pylori strains and culture

H pylori reference strain ATCC49503 (cagA$^+$, vacA s1a) was used in the experiment. The bacteria were plated onto Columbia agar containing 70 mL/L sheep blood, 10 μg/mL vancomycin, 2 μg/mL amphotericin B, and 20 μg/mL polymyxin B sulfate and incubated at 37 ℃ under microaerobic conditions[19]. After 3 d, the bacteria were harvested into 0.01 mol/L phosphate-buffer saline (PBS) and pelleted by centrifugation at 4 000 r/min for 10 min, and resuspended in antibiotic-free DMEM with 100 mL/L FBS to a concentration of 1×10^8 CFU/mL.

Co-culture of *H pylori* and HepG2 cells and protein extraction

For all experiments, *H pylori* (1×10^8 CFU) were added to HepG2 (1×10^6) at a bacteria:cells concentration of 100:1. Control cells were incubated with DMEM/100 mL/L FBS alone, and co-incubation was performed up to 6 h in triplicate. At the end of incubation, the majority of adherent bacteria were removed by several washes in ice-cold PBS. The cells were collected by trypsinization followed by centrifugation. Finally, the cells were lysed in 200 μL lysis buffer (8 mol/L urea, 2 mol/L thiourea, 40 g/L CHAPS, 40 mmol/L Tris, 65 mmol/L DTT, 5 mmol/L PMSF). The lysates were vortexed followed by incubation at room temperature for 30 min and then centrifuged at 15 000 *g* for 30 min at 4 ℃. The supernatant was transferred to a fresh tube and the concentration of the total protein was determined by the Bradford method. Aliquots were stored at -80 ℃ until use.

2-DE

2-DE was performed as described[20]. The first dimensional isoelectric focusing (IEF) was performed on precast 18-cm immobilized pH 3-10 gradient (IPG) strips at 20 ℃ using a IPGphor IEF Cell (Amersham Biosciences). Typically, 300 μg of total protein were mixed with a rehydration buffer containing 8 mol/L urea, 20 g/L CHAPS, 3 g/L DTT, 5 mL/L IPG buffer (pH 3-10) and a trace of bromophenol blue, to a total volume of 350 μL. The mixtures were loaded onto the IPG strip and focusing was carried out for 41 920 Vh. Following IEF, the gel strip was first equilibrated for 15 min in the equilibration buffer containing 50 mmol/L Tris-HCl (pH 8.8), 6 mol/L urea, 300 mL/L glycerol, 20 g/L SDS, 2 g/L DTT, and a trace of bromophenol blue. Then the gel strip was equilibrated for another in the same equilibration buffer, except that DTT was replaced with 30 g/L iodoacetamide. Second-dimensional SDS-PAGE was performed in 12.5% acrylamide gels using the ProTEAN II system (Bio-Rad) as described by manufacturer and Gorg[20]. After electrophoresis, the protein spots were visualized by silver nitrate.

Image analysis

The stained 2-DE gels were scanned with LabScan software on Imagescanner (Amersham Biosciences). ImageMaster 2D Elite 3.01 analysis software was used for spot-intensity calibration, spot detection, background abstraction, matching, and 1-D calibration. The reproducibility of spot position was calculated with Corbett's method[21]. Statistical analysis was carried out with SPSS for Windows 10.0 and Excel. To account for experimental variations, three gels were prepared for each group. The gel spot pattern of each gel was summarized in a standard after spot matching. Thus, we obtained one standard gel for each group. These standards were then matched to yield information about differences in abundance related to *H pylori* treatment (up- or downregulation of spots).

MALDI-TOF-MS

Protein spots were excised from preparative gels using biopsy punches and transferred to a 1.5-mL siliconized Eppendorf tube. Proteins were in gel digested as previously described[22]. The gel spots were destained in the destaining solution that consisted of 100 mmol/L $Na_2S_2O_3$ and 30 mmol/L $K_3Fe(CN)_6$ (V/V, 1:1). The protein-containing gel spots were reduced in the reduction buffer (100 mmol/L NH_4HCO_3 and 10 mmol/L DTT) for 1 h at 57 ℃ and then alkylated in the alkylation buffer (100 mmol/L NH_4HCO_3 and 55 mmol/L iodoacetamide) in the dark for 30 min at room temperature. The gel pieces were dried in a vacuum centrifuge. The dried gel pieces were incubated in the digestion solution that consisted of 40 mmol/L NH_4HCO_3 and 20 μg/mL proteomics grade trypsin for 24 h at 37 ℃. The peptide digest (1 μL) was mixed with 1 μL CCA matrix solution and 1 μL of this mixture was applied to the stainless steel plate and air dried. The samples were analyzed with Voyager DE STR MALDI-TOF Mass Spectrometer (Applied Biosystems, Cambridge, MA). The parameters were set up as follows: positive ion-reflector mode, accelerating voltage 20 000 V, grid voltage 68%, mirror voltage ratio 1.12, N_2 laser wavelength 337 nm, pulse width 3 ns, the number of laser shots 50, acquisition mass range 900-3 500 Da, delay 180 ns, and vacuum degree 4×10^{-7} Torr. A list of the corrected mass peaks was the peptide mass fingerprinting (PMF).

Database analysis

Proteins were identified with PMF data by searching software PeptIdent (http://www.expasypku.edu.cn). The searching parameters were set up as follows: acquisition mass ranges 900-3 500 Da, the mass tolerance was ±0.5 Da; the number of missed cleavage sites was allowed up to 1; the cysteine residue was modified as carbamidomethyl-cys; the minimum

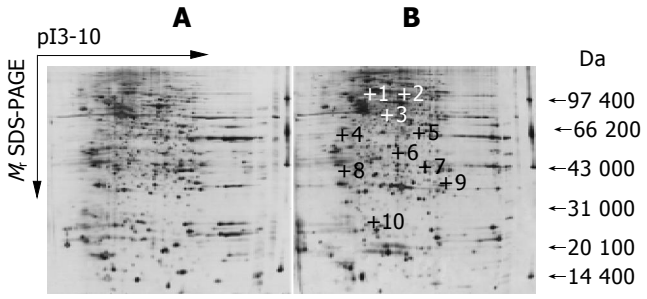

Figure 1 2-DE maps of untreated (**A**) and *H pylori*-treated HepG2 (**B**) cell proteins. The proteins from cells were extracted and separated on a pH 3-10 IPG strip, followed by a 12.5% SDS-polyacrylamide gel and silver staining. Spots that were found to be overexpressed have been annotated.

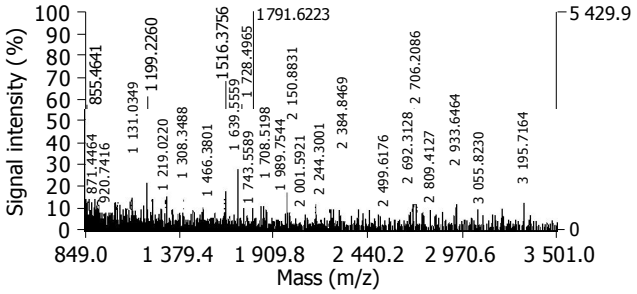

Figure 2 Peptide mass fingerprinting of the spot 10. The spot was in-gel digested with trypsin. After desalting, the peptide mixture was analyzed by MALDI-TOF-MS.

number of matched peptide was four; species was selected as *Homo sapiens* (humans); the peptide ion was $[M+H]^+$; the isotope masses were used; and the searching range was within the experimental p*I* value ±0.5 pH unit and experimental M_r ±20%.

RESULTS

2-D map and image analysis

Three different independent sets of experiments were carried out to compare the pattern of cellular protein expression in untreated and *H pylori*-treated HepG2 cells. The two photographs shown in Figure 1 depict the pattern of cellular proteins obtained after 2-DE of total cellular extracts from untreated and *H pylori*-treated HepG2 cells. For untreated HepG2 cells, a total of 988±94 spots were detected; for *H pylori*-treated HepG2 cells, a total of 996±68 spots were detected. Most of the spots were centralized in the area of pI 4-8 and M_r 31 000-97 000 Da. A total of 861 spots were matched between the 2-DE maps of *H pylori*-treated HepG2 cells and untreated HepG2 cells. This matching analysis revealed that 10 protein spots showed higher expression in the treated cells ($P<0.05$). The spots that clearly overexpressed in the treated cells were marked with a cross at the corresponding site in Figure 1.

MALDI-TOF-MS analysis and protein identification

These 10 differential protein spots were excised from the stained gels and digested in-gel with trypsin. The PMF was obtained by MALDI-TOF-MS. A representative PMF map of the spot 10 was showed in Figure 2. The monoisotopic peptide masses obtained from mass spectra were used to search the SWISS-PROT and TrEMBL database with PeptIdent software. The resulting protein was determined by comprehensively considering the corresponding experimental pI, M_r, the number of matched peptides, and the sequence coverage (Tables 1 and 2). Seven proteins were successfully identified. The data on all identified protein spots were described in Table 2; these proteins were involved in transcription regulation, signal transduction, metabolism and so on.

Table 1 Matching of protein spot-10 peptide mass fingerprint data with protein Q96AX2 in database

User mass	Matching mass	Mass (Da)	#MC	Modification	Position	Peptide
976.901	977.3638	0.4628	1	1xCys_CAM	215–222	RSSCCSFM
990.94	991.3795	0.4395	1	1xCys_PAM	215–222	RSSCCSFM
999.094	999.5332	0.4392	0		42–49	TCFLIQFK
1 006.907	1 007.3744	0.4674	1	1xCys_PAM,1xMSO	215–222	RSSCCSFM
1 167.021	1 166.5295	–0.4914	0	2xCys_CAM,1xGERA, 1xMSO	216–222	SSCCSFM
1 266.017	1 265.6091	–0.4078	1	1xCys_CAM,1xGERA, 1xMSO	215–222	RSSCCSFM
1 308.278	1 308.742	0.464	0	2xGERA	216–222	SSCCSFM
1 345.559	1 345.707	0.148	1		151–162	VIRSEDGETLAR
1 464.517	1 464.8431	0.3261	1	2xGERA	215–222	RSSCCSFM
1 466.362	1 466.8112	0.4492	0	2xCys_PAM,2xGERA, 1xMSO	216–222	SSCCSFM
1 516.378	1 516.7543	0.3763	0		122–133	AWLTEIHEYAQR
1 684.665	1 684.8249	0.1599	1		1–17	TGTPGAVATRD GEAPER
2 479.013	2 479.2207	0.2077	1	1xCys_CAM	18–41	SPPCSPSYDLTGK VMLLGDTGVGK

36.5% of sequence covered:

```
     1          11         21         31         41         51
     |          |          |          |          |          |
   1 TGTPGAVATR DGEAPERSPP CSPSYDLTGK VMLLGDTGVG KTCFLIQFKd gaflsgtfia  60
  61 tvgidfrnkv vtvdgvrvkl qiwdtagqer frsvthayyr daqallllyd itnkssfdni 120
 121 rAWLTEIHEY AQRdvvimll gnkadmsser VIRSEDGETL AReygvpfle tsaktgmnve 180
 181 laflaiakel kyraghqade psfqirdyve sqkkRSSCCS FM
```

Table 2 Proteins identified by MS

Spot	SWISS-PROT Accession No.	Peptides Matched	pI	M_r (Da)	Sequence coverage (%)	Protein identified
1	P05556	19/106	5.31	86 242	31.2	Chain 1: integrin β-1
3	P17252	7/28	6.61	76 764	39.9	Protein kinase C, alpha type
6	P48742	6/34	7.16	44 482	39.6	LIM/homeobox protein Lhx1
7	P20042	10/92	5.60	38 388	30.9	eIF-2-beta
8	P46734-3	6/37	7.08	39 940	35.0	MAP kinase kinase 3
9	P48059	8/44	8.43	37 251	36.3	PINCH protein
10	Q96AX2	13/86	5.96	24 684	36.5	Ras-related protein Rab-37

DISCUSSION

The detection that *Helicobacter* spp. could infect biliary tract and liver of humans has been reported by several studies in different settings. Fox *et al*[6], have shown the presence of *Helicobacter* spp. in the bile of Chileans with chronic cholecystitis. Avenaud and coworkers[3] have demonstrated by PCR the presence of genomic sequences of *Helicobacter* spp. in the liver of eight patients with hepatocellular carcinoma (HCC) without primary diagnosis of cirrhosis, and a further analysis by sequencing revealed that these species were *H pylori* and *H felis*. Similarly, Ponzetto[12] has reported the presence of cagA gene sequences obtained from the liver tissue of cirrhotic patients with HCC. Furthermore, Nilsson *et al*[2], have identified *H pylori* and *Helicobacter* spp. in human liver samples from patients suffering from PSC and PBC and recently in liver samples of patients with cholangiocarcinomas or HCC[5]. Of great interest is the fact that the gene sequence obtained from positive PCR of *Helicobacter* spp.-specific 16S rRNA was usually most analogous to *H pylori*. *Helicobacter* spp. has been successfully cultured from the liver of a patient with Wilson's disease by Queiroz and Santos[23]; the isolate is closely related to *H pylori* by biochemical and 16S rRNA analysis. Lately, Wang *et al*[24], followed-up C57BL/6 and Balb/cA mice infected by three different *H pylori* isolates. They found that one C57BL/6 mouse infected with *H pylori* strain 119p developed HCC after 23 mo. Taking the results together, we may conclude that, as in animals, *Helicobacter* species especially *H pylori* may colonize the liver of humans, which could have some sort of importance in the pathogenesis and in the development of some liver diseases.

The comparative proteomic study was performed between the untreated and *H pylori*-treated HepG2. Ten differential protein spots were selected to perform in-gel trypsin digestion and MALDI-TOF-MS-based PMF analysis. Seven of these proteins were successfully identified by MALDI-TOF-MS. Some of the identified proteins are the oncogene-encoded products and others are the regulatory proteins of transcription and signal transduction.

The integrins are a family of cell surface glycoproteins which mediated interactions of cells with the extracellular matrix and cells with cells. These integrin- mediated interactions influence many aspects of cell behavior including cell survival, cell adhesion, cell migration, as well as cell proliferation and differentiation. All integrins are heterodimers composed of two subunits, α and β. Integrin β-1 has been found to play an essential role in invasion and metastasis of HCC cells[25]. Liu *et al*, found that integrin β-1 gene was upregulated in HCC using cDNA microarray technology, which was consistent with RT-PCR and Northern blot analysis of integrin β-1 gene. Human hepatoma cell lines HepG2, Huh7, and HLE stably transfected with full-length integrin β-1 had overexpression of integrin β-1 and were protected from apoptosis induced by chemotherapeutic reagents via a mitogen-activated protein kinase (MAPK)-dependent pathway[26].

Protein kinase C (PKC) is a family of at least 11 structurally related phospholipid-dependent serine/threonine kinases and it plays crucial roles in transducing signals that regulate diverse cellular functions, including proliferation, differentiation, and apoptosis. The PKC family is divided into three subgroups based on differences in their structures and co-factor requirements. PKC-α is a member of the group A or classical PKCs (cPKCs). Review of the literatures has shown that the PKC signal transduction pathway plays an important role in the development of many diseases and, in particular, cancer[27]. PKC-α is an important tumor-promoting factor; as potential target for anticancer therapy, PKC-α is currently being studied[28].

Homeobox genes play fundamental roles in development. They can be subdivided into several subfamilies, one of which is the LIM-homeobox subfamily. The characteristic features of LIM-homeodomain proteins are double zinc finger motifs, called LIM domains, that are located N-terminally of the homeodomain. These proteins mediate protein-protein interactions and are of fundamental importance for cell differentiation, cytoskeletal remodeling and transcriptional regulation[29].

Eukaryotic translation initiation factor 2 (eIF-2) is a multimeric protein consisting of three dissimilar subunits termed α, β, and γ, which functions as a central switch in the initiation of protein synthesis. In its GTP-bound state it delivers the methionyl initiator tRNA (Met-tRNA(i)) to the small ribosomal subunit and releases it upon GTP hydrolysis following the recognition of the initiation codon[30]. PINCH protein is an effector of integrin and growth factor signaling, coupling surface receptors to downstream signaling molecules involved in the regulation of cell survival, cell proliferation and cell differentiation[31].

MAPK pathway is an important signal transduction pathway that transduces extracellular signals into intracellular responses and has been implicated in a wide array of physiological processes such as proliferation, differentiation, development, apoptosis, stress and inflammatory responses. The MAPK kinases (MAPKKs) are up-stream dual-specificity protein kinases which phosphorylate and activate MAPK on threonine and tyrosine residues[32].

Ras-related protein Rab-37 belongs to the small GTPase superfamily, Rab family. GTPases regulate a myriad of cellular functions including signal transduction, cytoskeletal organization and membrane trafficking. Rab family members are also widely involved in human tumorigenesis by overexpression[33,34].

The upregulation of these proteins suggests that the capacity of the tumor invasion is stronger. However, the exact mechanisms through which *H pylori* lead to the change of these proteins await further study.

Advances in 2D electrophoresis, MS, and bioinformatics now make possible the large-scale examination of protein expression patterns. These improved methods are used to identify proteins found to be upregulated in expression level in *H pylori*-treated HepG2 cells. The above findings could be valuable for further elucidating the etiological role of *Helicobacter* spp. infection in a variety of liver disorders.

REFERENCES

1 **Solnick JV,** Schauer DB. Emergence of diverse *Helicobacter* species in the pathogenesis of gastric and enterohepatic diseases. *Clin Microbiol Rev* 2001; **14**: 59-97
2 **Nilsson HO,** Taneera J, Castedal M, Glatz E, Olsson R, Wadstrom T. Identification of *Helicobacter pylori* and other *Helicobacter* species by PCR, hybridization, and partial DNA sequencing in human liver samples from patients with primary sclerosing cholangitis or primary biliary cirrhosis. *J Clin Microbiol* 2000; **38**: 1072-1076
3 **Avenaud P,** Marais A, Monteiro L, Le Bail B, Bioulac Sage P, Balabaud C, Megraud F. Detection of *Helicobacter* species in the liver of patients with and without primary liver carcinoma. *Cancer* 2000; **89**: 1431-1439
4 **Myung SJ,** Kim MH, Shim KN, Kim YS, Kim EO, Kim HJ, Park ET, Yoo KS, Lim BC, Seo DW, Lee SK, Min YI, Kim JY. Detection of *Helicobacter pylori* DNA in human biliary tree and its association with hepatolithiasis. *Dig Dis Sci* 2000; **45**: 1405-1412
5 **Nilsson HO,** Mulchandani R, Tranberg KG, Stenram U, Wadstrom T. *Helicobacter* species identified in liver from patients with cholangiocarcinoma and hepatocellular carcinoma. *Gastroenterology* 2001; **120**: 323-324
6 **Fox JG,** Dewhirst FE, Shen Z, Feng Y, Taylor NS, Paster BJ, Ericson RL, Lau CN, Correa P, Araya JC, Roa I. Hepatic *Helicobacter* species identified in bile and gallbladder tissue from Chileans with chronic cholecystitis. *Gastroenterology* 1998; **114**: 755-763
7 **Roe IH,** Kim JT, Lee HS, Lee JH. Detection of *Helicobacter* DNA in bile from bile duct diseases. *J Korean Med Sci* 1999; **14**: 182-186
8 **Ito K,** Nakamura M, Toda G, Negishi M, Torii A, Ohno T. Potential role of *Helicobacter pylori* in hepatocarcinogenesis. *Int J Mol Med* 2004; **13**: 221-227
9 **Silva CP,** Pereira-Lima JC, Oliveira AG, Guerra JB, Marques DL, Sarmanho L, Cabral MM, Queiroz DM. Association of the presence of *Helicobacter* in gallbladder tissue with cholelithiasis and cholecystitis. *J Clin Microbiol* 2003; **41**: 5615-5618
10 **Nilsson HO,** Castedal M, Olsson R, Wadstrom T. Detection of *Helicobacter* in the liver of patients with chronic cholestatic liver diseases. *J Physiol Pharmacol* 1999; **50**: 875-882
11 **Chen W,** Li D, Cannan RJ, Stubbs RS. Common presence of *Helicobacter* DNA in the gallbladder of patients with gallstone diseases and controls. *Dig Liver Dis* 2003; **35**: 237-243
12 **Ponzetto A,** Pellicano R, Leone N, Cutufia MA, Turrini F, Grigioni WF, D'Errico A, Mortimer P, Rizzetto M, Silengo L. *Helicobacter* infection and cirrhosis in hepatitis C virus carriage: is it an innocent bystander or a troublemaker? *Med Hypotheses* 2000; **54**: 275-277
13 **Fan XG,** Peng XN, Huang Y, Yakoob J, Wang ZM, Chen YP. *Helicobacter* species ribosomal DNA recovered from the liver tissue of chinese patients with primary hepatocellular carcinoma. *Clin Infect Dis* 2002; **35**: 1555-1557
14 **Peng XN,** Fan XG, Huang Y, Wang ZM, Chen YP. The study on relationship between *Helicobacter* infection and primary liver carcinoma. *Shijie Huaren Xiaohua Zazhi* 2002; **10**: 902-906
15 **Huang Y,** Fan XG, Chen YP, Li N, Tang LJ. Detection of *Helicobacter* species 16S rRNA gene in paraffin-embedded hepatocellular carcinoma tissues. *Shijie Huaren Xiaohua Zazhi* 2002; **10**: 877-882
16 **Fagoonee S,** Pellicano R, Rizzetto M, Ponzetto A. The journey from hepatitis to hepatocellular carcinoma. Bridging role of *Helicobacter* species. *Panminerva Med* 2001; **43**: 279-282
17 **Wilkins MR,** Sanchez JC, Gooley AA, Appel RD, Humphery-Smith I, Hochstrasser DF, Williams KL. Progress with proteome projects: why all proteins expressed by a genome should be identified and how to do it. *Biotechnol Genet Eng Rev* 1996; **13**: 19-50
18 **Pandey A,** Mann M. Proteomics to study genes and genomes. *Nature* 2000; **405**: 837-846
19 **Fan XG,** Chua A, Li TG, Zeng QS. Survival of *Helicobacter pylori* in milk and tap water. *J Gastroenterol Hepatol* 1998; **13**: 1096-1098
20 **Gorg A,** Obermaier C, Boguth G, Harder A, Scheibe B, Wildgruber R, Weiss W. The current state of two-dimensional electrophoresis with immobilized pH gradients. *Electrophoresis* 2000; **21**: 1037-1053
21 **Corbett JM,** Dunn MJ, Posch A, Gorg A. Positional reproducibility of protein spots in two-dimensional polyacrylamide gel electrophoresis using immobilised pH gradient isoelectric focusing in the first dimension: an interlaboratory comparison. *Electrophoresis* 1994; **15**: 1205-1211
22 **Chen P,** Xie JY, Liang SP. Identification of Protein Spots in Silver-stained Two-dimensional Gels by MALDI-TOF Mass Peptide Map Analysis. *Shengwu Huaxue Yu Shengwu Wuli Xuebao (Shanghai)* 2000; **32**: 387-391
23 **de Magalhaes Queiroz DM,** Santos A. Isolation of a *Helicobacter* strain from the human liver. *Gastroenterology* 2001; **121**: 1023-1024
24 **Wang X,** Willen R, Svensson M, Ljungh A, Wadstrom T. Two-year follow-up of *Helicobacter pylori* infection in C57BL/6 and Balb/cA mice. *APMIS* 2003; **111**: 514-522
25 **Masumoto A,** Arao S, Otsuki M. Role of beta1 integrins in adhesion and invasion of hepatocellular carcinoma cells. *Hepatology* 1999; **29**: 68-74
26 **Zhang H,** Ozaki I, Mizuta T, Matsuhashi S, Yoshimura T, Hisatomi A, Tadano J, Sakai T, Yamamoto K. Beta 1-integrin protects hepatoma cells from chemotherapy induced apoptosis via a mitogen-activated protein kinase dependent pathway. *Cancer* 2002; **95**: 896-906
27 **Rybczynska M,** Ksiazek K, Kaczmarek J. The role of PKC isoforms in tumorigenicity and apoptotic cell death. *Postepy Hig Med Dosw* 2000; **54**: 777- 796
28 **Roychowdhury D,** Lahn M. Antisense therapy directed to protein kinase C-alpha (Affinitak, LY900003/ISIS 3521): potential role in breast cancer. *Semin Oncol* 2003; **30**: 30-33
29 **Hobert O,** Westphal H. Functions of LIM-homeobox genes. *Trends Genet* 2000; **16**: 75-83
30 **Sonenberg N,** Dever TE. Eukaryotic translation initiation factors and regulators. *Curr Opin Struct Biol* 2003; **13**: 56-63
31 **Wang-Rodriguez J,** Dreilinger AD, Alsharabi GM, Rearden A. The signaling adapter protein PINCH is up-regulated in the stroma of common cancers, notably at invasive edges. *Cancer* 2002; **95**: 1387-1395
32 **Johnson GL,** Lapadat R. Mitogen-activated protein kinase pathways mediated by ERK, JNK, and p38 protein kinases. *Science* 2002; **298**: 1911-1912
33 **Pfeffer SR.** Rab GTPases: specifying and deciphering organelle identity and function. *Trends Cell Biol* 2001; **11**: 487-491
34 **He H,** Dai F, Yu L, She X, Zhao Y, Jiang J, Chen X, Zhao S. Identification and characterization of nine novel human small GTPases showing variable expressions in liver cancer tissues. *Gene Expr* 2002; **10**: 231-242

Science Editor Li WZ **Language Editor** Elsevier HK

PO Box 2345, Beijing 100023, China
www.wjgnet.com
wjg@wjgnet.com

ELSEVIER

World J Gastroenterol 2005;11(22):3490
World Journal of Gastroenterology ISSN 1007-9327

Acknowledgements to Reviewers of *World Journal of Gastroenterology*

Many reviewers have contributed their expertise and time to the peer review, a critical process to ensure the quality of *World Journal of Gastroenterology*. The editors and authors of the articles submitted to the journal are grateful to the following reviewers for evaluating the articles (including those were published and those were rejected in this issue) during the last editing period of time.

Pelayo Correa, Boyd Professor
Department of Pathology, Louisiana State University Health Science Center, 1901 Perdido St., New Orleans La 70112, United States

John Cuppoletti, Professor
Department of Molecular and Cellular Physiology, University of Cincinnati College of Medicine 231 Albert Sabin Way, Cincinnati OH 45267-0576, United States

Zong-Jie Cui, Professor
Institute of Cell Biology, Beijing Normal University, Beijing 100875, China

Da-Jun Deng, Professor
Department of Cancer Etiology, Peking University School of Oncology, 1 Da-Hong-Luo-Chang Street, Western District, Beijing 100034, China

Er-Dan Dong, Professor
Department of Life Science, Division of Basic Research in Clinic Medicine, National Natural Science Foundation of China, 83 Shuanqing Road, Haidian District, Beijng 100085, China

Amar Paul Dhillon, Professor
Department of Histopathology, Royal Free Hospital, Pond Street, London NW3 2QG, United Kingdom

Sheung-Tat Fan, Professor
Department of Surgery, The University of Hong Kong, Queen Mary Hospital, 102 Pokfulam Road, Hong Kong, China

Xue-Gong Fan, Professor
Xiangya Hospital, Changsha 410008, Hunan Povince, China

De-Wu Han, Professor
Shanxi Medical University, 86 Xinjian South Road, Taiyuan 030001, Shanxi Povince, China

Richard A Kozarek, M.D.
Department of Gastroenterology, Virginia Mason Medical Center, 1100 Ninth Avenue, P.O. Box 900, Seattle 98111-0900, United States

Shiu-Ming Kuo, M.D.
University at Buffalo, 15 Farber Hall, 3435 Main Street, Buffalo 14214, United States

Vasiliy Ivanovich Reshetnyak, Professor
Institute of General Reanimatology, 25-2, Petrovka Str., Moscow 107031, Russian Federation

Michael Steer, Professor
Department of Surgery, Tufts-Nemc, 860 Washington St, Boston, Ma 02111, United States

Qin Su, Professor
Department of Pathology, Cancer Hospital and Cancer Institute, Chinese Academy of Medical Sciences and Peking Medical College, PO Box 2258, Beijing 100021, China

Jonas Valantinas, M.D.
Professor of Gastroenterology, Vilnius University Hospital, Santariskiu 2, Vilnius LT-2600, Lithuania

Harry H-X Xia, M.D.
Department of Medicine, The University of Hong Kong, Pokfulam Road, Hong Kong, China

Jia-Yu Xu, Professor
Shanghai Second Medical University, Rui Jin Hospital, 197 Rui Jin Er Road, Shanghai 200025, China

Dong-Liang Yang, Professor
Department of Infectious Diseases, Tongji Hospital, Tongji Medical College, Huazhong University of Science and Technology, 1095 Jiefang Avenue, Wuhan 430030, Hubei Province, China

Xue-Biao Yao, Professor
Laboratory of Cell Dynamics, University of Science and Technology of China, 96 Jin Zhai Road, Hefei 230027, Anhui Province, China

Yuan Yuan, Professor
Cancer Institute of China Medical University, 155 North Nanjing Street, Heping District, Shenyang 110001, Liaoning Province, China

Zhi-Rong Zhang, Professor
West China School of Pharmacy, Sichuan University, 17 South Renmin Road, Chengdu 610041, Sichuan Povince, China

Xiao-Hang Zhao, Professor
State Key Laboratory of Molecular Oncology, Cancer Institute of Chinese Academy of Medical Sciences, 17 Panjiayuan, Chaoyangqu, Beijing 100021, China

Shu Zheng, Professor
Scientific Director of Cancer Institute, Zhejiang University, Secondary Affiliated Hospital, Zhejiang University, 88# Jiefang Road, Hangzhou 310009, Zhejiang Province, China

PO Box 2345, Beijing 100023, China
www.wjgnet.com
wjg@wjgnet.com

ELSEVIER

World J Gastroenterol 2005;11(22):Appendix 1
World Journal of Gastroenterology ISSN 1007-9327

Meetings

Major meetings coming up

Digestive Disease Week
106th Annual Meeting of AGA, The American Gastroenterology Association
May 14-19, 2005
www.ddw.org/
Chicago, Illinois

13th World Congress of Gastroenterology
September 10-14, 2005
www.wcog2005.org/
Montreal, Canada

13th United European Gastroenterology Week, UEGW
October 15-20, 2005
www.uegf.org/
Copenhagen, Denmark

American College of Gastroenterology Annual Scientific Meeting
October 28-November 2, 2005
www.acg.gi.org/
Honolulu Convention Center, Honolulu, Hawaii

Events and Meetings in the upcoming 6 months

World Congress on Gastrointestinal Cancer
June 15–18, 2005
Barcelona

Events and meetings in 2005

Canadian Digestive Disease Week Conference
February 26-March 6, 2005
www.cag-acg.org
Banff, AB

2005 World Congress of Gastroenterology
September 12–14, 2005
Montreal, Canada

International Colorectal Disease Symposium 2005
February 3–5, 2005
Hong Kong

13th UEGW meeting *United European Gastroenterology Week*
October 15–20, 2005
www.webasistent.cz/guarant/uegw2005/
Copenhagen-Malmoe

7th International Workshop on Therapeutic Endoscopy
September 10–12, 2005
www.alfamedical.com
Theodor Bilharz Research Institute

EASL 2005 the 40th annual meeting
April 13–17, 2005
www.easl.ch/easl2005/
Paris, France

Pediatric Gastroenterology, Hepatology and Nutrition
March 13, 2005
Jakarta, Indonesia

21st annual international congress *of Pakistan society of Gastroenterology & GI Endoscopy*
March 25–27, 2005
www.psgc2005.com
Peshawar

8th Congress of the Asian Society of HepatoBiliary Pancreatic Surgery
February 10–13, 2005
Mandaluyong, Philippines

APDW 2005 - Asia Pacific Digestive Week 2005
September 25–28, 2005
www.apdw2005.org
Seoul, Korea

World Congress on Gastrointestinal Cancer
June 15–18, 2005
Barcelona

British Society of Gastroenterology Conference (BSG)
March 14–17, 2005
www.bsg.org.uk
Birmingham

Digestive Disease Week *DDW 106th Annual Meeting*
May 15–18, 2005
www.ddw.org
Chicago, Illinois

70th ACG Annual Scientific Meeting and Postgraduate Course
October 28-November 2, 2005
Honolulu Convention Center, Honolulu, Hawaii

Events and Meetings in 2006

EASL 2006 - THE 41ST ANNUAL MEETING
April 26–30, 2006
Vienna, Austria

Canadian Digestive Disease Week Conference
March 4–12, 2006
www.cag-acg.org
Quebec City

XXX pan-american congress of digestive diseases *XXX congreso panamericano de anfermedades digestivas*
November 25-December 1, 2006
www.gastro.org.mx
Cancun

World Congress on Gastrointestinal Cancer
June 14–17, 2006
Barcelona, Spain

7th World Congress of the International Hepato-Pancreato-Biliary Association
September 3–7, 2006
www.edinburgh.org/conference
Edinburgh

71st ACG Annual Scientific Meeting and Postgraduate Course
October 20–25, 2006
Venetian Hotel, Las Vegas, Neveda

PO Box 2345, Beijing 100023, China
www.wjgnet.com
wjg@wjgnet.com

ELSEVIER

World J Gastroenterol 2005;11(22):Appendix 2-3
World Journal of Gastroenterology ISSN 1007-9327

Instructions to authors

GENERAL INFORMATION

World Journal of Gastroenterology (*WJG,* ISSN 1007-9327 CN 14-1219/R) is a weekly journal of more than 48 000 circulation, published on the 7th, 14th, 21st and 28th of every month.

Original Research, Clinical Trials, Reviews, Comments, and Case Reports in esophageal cancer, gastric cancer, colon cancer, liver cancer, viral liver diseases, *etc*., from all over the world are welcome on the condition that they have not been published previously and have not been submitted simultaneously elsewhere.

Published jointly by
The WJG Press and Elsevier Inc.

SUBMISSION OF MANUSCRIPTS

Manuscripts should be typed double-spaced on A4 (297×210 mm) white paper with outer margins of 2.5 cm. Number all pages consecutively, and start each of the following sections on a new page: Title Page , Abstract, Introduction, Materials and Methods, Results, Discussion, Acknowledgements, References, Tables, Figures and Figure Legends. Neither the Editors nor the Publisher is responsible for the opinions expressed by contributors. Manuscripts formally accepted for publication become the permanent property of The WJG Press and Elsevier Inc., and may not be reproduced by any means, in whole or in part without the written permission of both the Authors and the Publisher. We reserve the right to put onto our website and copy-edit accepted manuscripts. Authors should also follow the guidelines for the care and use of laboratory animals of their institution or national animal welfare committee.

Authors should retain one copy of the text, tables, photographs and illustrations, as rejected manuscripts will not be returned to the author(s) and the editors will not be responsible for the loss or damage to photographs and illustrations.

Online submission
Online submission is strongly advised. Manuscripts should be submitted through the Online Submission System at: http://www.wjgnet.com/index.jsp. Authors are highly recommended to consult the ONLINE INSTRUCTIONS TO AUTHORS (http://www.wjgnet.com/wjg/help/instructions.jsp) before attempting to submit online. Authors encountering problems with the Online Submission System may send an email describing the problem to wjg@wjgnet.com for assistance. If you submit manuscript online, do not make a postal contribution. A repeated online submission for the same manuscript is strictly prohibited.

Postal submission
Send 3 duplicate hard copies of the full-text manuscript typed double-spaced on A4(297×210 mm) white paper together with any original photographs or illustrations and a 3.5 inch computer diskette or CD-ROM containing an electronic copy of the manuscript including all the figures, graphs and tables in native Microsoft Word format or *.rtf format to:

World Journal of Gastroenterology
Apartment 1066 Yishou Garden,
58 North Langxinzhuang Road,
PO Box 2345, Beijing 100023, China
E-mail: wjg@wjgnet.com
http: //www.wjgnet.com

MANUSCRIPT PREPARATION

All contributions should be written in English. All articles must be submitted using a word-processing software. All submissions must be typed in 1.5 line spacing and in word size 12 with ample margins. The letter font is Tahoma. For authors originating from China, one copy of the Chinese translation of the manuscript is also required (excluding references). Style should conform to our house format. Required information for each of the manuscript sections is as follows:

Title page
Full manuscript title, running title, all author(s) name(s), affiliations, institution(s) and/or department(s) where the work was accomplished, disclosure of any financial support for the research, and the name, full address, telephone and fax numbers and email address of the corresponding author should be involved. Titles should be concise and informative (removing all unnecessary words), emphasize what is NEW, and avoid abbreviations. A short running title of less than 40 letters should be provided. List the author(s)' name(s) as follows: initials and/or first name, middle name or initial(s) and full family name.

Abstract
An informative, structured abstract of no more than 250 words should accompany each manuscript. Abstracts for original contributions should be structured into the following sections: AIM: Only the purpose should be included. METHODS: The materials, techniques, instruments and equipments, and the experimental procedures should be included. RESULTS: The observatory and experimental results, including data, effects, outcome, *etc*. should be included. Authors should present *P* value where necessary, and the significant data should accompany. CONCLUSION: Accurate view and the value of the results should be included.

The format of structured abstracts is at: http://www.wjgnet.com/wjg/help/11.doc

Key words
Please list 3-10 key words that could reflect content of the study.

Text
For most article types, the main text should be structured into the following sections: INTRODUCTION, MATERIALS AND METHODS, RESULTS and DISCUSSION, and should include appropriate Figures and Tables. Data should be presented in the body text or Figures and Tables, not both.

Illustrations
Figures should be numbered as 1, 2, 3 and so on, and mentioned clearly in the main text. Provide a brief title for each figure on a separate page. No detailed legend should be involved under the figures. This part should add into the text where the figures are applicable. Digital images: black and white photographs should be scanned and saved in TIFF format at a resolution of 300 dpi; color images should be saved as CMYK (print files) and not RGB (screen-viewing files). Place each photograph in a separate file. Print images: supply images of size no smaller than 126×76 mm printed on smooth surface paper; label the image by writing the Figure number and orientation using an arrow. Photomicrographs: indicate the original magnification and stain in the legend. Digital Drawings: supply files in EPS if created by Freehand and Illustrator, or TIFF from Photoshop. EPS files must be accompanied by a version in native file format for editing purposes. Scans of existing line drawings should be scanned at a resolution of 1200 dpi and as close as possible to the size at which they will appear when printed, not smaller. Please use uniform legends for the same subjects. For example: Figure 1 Pathological changes of atrophic gastritis after treatment. A: ...; B: ...;C: ...; D: ...; E: ...; F: ...; G: ...

Tables
Three-line tables should be numbered as 1, 2, 3 and so on, and mentioned clearly in the main text. Provide a brief title for each table. No detailed legend should be involved under the tables. This part should add into the text where the tables are applicable. The information should complement but not duplicate that contained in the text. Use one horizontal line under the title, a second under the column heads, and a third below the Table, above any footnotes. Vertical and italic lines should be omitted.

Notes in tables and illustrations
Data which is not statistically significant should not be noted. $^{a}P<0.05$, $^{b}P<0.01$ ($P>0.05$ should not be noted). If there are other series of *P* values, $^{c}P<0.05$ and $^{d}P<0.01$ are used; Third series of *P* values can be expressed as $^{e}P<0.05$ and $^{f}P<0.01$. Other notes in tables or under

illustrations should be expressed as ^1F, ^2F, ^3F; or some other symbols with a superscript (Arabic numerals) in the upper left corner. In a multi-curve illustration, each curve should be labeled with ●, ○, ■, □, ▲, △, *etc*. in a certain sequence.

Acknowledgments

Brief acknowledgments of persons who have made genuine contributions to the manuscripts and who endorse the data and conclusions are included. Authors are responsible for obtaining written permission to use any copyrighted text and/or illustrations.

References

Cited references should mainly be drawn from journals covered in the Science Citation Index (http://www.isinet.com) and/or Index Medicus (http://www.ncbi.nlm.nih.gov/PubMed) databases. Mention all references in the text, tables and figure legends, and set off by consecutive, superscripted Arabic numerals. References should be numbered consecutively in the order in which they appear in the text. Abbreviate journal title names according to the Index Medicus style (http://www.ncbi.nlm.nih.gov/entrez/query.fcgi?db=journals). Unpublished observations and personal communications are not listed as references. The style and punctuation of the references conform to ISO standard and the Vancouver style (5th edition); see examples below. Reference lists not conforming to this style could lead to delayed or even rejected publication status. Examples:

Standard jounal article (list all authors and include the PubMed ID [PMID] where applicable)

1 **Das KM,** Farag SA. Current medical therapy of inflammatory bowel disease. *World J Gastroenterol* 2000; 6: 483-489 [PMID: 11819634]

2 **Pan BR**, Hodgson HJF, Kalsi J. Hyperglobulinemia in chronic liver disease: Relationships between *in vitro* immunoglobulin synthesis, short lived suppressor cell activity and serum immunoglobulin levels. *Clin Exp Immunol* 1984; 55: 546-551 [PMID: 6231144]

3 **Lin GZ,** Wang XZ, Wang P, Lin J, Yang FD. Immunologic effect of Jianpi Yishen decoction in treatment of Pixu-diarrhoea. *Shijie Huaren Xiaohua Zazhi* 1999; 7: 285-287 [CMFAID:1082371101835979]

Books and other monographs (list all authors)

4 **Sherlock S,** Dooley J. Diseases of the liver and billiary system. 9th ed. Oxford: Blackwell Sci Pub, 1993: 258-296

Chapter in a book (list all authors)

5 **Lam SK.** Academic investigator's perspectives of medical treatment for peptic ulcer. In: Swabb EA, Azabo S. Ulcer disease: investigation and basis for therapy. New York: Marcel Dekker, 1991: 431-450

Electronic journal (list all authors)

6 **Morse SS.** Factors in the emergence of infectious diseases. Emerg Infect Dis serial online, 1995-01-03, cited 1996-06-05; 1(1):24 screens. Available from: URL: http//www.cdc.gov/ncidod/EID/eid.htm

PMID requirement

From the full reference list, please submit a separate list of those references embodied in PubMed, keeping the same order as in the full reference list, with the following information only: (1) abbreviated journal name and citation (e.g. *World J Gastroenterol* 2003;9(11): 2400-2403; (2) article title (e.g. Epidemiology of gastroenterologic cancer in Henan Province, China; (3) full author list (e.g. Lu JB, Sun XB, Dai DX, Zhu SK, Chang QL, Liu SZ, Duan WJ; (4) PMID (e.g. 14606064). Provide the full abstracts of these references, as quoted from PubMed on a 3.5 inch disk or CD-ROM in Microsoft Word format and send by post to The *WJG* Press. For those references taken from journals not indexed by *Index Medicus*, a printed copy of the first page of the full reference should be submitted. Attach these references to the end of the manuscript in their order of appearance in the text.

Inappropriate references

Authors should always cite references that are relevant to their article, and avoid any inappropriate references. Inappropriate references include those that are linked with a hyphen and the difference between the two numbers at two sides of the hyphen is more than 5. For example, [1-6], [2-14] and [1,3,4-10,22] are all considered as inappropriate references. Authors should not cite their own unrelated published articles.

Statistical data

Present as mean±SD and mean±SE.

Statistical expression

Express *t* test as *t*(in italics), *F* test as *F*(in italics), chi square test as χ^2 (in Greek), related coefficient as *r*(in italics), degree of freedom as γ(in Greek), sample number as *n*(in italics), and probability as *P*(in italics).

Units

Use SI units. For example: body mass, m(B) = 78 kg; blood pressure, p (B)=16.2/12.3 kPa; incubation time, t(incubation)=96 h, blood glucose concentration, c(glucose) 6.4±2.1 mmol/L; blood CEA mass concentration, p(CEA) = 8.6 24.5 μg/L; CO_2 volume fraction, 50 mL/L CO_2 not 5% CO_2; likewise for 40 g/L formaldehyde, not 10% formalin; and mass fraction, 8 ng/g, *etc*. Arabic numerals such as 23,243,641 should be read 23 243 641.

The format about how to accurately write common units and quantum is at: http://www.wjgnet.com/wjg/help/15.doc

Abbreviations

Standard abbreviations should be defined in the abstract and on first mention in the text. In general, terms should not be abbreviated unless they are used repeatedly and the abbreviation is helpful to the reader. Permissible abbreviations are listed in Units, Symbols and Abbreviations: A Guide for Biological and Medical Editors and Authors (Ed. Baron DN, 1988) published by The Royal Society of Medicine, London. Certain commonly used abbreviations, such as DNA, RNA, HIV, LD50, PCR, HBV, ECG, WBC, RBC, CT, ESR, CSF, IgG, ELISA, PBS, ATP, EDTA, mAb, can be used directly without further mention.

Italicization

Quantities: *t* time or temperature, *c* concentration, *A* area, *l* length, *m* mass, *V* volume.
Genotypes: *gyr*A, *arg* 1, *c myc*, *c fos*, *etc*.
Restriction enzymes: *Eco*RI, *Hin*dI, *Bam*HI, *Kbo* I, *Kpn* I, *etc*.
Biology: *Helicobacter pylori, H pylori, E coli, etc*.

SUBMISSION OF THE REVISED MANUSCRIPTS AFTER ACCEPTED

Please revise your article according to the revision policies of *WJG*. The revised version including manuscript and high-resolution image figures (if any) should be copied on a floppy or compact disk. Author should send the revised manuscript, along with printed high-resolution color or black and white photos, copyright transfer letter, the final check list for authors, and responses to reviewers by a courier (such as EMS) (submission of revised manuscript by e-mail or on the WJG Editorial Office Online System is NOT available at present).

Language evaluation

The language of a manuscript will be graded before sending for revision. (1) Grade A: priority publishing; (2) Grade B: minor language polishing; (3) Grade C: a great deal of language polishing; (4) Grade D: rejected. The revised articles should be in grade B or grade A.

Copyright assignment form

It is the policy of WJG to acquire copyright in all contributions. Papers accepted for publication become the copyright of WJG and authors will be asked to sign a transfer of copyright form. All authors must read and agree to the conditions outlined in the Copyright Assignment Form (which can be downloaded from http://www.wjgnet.com/wjg/help/9.doc).

Final check list for authors

The format is at: http://www.wjgnet.com/wjg/help/13.doc

Responses to reviewers

Please revise your article according to the comments/suggestions of reviewers. The format for responses to the reviewers' comments is at: http://www.wjgnet.com/wjg/help/10.doc

Proof of financial support

For paper supported by a foundation, authors should provide a copy of the document and serial number of the foundation.

Publication fee

Authors of accepted articles must pay publication fee.

PO Box 2345, Beijing 100023, China
www.wjgnet.com
wjg@wjgnet.com

ELSEVIER

World J Gastroenterol 2005;11(22):Appendix 4
World Journal of Gastroenterology ISSN 1007-9327

World Journal of Gastroenterology standard of quantities and units

Number	Nonstandard	Standard	Notice
1	4 days	4 d	In figures, tables and numerical narration
2	4 days	four days	In text narration
3	day	d	After Arabic numerals
4	Four d	Four days	At the beginning of a sentence
5	2 hours	2 h	After Arabic numerals
6	2 hs	2 h	After Arabic numerals
7	hr, hrs,	h	After Arabic numerals
8	10 seconds	10 s	After Arabic numerals
9	10 year	10 years	In text narration
10	Ten yr	Ten years	At the beginning of a sentence
11	0,1,2 years	0,1,2 yr	In figures and tables
12	0,1,2 year	0,1,2 yr	In figures and tables
13	4 weeks	4 wk	
14	Four wk	Four weeks	At the beginning of a sentence
15	2 months	2 mo	In figures and tables
16	Two mo	Two months	At the beginning of a sentence
17	10 minutes	10 min	
18	Ten min	Ten minutes	At the beginning of a sentence
19	50% (*V/V*)	500 mL/L	
20	50% (m/*V*)	500 g/L	
21	1 M	1 mol/L	
22	10 μM	10 μmol/L	
23	1N HCl	1 mol/L HCl	
24	1N H_2SO_4	0.5 mol/L H_2SO_4	
25	4rd edition	4^{th} edition	
26	15 year experience	15- year experience	
27	18.5 kDa	18.5 ku,18 500u or M_r18 500	
28	25 $g.kg^{-1}/d^{-1}$	25 g/(kg·d) or 25 g/kg per day	
29	6900	6 900	
30	1000 rpm	1 000 r/min	
31	sec	s	After Arabic numerals
32	1 pg $\cdot L^{-1}$	1 pg/L	
33	10 kilograms	10 kg	
34	13 000 rpm	13 000 *g*	High speed; *g* should be in italic and suitable conversion.
35	1000 *g*	1 000 r/min	Low speed. *g* cannot be used.
36	Gene bank	GenBank	International classified genetic materials collection bank
37	Ten L	Ten liters	At the beginning of a sentence
38	Ten mL	Ten milliliters	At the beginning of a sentence
39	umol	μmol	
40	30 sec	30 s	
41	1 g/dl	10 g/L	10-fold conversion
42	OD_{260}	A_{260}	"OD" has been abandoned.
43	One g/L	One microgram per liter	At the beginning of a sentence
44	*A*260 nm	A_{260}nm	*A* should be in italic.
	^bP<0.05	^aP<0.05	In Table, no note is needed if there is no significance in statistics: ^aP<0.05, ^bP<0.01 (no note if P>0.05). If there is a second set of P value in the same table, ^cP<0.05 and ^dP<0.01 are used for a third set: ^eP<0.05, ^fP<0.01.
45	**F*=9.87, §*F*=25.9, #*F*=67.4	^1F=9.87,^2F=25.9, ^3F=67.4	Notices in or under a table
46	KM	km	kilometer
47	CM	cm	centimeter
48	MM	mm	millimeter
49	Kg, KG	kg	kilogram
50	Gm, gr	g	gram
51	nt	N	newton
52	l	L	liter
53	db	dB	decibel
54	rpm	r/min	rotation per minute
55	bq	Bq	becquerel, a unit symbol
56	amp	A	ampere
57	coul	C	coulomb
58	HZ	Hz	
59	w	W	watt
60	KPa	kPa	kilo-pascal
61	p	Pa	pascal
62	ev	EV	volt (electronic unit)
63	Jonle	J	joule
64	J/mmol	kJ/mol	kilojoule per mole
65	10×10×10cm^3	10 cm×10 cm×10 cm	
66	N·km	KN·m	moment
67	$\bar{x}$±s	mean±SD	In figures, tables or text narration
68	Mean±SEM	mean±SE	In figures, tables or text narration
69	*im*	im	intramuscular injection
70	*iv*	iv	intravenous injection
71	Wang et al	Wang *et al.*	
72	EcoRI	*Eco*RI	*Eco* in italic and RI in positive. Restriction endonuclease has its prescript form of writing.
73	Ecoli	*E.coli*	Bacteria and other biologic terms have their specific expression.
74	Hp	*H pylori*	
75	Iga	*Iga*	writing form of genes
76	*igA*	IgA	writing form of proteins
77	-70 kDa	~70 ku	